

T
THE PETROLOGY AND GEOCHEMISTRY OF INTRUSIONS AT SELECTED NUNATAKS

IN THE AHLMANNRYGGEN AND GIAEVERRYGGEN,

WESTERN DRONNING MAUD LAND,

ANTARCTICA

/SR by

F.
JOHANNES REYNHARDT KRYNAUW.

D1986

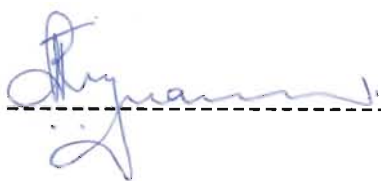
N Thesis (PhD, Geology) — University of Natal, Pietermaritzburg

Submitted in partial fulfilment of the requirements
for the degree of Doctor of Philosophy
in the Department of Geology and Mineralogy,
P University of Natal, Pietermaritzburg, S

(South Africa)

LIBRARY

I, JOHANNES REYNHARDT KRYNAUW, hereby declare that this thesis is my own original work, that all assistance and sources of information have been acknowledged, and that this work has not been presented to any other University for the purpose of a higher degree.



ABSTRACT

The mid-Proterozoic Borgmassivet intrusions of western Dronning Maud Land intrude Archaean granites and a volcano-sedimentary sequence, the Ritscherflya Supergroup. They are SiO_2 -rich ultramafic to mafic tholeiitic rocks which occur as layered bodies of unknown dimensions and sills up to 400 m thick. This thesis records detailed field, petrographic and whole rock geochemical studies on Borgmassivet intrusions at three widely-spaced localities within an area of approximately 20 000 km^2 in the Ahlmannryggen and Giaeverryggen.

- (i) Annandagstoppane-Juletoppane-Förstefjell area: The Annandagstoppane intrusions form part of a layered body or bodies, of which only a small part is exposed. They consist of a medium-grained 'main suite' of gabbro-norites and minor anorthosites, and a 'younger suite' of quartz diorite pegmatites, basaltic dykes, fine- to medium-grained gabbroic sills and minor albitite veins. The main suite rocks are ortho-cumulates in which plagioclase, orthopyroxene and clinopyroxene were primocrysts which crystallized in situ. The dykes and sills show typical basaltic and doleritic textures. Geochemical evidence suggests that the main and younger suites may be consanguineous.
- (ii) Robertskollen-Krylen area: The layered complex at Robertskollen comprises a lower, rhythmically layered ultramafic unit, overlain by a mafic unit. Olivine, orthopyroxene and clinopyroxene are the dominant cumulus phases in the ultramafic rocks, whereas plagioclase, orthopyroxene and clinopyroxene fractionation occurred during crystallization of the mafic rocks. Metastable co-existence of quartz with olivine and anomalous incompatible trace element characteristics of the Robertskollen complex suggest contamination of the magma(s) by crustal material. The Krylen intrusions show petrographic and geochemical characteristics similar to those

of the main suite at Juletoppane. A felsic dyke at Krylen may represent a rheomorphic product derived from Ritscherflya sediments.

(iii) Grunehogna-Jekselen area: The Grunehogna sill is a medium-grained diorite of unknown thickness, characterized by varying amounts of plagioclase and amphibole and a high Fe-Ti oxide content. It is overlain by a 50 m-thick quartz diorite pegmatite. The overlying 400 m-thick Kullen sill varies in composition from gabbro to gabbro and diorite and shows evidence for contamination by crustal material. Vugs, evidence for fusion, destruction of sedimentary structures and deformation in sedimentary contact zones and xenoliths and the abundance of pegmatites suggest that the sills intruded wet, unconsolidated or partially lithified sediments. The Jekselen complex consists of quartz diorites intruding Ritscherflya sediments. Amygdales in the upper zones of the complex indicate the subvolcanic nature of the intrusion.

Major, trace and rare earth element data of the Borgmassivet intrusions and the Straumshutane basalts (Watters, 1969a, 1969b, 1972, pers. comm., 1985) show a strong regional coherence, indicating that the rocks may be consanguineous. Abundance ratio patterns ('spidergrams') of the intrusions and basalts are identical. They are consistent with crustal contamination, possibly leucotonalite, of the magmas during ascent. The present distribution of the Borgmassivet intrusions and Straumshutane basalts reflects emplacement at stratigraphically higher levels within the Ritscherflya Supergroup from west to east. Previous radiometric isotope studies suggested that the intrusions are approximately 1700 to 1800 Ma in age, but recent investigations show that the isotopic data are poorly understood and have to be re-evaluated. Some of the isotope characteristics may result from crustal contamination and alteration effects during intrusion into water-saturated sediments.

ACKNOWLEDGEMENTS

I wish to thank the following persons and institutions:

My supervisors, Professor D.R. Hunter and Dr A.H. Wilson, for unfailing interest, expert advice and enthusiasm.

The Antarctic Division, Department of Transport, for logistical and financial aid, and the co-operation received from the Master, crew and ship's company of the MV S.A. Agulhas.

The Antarctic Programme, Marine and Earth Sciences Programmes of the FRD, CSIR, for co-ordination of the Antarctic Earth Sciences Programme.

The late Commandant R. Dean and the air crews who provided helicopter support. Despite working in isolated and often dangerous conditions one always felt to be in capable hands.

Professor V. von Brunn for advice and tremendous inspiration.

Dr A.R. Allen for advice and being my field partner during the 1981/82 field season, sometimes under trying conditions.

Mr P. Seyambu helped with preparation and did some of the geochemical analyses.

Dr B.R. Watters kindly made REE analyses available to me, which were done by N. Rogers at the Open University.

Mr R. Smith supplied major and trace element analyses of Archaean granitic rocks in the Piet Retief-Lüneburg area.

Mr D.I. Boden for his company and sense of humour as my field partner during the 1983/84 field season. His expert advice on the application of forestry techniques to the sampling of ultramafic rocks has been particularly useful.

Mr L.G. Wolmarans for his guidance with respect to the geology of western Dronning Maud Land and living in Antarctic conditions.

The Sanae teams and their leaders during my three field seasons. In particular, Dr D. Duthey and Dr A. Vermooten set very high standards and were of tremendous help to our field teams.

Similarly, I have enjoyed working with the members of the various South African Antarctic Earth Sciences Expeditions with which I have been associated. I wish to thank them for their support in the field, and the ability of most team members to contribute in some way to ensure that these Expeditions were successful.

Visitors to this Department have often had new ideas, or made suggestions which were very useful. In particular I wish to thank Professors C.J. Talbot and H.-J. Behr. Professor H.V. Eales kindly gave permission to quote from a paper by H.V. Eales and I.M. Reynolds. Professor K. Weber and G. Spaeth shared some of their latest ideas on the tectonic evolution of western Dronning Maud Land with us during a visit to the Research Vessel Polarstern.

E.P. Ferreira supplied information on the Schumacherfjellet and Högfonna Formations, and gave his permission to quote unpublished reports.

Dr J.M. Barton gave permission to quote unpublished Rb-Sr isotope data.

There are numerous other persons who have contributed to this project in various ways. I wish to thank them for their valuable discussions, advice, support in the field, acting as sounding boards to new (?) ideas, and various other ways in which they have contributed. Some of them are Professors H.L. Allsopp, T.N. Clifford and R.G. Cawthorn, Drs B.R. Watters, D. Bühmann, J.M. Barton, I. Evans and C. Harris, Messrs G.H. Grantham, P.B. Groenewald, D.M. Bristow, P. Mendonidis, D.W.W. Sleight, R.G. Smith, G. Snow, G. Brown, V. Preston, J.A. Versfeld, M. Peters, S.H. Auret, B. Hoal and R.T. Wonnacott. The technical support of P. Seyambu, P. Suthan, M. Seyambu, Mrs L. Le Roux and Mrs F. Richards was of a very high standard - thank you.

The kind and willing help from staff in Computer Services, University of Natal, Pietermaritzburg was much appreciated. Mrs B. Rimbault typed the manuscript with great patience. I owe a great debt to her. Thanks to Mrs L. Morley, who typed part of Chapter 4 for me.

My parents and father-in-law have given much support, materially and through encouragement, over the years. In no way can they be thanked adequately.

Finally, Paula and Mieke were at the receiving end. I do not think it will be possible to compensate for all the hours we should have spent together, but I will try my best.

CONTENTS

PAGE

ABSTRACT

ACKNOWLEDGEMENTS

CHAPTER 1	INTRODUCTION	1
	I. History of Research in Dronning Maud Land	1
	II. Geological Setting	5
	III. Previous Work on the Igneous Rocks in the Ahlmannryggen-Giaeverryggen-Borgmassivet Areas	8
	A. The Mafic-Ultramafic Intrusions	8
	B. The Straumsnutane and Fasettfjellet Formations	12
	C. Mafic and Ultramafic Dykes	13
	IV. Aims and History of this Investigation	14
	V. Selection of Study Areas and Thesis Organization	16
SECTION A	THE LAYERED COMPLEXES	19
CHAPTER 2	ANNANDAGSTOPPANE, JULETOPPANE AND FÖRSTEFJELL	20
	I. Geology of the Mafic Rocks	20
	A. The Main Suite	20
	B. The Younger Suite	23
	II. Petrography	27
	A. Petrography of the Main Suite	27
	B. The Annandagstoppane Basaltic Dykes	38
	C. The Juletoppane and Förstefjell Sill	38

II.	D. Fine-Grained Gabbroic Bodies, Juletoppane	41
	E. Pegmatites	41
	F. Albitite Veins	42
III.	Geochemical Characteristics	43
	A. Major and Trace Element Variation	43
	B. Interpretation	50
IV.	Study of a Detailed Section at Hammer Heads	51
	A. Field Description	51
	B. Petrography	52
	C. Plagioclase Grain Size Variation	54
	D. Geochemical Variation in the Hammer Heads Section	60
V.	Discussion	67
	A. Summary of Petrological Features in the Main Suite and the Hammer Heads Section	67
	B. Environment and Shape of Intrusions	69
	C. Regional Comparison of the Main Suite in the Different Areas	70
	D. Possible Mechanisms operating during Crystallization of the Main Suite	72
	E. Relationship of the Younger Suite to the Main Suite	77
CHAPTER 3	THE ROBERTSKOLLEN COMPLEX	79
I.	General Geology	79
	A. The Ultramafic Unit	81
	B. The Mafic Unit	84
	C. Dykes	86
II.	Petrography	86
	A. The Gully Section	86
	B. Regional Petrographic Variation	97

II.	C. The Pegmatites and Fine-Grained Bodies	98
III.	Geochemistry	100
	A. Regional Characterization of the Robertskollen Complex	100
	B. Geochemistry of Gully Section	105
IV.	Discussion	110
	A. Shape of the Complex	111
	B. Possible Assimilation of Crustal Material	112
	C. Magma Emplacement and Crystallization	116
V.	Conclusions	117
SECTION B	MAFIC SILLS AND GRANITIC INTRUSIONS IN THE AHLMANNRYGGEN	118
CHAPTER 4	THE GRUNEHOGNA INTRUSIONS AND THEIR CONTACT RELATIONSHIPS	119
I.	Introduction	119
II.	The Geology of the Grunehogna Nunataks	121
	A. The Sedimentary Succession	121
	B. The Mafic Sills	122
	C. Sediment/Sill Contact Relationships , Granitic Intrusions and Sedimentary Xenoliths	130
	D. Dykes	142
III.	Petrography	143
	A. Diorite Sills and Mafic Pegmatites	143
	B. The Grunehogna Granite and Granitic Bodies within Contact Zones	153
	C. Contact Zone Granosediments and Xenoliths	159
IV.	Geochemistry	167
	A. General Geochemical Features	168
	B. Comparison of Data Sets	179

V.	Discussion	183
A.	Intrusive Relationships	184
VI.	Conclusions	198
CHAPTER 5	KRYLEN NUNATAK	200
I.	Introduction	200
II.	Geology	200
III.	Petrography	201
A.	The Gabbronorite	201
B.	The Quartz Diorite	202
C.	Mela-Olivine Gabbronorite	203
D.	The Felsic Dyke	204
IV.	Geochemistry	205
V.	Conclusions	205
CHAPTER 6	THE JEKSELEN COMPLEX	206
I.	Introduction	206
II.	Geology	206
A.	The Jekselen Formation	206
B.	The Jekselen Subvolcanic Complex	207
III.	Petrography	210
IV.	Geochemistry	205
V.	Discussion and Conclusions	215
SECTION C	REGIONAL GEOCHEMISTRY AND SYNTHESIS	217
CHAPTER 7	REGIONAL GEOCHEMISTRY	218
I.	Introduction	218
II.	Regional Geochemical Variation	222

II.	A. Major and Trace Elements	222
	B. Rare Earth Element Compositions	229
	C. Abundance Ratios	232
	D. Interpretation of Abundance Ratios and ITER	232
III.	Conclusions	234
CHAPTER 8	SYNTHESIS AND CONCLUSIONS	235
	I. Synthesis	235
	II. Conclusions	240
REFERENCES		244
APPENDICES		267
	APPENDIX 1 SAMPLING AND ANALYTICAL TECHNIQUES	268
	APPENDIX 2 SAMPLE DESCRIPTIONS AND GEOCHEMISTRY	274
	APPENDIX 3 TABLES REFERENCED IN TEXT	318

CHAPTER 1 INTRODUCTION

This thesis reports petrological and geochemical research being conducted on some of the intrusions in the Ahlmannryggen and Giaeverryggen, western Dronning Maud Land, Antarctica (Figures 1.1, 1.2). The research forms part of the South African Antarctic Earth Sciences Programme, which receives logistical and financial support from the Department of Transport, on the advice of the South African Committee for Antarctic Research (SASCAR), CSIR. The area investigated is not well known, and has specific problems of logistic support and fieldwork. Hence a brief history of research in the area and a summary of the regional geology are given below.

I. History of Research in Dronning Maud Land

The first reported discovery of western Dronning Maud Land was during the Russian expedition of 1819 to 1821, led by F.F. von Bellingshausen and M.P. Lazarev. The ice-front of the Fimbulisen and Jelbartisen was sighted between about 1° and 3° W longitude, but no landings were made. More than 100 years elapsed before further scientific studies of this part of Antarctica were undertaken. A Norwegian expedition in 1930 under the leadership of H. Riiser-Larsen explored the ice-front from just east of the Greenwich Meridian to beyond Kapp Norvegia (71°20'S, 12°18'W). During this expedition mountains were discovered by Fin Lützow-Holm east of the Greenwich Meridian, about 200 km inland from the ice-front. This area of Antarctica was named Dronning Maud Land in honour of the Queen of Norway. The Norwegian expedition was followed during the 1938/39 austral summer by a German expedition, led by Alfred Ritscher, which completed an extensive aerial photographic survey, but no landings were made inland.

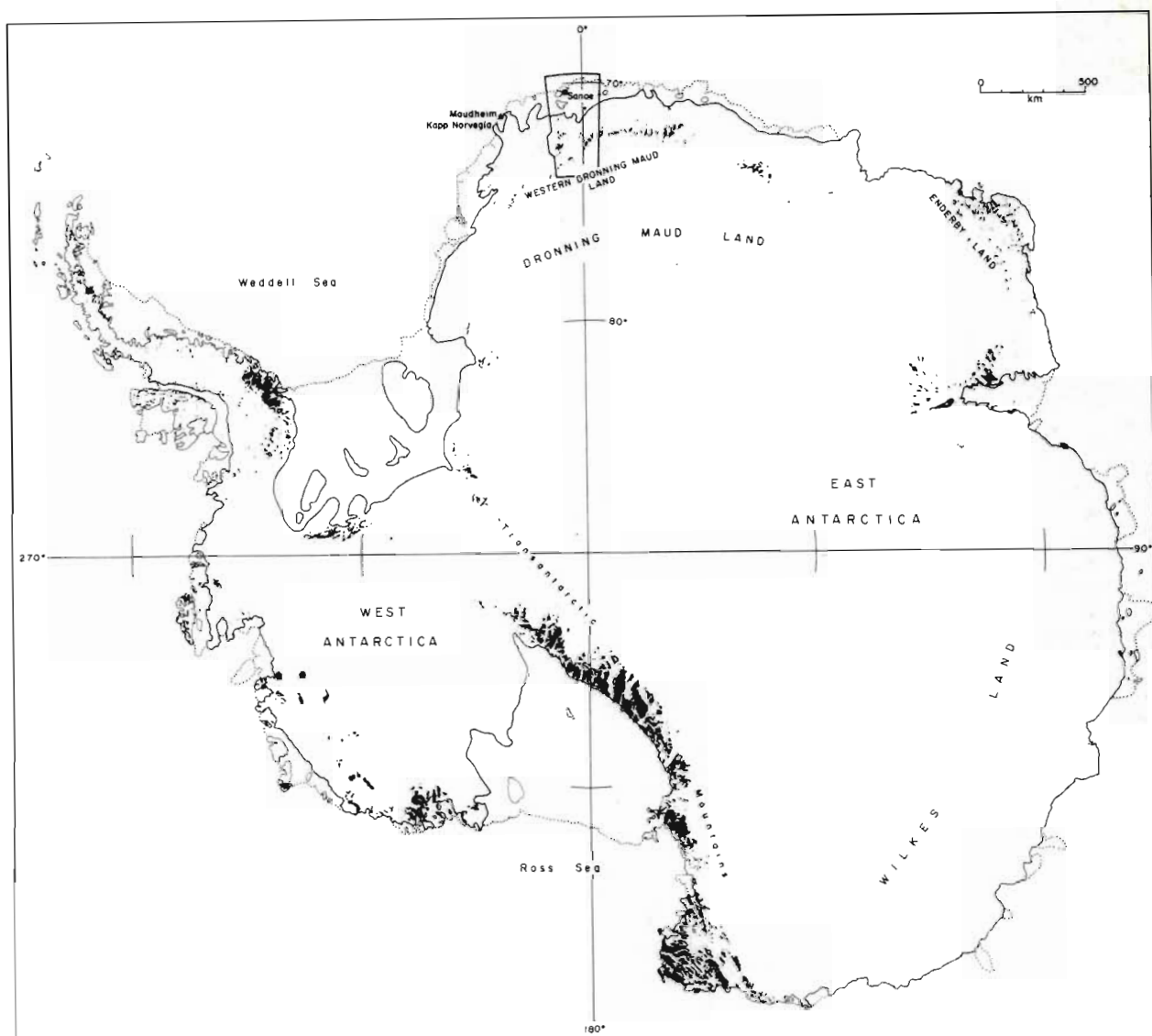


Figure 1.1 Locality map of the region studied by South African Antarctic Earth Sciences Expeditions (blocked area along 000°), showing outcrop distribution in the continent.

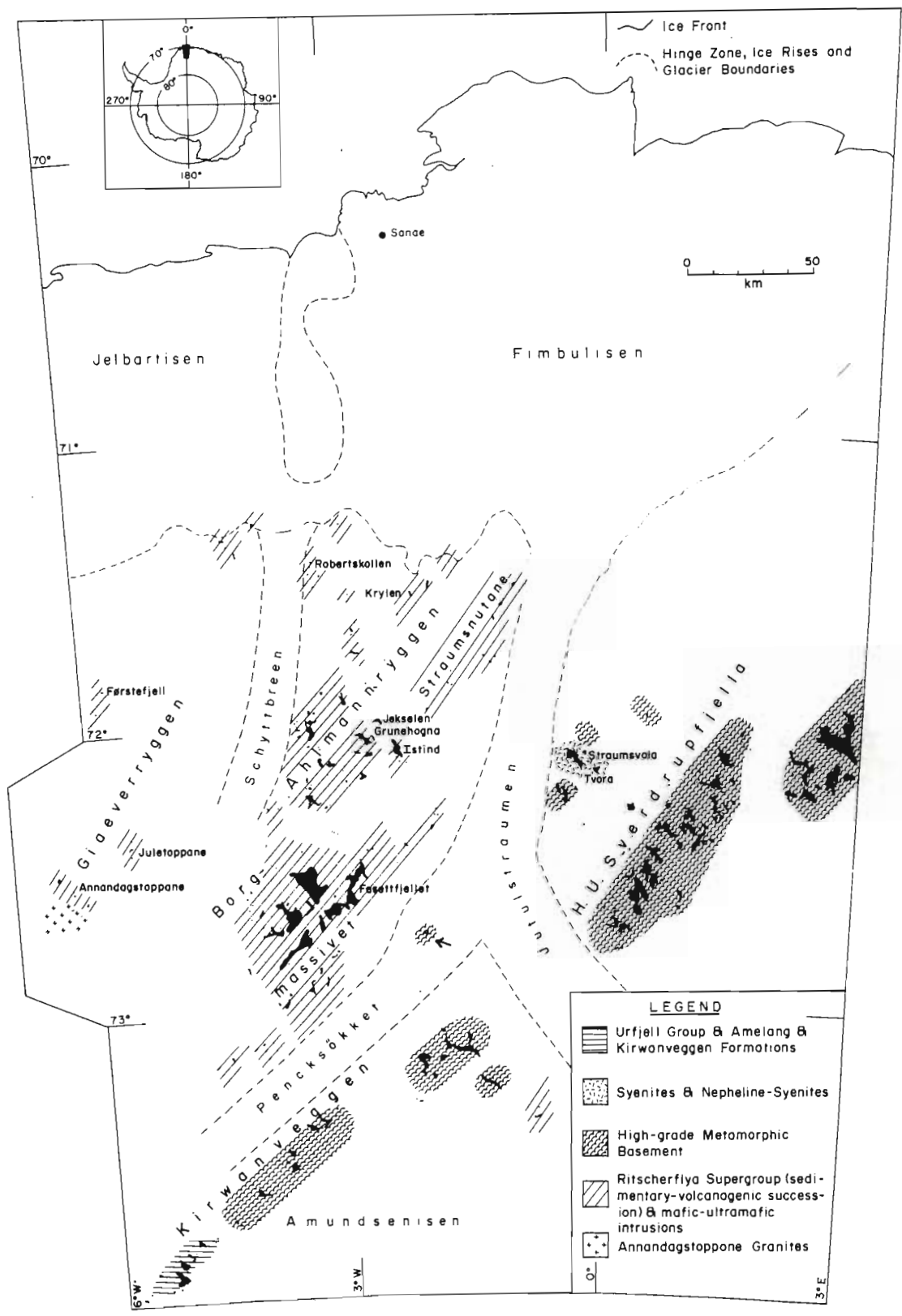


Figure 1.2 Generalized geology and localities of nunataks investigated during the current research project.

The first geological information about Dronning Maud Land was obtained by the joint Norwegian-British-Swedish Antarctic Expedition (NBSAE) which conducted oversnow and aerial surveys from 1949 to 1952 (Gjæver, 1954). The geological and topographic surveys traversed the area between the expedition's base at Maudheim (71°02'S, 10°55'W) and 1°30'E and as far south as 73°37'S. The geologists, E.F. Roots and A. Reece, mapped outcrops within an area of more than 50 000 km² during two summer seasons (Roots, 1953, 1954, 1969). Although this exploratory work was performed largely of a reconnaissance nature, the stratigraphic column which they established agrees in broad outline with that currently in use (Roots, 1969; Wolmarans and Kent, 1982).

South African involvement in Antarctic research followed the creation of the Scientific Committee on Antarctic Research (SCAR) of which South Africa has been a member since its inception in 1958. The first South African expedition accompanied by one geologist was mounted in 1960. In the period 1960 to 1975 most outcrops on nunataks in the area between 71° and 74° S, and 1° and 6° W were visited by geologists based at Sanae (Fig. 1.2). These geologists spent up to 14 months at Sanae, but the long periods of darkness and poor weather conditions restricted fieldwork to an average of 40 days annually. Nonetheless, the regional mapping completed between 1960 and 1975 has provided a sound foundation on which to base problem-orientated research.

Acquisition of a new research-relief vessel with the capacity to accommodate long-range helicopters resulted in a re-organization of the South African Antarctic Earth Sciences Research Programme. With this logistic support a greater involvement of University staff and research students was possible as the need to over-winter at Sanae was eliminated. Geological parties can travel south with the Sanae relief team, be air-lifted rapidly to the mountains, and return to Cape Town following completion of the take-over

period at Sanae. Geologists are thus able to spend about 30 to 40 days in the field during January and February every year. The first University geological team participated in the 1980/81 relief voyage. Since then as many as six teams have been engaged in detailed mapping during the summer seasons.

II. Geological Setting

Antarctica comprises two physiographic-structural provinces, Greater or East Antarctica and Lesser or West Antarctica (Figure 1.1). The former, which includes Dronning Maud Land, is underlain dominantly by Precambrian strata, and has been identified as the East Antarctic craton (Grikurov, 1982), or shield (Craddock, 1972). Ravich and Grikurov (1970) consider that East Antarctica consists of at least three crystalline shields or metamorphic complexes welded together by younger, late Precambrian to Palaeozoic mobile belts.

Approximately 2 per cent of the surface area of Antarctica is snow-free with the result that rock outcrops are confined to scattered nunataks. Outcrop in East Antarctica is confined to the Transantarctic Mountains, and a narrow zone along the rim of the continent. In Dronning Maud Land rock outcrops are found on nunataks that form an arcuate but discontinuous chain of mountains extending for 1 700 km from the eastern side of the Weddell Sea to east of Enderby Land (Figure 1.1), with an average exposed width of 75 km.

Four distinct terranes can be identified in western Dronning Maud Land (Figure 1.2), the geology of which has been summarized by Wolmarans and Kent (1982):

1. East and southeast of the Jutulstraumen and Pencksökket the H.U. Sverdrupfjella and Kirwanveggen are underlain by the polycyclically deformed, high-grade metamorphic rocks of the East Antarctic crystalline basement.
2. West and northwest of the Jutulstraumen and Pencksökket a relatively undisturbed sedimentary-volcanic sequence, the Ritscherflya Supergroup, forms the nunataks and mountains of the Borgmassivet, the Ahlmannryggen and the Giaeverryggen. The Ritscherflya Supergroup has been intruded extensively by the mafic Borgmassivet Intrusions, the ultramafic-mafic Robertskollen suite and the felsic Nils Jörgennutane suite.
3. At Annandagstoppane Archaean granite outcrops occur which have been dated at approximately 3200 Ma (Halpern, 1970; Barton, pers. comm., 1984) and 2800 Ma (Allsopp, reported in Elworthy, 1982; Auret, pers. comm. 1983). These granites may form the basement to the Ritscherflya Supergroup.
4. In the southwestern Kirwanveggen the crystalline basement is overlain by the Urfjell Group and the Amelang Formation. The Urfjell Group comprises a folded succession of quartzites and conglomerates, probably early Palaeozoic in age (Wolmarans and Kent, 1982). The Urfjell Group, in turn, is overlain by the Permian Amelang Formation, which consists of about 100 m of flat-lying sandstones with intercalated conglomerates and shales. The Amelang Formation is conformably overlain by more than 300 m of Jurassic basalts, the Kirwanveggen Formation.

The most important structural element in western Dronning Maud Land is the Pencksökket-Jutulstraumen dislocation between the high-grade metamorphic terrane to the east and the low-grade volcano-sedimentary sequence to the west (Figure 1.2). The Pencksökket trends approximately 045° until it joins the Jutulstraumen, whereafter the great outlet glacier trends approximately 032° .

At the junction a southern branch of the Jutulstraumen separates the Kirwanveggen from the H.U. Sverdrupfjella. Neethling (1970) states that the Pencksökkeet-Jutulstraumen system was offset en echelon to the northeast, but Landsat imagery shows that it is a single, slightly arcuate system. The Jutulstraumen is 300 km long and fills a trough which varies from 40 to 100 km in width. It is the second-largest drainage glacier of the Antarctic ice cap, the Lambert Glacier being the largest. Midbresrabben, near the junction of the Pencksökkeet and Jutulstraumen, is the only outcrop within the trough system, and comprises intensely sheared rocks and younger granites (Ravich and Soloviev, 1969; Grantham, pers. comm., 1985).

The nature of this structural feature is uncertain. Ravich and Soloviev (1969) consider the Pencksökkeet-Jutulstraumen system to be a graben of tectonic origin which is "a region of vigorous tectonic dislocations and apparently repeatedly the site of effusions and injection of magmatic masses of various compositions." These authors consider the onset of this tectonic activity was probably between 575 and 590 Ma. Neethling (1970) and Wolmarans and Kent (1982) refer to the feature as a rift. The latter authors suggest that rifting was initiated in the Proterozoic, with intermittent movement probably continuing until the Cainozoic. Soloviev (1972) and Declair and Van Autenboer (1982) consider the syenite bodies at Tvora and Straumsvola (Figure 1.2) to be restricted to deep regional faults, which characterize the tectonic contact zone between basement and platform deposits. Roots (1969) regards the Pencksökkeet as a zone of block faulting or a series of fault slices.

Estimates of the vertical displacement along the Pencksökkeet-Jutulstraumen rift vary considerably from about 600 to 1 500 m (Ravich and Soloviev, 1969) to 8 km (R.C. Wallace, quoted in Wolmarans and Kent, 1982).

To the west of the Ahlmannryggen and Borgmassivet is a glacier, the Schyttbreen, which is parallel to the Pencksökkeet-Jutulstraumen. The Schyttbreen may occupy another rift (Wolmarans, 1982; Wolmarans and Kent, 1982), but the evidence for this suggestion is tenuous.

III. Previous Work on the Igneous Rocks in the Ahlmannryggen-Giaeverryggen-Borgmassivet Areas

A The Mafic-Ultramafic Intrusions

The NBSA Expedition reported that the sediments of the Ritscherflya Supergroup had been intruded extensively by mafic rocks, which today form the dominant rock type of most nunataks in the Ahlmannryggen-Borgmassivet areas (Roots, 1953). They were named the *Borg Intrusions* (Roots, 1969).

During the first South African National Antarctic Expedition of 1960 V. von Brunn and J.J. la Grange investigated the nunataks in the northern Ahlmannryggen, including Robertskollen and Krylen (von Brunn, 1963, 1964). They discovered an ultramafic-mafic intrusion at Robertskollen in addition to the mafic rocks in the other nunataks they visited. Von Brunn provisionally correlated these rocks with the Jurassic Ferrar, Karoo and Tasmanian dolerites. The ultramafic rocks at Robertskollen were named the Roberts Knoll peridotite (Neethling, 1969). Neethling (1970, 1972a) accepted Roots' name of Borg Intrusions for all the mafic Precambrian sills in the Ahlmannryggen and Borgmassivet. He based his conclusions on the work of Pollak (1967), Neethling (1969), unpublished field reports in the South African Antarctic Earth Sciences Programme, and radiometric dating by McDougall (1969).

A number of plugs, dykes and irregular bodies in the mafic sills at Nils Jörgennutane and other localities were identified as syeno-diorites and named the *Jorgen syeno-diorite* (Neethling, 1969). Allsopp and Neethling (1970) suggest they are unrelated to, and younger than, the Borg intrusions, although Bredell (1976, 1982) regards these felsic intrusions as late differentiates of the Borg Intrusions and products of reaction between sediments and the mafic magmas.

Wolmarans and Kent (1982) describe the Borgmassivet Intrusions as all the relatively flat-lying mafic sills of Precambrian age which intruded the sedimentary-volcanogenic rocks of the Ritscherflya Supergroup. They use the terms *Robertskollen suite* and *Nils Jörgennutane suite* for the ultramafic and felsic phases respectively.

Annandagstoppane (72°33'S, 06°16'W), Juletoppane (72°23'S, 05°33'W) and Förstefjell (71°50'S, 05°43'W) were first visited by the NBSA Expedition in 1951 (Roots, 1954, 1969). A number of small nunataks, each less than 6 km² in extent, occur at the first two localities. Förstefjell is an isolated nunatak about 8 km north of Förstefjellsrabben in the northwestern Giaeveryggen (Figure 1.2). Annandagstoppane, identified incorrectly at the time as Juletoppane, was visited in the late nineteen sixties by Russian geologists. Their report of granite outcrops at Juletoppane, subsequently dated at 3,0 Ga (Halpern, 1970), led to a visit by a South African expedition in 1973 (Van Zyl, 1974).

Van Zyl reported that at Annandagstoppane the eastern and northern outcrops consist of dolerite, and the southwestern outcrops comprise granites, graphic granites and pegmatite (Figure 2.1). No contacts between the granitic and mafic rocks were observed. All the nunataks at Juletoppane (Figure 2.2)

comprise medium-grained dolerite, displaying well-developed magmatic layering. Pegmatitic pods and schlieren were found in places. The geology of Förstefjell has not been identified before but has been mapped as Borgmassivet Intrusions on Roots' (1969) map of the area. During the austral summers of 1980/81 and 1981/82 Annandagstoppane and Juletoppane were visited by South African Antarctic Earth Sciences teams. The mafic rocks were examined in detail in the field, followed by petrographic and geochemical studies which were reported by Krynauw (1983) and Krynauw et al. (1984). Förstefjell was visited briefly during the 1983/84 field season.

Relatively little petrographic work has been undertaken on the Borgmassivet Intrusions. Descriptions of specimens from limited areas or isolated nunataks are, however, available, e.g. von Brunn (1963) describes thin sections from the Robertskollen suite and the mafic rocks from the northern Ahlmannryggen, Aucamp (1972) describes the petrography of rocks from Grunehogna, and Bredell (1973) examined rocks from Jekselen and sills from the northeastern Borgmassivet.

Apart from the work of Neethling (1970, 1972b) and Bredell (1976), very little geochemical results have been reported to date. According to the regional studies, the Borgmassivet Intrusions comprise mainly quartz-normative tholeiites, which are considerably more silica-rich than the compositional range of most continental and oceanic basalts. Neethling recognizes two distinct differentiation trends.

The first trend is marked by an increase in SiO_2 , P_2O_5 and TiO_2 , with a concomitant decrease in FeO during the middle and late stages. These rocks were thought to be represented by the "more" differentiated intrusions, which have associated granophyres and exhibit rheomorphic phenomena.

The second trend is defined by a late-stage decrease in SiO_2 , and an increase in Fe_2O_3 . It was thought to be represented by the more massive intrusions which exhibit relatively little differentiation.

The oldest ages obtained to date on the Borgmassivet Intrusions vary from approximately 1700 to 1800 Ma (Allsopp and Neethling, 1970; Eastin et al., 1970; Elworth, 1982; Barton and Copperthwaite, 1983). Bredell (1976, 1982) proposes a reclassification of the mafic intrusions into the Krylen Intrusions (approximately 1700 Ma) and Ytstenut Intrusions (approximately 1000 Ma), based on reports by McDougall (1969), Allsopp and Neethling (1970) and Bredell (1973). Wolmarans and Kent (1982), however, believe that the Krylen and Ytstenut Intrusions could not be distinguished. They feel that there was insufficient evidence for a meaningful subdivision of the intrusive sills on the grounds of either lithology or age, and collectively describe the sills as the Borgmassivet Intrusives.

Rb-Sr data have yielded isochrons of 1800 Ma for the layered intrusion at Annandagstoppane, 1400 Ma for a diorite sill at Grunehogna, and 1200 Ma to 1000 Ma for rocks occurring at Robertskollen, Grunehogna and Jekselen (Barton and Copperthwaite, 1983; Barton, pers. comm., 1985). It has been suggested that not all of the isochron ages can reflect emplacement of the respective units, and there may be pseudoisochrons or meaningless isochrons (Barton, pers. comm., 1985).

Model ages of 1664 ± 50 Ma (Rb-Sr, Eastin et al., 1970) and approximately 1850 or 1400 Ma (Sm-Nd, Watters, pers. comm., 1984) have been obtained on the Straumsnutane basalts. Rb-Sr isochrons of 821 ± 50 Ma (Eastin et al., 1970) and approximately 850 Ma (Watters, pers. comm., 1984) have also been reported, in addition to an Rb-Sr model age of 1169 ± 35 Ma (Bowman, 1971) on a

Fasettfjellet andesite. The possible ages of 1600 to 1850 Ma suggest a genetic link between some of the extrusive and intrusive rocks of the Ahlmannryggen and Borgmassivet. Hence a brief description of the volcanic rocks from the Straumsnutane and Fasettfjellet is given below.

B The Straumsnutane and Fasettfjellet Formations

The volcanic rocks in the Straumsnutane were first reported by Roots (1953, 1969). He states that they are intermediate to basic in composition, often altered to "greenstones", and most were thought to be andesitic in composition. Butt (1962) and Roots (1953, 1969) report that most of the flows are amygdaloidal, and Butt notes that the lavas are more intensely sheared as the margins of the Jutulstraumen are approached. The occurrence of pillow lavas has been documented by Butt (1962) and Watters (1972). The latter author mapped the Straumsnutane during 1968/69, and subdivided the volcanic succession into four informal units. The succession was named the *Straumsnutane Formation* (Neethling, 1969, 1970). During the 1983/84 field season Watters remapped the area, and carried out sampling for research on major element, trace element and isotope geochemistry. He identified, mapped and sampled individual flows, and his preliminary results indicate that previous ideas about the stratigraphy of the Straumsnutane have to be revised considerably (Watters, pers. comm., 1984). He has shown that in the northern area the sequence has been folded into a complex series of anticlines and synclines trending north and northeast. He found that pillow lavas are distributed throughout the succession. His preliminary geochemical results indicate that the rocks are basaltic to basaltic-andesitic in composition, rather than andesitic, and that they are uniform with respect to major and trace element concentrations.

The volcanic succession at Fasettfjellet was discovered by Bastin (De Ridder and Bastin, 1968), and was examined by Watters (1969a, 1969b, pers. comm., 1984). Neethling (1970) named these rocks the *Fasett Volcanics* but the name was subsequently changed to the *Fasettfjellet Formation* (Wolmarans and Kent, 1982). The lava of the Fasettfjellet Formation displays an identical chemical character to the volcanic rocks from the Straumsnutane, the physical characteristics of the rocks from the two areas correspond closely, and the associated sediments are very similar, suggesting a close correlation between the two volcanic sequences (Neethling, 1970; Watters, pers. comm., 1984). The Fasettfjellet Formation conformably overlies the sedimentary Högfonna Formation.

C Mafic and Ultramafic Dykes

The Ritscherflya Supergroup and the Borgmassivet Intrusions have been intruded by mafic and ultramafic dykes (Wolmarans and Kent, 1982). These near-vertical dykes range in width from 30 cm to 30 m, and have probably intruded along pre-existing faults and joints. They are usually fine-grained, with chill margins, and are mainly dolerites and olivine-dolerites. Rare pyroxenite dykes have been described. Wolmarans and Kent (1982) consider them to be Triassic to Jurassic in age, although the possibility exists that some of them are feeder dykes to the Borgmassivet Intrusions.

Two types of dykes intrude the basalts of the Straumsnutane Formation (Watters, 1972). The first type averages 1 m and does not exceed 2 m in width. They are fine-grained rocks which exhibit basaltic textures. Vertical joints at right angles to their margins are invariably present. They all contain olivine phenocrysts, many of them up to 6 mm in length. The second set of dykes ranges from 2 to 14 m in width, and has a doleritic

texture. Fine- to medium-grained olivine-dolerite and basaltic dykes ranging in width from less than 30 cm to 2 m are common in the Ahlmannryggen (von Brunn, 1963; Aucamp, 1972).

IV. Aims and History of this Investigation

The research reported in this thesis is aimed at understanding the chemistry, source and petrogenesis of some of the intrusive rocks of the Ahlmannryggen. The volcanic rocks in the Straumsnutane are being investigated by B.R. Watters, University of Regina, Canada, and research on aspects of the isotope geochemistry of the intrusions is being conducted at the Bernard Price Institute, Johannesburg. The results from these three interrelated projects should contribute to an understanding of the nature of the sub-Antarctic mantle in western Dronning Maud Land. In addition, it is possible that rocks of the Ritscherflya Supergroup have been involved in the deformation and metamorphism of the high-grade metamorphic terranes of the H.U. Sverdrupfjella and the Kirwanveggen. If so, the chemical data reported here may serve as a basis for comparison between the Borgmassivet Intrusions and their metamorphosed equivalents. This, in turn, may be a useful indication of variation in subcrustal conditions across the Jutulstraumen tectonic zone.

However, owing to the regional nature and broad scope of the project, it has not been possible to undertake detailed studies on the mineralogy, mineral chemistry and REE characteristics of the rocks. These aspects are of vital importance for a full understanding of the petrogenesis of the intrusions. They will be treated in detail in follow-up projects.

The key questions to be considered in this thesis are:

1. What are the major geochemical and petrological characteristics of the Borgmassivet intrusions?
2. What are the genetic relationships (if any) of the different plutonic rock sequences?
3. What processes of differentiation or fractionation were operative?
4. To what extent have the various rocks been affected by metamorphic and/or metasomatic processes?
5. What relationship (if any) exists between the evolution of the Ritscherflya Supergroup and the igneous activity reflected by the Borgmassivet intrusions and the Straumsnutane basalts.

The history of the project can be summarized briefly:

1980/81 field season:

During January 1981 two days were spent at Krylen, Annandagstoppane, Jekselen, and Grunehogna, using a captive helicopter. Sampling was aimed at geochronological work by taking a number of samples from limited areas, rather than sampling for geochemical studies. However, these samples were analysed for major and trace elements, and some geochemical trends could be recognized already at this stage.

1981/82 field season:

During January and February 1982 Annandagstoppane, Juletoppane, Robertskollen and Grunehogna were investigated in more detail and a further 200 samples were collected.

1983/84 field season:

Based on earlier results, sections for detailed sampling were selected at Annandagstoppane and Robertskollen. Regional sampling was completed at Krylen, Grunehogna and Jekselen.

V. Selection of Study Areas and Thesis Organization

The original planning for this project had made provision for the sampling of most nunataks in the Ahlmannryggen and Giaeveryggen. However, after the 1980/81 field season it was recognized that each nunatak or nunatak area within these two regions may have unique geochemical and petrological characteristics. The only way to characterize the igneous rocks of the region was to study each nunatak in detail. It was decided to select six areas initially. These were: Annandagstoppane, Juletoppane, Robertskollen, Krylen, Grunehogna and Jekselen (Figure 1.2). A brief visit was paid to Förstefjell, which will be reported in this thesis. Selection of these nunataks was based on: (a) variation in field characteristics; (b) logistical considerations to dovetail field work within the overall Earth Sciences field programme; and (c) distribution of nunataks throughout the area.

The Annandagstoppane-Juletoppane-Förstefjell and Robertskollen areas (Figure 1.2) display characteristics of layered igneous complexes and have been grouped together in Section A of this thesis. Grunehogna comprises multiple sill intrusions into wet, unconsolidated sediments. Krylen may represent a sill, and Jekselen is a subvolcanic intrusion. The latter three nunataks have been grouped in Section B. An attempt to synthesize the regional characteristics of the intrusions has been made in Section C. The following information is presented in the Appendices: Sampling and analytical techniques and possible errors (Appendix 1), sample and petrographic descriptions and geochemical data (Appendix 2), and all tables referenced in the text (Appendix 3). The statistical treatment of geochemical data reported in Appendix 3 made use of the method of variable correlation ('reduced major axes', Tessier, 1948; Imbrie, 1956; Miller and Kahn, 1962).

Cumulus Terminology

The use of the terms cumulus and cumulate does not imply or exclude possible crystal settling, but is used in the sense of Irvine (1982) and Wilson (1982). Definition of cumulus terms as used in this thesis are as follows (Irvine, 1982):

Cumulate: An igneous rock characterized by cumulus framework of touching mineral crystals or grains, evidently formed and concentrated primarily through fractional crystallization.

Cumulus crystals: The fractionated crystals, which are typically subhedral to euhedral.

Postcumulus material: Crystals and grains that appear to have crystallized from intercumulus liquid in the interstices and pores of the cumulus framework, and that cement the cumulus crystals.

Cumulus crystallization stage: The formation of cumulus minerals.

Postcumulus processes: Those processes involved in solidification of the intercumulus liquid.

Orthocumulate: A cumulate in which abundant (mostly interstitial) postcumulus material is present, and in which cumulus minerals ideally exhibit much of their original crystallization forms. As a rule, postcumulus minerals make up 25 to 50 per cent (by volume) of orthocumulates.

Mesocumulate: A cumulate which has less postcumulus material than an orthocumulate, and in which cumulus grains adjoin in part along mutual interference boundaries developed through overgrowth. Postcumulus minerals make up 7 to 25 per cent of these rocks.

Adcumulate: A cumulate in which only minor amounts of postcumulus minerals are present (0 to 7 per cent) and mutual interference boundaries between are for the typical cumulus phases.

Petrographic terms used in this thesis are defined below (after MacKenzie et al., 1982).

Poikilitic texture: Relatively large crystals of one mineral enclose numerous smaller crystals of one, or more, other minerals, which are randomly orientated and generally, but not necessarily, uniformly distributed. The host crystal is known as an oikocryst, or enclosing crystal, and the enclosed crystals as chadacrysts.

Ophitic texture: This is a variant of poikilitic texture, in which the randomly arranged chadacrysts are elongate and are wholly, or partly, enclosed by the oikocryst. The commonest occurrence is of bladed crystals of plagioclase surrounded by subequant augite crystals in dolerite; however the texture is not confined to dolerites, nor to plagioclase and augite as the participating minerals.

Subophitic texture: The elongate chadacrysts are partly enclosed, and therefore penetrate the oikocrysts.

Intergranular texture: The spaces between plagioclase laths are occupied by one or more grains of pyroxene (± olivine and opaque minerals). Unlike ophitic texture, adjacent interrelated minerals are not in optical continuity and hence are discrete, small crystals. The feldspars may be in diverse, subradial or subparallel arrangement.

SECTION A

THE LAYERED COMPLEXES

CHAPTER 2 ANNANDAGSTOPPANE, JULETOPPANE AND FÖRSTEFJELL

I. Geology of the Mafic Rocks

No formal names exist for individual nunataks at Annandagstoppane and Juletoppane, but informal names are proposed here, which will be used in this thesis (Table 2.1 and Figures 2.1 and 2.2). The mafic rocks at Juletoppane and Annandagstoppane were divided into two groups by Krynauw et al. (1984), the 'main suite' and the 'younger suite'. This did not imply that the rocks from the two areas were necessarily related to one another, but the division was used to simplify description and discussion of these rocks.

A. The Main Suite

Maximum vertical exposure at Juletoppane and Förstefjell is 100 m, and at Annandagstoppane 50 m. Owing to the isolated nature of the outcrops and the small vertical exposures, no stratigraphic sequence has been established, and no attempt has been made to estimate thickness, size and shape of the main suite in the three areas.

Main suite rocks from Annandagstoppane comprise medium-grained norites, gabbros, gabbronorites and anorthositic gabbronorites in which modal variations in plagioclase, orthopyroxene and clinopyroxene define lenticular and discontinuous layers. In the northern outcrops at Viper's Hill, Bravo and Echo (Figure 2.1), the layers are rarely thicker than 5 to 10 cm. Truncated layers are locally present (Figure 2.3). In the southern outcrops at Hammer Heads it is not always possible to identify single units in the field owing to relatively small modal variations, although differential weathering on some weathered surfaces accentuates the layering. A homogeneous, porphyritic,

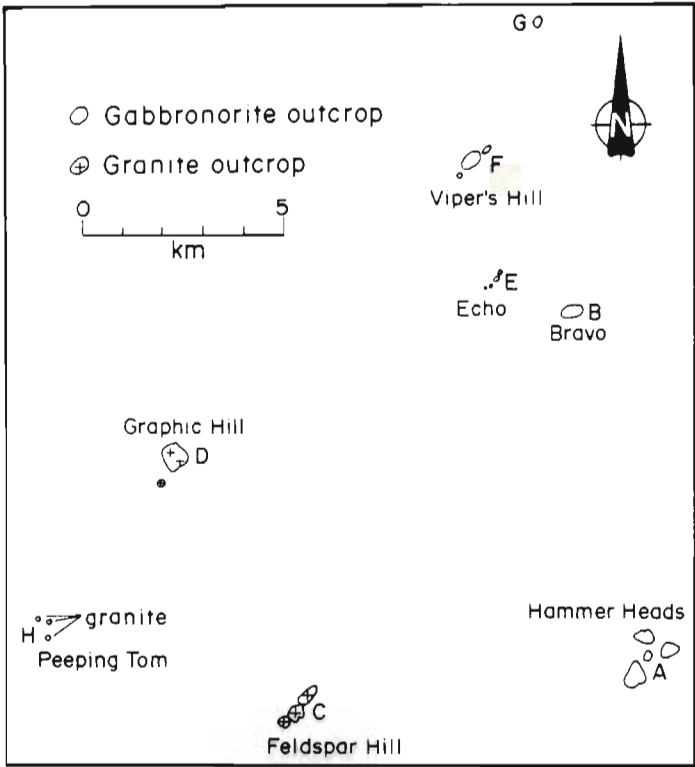


Figure 2.1 Distribution map of outcrops at Annandagstoppane, modified after Van Zyl (1974). Granite outcrops occur in the southwestern part of the area at Graphic Hill, Peeping Tom and Feldspar Hill.

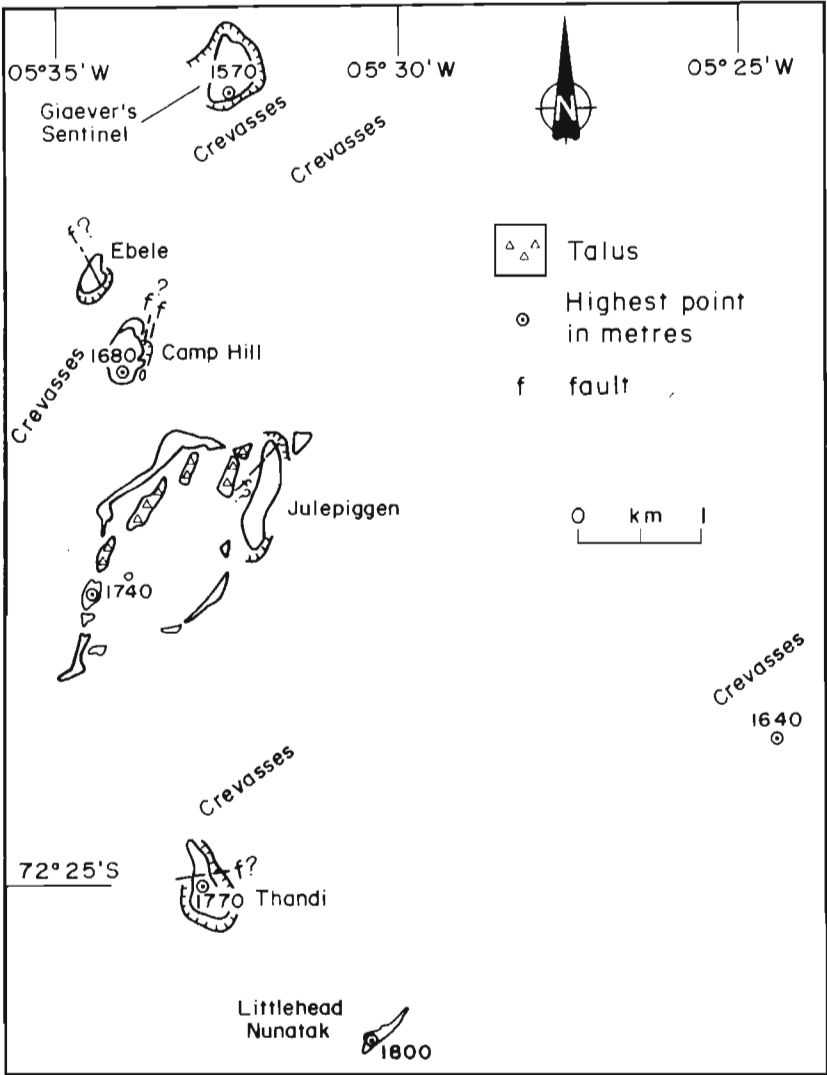


Figure 2.2 Distribution map of outcrops at Juletoppane, modified after Van Zyl (1974).

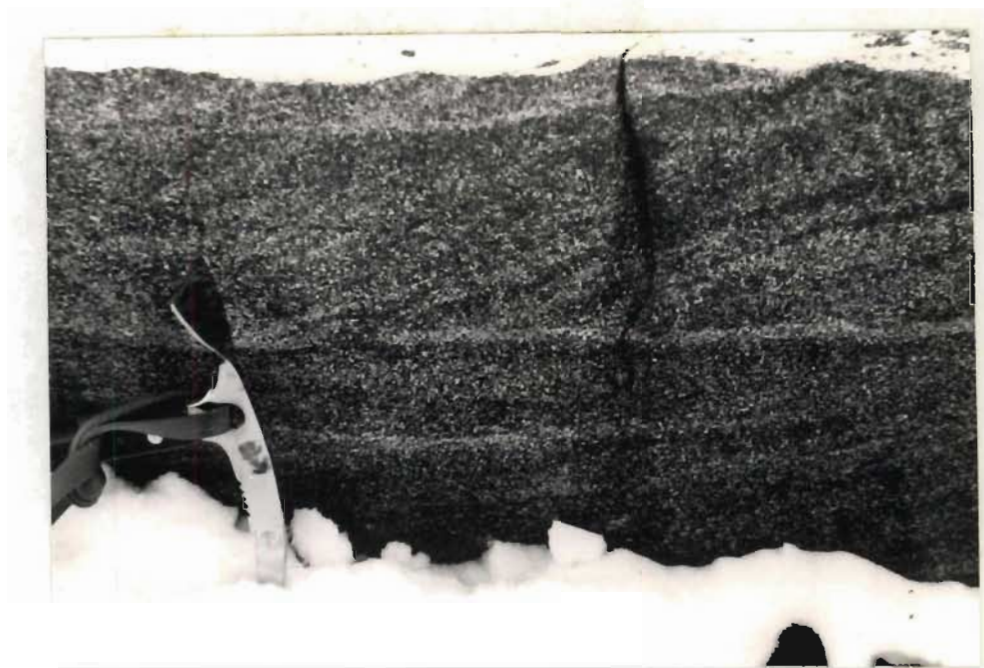


Figure 2.3 Truncated layering in gabbro-norite and norite at Viper's Hill, reminiscent of planar and trough cross-bedding. Length of ice axe head is 26 cm.



Figure 2.4 Load structures of anorthositic layers in norite, Viper's Hill. Length of ice axe head is 26 cm.

gabbro layer, about 15 to 20 m thick, occurs at Hammer Heads. At Juletoppane and Förstefjell the mafic rocks from the main suite comprise medium-grained gabbros and gabbronorites. The gabbroic rocks are very similar in appearance to those described at Annandagstoppane, with modal layering present, but with no evidence for truncation of layers. The layering is vertical at Förstefjell, with a strike of 355° . A homogeneous porphyritic gabbro layer, similar to that on Viper's Hill at Annandagstoppane, occurs in the upper parts of the two northern outcrops at Juletoppane (Gjaever's Sentinel and Ebele, Figure 2.2). Anorthosite lenses up to 10 cm thick and pods 15 to 20 cm in diameter occur locally at Viper's Hill. Some anorthosite lenses display slump or disruption structures (Figure 2.4). Relative changes in modal content among layers vary considerably. Contacts vary from sharp to gradational, but very little variation in grain size has been recorded.

B. The Younger Suite

Narrow, fine-grained basaltic dykes, less than 50 cm wide, cut the gabbroic rocks and the granites at Annandagstoppane (Figure 2.5). Outcrops of the dykes are rare, but abundant fragments of this rock are found in scree near most gabbro outcrops. Vertical columnar joints, perpendicular to the margins of the dykes occur abundantly in a dyke in the Archaean granite. The dip is vertical and it trends 325° .

Scree samples of albitite occur locally in the Annandagstoppane and Förstefjell nunataks. They may represent ice-transported material, but albitites in contact with gabbronorite have been found, suggesting local derivation. The contacts with the main suite rocks are sharp. Mafic pegmatites, as irregular pods and veins, occur throughout the Annandagstoppane and Juletoppane gabbros. The term "pegmatite" will be used in this thesis in

the sense of Jahns (1965), who applied the term to "holocrystalline rocks that are at least in part very coarse-grained, and whose major constituents include minerals typically found in ordinary igneous rocks, and in which extreme textural variations, especially in grain size, are characteristic." These pegmatites are mineralogically heterogeneous, even in hand specimen. Mineral assemblages vary from quartz-amphibole-biotite-plagioclase-K-feldspar to, less commonly, quartz-feldspar. Grain size ranges from less than 5 to 10 mm for most minerals, but locally acicular amphibole crystals are up to 15 cm in length. Chlorite-rich and feldspar-amphibole veins, usually less than 1 cm in thickness, are present locally.

A 25 to 30 m-thick fine- to medium-grained gabbro sill intrudes main suite rocks at Julepiggen in the Juletoppane area (Figure 2.6). The lower contact of the sill is not exposed, but the upper contact is horizontal and sharp, with no evidence of a chill zone. The exposed portion of the sill comprises a dark-grey, fine-grained rock which grades upwards into a medium-grained, light-grey gabbro. Fine- to medium-grained gabbroic bodies, similar in appearance to the upper part of the sill, are present in the main suite rocks at nunataks in the Juletoppane area. These bodies have irregular, pod-like shapes with sharp contacts, and are rarely larger than 3 m in diameter. A 30 to 40 m-thick fine- to medium-grained gabbro sill intrudes at the interface between main suite rocks and sediments. These sediments are possibly correlatives of the Ritscherflya Supergroup (Figure 2.7). The sill consists of a fine- to medium-grained dark-grey rock similar in appearance to the gabbro sill described at Juletoppane. Although generally conformable, the sill locally cuts across the sediments, which are contorted into an S-fold with a 1 m amplitude in one area.

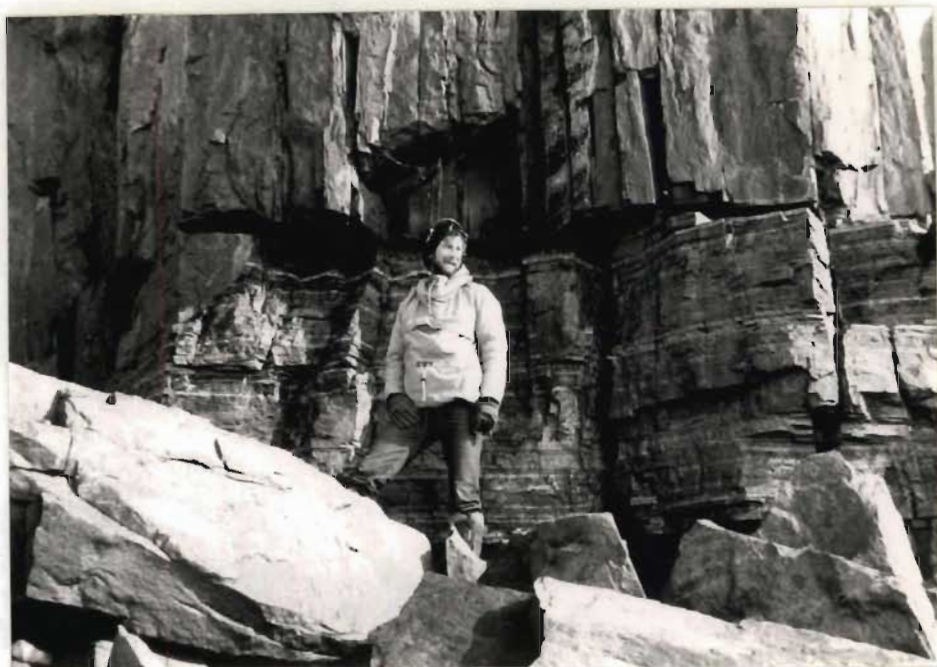


Figure 2.7 Gabbro sill intrusive into main suite and Ritscherflya (?) sediments at Förstefjell. Scale is 1.83 cm.

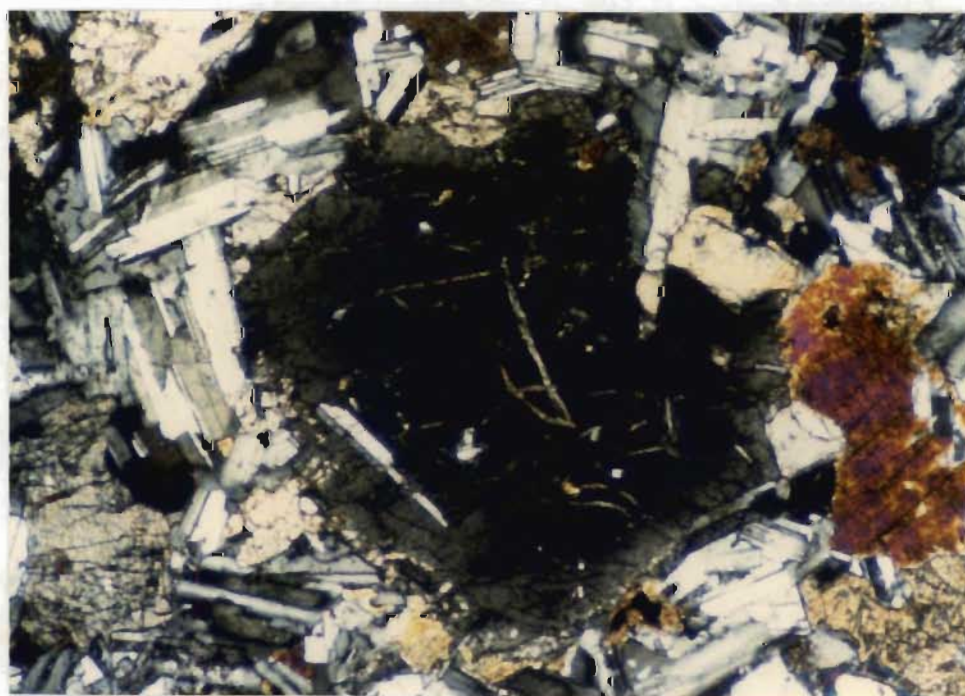


Figure 2.8 Photomicrograph of zoning in orthopyroxene of gabbro-norite at Hammer Heads. Crossed polars.

II. Petrography

A. Petrography of the Main Suite

Approximate modal compositions (Table 2.2), and limited mineral chemistry (based on optical measurements) are reported in this section. General petrographic features are summarized in Table 2.3. A more detailed study on a section at Hammer Heads is reported in section IV(B).

The typical gabbro-norite is a porphyritic rock with a poikilitic texture in which cumulus orthopyroxene and cumulus or postcumulus clinopyroxene phenocrysts are set in a matrix of zoned plagioclase and minor and trace amounts of interstitial postcumulus minerals. The orthopyroxene crystals are subhedral to euhedral, sections cut parallel to (001) being euhedral, and other sections typically subhedral. Sections parallel to (001) vary in size from 0.28 by 0.44 mm to 0.50 by 0.60 mm, and sections parallel and subparallel to (100) and (010) vary from 1.0 to 1.5 mm in length. Optical (2V) measurements indicate orthopyroxene compositions close to En_{70} . Locally the larger crystals exhibit evidence of zoning (Figure 2.8), primocrysts of orthopyroxene are in reaction relationship with clinopyroxene (Figure 2.9). This relationship was not observed in rocks in which both orthopyroxene and inverted pigeonite are present, and neither is it present in rocks containing orthopyroxene as the only Ca-poor pyroxene (Figure 2.10). The reaction relationship of orthopyroxene to clinopyroxene has been described elsewhere, e.g. in the Stillwater Complex (Jackson, 1961) and in the Great Dyke (Wilson, in prep.). It cannot be explained by following predicted crystallization paths in the system diopside-forsterite-silica (Bowen, 1914; Kushiro, 1972; Deer, Howie and Zussman, 1978), because the

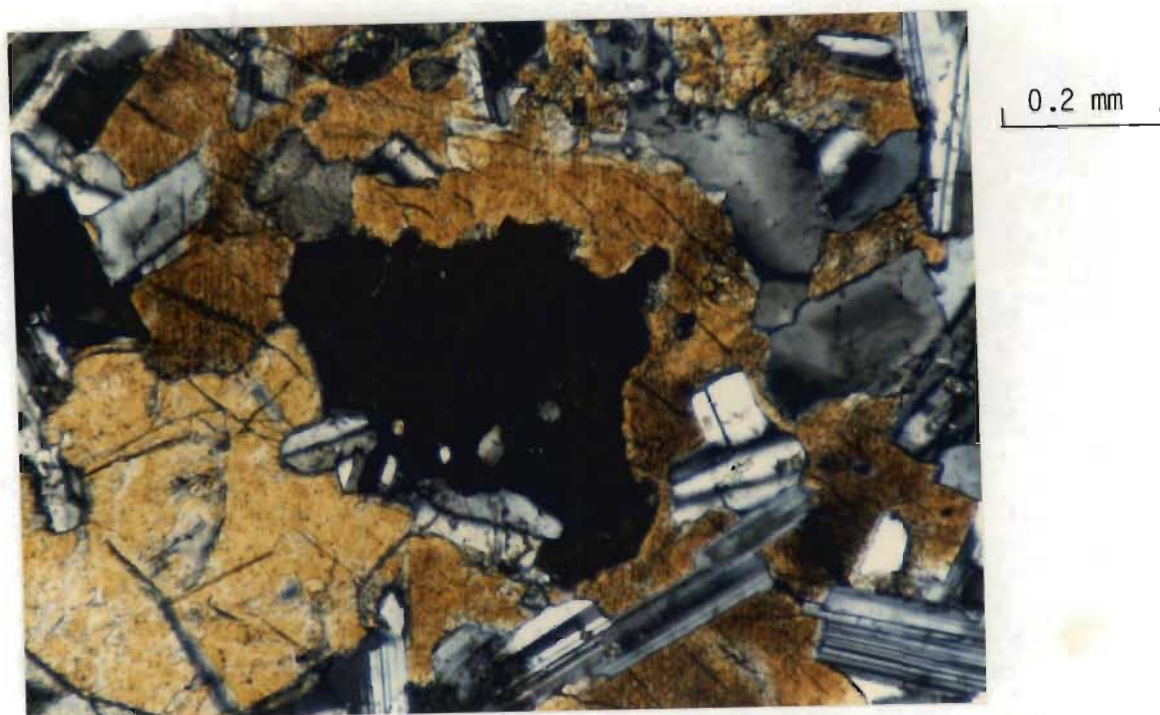


Figure 2.9 Photomicrograph of orthopyroxene reaction relationships with clinopyroxene, Hammer Heads. Crossed polars. Orthopyroxene is the dark mineral at the centre and is mantled by clinopyroxene.

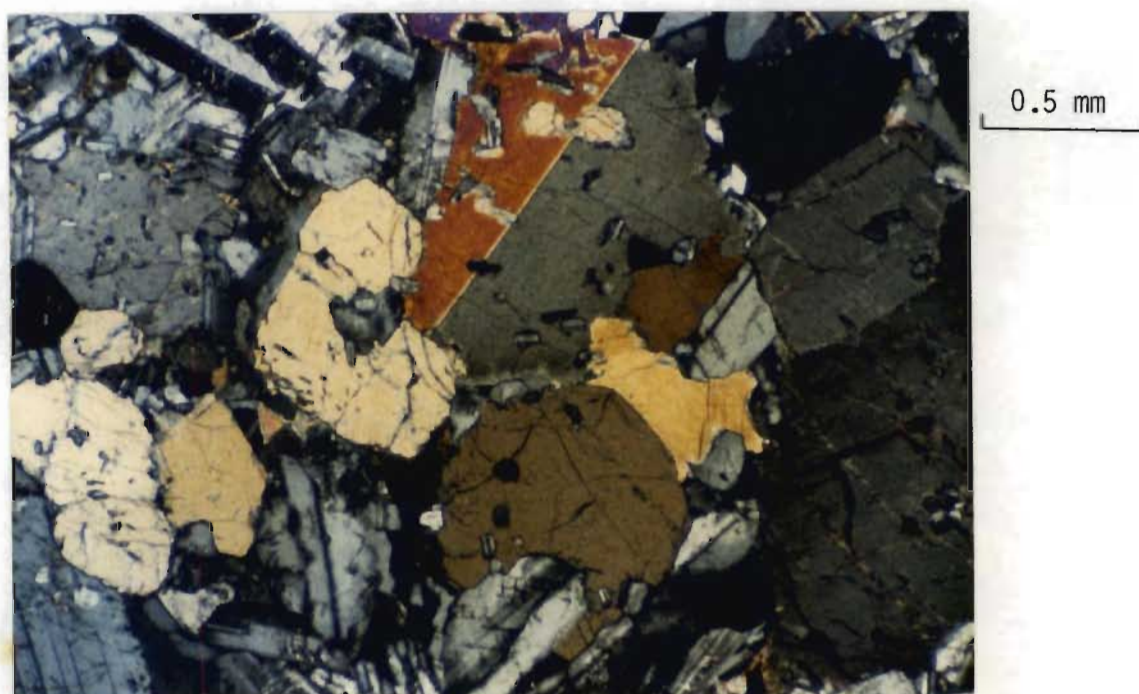


Figure 2.10 Photomicrograph of orthopyroxene primocrysts in gabbronorite, Viper's Hill. No reaction relationship is evident between orthopyroxene and clinopyroxene. Crossed polars. The euhedral minerals are orthopyroxenes. Clinopyroxene is twinned, or displays high interference colours.

complex phase relationships among orthopyroxene, pigeonite and clinopyroxene are not known in sufficient detail. At Bravo, and in the lower porphyritic layer at Hammer Heads many orthopyroxene cores are mantled by pigeonite (now inverted) (Figure 2.11). Locally the reaction affected entire grains. In some of the gabbro-norites at Viper's Hill there is only local evidence that orthopyroxene reacted with the magma to form pigeonite.

Cumulus orthopyroxene at Viper's Hill and Hammer Heads commonly occurs in clusters of six to eight grains and in some norite layers at Viper's Hill the orthopyroxene forms chains of five to ten crystals. Many of these chains are curved to define circular structures (Figure 2.12). Chain textures have been described from a number of layered intrusions (Jackson, 1961; Wager and Brown, 1968; von Gruenewaldt, 1970; Campbell, 1978). The latter author suggests that the chain textures are evidence for heterogeneous self-nucleation, and argues that they are more likely to have formed in situ rather than as chains which settled from higher levels in the magma. Eales and Reynolds (in press) describe branching chains of cumulus chromite in the Bushveld Complex, which can be used to determine the way-up of the layering. They argued that these delicate structures could only have been preserved during in situ crystallization and growth in the magma.

Inverted pigeonite is present in all main suite samples from Juletoppane and Förstefjell and locally from Annandagstoppane. Composite orthopyroxene-inverted pigeonite crystals occur in clusters at Juletoppane and form large grains up to 2 mm in diameter in places owing to re-equilibration and recrystallization. Most of the composite grains comprise a core of orthopyroxene mantled by inverted pigeonite, which is locally mantled by a second generation orthopyroxene (Figure 2.11). Both the second generation orthopyroxene and inverted pigeonite are in reaction relationship with



Figure 2.11 Photomicrograph of orthopyroxene mantled by inverted pigeonite, which is in turn mantled by orthopyroxene; gabbronorite, Hammer Heads. Crossed polars. In the top left-hand corner is evidence for a reaction relationship between the orthopyroxene mantle and clinopyroxene. Note the narrow, inner zone of blebby exsolution in the inverted pigeonite mantle.

0.5 mm

0.5 mm

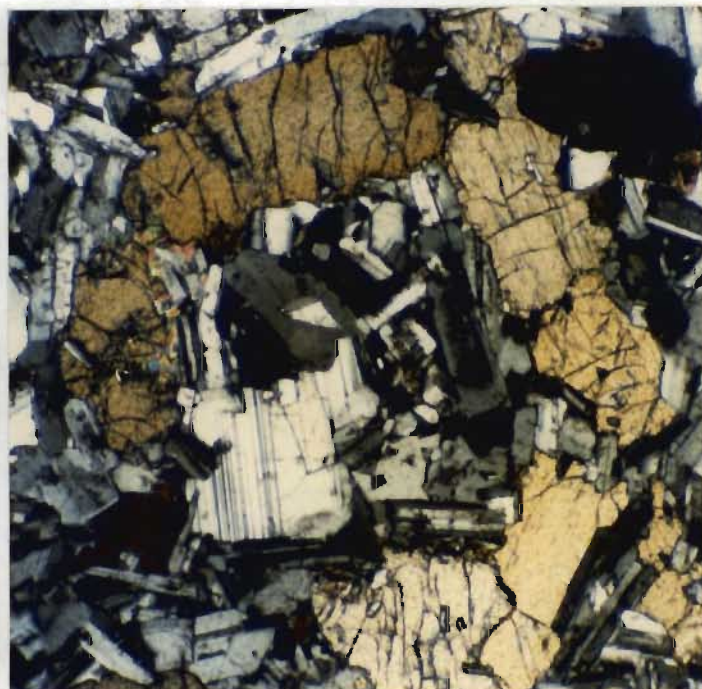
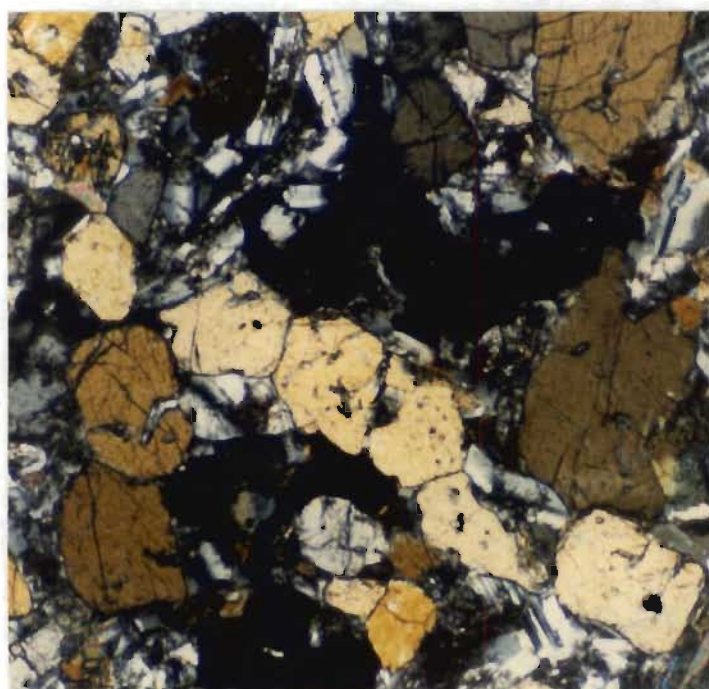


Figure 2.12 Photomicrographs of curved chains of orthopyroxene primocrysts, Viper's Hill (left) and Hammer Heads (right). Crossed polars.

clinopyroxene (Figures 2.11 and 2.13). There appears to be locally a sympathetic relationship between the presence of orthopyroxene mantles and that of plagioclase in some samples at Juletoppane. (Figure 2.14). Where plagioclase is enclosed or partly enclosed by an orthopyroxene mantle, an orthopyroxene zone free of inversion lamellae is present, resulting in embayments in the inverted pigeonite as shown in Figure 2.14. Similar features are found within the inverted pigeonite zone. Here plagioclase crystals are surrounded by a narrow zone of orthopyroxene free of inversion lamellae. In the same crystals which show these textures there are also plagioclase inclusions in the inverted pigeonite zones in contact with inversion lamellae. At least three different orientations of augite exsolution can be recognized in some grains of the inverted pigeonite, whereas other grains may show only one orientation. Two sets of lamellae at a small angle to each other are exhibited in association with a third blebby type of augite, which appears locally in the same grain. The latter type of exsolution is in optical continuity with augite mantles in reaction relationship with the pigeonite. In many cases where orthopyroxene cores are present the exsolved augite in the inner mantle has a blebby appearance over a narrow zone of 20 to 30 micron (Figure 2.11). The rest of the inverted pigeonite mantles consist of parallel exsolution lamellae in optical continuity with the exsolved blebs.

Plagioclase occurs in the matrix and as inclusions in cumulus orthopyroxene and postcumulus clinopyroxene. The plagioclase crystals in the matrix are lath-shaped euhedral to subhedral, varying considerably in size (Table 2.3). Rare megacrysts of plagioclase are present, but the proportion of megacrysts in main suite rocks in the Juletoppane area is higher than at Förstefjell and the Annandagstoppane area. Most of the plagioclase grains in the matrix show normal zoning from about An_{80} in the cores to An_{50-60} in the mantles.

Oscillatory zoning is common between the cores and mantles (Figure 2.15). The



Figure 2.13 Photomicrograph of inverted pigeonite in reaction relationship with clinopyroxene in gabbronorite at Viper's Hill. The clinopyroxene lamellae are in optical continuity with the clinopyroxene mantle. Crossed polars.



Figure 2.14 Photomicrograph of embayments in inverted pigeonite in the presence of plagioclase enclosed in orthopyroxene mantle, Juletoppane gabbronorite. Crossed polars.

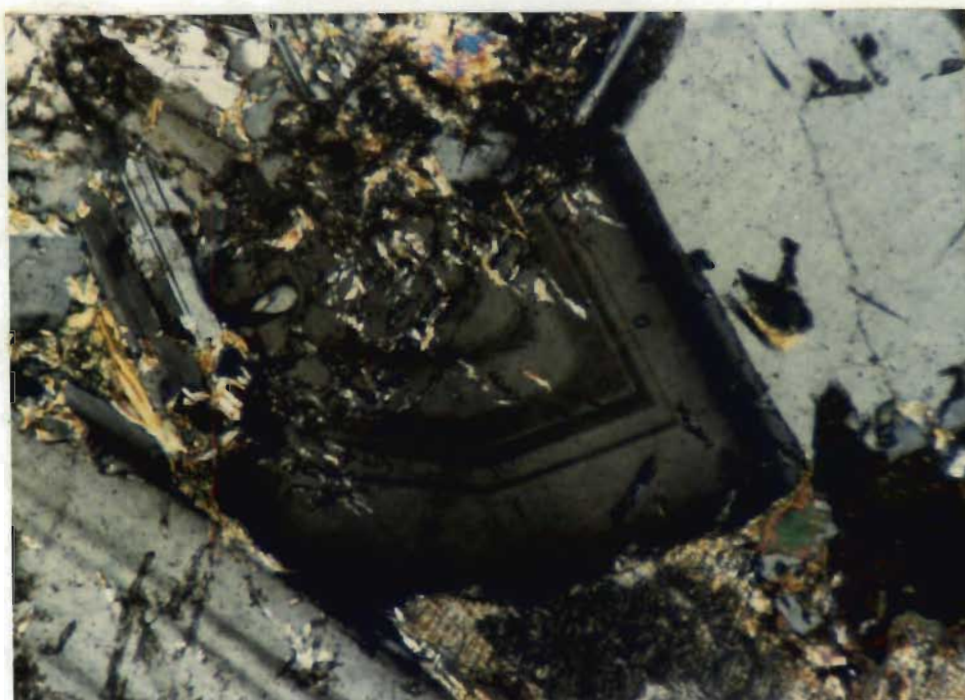


Figure 2.15 Photomicrograph of oscillatory zoning in plagioclase in gabbro-norite, Förstefjell. Crossed polars.



Figure 2.16 Photomicrograph of plagioclase chadacryst in cumulus orthopyroxene, norite, Viper's Hill. Crossed polars.

zoning in the plagioclase is evidence for extensive postcumulus growth. Plagioclase inclusions in cumulus orthopyroxene (Figure 2.16) occur as small laths. Postcumulus clinopyroxene oikocrysts invariably contain abundant plagioclase inclusions. Figure 2.17 shows that the size of the included plagioclase increases from the cores of the oikocryst to its margins. Similar features have been described by Wager (1961) and McBirney and Noyes (1979) who consider them to be indicative of in situ fractionation.

Grain size measurements of plagioclase inclusions in orthopyroxene and clinopyroxene were made, and compared with grain size distributions in the matrix in order to examine the characteristics of the mineral in the three different micro-environments, namely matrix, orthopyroxene and clinopyroxene. The data are presented as histograms in Figure 2.18. The most important features shown in these histograms are:

1. Grain sizes of plagioclase inclusions in orthopyroxene and clinopyroxene are markedly smaller than those in the matrix.
2. Width and length frequency distribution curves of plagioclase inclusions in orthopyroxene show that individual grains are smaller than those in clinopyroxene.
3. The range of grain sizes of plagioclase inclusions in clinopyroxene is greater than that of plagioclase included in orthopyroxene.
4. The frequency distribution curve of grain sizes of matrix plagioclase suggests there may be a bimodal size distribution.

Points 1 to 3 confirm that plagioclase nucleation was followed by orthopyroxene nucleation which, in turn, was followed by clinopyroxene crystallization. Growth of the latter mineral continued after postcumulus orthopyroxene growth had stopped, but the lack of plagioclase enclosed in clinopyroxene comparable in size to those in the matrix suggests that plagioclase growth continued after clinopyroxene growth had ceased. It is

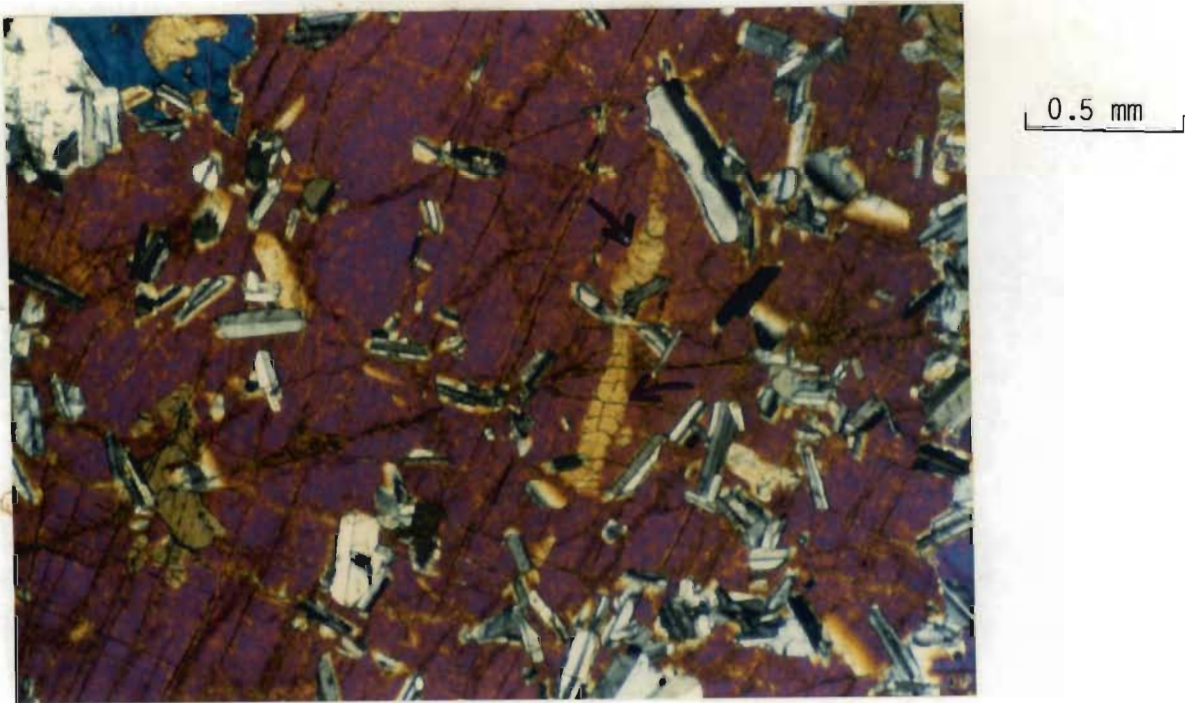


Figure 2.17 Photomicrograph of plagioclase crystals enclosed in clinopyroxene phenocryst. Plagioclase grain sizes increase towards the margins of the clinopyroxene. Remnant orthopyroxene (arrowed) represents a reaction between orthopyroxene and liquid to produce clinopyroxene. Crossed polars.

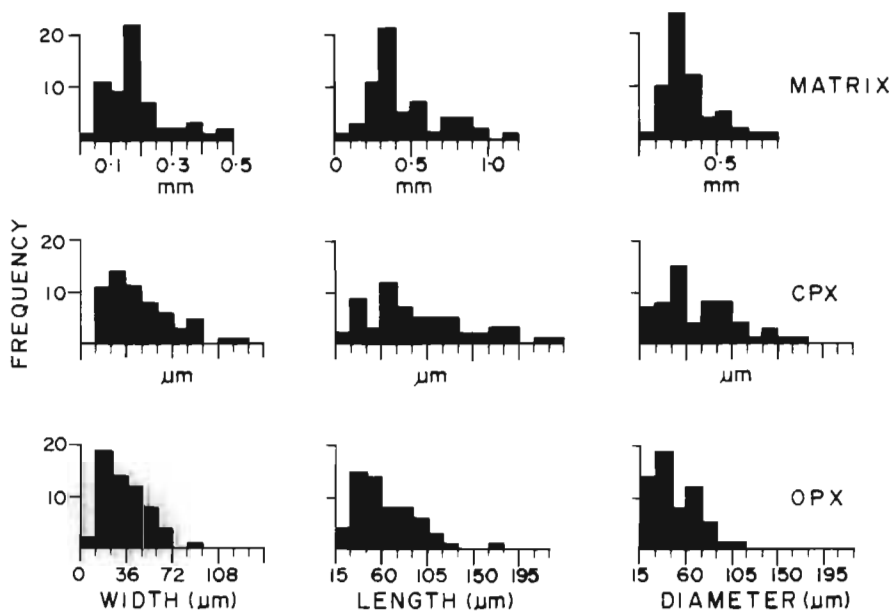


Figure 2.18 Comparison of plagioclase size distributions in sample A2/82 from Viper's Hill. "MATRIX": Plagioclase in matrix; "CPX": plagioclase inclusions in clinopyroxene; "OPX": plagioclase inclusions in orthopyroxene; \bar{x} : arithmetic mean. Note the spread in CPX values compared to OPX values.

likely that plagioclase growth, although slower than that of orthopyroxene and clinopyroxene, may have continued without interruption after its initial nucleation and only ceased at a very late stage.

Clinopyroxene habit is variable in different layers throughout the area, from interstitial grains to large oikocrysts although the modal content is relatively constant (Table 2.2).

Micrographic intergrowths of quartz and alkali feldspar (0.6 to 0.8 mm in diameter) with associated trace amounts of apatite needles and epidote are present as interstitial phases in nearly all the main suite rocks examined (Figure 2.19). However, sample A15/84 from Hammer Heads does not have micrographic intergrowths of quartz and alkali feldspar, but quartz and K-feldspar are present as discrete intercumulus phases up to 1.5 mm in diameter, in which apatite needles are enclosed locally (Figure 2.20). Magnetite occurs as an interstitial, anhedral mineral, which varies in size from 0.02 to 0.20 mm in diameter. Most grains have reacted with the postcumulus liquid or deuteric solutions to form biotite rims around the magnetite. Biotite also occurs in the matrix as interstitial grains.

Little evidence of deuteric alteration is found. Minor amounts of sericitization and saussuritization are present locally along cracks in plagioclase. In some plagioclase grains small patches of white mica (less than 0.2 mm in diameter) are present. Biotite has been altered locally to a green variety, and, in places, to chlorite, and the pyroxenes have been altered to tremolite/actinolite and chlorite along grain boundaries. Alteration of plagioclase and the pyroxenes may be present in the form of narrow (less than 1 mm) stringers, veinlets or irregular patches.



Figure 2.19 Photomicrograph of micrographic intergrowths of quartz and alkali feldspar, Viper's Hill. Crossed polars. The euhedral dark minerals are orthopyroxene crystals.

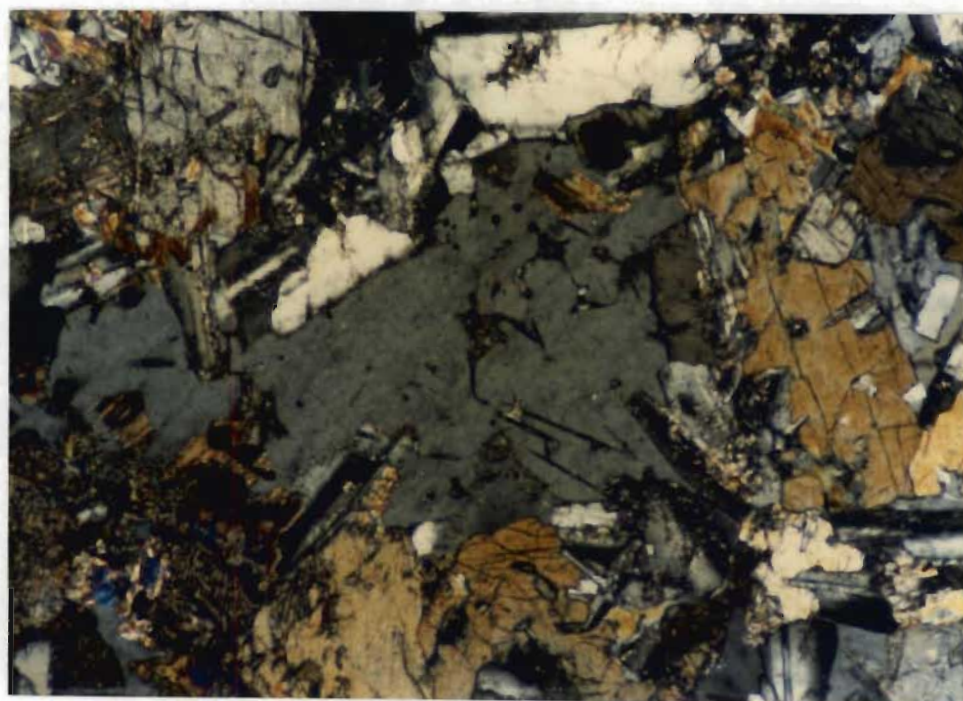


Figure 2.20 Photomicrograph of intercumulus quartz grain with enclosed apatite needles, sample A15/82, Hammer Heads. Crossed polars.

B. The Annandagstoppane Basaltic Dykes

The basaltic dykes are fine-grained glomeroporphyritic rocks with an intergranular texture in which aggregates of plagioclase microphenocrysts are set in a matrix of plagioclase, clinopyroxene and Fe-Ti oxides (Figure 2.21). The microphenocrysts are approximately 0.25 by 0.40 mm, and range in composition from An_{80} in the cores to An_{75} in the mantles. They vary from virtually unaltered, with minor sericitization along cracks, to pseudomorphs comprising white mica plates. Plagioclase in the matrix has a composition identical to that of the cores of the plagioclase phenocrysts. Intergranular clinopyroxene crystals are anhedral and rarely larger than 50 micron in diameter. Rare patches of tremolite/actinolite, chlorite and muscovite may represent uralitized clinopyroxene phenocrysts. Abundant disseminated anhedral Fe-Ti oxide grains up to 50 micron in diameter are characteristic of the basaltic dykes.

C. The Juletoppane and Förstefjell Sills

The sills at Juletoppane and Förstefjell are fine-grained gabbros and quartz gabbros with intergranular textures and varying amounts of plagioclase and quartz-alkali feldspar micrographic intergrowths (Table 2.4).

At the lowest exposed outcrop of the Juletoppane sill at Julepiggen the rock has an intergranular texture with a subparallel orientation of tabular plagioclase laths (Figure 2.22). Layering in thin section is defined by variations in plagioclase grain size, with individual layers or lenses as little as 6 mm in thickness. In fine-grained layers the plagioclase laths are approximately 0.08 by 0.30 mm and in the coarser-grained layers the grain size is approximately 0.20 by 0.60 mm. Anhedral clinopyroxene and inverted

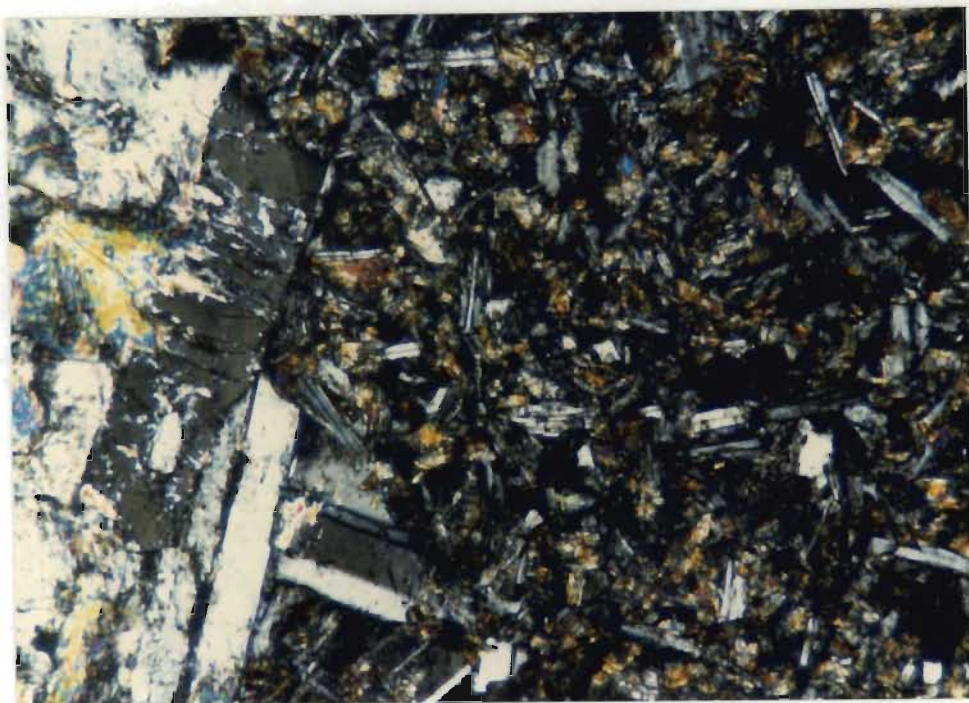


Figure 2.21 Photomicrograph of glomeroporphyritic intergranular texture in basaltic dyke. Crossed polars.

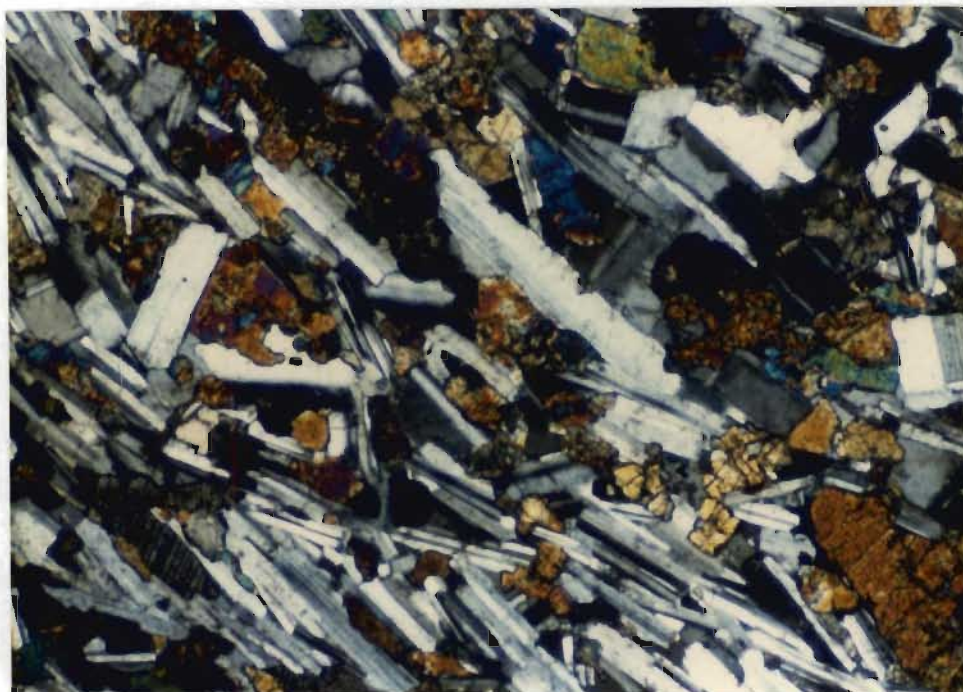


Figure 2.22 Photomicrograph of intergranular texture with subparallel orientation of plagioclase laths, Juletoppane sill. The pyroxenes are inverted pigeonite and clinopyroxene. Crossed polars.

pigeonite occur as interstitial minerals. Fe-Ti oxide grains are up to 1 mm in diameter. They show little alteration to biotite, and exhibit a poikilitic texture in which small (less than 0.10 mm in diameter) plagioclase and clinopyroxene inclusions occur. Micrographic intergrowths of quartz and alkali feldspar are rare. About twenty metres above the lower outcrop the rock has an intergranular to granular texture, with no apparent orientation of minerals, and plagioclase laths are about 0.25 to 0.75 mm in size.

Clinopyroxene and inverted pigeonite occur as intergranular phases, displaying a subophitic texture in which clinopyroxene phenocrysts partly enclose plagioclase laths. Abundant micrographic intergrowths of quartz and alkali feldspar occur in association with apatite needles and Fe-Ti oxides.

The petrographic textures of the sill at Förstefjell are similar to the upper part of the Juletoppane sill. The lower contact zone of the sill at Förstefjell has a subophitic intergranular texture, in which tabular plagioclase crystals commonly exhibit radiating textures and in places show arcuate outlines.

The length to width ratios are high, with average grain size approximately 0.2 by 0.65 mm. Clinopyroxene occurs as an intergranular phase and as phenocrysts (0.4 by 1.2 mm) which partly enclose plagioclase laths. Rare intergrowths of plagioclase and clinopyroxene were observed in a thin section. Fe-Ti oxide grains are present throughout in clusters, or locally in concentrations (30 micron wide) along the boundaries of plagioclase laths. Some plagioclase crystals contain bands (less than 10 micron thick) of these grains, which appear to be aligned parallel to crystallographic orientations in the plagioclase. Locally opaque minerals in the matrix have a dendritic habit, but they also occur as anhedral, disseminated Fe-Ti oxide grains, which have been altered to biotite in places. This latter type of oxide occurrence does not have the poikilitic habit described in the Juletoppane sill, but develops a skeletal texture. Interstitial phases comprise quartz, sericitized

alkali feldspar (in places as micrographic intergrowths) and apatite needles. Plagioclase crystals have been sericitized locally and clinopyroxene has been altered to tremolite/ actinolite, biotite, chlorite and Fe-Ti oxides.

D. Fine-grained Gabbroic Bodies, Juletoppane

The fine-grained gabbroic pods from Juletoppane have intergranular textures in which clinopyroxene and small amounts of inverted pigeonite are interstitial to plagioclase laths. Locally subophitic textures have developed in which plagioclase is partly enclosed by clinopyroxene laths. Modal contents are given in Table 2.4. Plagioclase grain sizes vary from 0.3 to 0.8 mm in diameter, and shows normal zoning from core to mantle, but with oscillatory zoning present in between. The Fe-Ti oxides vary from skeletal forms locally to grains of 0.6 to 0.8 mm in diameter, which contain plagioclase, clinopyroxene and biotite inclusions. Alteration to biotite is only found sporadically. Micrographic intergrowths of quartz and alkali feldspar are abundant, and apatite is commonly associated with the intergrowths as clusters of parallel needles. The gabbroic bodies show considerable deuteric alteration. Sericitization and saussuritization of plagioclase are common, and clinopyroxene and inverted pigeonite show abundant alteration to amphibole, biotite, chlorite and Fe-Ti oxides. Locally narrow (less than 0.1 mm) chlorite veins cut the rocks.

E. Pegmatites

Quartz-diorite pegmatites are mineralogically heterogeneous rocks showing considerable variation in grain size and texture. All the textures are granophyric, with plagioclase of approximately An_{50} at the cores of the

micrographic intergrowths of quartz and K-feldspar. Most of the plagioclase laths (1 by 4 mm) show some degree of sericitization. In some pegmatites acicular clinopyroxene crystals are up to 15 cm in length, and most of the crystals have been altered to tremolite/actinolite, biotite, chlorite and Fe-Ti oxides. Quartz is present as discrete grains (i.e. not intergrown with K-feldspar) in the matrix, in addition to its occurrence in micrographic intergrowths and as skeletal intergrowths with Fe-Ti oxides. The latter occur mostly in skeletal forms, and are also intergrown with biotite, chlorite and tremolite/actinolite. Locally the Fe-Ti oxides exhibit a triangular trellis pattern, caused by the alteration of magnetite to biotite in grains containing magnetite-ilmenite exsolution lamellae. The unaltered ilmenite lamellae define the trellis pattern (Reynolds, 1983). Apatite is a common accessory mineral. A green variety occurs in clusters and veinlets in which sections perpendicular to (001) are up to 0.1 mm in diameter. Metamict zircon is present locally, and is typically associated with quartz or biotite.

F. Albitite Veins

The albitite veins at Viper's Hill are characterized by granophyric intergrowths of albite and quartz developed around cores of albite. In contrast, the albitite veins at Echo have a granular texture and those at Hammer Heads have a poikilitic, porphyritic texture. Whereas quartz and albite are the dominant minerals present at Viper's Hill and Echo, quartz is present only rarely in the albitites at Hammer Heads. At the latter locality tremolite/actinolite form phenocrysts, but this mineral is absent at Viper's Hill. It is present in minor amounts as acicular grains at Echo. Where quartz is abundant, it is strained, exhibiting well-developed Boehm lamellae. Quartz grains in the matrix have complex, interlocking margins with albite. Anhedral albite grains (0.5 to 1 mm in diameter) at Viper's Hill display a

characteristic checkerboard twinning. Albite at Echo is present as anhedral laths, but at Hammer Heads the mineral occurs as anhedral grains (0.1 mm in diameter) and as anhedral to subhedral grains enclosed in tremolite/actinolite phenocrysts. Fluid inclusions are abundant in both the quartz and albite at Viper's Hill, the presence of which imparts a cloudy appearance to the latter mineral. Accessory minerals at Viper's Hill are skeletal grains of Fe-Ti oxides and minor amounts of epidote. Sphene is an important minor phase in the Hammer Heads albitites occurring as anhedral grains enclosed in the amphibole phenocrysts and in the matrix. Apatite and zircon are also present. Epidote, together with trace amounts of sphene and zircon, is present in the albitites at Echo, where chlorite is found locally intergrown with tremolite needles.

III. Geochemical Characteristics

Samples representing the rock types from Annandagstoppane, Juletoppane and Förstefjell were analyzed for major and trace elements in order to study their geochemical characteristics and to facilitate comparison among the three areas. In addition, 46 samples, taken vertically at one metre intervals at Hammer Heads, were analysed in order to study detailed variation over a 44 metre section. Results of the latter study are reported in Section IV.

A. Major and Trace Element Variation

General geochemical characteristics of the main and younger suites in the three areas are summarized in Figures 2.23 and 2.24 and Tables 2.5 and 2.6. Correlation coefficients given in the text refer to r^2 .

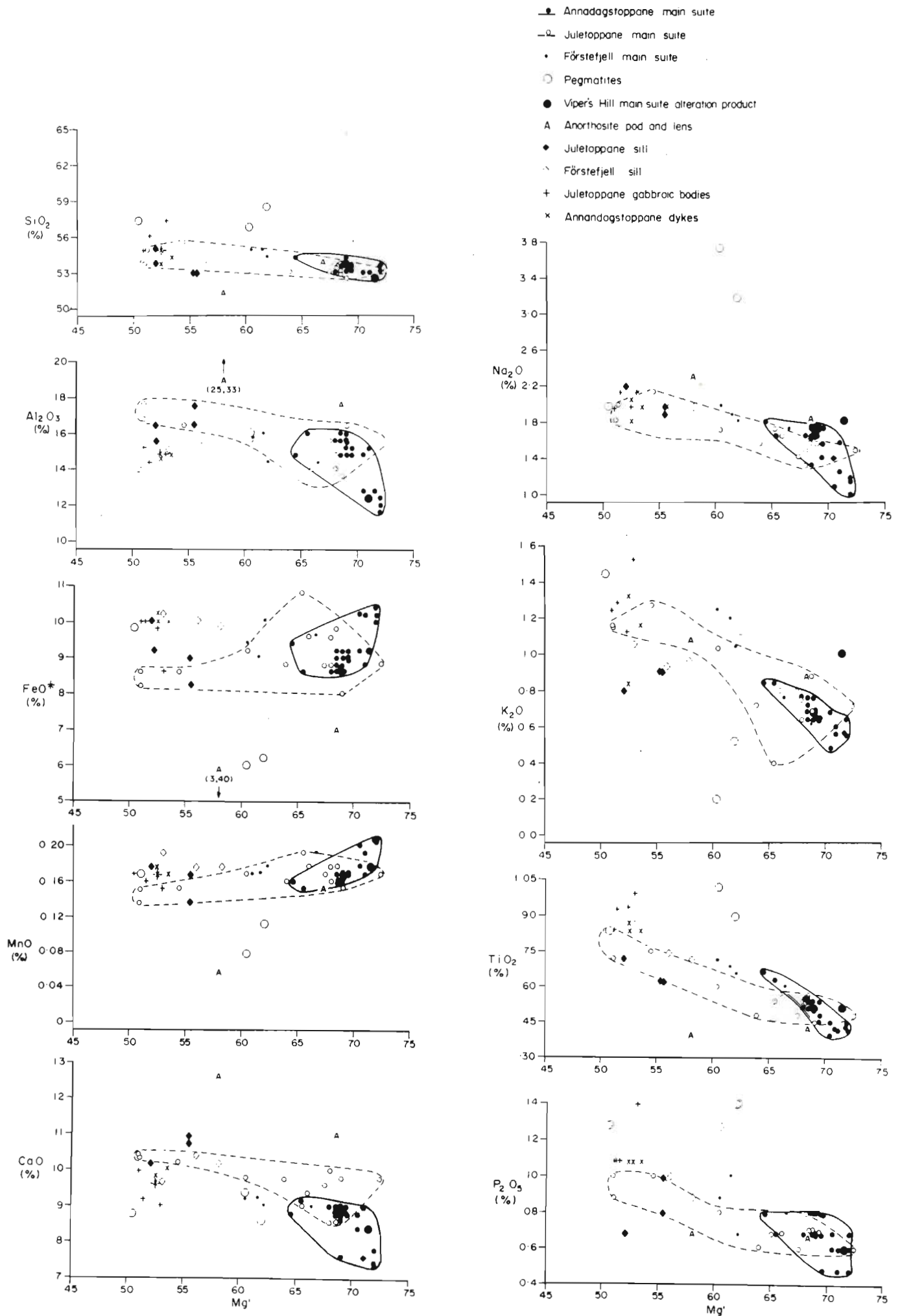


Figure 2.23 Regional variation of major elements with Mg' in the mafic intrusions at Annadagstoppane, Juletoppane and Förstefjell. Dashed line encloses field of Juletoppane data and solid line those of Annadagstoppane.

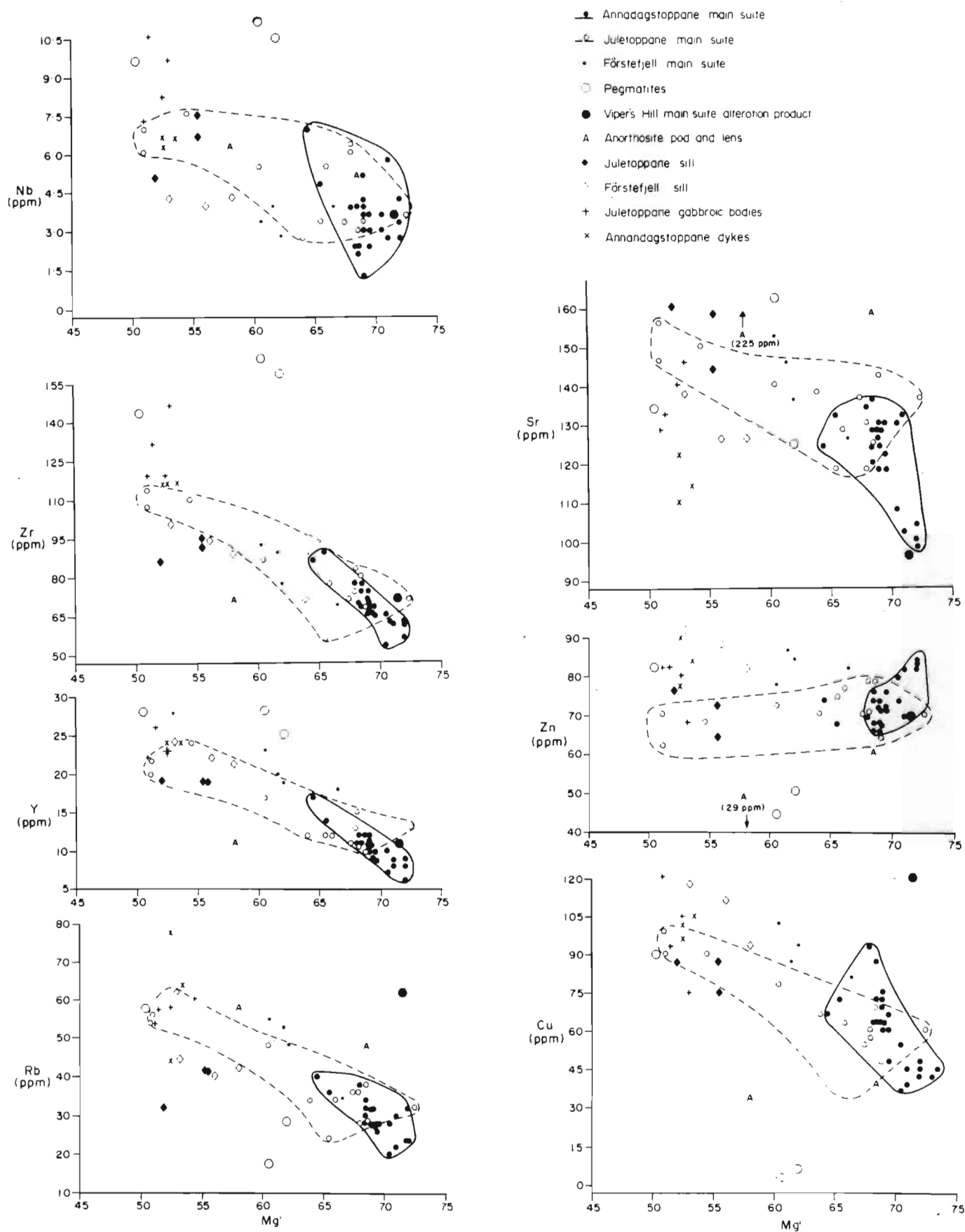


Figure 2.24 Regional variation of trace elements with Mg' in the mafic intrusions at Annandagstoppane, Juletoppane and Förstefjell.

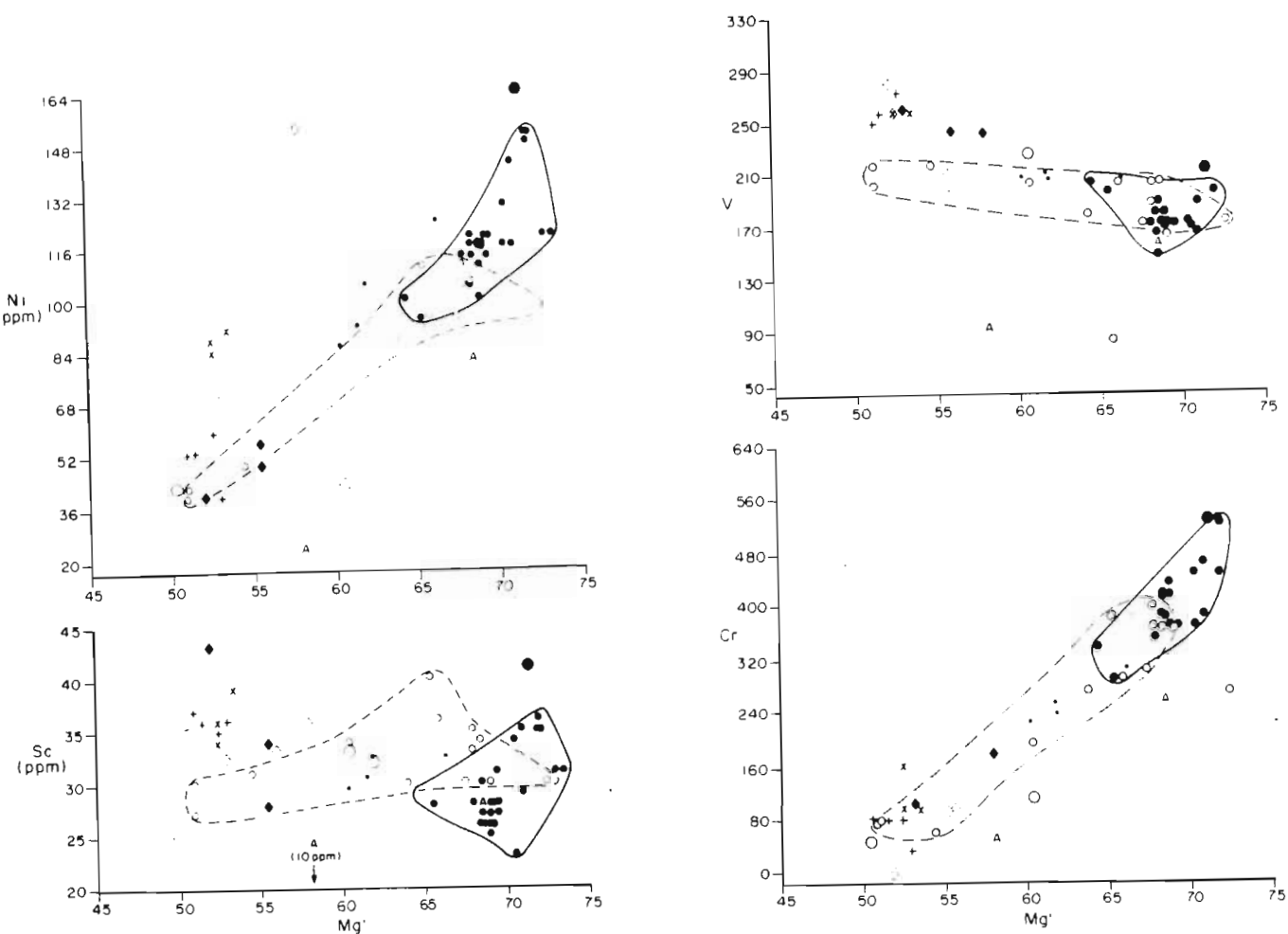


Figure 2.24 (continued)

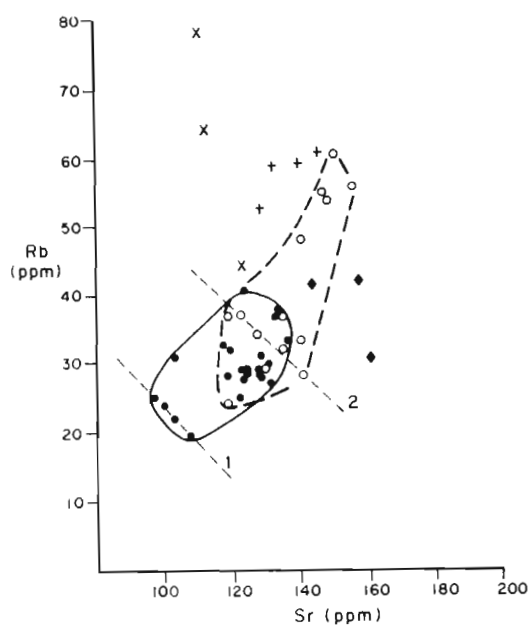


Figure 2.25 Regional variation of Rb with Sr in the mafic intrusions at Annandagstoppane, Juletoppane and Førstefjell. See text for discussion. 1: Variation at Viper's Hill; 2: Variation at Giaver's Sentinel. Symbols as in Figure 2.23.

Some of the most important features of the major and trace element geochemistry are

- (i) All the mafic rocks are quartz-normative tholeiites. They have a narrow range in SiO_2 contents, but the Mg-number (defined as $\text{Mg}' = 100 \text{ Mg}/(\text{Mg} + \text{Fe})$) shows a wide spread.
- (ii) Silica values decrease slightly with increasing Mg-number, but correlation is poor (Table 2.6).
- (iii) Alumina, CaO and Na_2O decrease with increasing Mg-number.
- (iv) Major element variation in the younger suite is greater than in the main suite, but variation is small within individual rock-types.
 - (a) The dykes have a narrow range in Mg-number and are slightly depleted in Al_2O_3 and CaO in relation to the compositional range of the Juletoppane main suite, and slightly enriched in FeO^* , MnO, TiO_2 and P_2O_5 , SiO_2 and Na_2O plot within the Juletoppane field. K_2O shows a larger variation than the other major elements.
 - (b) The fine-grained gabbroic bodies at Juletoppane and the Annandagstoppane dykes show essentially the same major element enrichment and/or depletion relative to the Juletoppane main suite field, although the data from the gabbroic bodies show a wider scatter on the variation diagrams. Data from the Juletoppane and Förstefjell sills have wider ranges for the Mg-numbers than the rocks of the younger suite. The data from the pegmatoids reflect the heterogeneous nature of these rocks, as the three samples analysed scatter considerably on the major element variation diagrams.
 - (c) The albitite geochemistry has not been indicated on Figure 2.23, because of the major differences in geochemical characteristics when compared with the other rocks in the area. The data are given in Appendix 2 (samples A9/82, A24/82 and A36/82). The most important

geochemical characteristics of the albitites are high concentrations of SiO_2 with very high $\text{Na}_2\text{O}/\text{K}_2\text{O}$ ratios between 212 and 351.

- (v) The trace element geochemical data of the Annandagstoppane, Juletoppane and Förstefjell main suites exhibit well-defined trends for the compatible and incompatible elements when plotted against Mg-number (Figure 2.24). The minor incompatible element oxides K_2O , TiO_2 and P_2O_5 and Nb, Zr, Y, Sr, Rb, Cu and V values increase with decreasing Mg-number. Chrome and Ni are compatible elements, showing marked increases with increasing Mg-number.
- (vi) Trace elements in the Annandagstoppane dykes show little variation, except for the mobile elements Sr and Rb. They are slightly enriched in Zr, Ni, Zn and Sc and depleted in Sr relative to the fields for these elements from the Juletoppane main suite.
- (vii) The Juletoppane sill shows little variation in trace elements compared to the dykes and gabbroic pods. Zr and Rb are depleted, and Y, Nb, Cu and Ni overlap the Juletoppane field.

The apparent incompatible behaviour of Sr appears to be anomalous, if plagioclase is a primocryst in the cumulus assemblage (Section II). The K_D of Sr in plagioclase in basaltic rocks is approximately 2.2 (e.g. Cox et al., 1979). Hence, if plagioclase was a major fractionating phase, Sr should have been removed by early-formed plagioclase, giving rise to lower concentrations of Sr in more evolved rocks, unless there is an increase in modal abundance of plagioclase with decreasing Mg-number. A positive correlation exists between Rb and Sr (Figure 2.25), but in specific layers, identified by dashed lines 1 (at Viper's Hill) and 2 (Glaever's Sentinel) negative correlations exist. These apparently opposing trends are important features of the petrogenesis of these rocks and represent a fine structure within the overall trend. The

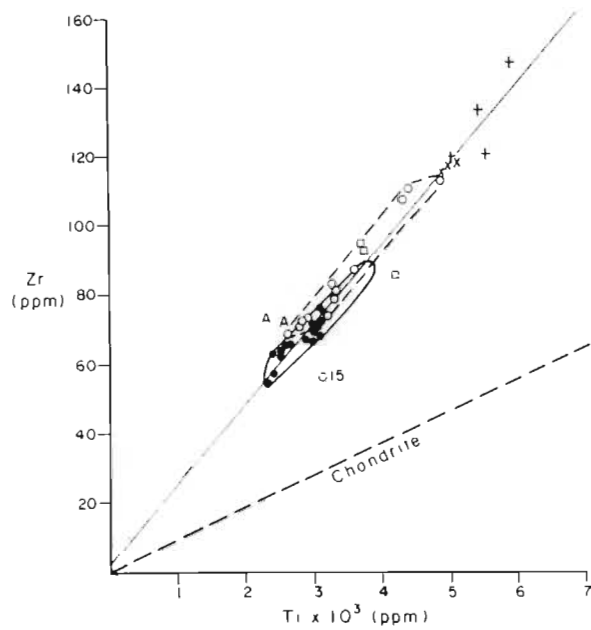


Figure 2.26 Variation of Zr with Ti in the Annandagstoppane, Juletoppane and F rsteffjell mafic intrusions. Symbols as for Figure 2.23. Correlation data are given in Table 2.6.

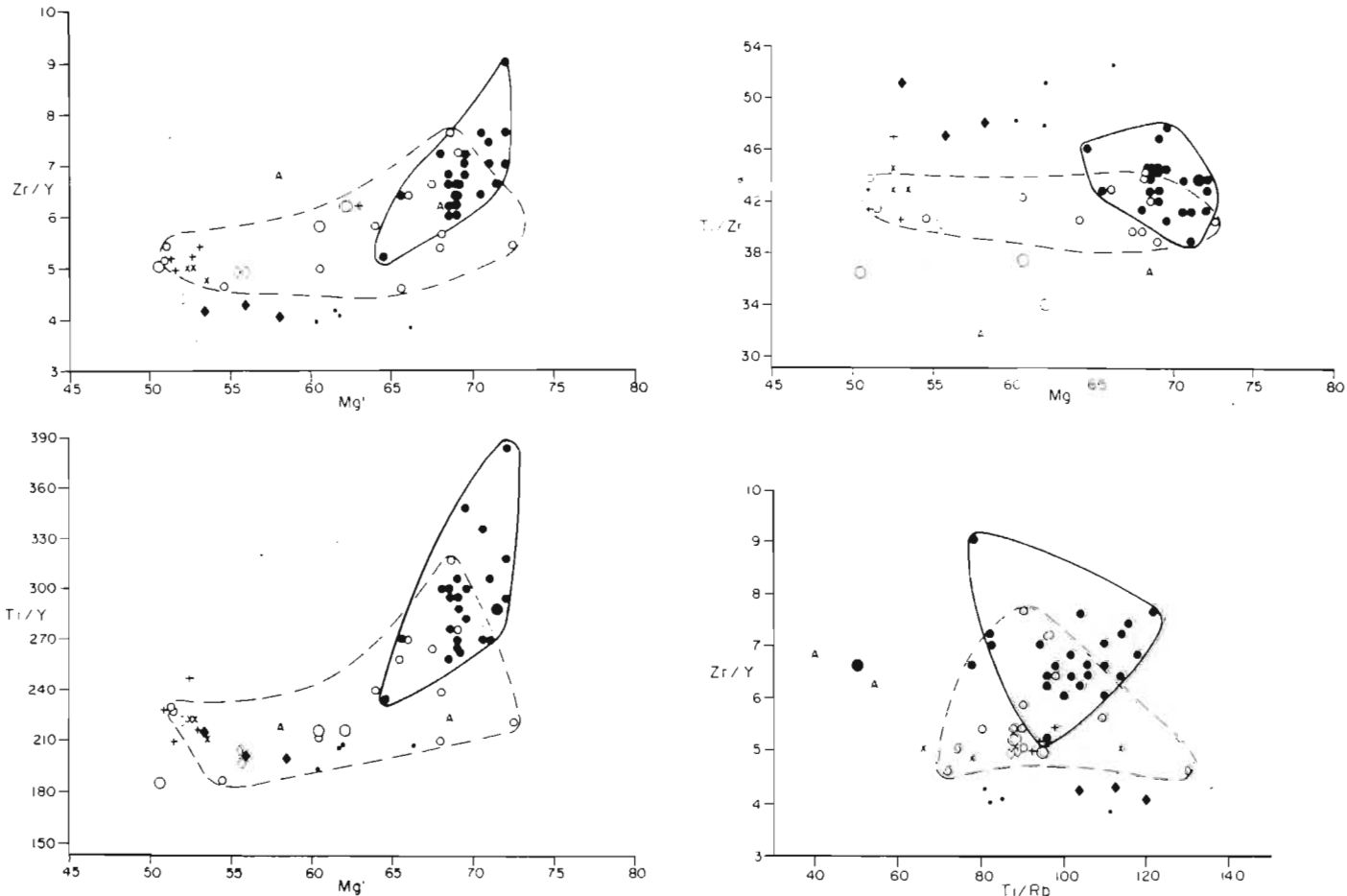


Figure 2.27 Trace element ratio variations in the mafic rocks from Annandagstoppane, Juletoppane and F rsteffjell. Symbols as for Figure 2.23.

rocks show very little evidence for deuteric or hydrothermal alteration and it is therefore assumed that the trends represent primary petrogenetic features.

Incompatible trace element diagrams, e.g. plots of Zr versus Ti (Figure 2.26), show strong correlations, in which significant overlap exists for the fields defined by the main suites of the different areas. These close correlations and extensive overlaps suggest a possible genetic relationship among the main suites of Annandagstoppane, Juletoppane and Förstefjell. However, geochemical similarity alone is insufficient to ascertain whether outcrops from different areas form part of a single intrusion (Mohr, 1983). Petrogenetic characteristics may be determined by comparing incompatible trace element ratios (Figure 2.27). The most important features on these diagrams are:

- (i) The fields defined by the different areas overlap.
- (ii) The variation diagrams Zr/Y and Ti/Y show positive variation with Mg⁺, but poor correlation for Ti/Zr and Mg⁺. This indicates that Y may be compatible with at least one of the primary cumulus phases in these rocks, or the observed variation may have resulted from different liquid compositions.

B. Interpretation

Great care has to be taken in the interpretation of compatible and incompatible element variation diagrams to take cognizance of or eliminate the effects of postcumulus processes and the presence of trapped liquid. However, with these limitations in mind, some preliminary conclusions can be drawn from the whole rock geochemical data.

The variation of the Mg-number in the main suite suggests that a considerable degree of fractionation had taken place during crystallization. However, the lack of coherent trends and relatively small range in SiO_2 values probably indicate the presence of a high liquid component in these cumulates (Wilson, pers. comm., 1985). The observed trends in K_2O , TiO_2 and P_2O_5 with Mg-number may reflect a progressively more evolved trapped liquid, resulting in the crystallization of increased amounts of postcumulus biotite, Ti-bearing oxide phases and apatite relative to the total postcumulus mineral content of the rocks. The significant overlap of major and trace element geochemical data and element ratios (Figures 2.23 to 2.27) indicates that a petrogenetic relationship between the main suite and younger suite may exist. Some fractionation may have occurred in the sills, but at present data are insufficient to evaluate this possibility adequately.

IV Study of a Detailed Section at Hammer Heads

The geochemical and petrographical data from Annandagstoppane, Juletoppane and Förstefjell serve to characterize the main and younger suite rocks, and to suggest that the main suites in these areas may be petrogenetically related. In order to evaluate the detailed crystallization history of the exposed rocks a 44 m section was sampled at 1 m intervals at Hammer Heads. Sample A0/84 was sampled at the snow line, and A44/84 at the 44 m level.

A Field Description

The Hammer Heads section comprises medium-grained gabbro-norites which show little textural and modal variation. The lower part of the succession (0 to 15 m) consists of a uniform, medium-grained, porphyritic gabbro-norite with phenocrysts of clinopyroxene. The upper part of the succession (16 to 44 m)

has poorly-defined layers, 2 to 3 m thick, defined by variable amounts of pyroxene and plagioclase. Lenticular anorthositic layers (up to 20 cm thick), are present locally. On the basis of these lithologies the succession can be divided into upper and lower units.

B Petrography

Modal proportions using the method of point counting recommended by Neilson and Brockman (1977) are summarized in Table 2.7 and Figure 2.28. Possible errors are discussed in Appendix 1.

Plagioclase modal content increases downwards in the upper unit, and shows a cyclic variation. In the lower unit modal content of the plagioclase shows wide oscillations among the layers but with no apparent overall decrease or increase with height. The cyclicity appears to be on a scale of 1 to 6 m for both the upper and lower units. Local deuteric alteration of plagioclase is present in sample A15/84, at the top of the lower unit and, to a lesser extent, in A14/84.

Orthopyroxene content decreases upwards through the lower 10 m of the lower unit, but increases through the rest of the section.

Inverted Pigeonite. In the lower unit the modal proportion of inverted pigeonite varies inversely with that of orthopyroxene, increasing slightly from 0 to 10 m and decreasing from the 10 to the 15 metre level. The mineral occurs in small amounts near the top of the upper unit, at the 42 m level, but apart from this one occurrence, is absent above the 25 m level. From 25 m downwards, small amounts of the mineral are present. The total Ca-poor pyroxene content (orthopyroxene plus inverted pigeonite) increases slightly from 0 m to the top of the upper unit.

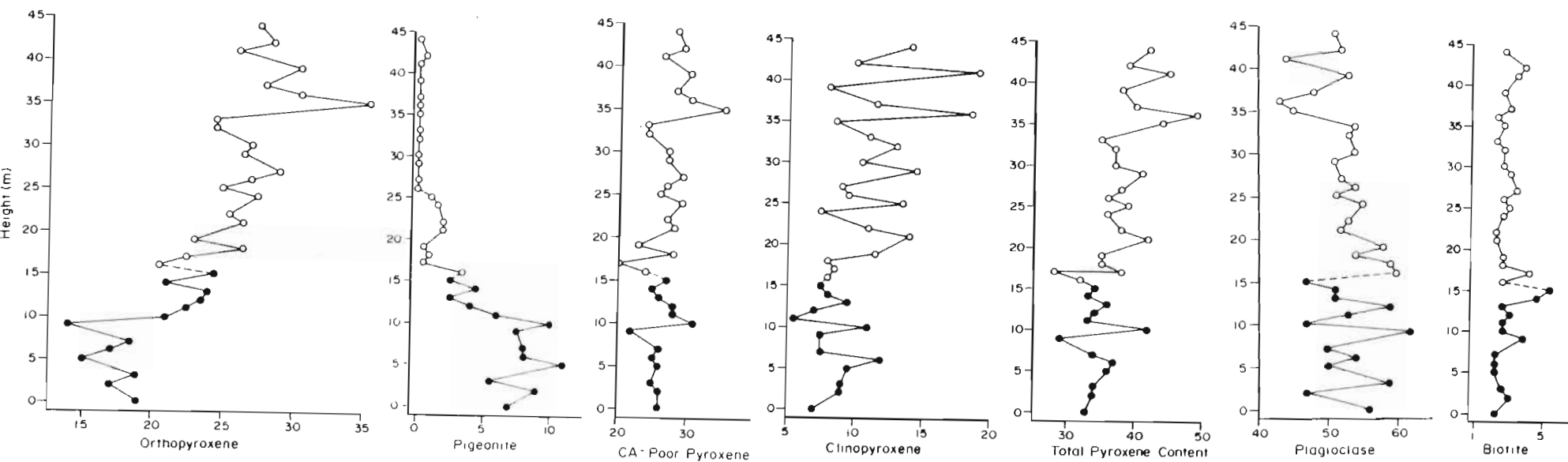


Figure 2.28 Variation in modal content of minerals (in volume per cent) with height in the Hammer Heads section. Solid circles: lower unit; open circles: upper unit.

Clinopyroxene. Variation in the modal proportions of clinopyroxene are greater in the upper unit than in the lower, particularly between 35 and 44 m, with an overall increase upwards in the sequence. In the lower unit the variation in clinopyroxene content is smaller, and there is no apparent overall increase or decrease downwards. A feature of the lower unit is the presence of clinopyroxene phenocrysts, which impart an ophitic texture to the rock.

Total pyroxene content (orthopyroxene plus inverted pigeonite plus clinopyroxene) increases upwards in the upper unit, and shows little overall change upwards in the lower unit, although there is considerable variation from 11 to 18 m.

Biotite. Little overall change is evident in biotite content, but a greater variation is present in samples at and near the contact between the upper and lower units. Sample A15/84, at the contact, contains over 5 per cent biotite. This sample shows a greater degree of Fe-Ti oxide-biotite reaction than the remainder of the section, in the development of wide biotite mantles around the oxide grains.

Micrographic intergrowths of quartz and K-feldspar are present in all samples, except in A15/84. In this rock quartz and K-feldspar occur as discrete intercumulus grains up to 1.5 mm in diameter (Figure 2.20).

C. Plagioclase Grain Size Variation

One of the features of layered complexes is layering defined by mineral grain size variation, and size-grading within layers (e.g. Wager and Deer, 1939; Hess, 1960; Jackson, 1961; Morse, 1969; Campbell et al., 1970; Campbell, 1978; McBirney and Noyes, 1979; Irvine, 1982). Plagioclase grain size analyses were conducted at 3 m intervals at the Hammer Heads section in an attempt to corroborate the cyclic units suggested by the modal data. Techniques and evaluation are discussed in Appendix 1.

Dowty (1980), Lofgren (1980) and Petersen (1985) have shown that crystal shape can give important information on the degree of supercooling during nucleation and crystallization in a magma. Histograms of 100 plagioclase grains in each thin section (Figure 2.29) were plotted for width, length and diameter (width + length)/2. Statistical data in Table 2.8 were obtained by making use of the SPSS FREQUENCIES routine (Nie et al., 1975) on the Sperry-Univac 1100 computer at the University of Natal.

The frequency distributions of plagioclase length are either bimodal, or show a very broad peak with high kurtosis values (e.g. samples A24/84, A30/84 and A42/84). Width distributions exhibit similar characteristics, although a number of samples (e.g. A0/84, A3/84, A21/84, A24/84 and A42/84) appear to be unimodal, with low kurtosis values. Diameter distributions are similar to the length distributions.

Variation of the size of parameters with height (Figure 2.30) can be summarized as follows:

- (i) The apparent mean width variation with height shows little deviation from the general trend from the base of the section to the top.
- (ii) Apparent mean length variation with height exhibits a regular cyclicity in the upper unit, but the average values remain constant.
- (iii) The apparent mean length and diameter increase regularly from the base to the top of the lower unit.
- (iv) The length/width ratios remain nearly constant throughout the section, with apparently anomalous values at 12 m (increased ratio) and 36 m (decreased ratio).

In order to investigate further the possibility that a bimodal size distribution in plagioclase exists in the Hammer Heads section, the size data

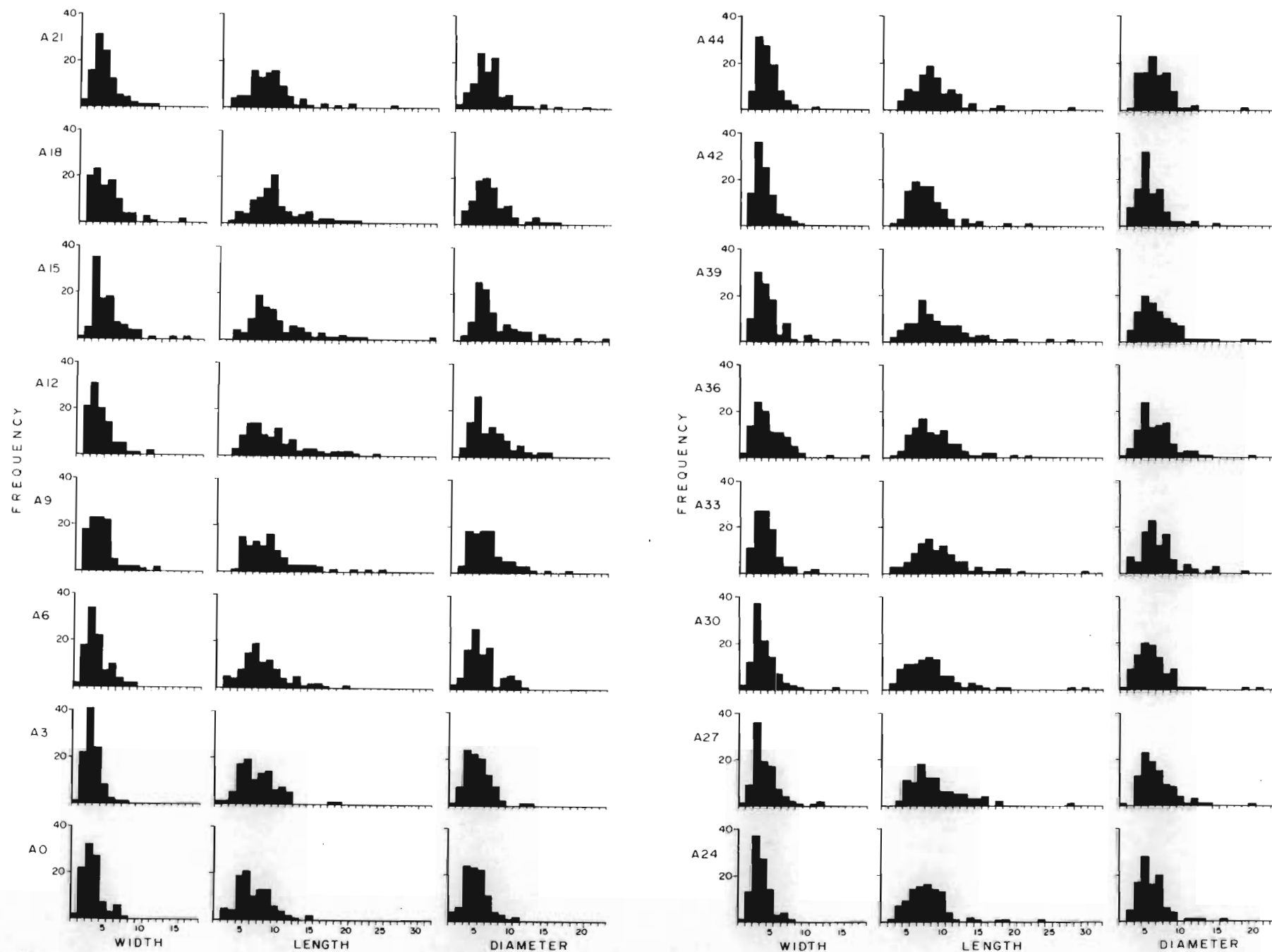


Figure 2.29

Frequency distributions of width, length and diameter of matrix grain classes in the Hammer Heads section. Intervals are 0.05 mm

in width, e.g. interval 5 equals 0.20 to 0.25 mm. See text for discussion.

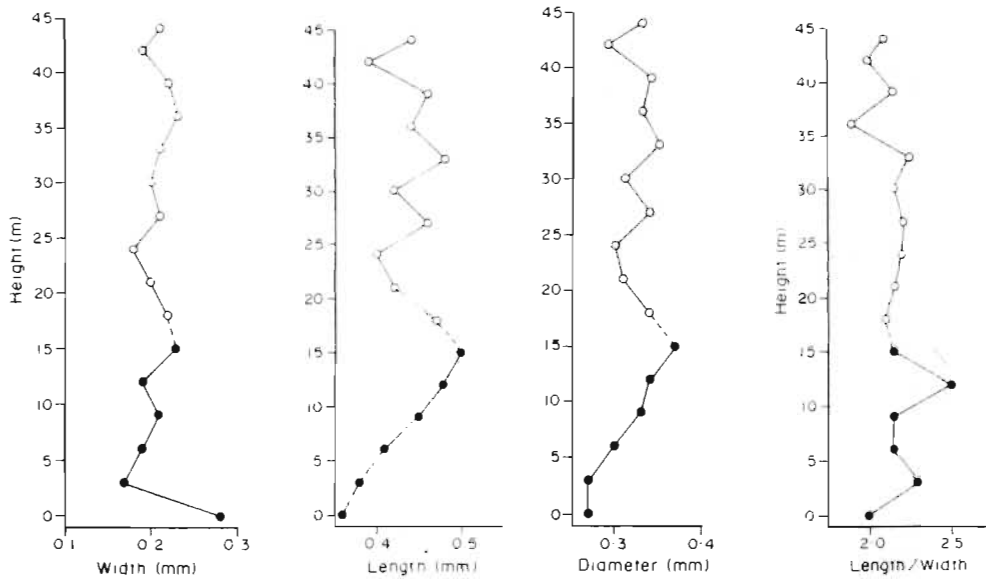


Figure 2.30 Variation of mean apparent width, length, diameter and length/width ratios of plagioclase in the Hammer Heads section. Solid circles: lower unit; open circles: upper unit.

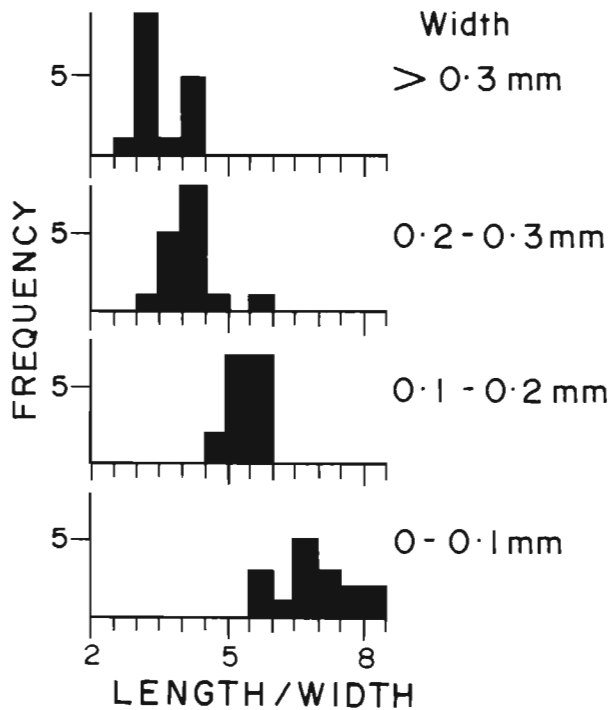


Figure 2.31 Frequency of apparent mean length/width ratios of plagioclase according to plagioclase width in all size-analysed samples, Hammer Heads section.

were classed into four categories by width, namely 0 to 0.1 mm (Class 1), 0.101 to 0.2 mm (Class 2), 0.201 to 0.3 mm (Class 3) and greater than 0.3 mm (Class 4). Mean length/width ratios in the different classes were determined for each of the analysed samples (Table 2.8). The results are depicted in Figure 2.31, which shows that there is a regular decrease of the ratio with increasing width (i.e. increasing grain size).

The mean ratios of the different classes for individual samples are depicted in Figure 2.32. It is assumed that Class 1 represents plagioclase primocrysts which were unaffected, or little affected by orthocumulus growth, and that Classes 2, 3 and 4 represent increasing amounts of orthocumulus growth. Class 1 shows marked fluctuations about the mean in the upper unit, whereas there is a nearly regular increase in the ratio from the base to 15 m in the lower unit. The trends in Classes 2, 3 and 4 are similar to those for Class 1, but the topmost sample (at 15 m) in the lower unit shows a decrease in the mean ratio relative to the remainder of this unit.

Nucleation density

A parameter that may be useful to explain some of the textural features of plagioclase in the Hammer Heads section is nucleation density. The number of plagioclase grains per square millimetre was measured in the matrices of two samples (A0/84 and A44/84), and as enclosed grains in orthopyroxene and clinopyroxene. Gray (1970) has argued that the number of crystals per unit area in a rock generally cannot be determined uniquely from thin section measurements owing to the sectioning effect. He showed that it may be possible to obtain relative values for Z , the total number of nuclei formed in a unit volume of a melt, but that this is valid only in special cases. For this reason the measurements reported here are semiquantitative. The results

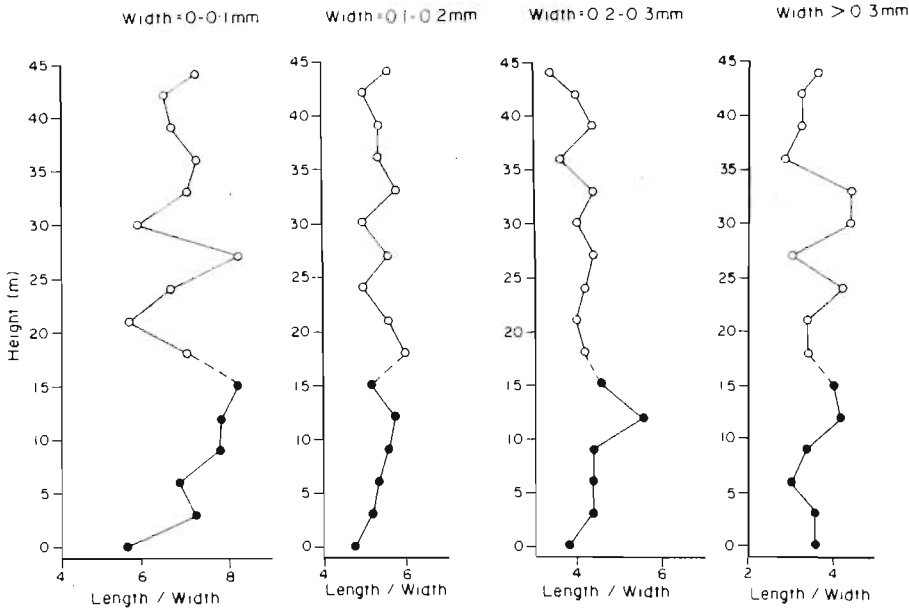


Figure 2.32 Length/width ratio variation of different width classes with height in the Hammer Heads section. Solid circles: lower unit; open circles: upper unit.

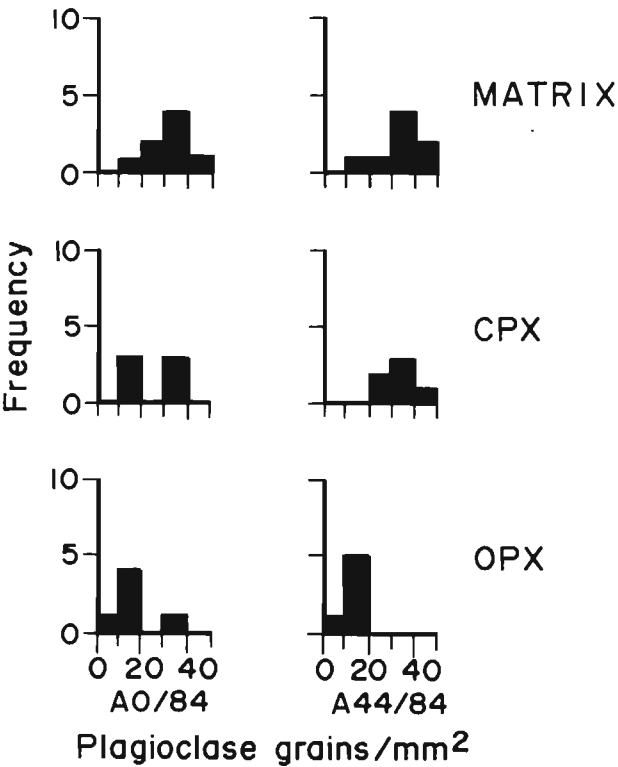


Figure 2.33 Frequency distribution of plagioclase grains/mm² as a function of nucleation density in samples A0/84 and A44/84. OPX: Frequency distribution of grains/mm² enclosed in orthopyroxene; CPX: Frequency distribution of grains/mm² enclosed in clinopyroxene; MATRIX: Frequency distribution of grains/mm² occurring in matrix.

are depicted in Figure 2.33. In sample A0/84 there is a clear bimodal distribution of grains enclosed in orthopyroxene and clinopyroxene. The matrix shows a near normal distribution, with a peak corresponding to the interval 30 to 40, and 10 to 20 where most orthopyroxene nucleation densities occur. Peaks corresponding to the interval 30 to 40 occur in the matrix and clinopyroxene nucleation densities of sample A44/84. Plagioclase grains enclosed in orthopyroxene define a nucleation density in the interval 10 to 20.

On the basis of this study it is suggested that a bimodal size distribution exists which is related to two separate periods of nucleation.

D Geochemical Variation in the Hammer Heads Section

The major and trace element geochemical variation with height in the Hammer Heads section is shown in Figures 2.34 and 2.35. Data are given in Appendix 2, and statistical parameters in Table 2.9.

The results displayed in Figures 2.34 and 2.35 can be discussed in terms of (i) the overall variation with height in the upper and lower units, and (ii) comparative geochemical behaviour of the different elements within cycles. Sample A15/84, at the top of the lower unit, appears to show anomalous behaviour on a number of diagrams, for which reason this sample will be discussed separately. A 10 cm-thick layer, which has a higher mafic mineral content than the adjacent rocks, occurs at 17 m. The data from a sample of this layer is included in Figures 2.34 and 3.34 and shown as a star.

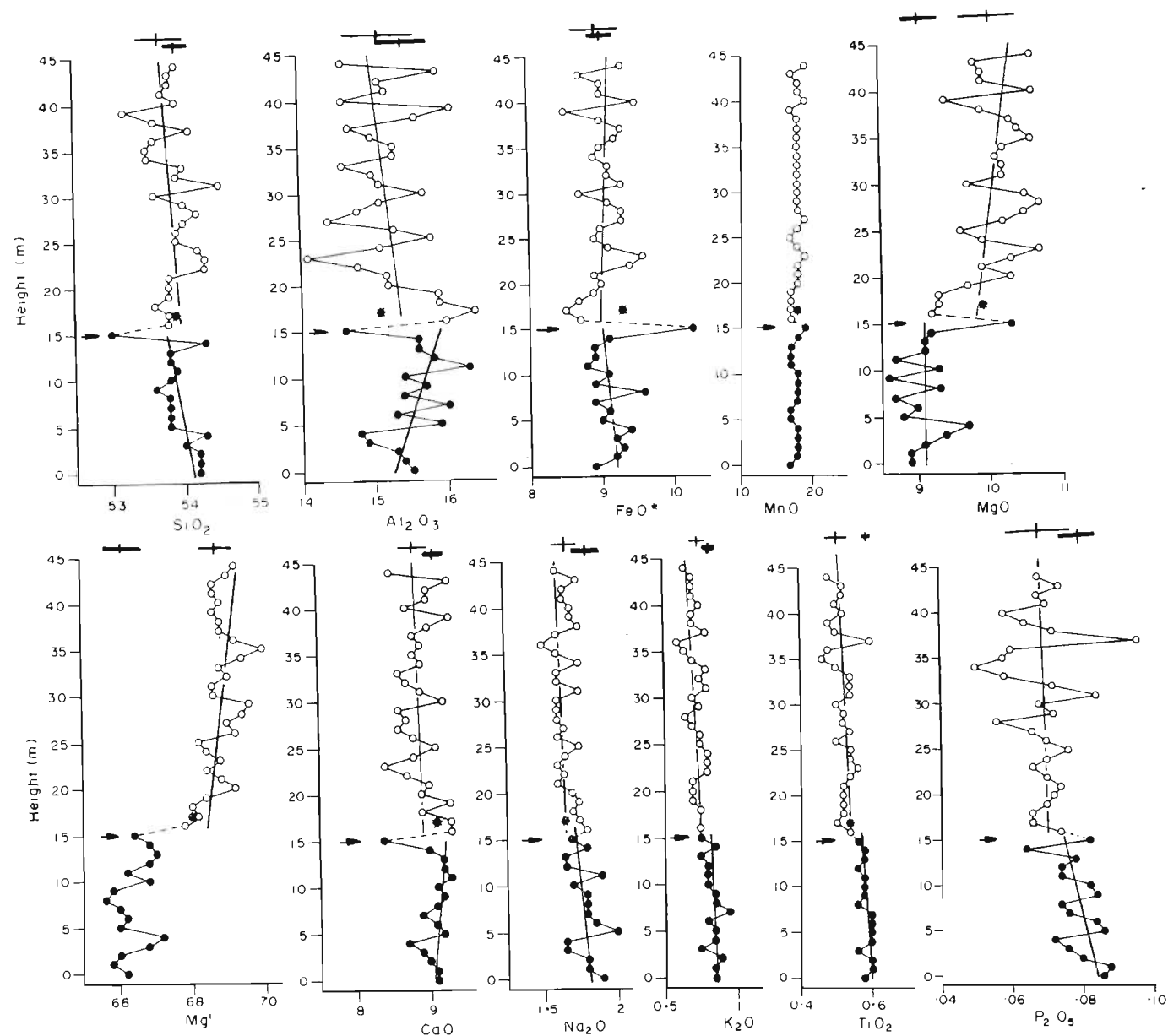


Figure 2.34

Major element and Mg' variation with height in the Hammer Heads section. Closed circles: lower unit; open circles: upper unit; heavy bar with vertical line: mean and standard deviation of lower unit; thin bar with vertical line: mean and standard deviation of upper unit; slopes are indicated by subvertical straight lines. A mafic layer at 17 m (star, see text) is included for comparison. Arrow: sample A15/84. Errors are discussed in Appendix 1.

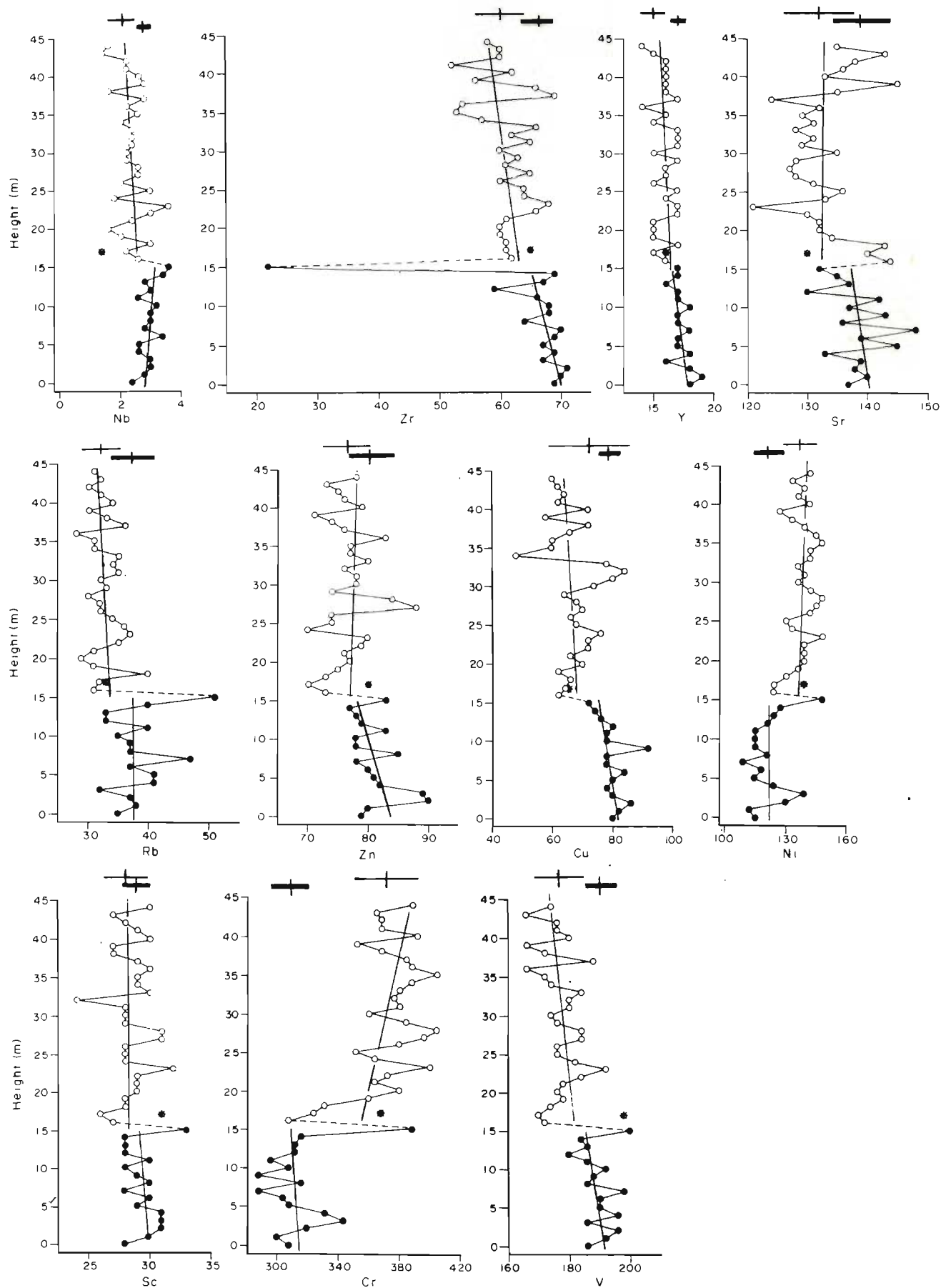


Figure 2.35

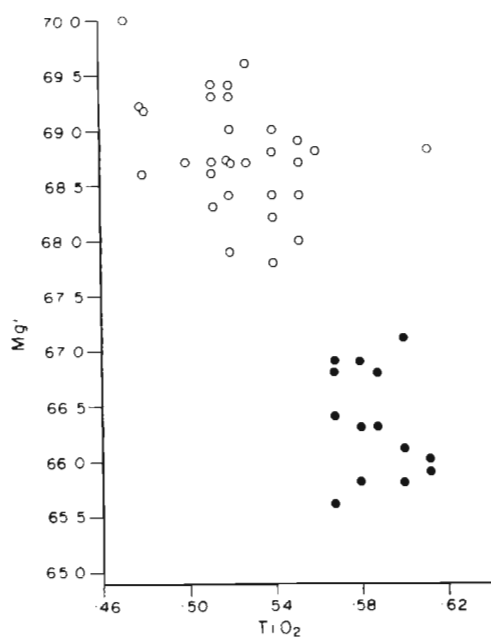
Trace element variation with height in the Hammer Heads section. Closed circles: lower unit; open circles: upper unit; A 10 cm mafic layer (star) at 17 m is included for comparison.

(i) Overall variation with height:

The major differences between the lower and upper units excluding sample A15/84, are:

- (a) TiO_2 values in the lower unit are consistently higher than in the upper unit, except for an anomalously high value at 37 m (Figure 2.36);
- (b) Mg-number increases upwards in both units, but shows a clear separation between them at the 15 m level;
- (c) Opposing trends within each unit are defined by variation with height in Al_2O_3 , MgO, CaO, Nb, Sr, Zn and Cr. Sr variation (Figure 2.35) can be described more appropriately as two broadly cusplate-shaped patterns: convex to the left in the upper unit and convex to the right in the lower.

The most striking geochemical feature of the Hammer Heads section is the overall increase in Mg-number with height, and the concomitant decrease in the incompatible elements K_2O , TiO_2 , P_2O_5 ; Zr, Y, Rb and Cu. Sample A15/84 appears to be part of the lower unit on the basis of its Mg-number, but its geochemistry shows a number of apparently anomalous features. The rock appears to be depleted in SiO_2 , Al_2O_3 (?), CaO, and particularly in Zr, and enriched in FeO^* , MgO, Rb, Ni, Sc, Cr and V (?) relative to the rest of the section and/or the lower unit (Figures 2.34 and 2.35). The depletion in Zr may suggest that A15/84 has a very low postcumulus mineral content relative to the rest of the section, but the petrographic investigation (Section IV.B) showed this is not the case. Furthermore, the P_2O_5 content, which is a reliable relative measure of the amount of postcumulus minerals in cumulate sequences, is higher in A15/84 than in the samples from the adjacent overlying 15 m and underlying 4 m of the section (Figure 2.34). This suggests that the



postcumulus mineral content in this sample is higher than in the adjacent section.

(ii) Comparative geochemical behaviour of elements with height: The compatible element oxides in the Hammer Heads section can be separated into two groups on the basis of sympathetic behaviour through the section. Group 1 oxides, consisting of Al_2O_3 , CaO and Na_2O , vary antipathetically with the oxides and trace elements of group 2, FeO , MgO , Ni and Cr . Group 2 oxides and elements vary sympathetically with total pyroxene content (Figure 2.28). The group 1 elements, however, cannot be related simply to modal plagioclase variations.

The incompatible minor and trace elements show broadly similar behaviour through the section. Small local fluctuations in variation of the elements with height occur which do not correspond to the trends of the other incompatible elements. These fluctuations may be the result of redistribution of intercumulus material (Tait et al., 1984; Kerr and Tait, 1985) or small-scale fractionation of intercumulus liquid (Barnes, 1986).

Variation of incompatible element ratios through the Hammer Heads section is given in Table 2.9 and Figure 2.31. Trace element ratios reported in Section III.B show that Zr and Rb were incompatible elements during fractional crystallization of the primary minerals in the Annandagstoppane rocks and they are therefore used as the denominators. The effects of A15/84 on the statistical evaluation are neglected, because of the anomalous geochemistry and petrographic features of this sample.

Rb/Zr , Cu/Zr and Ti/Zr increase upwards through both the upper and lower units of the sections and Cu/Rb , K/Rb and Ti/Rb decrease (Table 2.9). In the

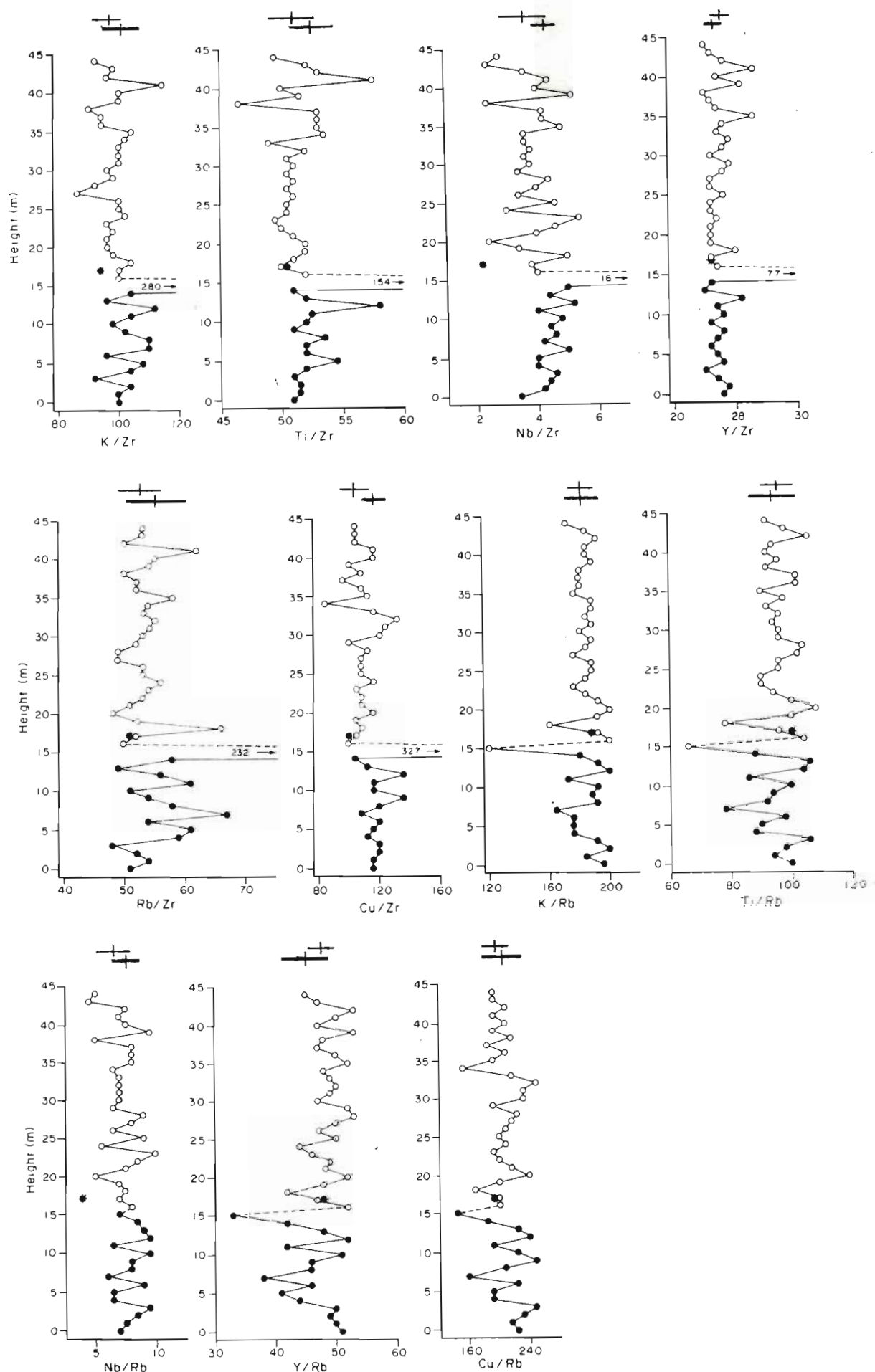


Figure 2.37

Trace element ratio variation with height in the Hammer Heads section. Solid circles: lower unit; open circles: upper unit. Errors are discussed in Appendix 1. The values for Nb/Zr, Cu/Zr, Nb/Rb, Y/Rb, and Cu/Rb have been multiplied by 100.

rest of the parameters reported here, opposite trends are found in the incompatible trace element variation with height, i.e. if the ratio increases upwards in the lower unit, it decreases upwards in the upper unit. Hence only the trends in the lower unit will be mentioned. Ratios that increase upwards in the lower unit are Nb/Zr, K/Zr and Nb/Rb, and those that decrease are Zn/Zr, Y/Rb and Zn/Rb. From the trends established it is clear that there is evidence of some degree of enrichment for some of the 'incompatible' elements relative to others.

V Discussion

A. Summary of Petrological Features in the Main Suite and at the Hammer Heads Section

- (i) Textural evidence suggests that primocryst formation in the main suite occurred in situ. Crystallization of cumulate assemblages in situ has been discussed and described by a number of authors, e.g. Campbell (1978), McBirney and Noyes (1979) and Wilson (1982). These authors as well as Irvine (1982) have redefined cumulus terminology in such a manner that the concept of in situ crystallization can be incorporated.
- (ii) There is limited evidence at Viper's Hill that convective currents caused local scouring, which suggests that the main body of magma was convecting. Therefore crystallization must have occurred in an environment isolated from the main body of magma.
- (iii) Two cyclic units were recognized in the Hammer Heads section based on variations in field characteristics, comparison of the Mg-numbers in the section and differences in mineralogical and geochemical variables.

- (iv) Plagioclase content decreases upwards in the upper unit, and increases upwards in the lower.
- (v) Total pyroxene content (orthopyroxene plus pigeonite plus clinopyroxene) increases upwards in the upper unit, but shows no significant change upwards in the lower unit.
- (vi) Al_2O_3 and CaO decrease upwards in the upper unit, but increase in the lower unit, whereas FeO and MgO show the reverse behaviour in the two units.
- (vii) The apparent mean length and diameter of plagioclase laths remains approximately constant in the upper unit, but shows a regular increase upwards in the lower unit. Furthermore, there is a bimodal distribution in the nucleation density of plagioclase and it is likely that two periods of plagioclase nucleation occurred.
- (viii) There are regular changes in length to width ratios for different width classes in the Hammer Heads section which reflect changing conditions in the degree of supercooling in the crystallizing magma (e.g. Dowty, 1980; Lofgren, 1980; Petersen, 1985).
- (ix) Studies of incompatible element ratios have shown there is no difference in absolute values between the upper and the lower units, although there are some differences in trends with height.
- (x) Sample A15/84, at the top of the lower unit, appears to be anomalous with respect to a number of petrographic and geochemical features in comparison with the upper and lower units. These features are:
 - (a) The rock apparently has a normal to high postcumulus mineral content when compared with the rest of the section.
 - (b) Biotite content is high, with a corresponding high Rb content.
 - (c) Quartz and K-feldspar occur as discrete grains in A15/84, whereas all samples in the rest of the section contain micrographic intergrowths of the two minerals.

- (d) Despite the relatively high postcumulus content the rock has a high Mg-number and a very low Zr content. It is depleted in SiO_2 , Al_2O_3 (?) and CaO , and enriched in FeO^* , MgO , P_2O_5 , Rb, Ni, Sc and Cr relative to the rest of the section and/or the lower unit.
- (e) Samples A15/84 and A14/84 show a higher degree of deuteritic alteration than the rest of the section.

B. Environment and Shape of Intrusions

Two lines of evidence suggest that the intrusions in the Annandagstoppane, Juletoppane and Förstefjell areas were emplaced close to the base of the Ritscherflya Supergroup:

- (i) Outcrops of Archaean granitoids believed to form the basement on which the Ritscherflya Supergroup was deposited occur in close proximity to the main suite rocks in the Annandagstoppane area; and
- (ii) Outcrops of sedimentary rocks correlated with the Ritscherflya Supergroup, occur approximately 100 m from the main suite at Förstefjell. The main suite and the sediments have been intruded by a younger sill.

The isolation of the nunataks from one another militates against determination of the geometry of the main suite intrusions.

C Regional Comparison of the Main Suite in the Different Areas

There are a number of macroscopic, microscopic and geochemical similarities among the main suite rocks at Annandagstoppane, Juletoppane and Förstefjell, which are summarized below:

- (i) Rhythmic layers defined by modal variations in orthopyroxene, clinopyroxene and plagioclase are present throughout the different areas;
- (ii) Grain sizes are similar;
- (iii) Orthopyroxene and plagioclase, and probably clinopyroxene and pigeonite, were primocryst phases.
- (iv) The mafic crystallization sequence orthopyroxene-pigeonite-second generation orthopyroxene-clinopyroxene occurs throughout the areas and reflects the same physico-chemical conditions that must have prevailed in the rocks from all three areas.
- (v) The main suite rocks are all orthocumulates with very high contents of postcumulus minerals;
- (vi) Major and trace element geochemistry, including compatible and incompatible variation and incompatible trace element ratios have markedly similar characteristics.

Krynauw et al. (1984) suggest that the Annandagstoppane and Juletoppane gabbroic rocks may form part of the same body, although they do point out that there are objections to this suggestion. The major criticism against direct correlation among the three areas in which main suite rocks occur are:

- (a) It will be shown in Chapter 7 that the lavas from the Straumshutane and all the Borgmassivet intrusions that were studied may be

consanguineous rocks on the basis of field relationships and geochemistry. Similarly, it is possible that Annandagstoppane, Juletoppane and Förstefjell represent different layered bodies, with similar geochemical characteristics. (b) Geochemical similarity alone may not be diagnostic to determine whether rocks in different areas form part of the same body or are even consanguineous. Different suites, derived from similar mantle sources, and having undergone similar processes, may show no significant geochemical differences in major, trace and rare earth element profiles (Mohr, 1983). (c) Preliminary Rb-Sr isotopic age determinations suggest there may be a difference in age between the main suites at Annandagstoppane and Juletoppane (Barton, pers. comm., 1983). Barton and Copperthwaite (1983) dated the Annandagstoppane gabbroic rocks at 1802 ± 100 Ma (isochron) with an initial $^{87}\text{Sr}/^{86}\text{Sr}$ ratio of 0.7034 ± 0.0009 . Subsequent analyses have confirmed the approximate 1800 Ma age (Barton, pers. comm., 1984). The Juletoppane gabbroic rocks yield errorchrons which suggest a significantly younger age for this intrusion. If this is confirmed, the two suites must be interpreted to reflect derivation from a common source at different times. However, more recent evaluation of data from the Borgmassivet intrusions has led Barton (pers. comm., 1985) to conclude that many of the data on these rocks may be false or pseudoisochrons.

Hence, a firm conclusion on the petrogenetic relationship cannot be reached until the isotope data on these rocks have been improved and are understood fully.

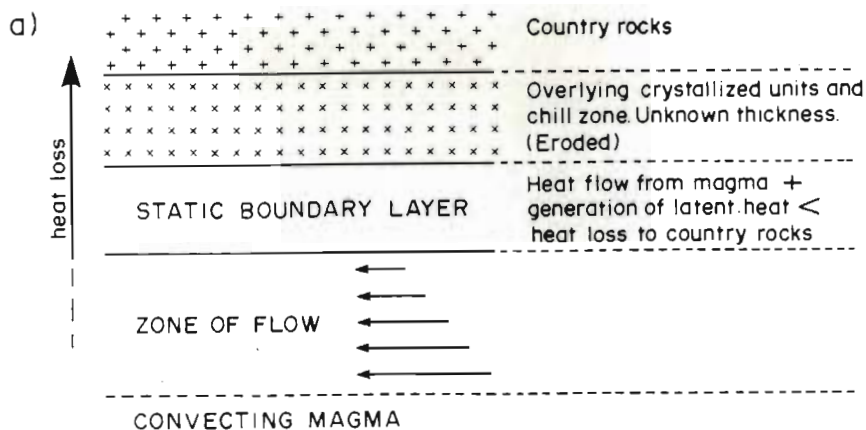
D. Possible Mechanisms Operating during Crystallization of the Main Suite

Models to account for the geochemical characteristics of the Hammer Heads section are constrained by the fact that the position of this section in the original stratigraphy of the Annandagstoppane intrusions is not known. The observed increase and cyclic variation in Mg-number upwards in the section, coupled with a sympathetic decrease in incompatible elements, may be a response to (a) crystallization near the top of the intrusion within a boundary layer (Campbell, 1978; McBirney and Noyes, 1979) and rhythmic nucleation of primocrysts (Maaløe, 1978); or (b) variation in the amount of trapped liquid (Barnes, 1986).

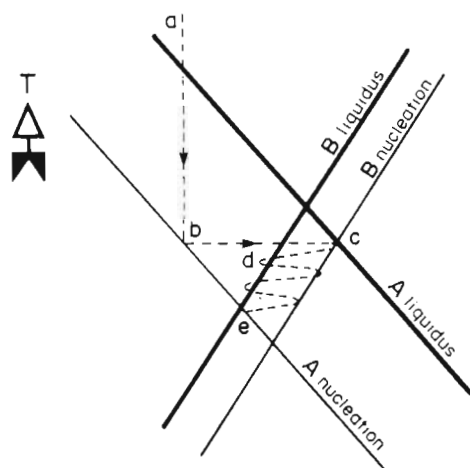
(i) Crystallization in a boundary layer

In situ crystallization occurs in boundary layers (McBirney and Noyes, 1979) near the margins of slowly cooling and convecting magmas (Figure 2.38).

The boundary layer consists of a static zone, where most crystallization occurs, and an interior zone of flow in which there is a steep velocity gradient between the static boundary layer and the interior of the magma. Rhythmic layering may be explained in terms of temperature and chemical concentration gradients which show different variations with time (Liesegang, 1896). A mechanism of oscillatory nucleation and diffusion-controlled crystallization affected by gravity leads to the development of double-diffusive convecting cells (McBirney and Noyes, 1979).



b) Fractionation of mineral 'A' dominating



c) Fractionation of mineral 'B' dominating

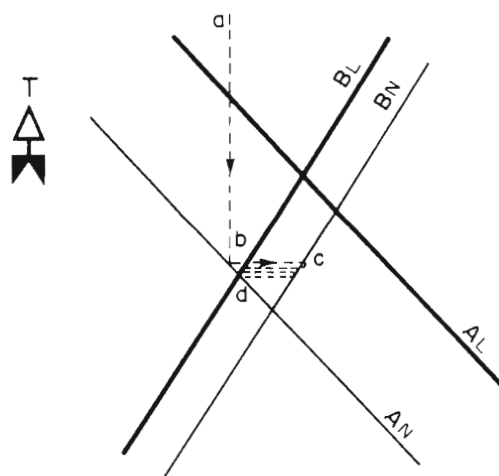


Figure 2.38

Diagrammatic representation of crystallization history in the Hammer Heads section, Annandagstoppane. (a) Development of static boundary layer adjacent to zone of flow and convecting magma. (b) and (c) Rhythmic nucleation after Maaløe (1978). "T" indicates increase in temperature. See text for discussion.

However, as an alternative to the development of double-diffusive convection cells, it is possible that rhythmic nucleation of plagioclase and the pyroxenes produced the observed layering. Nucleation of crystals in melts is usually heterogeneous (Chalmers, 1964) and requires a certain degree of supercooling. In the case of silicate melts, ΔT , the temperature interval between the liquidus and nucleation curves, may be substantial. The crystallization relationships for two crystalline phases, A and B, in a binary eutectic melt in which nucleation and growth of phase A dominated, are shown in Figure 2.38b (after Maaløe, 1978). A cooling melt with a composition at point 'a' forms nuclei of phase A at point 'b' on the nucleation curve of A. Release of latent heat may prevent a further drop in temperature, or may increase the temperature of the magma. Alternatively, if the rate of heat lost to the country rock is greater than the heat gained by the magma through release of latent heat, there will still be a reduction of the magma temperature, but at a lower rate than prior to crystallization. As mineral A grows it depletes the magma in the components of A. If the rate of growth of phase A is greater than the rate of diffusion of components of A through the magma, the composition of the magma will change along the path 'bc' in a distance $2r$ from the centre of each crystal of A with radius r (Nielsen, 1964). At point 'c' the nucleation curve of B is reached, and B starts to grow. If the liquidus of A is not crossed, A will continue to grow. It is assumed that the growth of B exceeds that of A at this point, so that the magma composition changes along 'cd'. At 'd' the liquidus of phase B is crossed, and B ceases to grow. Mineral A continues to grow, and the magma composition proceeds to change towards the nucleation curve of B. In this manner a rhythmic nucleation-growth condition is established

until point 'e' is reached, at which point a second pulse of nucleation of phase A occurs.

This mechanism may explain the rhythmic variation in plagioclase and orthopyroxene modal content at Hammer Heads, and may provide a mechanism for the second pulse of plagioclase crystallization. Local changes in magma composition will result in oscillatory zoned plagioclase, a feature observed throughout the main suite. If the starting magma composition is at point 'a' in Figure 2.38c, crystallization of phase B may dominate, or at least be relatively more important in the crystallization sequence than shown in Figure 2.38b. This may explain differences between the lower and upper units. The binary crystallization model presented above is probably oversimplified, because clinopyroxene was a fractionating phase in addition to plagioclase and orthopyroxene. Maaløe (1978) shows, however, that the same principles developed for the binary eutectic system can be applied in a ternary system and it is proposed that the above model is valid for primocryst nucleation and growth in the two units of the Hammer Heads section.

(ii) Effects of varying amounts of postcumulus liquid

Large amounts of liquid may be trapped in a magma undergoing fractional crystallization if large degrees of undercooling occur in a magma (Barnes, 1986). Hence liquid-rich assemblages may be present at and near the margin of an intrusion and primocryst-rich assemblages in the interior (Raedeke and McCullam, 1984). Barnes (1986) shows that the Mg-numbers of the whole rocks and those of primocryst phases are lowered with increasing contents of postcumulus liquid. Variation in the amount of postcumulus material in the

rocks of the Hammer Heads section may therefore be a viable alternative mechanism to explain the observed geochemical characteristics. Fractionation of the postcumulus liquid on the scale of about 1 m³ (Barnes, 1986) may have resulted in the observed cyclicity in incompatible trace element ratios.

(iii) Hammer Heads contact zone

The anomalous geochemistry and petrography of sample A15/84 from the Hammer Heads section are thought to reflect the properties of a zone enriched in deuteritic liquids which were trapped at the interface between two fractionating units. The low Zr content may reflect the effects of in situ fractionation of the postcumulus liquid as proposed by Barnes (1986). Further detailed studies across the contact between the upper and lower units are likely to elucidate such postcumulus processes.

(iv) Nucleation of second-generation plagioclase and orthopyroxene

Nucleation density and grain size analyses of plagioclase have shown that two pulses of plagioclase nucleation had occurred. Such a second nucleation pulse is possible if the rhythmic nucleation model of Maaløe (1978) is correct. Depletion of CaO in the micro-environment surrounding plagioclase is likely following nucleation and crystallization of plagioclase. If this depletion in calcium occurred at or near the surface of a growing pigeonite crystal a condition of constitutional supercooling would have developed. Thus orthopyroxene, and not pigeonite, would have become the stable crystallizing phase. The effect is seen in Figure 2.14 where orthopyroxene, rather than inverted pigeonite, occurs around enclosed plagioclase grains. This

effect would be locally developed, thus the mafic crystallization sequences

opx - pg - opx₍₂₎ - cpx; and

opx - pg - cpx

can exist in the same rock (opx: orthopyroxene; pg: pigeonite; opx₍₂₎: second-generation orthopyroxene; cpx: clinopyroxene).

E. Relationship of the Younger Suite to the Main Suite

The pegmatoids, veins and albitites found in the main suite rocks are considered to be deuteric and/or highly evolved products of main suite crystallization. They comprise very small volumes in the area, and little work has been done on them. The albitites may represent small volumes of immiscible Na₂O-rich liquids, which separated from the deuteric liquids. Some of them may represent vein fillings, and others, e.g. at Hammer Heads, are thought to be replacement products of main suite rocks.

The dykes show a narrow range in geochemical characteristics, but some fractionation has occurred in both the Juletoppane and Förstefjell sills. Variations in the degree of supercooling through the sills can be recognized petrographically in plagioclase textures. These textures include subparallel orientations of tabular laths, radiating or fan-shaped textures and arcuate outlines. The length to width ratios are very high. These textures are indicative of a high degree of supercooling (e.g. Dowty, 1980; Lofgren, 1980). Lofgren found that with a relatively low degree of supercooling the plagioclase crystals are tabular, but with an increase in the degree of supercooling the crystals may become acicular to skeletal to fan spherulitic. Acicular crystals are arcuate in many cases. Petersen (1985) has shown that

the orientation of plagioclase crystals is controlled by the degree of supercooling, and that fractionation may occur owing to variations in the degree of supercooling within a rapidly cooling magma. It is proposed that such fractionation may have occurred within the sills at Juletoppane and Førstefjell.

The geochemistry of the dykes, sills and gabbroic bodies show a close similarity on all the variation diagrams studied, and from the available evidence it is suggested that they are geochemically related to the main suite.

CHAPTER 3 THE ROBERTSKOLLEN COMPLEX

I. General Geology

A number of nunataks are spread over approximately 20 km² in the Robertskollen area (Figures 1.2 and 3.1). Provisional names for individual nunataks are given in Figure 3.1.

The rocks comprise ultramafic to mafic intrusions and mafic pegmatites, which have been intruded by a number of olivine dolerite and dolerite dykes. The ultramafic rocks, which underlie the mafic rocks, were described first by von Brunn (1963, 1964) from Tumble Ice and Petrel's Rest. During the present investigation ultramafic rocks were discovered in the eastern windscoop of Ice Axe Peak. No intrusive relationships with country or basement rocks have been observed, although ice-transported sedimentary rocks, probably derived from Ritscherflya sediments, are found on most of the nunataks.

Nomenclature. Rock names are based on modal proportions according to the method of Streckeisen (1976). Cumulus terminology is after Irvine (1982) as discussed in Chapter 1. The ultramafic and mafic rocks will be referred to as the ultramafic and mafic units, and both have been subdivided into zones, numbered in Roman numerals from the lowest exposures upwards at Ice Axe Peak (Figure 3.5). Subdivision of the units is based on petrographic and modal variations.

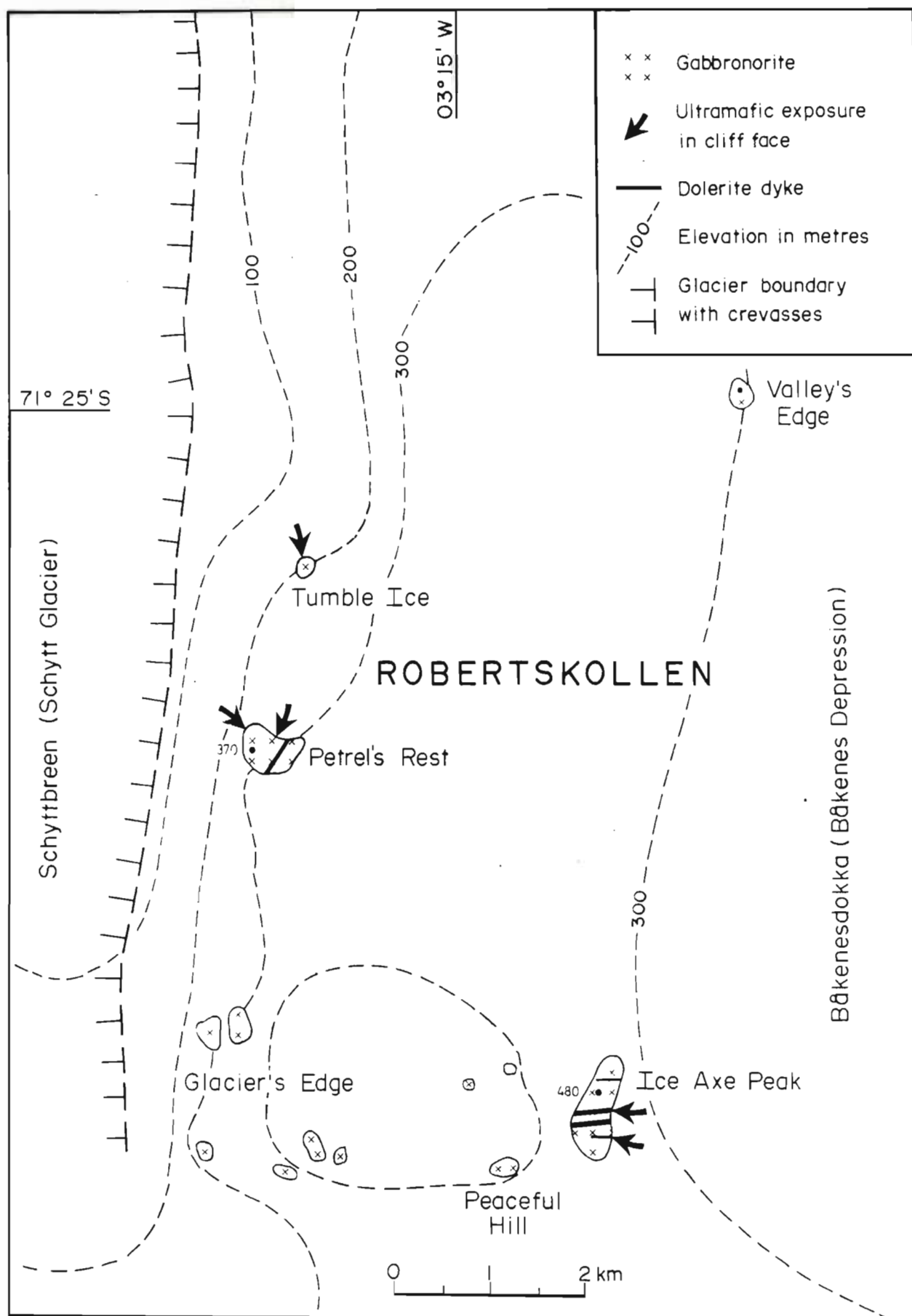


Figure 3.1 Distribution of nunataks and general geology of the Robertskollen Complex.

A. The Ultramafic Unit

Approximately 50 to 60 m of the ultramafic unit are exposed vertically at Tumble Ice, 15 to 20 m at Petrel's Rest and 50 m at Ice Axe Peak (Figures 3.2, 3.3 and 3.4). Little textural and mineralogical variation can be determined in hand specimen, although layering, defined by variation in the modal proportions of clinopyroxene, orthopyroxene and plagioclase, is accentuated on weathered surfaces. A detailed section along the southern gully (Gully Section) at Ice Axe Peak was sampled at 2 m intervals in the ultramafic unit and 2 to 4 m in the overlying mafic unit. The lithologies of these sections are shown in Figure 3.5.

Features common to the three sections are:

1. Mela-olivine gabbro-norite is the dominant rock type in the ultramafic unit;
2. A clinopyroxene-rich melagabbro-norite zone, which may be up to 10 m thick, occurs at the top of the ultramafic unit in each of the three exposures; and
3. The ultramafic unit is characterized by dominantly horizontal joints, and the overlying mafic unit by vertical joints.

The major differences are

1. Layers of mela-olivine norite and plagioclase-bearing lherzolite are present at Ice Axe Peak, and plagioclase-bearing wehrlite and plagioclase-bearing lherzolite were observed at Tumble Ice;



Figure 3.2

Ultramafic and mafic units exposed at Tumble Ice. Note the dominant vertical and horizontal joints in the mafic and ultramafic units respectively. Scale (arrowed) is 180 cm.



Olivine-bearing
melagabbonorite

Mela-olivine
gabbonorite

Melagabbonorite

Figure 3.3

Interlayered nature of the contact between the mafic and ultramafic units at Petrel's Rest. Scale is 14.5 cm in length.



Figure 3.4

Ultramafic and mafic units exposed at Ice Axe Peak. Maximum height of cliffs is 150 m. Arrows indicate two domes in the ultramafic unit.

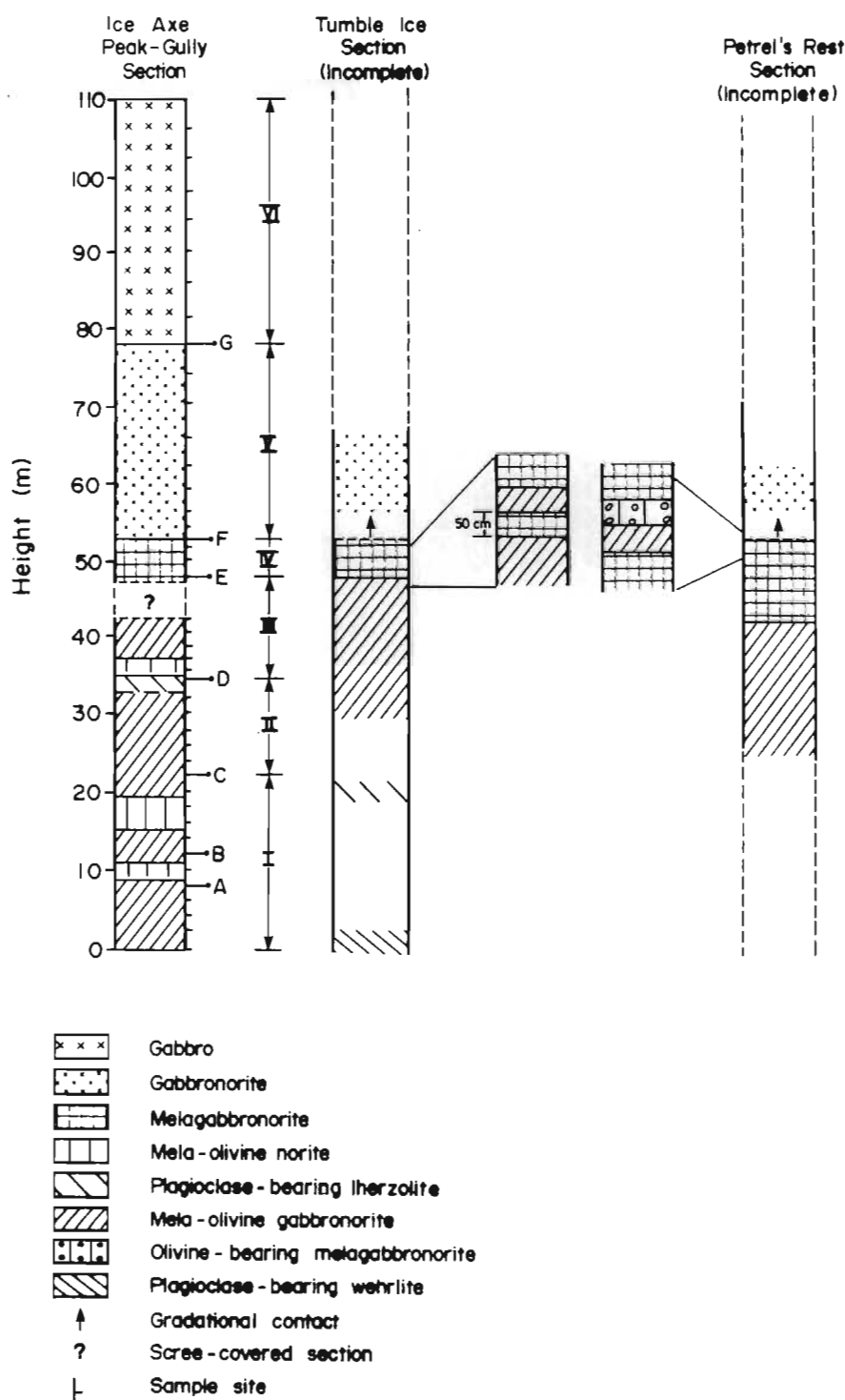


Figure 3.5

Summary of rock types and contact relationships of the mafic and ultramafic units at Ice Axe Peak, Tumble Ice and Petrel's Rest. Points A to G mark changes in petrographic, cumulate and/or geochemical characteristics in Gully Section. I to VI mark different zones as discussed in the text.

2. All the ultramafic rocks are medium-grained, but are relatively coarser at Tumble Ice and Petrel's Rest than at Ice Axe Peak;
3. The nature of the melagabbonorite and its contact with the overlying mafic rocks varies in detail. The melagabbonorite appears uniform at Ice Axe Peak, and has a sharp contact with the overlying gabbonorite. The contact is undulating, and locally shows cusate shapes, which are concave upwards, and small-scale diapiric structures (Figure 3.6), which protrude into the overlying layer. The melagabbonorite is interlayered with other rock types at Tumble Ice and Petrel's Rest (Figure 3.5). At Petrel's Rest the sequence upwards consists of 8 to 10 m of melagabbonorite, 30 to 50 cm of mela-olivine gabbonorite, approximately 30 cm of olivine-bearing melagabbonorite, and a melagabbonorite layer, which grades into the overlying gabbonorites.
4. The ultramafic-mafic contact at Tumble Ice and Petrel's Rest dips at approximately 5°NE , and the regional dip at Ice Axe Peak is approximately 10°E . The outcrops at the latter locality appear to define two broad domes (Figure 3.4).

B. The Mafic Unit

The mafic unit at Robertskollen shows little textural and mineralogical variation. Its maximum exposed thickness is at Ice Axe Peak, where approximately 150 m are present above the ultramafic-mafic contact. A description of this section is representative of the area. In the Gully Section, the first 25 m above the ultramafic rocks consist of medium-grained gabbonorites, which are overlain by gabbros. These rocks are mostly even-grained, but clinopyroxene phenocrysts are abundant in the uppermost 10 to 15 m below the peak. Small, irregular, fine-grained bodies are present locally

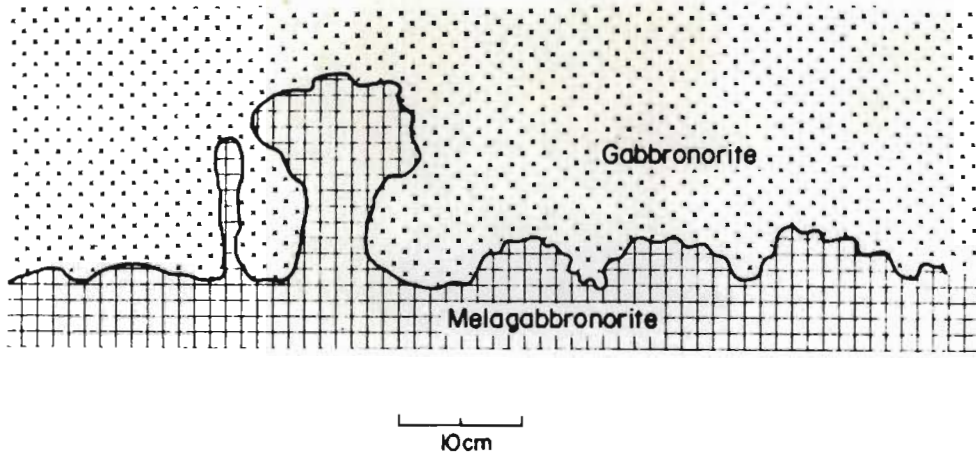


Figure 3.6 Details of the contact between the mafic and ultramafic units at Ice Axe Peak. Redrawn from photographs, approximately 200 m north of Gully Section.

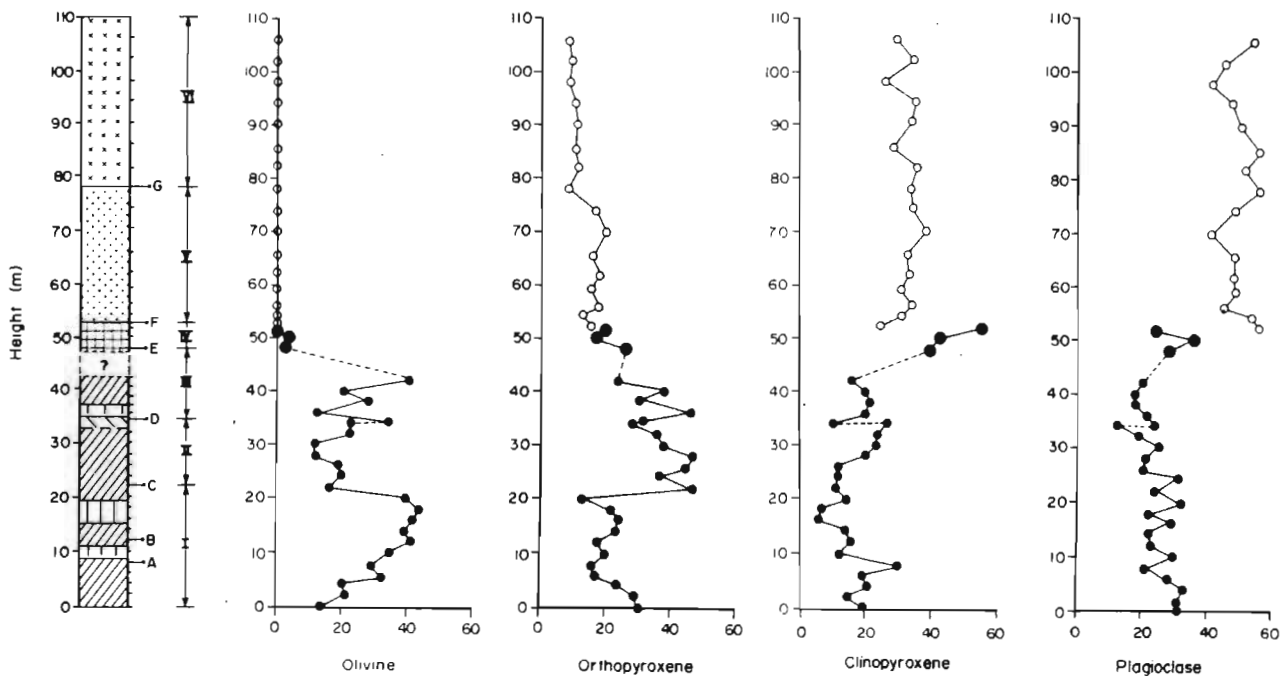


Figure 3.7 Variation in modal compositions (in per cent by volume) through Gully Section. See Appendix 1 for discussion on errors. Symbols in schematic section as for Figure 3.5. Small dots: ultramafic unit; Large dots: melagabbronorite; Open circles: mafic unit.

within these porphyritic rocks. At about 70 m above the ultramafic contact coarse-grained quartz diorite pegmatites appear, which increase in abundance upwards in the section to approximately 120 m above the contact. They occur as irregular masses with sharp contacts and as vein-like bodies which parallel both vertical and horizontal joints. The upper 30 m consists of a medium-grained porphyritic gabbro, which contains phenocrysts of clinopyroxene. Fine-grained gabbroic bodies with pod-like shapes and sharp contacts, rarely larger than 3 m in diameter, are present in this upper zone.

C. Dykes

Olivine dolerite and basaltic dolerite dykes, from 1 to 10 m in width, have been mapped at Ice Axe Peak and Snow Petrel's Rest (Figure 3.1). A 1 m-thick basaltic dyke in the southern part of Ice Axe Peak, striking approximately east-west, has a distinct mottled appearance, defined by differential weathering on the surface. The size of the individual patches defining the texture varies from 5 mm in diameter along the contacts of the sill to about 2 cm in the centre. The significance of the texture has not been determined, and requires further investigation.

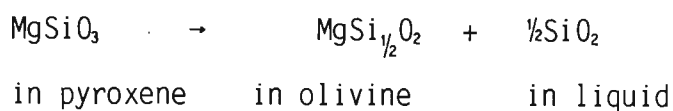
II. Petrography

A. The Gully Section

Gully Section at Ice Axe Peak represents the most complete sequence of the ultramafic and mafic rocks at Robertskollen. Modal compositions in the section are summarized in Table 3.1 and Figure 3.7. The symbols A to G in Figure 3.7 denote marked modal and textural changes. No detailed mineral

chemistry was determined, but optical observations suggest a fairly constant composition for plagioclase (cores of An_{70} and mantles of An_{50}) and orthopyroxene (En_{70}). Petrographic variation is summarized in Table 3.2.

Zone I (Figures 3.5 and 3.7); 0.0 to 22.0 m: Textures in the mela-olivine gabbronorites and mela-olivine norites of this zone vary from porphyritic and locally subpoikilitic to radiating and, rarely, to laminated. Euhedral chromite grains, seldom larger than 10 micron in diameter, occur as inclusions in olivine and orthopyroxene. Crystallization of chromite was followed by that of olivine, which occurs enclosed in plagioclase, clinopyroxene, phlogopite and, to a lesser extent, orthopyroxene. Grains enclosed in the former three minerals are rounded, anhedral to rarely euhedral, but in orthopyroxene most of the grains show typical reaction relationships such as corrosion and smaller grain sizes. However, there are rare grains which have retained euhedral shapes where they are partially enclosed by orthopyroxene, or appear to embay the orthopyroxene (Figure 3.8). These textures occur in Zone II as well, and indicate either a lack of reaction relationship between the two minerals, or suggest corrosion of the orthopyroxene, possibly by the reaction:



as proposed by Wilson (1982). Such a reaction may indicate metastable crystallization of olivine (Morse, 1980) or disequilibrium conditions caused by movement of intercumulus liquid (Tait et al., 1984).

Plagioclase occurs as subhedral laths up to 0.15 by 1.0 mm, which in places define radiating textures (Figure 3.9) or plagioclase spherulites (as defined by Mackenzie et al., 1982). In isolated cases the laths are curved.

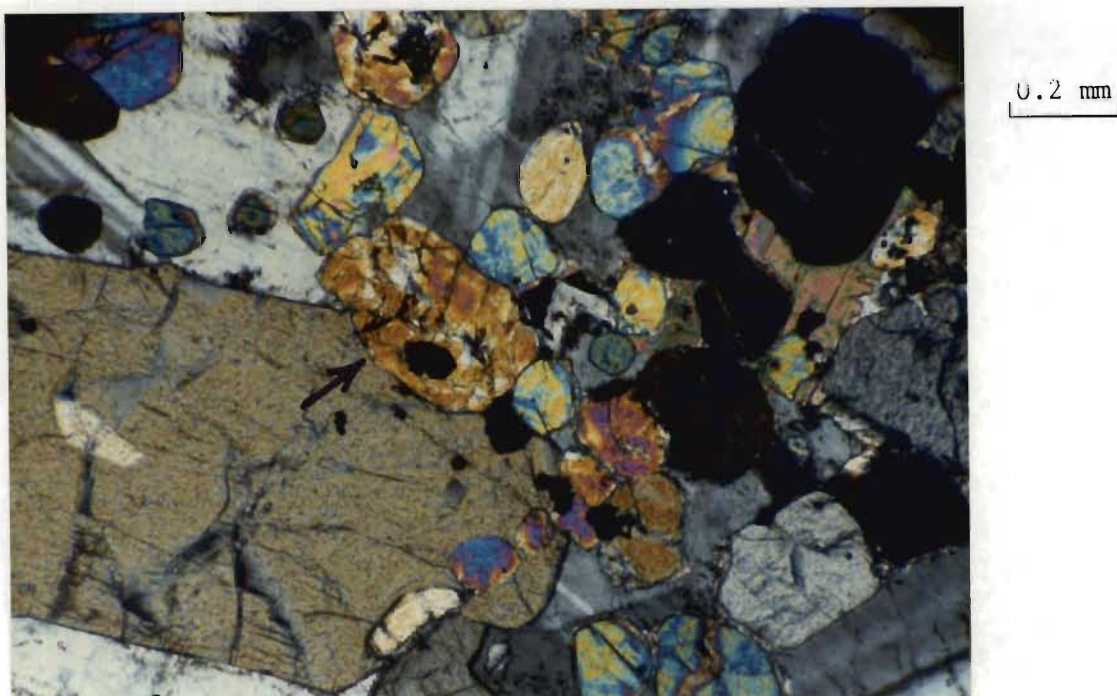


Figure 3.8 Photomicrograph of olivine (arrowed) apparently embaying orthopyroxene, ultramafic unit, Gully Section. Crossed polars.

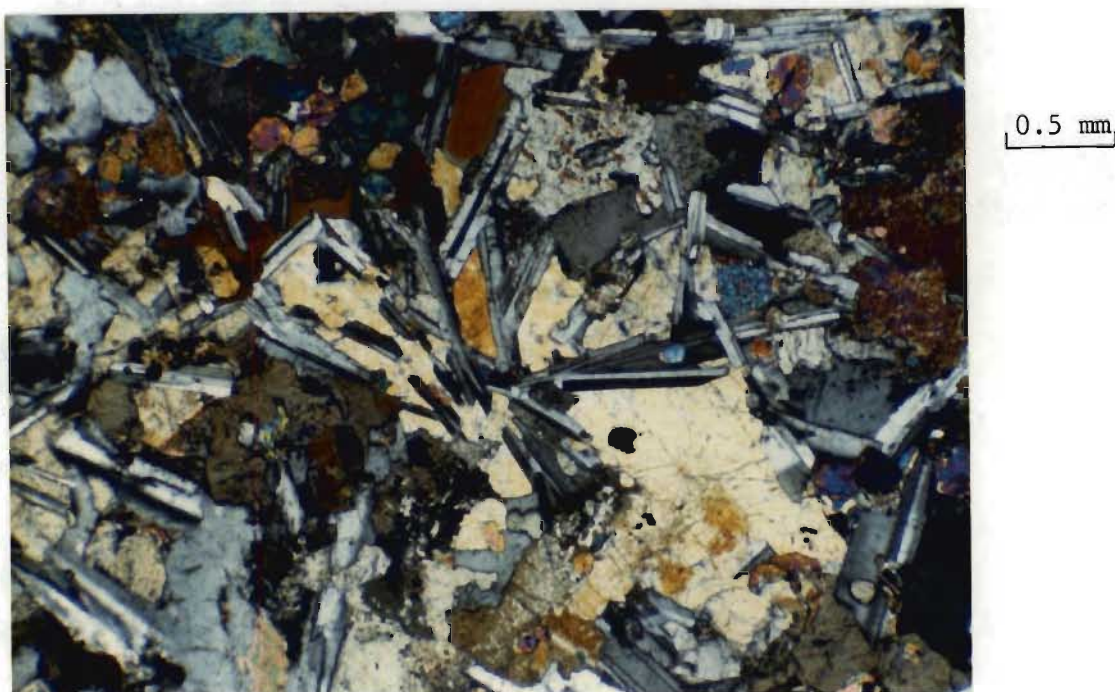


Figure 3.9 Photomicrograph showing radiating texture defined by plagioclase laths partially enclosed in orthopyroxene, ultramafic unit, Gully Section. Crossed polars.

Orthopyroxene occurs in the interstices, or encloses the spherulites subpoikilitically. Plagioclase laths bound these orthopyroxene megacrysts, resulting in some cases in a "wheel-and-spokes" texture as shown in Figure 3.10. Many of the laths have been corroded, resulting in splayed textures where orthopyroxene occurs in the embayed areas (Figure 3.11). The plagioclase spherulites are less abundant at 4 m above the snow line than elsewhere in the zone. Here pseudolaminations are defined by alternating orientations of plagioclase laths, which are subparallel to one another within each lamination. The alternate orientations among laminae are perpendicular to one another. The observation was tested by measuring the orientations of individual laths relative to the length of the thin section. The results for 100 measurements are given in the rose diagram in Figure 3.12, which clearly shows two preferential orientations. These results have to be tested further by measuring the orientation of the crystallographic axes, but it is clear that plagioclase at this level is preferentially orientated. The laths show limited normal zoning, but larger anhedral postcumulus grains are strongly zoned, and show oscillatory zoning.

Clinopyroxene and orthopyroxene are usually present as anhedral, postcumulus grains, which are interstitial to plagioclase laths, although rare phenocrysts up to 1.5 by 1 mm are present. Normal reaction relationships between the two minerals exist throughout the mafic and ultramafic units. Clinopyroxene contains exsolution lamellae of orthopyroxene, and is uralitized in some cases, with associated patchy alteration to phlogopite and Fe-Ti oxides. A central zone of clinopyroxene containing exsolved orthopyroxene, is mantled by clinopyroxene free of exsolution lamellae in rare cases. Magnesian-rich clinopyroxenes crystallize below the pigeonite-orthopyroxene inversion temperature, hence the exsolution lamellae consist of orthopyroxene (Deer et al., 1978). The zoned nature of the clinopyroxene in Gully Section is

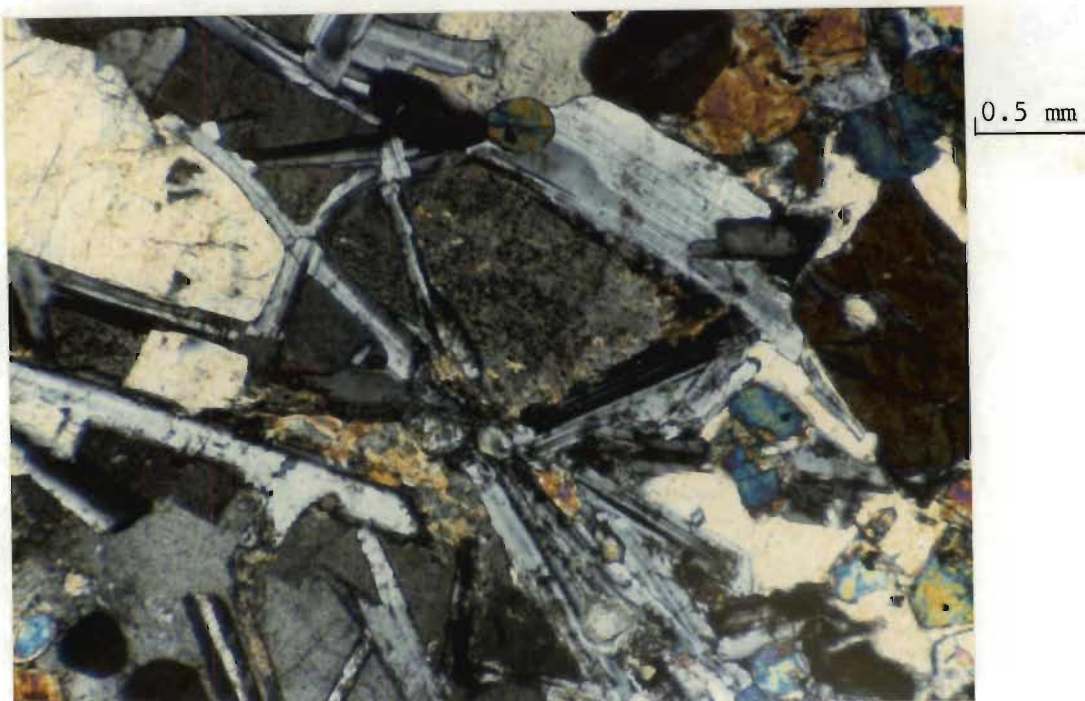


Figure 3.10 Photomicrograph of plagioclase-orthopyroxene relationships defining a "wheel-and-spokes" texture, ultramafic unit, Gully Section. Crossed polars.



Figure 3.11 Photomicrograph of embayed plagioclase enclosed in orthopyroxene, ultramafic unit, Gully Section. Crossed polars. The minerals with high birefringence are olivine and clinopyroxene (top right).

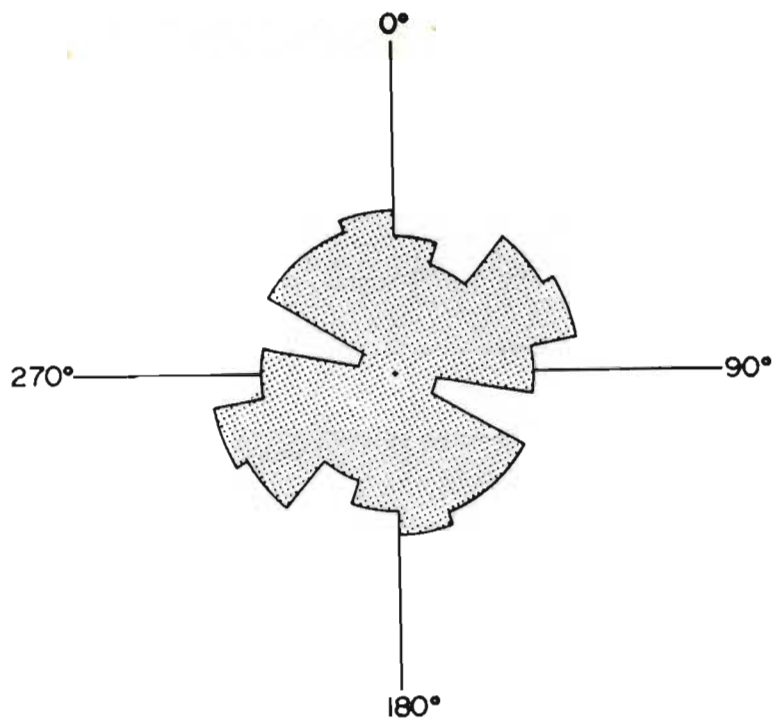


Figure 3.12 Rose diagram of orientations in plagioclase laths with length/width ratios $> 4:1$, ultramafic unit, Gully Section. Orientations 90° and 270° are parallel to the length of the thin section measured.

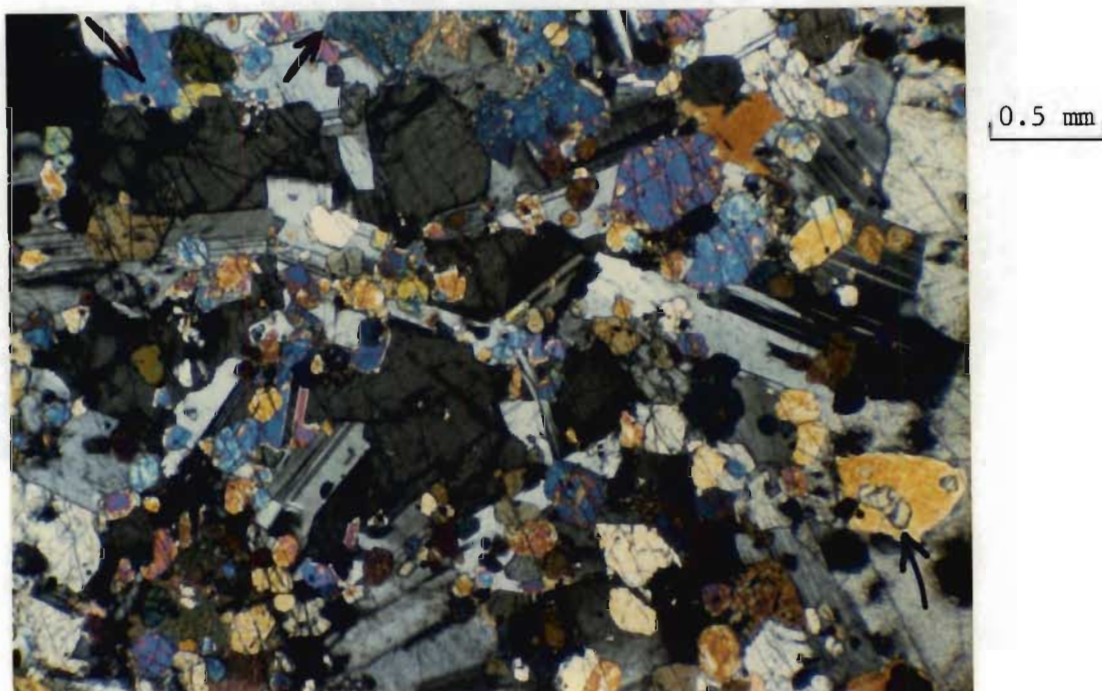


Figure 3.13 Photomicrograph of olivine-orthopyroxene distribution, ultramafic unit, Gully Section. Crossed polars. The orthopyroxene has low interference colours. Clinopyroxene is arrowed.

probably a reflection of increasing Fe-enrichment during crystallization. Phlogopite occurs in interstices and as an alteration product of Fe-Ti oxides and clinopyroxene. Its mode of occurrence remains similar throughout the ultramafic unit.

A locally marked increase in clinopyroxene content occurs at 8 m (point A, Figure 3.7) and above this point there is an apparent increase in zoned, postcumulus plagioclase relative to the plagioclase laths. The irregular distribution of olivine owing to its normal peritectic reaction relationship with orthopyroxene is marked in this zone, and remains a feature throughout the rest of the ultramafic unit (Figure 3.13). Point B (Figure 3.7) marks an increase in the amount and size (up to 10 mm by 5 mm) of postcumulus orthopyroxene phenocrysts relative to interstitial grains.

Modal variation in Zone I (Figure 3.7) shows a regular increase in olivine content, with a concomitant, inverse variation in orthopyroxene content, reflecting the reaction relationship between the two minerals. Modal clinopyroxene decreases upwards in this zone, apart from a marked increase at 8.0 m, and the total plagioclase content varies about a mean of 27 per cent.

Zone II (Figures 3.5 and 3.7); 22.0 to 34.0 m: Euhedral cumulus orthopyroxene grains (up to 0.8 by 1.5 mm in size) appear at 22.0 m (point C, Figure 3.7), concomitant with a sharp increase in total orthopyroxene and a decrease in olivine content. Small subhedral clinopyroxene grains (0.7 by 1.0 mm) occur locally at 22.0 m, but above this level they are euhedral and are considered to be cumulus grains. Postcumulus orthopyroxene phenocrysts are up to 1.0 by 2.3 mm, and show zoning to more Fe-rich mantles. These grains contain exsolved clinopyroxene lamellae and blebs, and inclusions of

serpentine after olivine. Postcumulus clinopyroxene lacks the coarse exsolved orthopyroxene lamellae present in this mineral in Zone I. The top of Zone II, point D, is marked by an increase in phlogopite content, uralitization and alteration of clinopyroxene to phlogopite and serpentinization of olivine. Modal content of olivine in this sections shows cyclic variation upwards, orthopyroxene and plagioclase decrease, and clinopyroxene increases.

Zone III (Figures 3.5 and 3.7); 34.0 to 42.0 m: The most important change in Zone III compared to Zone II is an increase in grain size of cumulus and postcumulus minerals. Cumulus orthopyroxene grains are as large as 1.5 mm in diameter and cumulus clinopyroxene is up to 2 mm, whereas locally developed postcumulus grains are 5 mm in diameter. The cumulus orthopyroxene occurs in clusters with very little postcumulus material in the interstices.

Modal variation in Zone III shows erratic variation in olivine and orthopyroxene upwards, with an overall decrease in the latter mineral and an apparent decrease in clinopyroxene content relative to Zone II.

Zone IV (Figures 3.5 and 3.7); 42.0(?) to 51.5 m: Zone IV is the uppermost zone in the ultramafic unit, and consists of melagabbro norite (Figure 3.14) containing less than 5 per cent olivine. Clinopyroxene and orthopyroxene both occur as primocrysts, and laths of strongly zoned plagioclase are present in this zone. Postcumulus clinopyroxene grains have been uralitized strongly and altered to phlogopite. Trace amounts of olivine and quartz, not in contact with one another, are present in the uppermost part of the zone; the quartz occurring as an interstitial mineral.

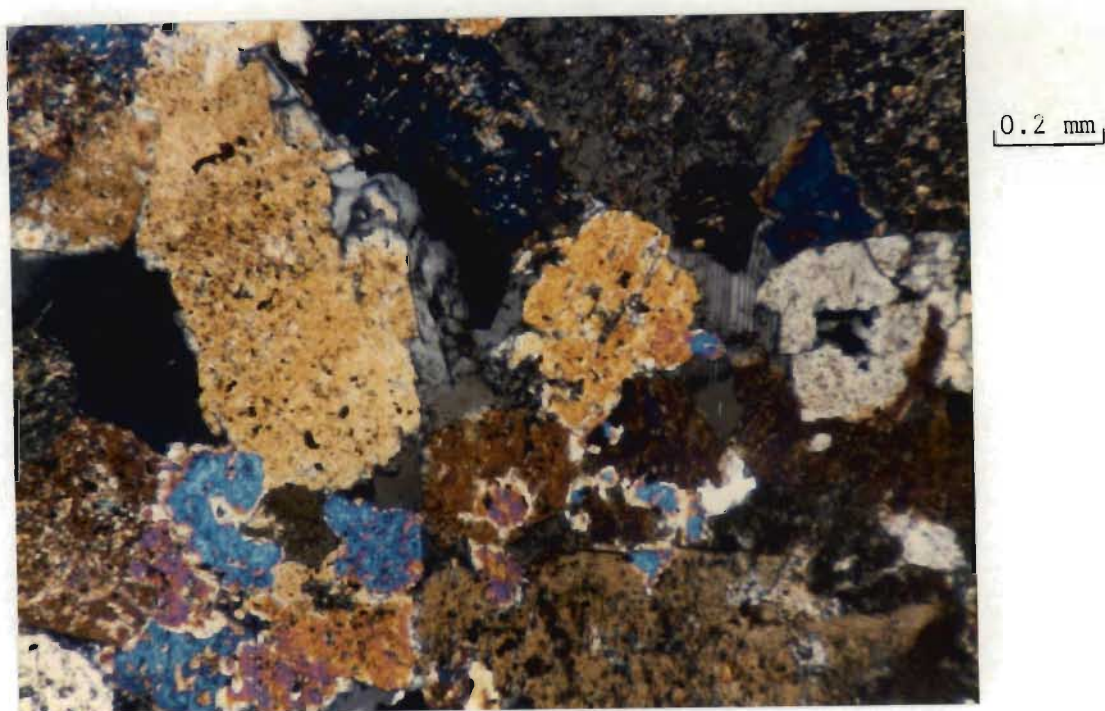


Figure 3.14 Photomicrograph of partially uralitized clinopyroxene in Zone IV, ultramafic unit, Gully Section. Crossed polars.

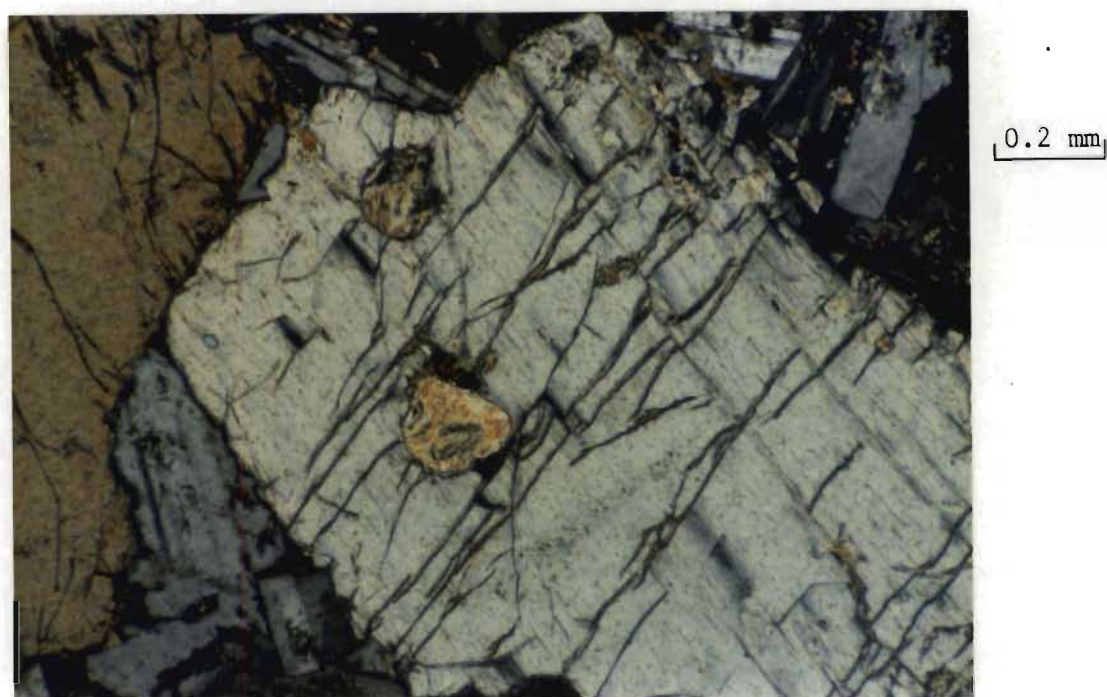


Figure 3.15 Photomicrograph of serpentine after olivine (?) enclosed in orthopyroxene, mafic unit, Gully Section. Crossed polars.

Alteration in the ultramafic unit: The ultramafic unit shows little alteration throughout the section, other than at the top of Zone II (point D) (Figure 3.5). Olivine is rarely partially serpentinized. Slight uralitization of clinopyroxene, associated with alteration to phlogopite and Fe-Ti oxides is present at this level. These alteration effects marginally increase upwards in the unit, and from about 22 m (point C) upwards some orthopyroxene grains are altered locally to phlogopite. Uralitization and alteration of clinopyroxene to phlogopite is more marked in the melagabbronorite of Zone IV than lower in the unit. The alteration of the pyroxenes within the section is interpreted to be the result of local increases in potassium in deuteritic liquids.

Zone V (Figures 3.5 and 3.7); 52.0 to 76 m: Zone V comprises the lower zone of the mafic unit, and shows a sharp increase in plagioclase content. Olivine is absent, apart from rare, serpentinized inclusions in orthopyroxene. Quartz is present in all samples, and there are marked textural changes compared to the ultramafic unit.

Anhedral phenocrysts of orthopyroxene and clinopyroxene up to 1 by 2 mm are set in a matrix of plagioclase, which varies from small, interstitial grains to subhedral, zoned laths of 0.4 by 2 mm at 52 m (point F, figure 3.5). The mafic minerals include anhedral orthopyroxene, clinopyroxene, biotite and Fe-Ti oxides, and small amounts of interstitial tremolite-actinolite needles, which are associated with uralitization of clinopyroxene. Small (0.3 to 0.5 mm) subhedral clinopyroxene and orthopyroxene grains are sporadically present. Two metres above point F subhedral orthopyroxene grains, each about 0.6 by 1.2 mm, form small clusters. Some of these grains contain plagioclase laths, whereas others contain rare serpentine inclusions (Figure 3.15) which are probably pseudomorphs after olivine. In many orthopyroxene grains no

inclusions are present. Higher in the zone the amount of plagioclase inclusions in orthopyroxene increases. Most clinopyroxene grains at this level are interstitial to plagioclase, although some of the phenocrysts contain plagioclase inclusions.

Quartz is present as anhedral, slightly corroded grains in the matrix and as interstitial patches of micrographic intergrowths with alkali-feldspar, and rarely as inclusions in biotite, chlorite, plagioclase and clinopyroxene. A slightly corroded quartz grain occurs enclosed in an orthopyroxene phenocryst at 58 m. Zircon, apatite and rutile(?) are locally enclosed in quartz throughout the mafic unit.

Minor to trace amounts of Fe-Ti oxides occur interstitially to plagioclase, orthopyroxene and clinopyroxene. In most cases the mineral has been altered to biotite.

Zone VI (Figures 3.5 and 3.7); 76.0 m to 110 m: A sharp reduction in modal orthopyroxene at 78.0 m (point G) marks the start of the gabbro zone. Other than this change there is little variation in texture compared to the underlying gabbro-norites. In the upper parts of the measured section the quartz content increases locally to 8 per cent at 98.0 and 102.0 m, and grain sizes of postcumulus orthopyroxene phenocrysts increase from about 1.0 by 1.5 mm to 2.0 by 4 mm. Local alteration of Fe-Ti oxides to sphene, in addition to the alteration to biotite has been observed. Apart from a decrease in orthopyroxene and an increase in plagioclase contents there is no evidence for small-scale layering in Zones V and VI.

Alteration in the mafic unit: Saussuritization of plagioclase cores and uralitization of clinopyroxene is much more marked in the mafic than in the ultramafic unit.

B. Regional Petrographic Variation.

The rocks overlying the Gully Section are intergranular quartz gabbros. Spherical micrographic to granophyric intergrowths of quartz and alkali feldspar are common and are up to 2 mm in diameter. Skeletal Fe-Ti oxides of a similar size are minor constituents, which show extensive alteration to biotite.

The porphyritic gabbro near the top of Ice Axe Peak is ophitic, and consists of anhedral clinopyroxene and orthopyroxene phenocrysts set in a matrix of euhedral orthopyroxene, intergranular clinopyroxene, plagioclase laths, minor amounts of phlogopite and Fe-Ti oxides, and trace amounts of very fine-grained micrographic quartz. The clinopyroxene phenocrysts are 3 to 5 mm in diameter, and enclose numerous plagioclase laths, similar to those described in the Annandagstoppane region (Chapter 2). The orthopyroxene phenocrysts are about 0.6 by 2 mm and contain moderate amounts of plagioclase inclusions.

The mafic unit shows little other regional variation at Robertskollen, except at Valley's Edge, where Von Brunn (1963) reported the presence of norite, which is overlain by orthopyroxene-free gabbro. This gabbro shows extensive hydrothermal alteration.

The major regional variation in the ultramafic unit is an increase in the size of constituent minerals at Tumble Ice and Petrel's Rest. Olivine grains are up to 1.2 mm in diameter, and cumulus orthopyroxene and clinopyroxene grains are up to 1.5 by 2.5 mm, and 1.0 by 1.4 mm in size respectively. In the

melagabbro at Petrel's Rest the cumulus clinopyroxene is up to 2.0 by 4.0 mm. Postcumulus orthopyroxene is up to 5 mm and clinopyroxene 4 mm in diameter locally.

Highly corroded and fragmented quartz grains occur in the melagabbro at Petrel's Rest in a rock containing fresh and serpentinized olivine (Figure 3.16). The material occurring in the embayments consists of strongly saussuritized plagioclase and associated epidote, biotite/phlogopite, and sericite. The coexistence of cumulus olivine and corroded quartz represents a disequilibrium situation which can be accounted for only by contamination of crustal material. The latter, fine-grained material occurs between orthopyroxene and quartz contacts.

C. The Pegmatites and Fine-Grained Bodies.

The coarse-grained phases at Robertskollen are quartz gabbro pegmatites, which are characterized by micrographic intergrowths of quartz, K-feldspar and plagioclase. Plagioclase laths show extensive saussuritization and sericitization, and clinopyroxene has been uralitized completely. Skeletal Fe-Ti oxide grains are common, and have been altered to biotite and, to a lesser extent, sphene and haematite along their margins. Apatite is a minor constituent, and trace amounts of zircon are present.

The fine-grained bodies at Ice Axe Peak are variolitic olivine-bearing dolerites. The groundmass consists of fans of diverging plagioclase needles with which orthopyroxene is intergrown, and clinopyroxene (Figure 3.17). Some needles partially enclose olivine grains, which are slightly corroded where they are in contact with orthopyroxene. The plagioclase fans diverge from the upper right to lower left of Figure 3.17, probably indicating heat flux in this direction (e.g. Mackenzie et al., 1982; Wilson, pers. comm., 1985).

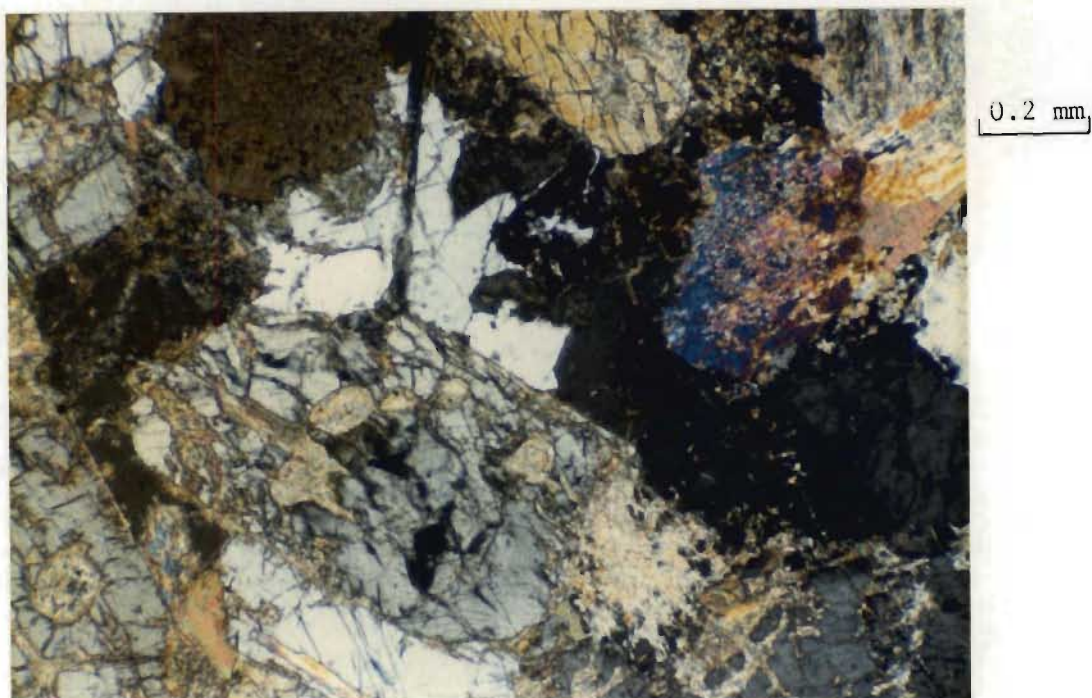


Figure 3.16 Photomicrograph of extensively corroded quartz grain adjacent to orthopyroxene which enclosed serpentinized olivine. Unaltered olivine is present in this thin section; melagabbronite, Petrel's Rest. Crossed polars.



Figure 3.17 Photomicrograph of texture of fine-grained phase from the top of Ice Axe Peak, showing orientated fans of plagioclase laths. The orientation of the apices of the fans indicates the direction of heat flux (Mackenzie et al, 1982; Wilson, pers. comm., 1985). Quartz and olivine grains are arrowed.

Microphenocrysts of clinopyroxene with highly irregular contacts are locally present, and trace amounts of quartz are present interstitially to plagioclase, orthopyroxene and clinopyroxene. Biotite is locally present as an interstitial mineral.

III. Geochemistry

A Regional Characterization of the Robertskollen Complex.

A total of 40 samples were analysed for major and trace elements, 23 from the ultramafic unit and 17 from the mafic unit. The Mg-number ($\text{Mg}/(\text{Mg} + \text{Fe}^{2+})$) will be used as the main reference parameter.

The mafic and ultramafic units at Robertskollen are quartz normative and olivine normative tholeiitic rocks respectively. Element and Mg-number characteristics of the two units are summarized in Table 3.3. Some of the most important features are the relatively high SiO_2 values in rocks with corresponding high MgO contents and Mg-numbers, (e.g. $\text{SiO}_2 = 53.57$ per cent with a corresponding Mg-number of 77.35), a wide range in Mg-number in the mafic unit (78.87 to 41.28), and high K_2O , Zr and Ba contents in the ultramafic rocks (up to 0.48 per cent K_2O , 43 ppm Zr and 124 ppm Ba). Ni and Cr among the compatible elements show the greatest depletion from the most ultramafic to the most felsic rocks.

Interelement Correlations

Variation diagrams of the major and trace elements analyzed are presented in Figure 3.18, and interelement correlations are given in Tables 3.4 and 3.5.

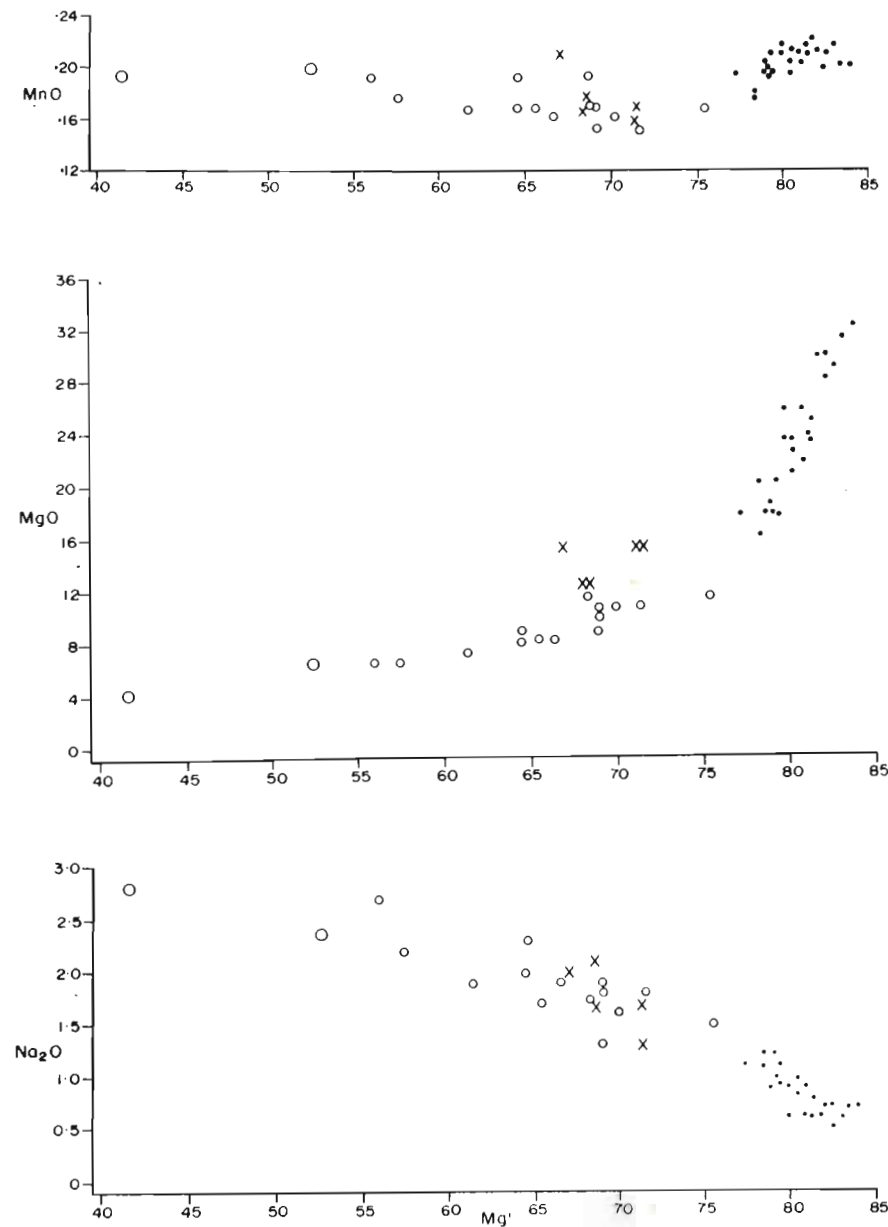
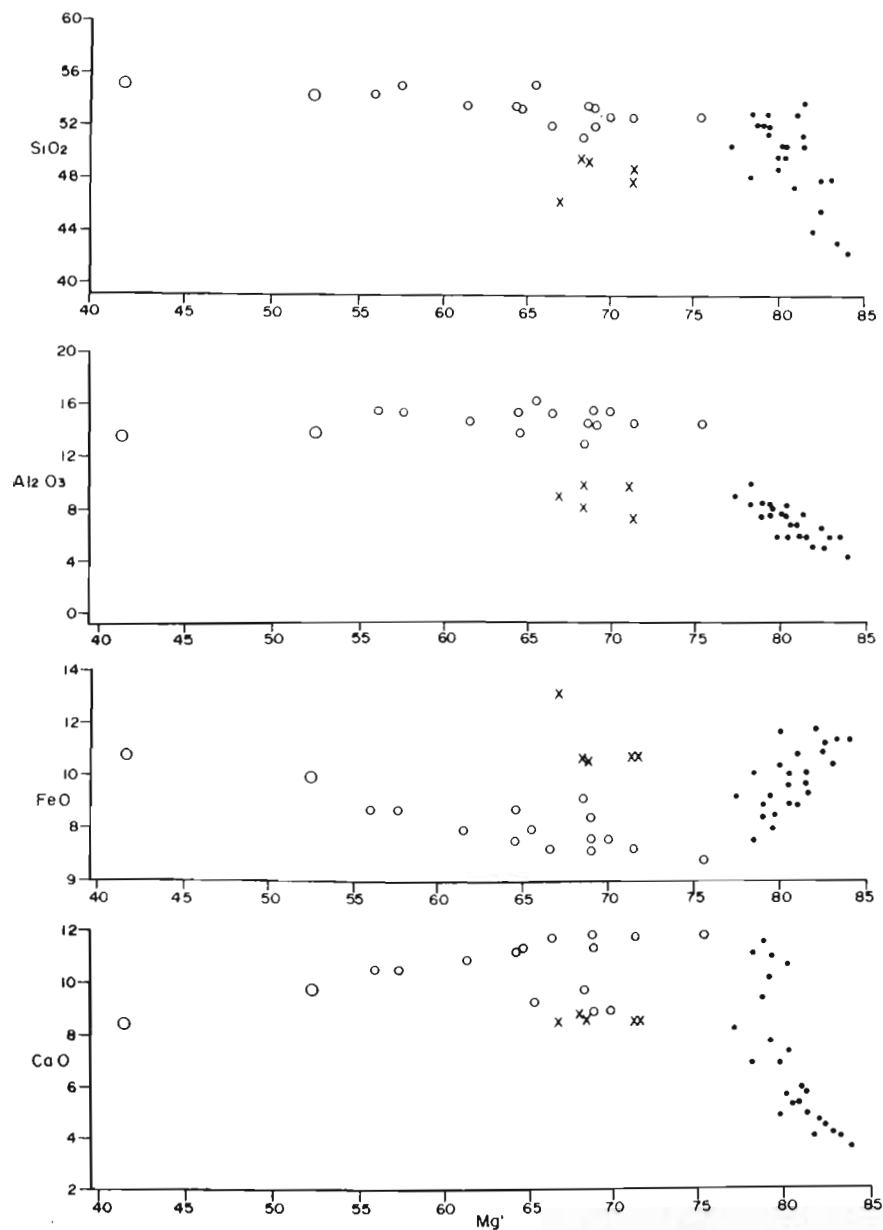


Figure 3.18 Regional variation in concentrations of major and trace elements in the mafic and ultramafic units at Robertskollen. Dots: ultramafic unit; Small circles: mafic unit; Large circles: pegmatite phases in mafic unit; Crosses: Jurassic (?) dykes. Major element data are in per cent by weight and trace elements in ppm. Errors are discussed in Appendix 1.

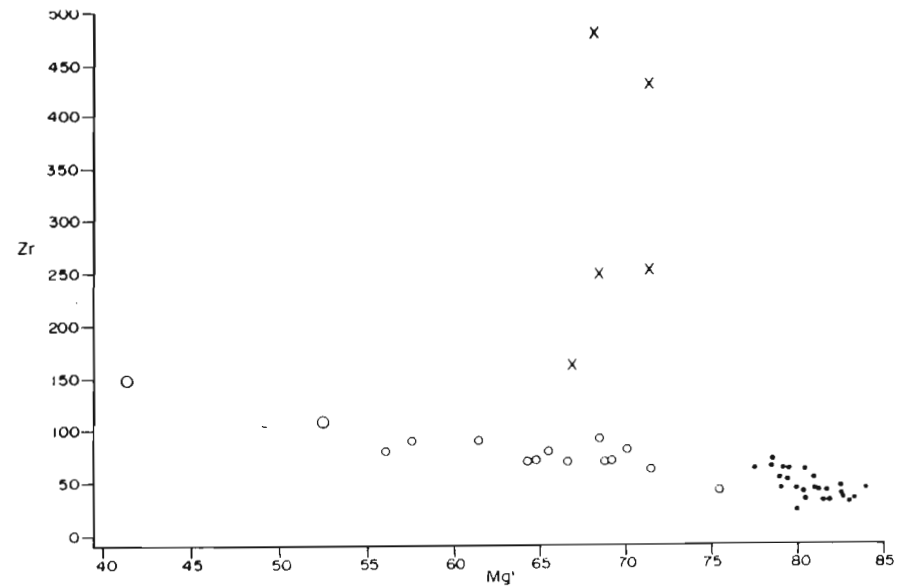
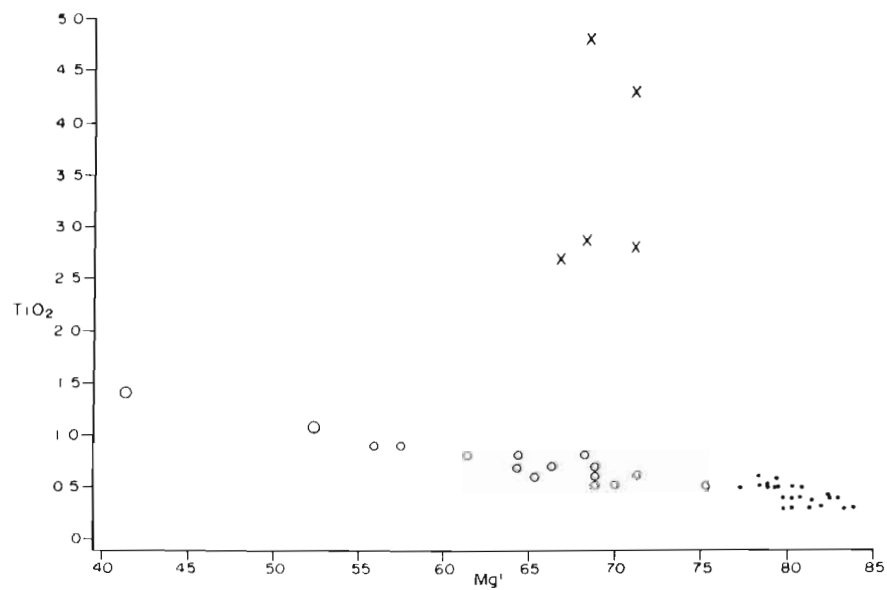
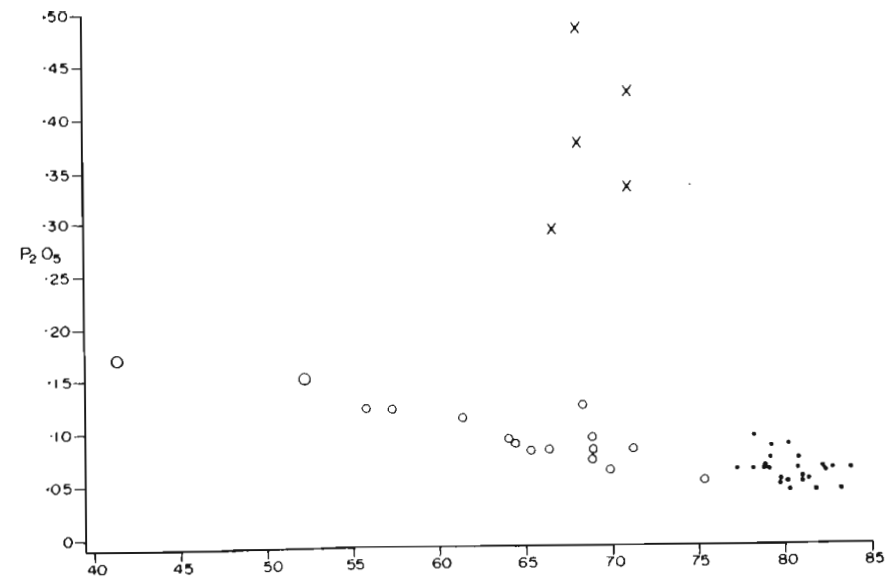
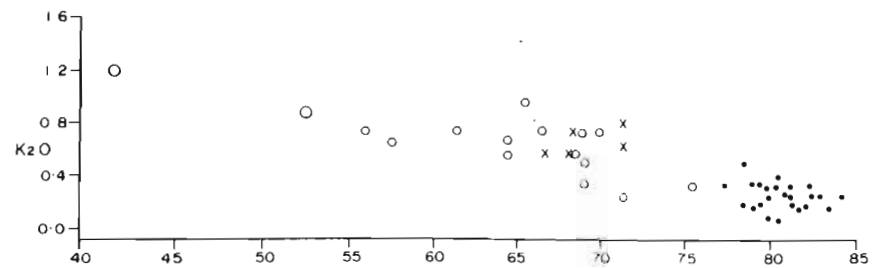


Figure 3.18 (continued)

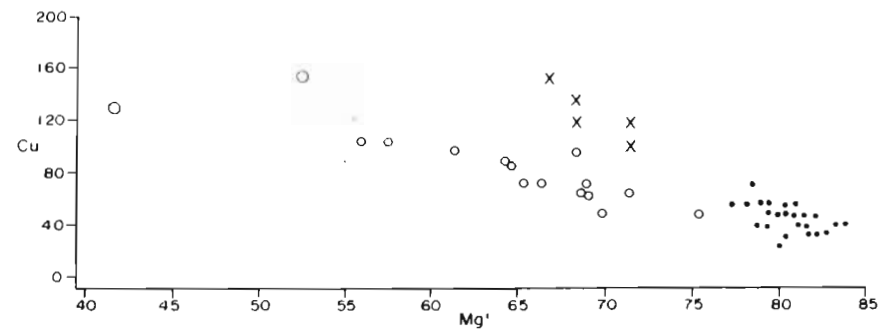
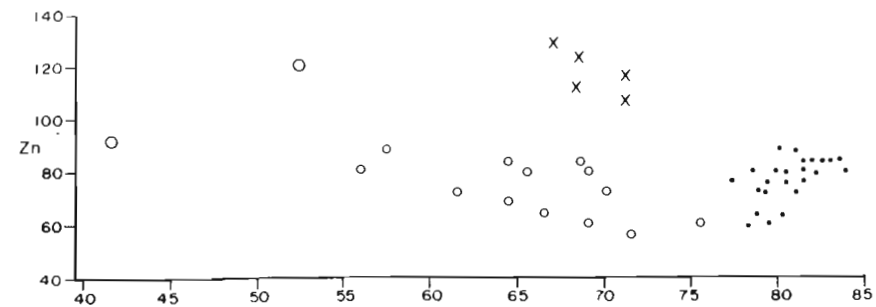
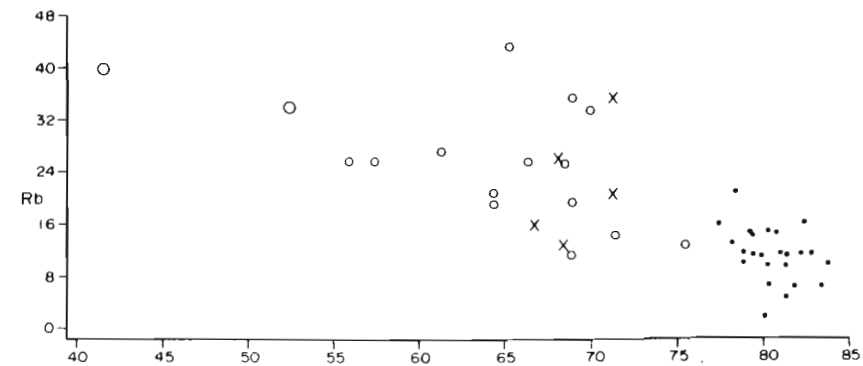
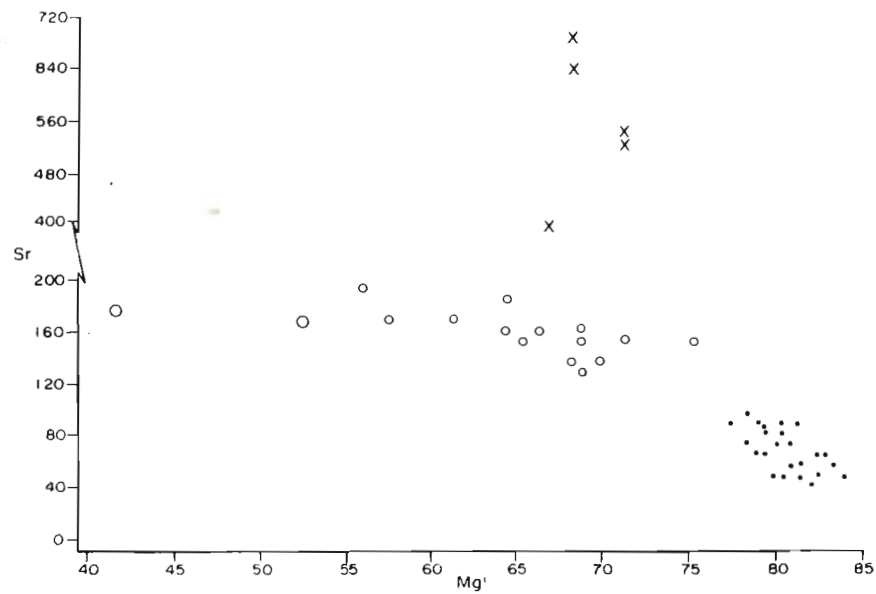
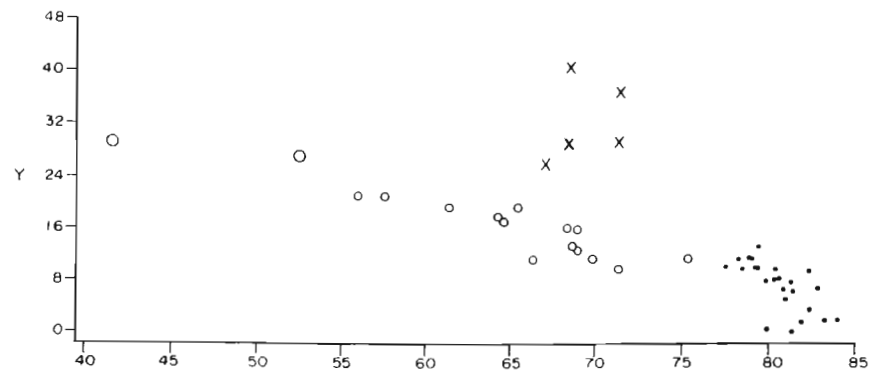
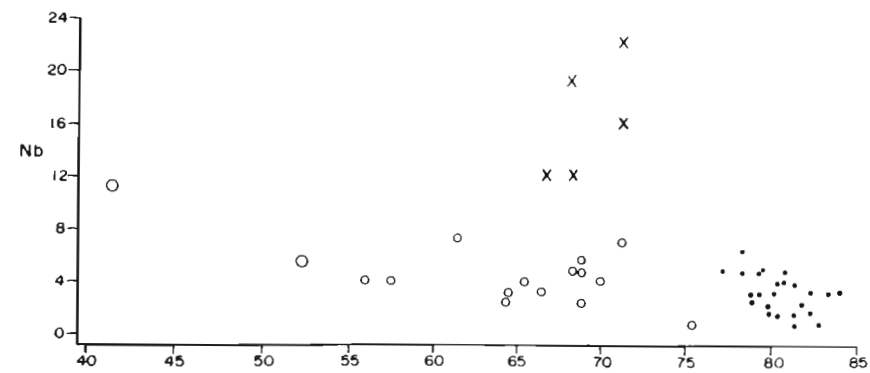


Figure 3.18 (continued)

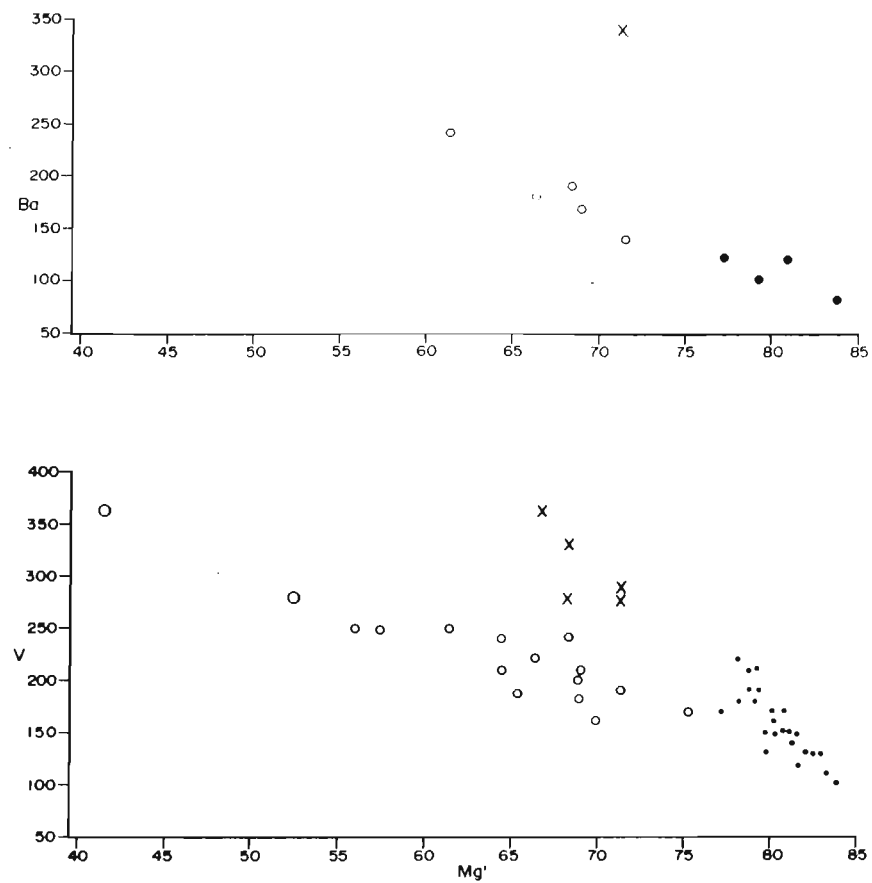
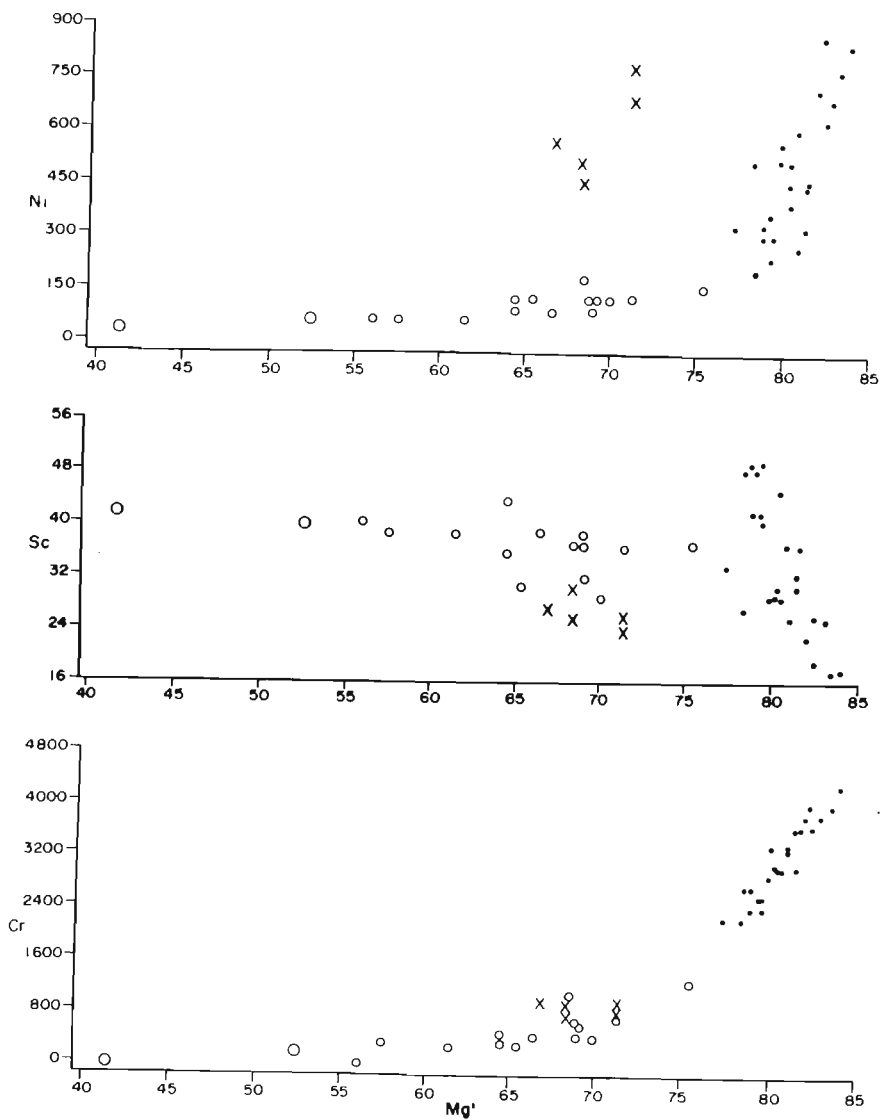


Figure 3.18 (continued)

The Robertskollen (Jurassic ?) dykes were not studied in detail, but geochemical data are shown for comparison on the variation diagrams.

Ultramafic unit: Mg-number correlation with most elements is low except with Al_2O_3 ($r^2 = 0.72$), Cr (.85), Ba (0.73) and V (0.66). Trace element correlations are similarly moderate or low, except Zr/ TiO_2 ($r^2 = 0.74$), Sr/Ba (0.95) and Rb/ Ba (0.97). During normal fractional crystallization of a magma the incompatible elements are concentrated into the liquid at approximately constant ratios, resulting in high interelement correlations. Hence the relatively poor correlations reported here appear to be anomalous and require further investigation.

Mafic unit: Mg-number shows a high negative correlation with most of the incompatible elements, including Na_2O and V. The exceptions are K_2O , with a moderate negative correlation ($r^2 = 0.63$), and Nb, Sr and Rb, which have low negative correlations with Mg-number. Interelement variations among incompatible elements are generally high, except where Nb, Sr and Rb are involved.

B Geochemistry of Gully Section

Major characteristics of geochemical variation in Gully Section (Figure 3.19) are:

- (i) SiO_2 varies antipathetically with MgO , FeO^* (total iron expressed as FeO) and modal olivine.
- (ii) The compatible trace elements, Ni and Cr, vary sympathetically with modal olivine in the ultramafic unit and with orthopyroxene in the mafic unit. Points (i) and (ii) indicate primary control of compatible element behaviour by cumulus mineralogy.

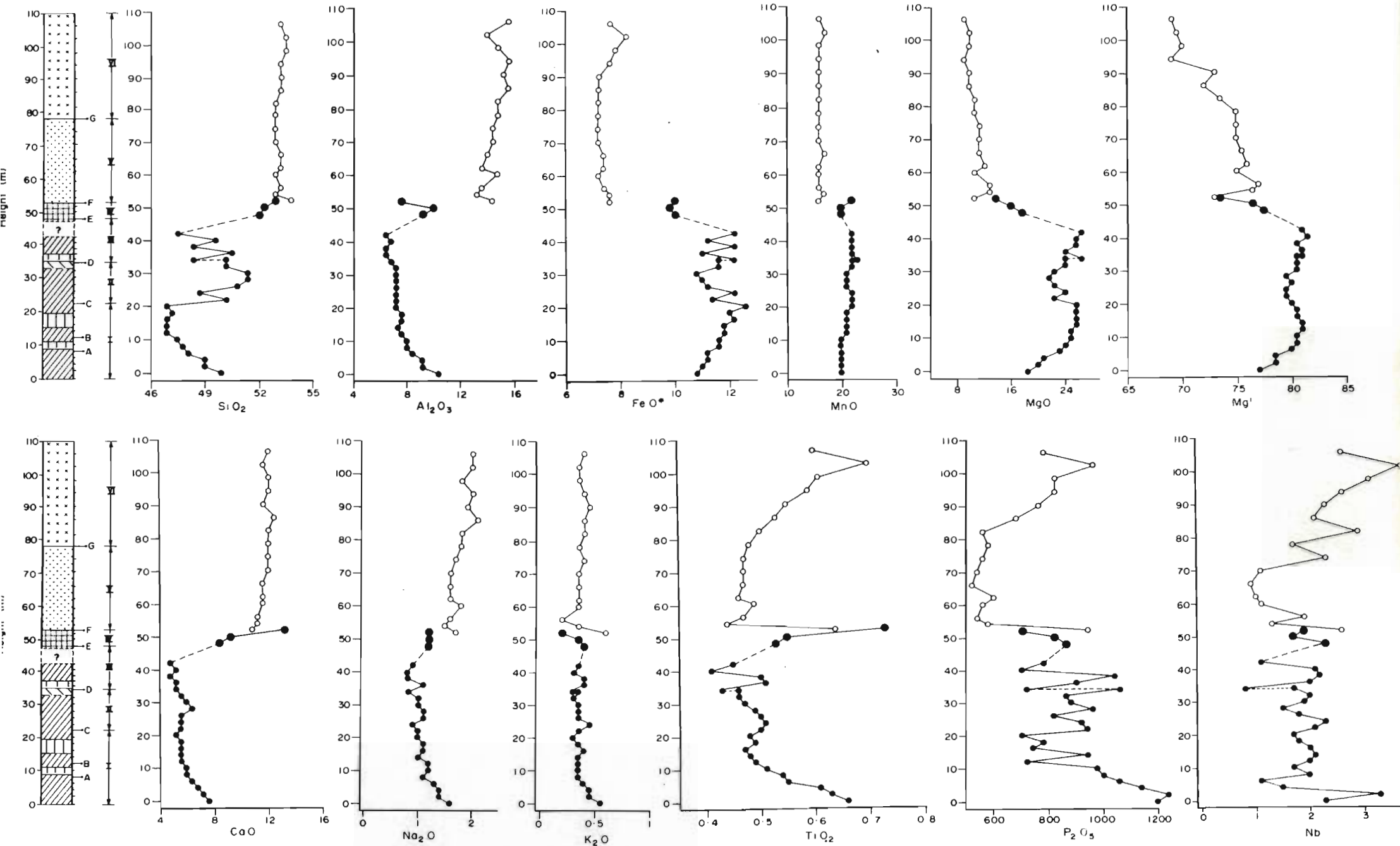


Figure 3.19 Major and trace element variations with height in Gully Section. Small dots: Ultramafic Unit; Large dots: Zone IV, Ultramafic Unit; Circles: Mafic Unit; symbols in schematic section as per Figure 3.5. Examples are discussed in Appendix 1.

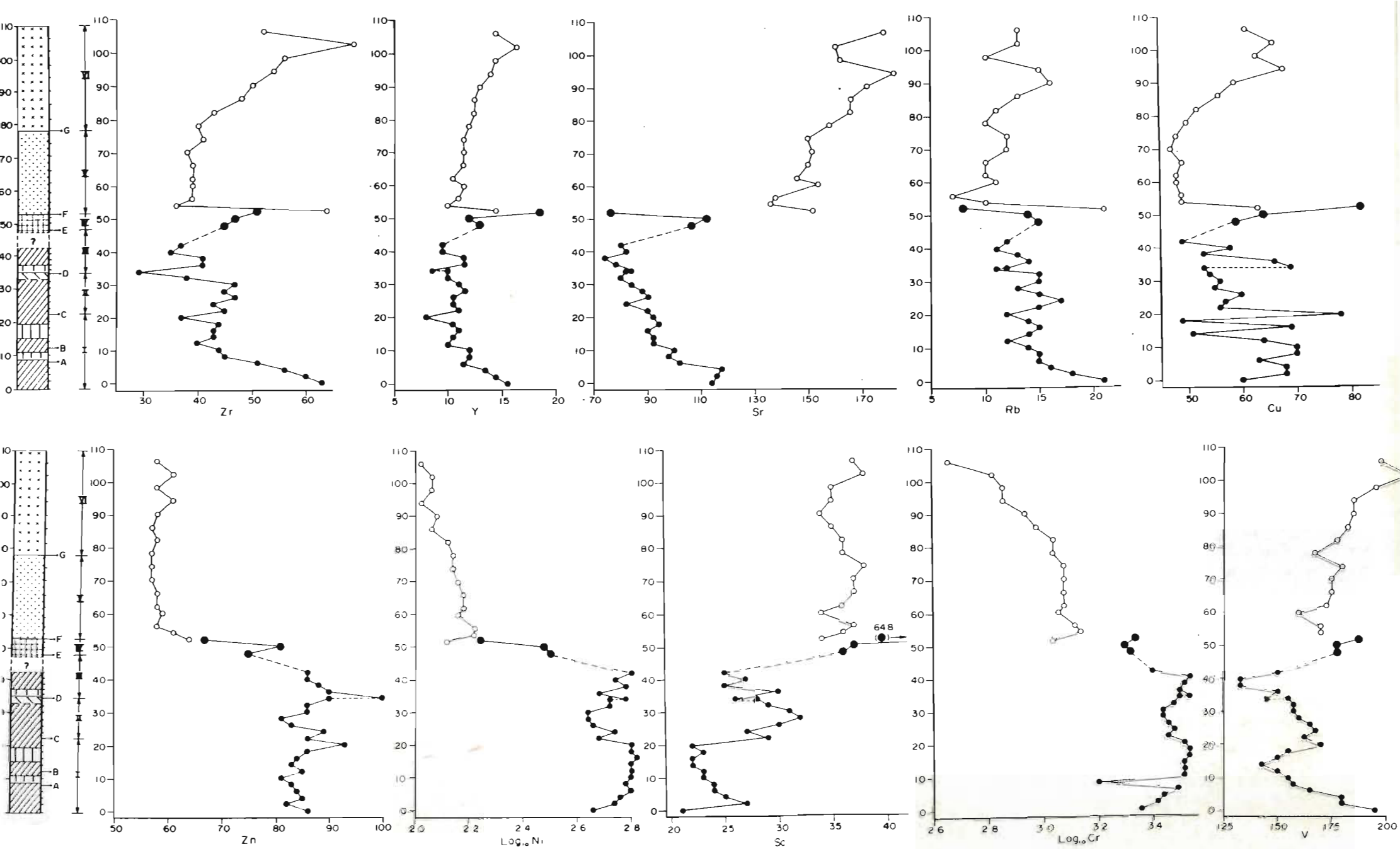


Figure 3.19 (Continued)

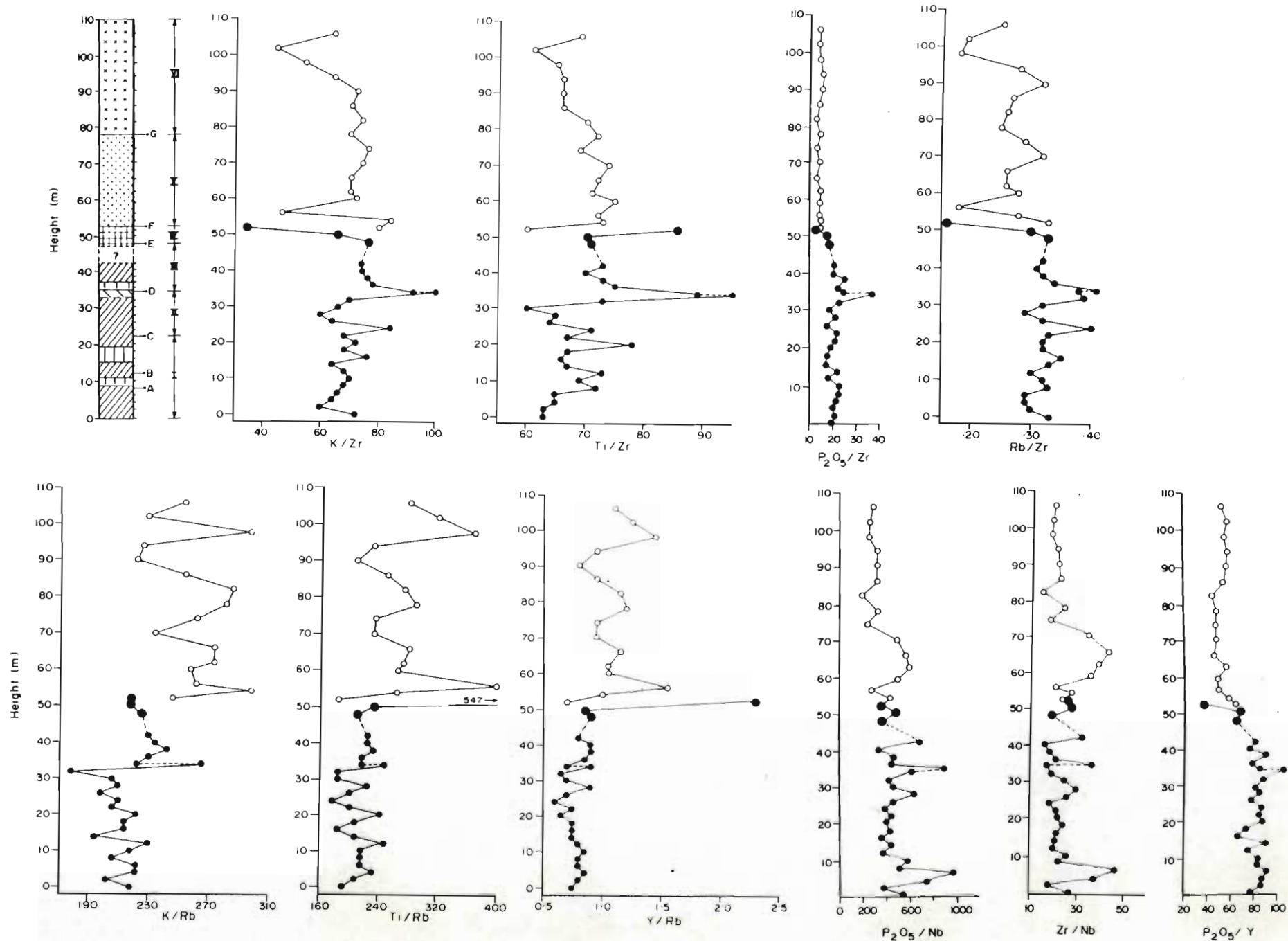


Figure 3.20 Variation in incompatible trace element ratios with height in Gully Section. Symbols in schematic section as for Figure 3.5. Small dots: ultramafic unit; Large dots: Zone IV, ultramafic unit; Circles:

- (iii) The Mg-number varies in two cycles with height in the ultramafic unit. The lowermost cycle is within Zone I, in which the Mg-number increases from 0 to 12 m and decreases from 12 to 22 m. The second cycle is from the base of Zone II at 22 m to the top of Zone IV. The Mg-number increases systematically through Zones II and III and decreases in Zone IV. The mafic unit shows a systematic decrease in Mg-number upwards to the top of Zone VI. The behaviour of the Mg-number through the section may be due to (a) fractional crystallization, (b) contamination of the Robertskollen magma(s), (c) variation in the amount of trapped liquid in the rock, (d) more than one magma pulse into the magma chamber, or (e) a combination of these factors.
- (iv) The incompatible elements decrease upwards in the ultramafic unit and show large variations through Zone IV, but they increase systematically upwards in the mafic unit. These trends result in a broad, cusped trend throughout the section, most clearly observed for TiO_2 , Zr and Y.
- (v) Some incompatible elements behave apparently anomalously in Zone IV. Ti, Zr and Cu increase upwards with decreasing Mg-number, but K_2O , P_2O_5 and Rb vary systematically with Mg-number and Ni.
- (vi) Samples from the top of Zone IV and the base of Zone V (the contact samples) show anomalous geochemical behaviour compared to the underlying and overlying rocks:
- The Mg-number is approximately 73 for both samples compared to 76 for the adjacent samples;
 - The contact samples show a marked increase in TiO_2 , Zr, Y and Cu compared to the adjacent samples; and
 - CaO and Sc are enriched in the ultramafic contact rock compared to the rest of the section, whereas K_2O , P_2O_5 , Nb, and Rb are enriched in the mafic contact rock.

- (vii) Incompatible trace element ratios show no essential differences between the mafic and ultramafic units (Figure 3.20), except in the K/Rb ratio. The irregular distribution of phlogopite and biotite through the section (Table 3.1) suggests remobilization of these two elements during deuteritic and/or hydrothermal processes.

IV DISCUSSION

Mineral chemistry data through Gully Section are required in order to establish a detailed petrogenetic model for the Robertskollen complex. Nevertheless, field, petrographic and whole rock geochemical data described here are adequate to provide a simple model for the evolution of the complex. It is proposed that the complex intruded sediments of the Ritscherflya Supergroup and, possibly, a granitic terrane. Stoping and assimilation of country rocks modified the geochemical characteristics of the Robertskollen magma. At least two major pulses of parent magma may have occurred during the evolution of the ultramafic unit, which influenced the geochemical and mineralogical variation throughout the complex, although some of the geochemical features may be explained by variation of the amount of trapped liquid.

A. Shape of the Complex

Three diagnostic features characterize the Robertskollen complex:

- (i) The section at Ice Axe Peak represents the maximum exposure of the Robertskollen complex in the Robertskollen area.
- (ii) The lowermost and uppermost outcrops have petrographic textures consistent with considerable degrees of undercooling (Dowty, 1980; Lofgren, 1980; Petersen, 1985). These textures include radiating or variolitic and laminated plagioclase laths.
- (iii) Plagioclase laths have been corroded near the base of Gully Section. It is suggested that metastable nucleation and crystal growth of the plagioclase released latent heat, which increased the temperature of the magma sufficiently for plagioclase to become unstable. Corrosion of the mineral by the magma was arrested by nucleation and growth of orthopyroxene.

The effects of undercooling and metastable nucleation of plagioclase suggest that the lowermost outcrops and the fine-grained phases near the top of Ice Axe Peak represent rocks at or near the floor and roof of the complex. The minimum thickness of the complex is therefore suggested to be 150 m at this locality.

The shape of the body cannot be determined, owing to the lack of contacts with country rocks in the outcrops. The concentration of pegmatites near the upper parts of the body, but not within the upper contact rocks, is a common feature in sheet-like bodies (e.g. Walker and Poldervaart, 1949), but whether the

Robertskollen complex intruded as a sill, phacolith or other sheet-like body is uncertain. The Schyttbreen, a north-flowing glacier to the west of Robertskollen (Figure 3.1) probably marks the site of major faults (Znachko-Yavorskii *et al.*, 1978; Wolmarans, 1982; Wolmarans and Kent, 1982), which further complicates the understanding of the geometry of the complex.

B. Possible Assimilation of Crustal Material

The following petrographic and geochemical characteristics must be accommodated in any model for the Robertskollen complex:

- (i) Quartz occurs in olivine-bearing rocks (Figures 3.16 and 3.17) and enclosed in orthopyroxene. These grains are interpreted to be xenocrysts derived from blocks of granitic or sedimentary material incorporated in the magma.
- (ii) The incompatible elements P, K and Rb decrease sympathetically with Mg-number and Ni in Zone IV, whereas Ti, Zr and Cu increase (Figure 3.19). The behaviour of K and Rb may be the result of deuteritic or hydrothermal mobilization, but that of P is anomalous.
- (iii) Incompatible trace element correlations are moderate or low.
- (iv) The ultramafic and mafic samples from the contact between Zones IV and V show apparently anomalous features (Figure 3.19): (a) The Mg-number for both samples is lower than in the adjacent samples above and below; (b) They show a marked increase in TiO_2 , Zr, Y and Cu compared to the adjacent samples; (c) CaO and Sc are enriched in the ultramafic contact rock, whereas K_2O , P_2O_5 and Nb are enriched in the mafic contact rock.
- (v) The Robertskollen mafic and ultramafic units have been dated at 1215 ± 128 Ma and 1181 ± 53 Ma respectively, showing no age difference (Barton

and Allsopp, pers. comm., 1983). Initial $^{87}\text{Sr}/^{86}\text{Sr}$ ratios of 0.7065 ± 0.0005 and 0.7057 ± 0.0003 for the mafic and ultramafic units respectively may reflect crustal contamination.

The petrographical and geochemical features described above are consistent with contamination of the magma by calcareous sedimentary xenoliths, stoped from overlying country rocks. It is suggested that stoped sedimentary blocks sunk into the evolved mafic magma until it reached the interface between the mafic and ultramafic units. Even if the ultramafic unit was not yet solidified, its density would have been higher than that of the sedimentary material (Daly et al., 1966; Oxburgh and McRae, 1984), preventing further sinking (Figure 3.21).

Eddies and effects of turbulence may have resulted in small amounts of xenocrystic material being partially mixed with the upper parts of the ultramafic liquid, leading to the presence of corroded quartz xenocrysts in olivine-bearing rocks. Two effects would have inhibited convection at the level where the stoped material had come to rest. The first effect is that the liquid would have lost heat to the stoped blocks and the second is that the SiO_2 content would have increased locally. The combined effect of these two factors would have led to increased viscosity, preventing further mixing with the overlying convecting magma. Thus a narrow (<1 m?) viscous layer enriched in SiO_2 , CaO, incompatible elements and possibly lower $\text{Mg}/(\text{Mg} + \text{Fe})$ ratios (?) may have formed overlying an ultramafic liquid. This layer is referred to below as the interface layer.

Competing diffusivities would have resulted in the establishment of a series of double-diffusive or multicomponent convection layers within a zone in the ultramafic liquid, and possibly in the interface layer (Turner, 1973, 1985;

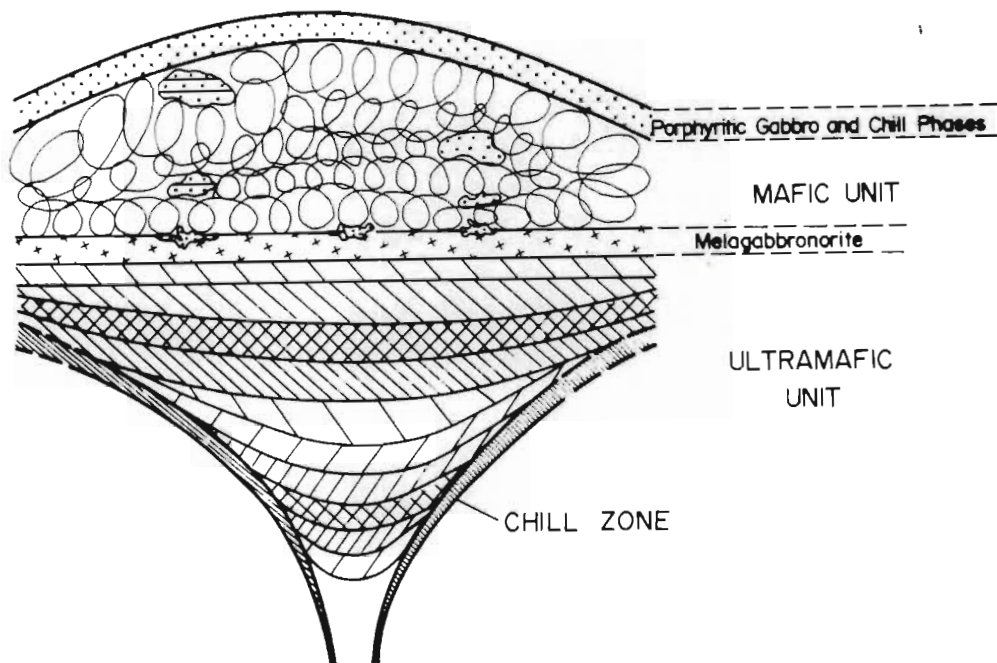


Figure 3.21 Schematic diagram of Robertskollen magma chamber during crystallization of the ultramafic unit. Not to scale. Stippled areas in mafic unit: Xenoliths of country rock.

Turner and Gustafson, 1978; McBirney and Noyes, 1979; Huppert and Turner, 1981; Sparks et al., 1984; Turner and Campbell, 1986). If the diffusive processes occurring across the double-diffusive layers were arrested (e.g. by the onset of crystallization) before the breakdown of individual layers, a stepwise element distribution can be expected within the zone affected by these processes, with higher SiO_2 , CaO and incompatible element contents and lower Mg/Fe ratios at the top than the bottom of the zone affected by the double diffusive convection processes.

The apparently anomalous distribution of P_2O_5 may be the result of a low diffusivity of this element in magmas. Assimilation of crustal material by a basalt magma is essentially a liquid state interdiffusion process (Watson, 1982). Selective contamination of elements is the result of varying diffusivities of ions and their relative affinities for magmas of different composition. However, phosphorus diffuses very slowly in melts containing little water, resulting in slow dissolution of apatite (Watson and Harrison, 1984). It can be assumed that the diffusivity of this element will remain lower than that of most other trace elements even under hydrous conditions. Hence, a contaminant rich in incompatible elements would have lead to an interface layer anomalously enriched in these elements, and an underlying mafic layer (Zone IV) enriched in those incompatible elements with the larger diffusivities. Enrichment effects would have decreased downwards owing to the double-diffusive effect.

C. Magma Emplacement and Crystallization.

Geochemical data permit identification of two features of the Robertskollen complex:

- (i) The Mg-number defines two cycles within the ultramafic unit, and decreases systematically upwards within the mafic unit (Figure 3.19);
- (ii) The incompatible elements define broadly cusped trends owing to their decrease upwards in the ultramafic unit and increase in the mafic unit.

These characteristics may be explained by variation in the postcumulus content of the rocks, by addition of magma to the chamber, or to a combination of these processes.

(a) The effect of intercumulus liquid

Large degrees of undercooling and consequent crystallization lead to liquid-rich assemblages at the margins of intrusions and to crystal-rich cumulates in the interior (Raedeke and McCallum, 1984; Barnes, 1986). A regular decrease in trapped liquid upwards in Gully Section would have resulted in a concomitant increase in Mg-number and decrease in incompatible element contents of the whole rock.

(b) Addition of magma to the chamber

The cyclicity of Mg-number through Gully Section suggests that a process in addition to simple variation in the amount of intercumulus material may have operated in the Robertskollen complex. The most likely process would have been the addition of magma pulses to the Robertskollen magma

after intrusion as proposed for a number of intrusions (Campbell, 1977; McBirney, 1980; Wilson, 1982; Irvine et al., 1983; Campbell and Turner, 1986; Turner and Campbell, 1986).

V. Conclusions

On the basis of field, petrographic and geochemical data it is concluded that

- (i) The evolution of the Robertskollen complex was affected by crustal contamination;
- (ii) Addition of magma pulses during crystallization may have occurred; and/or
- (iii) Regular variation in the amount of intercumulus liquid affected geochemical behaviour;
- (iv) Fractional crystallization of chromite, olivine, orthopyroxene and clinopyroxene occurred in the ultramafic unit and plagioclase, orthopyroxene and clinopyroxene in the mafic unit;
- (v) Metastable crystallization of plagioclase occurred under conditions of supercooling in the ultramafic unit;
- (vi) Models of the petrogenesis and evolution of the Robertskollen magma(s) will be enhanced considerably by detailed isotope studies ($^{87}\text{Sr}/^{86}\text{Sr}$ and stable isotopes) and information on mineral chemistry.

SECTION B

MAFIC SILLS AND GRANITIC INTRUSIONS

IN THE AHLMANNRYGGEN

CHAPTER 4 THE GRUNEHOGNA INTRUSIONS AND THEIR CONTACT RELATIONSHIPS

I Introduction

The Grunehogna nunataks ($72^{\circ}02'S$, $02^{\circ}40'W$, Figures 1.2 and 4.1) situated 25 km west of the Jutulstraumen in the Ahlmannryggen comprise good outcrops of complex mafic sills, which have been intruded by granitic and basaltic dykes. Contacts of the sills with their sedimentary country rocks are very well exposed and provide an opportunity to study intrusion mechanics and effects of the intrusions on these sediments. The highest peak at Grunehogna, Kullen, is 1 555 m above mean sea level, and rises about 450 m above the surrounding ice sheet. Large windscoops along the northern faces, and to a lesser extent along the southern slopes of the nunataks, allow access to the lower parts of the outcrops. A number of routes can be followed to the peaks along which continuous sections can be studied.

The subvolcanic intrusion at Jekselen lies about 11 km east-northeast of Grunehogna (Chapter 6). About 10 km south is the Preikestolen, which forms part of the Liljequisthorga nunataks, and comprises mafic sills and minor volumes of ultramafic rocks. Snow (1986) has shown that the sequence at Preikestolen is similar to that at Grunehogna, as described below.

GEOLOGY OF THE GRUNEHOGNA AREA

(Modified after Aucamp, 1972; Bredell, 1976)

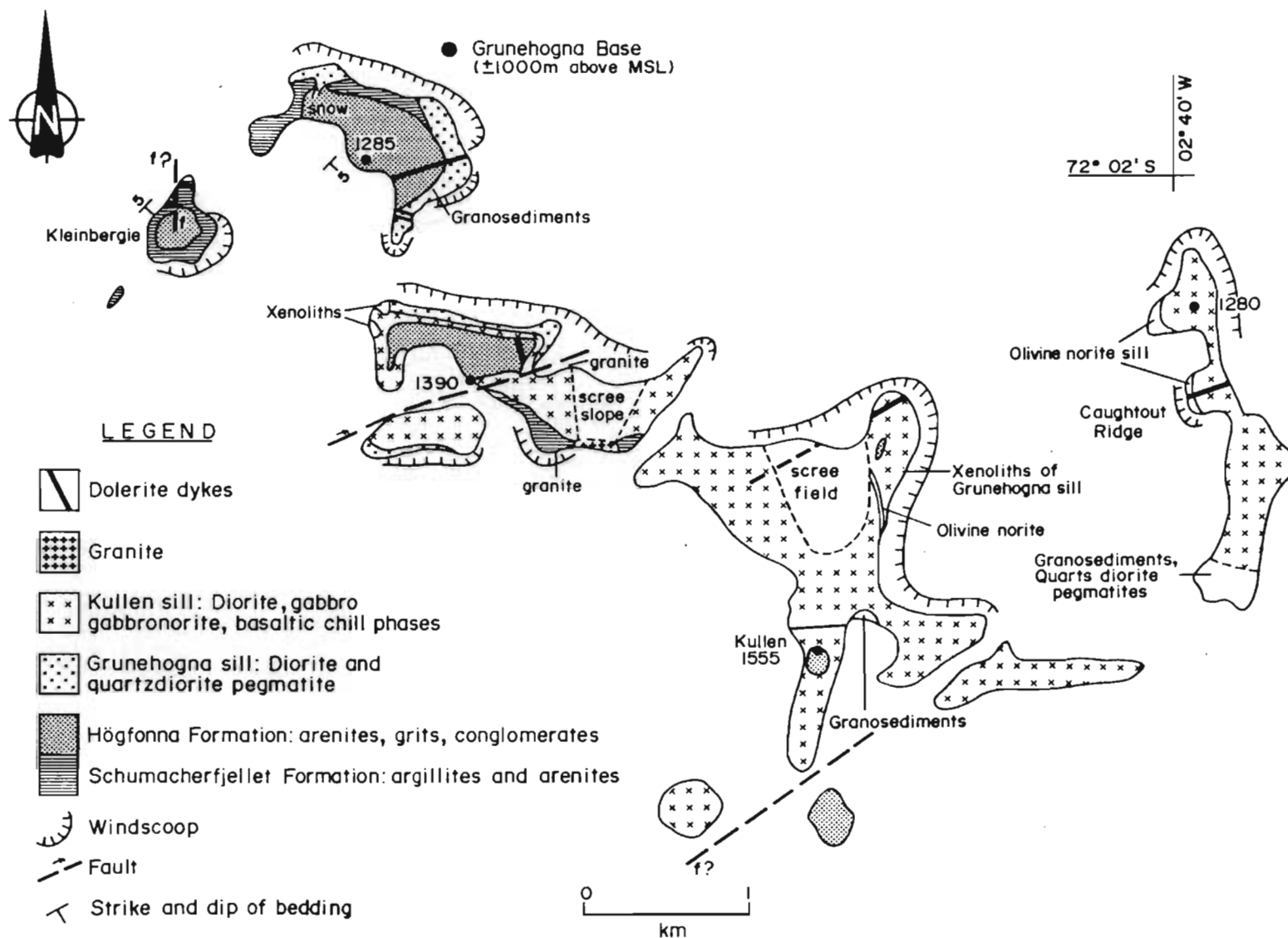


Figure 4.1 Geology of the Grunehogna and Kullen area, modified after Aucamp (1972) and Bredell (1976).

II The Geology of the Grunehogna Nunataks

Previous reports on the geology of Grunehogna and adjacent areas have been made by Roots (1953, 1969), Butt (1962, 1963), Neethling (1964, 1969b, 1970b, 1972a), Bredell (1976, 1982) and Wolmarans and Kent (1982). The first detailed geological mapping in the area was carried out by Aucamp (1972). The following descriptions of the clastic rocks and their sedimentology are based on these previous reports, and work currently in progress by E.P. Ferreira (1986a and b).

A. The Sedimentary Succession

The Ahlmannryggen Group (Table 4.1A and 4.1B) is the lowest, exposed group of the Ritscherflya Supergroup. The nature of the rocks underlying this group is unknown. The lower three formations of the Ahlmannryggen Group, the Pyramiden, Framryggen and Schumacherfjellet Formations, are predominantly argillaceous. The overlying Högfonna, Jekselen and Raudberget Formations are characterized by reddish arenites and the presence of volcanoclastic material. In the field the lower three formations are clearly demarcated from the upper units due to the colour contrast between the Schumacherfjellet and Högfonna Formations. These latter two formations are exposed in the Grunehogna nunataks at Kullen, and nunataks 1390, 1285 and Kleinbergie (Figure 4.1).

The Pyramiden, Framryggen and Schumacherfjellet Formations were mainly deposited in shallow water under low energy conditions, with some evidence of deposition under high current velocity conditions during the closing phases of sedimentation in the Schumacherfjellet Formation (Table 4.2). This latter formation is characterized by alternating yellowish-brown to grey arenites and dark-brown and purple to black argillites (mudstones) in which individual

layers, less than 50 cm thick, are laterally extensive. Periodic emergence is evident from the presence of desiccation cracks. Ferreira (1986a and b) considers the Schumacherfjellet Formation to represent a tidal flat environment.

The upper three units of the Ritscherflya Supergroup, the Högfonna, Jekselen and Raudberget Formations, overlie the Schumacherfjellet Formation conformably, and are made up of arenites and argillites, also deposited in shallow water. A general increase in energy conditions compared with the lower three formations is suggested by a higher arenite to argillite ratio and the presence of conglomerates (Table 4.1). The Högfonna Formation (Table 4.2), for example, comprises brown-grey to grey arenites which appear red when viewed from a distance, reddish-brown and purple to black argillites, extraformational conglomerates, mud-clast breccias and layers containing rip-up clasts. Mud-clasts commonly occur as channel-fill, in which the conglomerates and coarse-grained arenites contain a high volume of red jasper grains and pebbles. The dominant argillite in this formation is shale, with units up to 90 cm thick, whereas the arenites are up to 10 m thick. Upward-fining cycles of conglomerate, arenite and shale are present. Further data on the Ritscherflya Supergroup are summarized in Tables 4.1 and 4.2.

B. Mafic Sills

Two mafic sills, intrusive into the Schumacherfjellet and Högfonna Formations, are the dominant features of the Grunehogna nunataks. They are exposed best in the north faces of nunatak 1390 (Figure 4.2) and Kullen 1555 (Figure 4.3), and will be termed the Grunehogna and Kullen sills, respectively.



Figure 4.2

North face of nunatak 1390. A: Grunehogna sill; B: Grunehogna pegmatite; C: Basal zone, Kullen sill; D: Main Kullen sill; E: Chill zone.

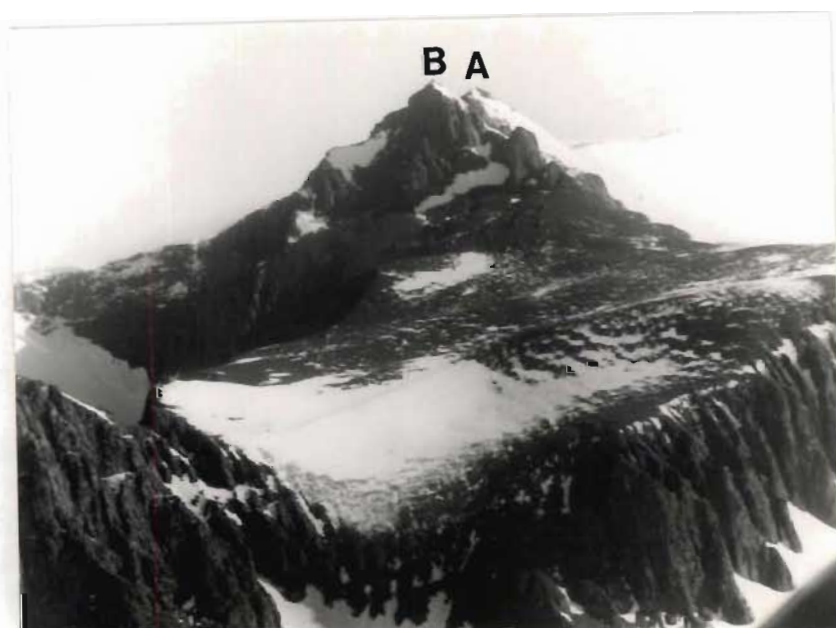


Figure 4.3

Kullen peak (point A), with scree field in foreground. Outcrops of Högfonna Formation overlie the Kullen sill at points A and B.

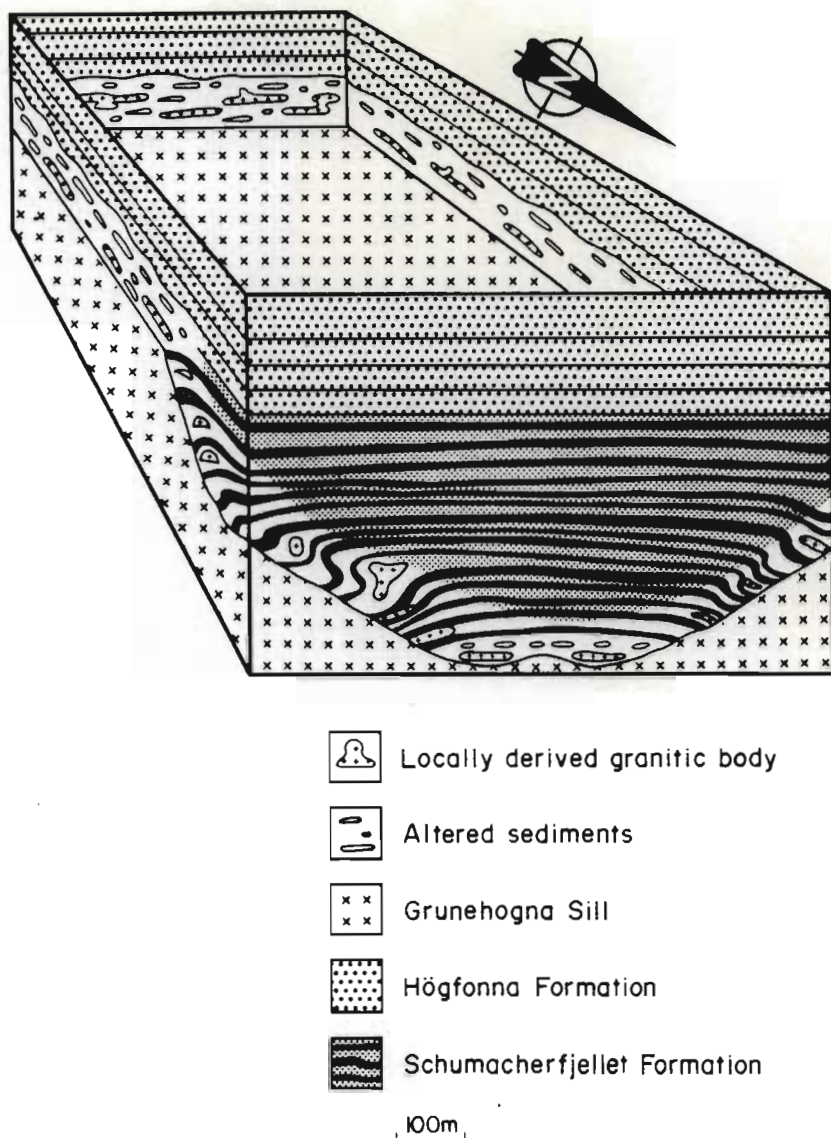


Figure 4.4 Schematic block diagram of Grunehogna sill-sediment relationships in the 1285 nunatak. See text for discussion.



Figure 4.5 Grunehogna pegmatite, 1390 north face. The dark minerals are hornblende, white laths are albite and brick-red areas consist of quartz.

The upper 50 to 55 metres of the Grunehogna sill are exposed above the snow line at nunatak 1390. Outcrops are present in the southernmost windscoop of 1390, in the eastern windscoop of Kullen, and in the northern and southern faces of 1285 (Figure 4.1). In the south face of 1285 the sill is concordant with the overlying, near-horizontal Högfonna sediments, but in the north face it transgresses the sediments of the Schumacherfjellet Formation in a north-plunging trough-shaped intrusion (Figures 4.1 and 4.4) with a 30 m (?) -thick, near-vertical apophysis. The Grunehogna sill is a medium-grained, melanocratic rock, comprising varying amounts of plagioclase and amphibole. A high oxide mineral content, estimated to be locally up to five per cent by volume, is characteristic. The plagioclase grains are oriented subparallel to define an igneous lamination in the exposed lower half of the sill in the 1390 north face. This igneous lamination is present throughout this lower section, and comprises lenticular layers with diffuse boundaries, 1 to 20 mm thick, which are defined by relative modal variations in plagioclase and pyroxene content. The contacts between the layers are usually diffuse. Little evidence of plagioclase alteration is present near the snow line at the 1390 north face, but upwards in the sill the grains appear cloudy, with a light-green tinge. From about 30 to 40 m above the snow line small, red patches, less than 1 cm in diameter, appear in the rock, and increase in abundance towards the upper contact with an overlying mafic pegmatite. These patches contain graphic and micrographic intergrowths of quartz and feldspar. Small vugs, lined with amphibole, epidote and chlorite are locally present in the upper parts of the sill near the contact with the sediments at nunatak 1285. Oval sedimentary xenoliths, not more than 20 cm in length, occur sparsely in the upper five metres of the sill. Patches of green-stained rocks are present along joints, cracks and vugs in the upper part of the Grunehogna sill, Grunehogna pegmatite and within sedimentary contact zones overlying the sill. The green mineral was identified as atacamite by Ferreira (1986a, 1986b).

A 50 - 55 m-thick mafic pegmatite, named the Grunehogna pegmatite, conformably overlies the Grunehogna sill in the 1390 north face (Figure 4.2). Its contacts with the underlying Grunehogna and overlying Kullen sills are sharp, and apart from the increase in pegmatitic phases upwards within the lower sill, there is no field evidence to link genetically this mafic pegmatite with either of the Grunehogna or Kullen sills. The rock is a mineralogically and texturally heterogeneous, coarse-grained quartz diorite pegmatite, consisting of tabular amphibole and plagioclase, quartz, red alkali feldspar and graphic intergrowths of quartz and alkali feldspar (Figure 4.5). High concentrations of epidote are present locally, which impart a light green cast to the rock. A crude layering, defined by variations in grain size and the proportions of plagioclase and amphibole, is evident throughout the pegmatite. The layers vary from about 50 cm to 4 m in thickness. A layered mafic pegmatite with a circular shape, about 3 m in diameter, is exposed within the Grunehogna sill in the southeast face of nunatak 1285. Its attitude cannot be determined, but its characteristics in hand specimen are the same as in the Grunehogna pegmatite.

The Kullen sill is a melanocratic, coarse-grained rock, gabbroic or, rarely, gabbro-noritic to dioritic in composition (Figures 4.2 and 4.6). In the 1390 north face it is 120 m thick but at Kullen a total thickness of 400 m is exposed. Snow (1986) reports a similar thickness for the Kullen sill at Preikestolen. The sill is mineralogically and texturally homogeneous on the 1390 north face, apart from chill phases which occur along the lower and upper contacts. At 1390 the central part of the sill consists of amphibole and sericitized and saussuritized plagioclase. The lower 3 m-thick basal zone at 1390 is fine- to medium-grained, with an igneous lamination defined by plagioclase-rich bands of diorite up to 5 mm in thickness, separated by laminae 2 to 3 cm thick with the same mineralogical



Figure 4.6 Texture of altered Kullen sill. Length of ice axe head is 26 cm.



Figure 4.7 Upper chill zone of Kullen sill in 1390 north face Z: Chill zone; H: Högfonna Formation; K: Apophysis of Kullen sill.

composition as the central part of the Kullen sill. The upper chill against the Högfonna sediments is a 1 m-thick fine-grained, melanocratic diorite (Figure 4.7). Apophyses of the Kullen sill, similar in hand specimen to the chill zone, transgress the overlying sediments at 1390 and approximately 250 m north of Kullen peak (Figure 4.8). These apophyses locally contain scattered phenocrysts of amphibole, 4 mm in diameter.

The Kullen sill is in contact with the Grunehogna sill along the eastern face of Kullen, with no intervening mafic pegmatite. Oval xenoliths of the Grunehogna sill, 10 cm to 2 m in length, are present at this locality at the base of the Kullen sill in a zone about 3 to 4 m thick. Samples of this basal zone appear similar in most other respects to the basal zone at the 1390 north face. Overlying the basal zone at Kullen is an approximately 300 m-thick mineralogically and texturally uniform zone, similar to that at the 1390 north face. Locally clinopyroxene, rather than amphibole, can be recognized in the rock. From here, up to the chill zone, which is about 1 to 2 m thick, the rock comprises layered gabbros consisting of thin (0.5 to 1 cm) lenticular layers defined by modal variations in plagioclase and clinopyroxene. Diffuse pegmatitic blebs are commonly present in the upper 50 m of this rock. In the southernmost windscoop of the Grunehogna 1390 area, the Kullen sill is in direct contact with the Grunehogna sill. No evidence of a chill zone is present in the Grunehogna sill, but the basal zone of the Kullen sill shows a distinct chill zone, approximately 50 cm in thickness.

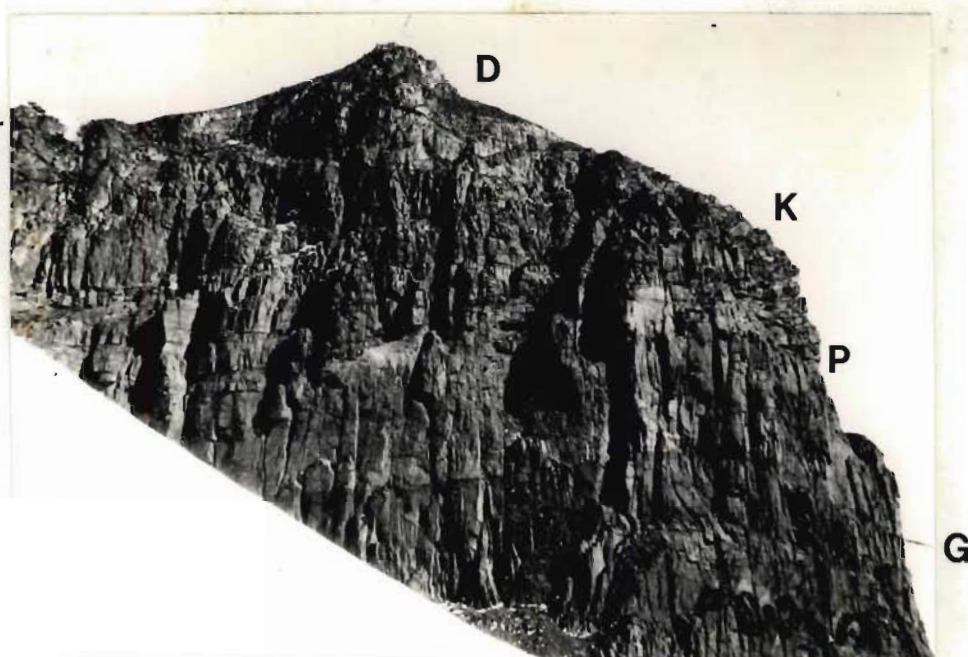


Figure 4.8 Apophyses of Kullen sill intruding overlying Högfonna Formation, 1390 northwest face. G: Grunehogna sill; P: Grunehogna pegmatite; K: Kullen sill; D: Zone in which apophyses intrude.



Figure 4.9 Contact zone, 1285 southeast face. The underlying dark rocks are the Grunehogna sill, and overlying dark rocks are coarse-grained arenites of the Högfonna Formation. Person is 2 m tall.

C. Sediment/Sill Contact relationships, Granitic Bodies and Sedimentary Xenoliths

A 3 m-thick zone between the upper contact of the Grunehogna sill and the sediments of the Högfonna Formation on the 1285 southeast face has an orange-red to reddish-brown colour when viewed from a distance (Figure 4.9), and was identified as a granodiorite by Bredell (1976). It will be referred to as the contact zone in this thesis. Within the contact zone are pinkish-red to orange-red, fine- to medium-grained rocks for which the field term granosediment is used. This term is proposed, because the contact zone rocks display textures gradational from typical fine-grained granites (sensu stricto) and granophyres to sedimentary rocks in which sedimentary structures can be recognized. Gradational between the granitic and sedimentary rocks are granosediments with a granitic appearance in hand specimen, but with a poorly-developed lamination defined by dark minerals. In some cases the granitic or sedimentary nature of the granosediments can only be established by petrographic studies. The mineralogy of these rocks is described in section III. Throughout the contact zone are beige to buff and brownish-grey sedimentary enclaves of medium-grained arenites in which lamination and rarely cross-bedding can be recognized (Figures 4.9, 4.10 and 4.11). The enclaves are tabular in shape, with oval, elongated cross-sections. Their boundaries are typically sharp, but locally may be diffuse. Elsewhere the enclaves grade into schlieren in the granosediment (Figure 4.12). Locally granosediment interfingers with the sedimentary lamination (Figure 4.12). Many enclaves are concentrically zoned in cross-section, reminiscent of Liesegang rings. The zonation comprises a dark-grey core in which well-defined sedimentary structures are preserved, enclosed by one or more rings of light-brown or buff-coloured rock in which sedimentary structures are poorly-defined or absent (Figure 4.13).



Figure 4.10 Sediment enclaves in contact zone, showing laminations and zoned nature, 1285 southeast face.



Figure 4.11 Possible cross-bedding in sediment enclave. Scale is 10 cm in length, 1285 southeast face.



Figure 4.12 Gradational nature of borders of sediment enclaves in granosediment and development of schlieren, 1285 southeast face.



Figure 4.13 Zoning in sediment enclave, 1285 southeast face.

A section across the contact zone was measured and sampled (Figure 4.14). Seven layers were recognized within the section, which are numbered CZ1, at the base of the zone, to CZ7 at the top. The latter layer includes sedimentary rocks in which vugs and granitic veinlets are present. This layer grades into typical sediments of the Högfonna Formation. The contact zone is laterally continuous in the exposure. The general features described below are constant, but contacts between horizons are rarely well-defined and some horizons such as CZ4 are lenticular. Dark minerals referred to below are chlorite, Fe-Ti oxides and rare pyrite.

Figure 4.14 shows a section from the upper part of the diorite to a sequence of coarse-grained arenites and grit bands. At 1 m below the contact the diorite is coarse-grained, and contains numerous patches of orange-red graphic intergrowths of quartz and alkali feldspar. From about -50 cm below the contact abundant epidote and graphic intergrowths in the sill give the rock a mottled bright green and red appearance. The contact with CZ1 is marked by a fine-grained epidote-rich band, but no chill zone is present. CZ1 is a fine- to medium-grained orange-red granitic layer which contains irregular cream-buff patches and concentrations (up to 2 cm in diameter) of epidote, oxide minerals and chlorite, local medium- to coarse-grained veins and patches composed of the assemblage quartz-feldspar-epidote-chlorite and sparse, round to oval arenitic schlieren (1 to 6 cm in diameter) in which crude laminations can be recognized. These schlieren have diffuse contacts and poorly- to well-defined layering of dark-grey, light-grey and pinkish red laminations. Colour variation is due to variations in the dark mineral and feldspar content of the schlieren.

SECTION OF CONTACT ZONE AT 1285 SOUTHEAST FACE

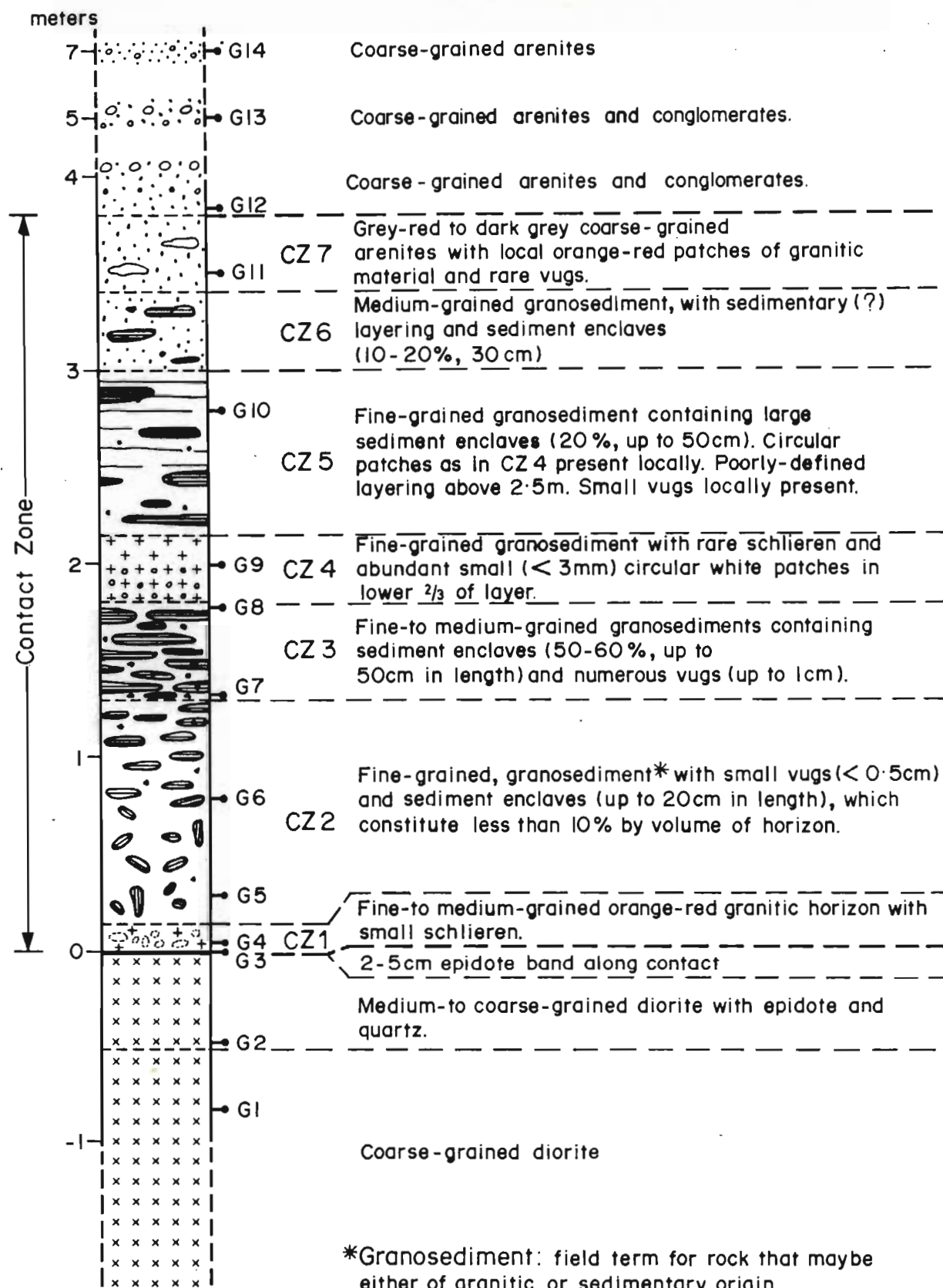


Figure 4.14 Description of section through contact zone of the Grunehogna sill along 1285 southeast face. Values in per cent and centimetres indicate volume per cent and average exposed length of sediment enclaves. "G" values are sample numbers given in Table 4.4.

CZ2 is a pinkish red to orange-red granosediment, with rare, small chlorite-epidote-quartz-lined vugs (less than 0.5 cm in diameter) and sedimentary enclaves up to 20 cm long, which constitute less than 10 per cent by volume of the layer. The enclaves are randomly oriented in the lower part of the layer but towards the top they are oriented subparallel to the regional dip of the overlying Högfonna sediments.

The CZ3 layer comprises fine- to medium-grained granosediment containing 50 to 60 per cent sedimentary enclaves, which are up to 50 cm long and are oriented parallel to the regional dip. Numerous vugs (up to 1 cm in diameter) occur in the granosediment and the enclaves. The CZ4 layer is a fine-grained granosediment with minor amounts of dark minerals, buff arenitic schlieren and no vugs. The lower two-thirds of this layer contains small (3 mm diameter) cream-white spheres, which constitute about 50 per cent of the rock, but which are absent in the upper part of the layer. Medium-grained granosediment in the CZ5 layer contains irregular sub-spherical, cream-white patches (up to 3 mm diameter) and sedimentary enclaves, up to 50 cm in length, make up less than 20 per cent of the rock. The sub-spherical patches are described in more detail in section III (SAPG texture). In the uppermost 1.5 m a wispy lamination is defined by concentrations of chlorite and oxide minerals (Figure 4.15). Vugs are rare in layer CZ6, in which the medium-grained granosediment exhibits a distinct sedimentary (?) lamination. Sedimentary enclaves, up to 30 cm long, make up between 10 and 30 per cent of the rock. Grey-red to dark-grey grits and arenites are present in layer CZ7. Rare vugs and the local presence of orange-red patches and veins of granitic material are the only features which suggest that these sediments form part of the contact zone. The contact of CZ7 with CZ6 is locally contorted, suggestive of



Figure 4.15 Wispy lamination in granosediment, 1285 southeast face.



Figure 4.16 S-fold in Schumacherfjellet Formation along contact with Grunehogna sill, 1285 north face. Person right of centre is 1.8 m tall.

soft-sediment slumping. Conglomerates and coarse-grained arenites overlies the CZ7 layer. The contact is well-defined, owing to the contrast between the medium-grained and coarse-grained rocks.

The sediments have been folded into S-type disharmonic folds with northerly plunges where the Grunehogna sill transgresses the Schumacherfjellet Formation at an angle of approximately 30° to 35° along the north face of 1285 (Figures 4.4 and 4.16). Two sets of transgressive contacts are found about 400 m apart along the western and eastern parts of the north face. (Figures 4.4 and 4.16). In the western outcrops the maximum amplitude of the folds is about 10 m, and in the eastern outcrops about 15 to 18 m. The attitudes of the S-type folds at both contacts show downward movement on the northern side of the sill. The sediments between the S-folds along the sill contacts are undisturbed. In the eastern outcrops, south of the north face, the deformation varies from tight to open S-folds (Figures 4.4 and 4.16) over a distance of about 30 to 40 m which has resulted in the creation of voids. These voids have been filled subsequently by small granitic bodies, each estimated to have volumes not exceeding 3 m^3 . Granosediments, sedimentary enclaves and granitic layers similar to those in the 1285 southeast contact zone are found within the sediments affected by this folding. Some of the granitic bodies along the north face of 1285 transgress sediments in which abundant granitic veins are present. Small (1 to 3 mm), disseminated concentrations of orange-red to brick-red quartz-feldspar bodies occur in many feldspar-rich arenite beds. They are concentrated locally below argillaceous bands, and may either form a granitic vein parallel to and at the base of the argillaceous layer (Figure 4.17) or break through the argillite and intrude overlying arenites as veins 2 to 5 mm thick. The veins locally exploit bedding planes, as well as small-scale intraformational faults with 1 to 15 cm displacements of the sedimentary laminations and beds, i.e. without affecting

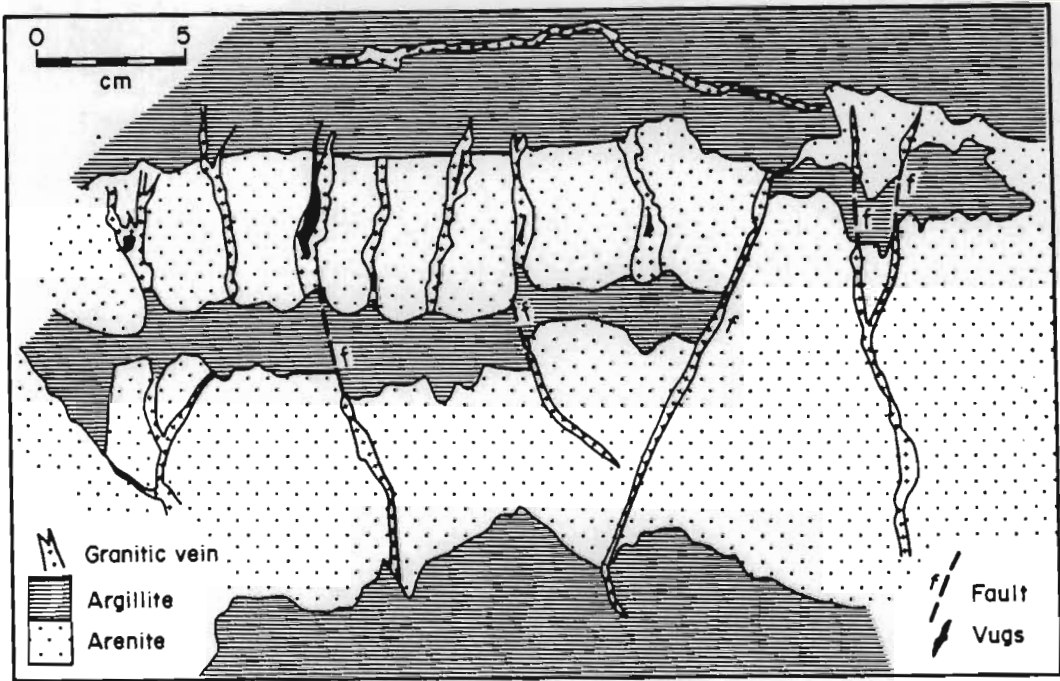


Figure 4.17 Relationships among granitic veinlets, argillites and arenites, 1285 north face.



Figure 4.18 Grunehogna granite (reddish brown) intruding Kullen sill (centre left) and Schumacherfjellet Formation. Person to right and below centre of photograph is 2.0 m tall.

overlying or underlying beds. However, the veins are found rarely within faults where argillaceous beds are transected. In many cases they are present in the continuations of the faults in arenites on both sides of argillaceous layers (Figure 4.17). Granosediment is also present in a 3 m-thick contact zone along the apophysis intruding Högfonna sediments along the north face of nunatak 1285.

Contact zones of the sediments with the Kullen sill vary in character. No discernible thermal effects were recognized in the field where the sill is in contact with overlying Schumacherfjellet sediments southeast of peak 1390. In the southern part of Caughtout Ridge (Figure 4.1), a "granodiorite" body was mapped by Aucamp (1972) and Bredell (1976). Most of the outcrop consists of a granodioritic to quartz diorite pegmatite, with smaller volumes of granosediment and quartz arenite. The contact of the pegmatite with the underlying Kullen sill is gradational over two to three metres. A 4 m-thick contact zone is present along the upper, conformable contact of the Kullen sill with Högfonna sediments at peak 1555. This zone is similar in appearance to the contact zone between the Grunehogna sill and Högfonna sediments at 1285. It contains granosediments, sedimentary enclaves and small vugs in similar proportions to those in the contact zone of the Grunehogna sill.

Small granite intrusions, other than those described above, and in all cases within 10 to 15 m of either the Grunehogna or the Kullen sills, have been reported by Aucamp (1972) and Bredell (1976). Both these authors describe a 300 m-wide 'granodiorite' intrusion approximately 600 m east of peak 1390. This geometry was based on the presence of small, irregular sill-like intrusions in the northern face of the 1390 outcrop and two granitic outcrops 800 m southeast of peak 1390. A scree slope along the northeastern flank of 1390 is covered in granitic debris, giving the impression of a large

intrusion, but no outcrops of granitic material occur there. The field relationships suggest small separate, granitic (not granodioritic) bodies spatially associated with the Grunehogna and Kullen sills. The granite southeast of Grunehogna intrudes both the Kullen sill and sediments of the Schumacherfjellet Formation (Figure 4.18), and is named the Grunehogna granite. This granite locally exploits bedding planes, resulting in downwarping of the sediments as shown in Figure 4.18. Both sill-like and dyke-like contacts with the sediments are found at this locality. The Grunehogna granite is a medium-grained orange-red rock which varies in hand specimen from a mineralogically homogeneous quartz-albite-K-feldspar rock with evenly disseminated chlorite and epidote to a granophyric granite containing about 30 to 40 volume per cent granophyric quartz-alkali feldspar intergrowths in spheres about 5 mm diameter, trace amounts of chlorite, and minor amounts of epidote.

Sedimentary xenoliths occur sparsely in the Grunehogna and Kullen sills. They are up to 15 m in diameter, and typically have rims of granitic composition around their margins. Some xenoliths show little evidence of deformation, but locally others are highly contorted, suggestive of deformation in an unconsolidated or partially consolidated medium (Figure 4.19). A large xenolith (?) was found 750 m northwest of peak 1390, at the contact between the Grunehogna pegmatite and the overlying Kullen sill. The chill zone of the Kullen sill is locally fragmented and mixed with brecciated sediment. This mixed breccia zone, which is 20 to 50 cm thick, is intruded by a later phase of the Kullen sill. The interpretation of these relationships is that an early-formed chill zone of the Kullen sill was brecciated prior to solidification of the main body of magma, apophyses of which intruded the breccia. The contact of the xenolith with the underlying pegmatite is obscured by snow.



Figure 4.19 Contorted laminations in sedimentary xenolith from the Grunehogna sill, 1285 southeast windscoop.

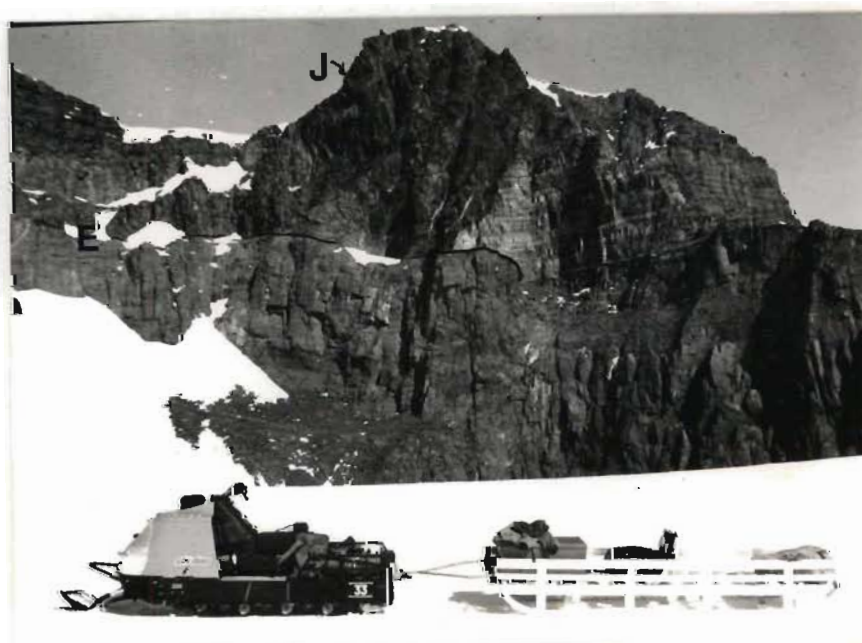


Figure 4.20 Dyke (arrow J) transgressed by Kullen sill along plane E \pm 300 m east-northeast of peak 1390. The dyke-sediment contacts are approximately vertical, but the oblique angle from which the dyke is viewed (looking towards west-southwest at north-south trending dyke) results in apparently irregular contacts.

D. Dykes

Dykes in the Grunehogna area have been described by Aucamp (1972), Bredell (1976) and Wolmarans and Kent (1982). Aucamp describes dolerite dykes and dolerite sheets, and quartz diorite, pyroxenite and olivine dolerite dykes, in addition to aphanitic mafic intrusive rocks spatially associated with faults. Although the dykes in the Grunehogna area do not form an integral part of this study, age relationships of two of the dykes at these localities were re-examined at nunatak 1285 and peak 1390. Aucamp described two dolerite dykes which he interpreted as being older than the Grunehogna and Kullen sills. The first dyke investigated is poorly exposed in a gully east of peak 1285 (Figure 4.1) and strikes WSW to ENE. Aucamp (1972) reported that no outcrops of this dyke were found in the sill, and concluded that it is the older intrusion. However, the area where the dyke is likely to transgress the sill is covered by scree and snow, and it is believed that the evidence is far too tenuous to deduce the relative ages of the dyke and the Grunehogna sill. The second dolerite dyke which occurs about 300 m east-northeast of peak 1390 (Figure 4.1) is approximately 15 m wide and strikes SSE to NNW. This dyke is cross-cut by the Kullen sill (Figure 4.20) and is therefore the oldest intrusion in the area.

III Petrography

A. Diorite Sills and Mafic Pegmatites

Modal data of representative samples from the Grunehogna and Kullen sills are given in Table 4.3, which indicates the approximate elevations at which the samples were collected. These elevations can be regarded only as relative indications of sample positions, because they were determined by altimeter, which could not be calibrated with a base camp monitor. Microclimate fluctuations are notorious in Antarctica (King, 1969; Dalrymple and Frostman, 1971), leading to possible large errors in elevations determined by this method.

The Grunehogna Sill.

The Grunehogna sill is a medium-grained diorite with a granular to locally intergranular texture, comprising plagioclase, clinopyroxene, hornblende, Fe-Ti oxides, K-feldspar and quartz (Figure 4.21). The top of the sill is a medium-grained granophyric quartz diorite, composed of sericitized and saussuritized plagioclase and hornblende laths, which are set in a fine-grained matrix of micrographic quartz intergrown with plagioclase, K-feldspar, aggregates of hornblende, chlorite, biotite, apatite and Fe-Ti oxides. The plagioclase laths show an increase in grain size from the lowest exposed outcrop upwards in the 1390 north face (Table 4.3). In the lower part of the sill all plagioclase grains show some degree of sericitization and saussuritization, which varies from sparse development along cracks to extensive alteration throughout grains. Higher in the sill alteration of plagioclase is pervasive, but sample G14/82, from about 5 m below the contact with the mafic pegmatite, contains some unaltered plagioclase. In the lower and upper samples the plagioclase shows normal zoning, with the composition

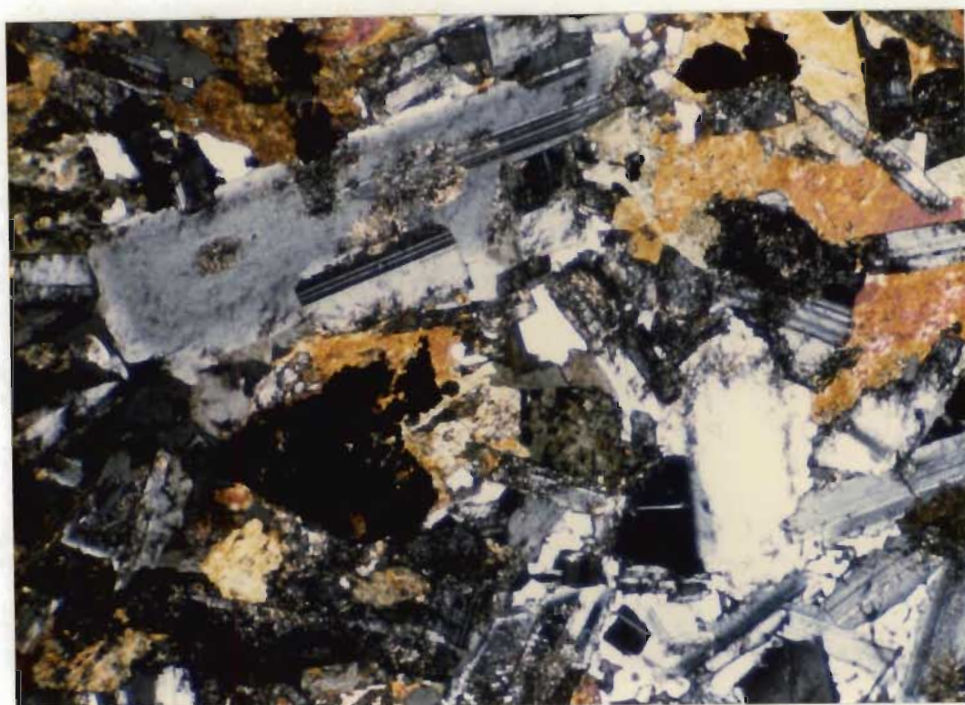


Figure 4.21 Photomicrograph of general texture of lowermost exposed Grunehogna sill, 1390 north face. Crossed polars. Minerals with high birefringence are uralitized pyroxenes, opaque minerals are Fe-Ti oxides.

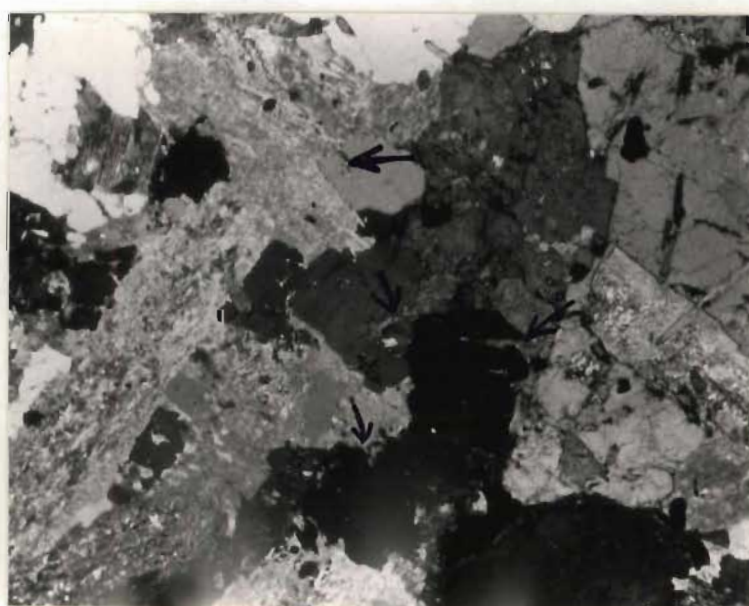


Figure 4.22 Photomicrograph of quartz grains (in extinction) in upper Grunehogna sill, showing vein-like embayments (arrowed) filled with plagioclase, K-feldspar and hornblende. Crossed polars.

ranging from about An_{45} in the cores to An_{35} in the outer rims. A narrow (20 micron) albitic mantle is present around many plagioclase grains. Rare antiperthite occurs in the lowest part of the sill.

Clinopyroxene (augite) is present only in sample A9/82 at the lowest exposed outcrop of the Grunehogna sill. The habit of the mineral varies from small, anhedral grains interstitial to plagioclase, to aggregates of approximately 1 mm, in which individual grains cannot be distinguished owing to extensive uralitization and sporadic alteration to chlorite. Individual grains exhibit a checkerboard appearance as a result of uralitization. Higher in the sill the mineral has been altered to hornblende grains lacking the checkerboard texture, and clinopyroxene remnants are rarely present. Small, interstitial euhedral hornblende grains occur locally, which may represent primary crystallization products from the magma, rather than alteration products from clinopyroxene. K-feldspar and quartz are sparsely present as interstitial, anhedral grains and as micrographic intergrowths in the lower part of the Grunehogna sill, but the modal content of quartz increases upwards in the sill (Table 4.3). The K-feldspar is microperthitic and has a reddish-brown cloudy appearance in thin section owing to the presence of finely disseminated exsolved haematite. Quartz intergrowths with both K-feldspar and plagioclase are locally strained, with development of Boehm lamellae. Fluid inclusions are numerous in the quartz grains. In the upper part of the sill the granophyric quartz exhibits vein-like embayments filled with plagioclase, K-feldspar or, rarely, hornblende and epidote (Figure 4.22).

The Grunehogna sill has a high content of Fe-Ti oxides, which ranges from 2.0 to 6.4 per cent by volume (Table 4.3). The oxides are ilmenite and haematite, occurring in the ratio 3:2. Ilmenite varies from subhedral to anhedral and no exsolution phases are present. Locally grains are poikilitic, enclosing

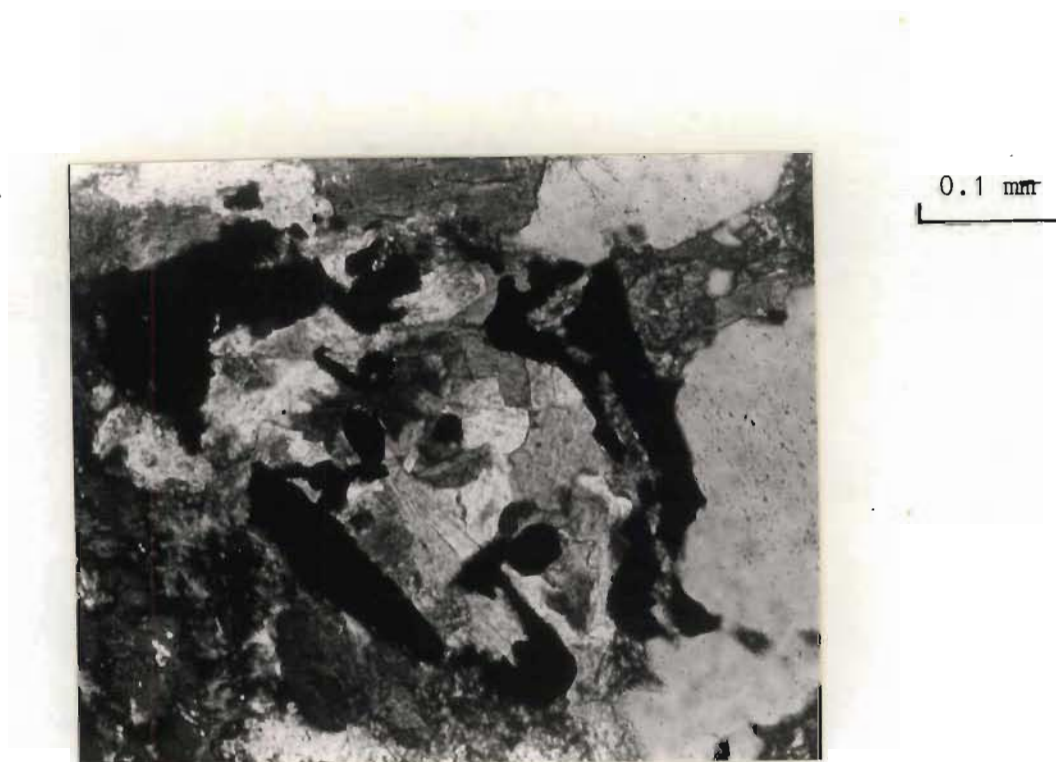


Figure 4.23 Photomicrograph of atoll microstructure of ilmenite in Grunehogna sill. Crossed polars. Opaque grains are ilmenite. The core of the structure consists mainly of chlorite.

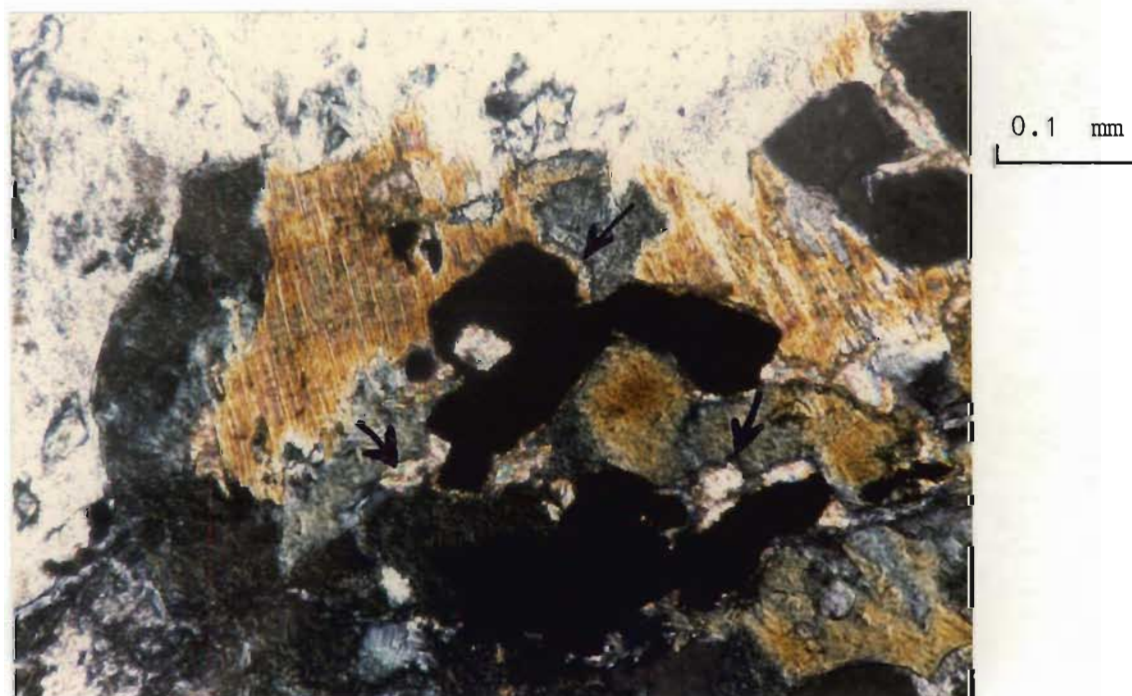


Figure 4.24 Photomicrograph of sphene (arrowed) along rim of ilmenite grains. Crossed polars. Biotite and uralitized pyroxene occur in association with the ilmenite.

amphibole, haematite or rarely quartz. In places the mineral forms symplectic intergrowths with quartz and/or amphibole, or atoll microstructures in which discrete grains of ilmenite define circular structures (Figure 4.23). Rod-like intergrowths of ilmenite with amphibole, plagioclase and, rarely, biotite occur in places, and, in the upper part of the sill, sphene is present along the rims of most oxide grains (Figure 4.24). Discrete, anhedral haematite grains are usually associated with ilmenite. A trellis pattern is defined by lamellae (<1 micron thick), which are probably composed of ilmenite. The presence of such trellis patterns have been interpreted as an indication that the haematite is a secondary product after magnetite-ulvöspinel solid solution (Haggerty, 1976a; Reynolds and Goldhaber, 1978; Ramdohr, 1980; Reynolds, 1983).

Biotite is sparsely present in association with Fe-Ti oxides, or intergrown with chlorite and, rarely, with hornblende. Alteration to muscovite along cleavage planes occurs rarely. In the upper part of the sill the biotite content increases, and the mineral is locally altered to epidote, which also occurs along cleavage planes (Figure 4.25). Epidote, apatite and, rarely, zircon are accessory minerals, but in the upper part of the sill the former two minerals are important minor constituents, which are intergrown with amphibole, or found in contact with quartz. Radiating tremolite/actinolite needles are sparsely present throughout the sill, and trace amounts of chalcopyrite-sphalerite intergrowths are associated with quartz and the Fe-Ti oxides.

The overlying Grunehogna pegmatite is a coarse-grained quartz diorite in which occur granophyric intergrowths of quartz with oligoclase or with microperthitic K-feldspar set in a coarse-grained matrix of oligoclase and hornblende. Skeletal Fe-Ti oxides are closely associated and intergrown with

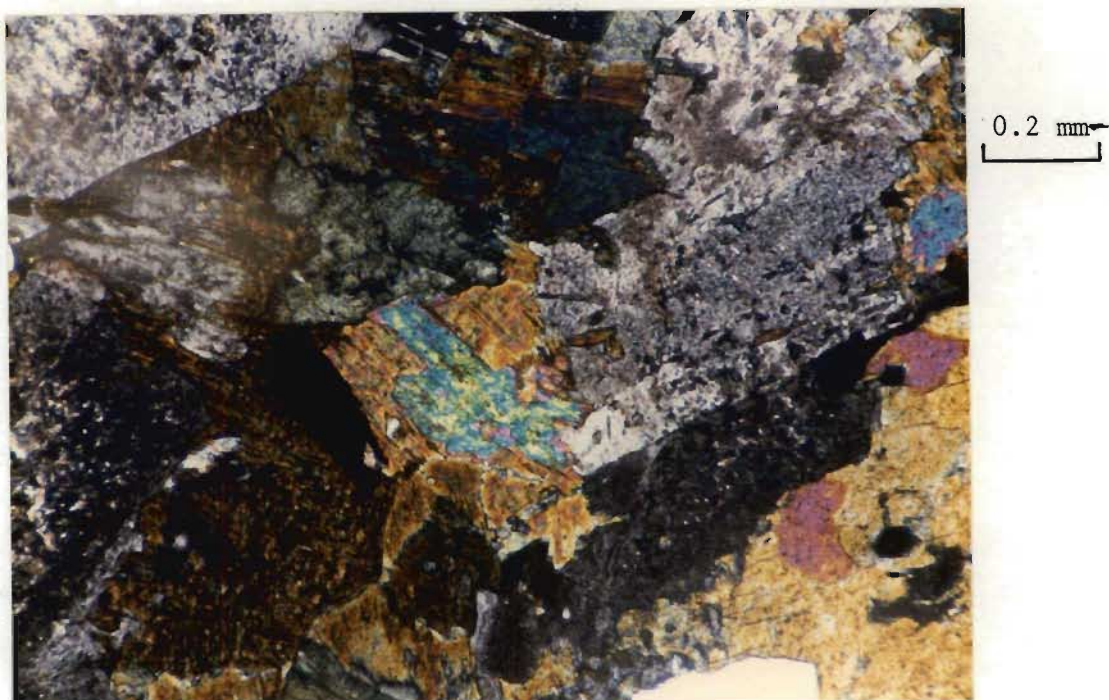


Figure 4.25 Photomicrograph of biotite altered to epidote (highly birefringent mineral at centre) in Grunehogna sill. Crossed polars.

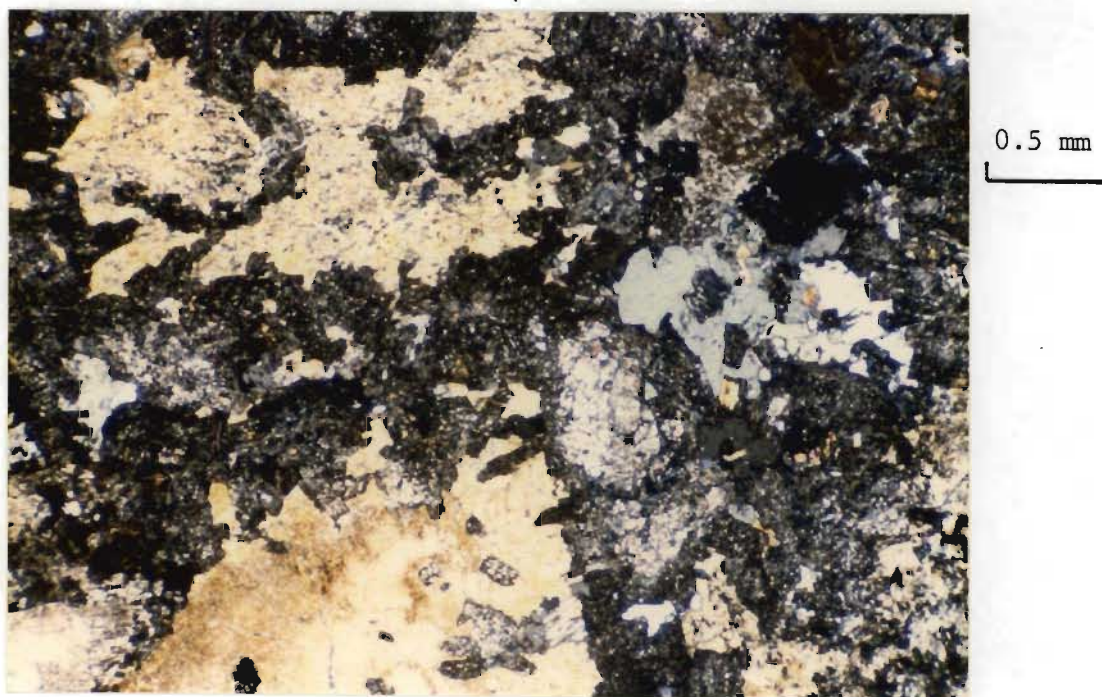


Figure 4.26 Photomicrograph of general texture of altered Kullen sill. Crossed polars. The mineralogy is quartz (white grains), sericitized plagioclase and uralitized pyroxene.

hornblende laths. These oxides have rims of sphene in many cases. Sphene, other than in the rims, chlorite, and tremolite/actinolite are abundant locally. Epidote and apatite are minor constituents, although the concentration of the former mineral varies greatly throughout the sill. Zircon is present in accessory amounts.

The Kullen sill.

The Kullen sill shows considerable textural and modal variation (Table 4.3), ranging from rocks with cumulus textures to those highly altered by deuteric or hydrothermal fluids in which cumulus textures cannot be recognized. A sample from the southernmost windscoop of Grunehogna, taken two metres above the lower contact of the Kullen sill, shows petrographic features similar to the Juletoppane gabbros (Chapter 2). The rock is a medium- to fine-grained gabbro-norite containing primocryst (?) phenocrysts of inverted pigeonite mantled by orthopyroxene, set in a matrix of normally zoned plagioclase ($An_{7.0}$ to $An_{6.0}$), augite and minor amounts of biotite, Fe-Ti oxides and micrographic intergrowths of quartz and alkali feldspar. Clinopyroxene-rich norites are present at and near the base of the Kullen sill at Preikestolen (Snow, 1986). These norites are petrographically very similar to the norites described from Viper's Hill at Annandagstoppane (Chapter 2).

In the main body of the sill at the 1390 north face, excluding the lower and upper chill zones, sericitization and saussuritization of plagioclase has proceeded to the extent that it is difficult to distinguish original grain boundaries. The pyroxenes have been altered and uralitized extensively to amphibole and chlorite (Figure 4.26). Epidote is an important minor constituent, occurring as disseminated grains and in saussuritized plagioclase. In the Kullen 1555 section, however, primary igneous textures

can be distinguished, although the sill shows sporadic alteration to the same extent as in the 1390 outcrop. In the lower part of the sill at Kullen (sample G64/82, Table 4.3), the composition is dioritic, with fine- to medium-grained granular and interstitial textures (as defined by MacKenzie *et al.*, 1982). Locally the rocks are porphyritic, with phenocrysts of partially uralitized augite laths (up to 0.4 by 5 mm). Sample G63/82 from higher in the sill than G64/82 (Table 4.3) shows an increase in the amount of uralitized augite phenocrysts. Plagioclase appears both as phenocrysts and as fine-grained granophyric intergrowths with quartz. The clinopyroxene phenocryst laths in sample G59/82 are up to 1 by 7 mm in size and have been altered extensively to hornblende. There is a considerable increase in the grain size of plagioclase in this rock compared to the rest of the section (Table 4.3). Near the top of the intrusion, below the upper chill zone, the sill is a porphyritic, granophyric quartz diorite with an ophitic texture in which augite phenocrysts contain numerous inclusions of plagioclase. Throughout the Kullen sill plagioclase shows partial to extensive sericitization and saussuritization. Compositions, which have been determined optically, vary from about An_{70} in the cores to An_{35} on the rims, with well-defined normal zoning, although reversed zoning is present sporadically in some grains. Altered pyroxene phenocrysts in the granophyric quartz diorite have a core of chlorite and/or serpentine, with a mantle of augite (Figure 4.27).

Fe-Ti oxides occur throughout the Kullen sill as poikilitic to skeletal grains, which are composed of mosaic intergrowths of ilmenite, haematite and rutile or pseudobrookite. These textures indicate strong oxidation of ilmenite (Haggerty, 1976a). Alteration of ilmenite to biotite and sphene is also common. Apatite and epidote are commonly present in the Kullen sill as

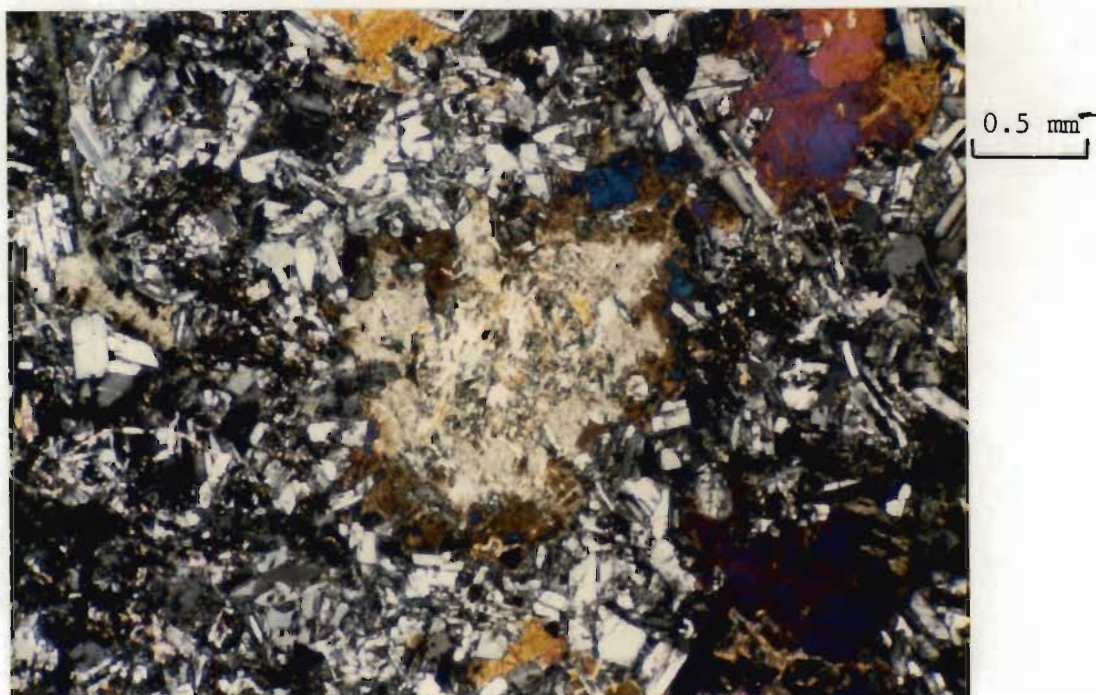


Figure 4.27 Photomicrograph of zoning in uralitized pyroxene, Kullen sill. Crossed polars.

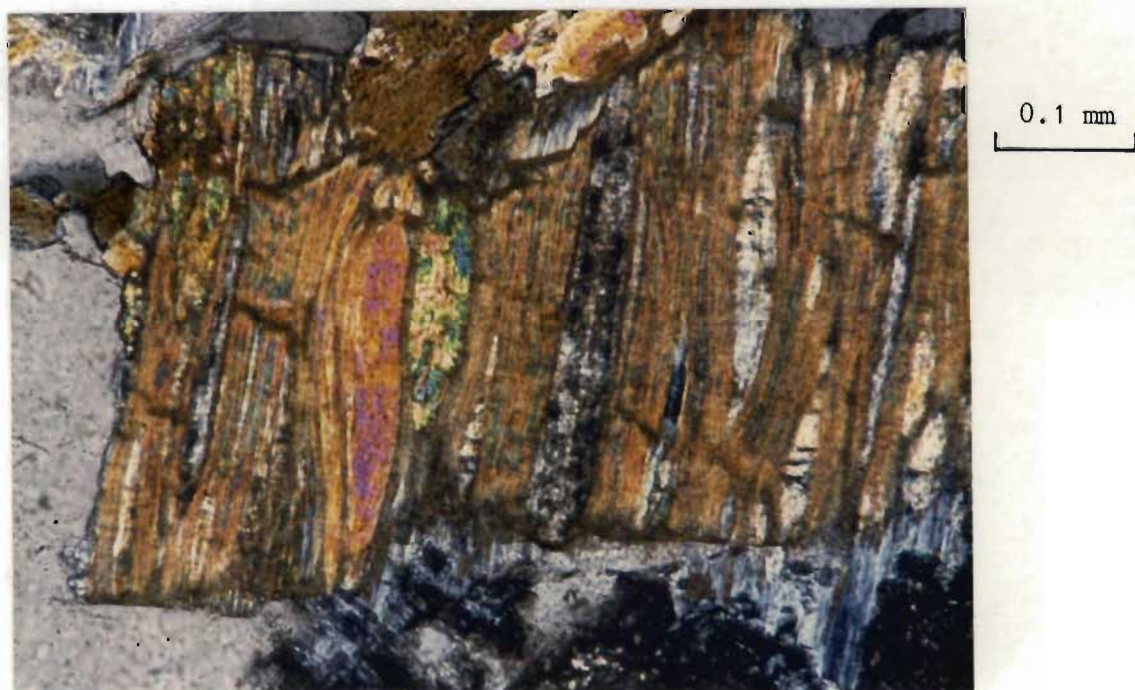


Figure 4.28 Photomicrograph of biotite alteration to epidote, zoisite/clinozoisite and chlorite, basal chill zone, Kullen sill. Crossed polars.

accessory minerals, but may occur locally as minor constituents. Chlorite occurs interstitially to plagioclase and pyroxene, and as alteration products of the pyroxenes and amphibole.

Kullen sill chill zones

The basal chill zone of the Kullen sill is a fine- to medium-grained, granophyric, granular diorite comprising anhedral hornblende (0.5 mm in diameter) and stubby sericitized and saussuritized plagioclase laths. Although the mineralogy is similar to the rest of the sill, in this zone there are small lenticular veins, 0.3 mm wide and 2 to 8 mm apart, aligned parallel to the basal contact. The composition of these veins is variable, being composed of (i) fine-grained quartz with zoisite needles, (ii) quartz, (iii) chlorite, or (iv) granophyric intergrowths of quartz and plagioclase. The zoisite needles form cones, with the apices of the cones situated on the walls of the veins. Biotite in the basal chill zone has been altered to epidote and zoisite, which occur along the cleavage planes, and chlorite, which forms mantles or irregular patches around the margins of the mineral. The epidote and zoisite occur either as discrete wedge-shaped laths, or with epidote in the centre, the laths surrounded by zoisite (Figure 4.28). The biotite cleavage is curved around the laths. It has not been established whether the alteration of biotite represents deuteric/hydrothermal action or a later metamorphic event.

Textures in the upper chill zones of the Kullen sill and its apophyses vary considerably. The chill zone in the 1390 section is a fine-grained porphyritic rock of basaltic to basaltic andesitic in composition. The matrix is granular. Plagioclase (0.6 by 1 mm) and amphibole (0.6 by 3 mm) microphenocrysts show considerable sericitization and saussuritization, but

are clearly recognizable. Alteration of plagioclase grains in the matrix is identical to that in the main body of the sill at peak 1390. Many quartz grains show extensive corrosion within the chill zones and, locally, in the main body of the sill (Figure 4.29a). Spherical to irregular patches of granophyric intergrowths are associated with strained quartz grains, which have been corroded by mixtures of very fine-grained chlorite, epidote, K-feldspar (?) and secondary (?) quartz. In many cases the strained quartz grains are present along the rims of the granophyric patches and appear to grade into the quartz in the granophyric intergrowths (Figures 4.29b and c). Elsewhere in the sill and in the apophyses, the chill zones are less altered, and in places biotite is present as a major constituent (approximately 10 per cent by volume). Fine-grained intergranular to porphyritic textures are also recognized in the upper chill zones. Radiating plagioclase laths are present in the intergranular matrix (Figure 4.30). This texture is particularly well-developed in an apophysis above the 1390 north face, which also shows a highly irregular distribution of Fe-Ti oxide patches (2 to 5 mm in diameter). Plagioclase is more extensively altered where it occurs with these patches than elsewhere in the same thin section (Figure 4.31).

B. The Grunehogna Granite and Granitic Bodies within Contact Zones

The granites occurring southeast of Grunehogna Peak 1390 are medium- to fine-grained rocks, which comprise the following textural types:

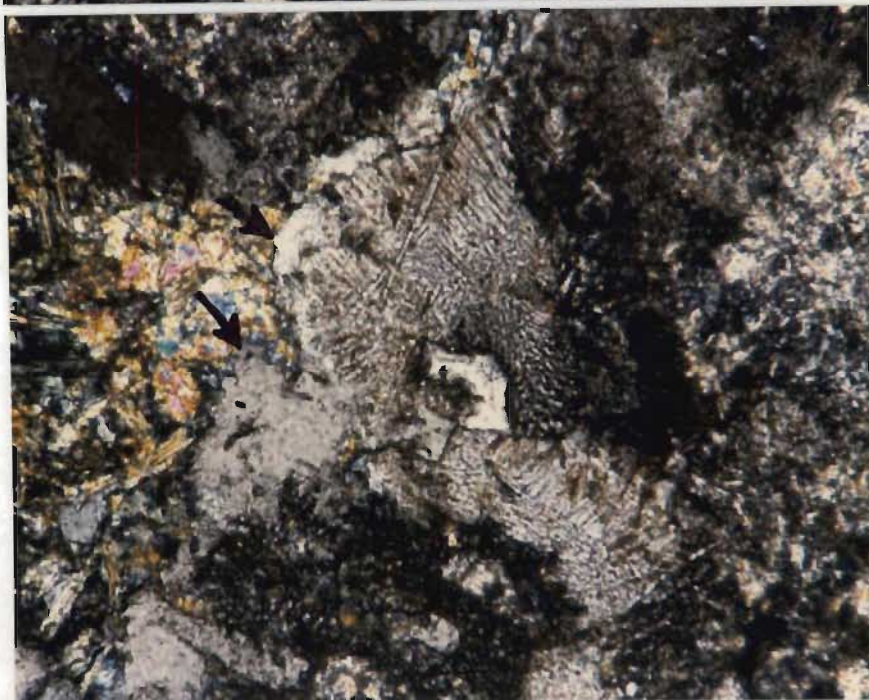
- (i) Granular granites (Figure 4.32);
- (ii) Granular granites, with minor, incipient development of granophyric textures (Figure 4.33);

(a)



0.1 mm

(b)



0.1 mm

(c)



0.1 mm

Figure 4.29(a) Photomicrograph of corroded quartz grain in Kullen sill. (4.29b and c). Strained quartz grains (arrowed) grading into granophyric intergrowths, upper chill zone, Kullen sill. Crossed polars.



0.5 mm

Figure 4.30 Photomicrograph of intergranular texture with radiating plagioclase laths in chill zone, Kullen sill. Crossed polars.



2 mm

Figure 4.31 Photomicrograph showing irregular distribution of Fe-Ti oxides in Kullen sill apophysis. Plane polarized light. The highest concentration is associated with a higher degree of secondary alteration of pyroxenes and plagioclase in the left half of the photograph.

- (iii) Granophyric granites, with local development of intergrowths of quartz and alkali feldspars;
- (iv) Granophyre (Figure 4.34).

The major minerals in types (i), (ii) and (iii) are anhedral quartz, microcline microperthite and subhedral albite laths, the latter mineral being affected by minor saussuritization. Quartz grains are strongly strained in places and embayed by albite in many cases. Microcline microperthite invariably contains a fine dusting of exsolved haematite, which imparts a reddish cast to the feldspar. Microcline is present rarely as euhedral grains, but more commonly as anhedral grains intergrown with quartz. Grains of sphene, up to 1.4 mm in length, are present sporadically in small concentrations (Figure 4.32). Chlorite and apatite are present in minor and trace amounts, and epidote is invariably present in association with chlorite, Fe-Ti oxides and albite. The Fe-Ti oxides form euhedral to skeletal grains, with the skeletal type displaying triangular trellis patterns. The oxides are found in association with chlorite, or, rarely, actinolite. There is a considerable variation in the grain size of the oxides within a single thin section and there is a suggestion of grain-size layering. The distribution of Fe-Ti grain sizes was determined for one sample. The resulting contour diagram further supports evidence of fine-scale layering (Figure 4.35).

Type (iv), the granophyre, consists of spherical intergrowths of alkali feldspar and quartz set in a granular matrix of quartz, microcline microperthite, albite, and accessory minerals (Figure 4.34). The intergrowths are 5 to 7 mm in diameter, and their centres are 10 to 12 mm apart. Quartz and albite constitute the cores, with quartz-K-feldspar intergrowths forming mantles. Quartz habit varies from cuneiform to



Figure 4.32 Photomicrograph showing general texture of Grunehogna granite. Light-grey to white mineral is quartz; K: K-feldspar; P: albite; SP: Sphene. Crossed polars.



Figure 4.33 Photomicrograph of local development of incipient granophyric texture in Grunehogna granite. Crossed polars.



Figure 4.34 Photomicrograph of granophyric texture in Grunehogna granophyre. White mineral: quartz; light-grey: albite; dark-grey in mantle: K-feldspar. Crossed polars.

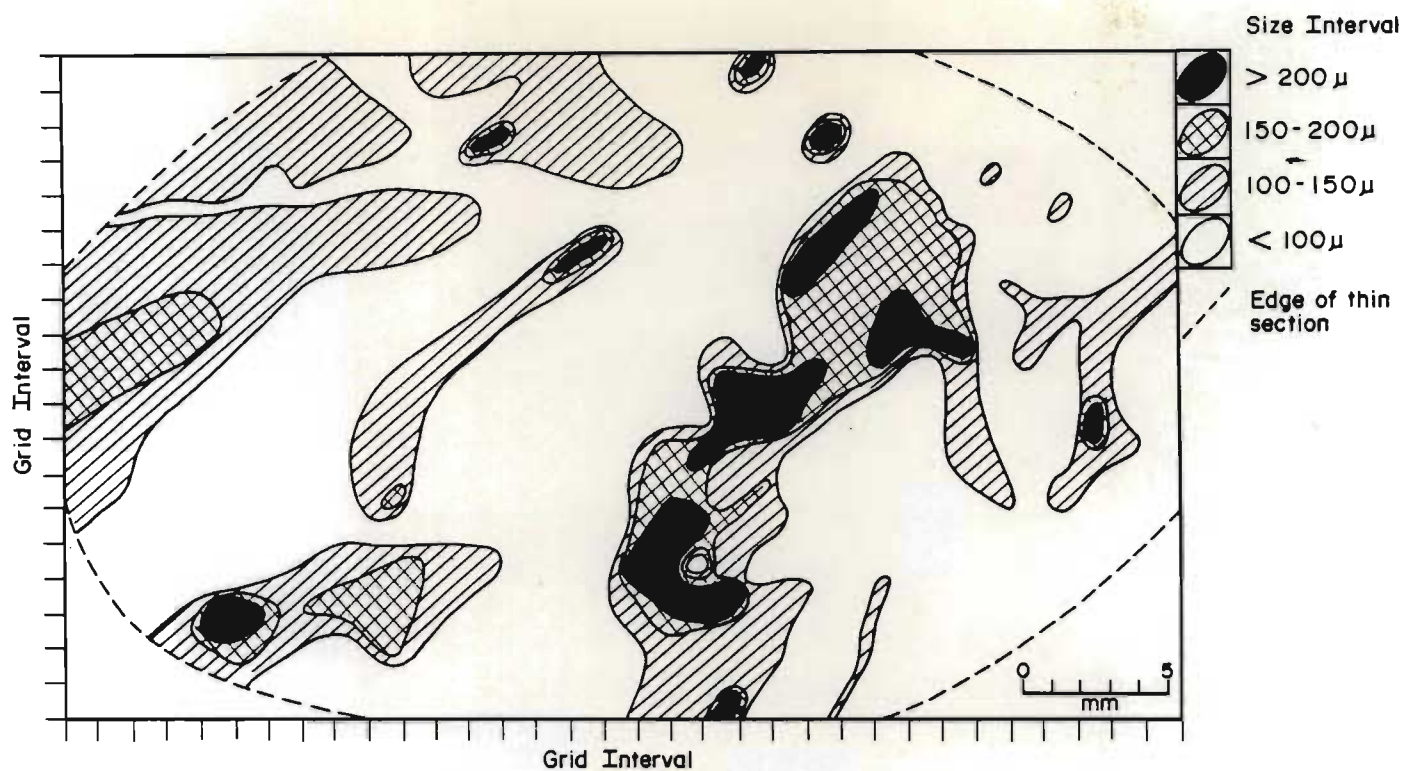


Figure 4.35 Contour diagram of variation in opaque mineral grain sizes in thin section of Grunehogna granite. An apparent trend from the bottom left to top right hand of the diagram suggests a crude layering or lamination defined by the opaque minerals (mainly Fe-Ti oxides).



Figure 4.36 Photomicrograph of granophyric texture in granosediment: quartz intergrown with albite and K-feldspar.

vermicular, arranged parallel in the core, but radial in the mantle of the intergrowths. Quartz increases in apparent grain size from less than 0.1 mm for individual "grains" in the cores to 0.5 mm in the mantles, although fine-grained intergrowths are present locally in the outer rims. Minor amounts of chlorite and Fe-Ti oxides are present in this rock, with only trace amounts of zircon, epidote, clinozoisite or zoisite, allanite and sphene. Chlorite in the matrix is interstitial to quartz and the feldspars, occurring as radiating, fan-shaped clusters. Epidote, clinozoisite or zoisite and rare allanite form aggregates which are irregularly distributed throughout the rock.

Microstructures in the small granitic bodies present in contact zones are identical to those in the Grunehogna granite, including mineralogy, grain size and variation from granular to granophyric types.

C. Contact Zone Granosediments and Xenoliths.

The sedimentary contact zones and xenoliths adjacent to and included in the Grunehogna and part of the Kullen sills show petrographic features which distinguish them from the regionally metamorphosed sedimentary rocks. Salient features of the metamorphic textures and grade of the Högfonna arenites and graywackes in the 1285 southeast outcrop will be described in order to compare them with the contact zone granosediments. Detailed petrographic descriptions have been given by Ferreira (1986a).

At 150 m above the upper contact of the Grunehogna sill the metamorphic assemblage is muscovite-chlorite-carbonate-(stilpnomelane ?)-(piemontite ?) which indicates very low-grade metamorphism (Winkler, 1976). The stilpnomelane was identified optically, but its occurrence has not been

confirmed. The mineral is rare, and was not found below 150 m. Albite is present in detrital grains which show extensive saussuritization with development of large amounts of piemontite. This reaction is interpreted as retrograde development of albite from plagioclase with higher anorthite contents. Quartz grains in contact with one another form poorly-defined triple junctions, although recrystallization and development of overgrowths are evident. At the 110 m level sphene occurs as an alteration product of Fe-Ti oxides and large (100 by 200 micron) flakes of muscovite have developed. Sphene increases in amount downwards in the succession. Triple junctions in quartz are better defined than in the overlying rocks, but do not approach 120° equilibration junctions (Spry, 1969). Very fine-grained, irregular silica veinlets with apparently random orientations transgress all the sediments below 110 m. Some of these veinlets appear to transgress quartz grains, suggesting solution of the original quartz grains by hydrothermal fluids. Detrital K-feldspar grains are present from 90 m down in the succession to approximately 20 m above the contact with the sill. Albite occurs as a secondary mineral in detrital, saussuritized grains in this section. The paragenesis carbonate-chlorite-haematite-albite-epidote-sphene occurs below 20 m, and is considered to represent high-temperature, low pressure metamorphism (Einsele, 1985). The haematite grains are evenly distributed in the rocks, and are anhedral to subhedral in shape with no trellis patterns. Trace amounts of ilmenite are intergrown with the haematite, but no other evidence for exsolution is present. The presence of haematite rather than pyrite, suggests an oxidizing environment.

Textures identified in the contact zones and xenoliths are defined below; and examples given in Figures 4.36 to 4.42.

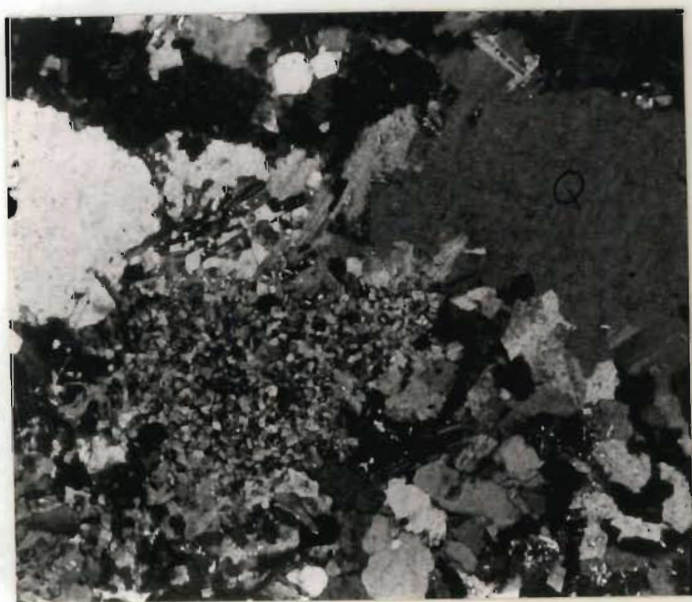
(i) Granophyric texture (Figure 4.36) comprises intergrowths of quartz, K-feldspar and albite. Various forms have been identified, as defined by Barker



Figure 4.37 Photomicrograph of pseudogranophyric texture in granosediment. Crossed polars.

.2 mm

.1 mm



(a)



(b)

Figure 4.38(a) Partially embayed quartz (PEQ texture) in granosediment, showing development of micro-aplite.
 (b) Detail of Figure 4.38(a). Q: quartz. Crossed polars.

(1970). Quartz habit varies from cuneiform to vermicular, and may be arranged in parallel, plumose or radiating forms. The mineral shows a uniform optical orientation over parts of the intergrowths, but albite and K-feldspar are present in discrete phases, which may be arranged in zones. Barker (1970) states that albite is commonly untwinned in the intergrowths he describes, but in the rocks described here, well-defined albite twinning is common. K-feldspar invariably contains a fine dusting of very fine-grained haematite, and, locally, microperthite can be identified.

(ii) Pseudogranophyric texture (Figure 4.37) consists of quartz grains forming skeletal or "exploded bomb" textures in which separate, angular grains are in optical continuity, with intervening material comprising albite and K-feldspar.

(iii) Embayment or corrosion textures in quartz: many quartz grains are embayed by very fine-grained (less than 20 micron), irregularly-shaped patches of quartz, K-feldspar and albite with minor amounts of muscovite and locally traces of epidote, chlorite and Fe-Ti oxides. Rare granophyric intergrowths are present in these micro-aplites. Four different embayment textures have been recognized, viz:

- (a) PEQ texture: Partially embayed quartz grains are embayed along their margins only (Figure 4.38);
- (b) EEQ texture: Extensively embayed quartz (Figure 4.39).

This texture varies considerably: some quartz grains show deeply scalloped margins within which micro-aplite, or alkali feldspar is present. In other cases the micro-aplite and alkali feldspar form lobes or branched lobes within the quartz grains. Textures transitional from PEQ to granophyric may be present.



Figure 4.39 Photomicrograph showing extensively embayed quartz (EEQ texture) in granosediment. Crossed polars.

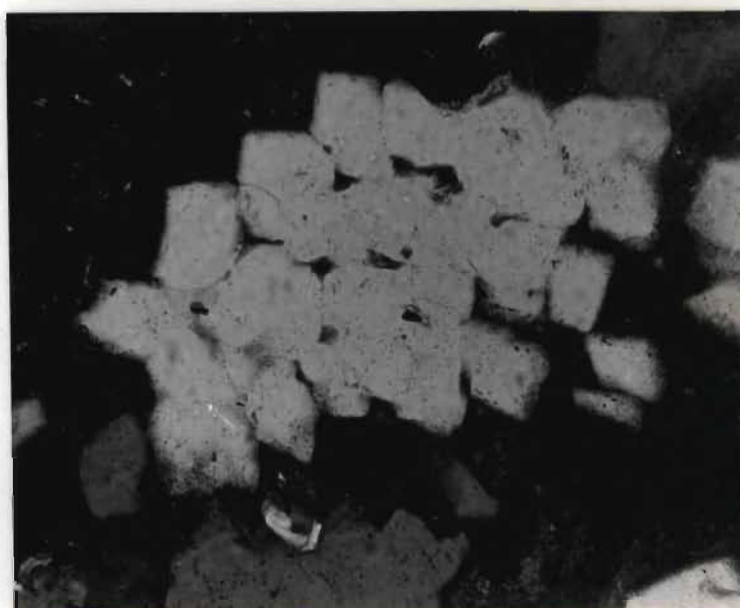


Figure 4.40 Photomicrograph showing amoeboid texture in quartz from granosediment. Crossed polars.

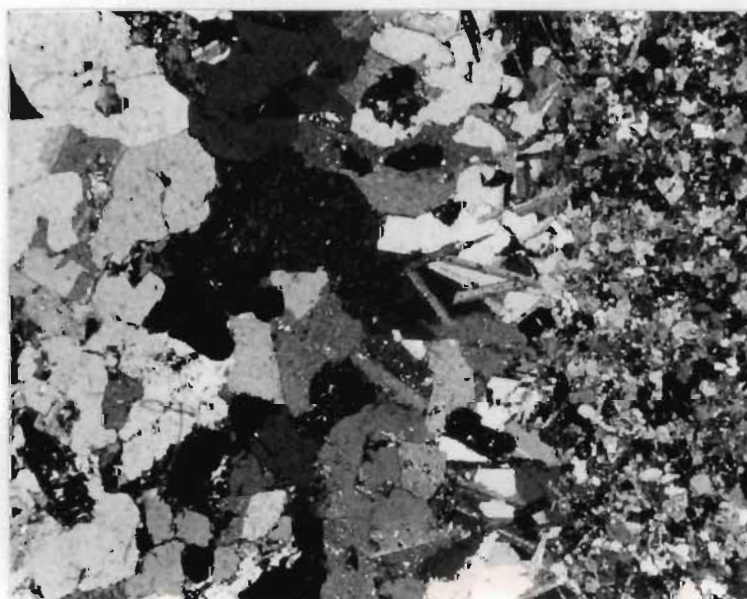


Figure 4.41 Photomicrograph showing sieve texture in quartz from xenolith in Grunehogna sill. Crossed polars.



2 mm

Figure 4.42 Photomicrograph of spherical aggregate of pseudogranophyric (SAPG) texture in granosediment (left half of photograph). Crossed polars.



1 mm

Figure 4.43 Photomicrograph of contact zone between small granitic body (left) and granosediment (right). Crossed polars.

- (c) Amoeboid texture has the appearance of separate quartz grains moulded together to form an "amoeboid" aggregate. The separate grains are in optical continuity (Figure 4.40).
- (d) Sieve texture contains patches within quartz grains filled by micro-aplite, muscovite or chlorite (Figure 4.41).

SAPG texture (spherical aggregates of pseudogranophyric texture) consists of spherical zones in which granophyric, pseudogranophyric and EEQ textures occur, with a matrix containing none or few of these features (Figure 4.42). The quartz in this matrix is usually recrystallized, with well-developed triple junctions at 120° . Amoeboid or partially embayed textures may be present locally.

The petrography of the sediments and granosediments up to 7 m above the sill contact in the 1285 SE contact is summarized in Table 4.4. The major identifiable difference between the metasediments and the contact zone is the appearance of abundant secondary K-feldspar in the granophyric intergrowths and as interstitial and large poikiloblastic grains. A fine dusting of exsolved haematite imparts a red colour to the contact zone. Concomitant with the increase of feldspar there is a decrease in muscovite, which is absent in the lower layers of the contact zone. In the upper part of the contact zone very fine needles of an unidentified mineral are present in the muscovite. The mineral may be fibrolite, but this has not been confirmed. The quantity and occurrence are very low and it is not possible to separate the material for X-ray diffraction identification.

PEQ textures are generally developed in the contact zone furthest away from the contact with the sill and granophyric textures and granitic bodies in the granosediments closest to the contact. However, granophyric granite has been

observed up to 2 m above the sill. Textural variation is clearly not a simple function of distance from the sill, although a broad relationship does exist. Layering in the sediments is defined by the alignment of rounded and subrounded Fe-Ti oxides, chlorite, trace amounts of sphene, rare pyrite cubes and epidote. These minerals also define a crude layering in the granosediments, although they tend to be more evenly distributed within these rocks than in the sediments. The petrography of the sedimentary enclaves in the granosediments varies in detail, but a core and mantle, or mantles, can commonly be recognized. Within the cores well-defined lamination is recognized by concentrations of rounded Fe-Ti oxide grains, sphene, chlorite and epidote. Quartz grains are recrystallized, with well-developed triple junctions at 120° and rare PEQ textures. The mafic minerals are more evenly distributed in the mantles, imparting a lighter colour in hand specimen, although crude layering can still be distinguished. PEQ textures become more common towards the margins of the enclaves, whereas the outer mantles show extensive EEQ and pseudogranophyric textures. Associated with the increase in EEQ texture is an increase in the amount of K-feldspar.

Features in granosediments other than in the 1285 SE contact zone are:

- (i) In some sedimentary layers the rocks show extensive recrystallization with local development of K-feldspar at the expense of muscovite, which encloses quartz and albite grains.
- (ii) Small veinlets with granular textures are abundantly developed in parts. They comprise quartz + K-feldspar + albite + muscovite + epidote + chlorite + sphene + allanite (rare).

(iii) Textures of the small granitic bodies are identical to those described in Section B. They have sharp contacts with the granosediments, although narrow (1,5 mm) contact zones may intervene between some of the granites and granosediments. In these zones a lamination 0,4 to 0,5 mm shows an increased development of embayment and pseudogranophryic textures compared to the rest of the granosediment. Adjacent to this lamination is a second one, about 1 mm thick, containing intergrowths of bladed albite and quartz which are orientated with their long axes perpendicular to the contact (Figure 4.43).

Xenoliths have similar textures to those described in the contact zones, but sieve textures are more abundant.

IV GEOCHEMISTRY

A total of 47 samples of the sills, granosediments and granites at Grunehogna were analyzed for major and trace elements. These include samples from the Grunehogna sill (6), Grunehogna pegmatite (3), Kullen sill and its chill phases (20), Grunehogna granites southeast of peak 1390 (5) and granosediments from nunatak 1285 (13). Major and trace element data are given in Appendix 2. Statistical data, including standard deviations and maximum, minimum and mean values of individual elements for the different groups of samples are given in Table 4.5. Statistical data for the Grunehogna pegmatites are not recorded, as only three whole rock analyses are available. Variable correlation ('reduced major axes', Tessier, 1948; Imbrie, 1956; Miller and Kahn, 1962) of selected element pairs were determined and are given in Tables 4.6, 4.7, 4.8 and 4.9.

A. General Geochemical Features

The Mg-number ($\text{Mg}/(\text{Mg} + \text{Fe}^{2+})$) will be used as a reference parameter for discussion of general geochemical features in the four main rock-types at Grunehogna, namely the Kullen and Grunehogna sills, Grunehogna granites, and granosediments from contact zones. The Mg-number is not petrogenetically significant when applied to sedimentary rocks, but is nevertheless useful for comparison of the various chemical groupings. Variation diagrams of all the major and trace elements analyzed are depicted in Figures 4.44 and 4.45, and variable correlation data of selected element pairs are given in Tables 4.6, 4.7, 4.8 and 4.9. Note that elements for which three or less determinations are available are excluded from the variable correlation tables.

The tholeiitic rocks comprising the Grunehogna and Kullen sills are quartz and hypersthene-normative. Table 4.5 shows a number of parameters which can be used to distinguish the two sills. Al_2O_3 , MgO, Ni and Cr are enriched and Mg-number values are higher in the Kullen relative to the Grunehogna sill. FeO, MnO, Na_2O , TiO_2 , Nb, Zr and Cu are enriched in the Grunehogna sill. The Grunehogna granites have low Mg-numbers and moderate to high SiO_2 values.

The normative An-Ab-Or diagram of O'Connor (1965), as adapted by Barker (1979), shows that the Grunehogna granites vary from granodiorite to granite in composition (Figure 4.46). Two samples of granosediment from the large xenoliths west of Grunehogna 1390 (Figure 4.1), which have typical granitic and granophyric petrographic textures, plot respectively in the trondhjemite and granite fields in Figure 4.46. Three samples of "granite" in granosediments from the 1285 contact zone show a more limited range in composition in the granite field, although one sample straddles the boundary between the granite and trondhjemite fields. Granosediments, which show

- + Grunehogna granite
- + Granosediments with granitic textures
- ⊕ Possibly contaminated Kullen sill
- Kullen sill
- ◊ Upper chill zones and apophyses, Kullen sill
- Grunehogna pegmatite
- Grunehogna sill
- △ Högfonna and Schumacherfjellet sediments and granosediments with sedimentary textures

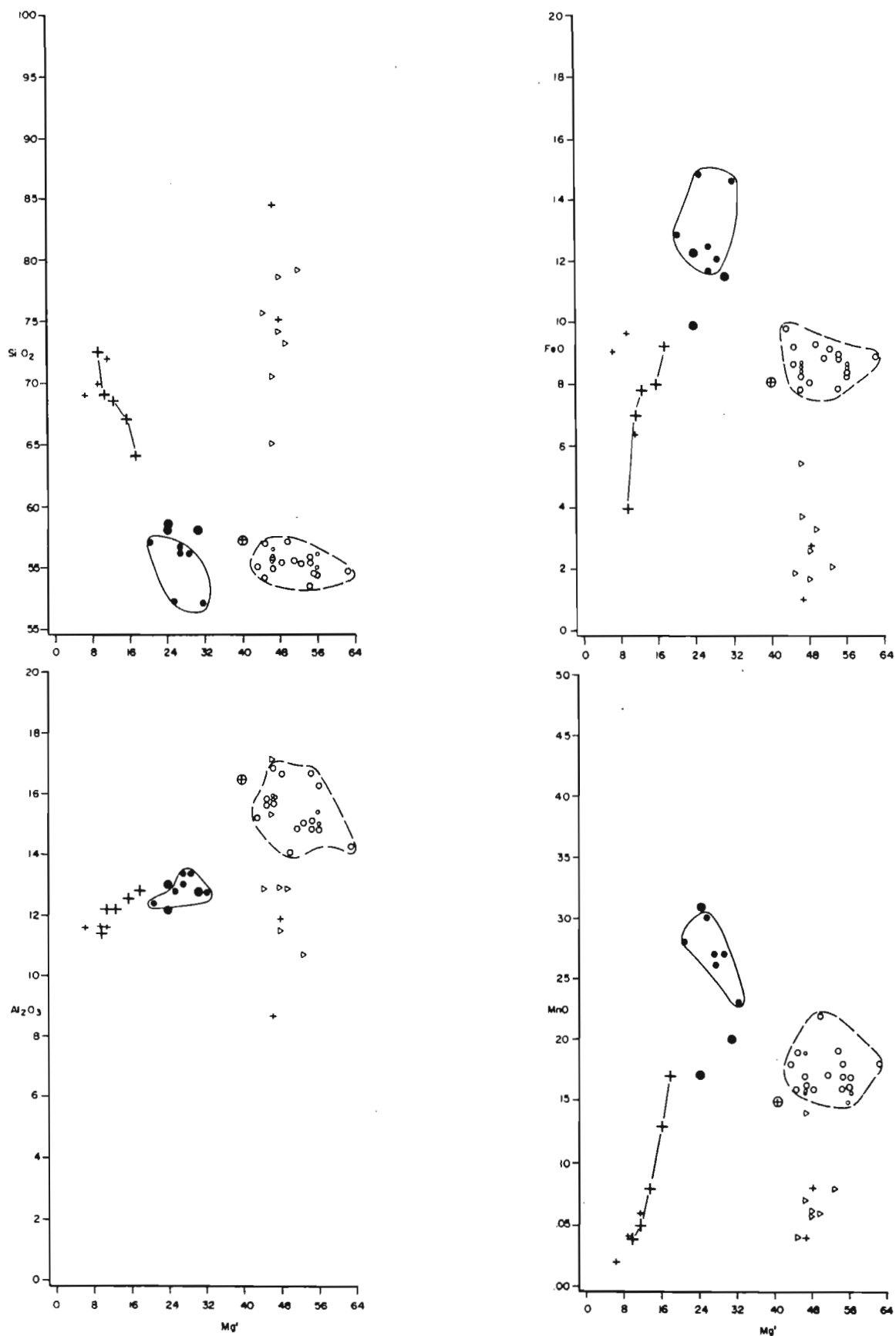


Figure 4.44 Mg-number variation with major and trace elements for various rock units at Grunehogna. Oxide values in per cent, trace element values in ppm.

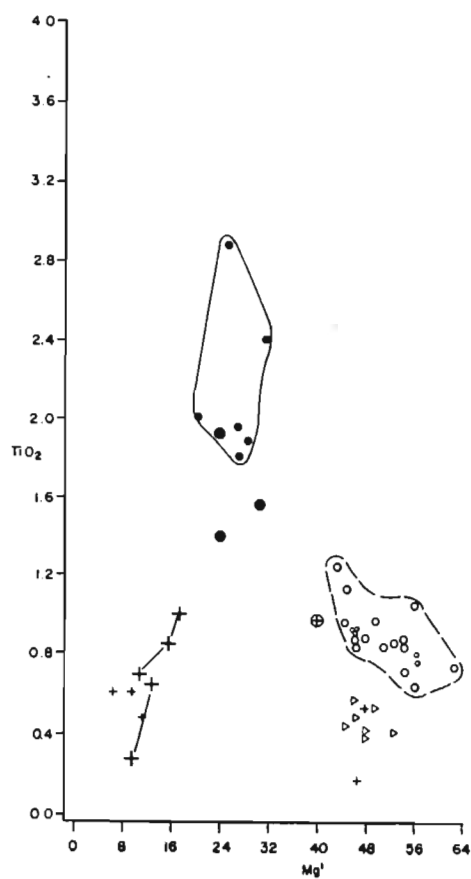
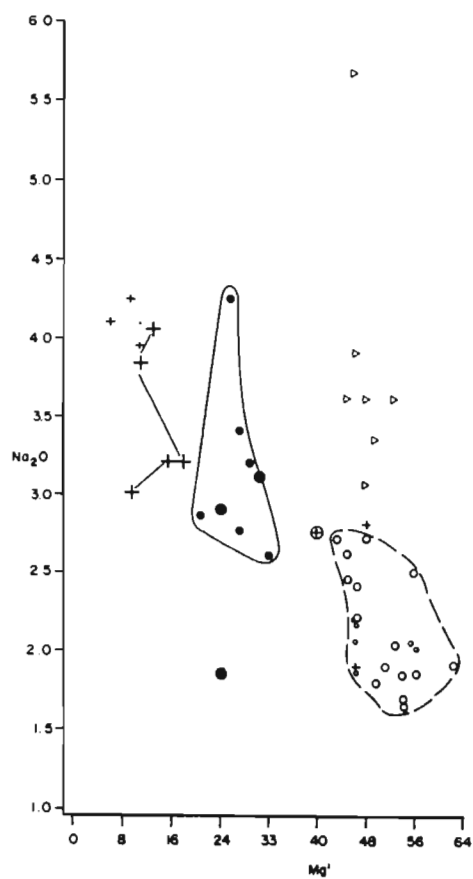
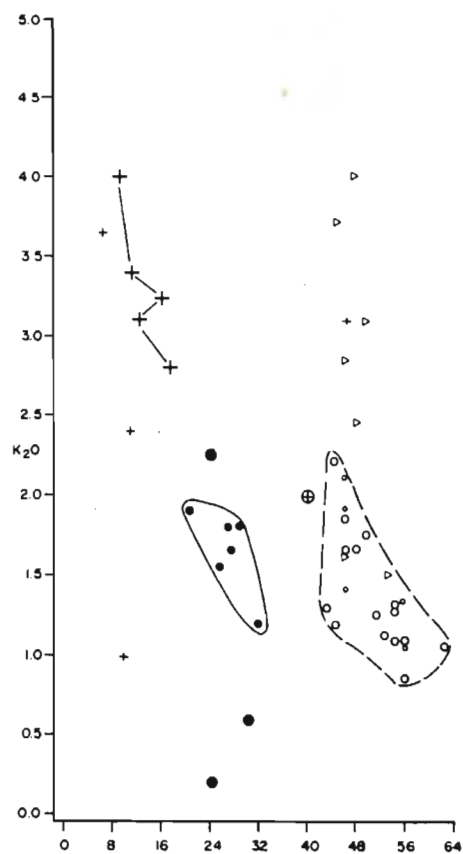
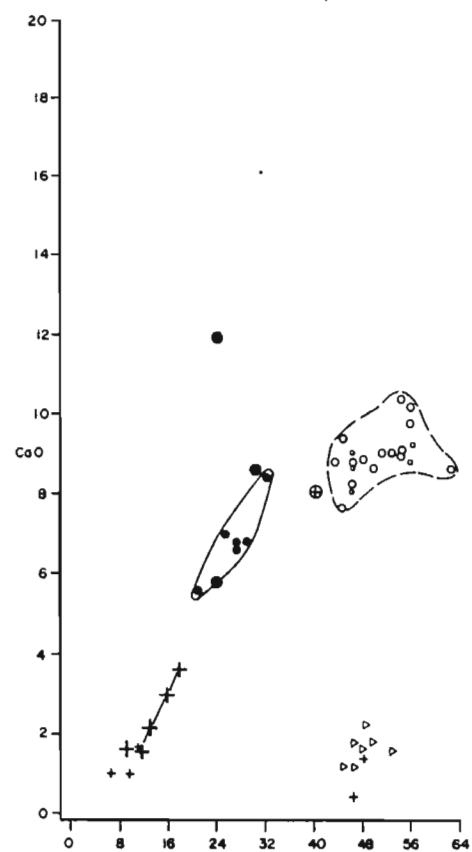


Figure 4.44 (Continued).

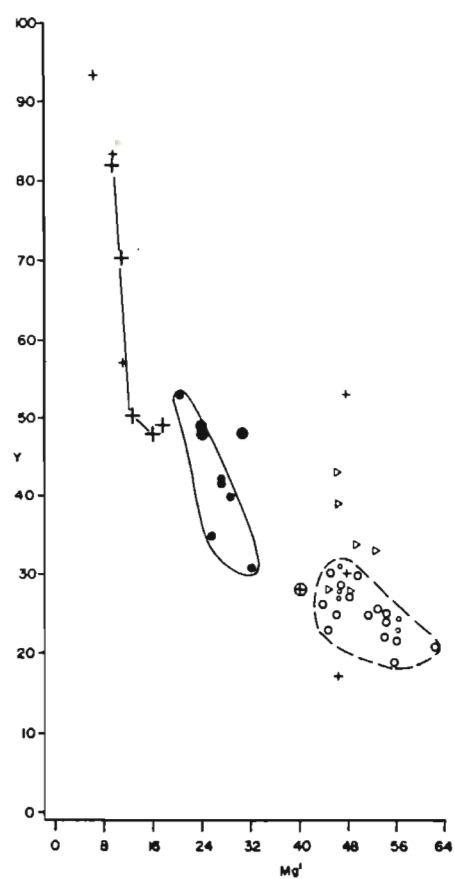
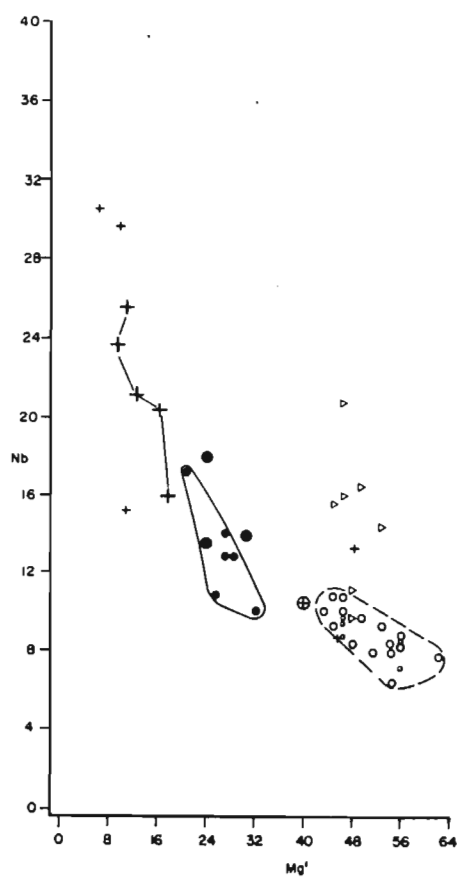
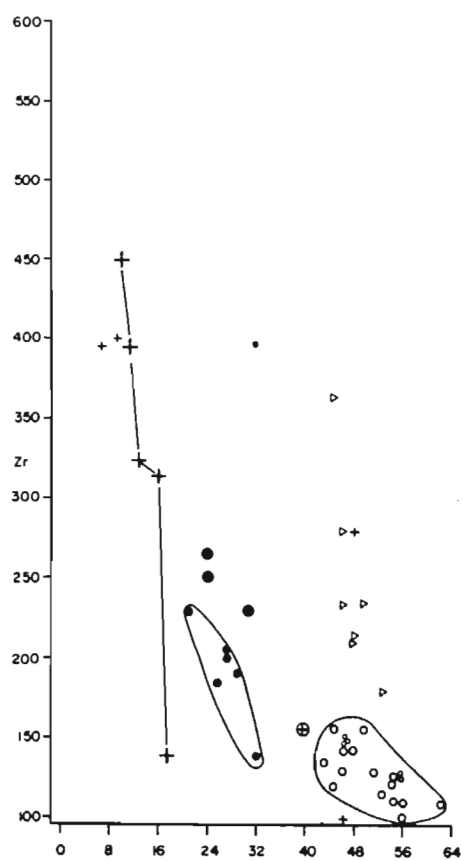
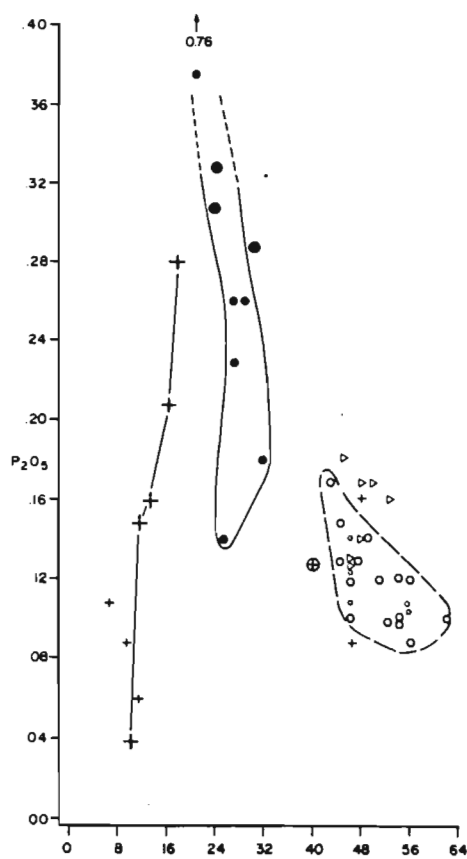


Figure 4.44 (Continued)

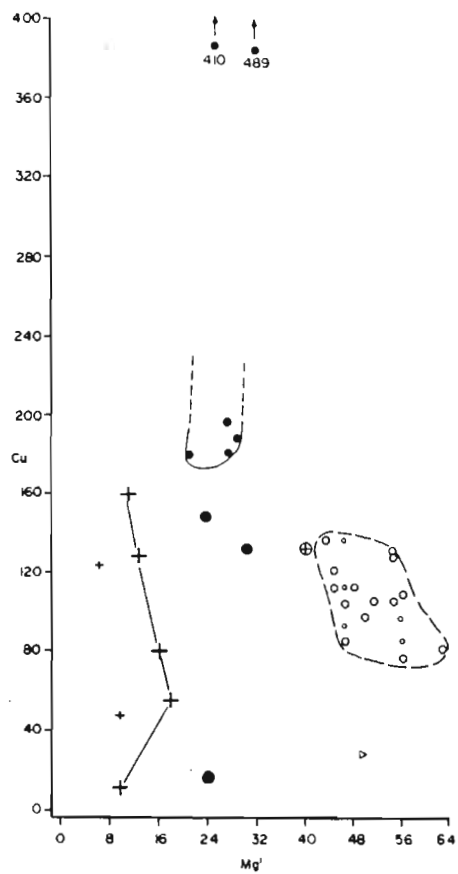
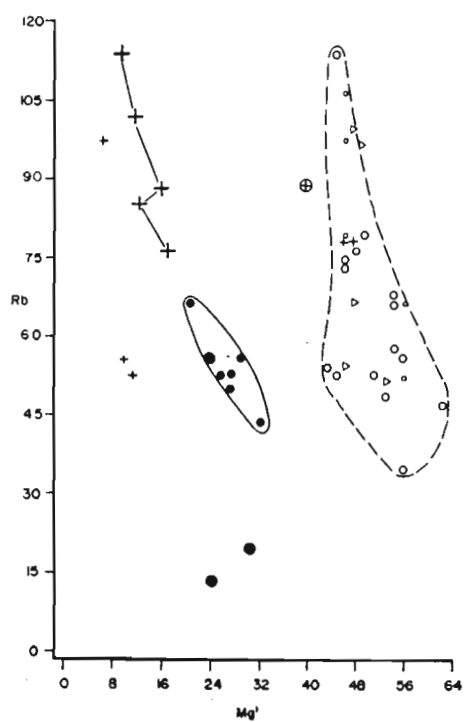
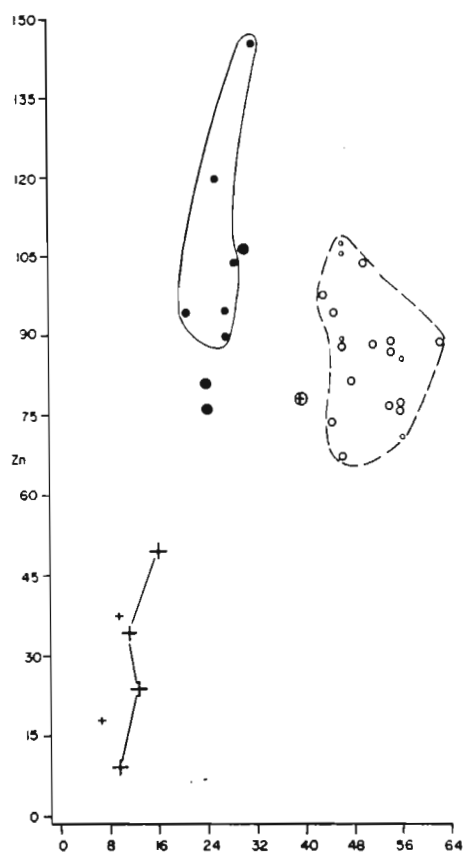
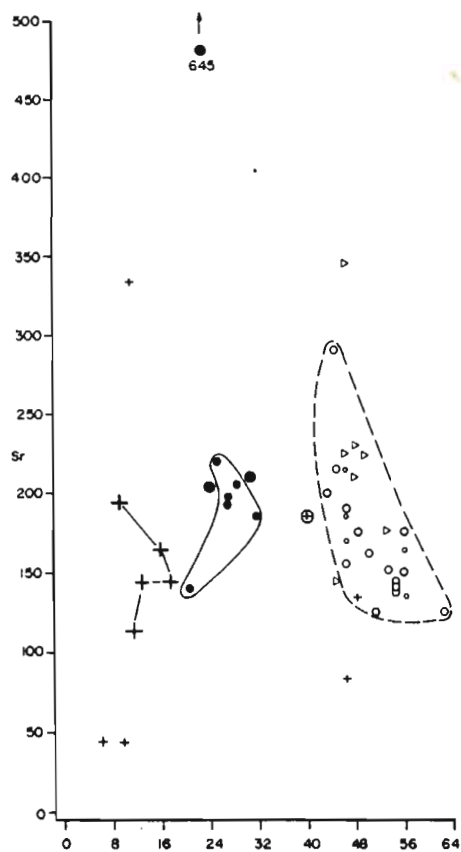


Figure 4.44 (Continued)

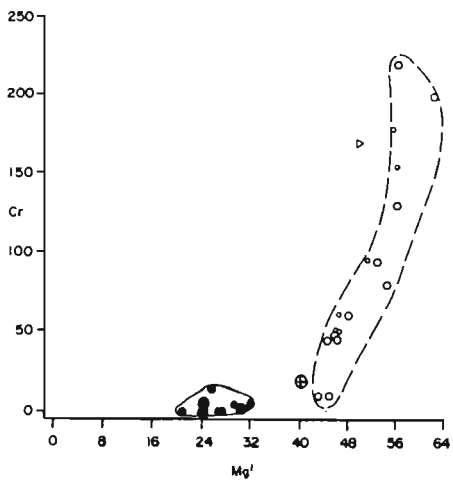
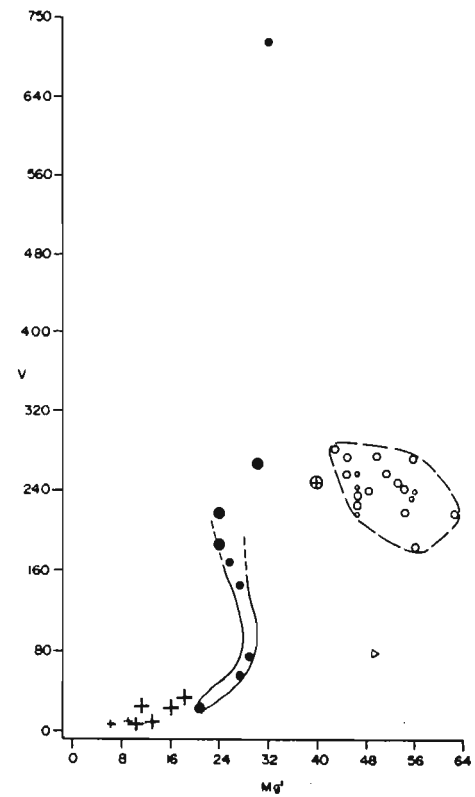
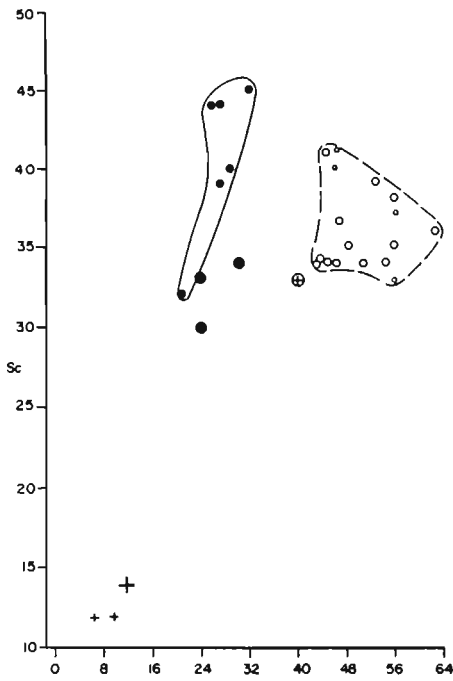
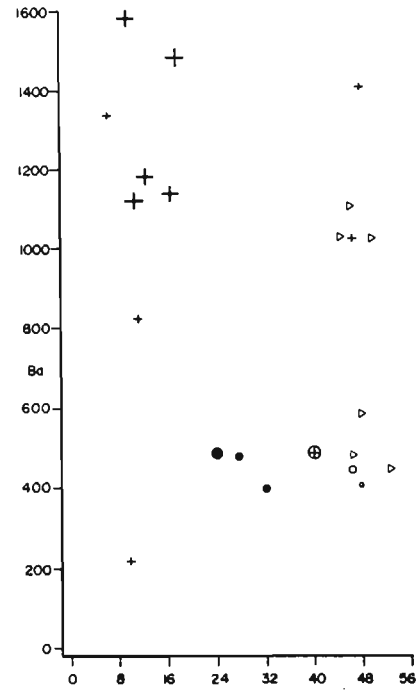
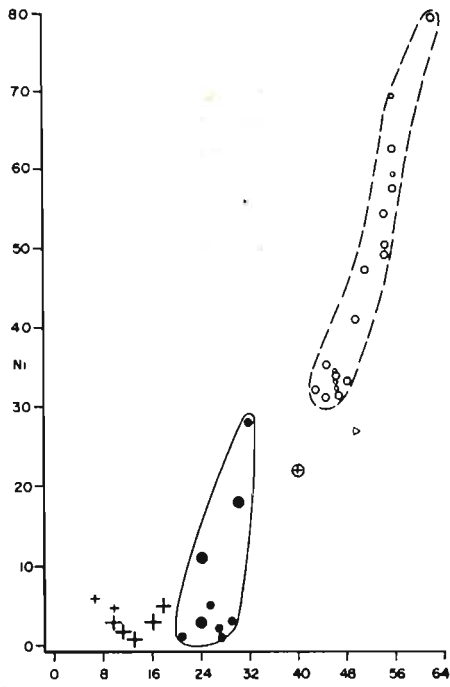


Figure 4.44 (Continued)

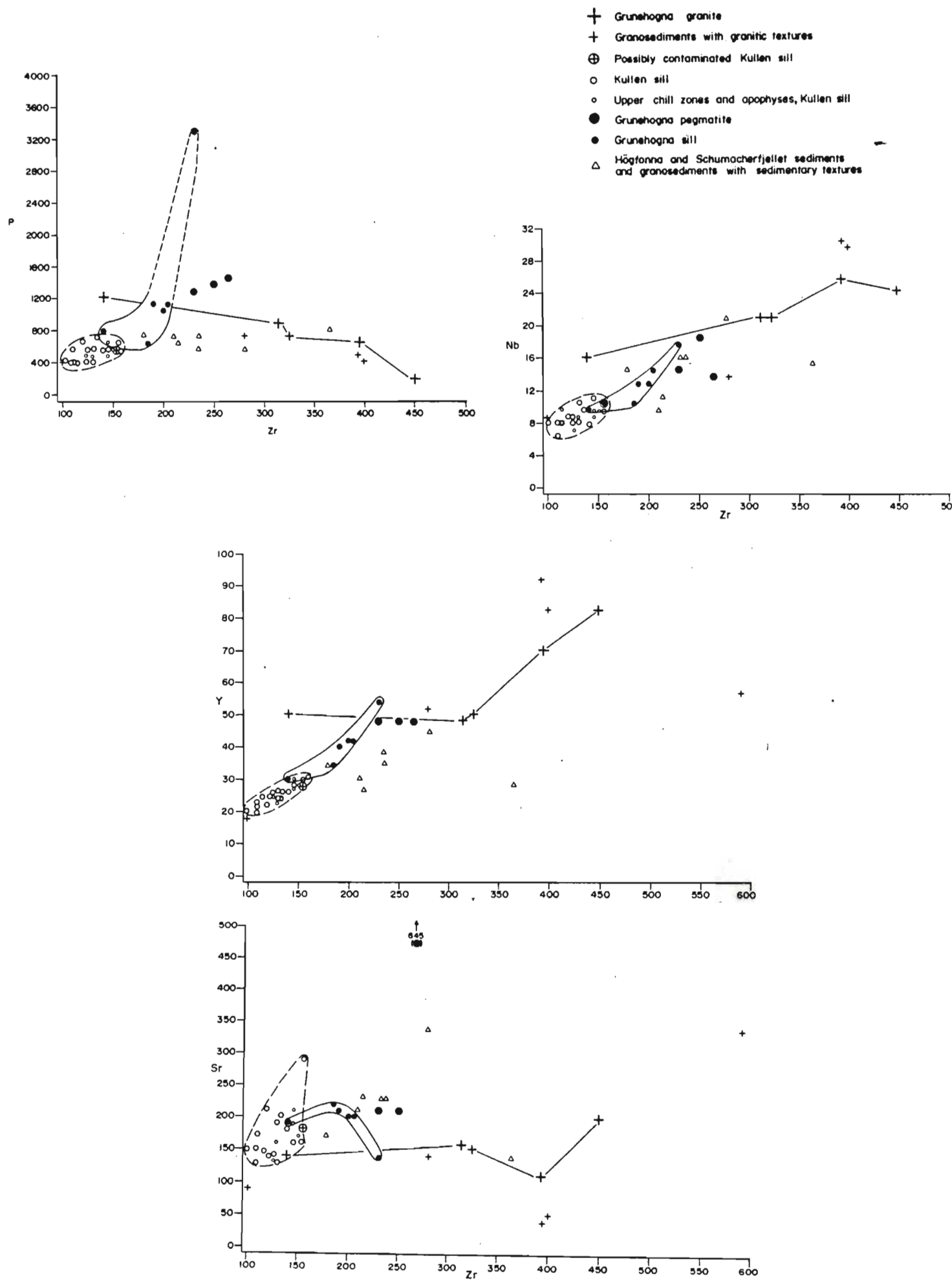


Figure 4.45

Selected minor and trace element variation diagrams for various rock units at Grunehogna. All values in ppm.

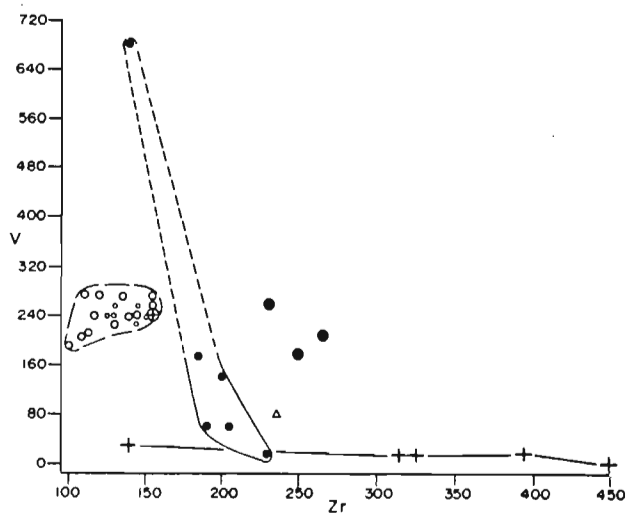
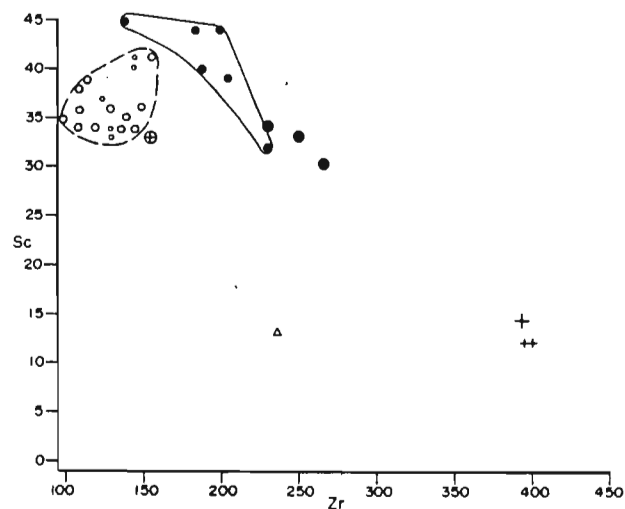
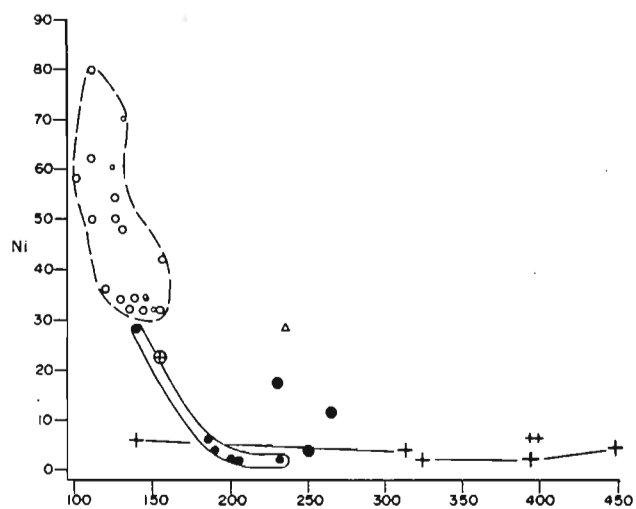
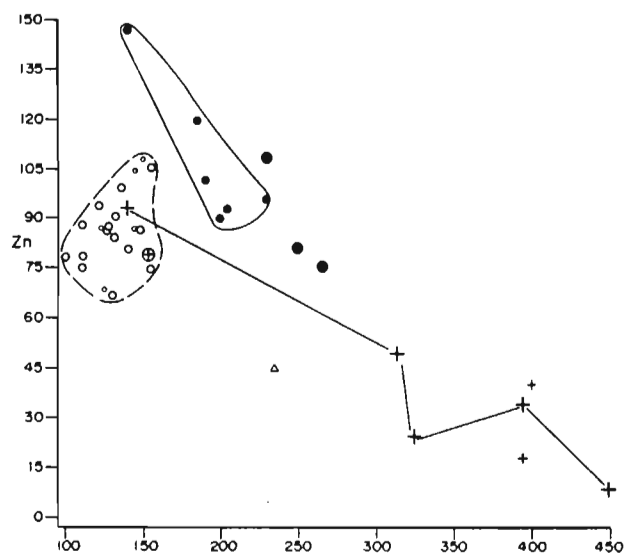
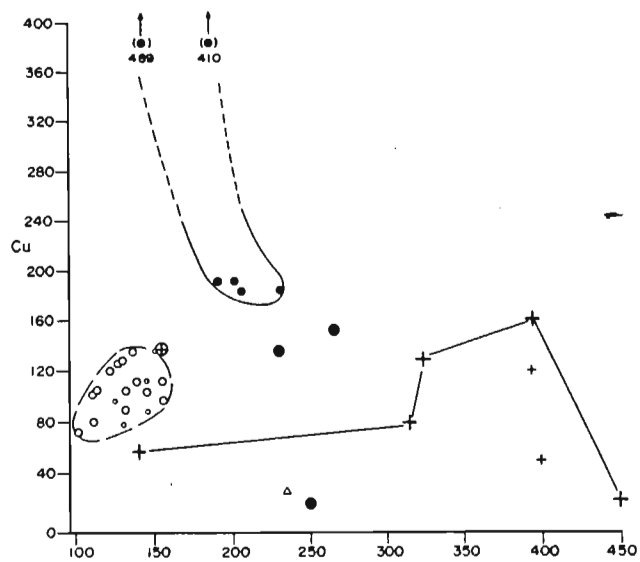
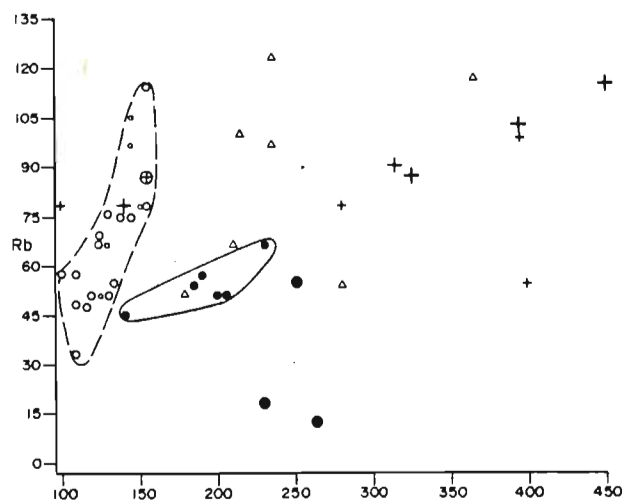


Figure 4.45 (Continued)

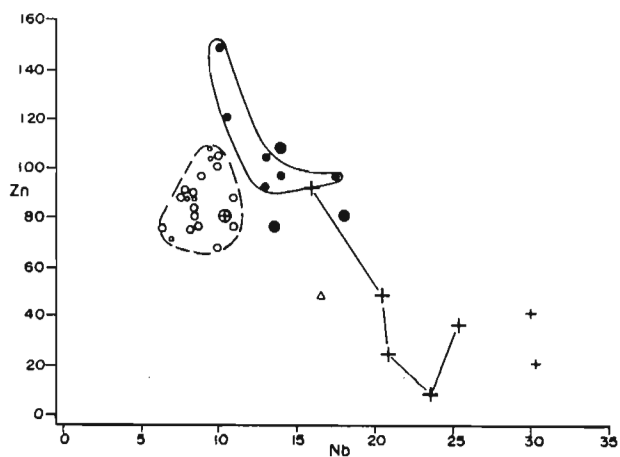
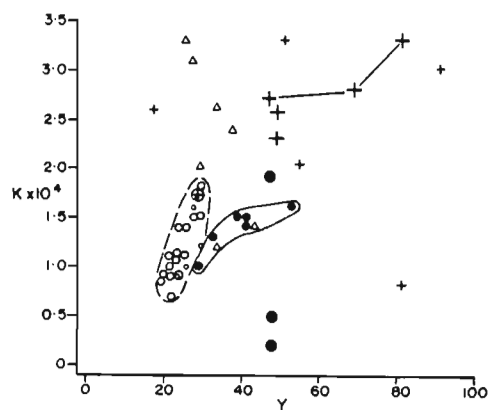
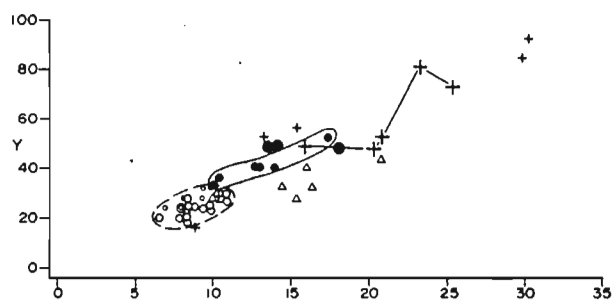
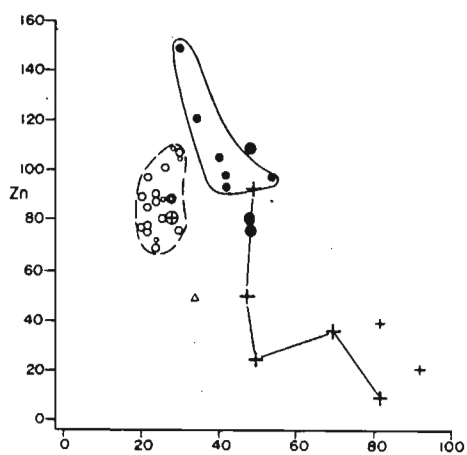
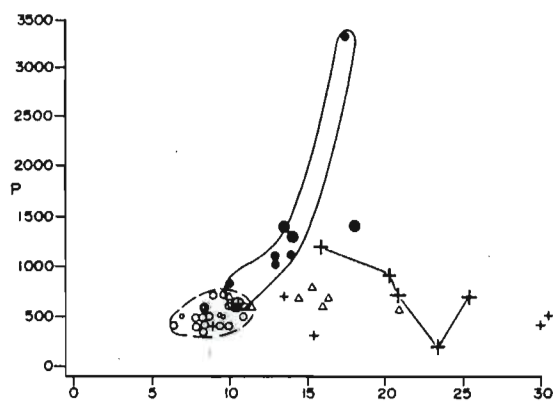
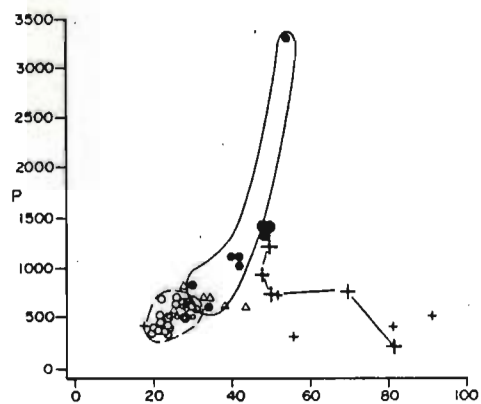
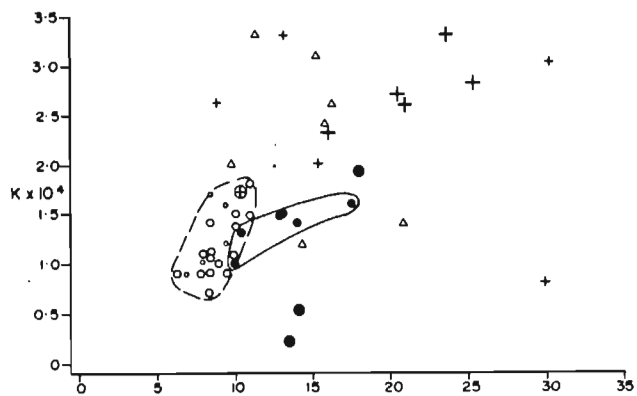


Figure 4.45 (Continued)

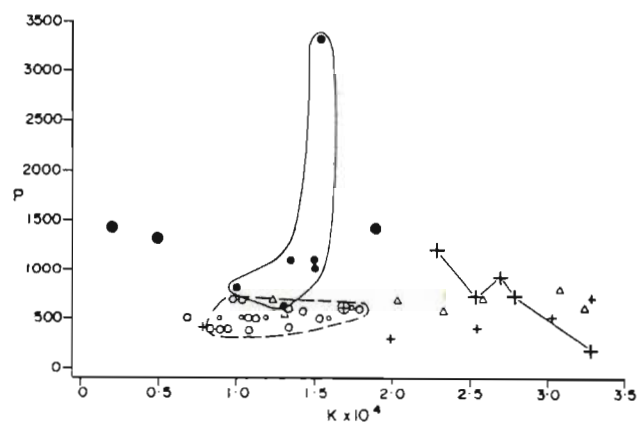
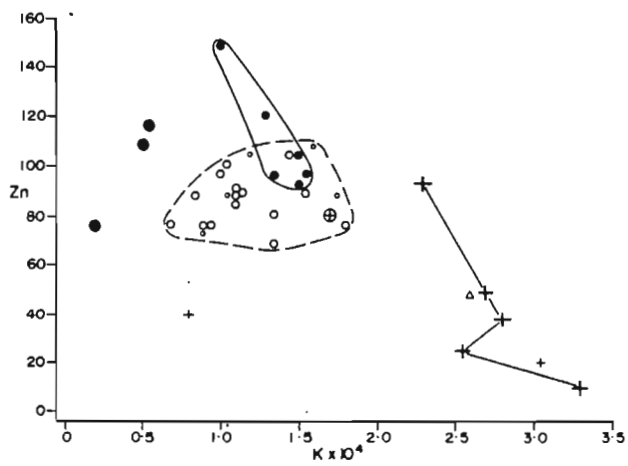
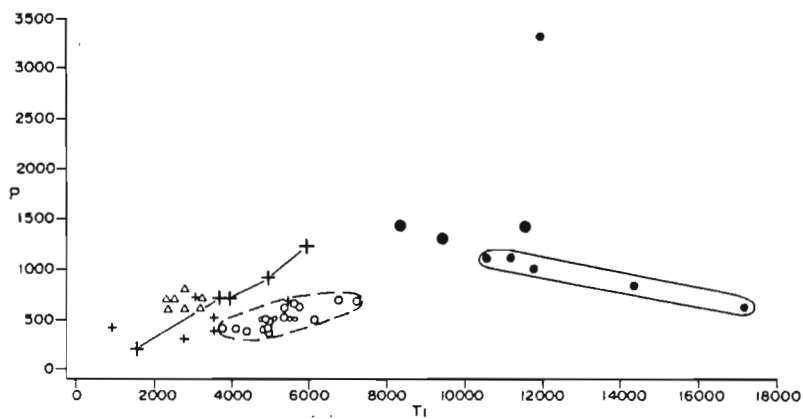
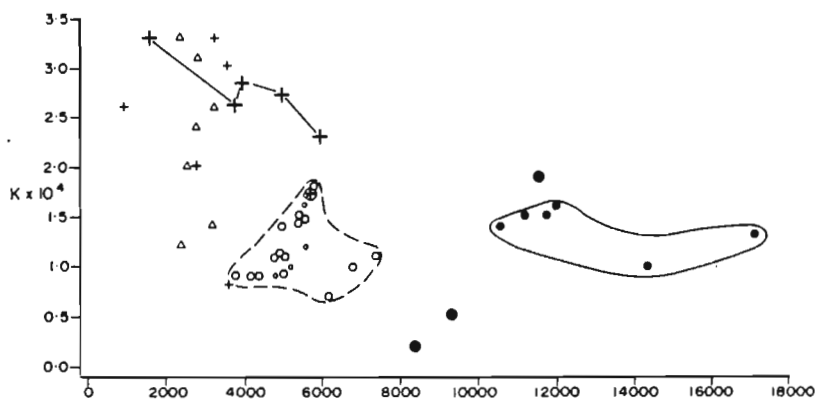


Figure 4.45 (Continued)

evidence of sedimentary laminations in hand specimens and/or thin section, plot in the trondhjemite and granite fields. However, none of the samples plotting in the trondhjemite fields can be classified as trondhjemites, because their major element characteristics do not correspond with those of trondhjemites as defined by Barker (1979).

Interelement correlations

In the Kullen sill most compatible and incompatible element pairs show poor correlation (Table 4.6), the exceptions being Mg-number variation with Ni ($r^2 \sim 0.9$), Zr variation with SiO_2 (negative correlation) and CaO, Zr variation with K_2O , Y and Rb, and Ti with P_2O_5 ($r^2 = 0.6$ to 0.9). Mg-number correlation with FeO is very low, suggesting that there is not a systematic variation of the Mg/Fe ratio through the sill. A sample of the Kullen sill taken on the contact with the xenolith west of peak 1390, has a slightly lower Mg-number and Ni content, compared to the other Kullen data. The geochemical data do not suggest significant contamination of this sample by the xenolith. Chill phases and apophyses do not show consistent geochemistry, but show variations similar to the rest of the Kullen sill data (Figures 4.44 and 4.45).

The Grunehogna sill shows a high negative correlation ($r^2 \sim 0.9$) of Zr with MgO and CaO (Table 4.7) and high positive correlation of Nb with Y. The essentially incompatible elements P_2O_5 , Nb, Zr, Y and, to a lesser extent Sr, have interelement correlations between 0.6 and 0.9, whereas Zn, Cu, Ni, Sc and V correlate negatively with the incompatible elements. Ti shows poorly-defined negative correlation with P_2O_5 , Nb, Zr, Y and Rb.

Interelement correlations in the Grunehogna granites are high in most cases (Table 4.8), except for element pairs involving Na_2O , Sr, Cu, Ni and Ba, and

Ti-Nb, Ti-Sr and Ti-Ba. P_2O_5 correlates positively with Mg-number and Ti, and negatively with Zr, Nb, Y and Rb. Granosediment data are given in Table 4.9 for comparison with the intrusive rocks.

B Comparison of Data Sets

The Grunehogna and Kullen Sills

Geochemical trends in Figures 4.44 and 4.45 show a number of features which suggest that the Kullen and Grunehogna sills may be derived either from different magmas and/or magma sources, or that they may represent different fractionation trends. Variation of Mg-number with Na_2O , K_2O and P_2O_5 defines parallel, but separate trends, and Rb-Zr, Zn-Zr and K-Y trends intersect along strongly divergent regression lines. However, K, Rb, Zn and Na_2O are highly mobile elements and therefore the data are open to different interpretations. Comparison of slopes given in Tables 4.6 and 4.7 has been made using the method of Imbrie (1956), as described by Miller and Kahn (1962).

The hypothesis being tested is that the difference between the two slopes is no greater than that expected by chance. The statistic Z is computed where Z is defined as

$$Z = \frac{K_1 - K_2}{\sqrt{S_{K_1}^2 + S_{K_2}^2}}$$

where K is the slope, and S_K is the standard error of the slope (Table 4.10).

Most of the slopes were found to be significantly different (95 per cent confidence level), using data from Murdoch and Barnes (1974, Table 3) for areas under the normal curve, tabulated by Z values. Data for which slopes were not shown to be significantly different were tested further by calculating the Z statistic for geologically meaningful values along the X-axis where the vertical difference between two growth lines is at a maximum.

A geologically meaningful value is considered to be a value which is possible to occur in both sets of data, e.g. Mg-number equal to 60. This Z value is computed by

$$Z = \frac{x_0 (K_1 - K_2) + (b_1 - b_2)}{\sqrt{S_{K_1}^2 (x_0 - \bar{x}_1)^2 + S_{K_2}^2 (x_0 - \bar{x}_2)^2}}$$

where x is the chosen value along the X-axis

K is the slope

b is the intercept on the Y-axis

S_K is the error in the slope and

\bar{x} is the mean of the data set (Table 4.10).

The combination of these two tests demonstrates that only Mg-number variation with MnO, MgO and Na₂O, and Zr variation with Na₂O show no significant differences between the Kullen and Grunehogna sills.

Geochemical variation within the two sills shows a large separation in fields on the AFM diagram (Figure 4.47), reflecting the high FeO and low MgO contents of the Grunehogna relative to the Kullen sill.

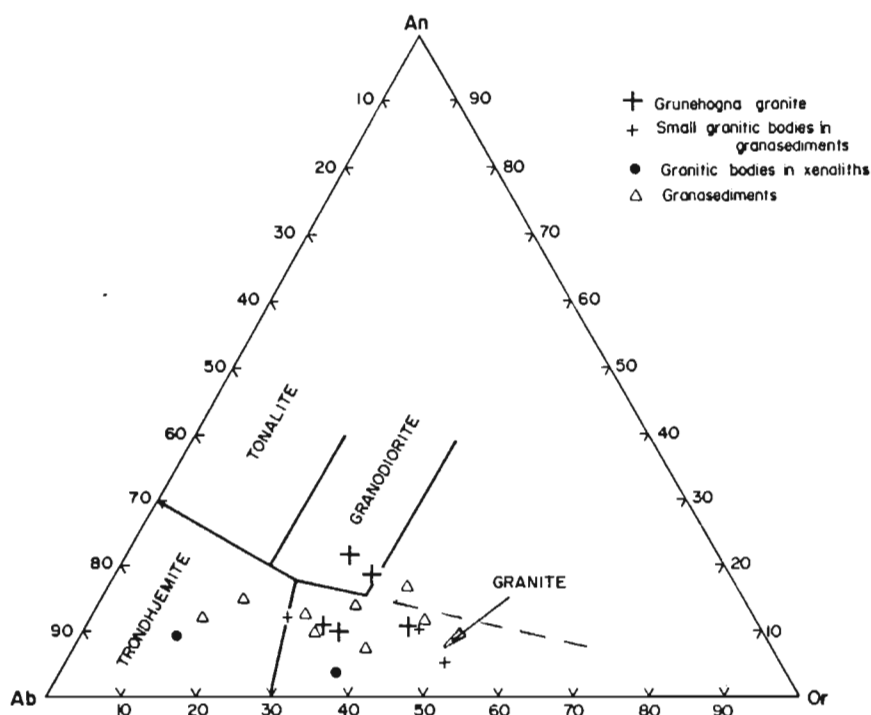


Figure 4.46 Normative An-Ab-Or ternary diagram (O'Connor, 1965), modified by Barker (1979).

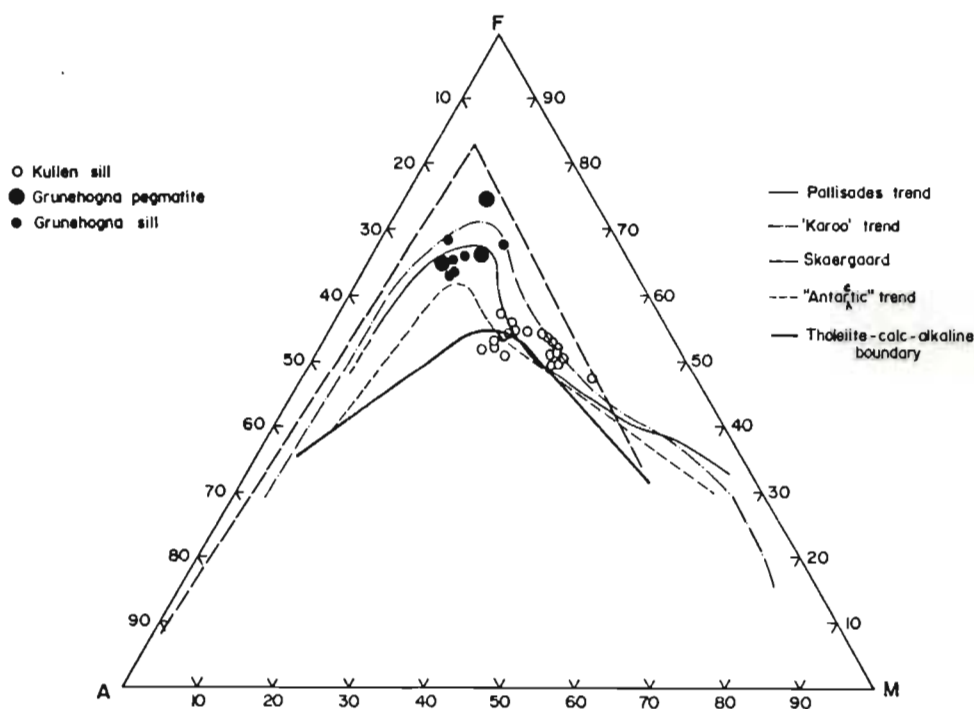


Figure 4.47 AFM diagram showing compositions of Grunehogna sill and pegmatite, and the Kullen sill. Tholeiite-calc-alkaline boundary after Irvine and Barager (1971), Palisades sill: Walker (1969a), "Karoo" trend: Walker (1969a) after Walker and Poldervaart (1949), Skaergaard: Wager and Brown (1968), "Antarctic" trend: Walker (1969a) after Gunn (1962, 1966), Hamilton (1965), Stephenson (1966).

The Grunehogna Pegmatite

Only three samples of the pegmatite from the 1390 north face are available, hence geologically meaningful variation cannot be computed. However, examination of Figures 4.44, 4.45 and 4.47 show that the geochemistry of the pegmatites more closely approximate that of the Grunehogna sill, except for variation diagrams involving Sr and K. One epidote-rich sample has a Sr content of 645 ppm compared with the mean of 191 ppm in the Grunehogna sill, and K-variation may be explained by the variation in the nature of the quartz-alkali feldspar intergrowths which varies from dominantly quartz-K-feldspar to dominantly quartz-oligoclase (Section IIIA).

The Grunehogna sill and Grunehogna granites

The Grunehogna granites appear to lie along extensions of trends within the Grunehogna sill on a number of variation diagrams in Figures 4.44 and 4.45, e.g. Mg-number variation with most of the major and trace elements. Table 4.11 lists Z values as described above, and shows that only Mg-number variation with SiO_2 , FeO, MgO, Na_2O , TiO_2 and Nb and variation of Nb with Sr and Rb are not significantly different in both slopes and growth lines at selected X_0 values. However, it can be argued that this comparison is not strictly valid, because variations in primocryst development and mineral chemistry are likely to result in changes in slopes on variation diagrams. Furthermore, the data bases are small, and removal of one sample may further influence slopes and growth lines. However, the parallel and intersecting nature of the trends in the Grunehogna sill and Grunehogna granites on variation diagrams such as Mg-number with Na_2O , MnO, P_2O_5 , Sr and Cu, K with Nb, and Zn with K, suggest that

the granites have not been derived from the Grunehogna sill. Quantitative modelling of the data is discussed in Chapter 7, where regional correlations of the igneous rocks in the Ahlmannryggen are examined.

Comparison of Grunehogna granites and small granitic bodies

Two of the small granitic bodies within granosediments at the 1285 southeast outcrops show compositions similar to the granosediments and Högfonna sediments on all variation diagrams in Figures 4.44 and 4.45. However, two granitic samples from a xenolith west of peak 1390 and one from the 1285 southeast face are very similar in composition to the Grunehogna granites. They have slightly higher FeO and Zn contents at the same Mg-numbers, and lower K₂O and Rb than the Grunehogna granites. On this sparse evidence it is not possible to distinguish the two granitic types.

V DISCUSSION

Field, petrographic and geochemical data of the intrusive and associated rocks at Grunehogna (excluding dykes) show that part of the petrogenetic history of the sills and some of the associated granitic bodies is closely related to the environment into which the sill were emplaced. This environment and the effects of intrusion upon the country rocks are discussed below, followed by discussions on the igneous history of the Grunehogna and Kullen sills.

A. Intrusive Relationships.

The Grunehogna sill is thought to have intruded water-saturated, partially consolidated or unconsolidated sediments at shallow levels (Krynauw, 1983). Features supporting this hypothesis are:

1. The development of large-scale drag folding in Schumacherfjellet sediments along planes where the sill transgresses these sediments, and extensive soft-sediment deformation in xenoliths;
2. Partial destruction of sedimentary structures and presence of sedimentary enclaves in granosediments;
3. The occurrence of vugs within contact zones;
4. Petrographic and field evidence for fusion of sediments within the contact zones;
5. The presence of apparently large volumes of pegmatites associated with the Grunehogna sill.

1. Evidence for soft-sediment deformation.

Francis (1982) proposes a mechanism for intrusion of sills into sedimentary basins, which suggests that ascent of magma occurs under moderate, continuous pressure along near-vertical fractures. The dykes thus formed do not reach the surface, but intrude laterally at intersections of the dykes with bedding planes. Magma intrusion is likely to be gravity controlled and thus emplacement occurs downwards towards the centre of the basin. Transgression of the sediments by the sills during this phase will probably be on a relatively small scale (Francis, 1982). If flow down low dips took place it is likely that

small variations in the regional dip could have a profound effect on intrusion dynamics. Stephenson and Griffin (1976) have described down-dip flow of lavas along slopes of only 0.3° . It is suggested that the Grunehogna magma intruded down-dip along or close to the interface between the Schumacherfjellet and Högfonna Formations. Local variations in dip caused pooling of magma, which differentially increased the mass of magma plus sediment on the underlying, still unconsolidated sediments. This resulted in very large-scale sagging or slumping of the Schumacherfjellet sediments, and transgression of the Grunehogna magma along an inclined plane in the order of 100m. The resulting soft-sediment deformation caused the development of the disharmonic folding seen along the 1285 north face (Figure 4.16). Sagging of lithified sediments has been proposed previously by Petraske et. al (1978) to account for the formation of laccoliths, and this mechanism is considered viable for the Grunehogna occurrences. Extensive soft-sediment deformation was described in large xenoliths in the Grunehogna sill, which were presumably stoped from the overlying sediments (Figure 4.19). The lack of similar features in the country rocks suggests that the xenoliths were still unconsolidated at the time of incorporation in the magma. Soft-sediment deformation was also described in the upper horizon of the contact zone along the 1285 southeast face, but this occurrence is more limited in extent and intensity and is not unequivocally related to the effects of sill intrusion.

2. Destruction of sedimentary structures.

Destruction of sedimentary structures and reconstitution of sediments in contact zones of andesite and rhyolite sills in parts of Britain have been described by Kokelaar (1982). He has shown that these effects were the result of fluidization of wet sediments during intrusion at pressures below

312 bars. Complete homogenization of sediments may be achieved, resulting in the rapid, local transport of fluidized sediment.

Kokelaar (1982) states that precise conditions for the onset of fluidization cannot be determined, but consideration of temperature - pressure - volume relationships of water (Figure 4.48) can indicate the favourable conditions for this mechanism. Heating at uniform pressure below the critical pressure causes an explosive expansion of water vapour on crossing the phase boundary, followed by relatively slow expansion at higher temperatures (Pathway A, Figure 4.48). The explosive expansion may cause momentary fluidization and flow of vapour. Pathway B, above the critical pressure, does not show this effect. Along Pathways C and D, explosive or rapid expansion may occur on crossing of the phase boundary. These latter two pathways represent conditions that may be encountered upon the opening of fractures. In wet sediments persistent vapour can be generated if a heat source is available to prevent condensation, resulting in fluidization and voluminous and/or long distance transport of sedimentary material. Owing to the development of an insulating carapace of vapour, the zone affected by fluidization remains fairly narrow, while the surrounding host remains unaffected until the water in it reaches the boiling temperature.

Within the contact zone of the Grunehogna sill there is no evidence for transport of sediment, but destruction of sedimentary structures did occur, as evidenced by the destruction, or partial destruction of laminations in granosediments. Sedimentary enclaves in which sedimentary structures are recognized represent centres where lithification or compaction has been initiated in an otherwise unconsolidated, water-saturated sediment. This partial lithification or compaction of the sediment may have prevented

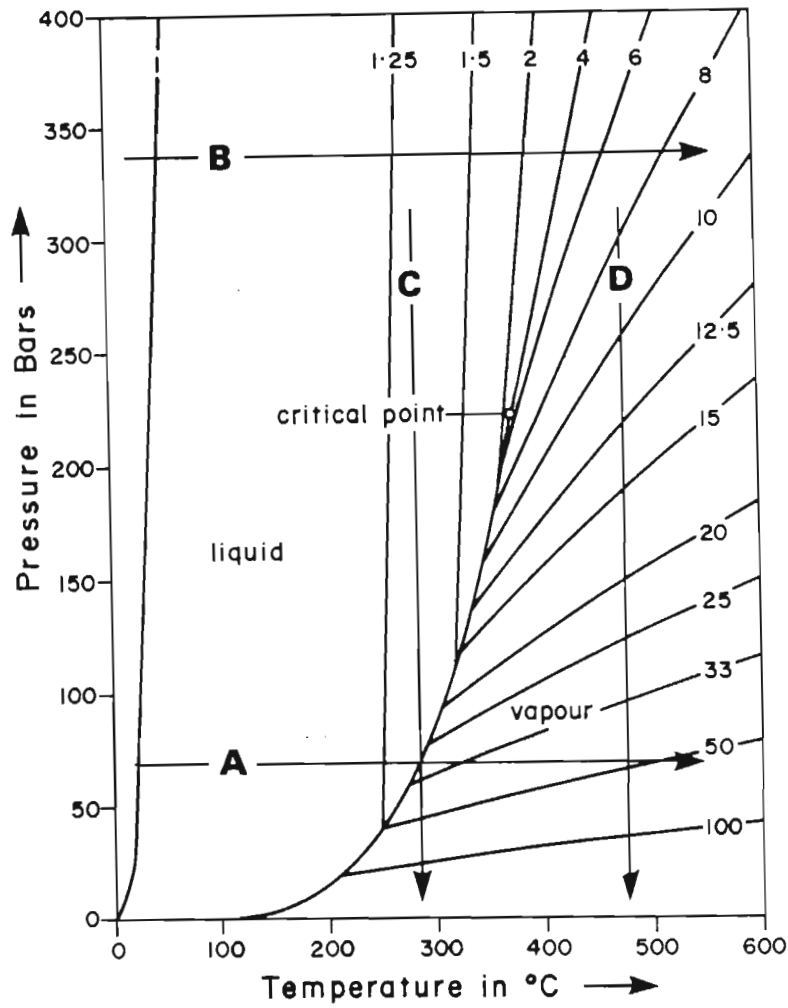


Figure 4.48

Variations in specific volume of water with temperature and pressure (after Kennedy and Holser, 1966; Kokelaar, 1982). Pathway A: Heating at uniform pressure below the critical pressure of water; Pathway B: Heating at uniform pressure above the critical pressure of water; Pathways C and D: Decrease in pressure at constant temperature.

transport of detrital material. The zoned nature of the enclaves reflects varying degrees of lithification and/or compaction.

3. Vugs in contact zones.

The presence of vugs within contact zones is further evidence that boiling took place in wet sediments during intrusion of the Grunehogna sill, and further constrains the level at which intrusion occurred. The critical point of pure water is at 221 bars (Figure 4.49). For sea water composition, the critical pressure would be 312 bars (Krauskopf, 1967; Kokelaar, 1982) and assuming a density of 2 g/cm^3 for wet sediments (Moore, 1962) this would correspond to a depth of 1.6 km. Thus the upper limits for the level of intrusion are between 1.1 and 1.6 km.

The exact nature of the environment of deposition of the sediments at Grunehogna is unknown, although the possibility of marine embayments alternating with braided river systems in the depositional environment has been suggested (Ferreira, 1986a, 1986b).

4. Fusion of sediments in contact zones.

Fusion of sediments in contact with intrusive bodies has been recognized since the early part of the century by a large number of workers (e.g. Du Toit, 1904, 1905, 1913, 1929; Harker, 1904; Bowen, 1910; Mennell, 1911; Hatch, 1912; Young, 1918; Hawkes, 1929; Mountain, 1935, 1936, 1943, 1944, 1945, 1960; Tomkeieff, 1940; Reynolds, 1940; Walker and Poldervaart, 1941, 1942a, 1942b, 1949; Poldervaart, 1944, 1946; Kent and Frankel, 1948; Frankel, 1950; Wells, 1951; Bailey, 1959; Ackerman and Walker, 1960; Wyllie, 1961; Smith, 1969; Kenyon, 1976). The fused rocks can be divided

into two major groups, namely (i) vitreous and semi-vitreous rocks or 'buchites' (as defined by Tomkeieff, 1940) and (ii) rocks with granophyric textures.

An example of the vitreous fusion products in sandstone associated with a picrite sill in Soay is described and discussed by Wyllie (1961). He proposed that the development of liquid, now seen as glass, resulted from decomposition of sericite and the fusion of quartz and feldspar. Fluxing was effected by volatiles migrating through the rock and by mutual fluxing between the quartz and feldspar where they were in contact with each other. Walker and Poldervaart (1949) believed that the local fusion and mobilization of sediments in contact with certain Karoo sills were caused by fluxing of sulphate and chloride ions. Subsequently, the glasses were shown to have high water-contents (Frankel, 1950), and Wyllie (1961) suggested that the fluxing action of water, associated with an increase in temperature, caused the fusion. The fluxes associated with the Soay picrite were thought to have originated initially as a result of decomposition of sericite, which opened passageways for further volatiles emanating from the magma.

Granophyric intergrowths in contact zones or in xenoliths have been described mainly in epizonal rocks (Barker, 1970). Authors such as Bowen (1910), Mennell (1911), Hawkes (1929), Wells (1951) and Bailey (1959) consider them to be products of crystallization from melts. An origin by metasomatic replacement has also been proposed (Daly, 1905; Gillson, 1927; Grout and Schwartz, 1933; Reynolds, 1936, 1950). Jahns et al (1969) produced granophyres experimentally from basalt by transport and redeposition of Si, Al, Na and K. The haematite-stained nature of the alkali feldspars and alteration of mafic minerals are common features in granophyric rocks (Barker, 1970). Furthermore, Taylor (1968) has shown that equilibration of oxygen

isotopes does not occur between alkali feldspar and coexisting quartz which Barker (1970) interprets as evidence for hydrothermal or deuteric alteration and oxygen exchange during the formation of the granophyric intergrowths. Barker also suggests as an alternative mechanism, rapid, magmatic crystallization of quartz and alkali feldspars to produce anhydrous granophyric intergrowths. These lead to the development of residual aqueous fluids, which cause alteration of earlier formed mafic minerals.

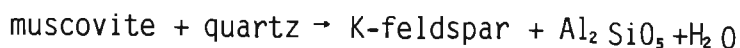
In the Grunehogna contact rocks the following factors have to be considered to understand the genesis of the granophyric rocks:

- (i) There is a regular gradation from slightly corroded quartz grains with small amounts of associated micro-aplite to granophyric intergrowths of quartz, K-feldspar and albite in rocks with granitic textures within the contact zone granosediments;
- (ii) The development of micro-aplite in sedimentary layers and mobilization of this material over short distances (tens of centimetres) to form granitic veinlets.

A mechanism of hydrothermal alteration may have operated initially after intrusion of the Grunehogna sill. It is possible that aqueous fluids from the sill could have supplied additional components such as K and Na ions, to the overlying sediments, with resultant hydrothermal alteration of the sedimentary minerals. This may have been followed by redeposition of Si, Al, Na and K ions virtually in situ to form the pseudogranophyric intergrowths. Fe^{3+} added from the magma, or more likely from local alteration of detrital magnetite, would have been deposited in solid solution with alkali feldspar as KFeSi_3O_8 (Ernst, 1960).

Although the above interpretation may be valid, the development of micro-aplite and its mobilization to form granitic veinlets suggest the presence of melt material. In the quartz-albite-orthoclase system with excess water (Winkler, 1976) melting takes place initially at approximately 800°C at 0.3 kilobar. If small amounts of anorthite are present, this temperature may increase by 10 to 20°C (Winkler et al, 1975). In contrast, the liquidus minimum temperature in the quartz-albite-orthoclase haplogranite system at 1 Kb H₂O drops from 750°C to 690°C by the addition of 1 per cent fluorine, and to 630°C with 4 per cent fluorine. Similarly, the minimum temperature is reduced to 660°C with the addition of 4.5 per cent B₂O₃ (Manning and Pichavant, 1983; Pichavant, 1984; Burnham and Nekvasil, 1986). Although no analyses for fluorine and boron have yet been done, it is possible that similar fluxes present in the sediments could have decreased the fusion temperature. This would be particularly true if part of the aqueous phase present in the sediments was sea water as proposed by Ferreira (1986a, 1986b). The thickness of the Grunehogna sill is unknown, but the volume of pegmatite, the scale of deformation associated with it, and the presence of a 3 m-thick contact zone along concordant contacts with the sediments suggest that the Grunehogna sill may be comparable in thickness to the Kullen sill, i.e. possibly 300 to 400 m. Temperatures of 800°C may therefore be a reasonable estimate of conditions within contact zone sediments at the time of intrusion of the Grunehogna sill.

In a water-saturated system containing quartz, muscovite and plagioclase melting would have occurred on a small scale, which can be seen now as micro-aplites along corroded quartz grain boundaries and small-volume granitic bodies. At the low pressures prevalent during intrusion of the Grunehogna sill the reaction:



may have occurred prior to melting (Winkler, 1976). Unfortunately phase relationships below 1 kilobar are not well-defined and it is possible that equilibrium would not have been reached before melting occurred. At the melting point in the water-saturated system, the reaction would have been:

Albite + K-feldspar + quartz + $H_2O \rightarrow$ Liquid (Tuttle and Bowen, 1958; Winkler, 1976). At low pressures the negative slope of the solidus in the water-saturated granite system is relatively flat and any slight release of pressure would result in instantaneous crystallization of the melt. Thus the melts formed within the Grunehogna sill contact zone could not have migrated far and the fact that they are confined to this zone is consistent with their formation in a water-saturated system. Similarly, where cracks may have developed, they were filled by melt material which would have crystallized very rapidly owing to the sudden release of pressure. In some cases melting may have occurred with no separation of melt from sediment, resulting in a "contaminated" granite which retained the chemical characteristics of the sediment from which it was derived.

The reason for the development of granitic, granophyric and aplitic textures, rather than the formation of a glass, may be explained by variation in the total volatile contents of the different intrusive environments. Within a water-saturated environment, transfer of material is relatively rapid, enhancing crystallization of the primary minerals on cooling from a melt. In systems where fluxes were obtained from the breakdown of hydrous phases such as sericite and/or emanations from the intruding magma the resulting melt products may be relatively dry. Such liquids are therefore more likely to produce glasses upon cooling.

The evidence for fusion of the sediments at Grunehogna at levels below 2 km contradicts the view of Patchett (1980) who believes that in the uppermost crust aqueous fluid circulation is the dominant effect of magma emplacement,

because partial melting does not occur at this level owing to the high temperature of granite minimum melting.

5. Apparent large volume of pegmatite.

Irregular concentrations and pods of pegmatites are present in the upper parts of the Grunehogna sill, which is overlain at Grunehogna 1390 by the 50 m-thick Grunehogna pegmatite. Similar relationships have been reported at Preikestolen nunatak (Snow, 1986), where the upper part of the Grunehogna sill is overlain by a 40 to 50 m-thick quartz diorite pegmatite. The field relationships and geochemical similarity suggest that the overlying pegmatite is a coarse-grained phase of the Grunehogna sill. It is absent in the eastern outcrops of Kullen and in nunatak 1285. Only the upper parts of the Grunehogna sill are exposed, and its thickness and aerial extent are unknown. It is therefore not possible to estimate the relative volume of pegmatite compared to that of the Grunehogna sill. However, in comparison with the Kullen sill, other Borgmassivet intrusions and typical Karoo sills (e.g. Walker and Poldervaart, 1949; Le Roex and Reid, 1978) the amount of pegmatitic material associated with the Grunehogna sill appears to be exceptionally high.

The large pegmatite volume indicates the presence of a high content volatiles in the Grunehogna magma. If the Grunehogna sill did intrude unconsolidated, water-saturated sediments these volatiles may represent meteoric water derived from the sediments, which were incorporated into the magma. Taylor (1979) speculates that the upper portions of certain magma chambers may become saturated with water by incorporation of meteoric water from country rocks. Such contamination most likely occurs by stoping or assimilation of hydrothermally altered roof rocks (Taylor, 1974). Oxygen and hydrogen isotope

studies on the Skaergaard intrusion have shown that very little water penetrated directly into the liquid magma (Taylor and Forester, 1979), but dehydration of stoped blocks of altered roof rocks did contribute some water to the magma. Taylor and Forester also suggest that small amounts of meteoric water diffused directly into the magma, which was responsible for the development of many gabbro pegmatite bodies in the Marginal Group of the Skaergaard intrusion. Walker and Poldervaart (1949) record pegmatites in Karoo sills in a few of the thickest intrusions, and note that they tend to occur in the proximity of xenolithic blocks. The inference may be drawn that the xenoliths provided volatiles which enhanced pegmatite crystallization. The presence of large xenoliths in the Grunehogna sill suggests a possible source of water. Furthermore, corroded quartz grains in both the Grunehogna and Kullen sills may be interpreted as xenocrysts, indicating some degree of magma contamination. Hence it is suggested that stoped blocks of wet, unconsolidated sediment contributed relatively large amounts of volatiles, mainly water, to the Grunehogna magma, which resulted in the development of an exceptionally large volume of pegmatite.

6. Contact relationships of the Kullen sill.

The Kullen sill is considered to be younger than the Grunehogna sill for the following reasons:

- (i) The Kullen sill has a chill zone where it is in contact with the Grunehogna sill;
- (ii) It contains xenoliths interpreted to be fragments of Grunehogna sill; and
- (iii) Thermal effects on the Schumacherfjellet and Högfonna sediments are much less marked than in the case of the Grunehogna sill.

Objections to this interpretation are:

- (a) Barton and Copperthwaite (1983) obtained an Rb-Sr isochron age of 1426 ± 87 Ma for the Kullen sill, and Barton (pers. comm, 1984) reported an Rb-Sr isochron age of 838 ± 112 Ma for the Grunehogna sill.
- (b) No hand specimens of the supposedly Grunehogna sill xenoliths have been obtained owing to sampling difficulty in the field, and the correlation therefore depends only on field identification.
- (c) It may be argued that the Kullen chill zone was developed in contact with sediments, and that the Grunehogna sill subsequently intruded between the Kullen sill and the sediments.

Contact relationships of the Kullen sill show much less evidence for intrusion into wet, unconsolidated sediments than the Grunehogna sill does. Along the upper contact of the Kullen sill with overlying Schumacherfjellet sediments south of peak 1390 the only thermal effects on the sediments is possibly minor evidence of baking. It appears that the Kullen sill intruded lithified sediments in this area. However, at Kullen peak a contact zone is present between the upper contact of the Kullen sill and Högfonna sediments. This zone is very similar in thickness and field characteristics to the one described at the southeast outcrops at nunatak 1285, adjacent to the Grunehogna sill. A mixed zone of quartz diorite pegmatite, granophyres and granosediments overlies the Kullen sill at Caughtout Ridge. It is therefore possible that the Kullen sill intruded subsequent to the Grunehogna sill when Schumacherfjellet sediments were already lithified, but Högfonna sediments were still unconsolidated or only partially lithified. These conclusions present a paradox in respect of the Rb-Sr isochron ages, which has not been solved to date, but, if there has been reaction between sills and sediments, then Rb-Sr data may well reflect incomplete rehomogenization.

7. Effects of intrusion into a water-saturated system

Both the Kullen and Grunehogna sills have been affected in various ways and degrees as a consequence of intrusion into a water-rich environment. It is likely that primary crystallization of ilmenite and haematite in the Grunehogna sill resulted from a high oxygen fugacity in the magma. The major source for increasing oxygen content of magmas is considered to be H_2O (Osborne, 1959; Hamilton et al., 1964; Burnham et al., 1969; Burnham and Davis, 1971), and it is therefore suggested that the departure from the crystallization path in the Grunehogna magma compared to the Kullen sill is a result of incorporation of water into the magma.

Enrichment of volatiles in the magma due to crystallization of the early formed phases led to the formation of small volumes of pegmatites in the upper parts of the Kullen sill, and probably to a certain amount of deuteric alteration. However, it is unlikely that this simple mechanism alone would have been responsible for the extensive alteration found throughout the sill. Based on the evidence presented and the discussion above it is suggested that the Kullen sill intruded after the Grunehogna sill, and enhanced an active hydrothermal convection system which had been established in the overlying sediments. A large number of authors have described similar effects at mid-ocean spreading centres and other intrusions, such as Skaergaard, and have shown that extensive subsolidus hydrothermal alteration of sills occurs when the hydrothermal liquids enter the solidified intrusions at temperatures in excess of $400^{\circ}C$ (eg. Taylor, 1974, 1979; Menzies and Seyfried, 1979; Taylor and Forrester, 1979; Einsele et al., 1980; Stakes and O'Neil, 1982; Einsele, 1985; Lonsdale and Becker, 1985). It is likely that the extensive alteration of the Kullen sill occurred as a result of similar hydrothermal action.

It may be argued that the alteration resulted from regional greenschist metamorphism, or alternatively as a result of extensive autometasomatic alteration such as described in the Kap Edvard Holm complex in Greenland (Elsdon, 1982). These possibilities have to be considered as serious alternatives to the model proposed above, but it is believed that the circumstantial evidence presented here favours the hydrothermal model. Hydrothermal convection associated with the Kullen and Grunehogna sills would have had two further important consequences. The first is that elements such as copper may have been scavenged from sediments and redeposited within the convection system. The green staining by atacamite in the upper parts of the Grunehogna sill and its contact zones may be the result of such hydrothermal action. The second consequence is that Rb-Sr isotope systematics may have been affected. Menzies and Seyfried (1979) have shown experimentally that Sr is removed from seawater during interaction with basalt glass. The Sr isotopic composition of the glassy basalt was increased from an initial $^{87}\text{Sr}/^{86}\text{Sr}$ value of 0.70260 to values between 0.70512 and 0.70842. Partial or incomplete isotopic equilibration in sills could therefore result in the generation of errorchrons or false isochrons.

8. The status of the Grunehogna granites.

The Grunehogna granites are intrusive into the Kullen sill, and are therefore the youngest intrusive rocks in the area, excluding the Jurassic (?) dykes. They are similar in hand specimen and petrography to the small-scale granitic bodies which represent fusion products in the contact zones associated with the Grunehogna sill. Barton and Copperthwaite (1983) report an Rb-Sr whole rock isochron age of 1008 ± 11 Ma for the Grunehogna granites. It is difficult to interpret the significance of this age, as the granites show extensive deuteric (?) alteration and epidotization. The isochron age may

thus represent a younger epidotization or metamorphic event, and not the age of intrusion.

The relationships of these rocks to the Borgmassivet intrusions are therefore still unclear, and further geochemical and isotope work on selected phases (such as granophyric intergrowths) will be required to resolve these problems.

VI CONCLUSIONS

The following model is proposed for intrusion of the Grunehogna and Kullen sills:

- (i) The Grunehogna sill intruded water-saturated, unconsolidated or partially lithified sediments of the Schumacherfjellet and Högfonna Formations, at shallow levels of less than, or at 0.3 kilobar.
- (ii) Large-scale, soft sediment slumping occurred where the sill transgressed sediments. Stoped sediments were similarly affected by soft-sediment deformation, and contributed small amounts of H_2O and possibly other volatiles to the Grunehogna magma.
- (iii) Heat flow from the magma was high enough to establish well-defined contact zones in which thermal effects included
 - (a) boiling of water, which resulted in partial destruction of sedimentary structures; (b) development of vugs; (c) fusion of sediments and small-scale mobilization of fused products, which crystallized as granitic veins and small granitic and granophyric bodies; and (d) development of high-temperature, low-pressure chlorite-haematite-albite-epidote-sphene assemblages.

- (iv) Addition of small amounts of water to the Grunehogna magma resulted in higher oxygen fugacities and primary crystallization of ilmenite and magnetite in the more evolved part of the Grunehogna sill. Owing to the higher volatile content of the Grunehogna magma, large volumes of mafic pegmatites were the final products of crystallization.
- (v) The Kullen sill post-dates the Grunehogna sill, and intruded when the Schumacherfjellet sediments were lithified, but Högfonna sediments were still unconsolidated or partially lithified. Contact thermal effects in Högfonna sediments were similar to those of the Grunehogna sill, but on a smaller scale. Contact effects on the Schumacherfjellet sediments were limited to recrystallization of existing minerals.
- (vi) Extensive subsolidus alteration of the Kullen sill is a result of hydrothermal alteration by circulating fluids in a hydrothermal convection system. This system was initially generated by the intrusion of the Grunehogna sill and enhanced by intrusion of the Kullen sill.
- (vii) The presence of corroded quartz grains in both sills may indicate reaction of magmatic quartz with deuteritic/hydrothermal fluids. An alternative is that these grains are xenocrysts derived by contamination of the magma by sediments.
- (viii) A study of fluid inclusions and stable isotope compositions of the sills and their wall rocks will make significant contributions to the understanding of the Grunehogna intrusive environment and effects on the evolution of the magmas.

CHAPTER 5 KRYLEN NUNATAK

I. Introduction

Krylen nunatak was visited in 1960 by von Brunn and la Grange (Von Brunn, 1963, 1964), and subsequently two brief visits were made during the 1980/81 and 1983/84 field seasons. Ten samples of the Borgmassivet intrusions, one of a Jurassic (?) dolerite dyke and one of a felsic dyke, were collected for isotope analyses along the upper 30 m of this nunatak. These samples were analyzed for major and trace elements during the current project. A further eight samples, collected during 1983/84, have been used for petrographic descriptions. Owing to the limited field work and small geochemical data base, this nunatak is described briefly, but very few inferences on the petrology and petrogenesis of the intrusions can be made. The geochemical data will be used for regional comparisons (Chapter 7).

II. Geology

Approximately 200 m of the Borgmassivet intrusions at Krylen are exposed along the north face of the nunatak. No contacts with country rocks have been observed. The lower exposed 150 m of the outcrop consist of light-grey, medium-grained gabbro-norite. Poorly-defined igneous laminations, defined by variations in the proportions of plagioclase and pyroxene in the rocks, can be recognized in places. The upper 50 m of the nunatak consist of grey to dark-grey quartz diorite, in which extensive alteration of plagioclase and pyroxene has occurred. A mela-olivine gabbro-norite layer, approximately 5 to 10 m thick, occurs about 15 m below Krylen peak within the upper zone.

A 50 cm-thick vertical felsic dyke and a 1 m-thick vertical dolerite dyke, trending 161° and 154° respectively, occur in the eastern part of the outcrop.

III. Petrography

A. The gabbronorite

The gabbronorites have a granular to seriate texture, composed of plagioclase, orthopyroxene, clinopyroxene, inverted pigeonite, quartz, Fe-Ti oxides and biotite. The textures and petrographic features of these rocks show much similarity to the Juletoppane gabbronorites (Chapter 2).

The plagioclase occurs as subhedral laths, which vary in size from 50 by 100 micron to 0.5 by 1.0 mm. They are strongly zoned from approximately An_{70} in the cores to An_{35} in the mantles. The plagioclase in the lowest exposures show little alteration, but higher in the sequence sericitization and saussuritization increase progressively.

Inverted pigeonite-orthopyroxene relationships are the same as at Juletoppane, i.e. the crystallization sequence orthopyroxene-pigeonite-orthopyroxene can be recognized as discussed in Chapter 2. The major difference compared with the Juletoppane rocks is that plagioclase is rarely enclosed in the composite orthopyroxene-pigeonite grains. Subhedral orthopyroxene laths are locally present, which also do not contain plagioclase inclusions. Although these laths may represent cumulus grains, no unequivocal cumulus textures have been recognized.

Clinopyroxene occurs as anhedral, stubby laths, up to 0.6 mm in diameter. In places they are interstitial to plagioclase, but in most cases their relationship with plagioclase and the Ca-poor pyroxenes defines a granular texture. No ophitic textures were found. Uralitization of the pyroxenes increases at the base of the outcrop, upwards.

Quartz is interstitial to plagioclase and the pyroxenes as single, anhedral grains, or as micrographic intergrowths with alkali feldspar. The micrographic intergrowths increase in abundance upwards in the outcrop. The Fe-Ti oxides form skeletal to poikilitic textures, with inclusions of biotite, quartz, and the primary minerals. Biotite occurs as mantles around the oxide grains in most cases. Minor amounts of chlorite are locally developed throughout the rocks.

B. The Quartz Diorite

The upper 50 m of the outcrop consist of altered granular, to seriate, to porphyritic granophyric quartz diorite. The plagioclase laths are up to 0.4 by 1.2 mm. Most of them have been saussuritized, extensively, but locally partially altered grains are present, which have compositions of less than An_{50} in their cores. Most of these grains are strongly zoned to An_5 in the mantles.

The pyroxenes have been uralitized extensively and Ca-poor pyroxenes cannot be distinguished from clinopyroxene. These uralitized grains are about 0.8 by 1.2 mm, but some phenocrysts may be up to 1 by 4 mm. The phenocrysts enclose plagioclase laths, defining subpoikilitic textures.

Abundant very fine-grained micrographic and granophyric intergrowths are interstitial to plagioclase and pyroxene. They define textures similar to those in the upper parts of the Kullen sill (Chapter 4), i.e. strained quartz grains grade into the intergrowths. They may thus represent xenocrysts, as discussed in Chapter 4. Fe-Ti oxides show extensive alteration to leucoxene, and trellis patterns are common. There is very little biotite in these rocks, most of the mineral occurring as narrow fringes to the Fe-Ti oxides. Apatite, occurring as needles, is a common accessory mineral, and chlorite is present at an alteration product of pyroxene. Chlorite also occurs in radiating fans, which are interstitial to quartz grains and granophyric intergrowths.

C. Mela-Olivine Gabbro-norite

The mela-olivine gabbro-norite within the upper zone consists of small (0.3 mm) olivine grains enclosed in clinopyroxene, which locally define subophitic textures, radiating plagioclase laths, orthopyroxene, chromite, Fe-Ti oxides and phlogopite.

Plagioclase laths are up to 0.1 by 0.6 mm in size and are saussuritized. Orthopyroxene has been uralitized and sericitized extensively. Clinopyroxene grains have been uralitized and locally replaced by phlogopite/biotite, whereas olivine grains have been serpentinized in places. The chromite grains are rarely larger than 20 to 30 micron in diameter and occur enclosed in olivine or in orthopyroxene. Fe-Ti oxide grains are enclosed in phlogopite/biotite, but show no further evidence of alteration.

D. The Felsic Dyke

A sample of felsic dyke from the north face of Krylen has a granular anhedral aplitic texture and consists of quartz, albite, microcline microperthite and albite with minor amounts of chlorite, sphene, epidote and zoisite/clinozoisite. Zircon and apatite are rare constituents in this rock. In general the rock is even-grained, with most grains about 0.5 mm in diameter, but there are locally finer grained patches of albite in which individual grains are about 2.5 mm in diameter. Concentrations of epidote and sphene are associated with these finer-grained patches. Quartz has been embayed partly to extensively by albite and microcline microperthite in a similar fashion as the granosediments described in Chapter 4.

Felsic material found as float at the top of Krylen nunatak is a fine-grained granular, anhedral rock consisting of quartz, K-feldspar and albite in which individual grains are less than 60 micron in diameter. The texture is very similar to the micro-aplites described in the granosediments at Grunehogna (Chapter 4). Fe-Ti oxides define narrow laminations, which are emphasized by small variations in grain size in different laminae. Zircon and sphene are minor constituents in this rock.

IV. Geochemistry

Geochemical data for individual samples from the upper 50 m of Krylen nunatak are given in Appendix 2. Table 5.1 summarizes statistical data of the geochemistry of these samples, excluding the felsic and dolerite dykes. If sample K11/81, the mela-olivine gabbro-norite, is excluded, the rocks show narrow ranges in element compositions, except for Zn and Cu. The inclusion of K11/81 results in much greater variation, particularly in Mg-number and Ni and Cr contents, as shown in Table 5.1.

V. Conclusions

The limited evidence presented above suggests that the Borgmassivet intrusions at Krylen show a number of similarities with the intrusions at Juletoppane, but much more detailed studies are required in order to determine the petrogenesis and detailed relationships to Borgmassivet intrusions elsewhere. The felsic dyke described above shows petrographic and geochemical similarities to the granosediments of Grunehogna, and may represent a rheomorphic dyke derived from Ritscherflya sediments. However, this possibility should also be tested much more rigorously before any firm conclusions are made.

CHAPTER 6 THE JEKSELEN SUBVOLCANIC COMPLEX

I. Introduction

Jekselen nunatak (Figure 1.2) is situated about 11 km east of Grunehogna (Chapter 4), and was visited briefly during the 1980/81 and 1983/84 field seasons. Ten samples from a 70 m section along the upper parts of the southeastern end of the nunatak were analysed for major and trace elements and studied petrographically. These analyses represent only a small part of the nunatak, and will be used for comparison with the regional data discussed in Chapter 7. Hence, aspects of the field relationships, petrography and geochemistry are described below, but few conclusions can be drawn.

II. Geology

The geology of Jekselen was first described by Neethling (1964) and Vaclavik (1971), neither of whom did any detailed mapping. Bredell (1976, 1982) mapped the nunatak and reinterpreted the geology of the area. Ferreira (1986) studied the sedimentary rocks of the Jekselen Formation in detail. The description below is based, in part, on the work of the latter two authors, and partly on the field work conducted during the current project.

A. The Jekselen Formation

The Jekselen Formation consists of large "rafts" or xenoliths which occur in the intrusive rocks in the upper parts of Jekselen nunatak. They appear to be isolated from one another, as the dips of the individual xenoliths vary considerably from about 50°(NW) to 65°(E). Neethling (1964) and Vaclavik (1971) interpret these sediments as downfaulted blocks. Vaclavik also

suggests that they have been folded, but the author concurs with Bredell (1976, 1982) and Ferreira (1986) that the Jekselen Formation is preserved as disoriented xenoliths, based on intrusive relationships discussed below.

The sediments comprise mudclast breccias and extraformational, jasper-bearing conglomerates at the base of sandstone layers. These latter rocks comprise quartz arenites and rare graywacke units. Silt and mudstones are subordinate. Planar cross-bedding is the most common sedimentary structure. Horizontal laminations and small-scale ripple marks, wavy lamination, current ripples and load structures are locally present.

Ferreira (1986a, 1986b) considers the depositional history of the Jekselen and Högfonna Formations to be similar, (Chapter 4), apart from a greater maturity of the sediments in the Jekselen Formation. He suggests that the Jekselen Formation was deposited in a low sinuosity braided channel environment. However, this can only be considered as a tentative model, owing to the absence of an undisturbed sedimentary succession.

B. The Jekselen Subvolcanic Complex

An approximately 300 m-thick section of the Complex is exposed at Jekselen. The base of the intrusion lies at an unknown depth below the snow line, but the upper contact with the sediments of the Jekselen Formation is exposed at various localities in the southeastern outcrops.

Bredell (1976, 1982) recognizes a continuous upward gradation from "plutonic" (medium- to coarse-grained) through "hypabyssal" to "volcanic" rocks, and divides the exposed section of the intrusion into five zones, namely the plutonic zone in the lowermost exposures, which is overlain by the plutonic-

hypabyssal transition zone, the hypabyssal zone, the hypabyssal-volcanic transition zone and the volcanic zone. Bredell's terms "plutonic", "hypabyssal" and "volcanic" are not appropriate, because they refer to textural changes within the same intrusive body and the usage of the term "volcanic" to denote fine-grained rocks in an intrusion is considered to be incorrect. Furthermore, the two transition zones, each about 5 to 10 m thick, reflect gradational textural changes within this intrusion, and should not be considered as separate zones. For the purpose of this discussion the medium- to coarse-grained rocks will be termed Zone I, the overlying medium-grained rocks Zone II, and the upper, fine-grained rocks which contain amygdalae, Zone III.

Zone I

An estimated 150 to 200 m of this zone is exposed at Jekselen. It consists of medium- to coarse-grained quartz diorite, quartz monzodiorite and locally granodiorite. The variation in composition defines a crude horizontal, lenticular layering, in which individual layers vary from 15 cm to 3 m in thickness. In places epidote occurs as a minor constituent, disseminated through the rock. Quartz, carbonate and epidote occur abundantly along joint surfaces, and epidote lenses are abundant. Bredell (1976) reports green copper carbonate staining and small amounts of limonite in some joint fillings.

Near the lowest exposed part of Zone I plagioclase and pyroxenes occur as stubby laths, but at higher stratigraphic levels both minerals become bladed, and, in parts, coarse-grained to pegmatitic. Near the contact with Zone II

lenses of fine- to medium-grained quartz diorite appear, which locally contain small amounts of disseminated sulphide, identified in hand specimen as pyrite and, rarely, chalcopyrite.

Zone II

Zone II consists of medium- to fine-grained quartz monzodiorite and quartz diorite, which contain bladed and acicular phenocrysts of clinopyroxene (identified as pigeonite by Bredell, 1976), showing no preferred orientation. Near the base of the Zone are coarse-grained lenses of quartz monzodiorite, but no further layering is encountered upwards. However, Bredell (1976) recognizes a lower subzone consisting of quartz monzodiorite and an upper quartz diorite subzone. Phenocryst lengths in the lower subzone are 8 to 10 mm in length, and 2 to 4 mm in the upper subzone.

Zone III

This zone consists of fine-grained porphyritic quartz andesite. Small, spheroidal amygdales from 1 to 5 mm in diameter, appear at the base of the zone. The amygdales increase upwards in frequency and size (up to 10 mm in diameter), concomitant with a reduction in grain size of both matrix and phenocrysts. In a zone about 1 m-thick along the contact with the Jekselen Formation the amygdales are up to 70 mm in diameter.

Contact Relationship between Zone III and the Jekselen Formation

The Jekselen Complex is intrusive into the Jekselen Formation. In places it transects the bedding of the sediments and a number of apophyses have been observed. An apophysis in the southeastern Jekselen protrudes about 8 m into the

Jekselen sediments, and has a marked concentration of amygdales along the contacts. In places the contact is sharp, with little apparent disturbance, but along most contacts the sediments and the intrusion have been brecciated. Numerous small (< 5 cm to 1 m) sedimentary xenoliths occur within parts of a 3 m-thick zone in the intrusive rocks, and locally there is intimate mixing of magma and sediment, resulting in a contorted, laminated rock (Figure 6.1).

III. Petrography

One sample from the lowermost exposures of Zone I was examined in thin section. It is a medium-grained granular to porphyritic, granophyric quartz monzodiorite, consisting of extensively uralitized clinopyroxene, sericitized and saussuritized plagioclase, anhedral quartz grains, granophyric intergrowths of quartz, plagioclase and alkali feldspar, and Fe-Ti oxides. Epidote occurs in minor quantities and apatite is commonly present as an accessory mineral.

The clinopyroxene varies from stubby laths of 0.4 by 0.8 mm, to phenocrysts of 0.8 by 4 mm. These laths have very irregular borders, and some contain cores of chlorite. Plagioclase is present as small laths, less than 1 mm in length, but the mineral has been altered to such an extent that its composition cannot be determined.

Quartz grains are strongly embayed and xenocryst textures such as those described in the Kullen sill (Chapter 4) are common, i.e. strained quartz grains grade into granophyric and micrographic intergrowths with plagioclase and K-feldspar.



Figure 6.1 Contortions in sediment-contaminated contact zone rock in the Jekselen complex.

The Fe-Ti oxides are very irregular in outline, are altered to leucoxene and exhibit trellis patterns. Small cubes, approximately 30 micron in diameter, are present locally, and are thought to be goethite and limonite pseudomorphs after pyrite.

Samples through the 50 m of Zone III have less K-feldspar and micrographic intergrowths are not as common as in the sample from Zone I. The Zone III rocks all contain quartz amygdales, but there is little evidence in thin section to suggest a regular increase in their size. At the base of this zone, they are less than 1 mm in diameter, and towards the centre of the zone the amygdales are about 0.5 mm. In the upper part they are up to 1.5 mm in diameter, but, as reported in the field description, they may be up to 70 mm along the upper contact. At the lowest level of the zone they are mantled by chlorite, but upwards in the succession only quartz is present in the amygdales.

Skeletal, or hopper-type, clinopyroxene needles form mantles to serpentine cores throughout the sampled section (Figure 6.2). These composite crystals are up to 1 mm wide and 4 mm long. The lengths do not appear to vary in size throughout the zone, but width decreases to less than 0.6 mm near the top of the zone. Inclusions of plagioclase occur abundantly in the composite crystals. Bredell (1976, 1982) identifies the clinopyroxene as pigeonite, but the mineral has a $2V$ of 30 to 35°, hence it is identified as augite. Plagioclase laths have been saussuritized and sericitized extensively. In places they form poorly-defined radial structures. Quartz occurs interstitially to plagioclase and clinopyroxene. The mineral is highly embayed, but granophyric and micrographic textures are much less common than in Zone I.

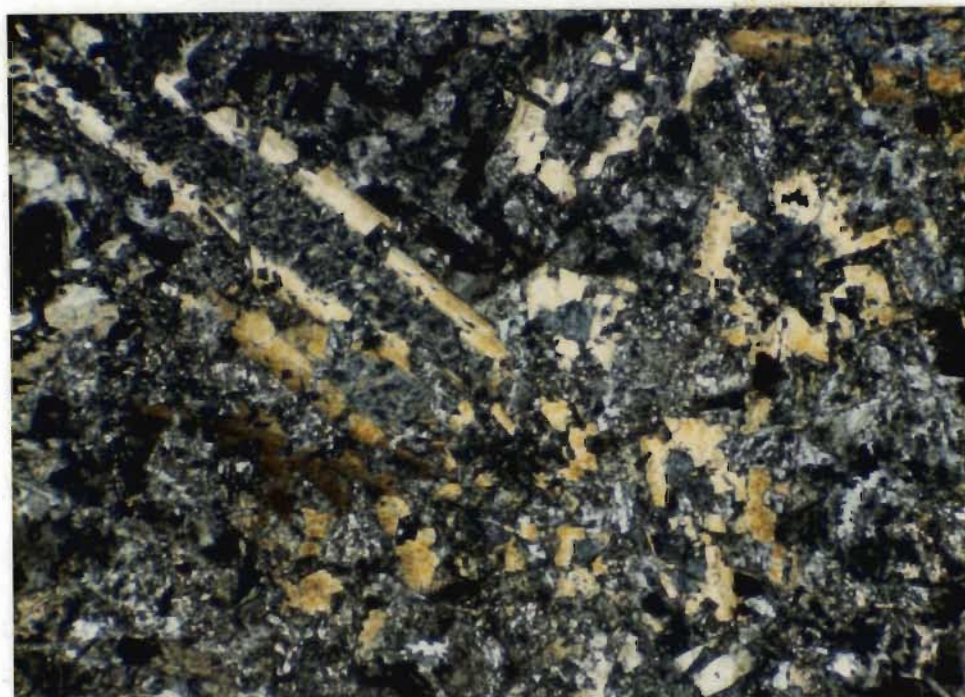


Figure 6.2 Photomicrograph of hopper-type clinopyroxene mantles over serpentine cores in Zone III of the Jekselen Complex. Crossed polars.

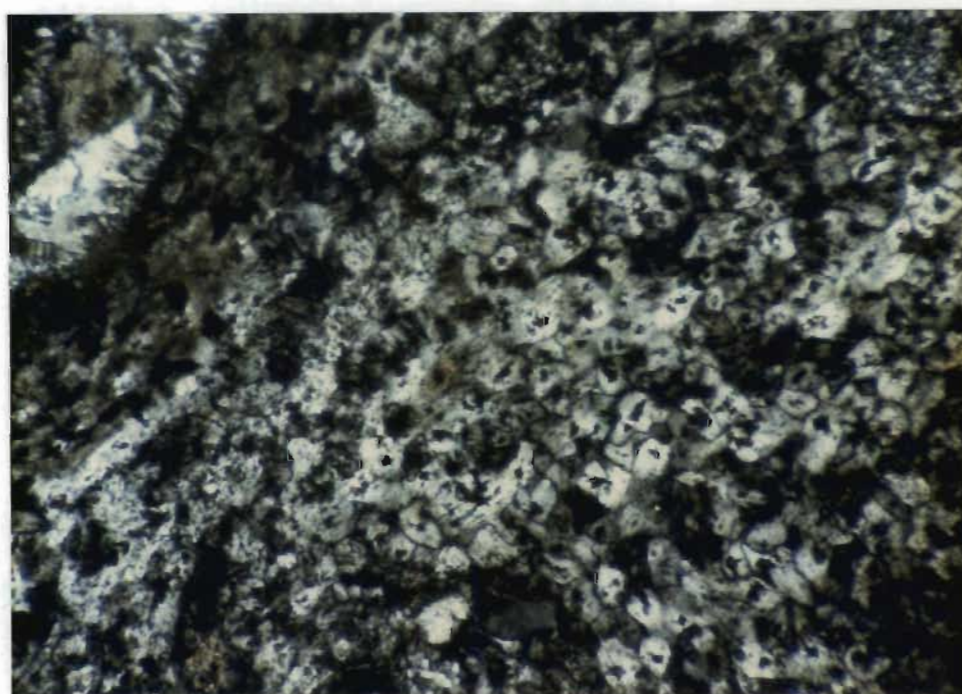


Figure 6.3 Photomicrographs of polygonal shapes with cores of Fe-Ti oxides in devitrified glass (?), Zone III contact zone, Jekselen Complex. Crossed polars.

Patches of devitrified glass occur throughout the zone, but increase markedly in amount upwards. The glass is cloudy and contains a fine dusting of opaque minerals. Slender, curved needles of plagioclase form fans or "horse's tail" textures, or locally festoon-type concentrations.

The zone has a fine-grained selvage, probably representing devitrified glass (intimately mixed with sedimentary material) where it is in contact with the Jekselen Formation. The sediments show extensive evidence of partial melting along quartz grain boundaries. These grains have complexly embayed margins along which occurs very fine-grained, micro-aplitic material texturally similar to that in the granosediments at Grunehogna (Chapter 4). The devitrified glass (?) consists of numerous polygons of fine, felty material. Each polygon has a core of an altered Fe-Ti oxide (Figure 6.3). It has not been established whether this devitrified glass represents a buchite derived from the sediments (Tomkeieff, 1940) or a glass derived from the magma.

Samples from the apophyses intruding the sediments have similar textures as Zone I, except that quartz is less common in the matrix and some serpentine may be pseudomorphic after olivine.

IV. Geochemistry

Major and trace element data for samples from Zone III and apophyses intruded into the Jekselen formation are given in Appendix 2. Statistical data are summarized in Table 6.1, which excludes sample J13/81, a sedimentary xenolith from one of the apophyses.

The rocks show a moderate range in SiO_2 (55.12 to 57.35) and Mg-number (55.16 to 59.27). The most striking feature of the data is the large range of Na_2O (1.65 to 5.61), K_2O (0.16 to 4.03), Sr (173 to 399), Rb (9 to 89) and Ba (109 to 1581) associated with the small variation in SiO_2 and Mg-number. The Jekselen geochemical data will be discussed further in comparison with the regional geochemistry of the Borgmassivet intrusions (Chapter 7).

V. DISCUSSION AND CONCLUSIONS

The intrusive nature of amygdaloidal rocks at Jekselen suggests that intrusion occurred at subvolcanic levels. The formation of gas bubbles in a magma depends on a number of variables, e.g. pressure, composition and temperature of the magma, and composition and concentration of the volatile phases present, which all affect the solubility of the volatiles (e.g. Fisher and Schmincke, 1984). The actual loss of H_2O and S volatiles by vesiculation in ocean-floor tholeiites occurs only at water depths less than 200 m (Moore and Schilling, 1973), although they exsolve slowly from cooling pillow interiors. Andesitic magmas are more viscous than basalts (Clark, 1966), but these magmas have higher water contents (Fischer and Schmincke, 1984). Therefore, with the limited evidence available it is not possible to determine accurately the level of intrusion for the Jekselen Complex, but qualitatively it can be stated that intrusion occurred at very shallow levels, probably less than 100 m below the surface.

The intimate mixing of magma and sediment along the upper contact of the intrusion and the large amounts of granophyric and micrographic intergrowths described in Zone I are evidence for extensive contamination of the Jekselen magma. This possibility is supported by the quartz textures described in this zone, which have been interpreted in the Kullen sill to represent xenocrysts

derived from sedimentary material. Oxburgh and McRae (1984) have shown that xenoliths sinking in a magma may be assimilated extensively, resulting in very marked changes in magma composition. Furthermore, the petrographic features in Zone I, including the presence of devitrified glass, amygdales, and clinopyroxene needles mantling chlorite and serpentine, in association with the contamination features and presence of sulphide minerals, suggest that the Jekselen Complex may be similar in its reactivity with its country rocks to the so-called Effingham-type dolerites described by Frankel (1969) and Absolom (1970). A detailed study of the Jekselen Subvolcanic Complex is therefore likely to contribute considerably to an understanding of assimilation processes in tholeiitic magmas.

SECTION C

REGIONAL GEOCHEMISTRY AND SYNTHESIS

CHAPTER 7 REGIONAL GEOCHEMISTRY

I. Introduction

All the Borgmassivet intrusions at selected nunataks in the Ahlmannryggen and Giaeverryggen are SiO_2 -rich tholeiitic rocks which have a number of geochemical similarities. Evidence for synemplacement contamination of magmas has been presented for the Grunehogna and Kullen sills and Robertskollen and Jekselen Complexes (Chapter 4). It is possible that the high SiO_2 and quartz content of the Annandagstoppane intrusions represent similar contamination. A comparison of the geochemistry for the different intrusions and the Straumsnutane basalts is presented in this chapter and a model for intrusion during the final stages of deposition in the Ritscherflya basin is proposed.

Major and trace element data are given in Appendix 2, including data on 176 Straumsnutane basalts and REE, Hf and Th analyses of selected samples from the Borgmassivet intrusions and Straumsnutane basalts supplied by Dr B.R. Watters of the University of Regina (pers. comm., 1985). Geochemistry of selected samples from the Lüneberg area in the Kaapvaal craton was supplied by R.G. Smith (pers. comm., 1986).

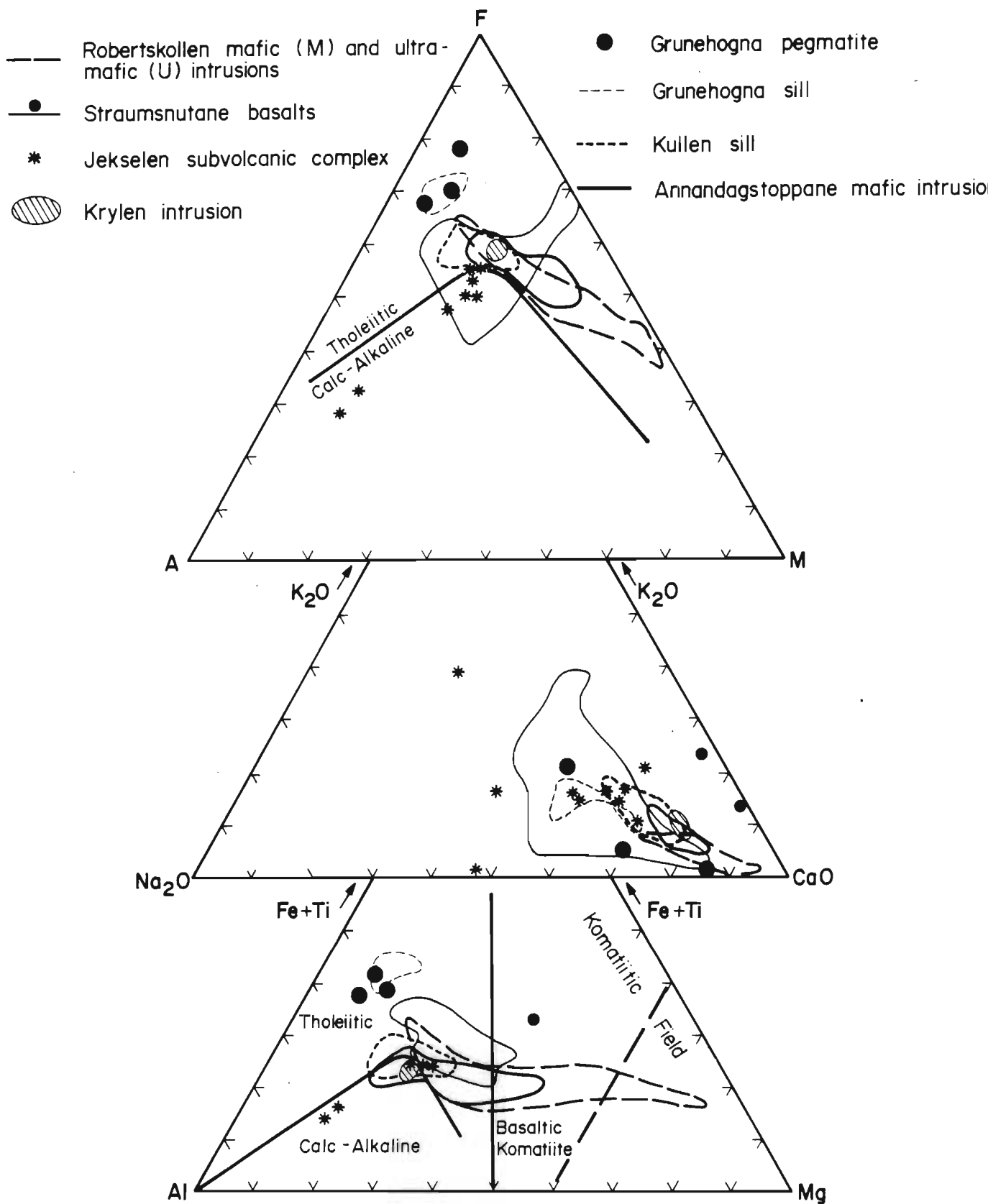


Figure 7.1

Ternary geochemical variation diagrams of Borgmassivet intrusions and Straumsnutane basalts.

(a) AFM diagram ($Na_2O + K_2O$ - total Fe as FeO - MgO ; boundary after Irvine and Barager (1971).

(b) K_2O - Na_2O - CaO diagram in weight per cent.

(c) Jensen diagram in cation proportions (Jensen, 1976).

Legend: lines enclose fields for different intrusions or lavas. Jekselen Complex indicated by stars. The smaller dots indicate basalts which plot outside the main basalt field.

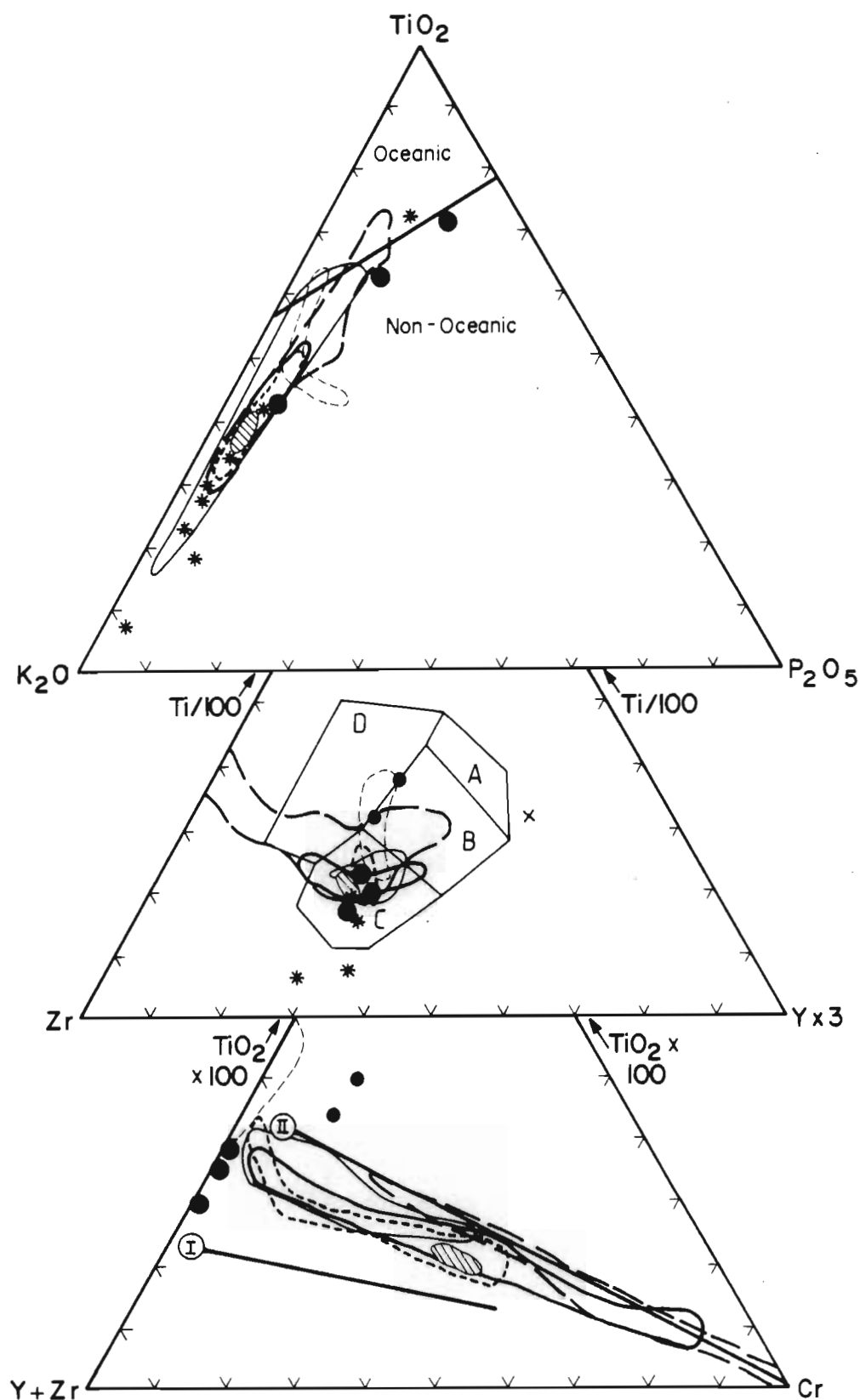


Figure 7.2

Ternary geochemical variation diagrams of Borgmassivet intrusions and Straumnsnutane basalts.

(a) TiO_2 - K_2O - P_2O_5 diagram (Pearce et al., 1975).

(b) $\text{Ti}/100$ - Zr - 3Y diagram (Pearce and Cann, 1973)

A: Low-K tholeiites; B: Ocean-floor basalts; C: Calc-alkali basalts; D: Within-plate basalts; X: Anomalous samples from Annandagstoppane.

(c) 100 TiO_2 - $(\text{Y} + \text{Zr})$ - Cr diagram (Davies et al., 1979). I: Archaean calc-alkaline trend; II: Archaean tholeiitic trend.

Legend as for Figure 7.1.

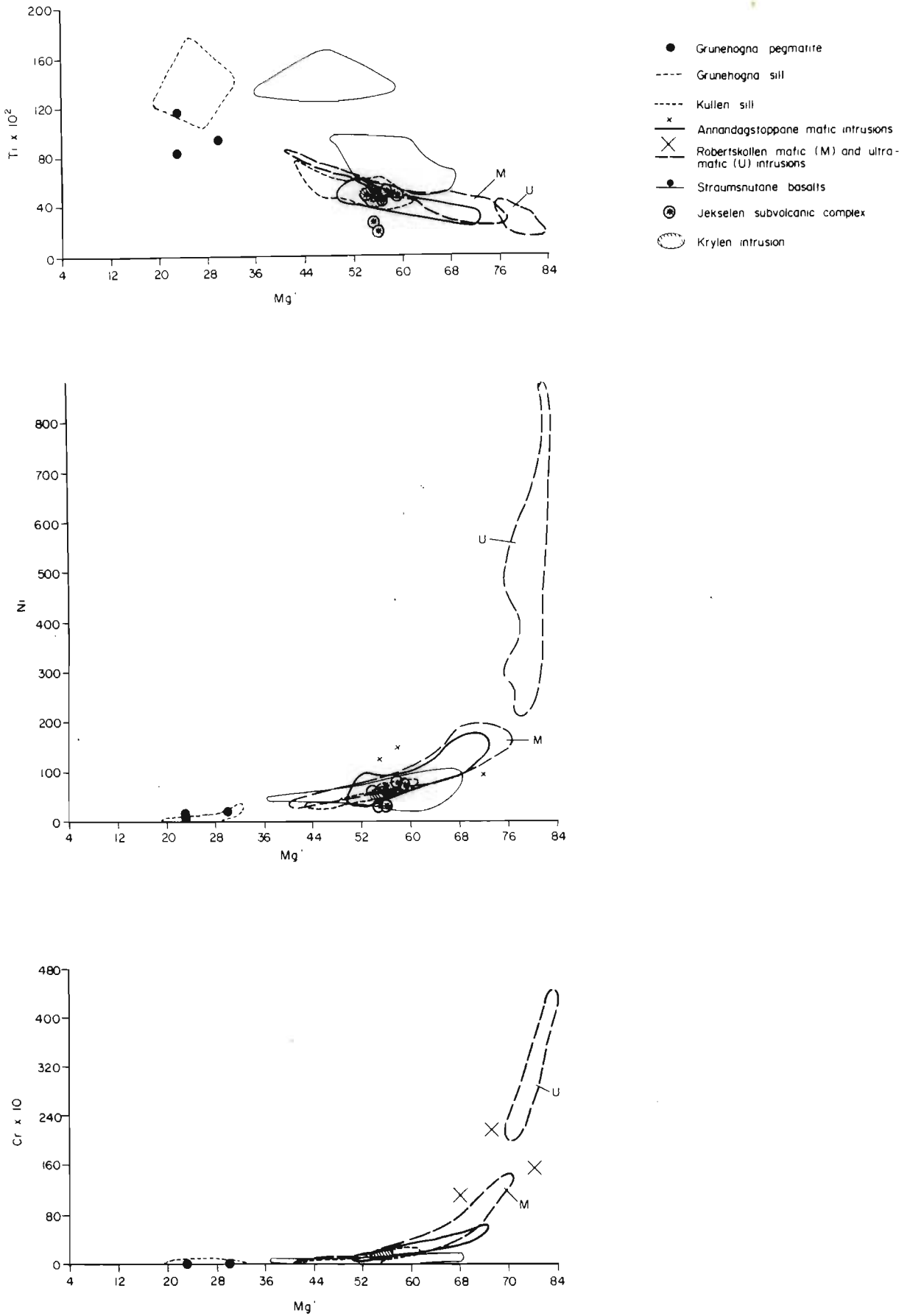


Figure 7.3 Ti, Ni and Cr variations with Mg-number ($Mg/(Mg + Fe^{2+})$) of Borgmassivet intrusions and Straumnsnutane basalts. Symbols for Annandagstoppane intrusions and Straumnsnutane basalts indicate values plotting outside the geochemical fields for these rocks.

II. Regional Geochemical Variation

A. Major and Trace Elements

Fields defined by interelement variations of compatible and incompatible elements of the Borgmassivet intrusions and Straumsnutane basalts overlap extensively (Figures 7.1, 7.2 and 7.3). The most primitive rocks examined are from the Robertskollen Ultramafic Unit, and the most evolved occur in the Straumsnutane basalts at nunataks Snökallen and eastern Trolljkeppiggen (Watters, pers. comm., 1985). These latter basalts, named here the Snökallen lavas, are characterized by high incompatible element (TiO_2 , P_2O_5 , Nb, Zr, Y and Cu) and low MgO contents compared to the rest of the Straumsnutane basalts.

Ternary variation diagrams (Figure 7.1)

Variation on the AFM diagram defines a well-constrained tholeiitic trend among the intrusive rocks, except the Jekselen samples, which plot in the calc-alkaline field. These latter samples apparently define a marked alkali enrichment trend, with concomitant depletion of Fe, and to a lesser extent, of Mg. The two samples with highest alkali contents are contaminated by sedimentary material as described in Chapter 6. The Straumsnutane basalts show considerable scatter from alkali-poor rocks in the tholeiitic field to samples with slightly enriched total alkalis which plot in the calc-alkaline field. The relative lack of variation within the intrusive rock series and the scatter of the Jekselen and Straumsnutane samples are further emphasized in the $\text{K}_2\text{O} - \text{Na}_2\text{O} - \text{CaO}$ diagram of Figure 7.1.

Variation in the Jensen cation diagram (Jensen, 1976) extends from the komatiitic field for the Robertskollen Ultramafic Unit to the tholeiite field for most of the intrusive rocks, with some overlap into the calc-alkaline field. The Straumsnutane basalts and Grunehogna sill are enriched in Fe + Ti relative to the other intrusive rocks. The two contaminated samples from the subvolcanic Jekselen intrusion, which are enriched in Al, plot within the calc-alkaline field.

Ternary diagrams using the incompatible elements K, Ti, Zr, Y and P, and the compatible element Cr have been used elsewhere to identify the tectonic setting of extrusive rocks (Pearce and Cann, 1973; Pearce et al., 1975; Davies et al., 1979). Field relationships discussed in Chapters 2, 4 and 6 indicate that the Borgmassivet intrusions are continental tholeiites. The ternary diagrams in Figure 7.2 confirm this conclusion and emphasize the similarity in geochemistry of the different intrusions and Straumsnutane basalts. The Borgmassivet intrusions and Straumsnutane basalts plot in the calc-alkali basalt and ocean-floor basalt fields on the Ti - Zr - Y diagram, which therefore appears to be anomalous. However, Holm (1982) points out that continental tholeiites also plot within these two fields. It is only the low-K tholeiites, ocean-floor basalts, calc-alkali basalts, ocean-island basalts and within-plate alkalic basalts which can be differentiated with the aid of this diagram.

Two-component variation

Examples of two-component regional variation are given in Figures 7.3 and 7.4. Incompatible element variation with Mg-number ($\text{Mg}/(\text{Mg} + \text{Fe}^{2+})$) shows enrichment of the incompatible elements (example being Ti in Figure 7.3) in the Straumsnutane basalts and Snökallen lavas compared with the intrusive

rocks at comparable Mg-numbers (between $Mg' = 37$ and 69). The compatible elements vary sympathetically with Mg-number as shown in the Ni and Cr diagrams (Figure 7.3). Examples of interelement variation among the incompatible elements are depicted in Figure 7.4, which shows a high degree of correlation and overlap of the different fields. Incompatible element correlations are summarized in Table 7.1. Most rock types show coherent trends with respect to the incompatible trace elements. The Grunehogna sill, the Jekselen samples and the Straumsnutane samples deviate from the general trend with respect to Ti and Zr. However, P_2O_5 , Sr, K_2O , Rb and Ba contents of the basalts scatter considerably on the variation diagrams. The examples of P_2O_5 and Sr are shown. Sr, K, Rb and Ba are highly mobile during surface alteration processes (e.g. Cann, 1970; Kay et al., 1970; Pearce and Cann, 1973; Pearce, 1975; Pearce et al., 1975; Wood et al., 1976; Davies et al., 1979). The work of Watters (1969a, 1969b, 1972, pers. comm., 1985) has shown that the Straumsnutane basalts have undergone post-extrusion alteration processes such as low-grade metamorphism, epidotization and probably some degree of weathering, and the scatter of Sr, K_2O , Rb and Ba contents on variation diagrams is to be expected. However, the variation in P_2O_5 is surprising in view of the work of Pearce et al. (1975) and Winchester and Floyd (1976) who have found that phosphorus is essentially immobile during metamorphism. If X_{CO_2} is significant in metamorphic fluids, high field strength elements may be mobile (Murphy and Hynes, 1986), but in view of the apparent variation in P_2O_5 compared to Ti, Y, Zr and Nb it is clear that more detailed work on the metamorphism of the Straumsnutane basalts is required.

The geochemical similarity among the different Borgmassivet intrusions and Straumsnutane basalts was evaluated further with the use of incompatible trace element ratios (Figure 7.5). The most striking features on these diagrams are:

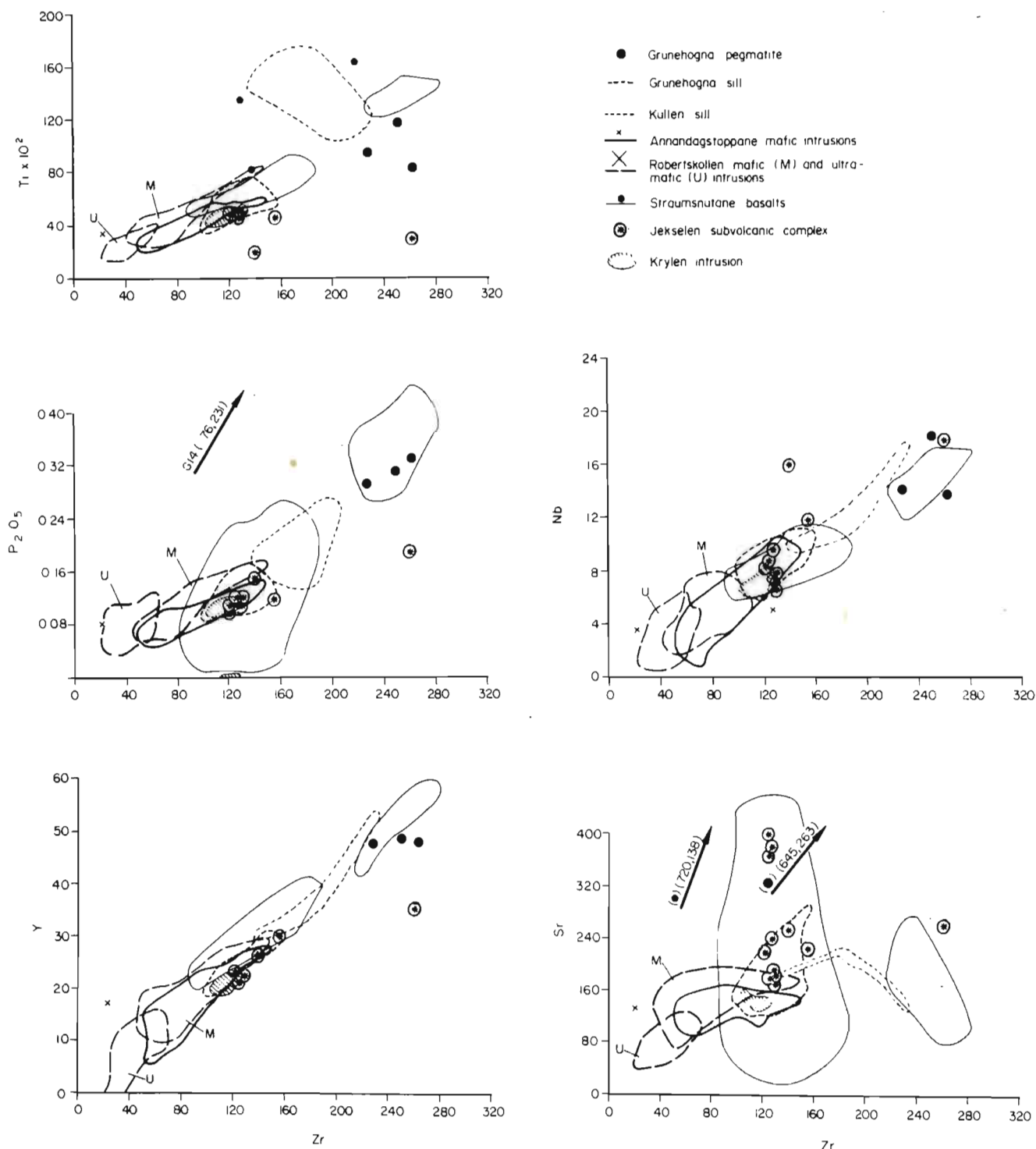


Figure 7.4 Selected incompatible element variation of the Borgmassivet intrusions and Straumsnutane basalts. Legend as for Figure 7.1. Arrows indicate points outside the limits defined by the axes of the diagrams. The first value in brackets given the "Y" value and the second gives the "X" value. G14 is from the Grunehogna sill.

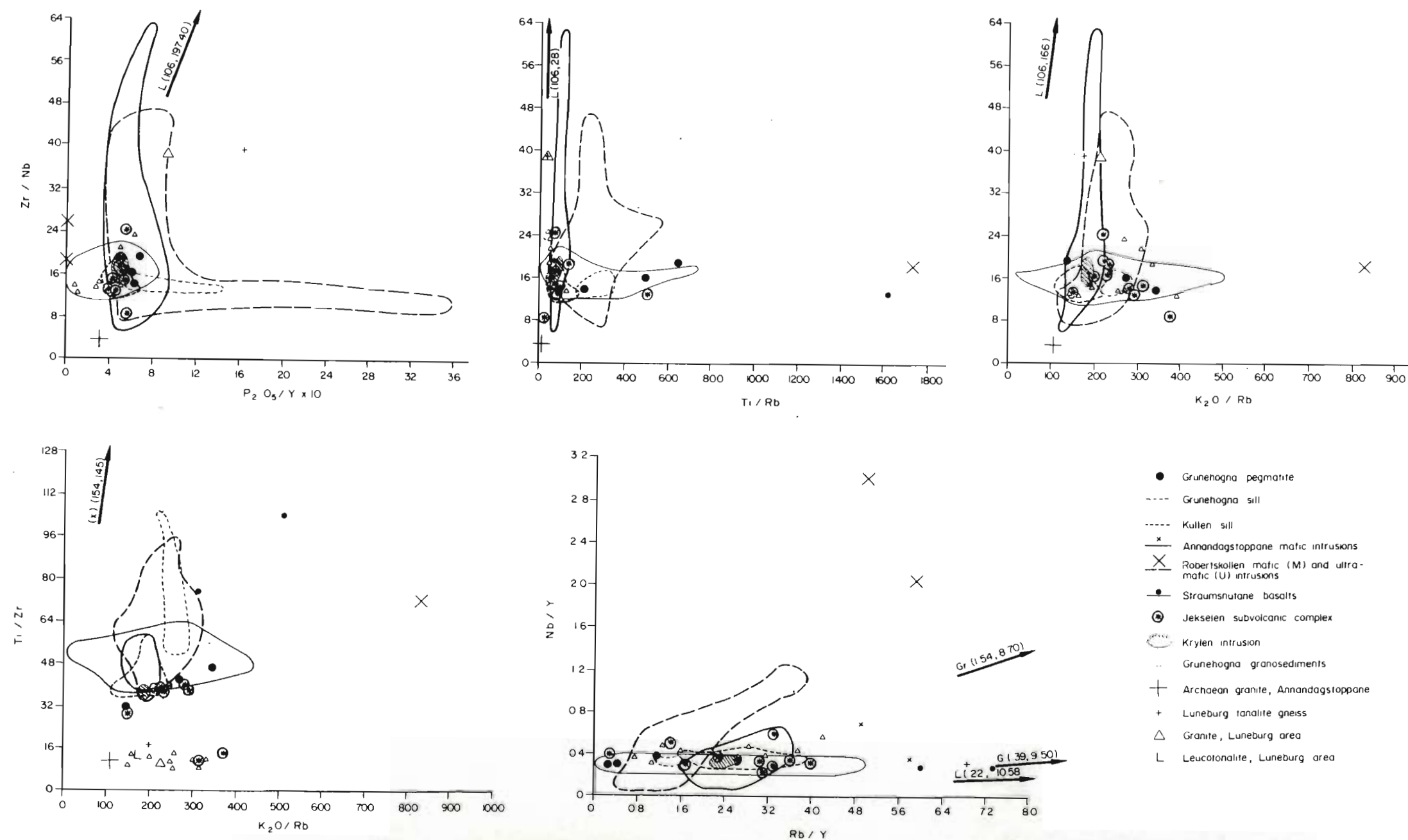


Figure 7.5

Selected incompatible trace element ratios of Borgmassivet intrusions and Straumnsnutane basalts. Added symbols to fields indicate samples plotting outside their geochemical fields. Arrows indicate plotted points outside the limits defined by the axes of the diagrams. The first value in brackets gives the "Y" and the second gives the "X" value. Gr: Archaean granite, Annandagstoppane; G: Granite, Lüneburg area. P_2O_5 / Y values are 10 times larger than indicated on the axis.

- (i) The extensive overlap among the intrusive and extrusive rocks;
- (ii) The wide range in Zr/Nb ratios of the Annandagstoppane and Robertskollen samples;
- (iii) The wide range in P_2O_5/Y and Ti/Zr ratios of the Robertskollen and Grunehogna samples; and
- (iv) The large variation in ratios involving K_2O and Rb.

Annandagstoppane incompatible trace element ratios (ITER): During the fractionation of mafic igneous rocks incompatible trace element ratios remain constant or nearly so. The wide range in Zr/Nb ratios of the Annandagstoppane rocks is therefore considered to be the result of factors other than fractional crystallization. In addition, the Nb/Y and Rb/Y ratios in these rocks define a poorly-constrained positive correlation. Yttrium may be partially compatible with clinopyroxene (K_D of Y in clinopyroxene = 0.5; Pearce and Norry, 1979), but the much smaller variation in P_2O_5/Y variation and lack of petrographic evidence for major clinopyroxene fractionation suggest a mechanism or mechanisms other than fractionation to explain this variation. It is important to note that K and Rb do not show evidence for mobilization in the Annandagstoppane rocks on interelement variation diagrams or in the K_2O/Rb ratio (Chapter 2 and Figure 7.5).

Robertskollen ITER: These rocks show very similar behaviour in incompatible element ratios to the Annandagstoppane rocks, except for a large variation in P_2O_5/Y , and considerable variation in Ti/Rb (Figure 7.5). The large variation in P_2O_5/Y results from five ultramafic samples, which contain very low concentrations of Y (less than 1.5 ppm). It is therefore difficult to judge the significance of the large P_2O_5/Y , Nb/Y and Rb/Y variations in these rocks.

Krylen intrusion and Kullen sill ITER: The Krylen intrusion and Kullen sill show very limited ITER variation, except for the Rb/Y ratio in the sill. The Kullen sill shows extensive evidence for hydrothermal alteration, but little K_2O/Rb variation compared to Robertskollen and the Straumsnutane basalts (Figure 7.5). Unless hydrothermal alteration affected K and Rb to exactly the same extent, the Rb/Y variation on Figure 7.5 should be considered as a result of processes or mechanisms other than post-intrusion alteration, such as fractional crystallization or contamination. Although there is evidence for more clinopyroxene fractionation in the Kullen sill than in the Annandagstoppane intrusions (Chapter 4), plagioclase and orthopyroxene are the dominant fractionating phases. Clinopyroxene fractionation in the Kullen sill therefore cannot account for the observed Rb/Y variation.

Grunehogna sill ITER: The Grunehogna sill ITER variation is limited, except for P_2O_5/Y and Ti/Zr. Evidence was presented in Chapter 4 that ilmenite was a fractionating phase in the Grunehogna sill, hence Ti cannot be considered as an incompatible element in this case. The P_2O_5/Y data (Figure 7.5) of this sill show that five of the six samples have a very limited variation (40.2 to 65.7), with a single sample from the top of the sill having a value of 142.3. This latter sample is enriched in micrographic intergrowths of quartz and alkali-feldspar, and probably represents crystallization of a volatile- and P_2O_5 -enriched liquid derived by fractional crystallization of the Grunehogna magma.

Straumsnutane basalt ITER: The Straumsnutane basalts show relatively small variations in Zr/Nb, Ti/Zr and Nb/Y, but large variation in ratios involving K and Rb.

As pointed out above K and Rb are highly mobile during alteration processes, and the ratio variations involving these elements may be artefacts of such post-extrusion mobilization. Hence, trace element ratios involving these elements cannot be used to define primary petrogenetic processes, except possibly for the Rb/Y variation in the Kullen sill as discussed above.

B. Rare Earth Element Compositions

Samples for rare earth element (REE) analysis were selected from different nunatak areas on the basis of Mg-number variation, i.e. one sample with a low and one with a high Mg-number were analysed where possible. The chondrite-normalized Straumsnutane basalt REE patterns are indistinguishable from those of the Borgmassivet intrusions (Figure 7.6). General characteristics are the following:

- (i) Light REE (LREE) have moderately steep and heavy REE (HREE) have flat slopes; $(\text{Ce/Yb})_{\text{cn}}$ ratios range from 3.0 to 4.3. These features indicate that garnet does not occur in the residue and that fractionation must have taken place at shallow levels;
- (ii) The range of REE contents and the LREE enrichment are typical of most continental tholeiites (Cullers and Graf, 1984);
- (iii) The ultramafic rock, R8/82, from Robertskollen, the most evolved samples of the Borgmassivet intrusions and the Straumsnutane basalts have small negative Eu anomalies. The anomaly in the ultramafic rock is assumed to reflect a very low modal plagioclase content, and the anomalies in the lavas and evolved intrusions reflect plagioclase fractionation, which also indicates shallow level fractionation.

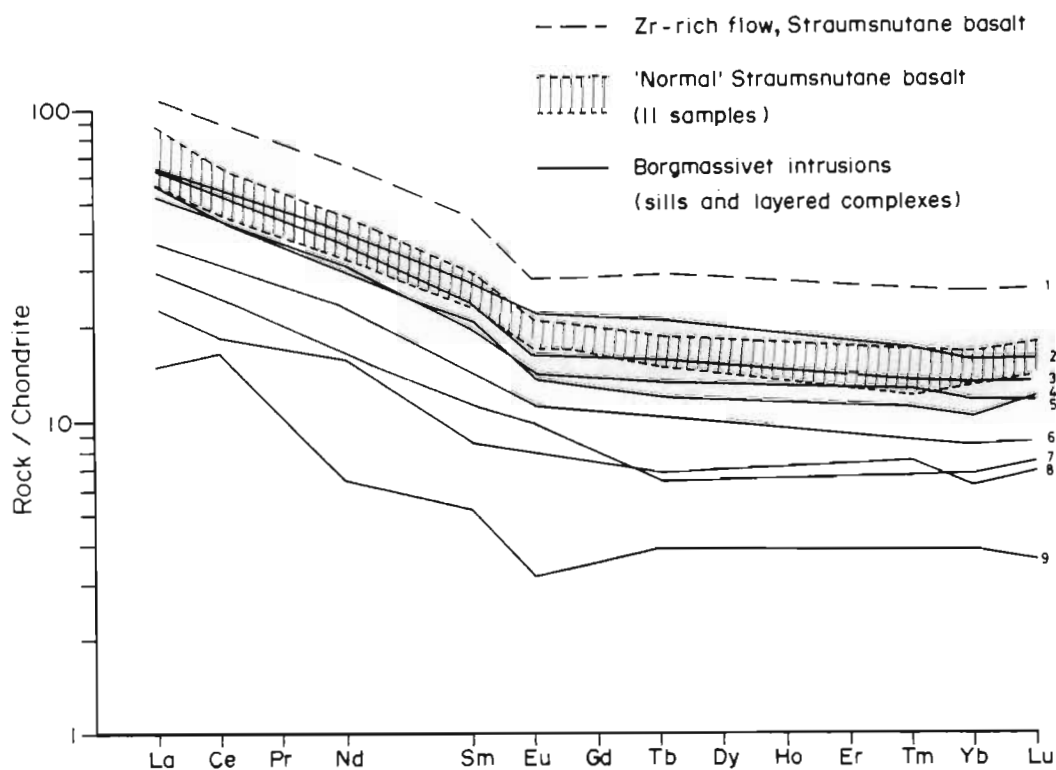


Figure 7.6

The range in chondrite-normalized REE abundances in the Borgmassivet intrusions and Straumnsnutane basalts. REE analysed are underlined. Normalizing factors for C-1 chondrites are from Taylor and McLennan (1981).

- 1: ET-11, Snökallen lava, eastern Trollkjellpiggen;
- 2: G9/82, Grunehogna sill;
- 3: G18/82, Kullen sill;
- 4: J19/81, Jekselen Complex;
- 5: JT10/82, Juletoppane;
- 6: A27/82, Annandagstoppane;
- 7: JT23/82, Juletoppane;
- 8: A14/82, Annandagstoppane;
- 9: R8/82, Ultramafic Unit, Robertskollen

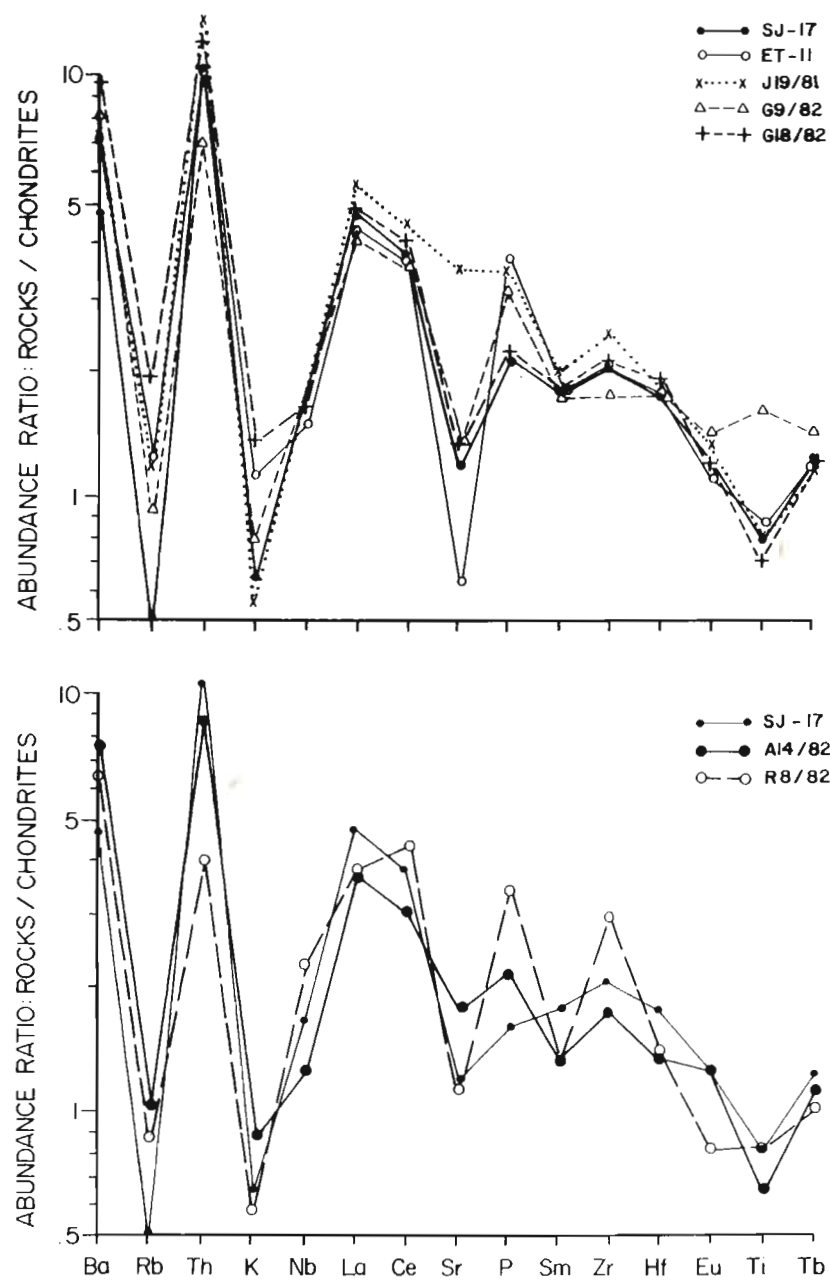
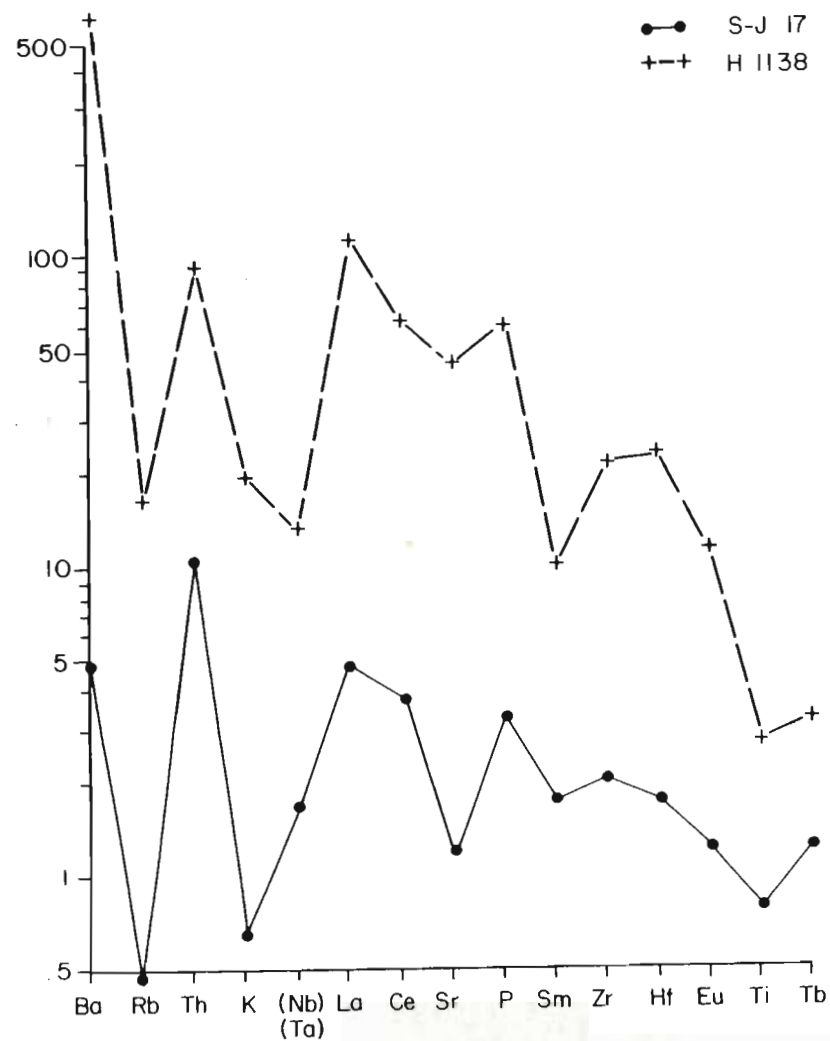


Figure 7.7

Abundance ratios (Element/Yb normalized to C1-chondrites) of Borgmassivet intrusions, Straumsnutane basalts and a leucotonalite, H1138, from the bimodal suite in Swaziland (Hunter et al., 1984). Straumsnutane basalt SJ-17 is used as



a reference on the diagrams. See text for discussion and normalizing factors. ET-11: Snökallen lava; J19/82: Jekselan Complex; G9/82: Grunenogna sill; G18/82: Kullen sill; A14/82: Annandagstoppane main suite; R8/82: Robertskollen Ultramafic Unit.

C. Abundance Ratios

A useful technique for comparing the Borgmassivet intrusions and lavas is the use of abundance ratios ("spidergrams") described by Thompson et al. (1982, 1983) and Dupuy and Dostal (1984). Incompatible element/Yb ratios are normalised to chondrites in order to decrease the effects of fractional crystallization and variable degrees of partial melting. The observed spidergrams obtained are therefore thought to reflect either source rock compositions, or the influence of processes such as crustal contamination.

Spidergrams of Borgmassivet intrusions and Straumsnutane basalts are shown in Figure 7.7. The patterns displayed by the various rock types approximate to one another very closely, with only minor deviations. The normalized ratios show an overall increase from Tb to Ba, with depletion of Nb, Sr, K and Rb. From Ba to La the patterns have W-shaped configurations, and a trough at Sr. The spidergrams are markedly similar to continental tholeiites described by Thompson et al. (1983, their Figure 2B) and Dupuy and Dostal (1984), but they also show differences. The most important similarities are that Nb and Sr are depleted and Th is enriched relative to La (Figure 7.7). The major difference is that Rb and K show considerable depletion on the spidergrams of the Borgmassivet and Straumsnutane rocks.

D. Interpretation of Abundance Ratios and ITER

Thompson et al. (1983) and Dupuy and Dostal (1984) compare the unique shape of continental tholeiite spidergrams to fusible rock types in continental crust and "average" continental crust. They conclude that the patterns are the

result of contamination by crustal material based on the general similarities of these spidergrams. The depletion in Sr could reflect plagioclase fractionation.

It may be argued that the similarities of spidergrams of the Borgmassivet intrusions and Straumsnutane basalts to the continental tholeiites described by Thompson et al. (1983) and Dupuy and Dostal (1984) reflect similar contamination of crustal material. However, the depletion of Rb and K in the spidergrams of the Antarctic rocks suggests that such contamination must reflect a particular rock type, rather than "average" crust. The presence of Archaean granite outcrops at Annandagstoppane suggests that the Ritscherflya Supergroup may be underlain by an Archaean granitoid terrane. In the absence of suitable isotope data further discussion has to be speculative, because of the limited evidence for this conclusion.

The most likely, widespread rock type in Archaean terranes that is depleted in Rb and Sr and has high Th contents relative to chondrites is leucotonalite. Hunter et al. (1984) report the geochemistry of leucotonalites which have very similar spidergram patterns to the Borgmassivet intrusions and Straumsnutane basalts. Their sample H1138 is shown for comparison with a Straumsnutane basalt ((SJ-17) in Figure 7.7. No Nb values were reported by these authors, and Ta is used instead of the similarity in geochemical behaviour of the two trace elements (Hunter, pers. comm., 1986). These patterns support the concept of contamination of the Borgmassivet intrusions by leucotonalite.

Some of the variation in incompatible trace element ratios (ITER) as discussed above may therefore be the result of contamination by crustal material. The ITER of granosediments and sediments from Grunehogna, a granite from Annandagstoppane and granitoid rocks from the Kaapvaal craton in the Lüneberg

area ($\pm 27^{\circ}20'S$, $30^{\circ}35'E$) are compared with ITER from the Borgmassivet intrusions and Straumsnutane basalts (Figure 7.5). The compositions of the sediments and granosediments show that if they were major contaminants, they are nevertheless unlikely to affect the ITER of the Borgmassivet intrusions to any degree. However, the Zr/Nb ratio indicates that variation in the Annandagstoppane and Robertskollen data is consistent with contamination of the Borgmassivet intrusions by leucotonalite.

III Conclusions

- (i) The major and trace element geochemistry of the Borgmassivet intrusions show marked similarities indicating a possible consanguineous relationship;
- (ii) The magmas were probably contaminated by crustal material, which may have been composed largely of leucotonalite.

CHAPTER 8 SYNTHESIS AND CONCLUSIONS

I. Synthesis

The geochemistry of the Borgmassivet intrusions and Straumsnutane basalts from selected nunataks in the Ahlmannryggen and Giaeverryggen shows regional coherence (Chapter 7). However, chemical homogeneity does not by itself prove conclusively that given rock types are consanguineous (Mohr, 1983). One of the problems of interpreting the geochemistry of the Ahlmannryggen igneous rocks is that the available Rb-Sr isotope data on these rocks are equivocal. A review of ages determined by this method was given in Chapter 1. Barton (pers. comm., 1985) suggests that the Borgmassivet intrusions may all be approximately 1200 Ma in age and that the ages older and younger than 1200 Ma may be pseudoisochrons reflecting the age of the source regions, or meaningless isochron trends which are mixing lines of strontium from two sources. Lutz and Srogi (1986) show on theoretical grounds that subsolidus hydrothermal alteration of rocks can cause systematic errors in age estimates if Sr addition is involved. The extensive hydrothermal alteration of the Kullen and Grunehogna sills and Straumsnutane basalts may have resulted in the generation of pseudoisochrons. De Paulo (1981) discusses the generation of pseudoisochrons as being the combined results of assimilation and fractionation. Lutz and Srogi (1986) show that only small proportional changes in Sr concentration are required to produce false ages and meaningless initial ratios. This may also be the case for the Borgmassivet intrusions (Barton, pers. comm., 1985).

Bearing in mind the limitations of the isotope data, it is suggested that the Borgmassivet intrusions and Straumsnutane basalts may be petrogenetically related mainly on the basis of the chemical homogeneity of the intrusive and extrusive rocks.

If this suggestion is correct a model for extensive igneous activity during the closing stages of deposition in the Ritscherflya basin can be proposed. The model is summarized in Figure 8.1. The cause of igneous activity has to remain conjectural at this stage.

A simplified scenario could be as follows:

- (i) The depositional environment in the Ritscherflya basin was largely fluvial, dominated by braided and meandering river and locally lacustrine systems (Bredell, 1973, 1976, 1982; Wolmarans and Kent, 1982; Swanepoel, pers. comm., 1984; Ferreira, 1986a, 1986b). The local presence of marine embayments was recognized by Ferreira (1986a, 1986b). Sediments were derived from the southwest, west and northwest and deposited in yoked basins, possibly related to block faulting (Wolmarans, 1982; Swanepoel, pers. comm., 1984; Ferreira, 1986a, 1986b).
- (ii) Volcanic activity commenced during upper Högfonna times, reflected by the presence of volcanoclastic sediments (De Ridder, 1970; Bredell, 1973, 1976, 1982; Wolmarans and Kent, 1982; Swanepoel, pers. comm., 1984; Ferreira, 1986a, 1986b).
- (iii) Increased volcanic activity culminated in the outpouring of the Straumsnutane basalts, which were largely subaerial flows. Local intercalations of pillowed basalts indicate that some subaqueous extrusions (marine and/or lacustrine) occurred (Watters, 1969a, 1969b, 1972, pers. comm., 1984).

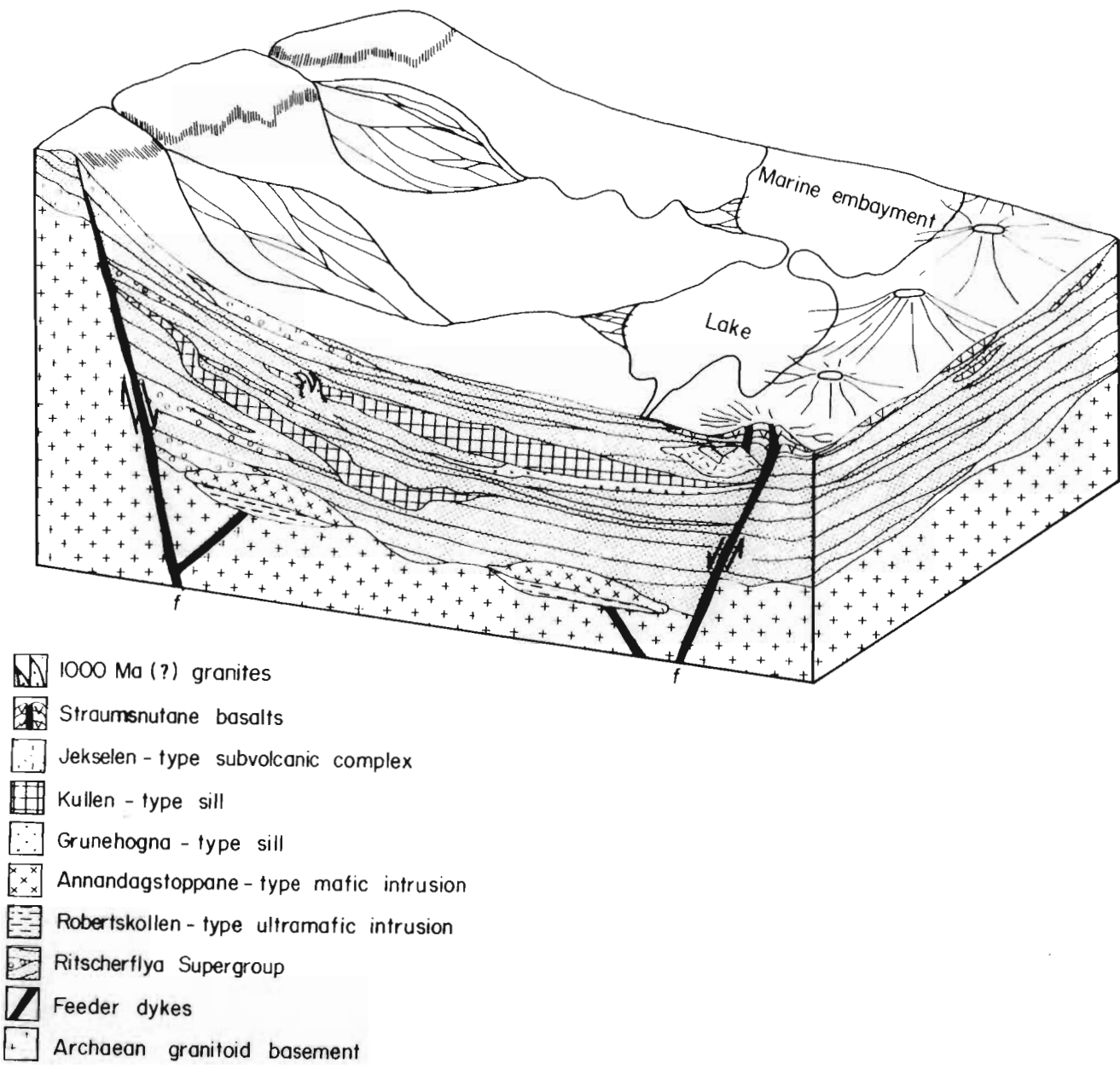


Figure 8.1 Proposed model of depositional and intrusive environment in the Ritscherflya Supergroup during late stages of basin development. Not to scale.

- (iv) Major faults near the western and eastern edges of the Ritscherflya basin acted as conduits for the Borgmassivet magmas which were generated in the upper mantle.
- (v) The presence of layered intrusions in the west at Annandagstoppane and limited outcrops of Archaean granites suggest that these intrusions were emplaced at or near the base of the Ritscherflya Supergroup. In contrast the Grunehogna and Kullen sills and Jekselen Complex were emplaced at shallow crustal levels. The Straumsnutane basalts in the northeastern Ahlmannryggen reflect largely subaerial extrusions that terminated Ritscherflya sedimentation. If the intrusions and extrusions are consanguineous as suggested by the geochemistry, the present distribution of the Borgmassivet intrusions and Straumsnutane basalts reflect stratigraphically higher levels from west to east (Figure 8.2). This conclusion is consistent with the concept that the present preservation of the Ritscherflya Supergroup (i.e. the oldest formations in the west and the youngest in the east) is a consequence of the presence of major faults with downthrows to the east (Wolmarans, 1982; Ferreira, 1986a, 1986b).

The Pencksökket-Jutulstraumen dislocation represents a major tectonic break with its downthrow side to the west. A number of large-scale faults parallel to the Pencksökket-Jutulstraumen have been recognized to the west of the Ahlmannryggen in the area bounded by 66° to 75°S and 0° to 30°W. These faults produced a series of blocks which are stepped down to the west and northwest (Hinz and Krause, 1982; K. Weber and G. Spaeth, pers. comm., 1986). At this stage of investigations in western Dronning Maud Land it is difficult to establish whether there is a direct tectonic link between the major faults represented by the Pencksökket-Jutulstraumen-type with downthrows to the west and the smaller-scale faults in the Ahlmannryggen, with their downthrows

W

E

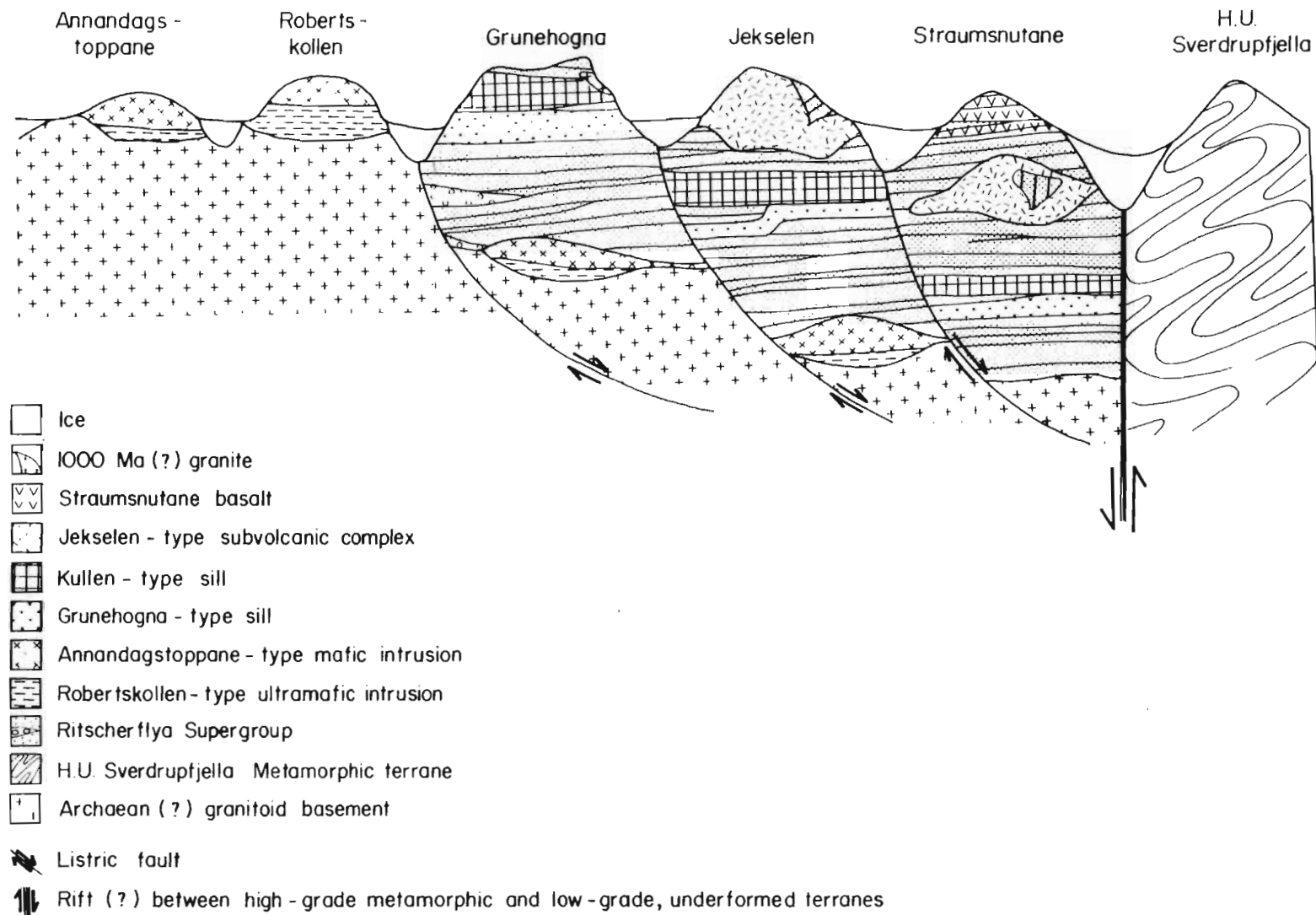


Figure 8.2 Diagrammatic east-west section of the Ritscherflya Supergroup and Borgmassivet intrusions from Annandagstoppane to the western H.U. Sverdrupfjella. Not to scale.

to the east. If they are linked it is tempting to speculate that western Dronning Maud Land is broken up into large tectonic blocks by the Pencksökket-Jutulstraumen-type faults, within which a series of smaller blocks exist which represent tectonic readjustment following, or synchronous, with the major faulting event.

II. Conclusions

The aims of this thesis are to understand the chemistry, source and petrogenesis of the Borgmassivet intrusions. The key questions are:

1. What are the major geochemical and petrological characteristics of the Borgmassivet intrusions?
2. What are the genetic relationships (if any) of the different plutonic rock sequences?
3. What processes of differentiation or fractionation were operative?
4. To what extent have the various rocks been affected by metamorphic and/or metasomatic processes?
5. What relationship (if any) exists between the evolution of the Ritscherflya Supergroup and the igneous activity reflected by the Borgmassivet intrusions and Straumsnutane basalts.

Although much more data on the mineral chemistry, isotope systems and rare earth element geochemistry of these rocks are required, some of these questions can be answered.

Question 1 The major geochemical and petrological characteristics of the Borgmassivet intrusions

The Borgmassivet intrusions are SiO_2 -rich continental tholeiites, some of which show evidence for synemplacement contamination. Some intrusions, e.g. the Grunehogna sill, intruded wet, unconsolidated or partially lithified sediments. Abundance ratios and incompatible trace element ratios suggest possible contamination of magmas by crustal material of leucotonalite composition prior to intrusions or extrusion, but more detailed research is required to test this possibility.

Question 2 Genetic Relationships

The regional geochemical coherence of the Borgmassivet intrusions and Straumnutane basalts suggests that they may be consanguineous.

Question 3 Processes of differentiation and fractionation

Petrographic data suggest that crystal fractionation was the dominant process during crystallization of the magmas. Initial primocrysts in the Robertskollen Complex were chromite, olivine, orthopyroxene and clinopyroxene. The Mafic Unit at Robertskollen and the rest of the Borgmassivet intrusions show dominantly plagioclase, orthopyroxene and, to a lesser extent, clinopyroxene fractionation.

Question 4 Metamorphic and/or metasomatic processes

The Kullen and Grunehogna sills were affected extensively by hydrothermal alteration. Other Borgmassivet intrusions, e.g. the Annandagstoppane intrusions and Robertskollen Complex show less evidence of alteration, although they have been altered locally by deuteric fluids.

Question 5 The relationship between the evolution of the Ritscherflya Supergroup and the Borgmassivet igneous activity

The Borgmassivet igneous event occurred during the final stages of the development of the Ritscherflya basin. The extrusive rocks form the uppermost formation of the Ritscherflya Supergroup. A genetic relationship between the igneous activity and basin development may therefore exist, but the exact nature of such a relationship is not yet known.

Suggestions for further work to test and refine the models presented for the regional properties and petrogenesis of individual intrusions are:

1. Detailed mineral chemistry and further REE data are required to refine the existing petrogenetic models;
2. Data on the chemistry of the sedimentary rocks, Sm-Nd, stable isotope and further Rb-Sr studies on the sediments and intrusions, coupled with fluid inclusion studies, will improve understanding of the assimilation effects in the Borgmassivet intrusions and may resolve some of the apparent paradoxes of existing Rb-Sr age determinations;
3. Further regional studies of the Borgmassivet intrusions in the Ahlmannryggen and Borgmassivet, and the intrusive mafic rocks in the high-grade metamorphic terrane of the H.U. Sverdrupfjella and

Kirwanveggen are required to compare the igneous history of the two areas with each other and with areas elsewhere in Antarctica and Gondwana.

It is hoped that the work reported in this thesis has made a contribution to the knowledge of the geology of western Dronning Maud Land, even if only to obtain a clearer understanding of the problems and questions facing researchers. This sentiment is expressed admirably by Douglas Adams (1979, 1980):

"The Answer to the Great Question ... Of Life, the Universe and Everything ... is ... Forty two" ... "- and so another, even bigger, computer had to be built to find out what the actual question was."

REFERENCES

- Abbey, S. (1980). Studies in "Standard Samples" for use in the general analysis of silicate rocks and minerals, Part 6: 1979 edition of "Usable" values. Geol. Surv. Can., Pap. 80-14, 30 pp.
- Absolom, S.S. (1970). Contaminated dolerites of Natal and Zululand. Petros, 2, 10-15.
- Ackerman, P.B., and Walker, F. (1960). Vitrification of arkose by Karroo dolerite near Heilbron, Orange Free State. Q. J. geol. Soc. London, 116, 239-254.
- Adams, D. (1979). The hitchhiker's guide to the Galaxy. Pan Books, London, 159 pp.
- Adams, D. (1980). The restaurant at the end of the universe. Pan Books, London, 186 pp.
- Allsopp, H.L., and Neethling, D.C. (1970). Rb-Sr isotopic ages of Precambrian intrusives from Queen Maud Land, Antarctica. Earth Planet. Sc. Lett., 8, 66-70.
- Arth, J.G. (1976). Behavior of trace elements during magmatic processes - A summary of theoretical models and their applications. J. Research U.S. geol. Surv., 4, 41-47.
- Aucamp, A.P.H. (1972). The geology of Grunehogna, Ahlmannryggen, western Dronning Maud Land. S. Afr. J. Antarct. Res., 2, 16-22.
- Bailey, E.B. (1959). Mobilization of granophyre in Eire and sinking of olivine in Greenland. Liverpool and Manchester geol. J., 2, 143-154.
- Barker, D.S. (1970). Compositions of granophyre, myrmekite, and graphic granite. Geol. Soc. Am. Bull., 81, 3339-3350.
- Barker, F. (1979). Trondhjemite: Definition, environment and hypotheses of origin, 1-12. In Barker, F., Ed., Trondhjemites, dacites, and related rocks. Elsevier, Amsterdam, 659 pp.

- Barnes, S.J. (1986). The effects of trapped liquid crystallization on cumulus mineral compositions in layered intrusions. Contrib. Mineral. Petrol., 93, 524-531.
- Barnes, S.J., and Naldrett, A.J. (1986). Geochemistry of the J-M (Howland) Reef of the Stillwater Complex, Minneapolis Adit area. II. Silicate mineral chemistry and petrogenesis. J. Petrol., (in press),
- Barton, J.M., Jr., and Copperthwaite, Y.E. (1983). Sr-isotopic studies of some intrusive rocks in the Ahlmann Ridge and Annandagstoppane, western Queen Maud Land, Antarctica, 59-62. In Oliver, R.L., James, P.R., and Jago, J.B. Antarctic Earth Science. Australian Academy of Sciences, Canberra. 697 pp.
- Bowen, N.L. (1910). Diabase and granophyre of the Gowganda Lake District, Ontario. J. Geol., 18, 658-674.
- Bowen, N.L. (1914). The ternary system diopside-forsterite-silica. Am. J. Sc. 4th ser. 38; 207-264.
- Bowman, J.R. (1971). Use of the isotopic composition of strontium and SiO₂ content in determining the origin of Mesozoic basalt from Antarctica. M.Sc. thesis (unpubl.), Ohio State Univ., U.S.A.
- Bredell, J.H. (1973). The geology of the Nashornet-Viddalskollen area, western Dronning Maud Land. S. Afr. J. Antarct. Res., 3, 2-10.
- Bredell, J.H. (1976). The Ahlmannryggen Group, the Viddalen Formation, and associated igneous rocks in the Viddalen area, western Dronning Maud Land, Antarctica. M.Sc. thesis (unpubl.), Univ. Pretoria.
- Bredell, J.H. (1982). The Precambrian sedimentary-volcanic sequence and associated intrusive rocks of the Ahlmannryggen, western Dronning Maud Land: A new interpretation, 591-597. In Craddock, C., Ed., Antarctic Geoscience. The University of Wisconsin Press, Madison. 1172 pp.

- Burnham, C.W., and Davis, M.F. (1971). The role of H_2O in silicate melts: pt. 1, P-V-T relations in the system $NaAlSi_3O_8-H_2O$ to 10 kilobars and 1000°C. Am. J. Sc., 270, 54-79.
- Burnham, C.W., Holloway, J.R., and Davis, M.F. (1969). Thermodynamic properties of water to 1000°C and 10,000 bars. Geol. Soc. Amer. Spec. Paper, 132, 1-96.
- Burnham, C.W., and Nekvasil, H. (1986). Equilibrium properties of granite pegmatite magmas. Amer. Miner., 71, 239-263.
- Butt, B.C. (1962). The geology of the Straumsnutane and Istind nunataks, western Queen Maud Land, Antarctica. Field report (unpubl.), Geological Survey of South Africa, Pretoria.
- Butt, B.C. (1963). Geological investigations of the second South African National Antarctic Expedition. Field Report (unpubl.). Geological Survey of South Africa, Pretoria.
- Campbell, I.H. (1977). A study of macro-rhythmic layering and cumulate processes in the Jimberlana Intrusion, Western Australia. Part 1: The upper layered series. J. Petrol., 18, 183-215.
- Campbell, I.H. (1978). Some problems with the cumulus theory. Lithos, 11, 311-323.
- Campbell, I.H., McCall, G.J.H., and Tyrwhitt, D.S. (1970). The Jimberlana norite, Western Australia - a smaller analogue of the Great Dyke of Rhodesia. Geol. Mag., 107, 1-12.
- Campbell, I.H., and Turner, J.S. (1986). The influence of viscosity on fountains in magma chambers. J. Petrol., 27, 1-30.
- Cann, J.R. (1970). Rb, Sr, Y, Zr and Nb in some ocean floor basaltic rocks. Earth Planet. Sc. Lett., 10, 7-11.
- Carlson, R.W., Lugmair, G.W., and MacDougall, J.D. (1981). Columbia River volcanism: the question of mantle heterogeneity or crustal contamination. Geochim. Cosmochim. Acta, 45, 2483-2499.

- Chalmers, B. (1964). Principles of solidification. Wiley, New York, 319 pp.
- Clark, S.P., Jr. (1966). Viscosity, 291-200. In Clark, S.P., Jr., Ed., Handbook of physical constants. Geol. Soc. Amer., Mem., 97, 587 pp.
- Cox, K.G., Bell., J.D., and Pankhurst, R.J. (1979). The interpretation of igneous rocks. George Allen and Unwin, London. 450 pp.
- Cox, K.G., and Hawkesworth, C.J. (1985). Geochemical stratigraphy of the Deccan Traps at Mahabaleshwar, western Ghats, India, with implications for open system magmatic processes. J. Petrol., 26, 355-377.
- Craddock, C. (1972). Antarctic tectonics, 449-455. In Adie, R.J. Ed., Antarctic Geology and Geophysics. Universitetsforlaget, Oslo. 876 pp.
- Cullers, R.L., and Graf, J.L. (1984). Rare earth elements in igneous rocks of the continental crust: predominantly basic and ultrabasic rocks, 237-274. In Henderson, P. Ed., Rare earth element geochemistry. Elsevier, Amsterdam, 510 pp.
- Dalrymple, P.C., and Frostman, T.O. (1971). Some aspects of the climate of interior Antarctica, 429-442. In Quan, L.O., Ed., Research in the the Antarctic. AAAS, Washington, D.C., 768 pp.
- Daly, R.A. (1905). The secondary origin of certain granites. Am. J. Sci., 4th Ser, 20, 185-216.
- Daly, R.A., Manger, G.E., and Clark, S.P., Jr. (1966). Density of rocks, 19-26. In Clark, S.P., Jr., Ed., Handbook of physical constants. Geol. Soc. Amer., Mem., 97, 587 pp.
- Davies, J.F., Grant, R.W.E., and Whitehead, R.E.S. (1979). Immobile trace elements and Archaean volcanic stratigraphy in the Timmins mining area, Ontario. Can. J. Earth Sc., 16, 305-311.
- Decleir, H., and Van Autenboer, T. (1982). Gravity and magnetic anomalies across Jutulstraumen, a major geologic feature in western Dronning Maud Land, 941-948. In Craddock, C. Ed., Antarctic Geoscience. The University of Wisconsin Press, Madison. 1172 pp.

- Deer, W.A., Howie, R.A., and Zussman, J. (1978). Rock-forming minerals. Volume 2A. Single-chain silicates, 2nd Edn. Longman, London. 668 pp.
- DePaulo, D.J. (1981). Trace element and isotopic effects of combined wallrock assimilation and fractional crystallization. Earth Planet. Sc. Lett., 53, 189-202.
- De Ridder, E., and Bastin, H. (1968). Preliminary report on the geology of the Borg Massif, western Queen Maud Land, Antarctica. Field report (unpubl.), Geological Survey of South Africa, Pretoria.
- Dostal, J., Dupuy, C., and Liotard, J.M. (1982). Geochemistry and origin of basaltic lavas from Society Islands, French Polynesia (south central Pacific Ocean). Bull. Volcanol., 45, 51-62.
- Dowty, E. (1980). Crystal growth and nucleation theory and the numerical simulation of igneous crystallization, 419-485. In Hargraves, R.B., Ed., The physics of magmatic processes. Princeton University Press, Princeton. 585 pp.
- Dupuy, C. and Dostal, J. (1984). Trace element geochemistry of some continental tholeiites. Earth Planet. Sc. Lett., 67: 61-69.
- Du Toit, A.L. (1904). Geological survey of Aliwal North, Herschel, Barkley East and part of Wodehouse. Cape geol. Comm. Ann. Repts. for 1904. 71-181.
- Du Toit, A.L. (1905). Geological survey of Glen Gray and parts of Queenstown and Wodehouse, including the Indwe area. Cape geol. Comm. Ann. Repts for 1905, 95-140.
- Du Toit, A.L. (1913). The geology of Mount Currie and Umzimkulu (Cape), and Alfred County (Natal). Union geol. Survey, Ann. Repts for 1913, 90-100.
- Du Toit, A.L. (1929). The geology of the major portion of East Griqualand (Matatiele), Explanation of sheet 35 (Cape), Union Geol. Survey.

- Eales, H.V., and Reynolds, I.M. (in press). Cryptic variations within chromitites of the Upper Critical Zone, northwestern Bushveld Complex. Econ. Geol.
- Eastin, R., Faure, G., and Neethling, D.C. (1970). The age of the Trollkjellrygg volcanics of western Queen Maud Land. Antarct. J. of the U.S., 5, 157-158.
- Einsele, G. (1985). Basaltic sill-sediment complexes in young spreading centers: Genesis and significance. Geology, 13, 249-252.
- Einsele, G., and 18 others. (1980). Intrusion of basaltic sills into highly porous sediments, and resulting hydrothermal activity. Nature, 283, 441-445.
- Elsdon, R. (1982). Autometasomatic alteration of gabbro, Kap Edvard Holm intrusive complex, East Greenland. Miner. Mag., 45, 219-225.
- Elworthy, T.P. (1982). Geochronology, 73-84. In Wolmarans, L.G. and Kent, L.E. Eds., S. Afr. J. Antarct. Res., Suppl. 2, 93 pp.
- Ernst, W.G. (1960). Diabase-granophyre relations in the Endion sill, Duluth, Minnesota. J. Petrol., 1, 286-303.
- Ferreira, E.P. (1986a). 'n Sedimentologies-stratigrafiese ondersoek van die sedimentêre gesteentes in die Ahlmannryggen, Antarktika. M.Sc. thesis. (unpubl.), Univ. Stellenbosch.
- Ferreira, E.P. (1986b). The sedimentology and stratigraphy of the Ahlmannryggen Group, Antarctica, 719-722. In Geocongress '86 Extended Abstracts. The 21st biennial congress of the Geological Society of South Africa, Johannesburg, 7th to 11th July, 1986, 1056 pp.
- Fisher, R.V., and Schmincke, H.-U. (1984). Pyroclastic rocks. Springer-Verlag, Berlin, 472 pp.
- Ford, A.B., and Boyd, W.W., Jr. (1968). The Dufek intrusion a major stratiform gabbroic body in the Pensacola Mountains, Antarctica. 23rd Int. geol. Congress, Prague, 1968, Proceedings, v. 2, 213-228.

- Francis, E.H. (1982). Magma and sediment - I. Emplacement mechanism of late Carboniferous tholeiite sills in northern Britain. J. geol. Soc. Lond., 139, 1-20.
- Frankel, J.J. (1950). A note on the vitrification of Karroo sediments by dolerite intrusions. Trans. R. Soc. S. Afr., 32, 287-293.
- Frankel, J.J. (1969). The distribution and origin of the Effingham rock type, a dolerite derivative of intermediate composition, in Natal and Zululand, South Africa, 149-173. In Larsen, L., Manson, V., and Prinz, M., Eds., Igneous and metamorphic geology. Geol. Soc. Amer. Mem., 115.
- Giaever, J. (1954). The White Desert. The Official Account of the Norwegian-British-Swedish Antarctic Expedition. Chatto and Windus, London. 304 pp.
- Gillson, J.L. (1927). Granodiorites in the Penn Oreille district in northern Idaho. J. Geol., 35, 1-31.
- Gray, N.H. (1970). Crystal growth and nucleation in two large diabase dikes. Can. J. Earth Sci., 7, 366-375.
- Greenman, N.N. (1951). On the bias of grain-size measurements made in thin section - a discussion. J. Geol., 59, 268-274.
- Grikurov, G.E. (1982). Structure of Antarctica and outline of its evolution, 791-804. In Craddock, C., Ed., Antarctic Geoscience. Proceedings of the Third Symposium on Antarctic Geology and Geophysics, Madison, 1977. The University of Wisconsin Press, Madison. 1172 pp.
- Grout, F.F., and Schwartz, G.M. (1933). The geology of the Rove Formation and associated intrusives in northeastern Minnesota. Minnesota geol. Surv. Bull., 24, 103 pp.
- Gunn, B.M. (1962). Differentiation in Ferrar dolerites, Antarctica. New Zealand J. Geol. Geophys., 5, 820-863.
- Gunn, B.M. (1966). Modal and element variations in Antarctic tholeiites. Geochim. Cosmochim. Acta., 30, 881-920.

- Haggerty, S.E. (1976a). Oxidation of opaque mineral oxides in basalts, Hg-1 - Hg-100. In Rumble, D., III, Ed., Reviews in Mineralogy. Volume 3: Oxide Minerals. Mineralogical Society of America, Washington, D.C., 300 pp.
- Haggerty, S.E. (1976b). Opaque mineral oxides in terrestrial igneous rocks, Hg-101 - Hg-300. In Rumble, D., III, Ed., Reviews in Mineralogy. Volume 3: Oxide Minerals. Mineralogical Society of America, Washington, D.C., 300 pp.
- Halpern, M. (1970). Rubidium-Strontium date of possibly three billion years for a granite rock from Antarctica. Science, 169, 977-978.
- Hamilton, D.L., Burnham, C.W., and Osborne, E. (1964). The solubility of water and effects of oxygen fugacity and water content on crystallization in mafic magmas. J. Petrol., 5, 21-29.
- Hamilton, W. (1965). Diabase sheets of the Taylor Glacier region, Victoria Land, Antarctica. U.S. Geol. Surv. Prof. Paper, 456-B, 71 pp.
- Harker, A. (1904). The Tertiary igneous rocks of Skye. Mem. geol. Surv. U.K., 245-246.
- Harrell, J.A., and Eriksson, K.A. (1979). Empirical conversion equations for thin-section and sieve derived distribution parameters. J. Sed. Pet. 49, 273-280.
- Hatch, F.H. (1912). Note on an interesting contact of dolerite with sandstone from the Eccabeds of Elandsplaagte, Natal. Ann. Natal Mus., 2, 393-395.
- Hawkes, L. (1929). On a partially fused quartz-feldspar rock and on a glomero-granular texture. Miner. Mag., 22, 163-173.
- Hess, H.H. (1960). The Stillwater Igneous Complex, Montana, a quantitative mineralogical study. Geol. Soc. Amer. Mem. 80. 230 pp.
- Hinz, K., and Krause, W. (1982). The continental margin of Queen Maud Land/ Antarctica: seismic sequences, structural elements and geological development. Geol. Jb., E23, 17-41.

- Holm, P.E. (1982). Non-recognition of continental tholeiites using the Ti-Y-Zr diagram. Contrib. Mineral. Petrol., 79, 308-310.
- Hunter, D.R., Barker, F., and Millard, H.T., Jr. (1984). Geochemical investigation of Archaean bimodal and Dwalile metamorphic suites, Ancient Gneiss Complex, Swaziland. Prec. Res., 24, 131-155.
- Huppert, H.E., and Turner, J.S. (1981). A laboratory model of a replenished magma chamber. Earth Planet. Sc. Lett., 54, 144-152.
- Imbrie, J. (1956). The place of biometrics in taxonomy. Bull. Amer. Mus. Nat. Hist., 108, art 2, 211-252.
- Irvine, T.N. (1970). Heat transfer during solidification of layered intrusions. 1. Sheets and Sills. Can. J. Earth Sci., 7, 1031-1061.
- Irvine, T.N. (1982). Terminology for layered intrusions. J. Petrol., 23, 127-162.
- Irvine, T.N., and Barager, W.R.A. (1971). A guide to the chemical classification of the common volcanic rocks. Can. J. Earth Sci., 8, 523-548.
- Irvine, T.N., Keith, D.W., and Todd, S.G. (1983). The J-M platinum-palladium reef of the Stillwater Complex, Montana: II. Origin by double-diffusive convective magma mixing and implications for the Bushveld Complex. Econ. Geol., 78, 1287-1334.
- Irving, A.J. (1978). A review of experimental studies of crystal/liquid trace element partitioning. Geochim. Cosmochim. Acta, 42, 743-770.
- Jackson, E.D. (1961). Primary textures and mineral associations in the ultramafic zone of the Stillwater complex, Montana. USGS Prof. Paper, 358, U.S. Government Printing Office, Washington. 106 pp.
- Jahns, R.H. (1955). The study of pegmatites, 1025-1135. In Bateman, A.M., Ed., Fiftieth Anniversary Volume, Economic Geology. Economic Geology Publishing Co., Lancaster, Pa.

- Jahns, R.H., Martin, R.F., and Tuttle, O.F. (1969). Origin of granophyre in dikes and sills of tholeiitic diabase. (Abstract). Amer. geophys. Union Trans., 50, 337.
- Jensen, L.S. (1976). A new cation plot for classifying sub-alkalic volcanic rocks. Ontario Division of Mines, Misc. Pap., 66 pp.
- Kay, R., Hubbard, N.J., and Gast, P.W. (1970). Chemical characteristics and origin of oceanic ridge volcanic rocks. J. Geophys. Res., 75, 1585-1614.
- Kennedy, G.C., and Holser, W.T. (1966). Pressure-volume-temperature and phase relations of water and carbon dioxide, 371-383. In Clark, S.P., Ed., Handbook of physical constraints. Mem. geol. Soc. Amer., 97, 587 pp.
- Kent, L.E., and Frankel, J.J. (1948). Studies on Karroo dolerites. (4) On intrusions of glass in dolerite. Trans. geol. Soc. S. Afr., 51, 179-193.
- Kenyon, A.K. (1976). Reaction phenomena between Karroo dolerite and Cave Sandstone xenoliths in the Birds River Complex. M.Sc. thesis (unpubl.), Rhodes Univ., Grahamstown, 166 pp.
- Kerr, R.C., and Tait, S.R. (1985). Convective exchange between pore fluid and an overlying reservoir of denser fluid: a post-cumulus process in layered intrusions. Earth Planet. Sc. Lett., 75, 147-156.
- King, H.G.R. (1969). The Antarctic. Blandford Press, London, 276 pp.
- King, R.P. (1983). Stereological methods for the prediction and measurement of mineral liberation. Spec. Publ. geol. Soc. S. Afr., 7, 443-447.
- Kokelaar, B.P. (1982). Fluidization of wet sediments during the emplacement and cooling of various igneous bodies. J. geol. Soc. Lond., 139, 21-33.
- Krauskopf, K.B. (1967). Introduction to geochemistry. McGraw Hill, New York, 721 pp.
- Krumbein, W.C., and Pettijohn, F.J. (1938). Manual of sedimentary petrography. Appleton-Century-Crofts, Inc., New York. 549 pp.

- Krynauw, J.R. (1983). Preliminary report on the geochemistry and petrology of some igneous rocks in the Ahlmannryggen and Giaeverryggen, western Dronning Maud Land, Antarctica, 63. (Abstract). In Oliver, R.L., James, P.R. and Jago, J.B. Eds., Antarctic Earth Science. Australian Academy of Science, Canberra. 697 pp.
- Krynauw, J.R., Dean, R.A., and Johnson, A.W. (1982). The use of helicopters for geological research in Dronning Maud Land, Antarctica. J. AeSSA/SAIAeA, 3, 36-43.
- Krynauw, J.R., Hunter, D.R., and Wilson, A.H. (1984). A note on the layered intrusions at Annandagstoppane and Juletoppane, western Dronning Maud Land. S. Afr. J. Antarct. Res., 14, 2-10.
- Kushiro, I. (1972). Determination of the liquidus relations in synthetic silicate systems with electron probe analysis: the system forsterite-diopside-silica at 1 atmosphere. Amer. Miner., 57, 1260-1271.
- Kyle, P.R., Pankhurst, R.J., and Bowman, J.R. (1983). Isotopic and chemical variations in Kirkpatrick Basalt Group rocks from southern Victoria Land, 234-237. In Oliver, R.L., James, P.R., and Jago, J.B., Eds., Antarctic Earth Science. Australian Academy of Science, Canberra, 697 pp.
- Le Roex, A.P., and Reid, D.L. (1978). Geochemistry of Karroo dolerite sills in the Calvinia district, western Cape Province, South Africa. Contrib. Mineral. Petrol., 66, 351-360.
- Liesegang, R.E. (1896). Über einige Eigenschaften von Gallerten. Naturw. Wochschr., 11, 353-362.
- Lofgren, G.E. (1980). Experimental studies on the dynamic crystallization of silicate melts, 487-551. In Hargraves, R.B., Ed., Physics of magmatic processes. Princeton University Press, Princeton. 585 pp.
- Lonsdale, P., and Becker, K. (1985). Hydrothermal plumes, hot springs, and conductive heat flow in the Southern Trough of Guaymas Basin. Earth Planet. Sc. Lett., 73, 211-225.

- Lutz, T.M., and Srogi, L.A. (1986). Biased isochron ages resulting from subsolidus isotope exchange: A theoretical model and results. Chem. Geol., 56, 63-72.
- Maaløe, S. (1978). The origin of rhythmic layering. Min. Mag., 42, 337-345.
- MacKenzie, W.S., Donaldson, C.H., and Guilford, C. (1982). Atlas of igneous rocks and their textures. Longman, Harlow. 148 pp.
- Manning, D.A.C., and Pichavant, M. (1983). The role of fluorine and boron in the generation of granitic melts. In Atherton, M.P., and Gribble, C.D., Eds, Migmatites, Melting and Metamorphism. Proceedings of the Geochemical Group of the Mineralogical Society. Shiva Geological Series. Cheshire, U.K., 326 pp.
- McBirney, A.R. (1980). Mixing and unmixing of magmas. J. Volcanol. Geotherm. Res., 7, 357-371.
- McBirney, A.R., and Noyes, R.M. (1979). Crystallization and layering of the Skaergaard intrusion. J. Petrol., 20, 487-554.
- McCallum, I.S., and Charette, M.P. (1978). Zr and Nb partition coefficients: Implications for the genesis of mare basalts, KREEP, and sea floor basalts. Geochim. Cosmochim. Acta, 42, 859-869.
- McDougall, I. (1969). Potassium-argon dates on minerals from dolerites from western Queen Maud Land, Antarctica. Appendix to Neethling, D.C. (1969), Pre-Gondwana sedimentary rocks of Queen Maud Land, Antarctica, 1153-1162. In Gondwana Stratigraphy, IUGS Symposium, Buenos Aires, 1967. UNESCO, Paris.
- Mennell, F.P. (1911). Observation on some basic dykes and their bearing on certain problems of rock genesis. Geol. Mag., 8, 10-15.
- Menzies, M., and Seyfried, W.E., Jr. (1979). Basalt-seawater interaction: trace element and strontium isotopic variations in experimentally altered glassy basalt. Earth Planet. Sc. Lett., 44, 463-472.

- Miller, R.L., and Kahn, J.S. (1962). Statistical analysis in the geological sciences. John Wiley and sons, New York. 483 pp.
- Mohr, P. (1983). Ethiopian flood basalt province. Nature, 303, 577-584.
- Moore, D.G. (1962). Bearing strength and other physical properties of shallow and deep-sea sediments from the North Pacific. Bull. geol. Soc. Amer., 73, 1163-1166.
- Moore, J.G., and Schilling, J.G. (1973). Vesicles, water and sulfur in Reykjanes Ridge basalts. Contr. Mineral. Petrol., 41, 105-118.
- Morse, S.A. (1969). The Kiglapait Layered Intrusion, Labrador. Mem. Geol. Soc. Amer., 112. 146 pp.
- Mountain, E.D. (1935). Syntectic phenomena in Karroo dolerite at Coedmore quarries, Durban. Trans. geol. Soc. S. Afr., 38, 93-112.
- Mountain, E.D. (1936). Anatectic veins at Gonubie River mouth. S. Afr. J. Sci., 33, 248-253.
- Mountain, E.D. (1943). The dikes of the Transkei gaps. Trans. geol. Soc. S. Afr., 46, 55-74.
- Mountain, E.D. (1944). Further examples of syntaxis by Karroo dolerite. Trans. geol. Soc. S. Afr., 47, 107-121.
- Mountain, E.D. (1945). The geology of East London, C.P. Trans. geol. Soc. S. Afr., 48, 31-42.
- Mountain, E.D. (1960). Felsic material in Karroo dolerite. Trans. geol. Soc. S. Afr., 63, 137-151.
- Murdoch, J., and Barnes, J.A. (1974). Statistical tables for science, engineering, management and business studies. 2nd revised Edn, Macmillan, London. 46 pp.
- Murphy, J.B., and Hynes, A.J. (1986). Contrasting secondary mobility of Ti, P, Zr, Nb and Y in two metabasaltic suites in the Appalachians. Can. J. Earth Sc., 23, 1138-1144.

- Neethling, D.C. (1964). The geology of the Zukkertoppen nunataks, Ahlmannryggen, western Dronning Maud Land, 378-389. In Adie, R.J., Ed., Antarctic geology. North-Holland Publishing Co., Amsterdam. 758 pp.
- Neethling, D.C. (1969a). Pre-Gondwana sedimentary rocks of Queen Maud Land, Antarctica, 1153-1162. In Gondwana Stratigraphy, IUGS Symposium, Buenos Aires, 1967, UNESCO, Paris.
- Neethling, D.C. (1969b). The geology of the Ahlmann Ridge, western Queen Maud Land. Amer. Geogr. Soc., Map folio series, 12, sheet 7.
- Neethling, D.C. (1970). South African Earth Science Exploration of western Queen Maud Land, Antarctica. Ph.D. thesis (unpubl.), Univ. Natal.
- Neethling, D.C. (1972a). Age and correlation of the Ritscher Supergroup and other Precambrian rock units, Dronning Maud Land, 547-556. In Adie, R.J. Ed., Antarctic Geology and Geophysics. 1970, Universitetsforlaget, Oslo. 876 pp.
- Neethling, D.C. (1972b). Comparative geochemistry of Proterozoic and Palaeo-Mesozoic tholeiites of western Dronning Maud Land. In Adie, R.J. Ed., Antarctic Geology and Geophysics. Proceedings of the Second International Symposium on Antarctic Geology and Solid Earth Geophysics, Oslo, 1970, Universitetsforlaget, Oslo. 876 pp.
- Neilson, M.J., and Brockman, G.F. (1977). The error associated with point-counting. Amer. Miner., 62, 1238-1244.
- Nie, N.H., Hull, C.H., Jenkins, J.G., Steinbrenner, K., and Bent, D.H. (1975). SPSS. Statistical package for the Social Sciences, 2nd Edn. McGraw Hill, New York. 675 pp.
- Nielsen, A.E. (1964). Kinetics of precipitation. Pergamon Press, Oxford. 151 pp.
- Norrish, K., and Hutton, J.T. (1969). An accurate X-ray spectrographic method for analysis of a wide range of geological samples. Geochim. Cosmochim. Acta, 33, 431-453.

- O'Connor, J.T. (1965). A classification for quartz-rich igneous rocks based on feldspar ratios. U.S. Geol. Surv. Prof. Pap., 525-B, 79-84.
- Osborne, E.F. (1959). Role of oxygen pressure in the crystallization and differentiation of basaltic magma. Am. J. Sc., 257, 609-647.
- Oxburgh, E.R., and McRae, T. (1984). Physical constraints on magma contamination in the continental crust: an example, the Adamello complex. Phil. Trans. R. Soc. Lond., Ser. A, 310, 457-472.
- Patchett, P.J. (1980). Thermal effects of basalt on continental crust and crustal contamination of magmas. Nature, 283, 559-561.
- Pearce, J.A. (1975). Basalt geochemistry used to investigate post tectonic environments in Cyprus. Tectonophysics, 25, 41-68.
- Pearce, J.A., and Cann, J.R. (1973). Tectonic setting of basic volcanic rocks determined using trace element analyses. Earth Planet. Sc. Lett., 19, 290-300.
- Pearce, J.A., and Norry, M.J. (1979). Petrogenetic implications of Ti, Zr, Y and Nb variations in volcanic rocks. Contrib. Mineral. Petrol., 69, 33-47.
- Pearce, T.H. (1968). A contribution to the theory of variation diagrams. Contrib. Mineral. Petrol., 19, 142-157.
- Pearce, T.H. (1970). Chemical variations in the Palisade Sill. J. Petrol., 11, 15-32.
- Pearce, T.H., Gorman, B.E., and Birkett, T.C. (1975). The TiO_2 - K_2O - P_2O_5 diagram: a method of discriminating between oceanic and non-oceanic basalts. Earth Planet. Sc. Lett., 24, 419-426.
- Petersen, J.S. (1985). Columnar-dendritic feldspars in the lardalite intrusion, Oslo region, Norway: 1. Implications for unilateral solidification of a stagnant boundary layer. J. Petrol., 26, 223-252.
- Petrasko, A.K., Hodge, D.S., and Shaw, R. (1978). Mechanics of emplacement of basic intrusions. Tectonophysics, 46, 41-63.

- Pichavant, M. (1984). The effect of boron on liquidus phase relationships in the system Qz-Ab-Or-H₂O at 1kb. (abs) EOS (Transactions of the American Geophysical Union), 65, 298.
- Poldervaart, A. (1944). The petrology of the Elephant's Head dike and the New Amalfi sheet (Matatiele). Trans. R. Soc. S. Afr., 30, 85-119.
- Poldervaart, A. (1946). The petrology of the Mount Arthur Complex (East Griqualand). Trans. R. Soc. S. Afr., 31, 83-110.
- Pollak, W.H. (1967). The geology of the south-eastern portion of the Ahlmann Ridge, western Queen Maud Land, Antarctica. Field report (unpubl.), Geological Survey of South Africa, Pretoria.
- Raedeke, L.D., and McCallum, I.S. (1984). Investigations in the Stillwater Complex, part II. Petrology and petrogenesis of the ultramafic series. J. Petrol., 25, 395-420.
- Ramdohr, P. (1980). The ore minerals and their intergrowths, 2nd Edn. Pergamon Press, Oxford. 1205 pp.
- Ravich, M.G., and Soloviev, D.S. (1969). Geology and petrology of the mountains of central Queen Maud Land (Eastern Antarctica). Transl. from Russian, 1966. Israel Program for Scientific Translations, Jerusalem. 348 pp.
- Ravich, M.G., and Grikurov, G.E. (1970). Main features of the tectonics of Antarctica. Internat. geol. rev., 12, 1297-1309.
- Reynolds, D.L. (1936). Demonstrations in petrogenesis from Kiloran Bay, Colonsay. I. The transfusion of quartzite. Miner. Mag., 24, 367-407.
- Reynolds, D.L. (1940). Contact metamorphism by a tertiary dyke at Waterfoot, Co. Antrim. Geol. Mag., 77, 461-469.
- Reynolds, D.L. (1950). The transformation of Caledonian granodiorite to Tertiary granophyre on Slieve Gullion, Co. Armagh, N. Ireland. 18th Internat. geol. Congr., pt 3, 20-30.

- Reynolds, I.M. (1983). The iron-titanium oxide mineralogy of Karoo dolerite in the eastern Cape and southern Orange Free State. Trans. geol. Soc. S. Afr., 86, 211-220.
- Reynolds, R.L., and Goldhaber, M.B. (1978). Iron-titanium oxide minerals and associated alteration phases in some uranium-bearing sandstones. J. Res. U.S. geol. Surv., 6, 707-714.
- Rollinson, H.R., and Roberts, C.R. (1986). Ratio correlations and major element mobility in altered basalts and komatiites. Contrib. Mineral. Petrol., 93, 89-97.
- Roots, E.F. (1953). Preliminary note on the geology of western Dronning Maud Land. Norsk geologisk Tidsskr., 32, 18-33.
- Roots, E.F. (1954). Journeys of the topographical-geological party, 1950-51, 245-280. In Giaever, J. The White Desert. Chatto and Windus, London, 304 pp.
- Roots, E.F. (1969). Geology of western Queen Maud Land. In Bushnell, V.C. and Craddock, C., Eds., Geologic Maps of Antarctica. Antarctic Map Folio Series, 12, PlVI.
- Salpas, P.A., Haskin, L.A., and McCallum, I.S. (1983). Stillwater anorthosites: a lunar analog? Proc. Lunar Planet Sc. Conf., 14th, J. Geophys. Res., 88, Suppl: B27-B39.
- Salpas, P.A., Haskin, L.A., and McCallum, I.S. (1984). The scale of compositional heterogeneities in Stillwater anorthosites An - I and An -II. Lunar Planet. Sc., XV, 713-714.
- Shaw, D.M., Dostal, J., and Keays, R.R. (1976). Additional estimates of continental surface Precambrian shield composition in Canada. Geochim. Cosmochim. Acta, 40, 73-83.
- Smith, D.G.W. (1969). Pyrometamorphism of phyllites by a dolerite plug. J. Petrol., 10, 20-55.

- Snow, G.B. (1986). The geology, geochemistry and petrography of the Preikestolen intrusions, southern Ahlmannryggen, Dronning Maud Land, Antarctica. Honours project (unpubl.), Univ. Natal, Pietermaritzburg.
- Soloviev, D.S. (1972). Platform magmatic formations of East Antarctica, 531-538. In Adie, R.J. Ed., Antarctic Geology and Geophysics. Universitetsforlaget, Oslo. 876 pp.
- Sparks, R.S.J., Huppert, H.E., and Turner, J.S. (1984). The fluid dynamics of evolving magma chambers. Phil. Trans. R. Soc. Lond., Ser. A, 310, 511-534.
- Spry, A. (1969). Metamorphic textures. Pergamon Press, Oxford, 350 pp.
- Stakes, D.S., and O'Neil, J.R. (1982). Mineralogy and stable isotope geochemistry of hydrothermally altered oceanic rocks. Earth Planet. Sc. Lett., 57, 285-304.
- Stephenson, P.J. (1966). Geology: (1) Theron Mountains, Shackleton Range and Whichaway Nunataks. Trans-Antarctic Expedition 1955-1958 Scientific Reports, 8.
- Stephenson, P.J., and Griffin, T.J. (1976). Some long basaltic flows in north Queensland, 41-51. In Johnson, R.W., Ed., Volcanism in Australasia. Elsevier, Amsterdam, 405 pp.
- Sun, S.S., Nesbitt, R.W., and Sharaskin, A.Ya. (1979). Geochemical characteristics of mid-ocean ridge basalts. Earth Planet. Sc. Lett., 44, 119-138.
- Tait, S.R., Huppert, H.E., and Sparks, R.S.J. (1984). The role of compositional convection in the formation of adcumulate rocks. Lithos, 17, 139-146.
- Taylor, H.P., Jr. (1968). The oxygen isotope geochemistry of igneous rocks. Contrib. Mineral. Petrol., 19, 1-71.

- Taylor, H.P., Jr. (1974). Oxygen and hydrogen isotope evidence for large-scale circulation and interaction between ground waters and igneous intrusions with particular reference to the San Juan volcanic field, Colorado, 299-324. In Hofmann, A.W., Giletti, B.J., Yoder, H.S., Jr., and Yund, R.A. Eds., Geochemical transport and kinetics. Carnegie Institution, Washington, D.C.
- Taylor, H.P., Jr. (1979). Oxygen and hydrogen isotope relationships in hydrothermal mineral deposits, 236-277. In Barnes, H.L., Ed., Geochemistry of hydrothermal ore deposits, 2nd Edn. John Wiley & Sons, New York, 798 pp.
- Taylor, H.P., Jr. and Forester, R.W. (1979). An oxygen and hydrogen isotope study of the Skaergaard intrusion and its Country rocks: a description of a 55-M.Y. old fossil hydrothermal system. J. Petrol., 20, 355-419.
- Taylor, S.R. (1964). Trace element abundances and the chondritic earth model. Geochim. Cosmochim. Acta, 28, 1273-1285.
- Taylor, S.R., and McLennan, S.M. (1981). The composition and evolution of the continental crust: rare earth element evidence from sedimentary rocks. Phil. Trans. R. Soc. Lond., A301, 381-399.
- Tessier, G. (1948). La relation d'allometrie, sa signification statistique et biologique. Biometrics, 4, 14-52.
- Thompson, R.N. (1982). Magmatism of the British Tertiary volcanic province. Scott. J. Geol., 18, 49-107.
- Thompson, R.N., Dickin, A.P., Gibson, I.L., and Morrison, M.A. (1982). Elemental fingerprints of isotopic contamination of Hebridean Palaeocene mantle-derived magmas by Archaean sial. Contrib. Mineral. Petrol., 79, 159-168.

- Thompson, R.N., Morrison, M.A., Dickin, A.P., and Hendry, G.L. (1983). Continental flood basalts ... arachnids rule OK?, 158-185. In Hawkesworth, C.J., and Norry, M.J., Eds., Continental basalts and mantle xenoliths. Shiva Publishing Limited, Nantwich, UK. 272 pp.
- Tomkeieff, S.I. (1940). The dolerite plugs of Tieveragh and Tievebulliagh near Cushendall, Co. Antrim, with a note on buchite. Geol. Mag., 77, 54-64.
- Turner, J.S. (1973). Buoyancy effects in fluids. Cambridge University Press, London, 367 pp.
- Turner, J.S. (1980). A fluid-dynamic model of differentiation and layering in magma chambers. Nature, 285, 213-215.
- Turner, J.S. (1985). Multicomponent convection. Ann. Rev. Fluid. Mech., 17, 11-44.
- Turner, J.S., and Campbell, I.H. (1986). Convection and mixing in magma chambers. Earth-Sc. Rev., 23, 255-352.
- Turner, J.S., and Gustafson, L.B. (1978). The flow of hot saline solutions from vents in the sea floor: some implications for exhalative and other ore deposits. Econ. Geol., 73, 1082-1100.
- Tuttle, O.F., and Bowen, N.L. (1958). Origin of granite in the light of experimental studies in the system $\text{NaAlSi}_3\text{O}_8\text{-KAlSi}_3\text{O}_8\text{-SiO}_2\text{-H}_2\text{O}$. Geol. Soc. Amer. Mem., No. 74.
- Van Zyl, C.Z. (1974). Notes on the geology of Juletoppane and Annandagstoppane, western Queen Maud Land, Antarctica. Field report, (unpubl), Geological Survey of South Africa, Pretoria.
- Von Brunn, V. (1963). Scientific studies in western Dronning Maud Land, Antarctica, 1960. M.Sc. thesis (unpubl.), Univ. Cape Town.

- Von Brunn, V. (1964). Note on some basic rocks in western Dronning Maud Land, Antarctica, 415-418. In Adie, R.J., Ed., Antarctic Geology. North Holland Publishing Co., Amsterdam.
- Von Gruenewaldt, G. (1970). On the phase-change orthopyroxene-pigeonite and the resulting texture in the Main and Upper Zones of the Bushveld Complex in the eastern Transvaal. Spec. Publ. geol. Soc. S. Afr., 1, 67-73.
- Wager, L.R. (1961). A note on the origin of ophitic texture in the chilled olivine gabbro of the Skaergaard intrusion. Geol. Mag., 98, 353-366.
- Wager, L.R., and Brown, G.M. (1968). Layered igneous rocks. Oliver and Boyd, Edinburgh. 588 pp.
- Wager, L.R., and Deer, W.A. (1939). Geological investigations in East Greenland; pt 3 - The petrology of the Skaergaard intrusion, Kangerdlugssauq, East Greenland. Meddelelser om Grønland, 105, 335 p.
- Walker, F., and Poldervaart, A. (1941). The Hangnest dolerite sill, S.A. Geol. Mag., 78, 429-450.
- Walker, F., and Poldervaart, A. (1942a). The petrology of the Karroo dolerites between Sutherland and Middelburg, C.P. Trans. geol. Soc. S. Afr., 45, 55-64.
- Walker, F., and Poldervaart, A. (1942b). The metasomatism of Karroo sediments by dolerite. Trans. R. Soc. S. Afr., 29, 285-307.
- Walker, F., and Poldervaart, A. (1949). Karroo dolerites of the Union of South Africa. Bull. geol. Soc. Amer., 60, 591-706.
- Walker, K.R. (1969a). A mineralogical, petrological, and geochemical investigation of the Palisades Sill, New Jersey. In Larsen, L., Manson, V., and Prinz, M. Igneous and Metamorphic Geology, 175-187. Geol. Soc. Amer. Bull., 115. 561 pp.
- Walker, K.R. (1969b). The Palisades Sill, New Jersey - A re-investigation. Geol. Soc. Amer. Spec. Paper 111. 178 pp.

- Watson, E.B. (1982). Basalt contamination by continental crust: some experiments and models. Contrib. Mineral. Petrol., 80, 73-87.
- Watson, E.B., and Harrison, T.M. (1984). Accessory minerals and the geochemical evolution of crustal magmatic systems: a summary of prospectus of experimental approaches. Phys. Earth Planet. Int., 35, 19-30.
- Watters, B.R. (1969a). Notes on the geology of Framryggen, Nunatak 1705, Trioen, Knallen, Tendegga and Fasettfjellet, Ahlmann Ridge. Field report (unpubl.), Geological Survey of South Africa, Pretoria.
- Watters, B.R. (1969b). The Trollkjellryg volcanic formation of the Ahlmann Ridge, western Queen Maud Land, Antarctica. Field report (unpubl.), Geological Survey of South Africa, Pretoria.
- Watters, B.R. (1972). The Straumsnutane volcanics, western Dronning Maud Land. S. Afr. J. Antarct. Res., 2, 23-31.
- Wells, M.K. (1951). Sedimentary inclusions in the hypersthene-gabbro, Ardnamurchan, Argyllshire. Miner. Mag., 29, 715-736.
- Wilson, A.H. (1982). The geology of the Great 'Dyke', Zimbabwe: The ultramafic rocks. J. Petrol., 23, 240-292.
- Wilson, A.H. (in prep.) The geology of the Great Dyke, Zimbabwe: Chemical and textural cyclic units within the uppermost (P1) pyroxenite and the nature of the mafic/ultramafic contact of the Hartley Complex.
- Winkler, H.J.F. (1976). Petrogenesis of metamorphic rocks, 4th Edn. Springer-Verlag, New York, 334 p.
- Winkler, H.G.F., Boese, M., and Marcopoulos, T. (1975). Low temperature granitic melts. Neues Jb. Miner. Monatshefte, 245-269.
- Wolmarans, L.G. (1982). Subglacial morphology of the Ahlmannryggen and Borgmassivet, western Dronning Maud Land, 963-968. In Craddock, C., Ed., Antarctic Geoscience. University of Wisconsin Press, Madison, 1172 pp.

- Wolmarans, L.G. and Kent, L.E. (1982). Geological investigations in western Dronning Maud Land, Antarctica - a synthesis. S. Afr. J. Antarc. Res., Suppl. 2, 93 pp.
- Wolmarans, L.G., and Krynauw, J.R. (1981a). Reconnaissance geological map of the Ahlmannryggen area, western Dronning Maud Land, Antarctica. Sheet 1 of a series of 3. SASCAR, Pretoria, 1981.
- Wolmarans, L.G., and Krynauw, J.R. (1981b). Reconnaissance geological map of the Bormassivet area, western Dronning Maud Land, Antarctica. Sheet 2 of a series of 3. SASCAR, Pretoria, 1981.
- Wolmarans, L.G., and Krynauw, J.R. (1981c). Reconnaissance geological map of the Kirwanveggen area, western Dronning Maud Land, Antarctica. Sheet 3 of a series of 3. SASCAR, Pretoria, 1981.
- Wood, D.A., Gibson, I.L., and Thompson, R.N. (1976). Elemental mobility during zeolite facies metamorphism of the Tertiary basalts of eastern Iceland. Contrib. Mineral. Petrol., 55, 241-254.
- Wood, D.A., Tarney, J., Varet, J., Saunders, A.D., Bougault, H., Joron, J.L., Treuil, M., and Cann, J.R. (1979). Geochemistry of basalts drilled in the North Atlantic by IPOD Leg 49: implications for mantle heterogeneity. Earth Planet. Sc. Lett., 42, 77-97.
- Wyllie, P.J. (1961). Fusion of Torridonian sandstone by a picrite sill in Soay (Hebrides). J. Petrol., 2, 1-37.
- Young, A. (1918). Fusion of Karroo grits in contact with dolerite intrusions. R. Soc. S. Afr. Min. Meeting, October 30, 1918.
- Znachko-Yavorskii, G.A., Kurinin, R.G., and Grikurov, G.E. (1978). Tectonic Map of Antarctica 1:10 000 000 sheet. Research Institute of the Geology of the Arctic, Complex "Sevmorgeo", Ministry of Geology of the USSR, Moscow.

APPENDICES

APPENDIX 1

SAMPLING AND ANALYTICAL TECHNIQUES

Two hundred and seventy-four samples of the Borgmassivet intrusions and Jurassic (?) dykes were analysed for major and trace elements as given in Appendix 2. No research was done on the Jurassic dykes, which are included here for comparison. The major and trace element data of 176 Straumsnutane basalts determined by Watters (pers. comm., 1985) are included in Appendix 2, but little information on operating conditions is available. All analyses done at the University of Natal, Pietermaritzburg were by X-ray fluorescence spectrometry. REE, Th and Hf analyses were done by Neutron activation analyses (Watters, pers. comm., 1985).

Sample Collection

Sample suites from the Antarctic terrain can seldom be considered as truly representative owing to the paucity of outcrop and difficult accessibility in many cases. It was attempted to sample individual nunataks along vertical profiles where possible. Most Borgmassivet intrusions are fine- to medium-grained and the sample sizes of 5 Kg can be considered as representative of a particular sampling site. Samples of coarse-grained rocks, such as pegmatites, were about 10 Kg. In the case of the pegmatites, which are texturally and chemically heterogeneous rocks, it is possible that this sampling size was too small to avoid sampling error altogether. However, sampling size was constrained by logistic considerations.

Sample Preparation

Weathered material was removed from samples in the field as far as possible. Any remaining excess material was removed and samples were reduced to fragments of 5 to 10 cm in diameter by using a hydraulic sample splitter with hardened steel cutters. The fragments were scrubbed under running water before being cleaned in an ultrasonic cleaner for 60 seconds. They were rinsed in distilled water supplied by the Department of Chemistry at the University of Natal, after which they were dried at 100°C for 1 hour. The fragments were then crushed by a jaw crusher with hardened steel jaws to fragments less than 1 cm in diameter. The crushed sample was reduced to approximately 100 g by the cone-and-quartering technique, and then milled to a fine powder in a swing mill ("siebtechnik"). Both vidiasteel and tungsten carbide swing mills were used. The jaw crusher was cleaned by brushing the jaw surfaces with a wire brush and washing with acetone, following by vacuum cleaning. At the start of a sample run the jaw crusher was "washed" with a sample representative of the run. A run consisted of samples of similar compositions, e.g. gabbros and gabbronorites of Annandagstoppane were included in one run, but anorthosites from the same area were part of an "anorthosite" run. The swing mill was cleaned in a similar way, but quartz was used first to clean the mill after samples with high chlorite or serpentine contents were milled.

Sample Preparation for X-Ray Spectrometry

Borgmassivet Intrusions

Most of the major and minor elements were analysed using the lithium tetraborate fusion method of Norrish and Hutton (1969). Analyses of Na_2O on samples suffixed "/81", P_2O_5 on samples from the Hammer Heads and Gully

sections and all the trace elements except REE, Th and Hf, were done on pressed powder pellets.

Preparation of Norrish fusion discs:

Silica crucibles were cleaned in dilute solution of HCl. Approximately 0.5 g of sample was weighed into the crucibles and dried at 100°C. The crucibles with samples were placed in a furnace at 1000°C for 4 hours and allowed to cool in a desiccator. The spectroflux used for the fusion discs was preheated in Pt crucibles at 1000°C, and $\pm 0,4$ g of the ashed sample was added as near as possible to the ratio of weight sample : weight flux = 2.2. Fusion was effected at 1000°C, and the product was cast in a brass dye maintained at 250°C. Annealing occurred for ± 3 hours on a heated asbestos plate and then allowed to cool gradually. The flux used was Johnson Mathie Spectroflux 105. Each new batch of flux was homogenized and a new set of standards was made up.

Pressed powder pellets:

Approximately 10 g of sample was mixed with 1 ml Mowiol solution in an agate mortar. Compression was at 10 tonnes in a position cylinder for ± 5 seconds. Hardening occurred at 120°C for ± 8 hours.

X-Ray Fluorescence Spectrometry:

X-ray fluorescence spectrometry was done on a Philips PW1410 spectrometer in the Department of Soil Science at the University of Natal, Pietermaritzburg. Calibrations were controlled with international standards and in-house synthetic standards and blanks. International standards used were NIM-D,

NIM-G, NIM-L, NIM-N, NIM-P, NIM-S, AGV, BR-1, BCR-1, DTS-1, G-2, GSP-1, JB-1, PCC-1 and W-1. Internationally accepted standard values were from Abbey (1980). Dr A.H. Wilson of the Department of Geology, University of Natal, Pietermaritzburg compiled the computer programs used for reduction of count data and calculation of mass absorption coefficients.

Data on Straumsnutane basalts

Major and trace element analyses were done by Dr B.R. Watters on pressed powder pellets using X-ray fluorescence spectrometry at the Open University. Details of sample preparation and potential errors can be obtained from Dr B.R. Watters, Department of Geology, University of Regina, Regina, Saskatchewan, Canada.

Precision of XRF Analyses

Precision of X-ray fluorescence major and trace element analyses is summarized below:

Major elements:

SiO ₂ :	$\pm 0.3\%$ at 50%	Al ₂ O ₃ , CaO, FeO:	$\pm 1\%$ at 15%
MgO :	$\pm 0.2\%$ at 20%	Na ₂ O :	0.15% at 4%
K ₂ O :	0.05% at 4%	MnO :	0.03% at 0.5%
TiO ₂ :	$\pm 0.01\%$ at 1.5%	P ₂ O ₅ :	0.03% at 0.5%
P ₂ O ₅ on pressed pellets: $\pm 5\%$ at 200 to 1000 ppm			

Trace elements:

Nb,Y: 0 - 200 ppm:	$\pm 5\%$		
Zr: 0 - 200 ppm:	$\pm 2\%$;	200 - 500 ppm:	$\pm 5\%$
Sr, Rb: 0 - 500 ppm:	$\pm 5\%$		
Cr, Ni: 0 - 500 ppm:	$\pm 5\%$;	500 - 2000 ppm:	$\pm 10\%$

Zn, Cu:	0 - 200 ppm:	$\pm 50\%$
Sc:	0 - 50 ppm:	$\pm 2\%$
V:	0 - 300 ppm:	$\pm 5\%$
Ba:	0 - 500 ppm:	$\pm 10\%$

Oxidation State of Iron

X-ray fluorescence analyses determine the total amount of iron in a rock. In order to distinguish between Fe^{2+} and Fe^{3+} wet chemical methods are required, which are not available at present.

A standard ratio of $\text{Fe}^{2+} : \text{Fe}^{3+} = 9 : 1$ was used in this project in order to compare the data from different nunataks. Factors such as the primary $\text{Fe}^{2+} : \text{Fe}^{3+}$ ratio of the magma, degree of crustal contamination and interaction with groundwater would have affected the final $\text{Fe}^{2+} : \text{Fe}^{3+}$ in the Borgmassivet intrusions. Hence, it is very important that wet chemical methods are used in future studies in order to determine the correct ratio.

Modal Analysis

The method of modal analysis used for this project was that of Neilson and Brockman (1977). Data were collected as a series of 12 sets of 36 points each. Typical errors were the following

Volume per cent	5	:	$\pm 1.5\%$
	5 - 20	:	$\pm 5\%$
	20 - 50	:	$\pm 7\%$

Grain Size Analysis

The analysis of grain sizes in thin and polished sections has been investigated and discussed by various authors (e.g. Krumbein and Pettijohn, 1938; Harrell and Erikssen, 1979). These authors assume spherical grains and make appropriate corrections to determine true grain size. In the case of grain size determinations in ores the most important factor is mineral liberation size, in which predictions are made of ore liberation as a function of particle mesh size (King, 1983). Empirical correction equations may produce correction factors as high as 30 per cent.

Jackson (1961) represents the maximum and minimum diameters of non-equidimensional grains in the Stillwater Complex in terms of the apparent diameter. He quotes Greenman (1951) who showed there was doubt as to the applicability of sectioning corrections to grains not spherical or ellipsoidal in shape. Jackson (1961) emphasizes that his techniques should be used only for comparative purposes within a single intrusion. In a study of apparent diameters of tabular grains compared to the true diameters of orientated grains Wilson (pers. comm., 1985) found that a correction for sectioning of only 11 to 12 percent is required for tabular grains as opposed to the theoretical correction of 20 to 25 per cent for spherical grains.

Some evidence of size bimodality exists (Figure 2.29, Chapter 2). In order to determine distribution parameters correctly, at least one of the populations must be known accurately. Slight changes in means and shapes of frequency distributions can cause considerable change in the shape of the combined frequency distribution curves, and the combined mean. Therefore the comparative approach of Jackson has been followed, with no corrections having been made for the sectioning effects.

APPENDIX 2

SAMPLE DESCRIPTIONS AND GEOCHEMISTRY

Sample descriptions and geochemical data of analysed samples are summarized in Tables A2.1 and A2.2. The thin sections and samples are stored in the Department of Geology and Mineralogy , University of Natal, Pietermaritzburg. Thin sections of Straumnsnutane basalts are stored in the Department of Geology, University of Regina, Regina, Canada. Data on Straumnsnutane basalts and all REE analyses were supplied by Watters (pers. comm., 1985). Table A2.3 summarizes REE and related data, and analyses on one Annandagstoppane granite and three Lüneburg granitic rocks are given in Table A2.4. The Lüneburg data were supplied by Smith (pers. comm., 1986). Further reduction of data, including norm calculations are available from The Head, Department of Geology and Mineralogy, University of Natal, P.O.Box 375, Pietermaritzburg, 3200. These data reductions make use of a program developed by Wilson (pers. comm., 1981). An example is given in Table A2.5.

The following abbreviations are used in Table A2.1:

ap: apatite	Ht: Height	plag: plagioclase
bi: biotite	inv.pg: inverted	py: pyrite
chl: chlorite	pigeonite	q: quartz
cpx: clinopyroxene	Kf: K-feldspar	serp: serpentine
ep: epidote	l.t.: less than	sph: sphene
Fe-Ti: Fe-Ti oxides	ms: white mica	tm: tremolite-actinolite
g-q: granophyric	ol: olivine	zr: zircon
intergrowths of quartz and alkali feldspar	opx: orthopyroxene	
	pg: pigeonite	

TABLE A2.1
HAND SPECIMEN AND PETROGRAPHIC DESCRIPTIONS OF CHEMICALLY ANALYSED SAMPLES

SAMPLE NUMBERS	LOCALITY	HAND SPECIMEN: TEXTURE AND NAME	TEXTURE	CONSTITUENT MINERALS	COMMENTS
<u>ANNANDAGSTOPPANE</u>					
A1/81 to A10/81 (10 samples)	Hammer Heads	Porphyritic medium-grained gabbronorite	Porphyritic rock with an ophitic and poikilitic texture in which postcumulus phenocrysts are set in a matrix of cumulus orthopyroxene and plagioclase, and postcumulus Fe-Ti oxides, biotite, micrographic intergrowths of quartz and alkali feldspar, and rare apatite.	Major: opx, cpx, plag. Minor: Fe-Ti, bi, g-q, ap.	Short chains consisting of opx crystals locally. Zoning in plagioclase and opx. Minor deuteric alteration.
A11/81	Hammer Heads	Fine-grained dark-grey basaltic dyke.	Fine-grained glomeroporphyritic rock with an intergranular texture in which aggregates of plag phenocrysts are set in a matrix of plag, cpx and Fe-Ti.	Major: plag, cpx Minor: Fe-Ti, ms, (tm), (chl), (py).	Local deuteric and/or hydrothermal alteration.
A12/81 and A13/81	Hammer Heads	Veined medium-grained gabbronorite.	As A1/81; pyroxenes extensively uralitized, plag partially sericitized	As A1/81 + sericite and uralite.	
A14/81	Hammer Heads	Medium-grained gabbro-norite.	As A1/81, except opx not normally euhedral. Opx has reaction relationships with pg (now inverted) and cpx. Opx is mantled by inv. pg, which is in turn mantled by a 2nd generation opx. Mantles of cpx commonly occur over the 2nd generation opx.	As A1/81 + inv. pg	
A1/82 and A2/82	Viper's Hill	Medium-grained gabbro-norite.	As A1/81.		Euhedral crystals of opx form clusters and short chains.
A3/82	Viper's Hill	As A1/82	As A1/81 and A1/82, but plag has been sericitized completely and opx has been uralitized extensively. Small amounts of uralitized cpx are present.	Sericite, chl, uralite	
A5/82	Viper's Hill	Medium-grained, mottled anorthosite pod	Medium-grained granular anorthosite containing rare interstitial opx and cpx, and narrow lamellae (l.t. 0.5 mm) which are noritic in composition.	Major: plag, (cpx), (opx). Minor: (g-q)	Plag laths are locally in subparallel orientation.
A7/82	Viper's Hill	Basaltic dyke	As A1/81		Samples not <u>in situ</u>
A9/82	Viper's Hill	Fine- to medium-grained cream-white albitite.	Granophyric quartz albitite composed essentially of quartz and albite, which are intergrown with each other and occur as discrete grains. Quartz is highly strained and ab shows checker board twinning.	Major: Ab, q. Minor: Chl, Fe-Ti.	Samples not <u>in situ</u>
A14/82, A16/82 A17/82, A21/82	Viper's Hill	Medium-grained norite.	As A1/81 and A1/82.		

SAMPLE NUMBERS	LOCALITY	HAND SPECIMEN: TEXTURE AND NAME	TEXTURE	CONSTITUENT MINERALS	COMMENTS
A22/82	Viper's Hill	Mottled anorthosite pod	Porphyritic medium-grained rock consisting of postcumulus poikilitic phenocrysts of cpx and inv.pg set in a matrix of orthocumulus plag. Mottling is caused by irregular distribution of mafic minerals and plag.	Major: plag Minor: cpx, inv.pg, bi, chl. Mottles: Major: cpx, inv.pg, plag.	Deuteric alteration of plag and pyroxenes is common.
A23/82	Echo	As A1/81 and A1/82			
A24/82	Echo	As A9/82	Granular texture	As A9/82 + tm, ep, sph, zr	No apatite in this rock
A25/82, A27/82	Echo Bravo	As A1/81 and A1/82	As A14/81		
A30/82	Bravo	As A11/81			
A34/82	Hammer Heads	As A1/81 + abundant cpx phenocrysts	As A1/81, but small amounts of inv.pg present. Postcumulus cpx phenocrysts are up to 6 mm in diameter.		
A36/82	Hammer Heads	Albitite	Phenocrysts of tremolite-actinolite set in matrix of albite.	Major: ab, (tm). Minor: zr, ap	Relatively high ap content.
A38/82, A39/82	Hammer Heads	As A14/81			
	<u>Hammer Heads Section</u>				
Ht = 0 to 14 m	Lower unit	As A34/82	As A14/81, but phenocrysts are more abundant.		Bi content increases at 14 m
Ht = 15 m	Uppermost sample in lower unit	As A14/81	Quartz and Kf present as discrete grains.	Bi up to 5 %	Deuteric alteration common.
Ht = 16 to 44 m	Upper unit	As A1/81			Small amounts of inv.pg present below 26 m.
<hr/>					
	<u>JULETOPPANE</u>				
JT1/82	Julepiggen	Granophyric pegmatite	Coarse-grained anhedral granophyric pegmatite consisting of graphic intergrowths of q and ab in a matrix of uralitized cpx, symplectic intergrowths of q and Fe-Ti, bi and tm. Clusters and veinlets of green ap present locally.	Major: q, plag, cpx, (Fe-Ti), (bi), (tm). Minor: ap, chl.	Albite extensively sericitized.
JT4/82	Julepiggen	Fine- to medium-grained gabbro pod.	Fine- to medium-grained intergranular texture in which euhedral laths of plag occur with interstitial cpx and inv.pg.	Major: plag, cpx, inv.pg. Minor: Fe-Ti, bi, g-q, chl, ap, ms, tm.	Extensive uralitization, locally sericitization and suassuritization.

SAMPLE NUMBERS	LOCALITY	HAND SPECIMEN: TEXTURE AND NAME	TEXTURE	CONSTITUENT MINERALS	COMMENTS
JT7/82	Julepiggen	As JT4/82	Fine- to medium-grained subophitic intergranular texture.	As JT4/82; chl minor	Fe-Ti alteration to leucoxene.
JT8/82	Julepiggen	Medium-grained gabbro-norite	Composite opx megacrysts mantled by inv.pg, rarely mantled in turn by opx, set in orthocumulate matrix of plag, cpx, bi, Fe-Ti and g-q.	Major: opx, cpx, inv.pg and plag. Minor: g-q, Fe-Ti, bi, chl, ap, ep, tm.	
JT11/82	Julepiggen	As JT1/82			Very little apatite.
JT12/82	Thandi	As A14/81	As A14/81 + presence of euhedral opx.		
JT13A,13B/82	Thandi	Granophyric pegmatite	Similar to JT1/82; all cpx extensively uranitized. Ep and sph common.	As JT1/82; less g-q and ap. Ep and sph common.	Extensive euhedral alteration.
JT15/82	Thandi	Medium-grained norite	As A14/81, with large megacrysts of anhedral inv.pg, no identifiable primocrysts of opx, and l.t. 10 % cpx.		Chloritization of cpx and inv.pg is common.
JT17/82	Julepiggen	Fine-grained gabbroic sill	Fine-grained gabbroic texture of plag laths with interstitial cpx and rare inv.pg.	Major: plag, cpx, (inv.pg). Minor: g-q, Fe-Ti, (bi)	
JT18/82 JT20,22,23/82	Julepiggen Gjaever's Sentinel	Medium-grained norite/ gabbro-norite	As JT15/82		
JT24/82	Ebele	Fine- to medium-grained gabbroic pod.	As JT4/82		Less alteration than JT4/82
JT25,26,27/82	Ebele	As JT20/82	As JT15/82		
JT28/82	Camp Hill	Medium-grained norite.	As A1/81, with less than 10 % cpx.	Major: plag, opx, (cpx). Minor: inv.pg, Fe-Ti, bi, g-q.	
JT29/82	Camp Hill	Fine-grained quartz gabbro pod.	Fine-grained porphyritic/ophitic texture, with intergranular matrix. G-q make up to 20 % of the rock.	Major: plag, cpx, g-q. Minor: Fe-Ti, bi, ap.	
JT30/82	Julepiggen	Fine-grained gabbroic sill.	As JT17/82		
JT31/82	Julepiggen	As JT17/82	As JT17/82, but plag laths in sub-parallel orientation.		
<u>FÖRSTEFJELL</u>					
F1,7,8,9/82		As JT15/82	As JT15/82, but cpx more abundant (20 to 25 % in F1/82).		
F2,3,4/82		As JT17/82			

SAMPLE NUMBERS	LOCALITY	HAND SPECIMEN: TEXTURE AND NAME	TEXTURE	CONSTITUENT MINERALS	COMMENTS
<u>ROBERTSKOLLEN</u>					
Ht = 0 to 20 m	Zone I, Gully Section	Medium-grained mela-olivine gabbro-norite and mela-olivine norite	Porphyritic, locally subpoikilitic to radiating and rarely laminated textures. Euhedral chromite enclosed in ol and opx. Euhedral ol is enclosed in plag, cpx and phlogopite, and anhedral ol occurs in opx. Ol-opx show reaction relationships, but rare euhedral ol is partly enclosed locally by opx. Plag shows textures consistent with high degrees of supercooling and metastable nucleation. Opx and cpx are anhedral and occur interstitially to plag, or enclose plag locally. Phlogopite occurs in interstices and as an alteration product of Fe-Ti oxides and cpx.	Major: ol, opx, cpx, (plag). Minor: Fe-Ti, phlogopite	
Ht = 22 to 32 m	Zone II, Gully Section	Medium-grained mela-olivine gabbro-norite and plagioclase-bearing lherzolite.	Euhedral cumulus opx appears at 22 m, with sharp increase in modal opx and decrease in ol content. Subhedral cpx occurs at 22 m as an interstitial mineral, but above this level it is euhedral. Postcumulus megacrysts of opx show zoning to more Fe-rich mantles. There is an increase in phlogopite content at 34 m in the plagioclase-bearing lherzolite.	As above	
Ht = 34 to 40 m	Zone III, Gully Section	Medium-grained mela-olivine norite (at base) and mela-olivine gabbro-norite.	General increase in grain size relative to Zone II. Textures similar.	As above	
Ht = 42 to 51.5 m	Zone IV, Gully Section	Medium-grained mela-gabbro-norite.	Granular rock with cpx and opx primocrysts. Strongly zoned plag laths are locally present. Rare quartz grains are highly corroded.	Major: cpx, opx Minor: plag, ol, (q), phlogopite, tm.	Extensive uranization
Ht = 52 76 m	Zone V, Gully Section	Medium-grained gabbro-norite	Anhedral phenocrysts of opx and cpx are set in a matrix of plag, opx, cpx, bi and Fe-Ti. Micrographic intergrowths of q and Kf are common. Rare ol occurs at the base of the zone.	Major: opx, cpx, plag. Minor: bi, Fe-Ti, tm, ap, g-q.	
Ht = 78 106 m	Zone VI, Gully Section	Medium-grained quartz gabbro	Textures similar to Zone V, but increase in q and decrease in opx.		
R1/82	Glacier's Edge	Medium-grained gabbro-norite	Anhedral megacrysts of opx and cpx are set in a matrix of plag, opx, cpx, bi and Fe-Ti oxides. Quartz is present as interstitial, anhedral grains and in g-q.	As Zone V, Gully Section	Deuteric alteration common.

SAMPLE NUMBERS	LOCALITY	HAND SPECIMEN: TEXTURE AND NAME	TEXTURE	CONSTITUENT MINERALS	COMMENTS
R2/82	Tumble Ice contact zone	Medium- to coarse-grained melagabbro-norite.	As Zonell, Gully Section		
R3/82	Tumble Ice contact zone	Medium- to coarse-grained mela-olivine gabbro-norite.	As Zone II, Gully Section		
R4/82	Tumble Ice contact zone	Medium- to coarse-grained melagabbro-norite	As Zone II, Gully Section		
R5/82	Tumble Ice ultra-mafic unit	Medium- to coarse-grained mela-olivine gabbro-norite	As Zone II, Gully Section		
R6/82	Tumble Ice, mafic unit	Medium-grained gabbro-norite	As Zone V, Gully Section, but less quartz.		
R7/82	Tumble Ice, ultra-mafic unit	Medium- to coarse-grained plagioclase-bearing hornblende	As Zone II, Gully Section		
R8/82	Tumble Ice, ultra-mafic unit	Medium- to coarse-grained plagioclase-bearing hornblende	As Zone II, but much more ol present.		
R14,15/82	Tumble Ice, mafic unit	Medium-grained gabbro-norite	As Zone V, Gully Section		
R16/82	Tumble Ice, mafic unit	Medium-grained quartz gabbro	As Zone VI, Gully Section		
R20/82	Ice Axe Peak	Fine-grained mottled Jurassic(?) dyke	Not determined		
R23/82	Zone I, Gully Section				
R25/82	Zone II, Gully Section				
R26/82	Zone III, Gully Section				
R27/82	Zone IV, Gully Section				
R31/82	Peaceful Hill	Pegmatitic quartz gabbro	As Zone VI	Trace amounts of zircon	
R33,35/82	Petrel's Rest	Medium- to coarse-grained mela-olivine gabbro-norite	As zone II, Gully Section		
R35/82	Petrel's Rest	As Zone IV, Gully Section			

SAMPLE NUMBERS	LOCALITY	HAND SPECIMEN: TEXTURE AND NAME	TEXTURE	CONSTITUENT MINERALS	COMMENTS
R36A/82	Petrel's Rest contact zone	Coarse-grained mela-olivine gabbronorite	As Zone IV, Gully Section		
R36B/82	Petrel's Rest contact zone	Coarse-grained ol-bearing melagabbronorite	As Zone IV, Gully Section		
R37/82	Petrel's Rest contact zone	Medium-grained melagabbronorite	As Zone IV, Gully Section		
R38/82	Petrel's Rest ultramafic unit	Coarse-grained mela-olivine gabbronorite	As Zone III, Gully Section, with rare, corroded quartz grains		
R39/82	Petrel's Rest	Fine- to medium-grained Jurassic(?) dyke	Not determined		
R40/82	Top of Ice Axe Peak	Porphyritic medium-grained gabbro	As Zone V, with cpx phenocrysts defining a porphyritic/ophitic texture		
R42/82	Top of Ice Axe Peak	Medium-grained quartz gabbro	As Zone VI, Gully Section		
R43/82	Top of Ice Axe Peak	Fine-grained doleritic chill zone(?).	Variolitic ol-bearing dolerite with a groundmass of fans of plag needles, with cpx in interstices and opx intergrown with needles. Metastable quartz is present.	Major: plag, cpx, opx, (ol) Minor: q, bi	
<u>GRUNEHOGNA</u>					
G9/82 to G14/82	North face, Grunehogna main peak: Grunehogna sill	Medium-grained melano-cratic diorite	Medium-grained granular to locally intergranular texture, consisting of plag, cpx, hornblende, Fe-Ti, Kf and q. Plag strongly zoned, Kf micro-perthitic owing to high haematite content. Fe-Ti up to 5 %.	Major: plag, cpx, hornblende, (Fe-Ti). Minor: Kf, q, g-q, (bi), ap, zr, ep, sph.	Seritization, uralitization and modal g-q increase from G9 to G14/82.
G15, 16A, 16B/82	North face, Grunehogna main peak: Grunehogna pegmatite	Coarse-grained quartz diorite pegmatite, locally with high ep content.	G-q set in matrix of plag and hornblende, which is locally intergrown with skeletal Fe-Ti.	Major: G-q, plag, hornblende Minor: Fe-Ti, sph, chl, tm, ep, ap, zr.	
G17/82	North face, Grunehogna main peak: Base of Kullen sill.	Fine- to medium-grained diorite	Fine- to medium-grained granular diorite, consisting of anhedral hornblende and stubby sericitized and saussuritized plag laths.	Major: plag, hornblende Minor: q, g-q, ep, chl, bi, sph, zr.	Presence of q and q + ep veinlets.
G18/82	North face, Grunehogna main peak: Kullen sill	Medium-grained diorite	Extensively sericitized and uralitized rock in which primary textures cannot be recognized and ep is an important minor constituent.	Major: plag, sericite, tm. Minor: g-q, ep, sph, chl	
G19/82	1285 south	fine-grained Jurassic(?) dyke	Not discussed in text		

SAMPLE NUMBERS	LOCALITY	HAND SPECIMEN: TEXTURE AND NAME	TEXTURE	CONSTITUENT MINERALS	COMMENTS
G28,29,31/82	West peak: chill zones and apophyses, Kullen sill.	Fine-grained basaltic rocks, locally containing cpx phenocrysts.	Fine-grained, locally variolitic, intergranular to porphyritic textures defined by microphenocrysts of tm and radiating plag laths in places. Irregular distribution of Fe-Ti.	Major: plag, tm, (g-q) Minor: q, ep, bi, Fe-Ti, Kf.	Quartz grades into g-q textures and may represent xenocrysts. Extensive sericitization and uralitization in places.
G32/82	As G18/82				
G33,34/82	North face, Grunehogna main peak: Kullen chill zones and apophyses	As G28/82			
G35,36/82	North face, Grunehogna main peak.	Intimate mixture of Kullen chill zone and sedimentary material.	Sedimentary material is granophyric. Not discussed in text.		
G50/82	Western Grunehogna	Orange-red medium-grained granosediment	Granosediment textures as defined in Chapter 4.	Major: q, albite, Kf, (ep), (Fe-Ti) Minor: sph, chl, tm, carbonate, ms	
G51,52/82	Western Grunehogna	Medium-grained light-grey to orange-red granophyre.	Spherical granophyric intergrowths of q, albite and Kf are set in a granular matrix of q, microcline, albite and accessory minerals. Fe-Ti up to 3 to 4 %.	Major: q, Kf, albite, (Fe-Ti) Minor: chl, ms, sph, ep, zr	Small (l.t. 5 mm) vugs present.
G53/82	Western Grunehogna Kullen sill	Medium-grained diorite	As G18/82		
G58 to G61/82 G63,64,65,67/82	North section, Kullen peak, Kullen sill.	Melanocratic medium-to coarse-grained gabbro and diorite.	Textures range from similar to A18/82 to those with primary igneous textures. These are fine- to medium-grained granular and interstitial to porphyritic, with phenocrysts of uralitized cpx. Plag occurs as phenocrysts, laths in the matrix and in g-q. Locally the rock becomes granophyric. Fe-Ti occurs as poikilitic to skeletal grains.	Major: plag, cpx, tm Minor: q, g-q, chl, ms, ap, ep, Fe-Ti.	
G66/82	North section, Kullen peak, Kullen sill	Fine-grained chill zone	As G 28/82		
G200/81	Grunhogna south	Medium-grained orange-red granite	Medium-grained granular granite consisting of q, microcline microperthite, albite and accessory minerals. Kf contains exsolved haematite.	Major: q, Kf, plag Minor: ms, ep, chl, tm, Fe-Ti, zr, ap, sph.	
G4,5,30,37,38,432 44,49/82	Grunehogna sill contact zones	Orange-red medium-grained granosediments	Granosediment textures as defined in Chapter 4.		

SAMPLE NUMBERS	LOCALITY	HAND SPECIMEN: TEXTURE AND NAME	TEXTURE	CONSTITUENT MINERALS	COMMENTS
G431/82	1285 south grano-sediment contact zone	As G200/81			
G11,12,3/81	Grunehogna south	As G58/82			
G21,22/81	Grunehogna south	As G58/82, but with chlorite veinlets	Not discussed in text		
G5,6,9/81	Grunehogna south	As G200/81			
G10/81	Grunehogna south	As G51/82			
<u>KRYLEN</u>					
K1 - 5, 8 - 10/81 K12/81	Top of nunatak	Grey to dark-grey quartz diorite	Medium-grained granular to seriate texture, comprising plag, opx, cpx, inv.pg, q, Fe-Ti and bi. Textures very similar to Juletoppane gabbro-norites, including opx-inv.pg-2nd opx crystallization.	Major: plag, opx, cpx (q) Minor: Fe-Ti, bi, ap, ep, (zr)	Considerable sericitization of plag and urolitization
K6/81	Top of nunatak	Felsic dyke	As G50/82		
K7/81	Top of nunatak	Jurassic(?) dyke	Not discussed in text		
K11/81	Top of nunatak	Medium-grained melagabbro-norite	Medium-grained granular to ophitic textures, consisting of ol grains enclosed in cpx, radiating plag laths, opx, chromite, Fe-Ti and phlogopite.		
<u>JEKSELEN</u>					
J9,16 - 19/81	Zone III, SE Jekselen	Fine-grained amygdaloidal porphyritic quartz andesite	Fine-grained amygdaloidal porphyritic rocks in which skeletal or hopper cpx needles form mantles over serp cores. These phenocrysts are set in a matrix of plag laths which locally are in poorly defined radial structures. Patches of devitrified glass (?) occur in which curved plag needles form fans or "horse's tails" structures and rarely festoons. Highly corroded quartz grains are interstitial to plag and cpx. G-q are rare. Quartz amygdaloids are locally present.	Major: plag, cpx Minor: q, (g-q), chl, serp, ap, ep	Extensive saussuritization, sericitization and urolitization.

SAMPLE NUMBERS	LOCALITY	HAND SPECIMEN: TEXTURE AND NAME	TEXTURE	CONSTITUENT MINERALS	COMMENTS
J11 to 14/81	Apophyses, SE Jekselen	Fine-grained amyg- daloidal quartz monzodiorite	Porphyritic to granophyric rock in which stubby laths of uralitized cpx megacrysts occur in a matrix of sericitized and saussuritized plag, interstitial, corroded q, g-q, Kf, Fe-Ti, ap, ep and chl. The cpx contains cores of chl in places. Small serpentinized pseudomorphs after ol(?) occur rarely.	Major: plag, cpx Minor: q, g-q, Kf, chl, Fe-Ti, ep, ap, tm, ms.	
J15/81	Upper contact with sediments, Zone III, SE Jekselen	Fine-grained selvage of intimately mixed andesite and sediment	Devitrified glass (?) occurring as numerous polygons of fine, felty material occurs in association with arenitic sediment in which the textures are similar to those in the grano- sediments described in Chapter 4.	Major: q, ms(?), carbonate, devitrified glass Minor: Fe-Ti, chl	

TABLE A2.2

MAJOR AND TRACE ELEMENT GEOCHEMISTRY

WHOLE ROCK GEOCHEMICAL DATA OF ANNANDAGSTOPPANE INTRUSIONS

MAJOR ELEMENTS IN WEIGHT PER CENT													TRACE ELEMENTS IN PPM											
SiO2	Al2O3	Fe2O3	FeO	MnO	MgO	CaO	Na2O	K2O	TiO2	P2O5	TOTAL	LOI	NB	ZR	Y	SR	RB	ZN	CU	NI	SC	CR	BA	V
A1.82 52.92	15.13	.97	7.89	.17	10.71	8.96	1.59	.62	.4055	.0600	99.43	.17	5.6	63	9.0	131	30	69	45	116	29.3	377	ND	161
A2.82 52.87	12.34	1.12	9.06	.21	13.03	7.84	1.19	.64	.4060	.0600	98.77	.10	4.3	56	6.3	103	31	81	43	147	34.6	453	ND	177
A3.82 52.66	12.61	1.02	8.24	.18	11.53	8.40	1.80	1.02	.5109	.0600	98.03	3.62	3.7	70	10.7	97	62	70	120	164	41.0	520	194	211
A5.82 51.15	25.33	.38	3.06	.06	2.35	12.54	2.29	1.07	.3854	.0700	98.69	1.07	6.3	72	10.7	225	58	29	33	22	10.3	55	263	88
A7.82 54.12	14.95	1.12	9.03	.17	5.82	10.05	1.94	1.17	.8273	.1100	99.31	.69	6.7	116	23.7	114	64	85	104	91	38.5	101	247	257
A9.82 76.84	12.72	.11	.89	.01	.44	.47	7.01	.02	.2463	.0200	98.78	.66	19.6	130	11.4	31	5	8	3	3	.4	9	10	6
A14.82 52.71	12.93	1.12	9.10	.20	12.25	8.47	1.11	.50	.3926	.0600	98.84	-.17	3.1	54	7.0	108	19	79	37	130	34.4	443	146	173
A16.82 53.59	11.88	1.16	9.41	.21	13.62	7.43	1.16	.57	.4365	.0700	99.54	-.07	3.2	62	8.9	100	24	85	49	150	35.9	528	ND	177
A17.82 53.17	12.28	1.13	9.18	.19	12.59	7.67	1.26	.57	.4272	.0500	98.52	.06	2.7	62	8.4	103	22	82	40	141	34.6	468	ND	183
A21.82 53.84	11.44	1.14	9.25	.21	13.44	7.50	1.03	.57	.4298	.0500	98.90	.00	2.8	62	8.1	97	25	83	46	152	34.5	531	ND	190
A22.82 53.01	17.46	.78	6.32	.15	7.69	10.94	1.77	.90	.4335	.0700	99.52	.67	5.1	71	11.6	158	48	59	38	82	27.6	261	ND	150
A23.82 52.82	14.62	1.01	8.16	.17	10.45	8.92	1.42	.63	.4362	.0500	98.69	.22	2.3	65	9.2	129	28	71	47	112	31.2	370	ND	170
A24.82 74.15	13.04	.07	.58	.01	.55	.77	7.69	.03	.2273	.0200	97.14	.45	36.5	115	18.4	38	4	3	1	5	2.4	15	ND	11
A25.82 53.09	14.62	1.01	8.21	.18	10.93	8.79	1.43	.67	.4477	.0700	99.45	.11	3.7	65	10.0	131	28	73	55	115	22.5	373	ND	170
A27.82 53.06	15.83	.96	7.76	.15	8.27	9.16	1.67	.86	.6271	.0700	98.42	.09	4.7	88	14.0	133	37	68	71	94	27.9	281	208	196
A30.82 53.81	14.72	1.13	9.14	.18	5.71	9.67	1.84	1.32	.8628	.1100	98.49	.49	6.6	117	23.6	111	78	89	102	87	35.7	96	ND	261
A34.82 53.70	14.66	1.01	8.15	.17	10.09	8.80	1.62	.75	.5521	.0800	99.58	.11	3.1	75	12.4	117	33	71	64	117	27.7	366	ND	180
A36.82 65.53	14.80	.21	1.70	.03	3.53	3.49	8.49	.04	.8670	.1600	98.85	.66	18.1	246	20.9	31	4	9	0	33	20.9	127	ND	80

WHOLE ROCK GEOCHEMICAL DATA OF ANNANDAGSTOPPANE INTRUSIONS

MAJOR ELEMENTS IN WEIGHT PER CENT													TRACE ELEMENTS IN PPM											
SIO2	AL2O3	FE2O3	FE0	MNO	MGO	CAO	NA2O	K2O	TIO2	P2O5	TOTAL	LOI	NB	ZR	Y	SR	RB	ZN	CU	NI	SC	CR	BA	V
A38.82 53.37	14.68	1.00	8.12	.17	10.02	8.79	1.36	.76	.5465	.0700	98.89	.01	3.9	76	11.0	120	32	73	86	120	29.9	387	ND	182
A39.82 53.16	15.63	.96	7.79	.16	9.38	8.94	1.63	.78	.5207	.0700	99.02	.02	4.0	76	10.5	134	38	70	92	113	27.8	348	207	171
A1.81 53.58	15.06	1.00	8.13	.17	10.48	8.73	1.70	.63	.4900	.0800	100.05	.10	2.9	66	9.7	122	25	73	60	118	26.7	ND	ND	0
A2.81 53.90	15.81	.98	7.91	.16	9.72	9.03	1.72	.66	.5100	.0700	100.47	.10	2.5	69	10.4	128	29	69	64	112	26.8	414	ND	146
A3.81 53.40	14.92	1.02	8.28	.17	10.47	8.79	1.58	.65	.5300	.0700	99.88	.36	3.5	67	9.2	119	28	76	67	119	27.5	ND	ND	0
A4.81 53.50	14.80	1.02	8.24	.17	10.35	8.68	1.70	.68	.5100	.0800	99.73	.19	1.1	69	10.3	123	28	72	69	118	27.7	428	ND	169
A5.81 53.56	15.99	.96	7.79	.16	9.68	9.08	1.72	.65	.5100	.0700	100.17	.12	5.0	66	10.0	128	31	67	62	110	25.8	ND	ND	0
A6.81 53.35	15.80	.97	7.82	.16	9.56	9.03	1.78	.71	.5300	.0700	99.78	.16	2.2	72	11.4	136	33	65	73	104	25.6	390	ND	165
A7.81 53.24	15.40	.98	7.97	.17	10.02	8.86	1.70	.69	.5200	.0800	99.63	.11	3.5	70	10.8	130	27	74	73	115	26.6	ND	ND	0
A8.81 53.91	15.73	.96	7.77	.16	9.68	9.02	1.69	.68	.5000	.0700	100.17	.18	3.8	69	11.1	125	29	69	75	115	25.9	417	ND	167
A9.81 53.68	15.64	.96	7.80	.17	9.64	7.54	1.70	.67	.5000	.0800	98.38	.14	4.1	71	11.3	129	28	65	61	101	24.5	ND	ND	0
A10.81 53.59	14.96	1.02	8.22	.18	10.13	8.75	1.66	.68	.5300	.0800	99.80	.12	2.5	74	12.3	124	29	76	62	116	26.2	416	ND	174
A11.81 54.61	14.96	1.12	9.06	.17	5.65	9.79	2.08	.85	.8400	.1100	99.24	.91	6.4	117	22.9	123	44	78	95	85	34.4	152	ND	257
A12.81 54.25	15.48	.78	6.35	.11	9.79	9.46	1.62	1.02	.5400	.0900	99.49	1.85	3.8	77	11.4	126	63	51	44	119	31.2	438	ND	177
A13.81 53.46	16.53	.74	5.98	.11	9.03	9.77	1.78	.84	.5400	.1200	98.90	2.57	5.5	73	15.3	141	59	45	43	119	31.0	419	ND	174
A14.81 54.12	14.93	1.04	8.46	.16	8.59	8.88	1.78	.86	.6500	.0800	99.55	.22	7.0	85	16.6	124	41	73	66	101	28.8	339	ND	199

WHOLE ROCK GEOCHEMICAL DATA OF HAMMER HEADS SECTION

MAJOR ELEMENTS IN WEIGHT PER CENT

MAJOR ELEMENTS IN WEIGHT PER CENT												TRACE ELEMENTS IN PPM												
SiO2	Al2O3	Fe2O3	FEO	MNO	MGO	CAO	NA2O	K2O	TiO2	P2O5	TOTAL	LOI	NB	ZR	Y	SR	RB	ZN	CU	NI	SC	CR	BA	V
HEIGHT = 0.0																								
54.16	15.48	.99	8.04	.17	8.87	9.08	1.89	.83	.5876	.0852	100.18	.00	2.4	69	17.5	137	35	79	79	116	28.1	308		ND 186
HEIGHT = 1.0																								
54.19	15.36	1.02	8.27	.18	8.94	9.11	1.80	.85	.5975	.0890	100.41	.00	2.9	70	18.8	140	38	80	81	113	29.6	301		ND 191
HEIGHT = 2.0																								
54.19	15.27	1.04	8.39	.18	9.11	9.03	1.80	.89	.6122	.0806	100.59	.00	3.1	71	17.5	138	37	90	86	130	30.8	321		ND 196
HEIGHT = 3.0																								
53.99	14.89	1.03	8.31	.18	9.41	8.92	1.66	.74	.5711	.0760	99.78	.00	3.1	67	16.2	139	32	89	80	138	30.5	344		ND 186
HEIGHT = 4.0																								
54.27	14.80	1.04	8.44	.18	9.66	8.73	1.64	.86	.5998	.0725	100.29	.00	2.7	69	18.2	133	41	82	78	125	31.0	333		ND 196
HEIGHT = 5.0																								
53.84	15.89	1.00	8.10	.17	8.81	9.18	2.01	.87	.6072	.0851	100.56	.00	2.7	67	17.2	145	41	81	79	115	29.2	307		ND 190
HEIGHT = 6.0																								
53.85	15.33	1.01	8.18	.17	8.97	9.11	1.84	.79	.6033	.0834	99.94	.00	3.4	69	17.1	139	37	80	84	117	29.6	302		ND 189
HEIGHT = 7.0																								
53.84	16.01	.99	8.03	.18	8.73	8.92	1.78	.93	.6124	.0764	100.10	.00	2.9	70	17.5	148	47	78	77	110	28.4	289		ND 197
HEIGHT = 8.0																								
53.81	15.44	1.07	8.66	.18	9.25	9.11	1.79	.85	.5710	.0741	100.81	.00	3.0	64	16.9	136	37	85	77	121	30.0	314		ND 186
HEIGHT = 9.0																								
53.65	15.66	.99	7.99	.18	8.64	9.19	1.82	.84	.5777	.0834	99.62	.00	3.0	68	17.1	143	37	78	92	114	28.9	289		ND 188
HEIGHT = 10.0																								
53.85	15.38	1.01	8.19	.18	9.25	9.07	1.71	.81	.5874	.0824	100.12	.00	3.3	68	18.2	137	35	78	78	116	28.4	309		ND 192
HEIGHT = 11.0																								
53.93	16.35	.98	7.91	.17	8.73	9.26	1.91	.82	.5773	.0742	100.71	.00	2.6	66	16.5	142	40	83	77	116	30.2	294		ND 186
HEIGHT = 12.0																								
53.85	15.84	.99	8.01	.17	9.06	9.16	1.65	.79	.5661	.0736	100.16	.00	3.1	59	16.8	130	33	79	80	120	28.2	310		ND 180
HEIGHT = 13.0																								
53.83	15.56	.99	7.99	.17	9.07	9.22	1.64	.77	.5803	.0784	99.90	.00	2.9	67	16.2	137	33	78	75	125	28.1	311		ND 186
HEIGHT = 14.0																								
54.27	15.59	1.01	8.15	.18	9.21	9.02	1.80	.87	.5937	.0650	100.76	.00	3.4	69	16.7	135	40	77	73	126	28.0	314		ND 184
HEIGHT = 15.0																								
53.00	14.62	1.15	9.29	.19	10.32	8.44	1.68	.74	.5669	.0820	100.08	.00	3.6	22	17.2	132	51	83	72	149	33.0	386		ND 199
HEIGHT = 16.0																								
53.76	16.01	.96	7.80	.17	9.21	9.27	1.82	.74	.5379	.0748	100.35	.00	2.5	62	15.6	144	31	73	62	124	26.8	309		ND 171
HEIGHT = 17.0																								
53.81	15.13	1.03	8.34	.18	9.93	9.13	1.65	.74	.5485	.0655	100.55	.00	1.4	65	15.6	130	33	80	64	139	30.7	367		ND 198

WHOLE ROCK GEOCHEMICAL DATA OF HAMMER HEADS SECTION

MAJOR ELEMENTS IN WEIGHT PER CENT

TRACE ELEMENTS IN PPM

SiO2	Al2O3	Fe2O3	FEO	MNO	MGO	CAO	NA2O	K2O	TiO2	P2O5	TOTAL	LOI	NB	ZR	Y	SR	RB	ZN	CU	NI	SC	CR	BA	V
HEIGHT = 17.0																								
53.86	16.40	.95	7.67	.17	9.27	9.25	1.77	.74	.5073	.0669	100.65	.00	2.3	61	15.2	140	32	70	63	124	26.2	322	ND	169
HEIGHT = 18.0																								
53.64	15.95	.96	7.80	.17	9.27	8.94	1.69	.77	.5209	.0660	99.78	.00	3.0	61	16.9	143	40	73	66	129	28.1	332	ND	174
HEIGHT = 19.0																								
53.82	15.90	.99	8.00	.17	9.70	9.25	1.74	.71	.5249	.0702	100.88	.00	2.1	60	15.2	134	31	75	62	135	27.6	360	ND	178
HEIGHT = 20.0																								
53.75	15.23	1.00	8.10	.18	10.26	8.90	1.69	.70	.5218	.0716	100.40	.00	1.5	60	14.5	132	29	77	67	129	29.1	380	ND	176
HEIGHT = 21.0																								
53.80	15.20	.99	8.04	.18	9.91	8.98	1.60	.71	.5221	.0731	100.01	.00	2.4	61	15.4	132	31	76	66	138	29.2	362	ND	178
HEIGHT = 22.0																								
54.31	14.84	1.05	8.49	.18	10.29	8.66	1.65	.78	.5487	.0707	100.87	.00	3.0	66	17.0	130	35	79	71	139	29.3	371	ND	184
HEIGHT = 23.0																								
54.27	14.13	1.07	8.68	.19	10.74	8.39	1.58	.79	.5614	.0657	100.47	.00	3.7	68	16.9	121	37	80	71	149	31.6	399	ND	192
HEIGHT = 24.0																								
54.16	15.11	1.01	8.18	.18	9.93	8.80	1.66	.79	.5374	.0701	100.43	.00	1.9	64	16.4	133	36	70	75	134	28.4	362	ND	181
HEIGHT = 25.0																								
53.88	15.78	.99	8.00	.17	9.64	9.08	1.75	.77	.5434	.0766	100.68	.00	3.0	64	16.6	136	34	74	68	130	27.5	353	ND	175
HEIGHT = 26.0																								
53.93	15.33	1.00	8.07	.18	10.22	8.81	1.61	.73	.5141	.0707	100.46	.00	2.1	60	14.6	131	32	74	66	141	28.2	381	ND	176
HEIGHT = 27.0																								
54.03	14.37	1.04	8.41	.19	10.47	8.59	1.66	.68	.5542	.0661	100.06	.00	2.6	65	16.4	128	32	88	70	146	30.6	395	ND	184
HEIGHT = 28.0																								
54.17	14.80	1.04	8.39	.18	10.69	8.68	1.60	.67	.5239	.0562	100.80	.00	2.7	61	16.2	127	30	84	68	149	30.7	403	ND	184
HEIGHT = 29.0																								
54.02	15.11	1.01	8.16	.18	10.48	8.65	1.61	.75	.5253	.0728	100.57	.00	2.2	63	16.7	128	33	74	64	141	28.3	385	ND	175
HEIGHT = 30.0																								
53.62	15.72	.97	7.87	.18	9.67	9.20	1.62	.69	.5113	.0678	100.12	.00	2.3	60	15.1	135	32	78	73	135	27.8	360	ND	173
HEIGHT = 31.0																								
54.50	15.06	1.03	8.32	.18	10.23	8.86	1.74	.79	.5507	.0843	101.34	.00	2.4	65	16.7	129	35	78	80	139	28.4	380	ND	180
HEIGHT = 32.0																								
53.92	15.02	1.01	8.19	.18	10.21	8.71	1.61	.75	.5382	.0724	100.21	.00	2.4	62	16.7	131	34	76	83	136	23.7	376	ND	180
HEIGHT = 33.0																								
54.00	14.57	1.01	8.19	.18	10.15	8.65	1.58	.79	.5401	.0586	99.72	.00	2.4	66	17.4	128	35	80	77	143	30.0	381	ND	184
HEIGHT = 34.0																								
53.48	15.30	.99	8.02	.18	10.23	8.89	1.73	.70	.5095	.0498	100.08	.00	2.0	57	14.5	131	31	77	48	141	29.0	388	ND	174

WHOLE ROCK GEOCHEMICAL DATA OF HAMMER HEADS SECTION

MAJOR ELEMENTS IN WEIGHT PER CENT

SiO ₂	Al ₂ O ₃	Fe ₂ O ₃	FeO	MnO	MgO	CaO	Na ₂ O	K ₂ O	TiO ₂	P ₂ O ₅	TOTAL	LOI	NB	Zr	Y	SR	RB	ZN	CU	Ni	SC	CR	BA	V
HEIGHT = 35.0																								
53.53	15.34	1.00	8.08	.18	10.56	8.80	1.58	.66	.4736	.0587	100.26	.00	2.5	53	15.6	129	31	77	59	147	29.3	405	ND	171
HEIGHT = 36.0																								
53.63	15.05	1.02	8.26	.18	10.41	8.86	1.48	.61	.4780	.0597	100.04	.00	2.3	54	14.0	132	28	83	59	144	29.5	389	ND	166
HEIGHT = 37.0																								
54.06	14.73	1.03	8.33	.18	10.32	8.82	1.60	.78	.6069	.0969	100.55	.00	2.9	69	16.9	124	36	76	66	139	28.4	384	ND	188
HEIGHT = 38.0																								
53.57	15.57	1.00	8.06	.18	9.94	8.97	1.73	.71	.5114	.0713	100.31	.00	1.6	66	15.6	135	33	74	71	133	27.4	368	ND	172
HEIGHT = 39.0																								
53.22	16.08	.95	7.69	.17	9.43	9.32	1.72	.68	.4764	.0639	99.80	.00	2.9	56	15.6	145	30	71	57	127	27.4	352	ND	165
HEIGHT = 40.0																								
53.86	14.61	1.06	8.57	.19	10.57	8.69	1.69	.75	.5239	.0575	100.57	.00	2.5	62	16.3	133	34	79	71	142	29.9	392	ND	180
HEIGHT = 41.0																								
53.66	15.23	1.00	8.08	.18	9.94	8.97	1.67	.71	.5023	.0692	100.01	.00	2.3	52	15.5	136	32	76	61	137	28.5	367	ND	175
HEIGHT = 42.0																								
53.76	15.07	1.00	8.06	.18	9.91	9.00	1.64	.70	.5264	.0681	99.91	.00	2.2	60	15.8	138	30	75	63	138	28.4	369	ND	175
HEIGHT = 43.0																								
53.76	15.92	.97	7.82	.17	9.78	9.25	1.76	.71	.5176	.0740	100.73	.00	1.4	60	15.1	143	32	73	62	134	27.1	363	ND	165
HEIGHT = 44.0																								
53.86	14.62	1.03	8.37	.19	10.56	8.53	1.59	.64	.4830	.0683	99.94	.00	1.6	58	14.4	135	31	78	60	141	29.5	386	ND	173

WHOLE ROCK GEOCHEMICAL DATA OF JULETOPPANE INTRUSIONS

MAJOR ELEMENTS IN WEIGHT PER CENT													TRACE ELEMENTS IN PPM											
SiO2	Al2O3	Fe2O3	FeO	MnO	MgO	CaO	Na2O	K2O	TiO2	P2O5	TOTAL	LOI	NB	ZR	Y	SR	RB	ZN	CU	NI	SC	CR	BA	V
JT1.82																								
57.55	13.52	1.28	10.39	.18	2.96	7.47	2.27	1.91	1.3327	.1500	99.01	.76	10.9	170	34.1	143	85	96	159	17	33.3	ND	ND	309
JT4.82																								
56.21	14.34	1.11	8.96	.16	5.37	9.19	2.13	1.27	.9171	.1100	99.77	.43	10.4	132	26.0	133	59	81	93	51	36.2	74	ND	257
JT7.82																								
55.00	14.75	1.09	8.79	.17	5.48	9.67	1.99	1.13	.9265	.1100	99.11	1.06	8.2	120	22.8	140	58	80	105	58	34.7	77	ND	271
JT8.82																								
53.15	15.62	1.03	8.31	.17	7.09	9.87	1.76	1.04	.6054	.0800	98.73	.33	5.4	87	17.4	141	49	73	78	74	33.0	193	239	201
JT9.82																								
55.15	16.28	.96	7.79	.15	5.19	10.14	2.12	1.28	.7400	.1000	99.90	.42	7.5	110	23.6	150	61	68	91	48	30.6	71	ND	219
JT10.82																								
53.90	17.51	.91	7.35	.14	4.30	10.36	1.78	1.17	.8263	.1000	98.35	.67	6.8	113	22.0	156	56	61	89	41	27.1	75	301	220
JT11.82																								
57.18	13.93	1.08	8.77	.17	5.04	8.72	1.96	1.45	.8533	.1300	99.28	1.03	9.5	142	27.8	133	58	82	89	44	35.9	52	ND	231
JT12.82																								
53.90	13.87	1.06	8.62	.18	10.38	8.63	1.34	.78	.5428	.0700	99.37	.09	6.2	82	15.3	119	37	78	60	109	32.6	375	ND	185
JT13.82																								
56.51	16.08	.66	5.31	.08	4.56	9.37	3.72	.21	1.0087	.1300	97.64	2.39	11.2	163	27.8	162	18	44	3	42	33.8	107	ND	226
JT13.82																								
58.27	15.26	.68	5.51	.11	5.04	8.67	3.14	.52	.9063	.1400	98.25	2.69	10.5	158	25.3	125	28	51	6	47	32.0	ND	ND	0
JT15.82																								
53.02	13.30	1.21	9.79	.19	10.41	9.06	1.69	.41	.5262	.0700	99.68	.84	3.4	56	12.2	119	24	73	35	110	40.3	386	ND	83
JT17.82																								
52.81	16.22	1.00	8.12	.17	5.68	10.81	1.90	.92	.6187	.0800	98.33	.32	7.6	94	18.7	144	42	71	88	55	34.3	93	ND	208
JT18.82																								
52.91	17.70	.90	7.30	.14	5.13	11.03	1.94	.91	.6256	.1000	98.69	.42	6.6	92	18.6	158	42	64	76	49	28.4	101	ND	190
JT20.82																								
53.32	14.63	.98	7.96	.16	9.59	10.10	1.51	.66	.5338	.0700	99.51	.23	5.9	74	13.4	129	29	71	57	103	35.1	400	ND	203
JT22.82																								
52.98	15.69	.97	7.85	.17	11.76	9.89	1.46	.71	.4724	.0600	102.01	.23	3.6	71	12.9	135	32	70	60	94	30.3	274	ND	170
JT23.82																								
52.44	16.38	.89	7.22	.15	9.06	9.89	1.55	.67	.4465	.0700	98.77	.37	3.3	68	9.6	141	28	63	48	93	29.5	363	177	158
JT24.82																								
57.05	14.79	.95	7.70	.15	4.90	9.03	2.13	1.54	.9899	.1400	99.37	.49	9.5	147	27.5	146	61	68	75	40	35.8	28	ND	261
JT25.82																								
53.24	15.72	.98	7.93	.17	9.14	9.70	1.42	.79	.4746	.0600	99.62	.25	3.4	72	10.9	135	37	70	55	93	30.1	309	ND	169

WHOLE ROCK GEOCHEMICAL DATA OF JULETOPPANE INTRUSIONS

MAJOR ELEMENTS IN WEIGHT PER CENT													TRACE ELEMENTS IN PPM												
SiO2	Al2O3	Fe2O3	FeO	MnO	MgO	CaO	Na2O	K2O	TiO2	P2O5	TOTAL	LOI	NB	ZR	Y	SR	RB	ZN	CU	NI	SC	CR	BA	V	
JT26.82																									
53.48	13.42	1.08	8.77	.18	10.76	8.57	1.56	.90	.5626	.0800	99.36	.31	2.9	81	10.7	123	37	78	68	102	33.6	360	ND	204	
JT27.82																									
54.04	13.83	1.06	8.56	.18	9.31	9.50	1.67	.79	.5551	.0700	99.57	.25	5.3	78	12.3	128	34	76	63	94	35.8	290	ND	200	
JT28.82																									
52.74	16.18	.97	7.83	.16	7.84	9.87	1.60	.73	.4926	.0600	98.47	.32	2.6	72	12.3	139	33	71	67	87	30.1	272	ND	178	
JT29.82																									
54.57	16.85	.96	7.80	.15	4.52	10.38	1.98	1.15	.7324	.0900	99.18	.53	6.1	107	19.5	147	55	69	98	43	30.1	73	220	200	
JT30.82																									
54.79	15.06	1.11	9.03	.17	5.26	10.03	1.94	1.24	.8480	.1100	99.59	.39	7.2	119	22.4	129	53	82	119	51	36.5	86	ND	249	
JT31.82																									
53.41	15.48	1.11	8.98	.18	5.47	10.30	2.23	.79	.7063	.0700	98.73	-.14	5.1	85	19.3	161	31	76	88	40	42.6	7	257	278	

WHOLE ROCK GEOCHEMICAL DATA OF FÖRSTEFJELL INTRUSIONS

MAJOR ELEMENTS IN WEIGHT PER CENT													TRACE ELEMENTS IN PPM											
SiO2	Al2O3	Fe2O3	FeO	MnO	MgO	CaO	Na2O	K2O	TiO2	P2O5	TOTAL	LOI	Nb	Zr	Y	Sr	Rb	Zn	Cu	Ni	Sc	Cr	Ba	V
F1.H4 54.86	15.65	1.04	8.43	.17	7.18	9.12	2.00	1.24	.7300	.0900	100.51	.00	3.4	91	22.3	152	53	78	102	85	29.1	223	ND	209
F2.H4 54.81	14.97	1.14	9.20	.19	5.88	9.65	2.13	1.05	.8600	.1000	99.98	.00	4.1	100	23.3	137	43	91	116	70	31.9	105	ND	258
F3.H4 53.84	15.28	1.09	8.85	.18	6.88	10.27	1.94	.98	.7100	.0900	100.11	.00	4.3	88	21.0	125	41	81	94	151	35.0	179	ND	240
F4.H4 54.47	15.13	1.11	8.97	.18	6.38	10.36	1.99	.93	.7400	.1000	100.36	.00	3.9	95	21.6	125	39	87	111	126	33.4	151	ND	244
F7.H4 54.30	14.55	1.10	8.91	.18	8.12	8.94	1.77	1.03	.6700	.0700	99.64	.00	2.8	78	18.8	135	47	84	92	104	31.8	234	ND	215
F8.H4 54.10	14.54	1.06	8.59	.19	9.49	8.96	1.70	.78	.6100	.0800	100.10	.00	3.8	69	17.2	126	33	82	82	124	31.7	310	ND	206
F9.H4 54.78	15.91	1.01	8.15	.17	7.37	9.26	1.90	1.20	.7000	.1000	100.55	.00	3.8	88	19.9	145	52	85	86	92	30.4	250	ND	205

WHOLE ROCK GEOCHEMICAL DATA OF GULLY SECTION, ROBERTSKOLLEN INTRUSIONS

MAJOR ELEMENTS IN WEIGHT PER CENT													TRACE ELEMENTS IN PPM											
SiO2	Al2O3	Fe2O3	FeO	MnO	MgO	CaO	Na2O	K2O	TiO2	P2O5	TOTAL	LOI	NB	ZR	Y	SR	RB	ZN	CU	NI	SC	CR	BA	V
HEIGHT = .0 M																								
49.84	10.22	1.21	9.79	.20	18.39	7.71	1.64	.55	.6600	.1208	100.33	.00	2.3	63	15.5	114	21	86	60	459	21.0	2329	ND	194
HEIGHT = 2.0 M																								
49.13	9.31	1.22	9.92	.20	20.19	7.07	1.41	.44	.6300	.1247	99.64	.00	3.3	60	14.5	115	18	82	68	538	26.5	2669	ND	179
HEIGHT = 4.0 M																								
48.94	9.22	1.24	10.07	.20	20.76	6.92	1.37	.43	.6100	.1147	99.87	.00	1.5	56	13.3	117	16	85	68	572	25.2	2803	ND	180
HEIGHT = 6.0 M																								
48.15	8.51	1.25	10.16	.20	22.85	6.38	1.33	.40	.5500	.1069	99.89	.00	1.1	51	11.7	101	15	84	63	623	23.8	3091	ND	164
HEIGHT = 8.0 M																								
47.85	8.05	1.29	10.41	.20	23.85	6.08	1.13	.37	.5400	.1003	99.87	.00	2.0	45	12.2	97	15	83	70	611	23.8	1570	ND	158
HEIGHT = 10.0 M																								
47.62	8.13	1.30	10.51	.20	24.48	5.96	1.18	.37	.5100	.0989	100.36	.00	1.7	44	11.9	99	14	81	70	625	23.3	3284	ND	155
HEIGHT = 12.0 M																								
47.03	7.76	1.32	10.65	.21	25.19	5.73	1.19	.33	.4900	.0725	99.97	.00	2.0	40	9.9	92	12	85	64	635	22.5	3368	ND	150
HEIGHT = 14.0 M																								
46.99	6.16	1.31	10.57	.21	25.48	5.59	1.00	.33	.4800	.0944	98.21	.00	2.1	43	10.5	92	14	83	51	638	22.4	3276	ND	143
HEIGHT = 16.0 M																								
46.88	7.43	1.36	11.05	.21	25.86	5.50	1.09	.39	.4700	.0734	100.31	.00	2.0	43	11.2	89	15	84	69	650	22.0	3453	ND	151
HEIGHT = 18.0 M																								
47.16	7.56	1.33	10.81	.21	25.44	5.59	1.09	.36	.4900	.0785	100.12	.00	1.8	44	10.7	94	14	86	49	630	23.0	3431	ND	155
HEIGHT = 20.0 M																								
46.83	7.19	1.40	11.31	.22	25.46	5.38	.96	.32	.4800	.0705	99.62	.00	1.7	37	8.1	92	12	93	78	640	21.8	3291	ND	169
HEIGHT = 22.0 M																								
50.17	7.36	1.27	10.31	.22	22.63	5.73	.97	.37	.5000	.0940	99.62	.00	2.1	45	11.1	89	15	86	56	482	28.7	2890	ND	163
HEIGHT = 24.0 M																								
48.57	7.29	1.36	11.01	.22	24.08	5.52	.93	.43	.5100	.0920	100.01	.00	2.3	43	10.6	82	17	89	57	560	26.6	2999	ND	167
HEIGHT = 26.0 M																								
50.91	7.34	1.25	10.11	.21	22.58	5.64	1.12	.36	.5000	.0824	100.10	.00	1.8	47	10.7	89	15	83	60	453	29.7	2886	ND	165
HEIGHT = 28.0 M																								
51.47	7.19	1.22	9.88	.21	21.82	6.22	1.09	.33	.4900	.0957	100.02	.00	1.5	45	11.4	88	13	81	55	431	32.3	2695	ND	161
HEIGHT = 30.0 M																								
51.39	7.31	1.19	9.66	.21	22.11	6.10	.97	.37	.4700	.0882	99.87	.00	1.9	47	10.8	84	15	86	56	435	31.3	2814	ND	157
HEIGHT = 32.0 M																								
50.14	7.31	1.28	10.40	.22	24.07	5.44	1.00	.32	.4600	.0868	100.73	.00	2.0	38	10.0	79	15	86	54	523	29.2	3083	ND	157
HEIGHT = 34.0 M																								
50.32	6.67	1.30	10.50	.22	24.02	5.25	.82	.35	.4600	.1058	100.02	.00	1.7	29	10.1	82	11	90	53	513	28.0	3180	ND	156

WHOLE ROCK GEOCHEMICAL DATA OF GULLY SECTION, ROBERTSKOLLEN INTRUSIONS

MAJOR ELEMENTS IN WEIGHT PER CENT														TRACE ELEMENTS IN PPM										BA	V
SiO2	Al2O3	Fe2O3	FeO	MnO	MgO	CaO	Na2O	K2O	TiO2	P2O5	TOTAL	LOI		Nb	Zr	Y	Sr	Rb	Zn	Co	Ni	Sc	Cr		
HEIGHT = 34.5 M 48.39	6.61	1.35	10.90	.23	26.05	5.13	.78	.32	.4300	.0711	100.26	.00		.8	29	8.4	84	12	100	69	615	26.0	3535	ND	146
HEIGHT = 36.0 M 50.56	6.48	1.23	9.95	.22	23.85	5.32	1.10	.39	.5100	.0910	99.70	.00		2.0	41	11.6	77	14	90	66	485	30.4	3141	ND	149
HEIGHT = 38.0 M 48.29	6.31	1.36	11.01	.22	25.53	4.94	.85	.38	.5000	.1042	99.49	.00		2.2	41	11.6	74	13	88	53	603	24.9	3349	ND	132
HEIGHT = 40.0 M 49.64	6.97	1.24	10.06	.22	25.23	5.12	.78	.31	.4100	.0706	100.05	.00		2.1	35	9.7	81	11	86	58	545	27.0	3438	ND	133
HEIGHT = 42.0 M 47.41	6.48	1.36	11.03	.22	26.51	4.97	.94	.33	.4500	.0778	99.78	.00		1.1	37	9.6	79	12	86	49	641	24.7	3537	ND	150
HEIGHT = 48.0 M 52.13	9.35	1.11	9.00	.20	17.51	8.30	1.20	.41	.5300	.0856	99.83	.00		2.3	45	13.2	105	15	75	59	318	35.5	2078	ND	177
HEIGHT = 50.0 M 52.27	9.95	1.10	8.88	.20	16.39	9.16	1.21	.37	.5500	.0821	100.16	.00		1.7	47	12.2	112	14	81	64	298	37.2	1993	ND	178
HEIGHT = 51.5 M 52.94	7.57	1.10	8.93	.22	13.92	13.28	1.19	.21	.7300	.0695	100.16	.00		1.9	51	18.6	76	8	67	82	174	64.8	2156	ND	350
HEIGHT = 52.0 M 53.69	14.49	.84	6.77	.16	10.17	10.89	1.74	.62	.6400	.0944	100.10	.00		2.6	64	14.7	152	21	64	63	131	34.3	1116	ND	188
HEIGHT = 54.0 M 52.99	13.39	.85	6.85	.17	12.66	11.21	1.53	.36	.4400	.0571	100.51	.00		1.3	36	10.0	136	10	61	49	168	35.5	1373	ND	170
HEIGHT = 56.0 M 53.12	13.45	.83	6.71	.16	12.52	11.29	1.60	.22	.4700	.0548	100.42	.00		1.9	39	10.9	138	7	58	49	167	36.6	1328	ND	170
HEIGHT = 59.0 M 53.04	14.66	.80	6.44	.16	10.71	11.72	1.76	.34	.4900	.0562	100.18	.00		1.1	39	11.3	154	11	59	48	143	34.0	1163	ND	161
HEIGHT = 62.0 M 53.09	13.80	.82	6.64	.16	11.74	11.63	1.60	.33	.4600	.0604	100.33	.00		1.0	39	10.6	145	10	58	48	149	36.3	1205	ND	173
HEIGHT = 66.0 M 53.08	14.14	.82	6.64	.17	11.60	11.61	1.63	.33	.4700	.0525	100.54	.00		.9	39	11.7	149	10	58	49	148	37.0	1210	ND	175
HEIGHT = 70.0 M 53.00	14.29	.81	6.54	.16	10.87	11.89	1.62	.34	.4700	.0548	100.04	.00		1.1	38	11.4	152	12	57	47	143	37.2	1192	ND	174
HEIGHT = 74.0 M 53.05	14.40	.81	6.55	.16	11.07	11.84	1.73	.38	.4700	.0551	100.52	.00		2.3	41	11.5	150	12	57	48	141	38.0	1182	ND	181
HEIGHT = 78.0 M 53.03	14.82	.79	6.40	.16	10.69	11.91	1.81	.34	.4800	.0578	100.49	.00		1.7	40	11.9	158	10	57	50	137	35.7	1110	ND	168
HEIGHT = 82.0 M 53.02	14.83	.81	6.55	.16	10.27	11.95	1.80	.38	.5000	.0565	100.33	.00		2.9	43	12.5	165	11	58	52	133	36.4	1092	ND	178

WHOLE ROCK GEOCHEMICAL DATA OF GULLY SECTION, ROBERTSKOLLEN INTRUSIONS

MAJOR ELEMENTS IN WEIGHT PER CENT														TRACE ELEMENTS IN PPM											
SiO2	Al2O3	Fe2O3	FeO	MnO	MgO	CaO	Na2O	K2O	TiO2	P2O5	TOTAL	LOI		Nb	Zr	Y	Sr	Rb	Zn	Cu	Ni	Sc	Cr	Ba	V
HEIGHT = 86.0 M																									
53.07	15.79	.80	6.46	.16	9.39	12.25	2.07	.40	.5300	.0679	100.99	.00		2.1	48	12.3	166	13	57	56	115	35.1	936	ND	183
HEIGHT = 90.0 M																									
53.24	15.31	.82	6.46	.16	9.69	11.79	1.94	.43	.5500	.0761	100.47	.00		2.3	50	13.0	171	16	58	59	118	34.1	855	ND	185
HEIGHT = 94.0 M																									
53.24	15.75	.84	6.81	.16	8.53	11.88	2.04	.41	.5900	.0818	100.33	.00		2.6	54	13.9	181	15	61	68	104	34.9	712	ND	185
HEIGHT = 98.0 M																									
53.36	14.93	.87	7.03	.16	9.27	11.96	1.82	.36	.6100	.0830	100.45	.00		3.1	56	14.4	161	10	58	63	113	35.3	724	ND	195
HEIGHT = 102.0 M																									
53.46	14.12	.91	7.37	.17	9.53	11.44	1.97	.36	.7000	.0969	100.13	.00		3.7	69	16.3	160	13	61	66	113	38.4	657	ND	210
HEIGHT = 106.0 M																									
53.24	15.54	.85	6.89	.16	8.51	12.14	2.04	.40	.6000	.0777	100.45	.00		2.6	52	14.3	177	13	58	61	104	36.9	454	ND	198

WHOLE ROCK GEOCHEMICAL DATA OF ROBERTSKOLLEN INTRUSIONS

MAJOR ELEMENTS IN WEIGHT PER CENT													TRACE ELEMENTS IN PPM											
SiO2	Al2O3	Fe2O3	FeO	MnO	MgO	CaO	Na2O	K2O	TiO2	P2O5	TOTAL	LOI	NB	Zr	Y	Sr	Rb	Zn	Cu	Ni	SC	CR	BA	V
R1.82 51.93	15.08	.90	7.30	.16	8.05	11.41	1.90	.70	.6670	.0800	98.18	1.25	3.5	71	11.8	163	26	62	69	84	39.0	549	176	215
R2.82 53.57	6.00	1.16	9.39	.22	22.92	5.54	.57	.19	.3453	.0500	99.96	.22	1.4	36	.0	50	5	76	38	335	37.6	3698	ND	154
R3.82 49.18	5.27	1.41	11.42	.22	25.62	4.78	.59	.10	.2881	.0500	98.93	.28	1.3	24	.0	45	1	87	22	555	29.1	3420	ND	130
R4.82 52.88	6.20	1.09	8.85	.20	21.30	5.34	.89	.25	.4825	.0600	97.54	.23	4.5	49	5.8	57	12	73	48	265	37.5	3391	ND	165
R5.82 50.29	5.79	1.22	9.86	.21	24.50	4.97	.63	.19	.3701	.0500	98.08	.41	4.1	40	5.7	54	10	78	38	436	32.1	3661	ND	148
R6.82 52.61	6.89	.97	7.85	.19	17.32	10.61	.98	.20	.5289	.0700	98.22	.44	4.6	56	10.3	64	12	61	47	225	49.6	2420	99	213
R7.82 43.17	5.54	1.37	11.06	.20	31.14	3.94	.75	.18	.3012	.0400	97.69	.17	3.6	34	1.2	56	6	83	36	778	16.9	4012	ND	105
R8.82 42.49	4.37	1.36	11.03	.20	32.31	3.70	.66	.21	.3117	.0600	96.70	1.40	3.5	38	1.7	45	10	80	37	846	17.2	4363	79	104
R14.82 52.94	14.30	.89	7.18	.15	10.08	11.51	1.80	.26	.5699	.0800	99.76	.89	7.2	63	10.4	148	14	54	62	118	36.8	832	138	188
R15.82 51.70	14.93	.87	7.05	.15	8.75	11.60	1.91	.48	.5803	.0700	98.09	.75	5.9	68	13.0	161	20	61	61	100	37.3	577	168	195
R16.82 53.73	14.61	1.01	8.18	.17	7.32	10.90	1.92	.69	.8161	.1100	99.46	1.00	7.6	89	18.9	170	27	73	92	72	38.1	339	237	246
R20.82 48.12	7.35	1.31	10.62	.16	14.88	8.22	1.35	.67	4.3070	.4200	97.41	2.07	22.3	425	37.4	541	35	114	120	689	26.4	932	337	293
R23.82 48.25	9.31	1.23	9.92	.18	20.13	6.97	1.18	.48	.6142	.0900	98.35	1.28	4.9	68	9.5	95	21	80	68	503	27.0	2721	ND	183
R25.82 49.52	7.05	1.24	10.05	.20	22.94	5.63	.85	.37	.5130	.0800	98.44	.48	3.6	55	8.4	78	15	80	54	512	28.5	3091	ND	158
R26.82 47.19	6.40	1.34	10.88	.21	25.92	5.12	.61	.27	.4468	.0700	98.46	.90	4.1	42	5.1	73	14	89	55	605	25.1	3436	116	145
R27.82 50.68	8.97	1.15	9.34	.19	17.90	8.00	1.15	.34	.4997	.0600	98.28	.39	5.0	57	9.7	90	16	76	59	327	33.7	2190	124	170
R31.82 55.09	13.79	1.34	10.85	.19	4.28	8.28	2.78	1.22	1.3892	.1700	99.38	1.08	11.1	146	29.3	177	40	90	131	33	42.4	2	ND	359
R33.82 47.86	5.18	1.31	10.62	.21	27.96	4.54	.50	.26	.3579	.0600	98.86	1.20	3.4	43	3.1	49	12	81	35	622	26.3	3609	ND	130

WHOLE ROCK GEOCHEMICAL DATA OF ROBERTSKOLLEN INTRUSIONS

MAJOR ELEMENTS IN WEIGHT PER CENT

MAJOR ELEMENTS IN WEIGHT PER CENT													TRACE ELEMENTS IN PPM												
SiO2	Al2O3	Fe2O3	FEO	MNO	MGO	CAO	NA2O	K2O	TiO2	P2O5	TOTAL	LOI	NB	ZR	Y	SR	RB	ZN	CU	NI	SC	CR	HA	V	
R35.82																									
44.04	4.48	1.42	11.52	.21	29.75	3.87	.71	.16	.2791	.0400	96.48	.08	2.4	33	2.0	42	7	84	28	707	22.6	3899	ND	116	
R361.82																									
50.57	5.88	1.09	8.84	.19	20.80	10.22	.55	.11	.3331	.0400	98.62	.48	4.4	34	7.8	49	7	65	28	389	45.1	2993	ND	169	
R362.82																									
51.80	7.17	1.02	8.24	.19	17.51	11.03	.93	.13	.4791	.0600	98.56	.22	3.5	46	11.4	66	9	62	42	295	48.6	2359	ND	207	
R37.82																									
52.45	8.33	.96	7.73	.18	15.92	11.00	1.12	.20	.5354	.0600	98.49	.37	6.2	57	11.2	73	13	61	57	220	48.4	2280	ND	219	
R38.82																									
51.39	7.85	1.02	8.26	.19	17.87	9.89	.94	.29	.4756	.0800	98.26	.54	5.2	58	9.3	78	14	72	40	307	41.3	2639	ND	183	
R39.82																									
48.76	9.35	1.32	10.67	.17	14.92	8.28	1.71	.81	2.7959	.3300	99.12	.31	15.9	245	29.0	529	21	106	107	768	24.1	834	ND	278	
R40.82																									
52.98	15.15	.95	7.69	.16	10.09	8.62	1.60	.76	.4680	.0600	98.53	.52	3.8	76	11.2	133	34	72	51	121	29.0	494	ND	160	
R42.82																									
53.90	14.37	1.01	8.21	.17	10.25	8.66	1.33	.75	.5330	.0800	99.26	1.17	5.1	73	12.2	126	35	79	64	124	32.6	484	ND	178	
R43.82																									
51.11	12.55	1.14	9.26	.19	11.43	9.55	1.71	.53	.8144	.1200	98.40	.68	5.1	90	15.5	135	25	82	93	178	36.3	1093	194	235	

WHOLE ROCK GEOCHEMICAL DATA OF GRUNEHOGNA INTRUSIONS

MAJOR ELEMENTS IN WEIGHT PER CENT													TRACE ELEMENTS IN PPM												
SiO2	Al2O3	Fe2O3	FeO	MNO	MGO	CAO	NA2O	K2O	TiO2	P2O5	TOTAL	LOI		NB	ZR	Y	SR	RB	ZN	CU	NI	SC	CR	BA	V
G9.82																									
51.87	12.72	1.81	14.65	.23	3.93	8.45	2.60	1.18	2.4124	.1800	100.03	.02		10.0	138	30.7	187	44	146	489	28	44.9	7	402	693
G10.82																									
56.25	13.10	1.54	12.44	.27	2.62	6.66	2.73	1.78	1.9556	.2300	99.58	.02		12.9	202	41.5	196	52	90	194	1	43.8	ND	ND	142
G11.82																									
51.75	12.78	1.82	14.73	.30	2.83	7.10	4.23	1.56	2.8693	.1400	100.11	.02		10.7	183	34.8	222	53	120	410	5	43.6	17	ND	169
G12.82																									
56.05	13.42	1.49	12.09	.27	2.73	6.80	3.20	1.80	1.8778	.2600	99.99	.02		12.8	190	39.6	206	56	103	189	3	40.2	6	ND	70
G13.82																									
55.80	13.48	1.44	11.68	.26	2.53	6.79	3.42	1.65	1.7801	.2600	99.09	.02		14.1	204	41.4	195	50	94	180	2	38.5	2	479	58
G14.82																									
56.86	12.45	1.58	12.83	.28	1.89	5.68	2.85	1.88	2.0170	.7600	99.08	.02		17.4	231	53.4	139	66	95	180	1	31.7	ND	ND	22
G15.82																									
57.95	12.95	1.52	12.29	.31	2.16	5.82	2.91	2.27	1.9400	.3100	100.43	.00		18.1	251	48.7	207	55	81	16	3	33.5	3	489	183
G16.82																									
58.03	12.72	1.40	11.37	.20	2.76	8.58	3.11	.62	1.5646	.2900	100.64	.02		14.1	228	47.6	212	19	107	133	18	34.0	2	ND	260
G16.82																									
58.34	12.18	1.20	9.76	.17	1.66	12.10	1.85	.22	1.3850	.3300	99.19	.02		13.7	263	47.9	645	13	76	148	11	29.9	ND	ND	215
G17.82																									
55.23	15.02	1.12	9.06	.19	5.65	9.01	2.02	1.11	.8383	.1000	99.35	.03		9.4	113	24.6	149	48	0	0	0	39.0	94	ND	244
G18.82																									
55.37	16.60	1.00	8.06	.16	4.24	8.76	2.72	1.64	.8846	.1300	99.56	.03		8.3	139	26.6	175	76	81	112	33	35.0	60	404	238
G19.82																									
51.21	13.18	1.54	12.43	.22	5.04	9.39	2.80	.69	2.2280	.2500	98.98	.03		11.1	173	30.3	278	24	115	207	65	26.7	74	ND	470
G28.82																									
56.41	15.81	1.05	8.47	.16	4.12	8.67	2.03	1.91	.9346	.1200	99.68	.03		9.7	148	28.2	169	79	107	136	32	35.5	52	431	240
G29.82																									
55.61	15.87	1.05	8.49	.16	4.17	7.95	2.17	1.42	.9186	.1100	97.92	.03		9.6	146	30.5	186	106	105	91	34	39.6	51	ND	253
G31.82																									
56.13	15.66	1.05	8.51	.19	4.10	8.24	2.18	2.09	.9267	.1400	99.22	.02		8.7	145	27.3	214	97	88	113	33	41.2	59	ND	219
G32.82																									
55.19	16.10	1.02	8.25	.16	3.99	9.06	1.84	1.86	.8883	.1200	98.48	.03		10.9	144	28.2	156	74	88	104	32	34.4	47	ND	240
G33.82																									
57.01	15.74	1.06	8.57	.16	3.98	7.51	2.61	2.18	.9580	.1300	99.91	.03		10.8	156	29.6	289	114	74	112	31	41.3	47	ND	257
G34.82																									
55.18	15.36	1.05	8.52	.15	5.93	9.24	2.02	1.07	.7877	.1100	99.42	.04		7.0	127	24.1	134	52	70	96	59	37.4	156	ND	241

WHOLE ROCK GEOCHEMICAL DATA OF GRUNEHOGNA INTRUSIONS

MAJOR ELEMENTS IN WEIGHT PER CENT

TRACE ELEMENTS IN PPM

	SiO2	Al2O3	FE2O3	FeO	MNO	MGO	CAO	NA2O	K2O	TiO2	P2O5	TOTAL	LOI	NB	ZR	Y	SR	RB	ZN	CU	NI	SC	CR	BA	V
G35.82																									
70.52	12.31	.58	4.71	.07	1.05	3.13	2.18	3.68	.7714	.2300	99.23	.02	18.5	322	51.6	247	110	44	73	4	17.8	5	1097	39	
G36.82																									
59.75	12.76	1.34	10.85	.24	2.33	5.34	2.53	2.65	1.5661	.1800	99.54	.02	12.4	221	41.4	148	106	121	212	11	39.7	4	ND	403	
G50.82																									
72.81	12.80	.40	3.21	.06	1.74	1.74	3.35	3.12	.5178	.1700	99.92	.04	16.4	233	33.6	225	96	46	26	27	12.6	169	1020	77	
G51.82																									
69.88	11.58	1.18	9.57	.04	.55	1.00	4.25	.98	.6088	.0900	99.73	.02	29.8	401	82.4	47	55	38	48	5	11.8	1	214	4	
G52.82																									
69.23	11.51	1.11	8.95	.02	.32	.98	4.11	3.66	.5904	.1100	100.59	.02	30.3	393	92.6	43	98	18	123	6	12.3	ND	1333	5	
G53.82																									
56.98	16.42	.99	8.05	.15	3.06	7.91	2.73	2.02	.9459	.1300	99.39	.03	10.5	153	28.0	183	88	79	132	22	32.5	19	489	246	
G58.82																									
54.40	14.75	1.04	8.44	.16	6.12	9.81	2.49	.87	1.0248	.1200	99.22	.05	8.4	110	21.6	173	34	77	107	62	37.6	219	ND	269	
G59.82																									
55.00	15.16	1.21	9.80	.18	4.17	8.77	2.70	1.29	1.2447	.1700	99.69	.02	10.0	136	25.9	198	54	98	136	32	34.3	8	ND	276	
G60.82																									
54.04	15.62	1.13	9.16	.19	4.28	9.41	2.45	1.22	1.1341	.1500	98.78	.02	9.1	118	22.7	214	52	94	119	35	34.3	8	ND	271	
G61.82																									
55.36	16.81	.97	7.83	.17	3.92	8.85	2.38	1.65	.8344	.1000	98.87	.03	10.1	132	24.5	192	74	67	85	34	36.3	50	ND	224	
G63.82																									
54.61	16.27	1.02	8.27	.17	6.09	10.22	1.87	1.06	.6292	.0900	100.30	.04	8.3	100	19.0	148	56	77	74	57	34.7	131	ND	186	
G64.82																									
53.62	16.70	.96	7.77	.16	5.29	10.31	1.86	1.12	.7197	.1000	98.61	.03	6.3	108	21.6	147	57	76	104	49	33.9	82	ND	212	
G65.82																									
54.71	14.17	1.10	8.88	.18	8.00	8.54	1.88	1.04	.7104	.1000	99.31	.05	7.8	110	20.8	127	47	88	80	79	35.7	199	ND	214	
G66.82																									
55.79	15.08	1.04	8.40	.16	5.97	8.74	2.07	1.35	.7953	.1100	99.51	.04	8.6	128	22.7	164	66	85	83	69	33.2	179	ND	235	
G67.82																									
55.30	14.74	1.10	8.88	.17	5.32	9.06	1.88	1.24	.8599	.1200	98.67	.03	8.0	131	25.1	127	52	89	105	47	33.7	95	ND	254	
G200.81																									
68.87	12.21	.86	6.95	.05	.52	1.52	3.87	3.39	.6712	.1500	99.06	.02	25.5	393	70.3	113	102	34	161	2	13.8	ND	1126	21	
G4.82																									
74.82	11.72	.33	2.65	.08	1.40	1.33	2.80	3.98	.5400	.1600	99.81	.00	13.3	281	52.8	136	78	0	0	0	.0	ND	1408	0	
G5.82																									
84.67	8.57	.13	1.02	.04	.51	.49	1.90	3.08	.1800	.0900	100.68	.00	8.8	101	17.4	85	78	0	0	0	.0	ND	1015	0	

WHOLE ROCK GEOCHEMICAL DATA OF GRUNEHOGNA INTRUSIONS

MAJOR ELEMENTS IN WEIGHT PER CENT

TRACE ELEMENTS IN PPM

	SiO ₂	Al ₂ O ₃	Fe ₂ O ₃	FeO	MnO	MgO	CaO	Na ₂ O	K ₂ O	TiO ₂	P ₂ O ₅	TOTAL	LOI	Nb	Zr	Y	Sr	Rb	Zn	Cu	Ni	SC	CR	BA	V
G30.82 73.77	12.86	.31	2.51	.06	1.26	2.16	3.04	3.94	.4100	.1400	100.46	.00	11.4	213	26.5	228	99	0	0	0	0	.0	ND	ND	0
G37.82 78.32	11.31	.19	1.52	.06	.79	1.53	3.59	2.44	.4200	.1700	100.34	.00	9.8	209	29.6	211	66	0	0	0	0	.0	ND	5/1	0
G38.82 75.36	12.78	.22	1.74	.04	.79	1.11	3.61	3.71	.4600	.1800	100.00	.00	15.5	363	27.7	144	116	0	0	0	0	.0	ND	1012	0
G431.82 72.16	11.66	.79	6.44	.06	.45	1.53	3.96	2.39	.4700	.0600	99.97	.00	15.3	589	56.7	337	53	0	0	0	0	.0	ND	823	0
G432.82 65.17	17.07	.66	5.34	.14	2.54	1.71	5.63	1.65	.5500	.1300	100.59	.00	20.9	280	43.3	344	54	0	0	0	0	.0	ND	490	0
G44.82 70.54	15.26	.45	3.63	.07	1.81	1.28	3.88	2.85	.4800	.1300	100.38	.00	16.0	234	38.9	225	123	0	0	0	0	.0	ND	1096	0
G49.82 78.91	10.52	.25	2.04	.08	1.32	1.56	3.62	1.48	.4100	.1600	100.35	.00	14.6	180	33.0	174	51	0	0	0	0	.0	ND	436	0
G11.81 55.41	15.03	1.08	8.76	.17	5.98	8.93	1.68	1.31	.8500	.1000	99.30	.00	8.5	123	24.9	142	66	88	127	54	.0	ND	ND	240	0
G12.81 55.65	14.86	1.10	8.90	.18	5.89	9.01	1.67	1.31	.8400	.1200	99.53	.00	7.9	123	23.7	140	68	87	128	50	.0	ND	ND	0	0
G21.81 57.78	13.66	1.30	10.52	.23	3.43	7.15	2.07	1.53	1.2300	.1700	99.07	.00	11.2	187	39.2	152	71	132	104	19	.0	ND	ND	313	0
G22.81 63.70	12.98	1.06	8.58	.13	1.61	6.58	2.98	.60	1.1400	.2400	99.60	.00	19.6	276	47.3	136	28	76	74	6	.0	ND	ND	0	0
G3.81 56.90	14.02	1.14	9.22	.22	4.99	8.63	1.81	1.76	.9500	.1400	99.78	.00	9.8	153	30.4	162	79	104	97	41	.0	ND	ND	271	0
G5.81 64.09	12.76	1.15	9.28	.17	1.12	3.60	3.21	2.79	1.0100	.2800	99.46	.00	16.2	141	49.0	144	77	93	54	5	.0	ND	1486	34	0
G6.81 66.92	12.66	1.00	8.10	.13	.89	3.00	3.19	3.23	.8400	.2100	100.17	.00	20.5	317	47.9	164	89	49	81	3	.0	ND	1145	23	0
G9.81 68.26	12.23	.96	7.81	.08	.63	2.19	4.03	3.08	.6300	.1600	100.06	.00	21.0	323	50.2	147	86	24	128	1	.0	ND	1177	11	0
G10.81 72.25	11.32	.50	4.04	.04	.26	1.59	2.99	4.00	.2700	.0400	97.30	.00	23.7	452	81.6	195	114	9	13	3	.0	ND	1580	5	0

WHOLE ROCK GEOCHEMICAL DATA OF KRYLEN INTRUSIONS

MAJOR ELEMENTS IN WEIGHT PER CENT												TRACE ELEMENTS IN PPM												
SiO2	Al2O3	Fe2O3	FeO	MnO	MgO	CaO	Na2O	K2O	TiO2	P2O5	TOTAL	LOI	Nb	Zr	Y	Sr	Rb	Zn	Cu	Ni	SC	CR	BA	V
K1.81																								
55.49	15.11	1.06	8.59	.18	5.90	9.03	1.64	1.44	.8200	.1200	99.38	1.57	8.2	122	23.4	140	67	102	94	52	34.3	167	321	219
K2.81																								
55.02	15.30	1.05	8.54	.18	6.29	9.20	1.68	1.11	.7500	.1000	99.22	1.41	7.7	120	22.5	138	52	80	93	56	31.9	182	ND	204
K3.81																								
54.76	15.89	1.02	8.22	.17	5.63	9.74	1.77	1.08	.7500	.1100	99.14	1.09	6.1	119	21.9	148	49	63	78	48	30.8	151	ND	211
K4.81																								
54.62	15.17	1.04	8.46	.17	5.62	9.51	1.61	1.17	.8400	.0000	98.21	1.29	8.0	125	22.1	140	55	86	91	50	33.1	145	288	211
K5.81																								
55.49	15.63	1.02	8.30	.17	5.70	9.72	1.64	1.09	.7800	.1000	99.64	1.14	7.0	122	22.8	144	50	84	90	50	34.2	149	ND	213
K6.81																								
76.05	11.77	.26	2.13	.03	1.13	1.67	5.36	.21	.5800	.0800	99.27	.78	18.2	322	32.6	161	13	15	1	23	10.8	358	29	66
K7.81																								
47.89	8.73	1.58	12.81	.18	14.27	8.38	1.74	.42	3.2900	.3100	99.60	.63	10.9	213	28.7	309	12	127	130	681	23.8	725	128	331
K8.81																								
55.01	16.12	1.01	8.22	.17	5.85	9.96	1.66	1.00	.7400	.0000	99.74	.93	7.3	115	21.5	147	48	80	87	53	31.8	147	ND	204
K9.81																								
54.38	16.53	.98	7.96	.17	5.91	9.86	1.73	1.04	.6900	.1000	99.35	1.09	6.7	105	19.1	156	46	84	39	53	32.6	159	280	202
K10.81																								
55.24	14.76	1.05	8.54	.17	6.24	9.78	1.52	1.18	.8100	.1100	99.40	1.31	6.4	116	19.3	132	51	96	67	59	38.0	158	ND	235
K11.81																								
48.56	9.52	1.17	9.48	.17	20.69	7.34	1.38	.61	.7000	.0000	99.62	2.24	4.1	70	11.3	95	26	67	54	814	23.3	2897	158	186
K12.81																								
54.86	16.08	1.00	8.07	.17	5.98	9.95	1.72	1.07	.7200	.1000	99.72	.93	6.4	108	21.0	147	50	80	80	52	33.0	150	277	201

WHOLE ROCK GEOCHEMICAL DATA OF JEKSELEN INTRUSIONS

MAJOR ELEMENTS IN WEIGHT PER CENT

TRACE ELEMENTS IN PPM

SiO ₂	Al ₂ O ₃	Fe ₂ O ₃	FeO	MnO	MgO	CaO	Na ₂ O	K ₂ O	TiO ₂	P ₂ O ₅	TOTAL	LOI	Nb	Zr	Y	Sr	Rb	Zn	Cu	Ni	SC	CR	BA	V
J9.81			8.42	.17	6.11	8.28	2.41	1.39	.7884	.1000	99.17	2.63	8.2	122	23.1	220	61	84	81	69	31.6	ND	314	226
55.59 14.87	1.04																							
J11.81			8.36	.15	5.77	7.87	1.65	2.51	.8000	.1200	98.46	2.52	7.5	129	22.3	193	89	82	82	59	30.9	ND	ND	218
55.36 14.84	1.03																							
J12.81			8.18	.16	6.56	5.64	3.12	1.94	.8300	.1100	99.89	2.72	7.3	128	22.3	244	68	91	101	68	32.3	ND	ND	219
57.19 15.15	1.01																							
J131.81			3.22	.07	2.32	2.63	3.65	4.03	.3300	.1500	101.06	2.95	16.1	140	26.8	256	89	35	6	33	9.3	ND	1581	55
70.34 13.92	.40																							
J132.81			3.49	.08	2.44	4.90	4.66	1.89	.4700	.1900	100.19	4.13	17.8	261	35.2	264	50	41	42	32	10.3	ND	800	75
68.59 13.05	.43																							
J141.81			8.40	.17	6.76	6.72	3.29	1.92	.8100	.1100	99.55	2.59	9.7	127	24.6	381	55	87	91	76	34.3	ND	ND	232
55.12 15.21	1.04																							
J142.81			8.39	.18	6.85	6.73	3.24	1.83	.8200	.1100	99.24	2.54	8.7	124	23.5	399	54	87	89	73	30.0	ND	ND	213
55.23 14.82	1.04																							
J15.81			7.64	.16	5.92	4.97	5.61	.16	.7500	.1200	100.35	6.06	11.8	155	30.3	227	9	61	14	62	32.6	ND	109	218
57.35 16.73	.94																							
J16.81			8.47	.17	6.17	7.14	2.57	2.01	.8200	.1100	99.54	2.64	6.7	129	22.5	186	74	90	85	63	31.9	ND	ND	225
55.78 15.25	1.05																							
J17.81			8.44	.16	5.94	7.84	2.38	2.00	.8300	.1200	100.15	2.62	7.9	130	23.1	173	83	89	85	61	30.7	ND	431	228
56.21 15.19	1.04																							
J18.81			8.38	.16	5.97	7.97	2.65	1.78	.8100	.1200	100.33	2.66	5.2	127	22.1	183	69	85	77	61	31.5	ND	ND	223
56.59 14.87	1.03																							
J19.81			8.20	.15	5.51	8.86	2.89	1.02	.8100	.1100	99.80	2.49	6.6	125	21.5	369	37	58	71	58	31.9	ND	239	217
56.23 15.01	1.01																							

WHOLE ROCK GEOCHEMICAL DATA OF STRAUMSNUTANE VOLCANICS

MAJOR ELEMENTS IN WEIGHT PER CENT												TRACE ELEMENTS IN PPM												
SiO2	Al2O3	Fe2O3	FeO	MnO	MgO	CaO	Na2O	K2O	TiO2	P2O5	TOTAL	LOI	Nb	Zr	Y	Sr	Rb	Zn	Cu	Ni	SC	CR	BA	V
ES-1 55.65	13.59	1.03	8.35	.16	7.13	6.24	3.77	2.25	1.0555	.1672	99.39	2.29	10.0	150	29.0	152	79	79	94	62	.0	67	603	227
ES-4 54.08	14.14	1.03	8.36	.17	9.86	4.61	2.59	3.47	1.0390	.2469	99.59	3.15	10.0	160	32.0	83	127	104	58	72	.0	73	1172	226
ES-6 55.38	14.30	1.05	8.53	.14	6.74	6.84	2.54	2.85	1.0405	.1442	99.57	2.32	11.0	154	33.0	209	144	89	101	61	.0	70	558	227
ES-7 52.99	14.07	1.17	9.50	.19	7.90	6.86	3.46	1.85	1.4714	.2248	99.69	2.83	9.0	167	34.0	68	55	106	118	63	.0	96	510	286
ES-8 54.30	13.81	1.15	9.34	.16	6.96	6.58	3.52	2.28	1.1638	.1974	99.46	2.34	10.0	164	36.0	188	72	98	119	59	32.2	89	641	260
ES-9 54.98	14.39	1.20	9.70	.14	5.94	7.71	2.08	2.14	1.1440	.1340	99.56	2.13	10.0	170	34.0	203	101	93	130	57	.0	96	485	271
ES-11 53.78	13.92	1.16	9.42	.18	8.31	4.79	3.06	3.20	1.4022	.2389	99.46	2.93	9.0	165	39.0	57	115	111	103	67	.0	97	1097	278
ES-12 53.36	13.90	1.26	10.22	.18	7.77	6.73	3.19	1.46	1.4740	.2135	99.77	2.90	10.0	175	37.0	132	50	116	130	62	.0	90	425	272
ES-14 54.19	13.55	1.14	9.24	.18	8.43	5.14	2.36	3.65	1.3415	.2392	99.46	2.99	9.0	174	36.0	73	136	112	124	62	.0	97	1163	278
ES-16 54.47	13.40	1.17	9.47	.16	6.87	6.99	3.67	1.97	1.1635	.1559	99.47	2.16	11.0	167	35.0	106	68	84	180	66	.0	97	490	293
ES-18 56.74	14.96	1.08	8.71	.13	5.40	5.60	1.97	3.95	1.0764	.1625	99.77	1.86	10.0	165	37.0	138	271	91	108	59	.0	99	602	266
ES-19 54.99	13.19	1.19	9.68	.16	7.15	7.57	2.70	1.64	1.2040	.1338	99.62	3.02	9.0	167	35.0	55	53	97	95	60	.0	93	391	275
ES-20 54.22	13.43	1.13	9.11	.17	7.38	5.90	3.57	3.12	1.2663	.1972	99.49	1.93	9.0	174	38.0	100	115	96	72	66	.0	84	948	278
ES-21 53.38	13.64	1.12	9.05	.23	7.95	6.99	4.58	1.09	1.4340	.2253	99.67	2.50	10.0	172	34.0	94	29	92	100	67	.0	73	231	243
ES-22 55.68	13.73	1.16	9.40	.15	7.40	4.87	3.10	2.75	1.1261	.1860	99.55	2.69	9.0	167	37.0	57	112	104	127	64	.0	94	773	225
ES-24 53.28	14.25	1.17	9.49	.17	8.11	5.41	2.40	3.91	1.4617	.2318	99.89	2.89	9.0	184	40.0	81	147	110	126	70	.0	98	1339	296
ES-25 54.04	13.72	1.22	9.86	.18	7.78	6.66	2.94	1.85	1.1447	.1856	99.57	2.35	8.0	173	37.0	196	78	100	114	70	.0	111	506	255
ES-26 54.14	13.74	1.15	9.32	.16	7.59	5.78	3.40	3.01	1.3657	.1821	99.84	2.31	10.0	187	40.0	130	120	98	34	68	.0	94	839	261

WHOLE ROCK GEOCHEMICAL DATA OF STRAUMSUTANE VOLCANICS

MAJOR ELEMENTS IN WEIGHT PER CENT													TRACE ELEMENTS IN PPM											
SiO2	Al2O3	Fe2O3	FeO	MnO	MgO	CaO	Na2O	K2O	TiO2	P2O5	TOTAL	LOI	Nb	Zr	Y	Sr	Rb	Zn	Cu	Ni	SC	CR	BA	V
ES-28																								
54.32	13.38	1.16	9.40	.17	7.74	5.76	3.51	2.60	1.2276	.1977	99.46	2.22	10.0	176	40.0	149	92	103	152	65	.0	96	856	276
ES-29																								
54.74	13.01	1.21	9.84	.18	7.25	8.55	2.23	1.30	1.1856	.1134	99.60	2.84	9.0	168	31.0	212	53	93	110	59	32.2	77	466	236
ES-30																								
55.86	13.01	1.22	9.89	.16	6.88	7.44	2.33	1.51	1.1847	.1236	99.61	2.77	10.0	170	33.0	220	63	98	100	64	.0	73	545	235
BN-1																								
54.83	13.09	1.07	8.64	.18	9.24	4.96	3.29	3.04	1.0644	.1757	99.56	2.80	8.0	147	33.0	124	111	92	10	84	.0	68	1104	227
BN-4																								
52.87	13.07	1.06	8.62	.22	10.75	5.51	3.91	2.22	1.0483	.2076	99.50	3.21	8.0	144	33.0	158	65	99	15	87	.0	73	563	234
BN-6																								
54.49	12.95	1.11	8.99	.19	8.51	7.09	3.90	1.38	.9901	.1327	99.73	2.78	9.0	143	32.0	138	50	84	25	83	36.3	70	443	240
BN-7																								
50.91	14.07	1.23	9.98	.18	10.22	7.75	3.51	.75	.9877	.1426	99.74	3.75	7.0	103	27.0	132	28	87	100	96	.0	140	404	248
BN-11																								
52.36	14.10	1.16	9.42	.18	8.00	9.65	2.69	1.01	.9369	.0824	99.58	2.38	8.0	116	26.0	229	56	78	104	95	.0	121	230	242
BN-15																								
51.75	13.39	1.13	9.18	.21	9.61	7.95	3.46	1.57	1.0892	.1660	99.50	3.31	8.0	131	28.0	42	43	83	105	85	.0	68	423	256
SJ-1																								
54.86	14.78	1.19	9.67	.15	5.89	7.93	2.08	1.94	1.1183	.1322	99.75	1.91	9.0	165	34.0	155	79	95	124	72	.0	121	474	262
SJ-2																								
55.11	12.80	1.24	10.02	.16	6.70	7.81	2.84	1.41	1.3795	.1441	99.62	2.36	11.0	168	36.0	244	43	92	76	62	.0	90	361	274
SJ-3																								
53.63	13.35	1.27	10.26	.18	8.10	6.42	2.92	1.77	1.3720	.2079	99.47	3.09	10.0	179	41.0	109	51	109	24	62	.0	89	440	257
SJ-4																								
54.93	12.93	1.14	9.25	.18	8.77	5.54	2.62	2.69	1.1897	.1983	99.44	3.00	11.0	166	34.0	54	88	104	11	67	.0	95	656	248
SJ-6																								
55.08	13.31	1.15	9.33	.17	6.88	7.22	3.26	1.78	1.1432	.1455	99.48	2.14	10.0	166	35.0	232	67	94	107	68	32.4	81	536	255
SJ-8																								
55.96	12.55	1.17	9.47	.21	8.57	4.86	2.62	2.76	1.2172	.2166	99.60	2.72	9.0	173	37.0	62	90	106	130	50	.0	21	815	259
SJ-10																								
53.00	14.12	1.29	10.47	.18	8.01	5.89	3.55	1.58	1.4528	.2235	99.78	2.80	10.0	159	35.0	180	60	101	117	83	.0	72	522	272
SJ-13																								
55.87	10.98	1.25	10.13	.17	8.47	11.74	.00	.00	1.0956	.0307	99.74	4.93	7.0	125	28.0	18	0	87	94	68	.0	61	74	229
SJ-14																								
55.29	14.10	1.12	9.09	.15	7.16	6.63	2.58	2.66	.9768	.1410	99.90	2.22	9.0	141	29.0	221	143	100	104	77	.0	62	649	259

WHOLE ROCK GEOCHEMICAL DATA OF STRAUMSUTANE VOLCANICS

MAJOR ELEMENTS IN WEIGHT PER CENT												TRACE ELEMENTS IN PPM													
SiO2	Al2O3	FeO	MnO	MgO	CaO	Na2O	K2O	TiO2	P2O5	TOTAL	LOI	Nb	Zr	Y	Sr	Rb	Zn	Cu	Ni	SC	CR	BA	V		
SJ-17	54.67	12.27	1.17	9.45	.19	9.41	8.60	2.07	.84	1.0552	.1015	99.82	3.37	9.0	140	30.0	163	19	101	58	77	36.0	67	204	261
SJ-19	54.05	13.21	.98	7.95	.15	9.60	5.97	2.64	4.25	.8620	.1420	99.81	2.71	6.0	114	25.0	113	121	74	25	95	.0	135	1012	259
SJ-20	54.96	13.83	1.00	8.07	.14	8.94	5.18	2.64	3.75	.8691	.1449	99.52	2.69	7.0	103	26.0	122	156	88	25	99	.0	119	876	242
FT-1	53.99	13.07	1.20	9.72	.18	8.38	7.60	2.83	1.33	.9623	.1360	99.40	3.16	7.0	139	30.0	126	45	97	120	77	35.6	74	397	268
FT-2	55.14	13.75	1.18	9.56	.17	6.68	7.97	2.07	1.88	.9567	.1040	99.45	2.10	8.0	137	31.0	217	81	100	115	77	.0	66	455	263
FT-3	53.28	13.42	1.20	9.70	.22	8.27	7.38	4.33	.58	1.1178	.1641	99.66	2.90	8.0	139	31.0	164	11	97	63	76	37.0	70	271	272
FT-4	51.98	14.65	1.23	9.96	.21	8.75	5.95	4.44	1.02	1.1820	.2261	99.59	2.13	9.0	138	35.0	202	22	101	41	79	.0	69	445	293
SN-1(A)	53.48	13.09	1.40	11.31	.19	5.28	7.22	3.29	1.62	2.2213	.2724	99.37	2.17	14.0	231	49.0	159	49	125	228	58	.0	69	516	311
SN-1(B)	53.31	13.37	1.40	11.31	.19	5.45	7.17	3.37	1.65	2.2144	.2857	99.73	2.17	15.0	227	50.0	161	47	123	223	49	.0	63	547	306
SN-2	50.52	15.24	1.40	11.31	.19	5.47	5.56	4.38	2.66	2.4677	.3804	99.57	1.83	17.0	280	57.0	106	140	140	406	56	.0	70	684	333
SN-3	50.59	15.02	1.42	11.51	.18	5.10	5.59	4.21	2.90	2.4515	.3651	99.35	1.61	17.0	277	59.0	106	152	132	447	56	.0	61	758	346
SN-5(A)	54.61	14.52	1.35	10.91	.12	3.74	5.24	2.99	3.60	2.1687	.2788	99.53	1.66	15.0	249	53.0	187	184	119	199	53	.0	58	636	316
SN-5(B)	54.11	14.05	1.39	11.27	.14	4.24	5.32	2.98	3.44	2.3010	.2992	99.55	1.66	17.0	251	52.0	159	175	126	254	49	.0	56	659	324
SN-6	54.22	14.44	1.38	11.20	.14	4.00	5.69	3.11	3.12	2.1706	.3043	99.79	1.34	15.0	249	51.0	233	144	122	198	49	.0	56	589	314
SN-7(A)	54.15	14.48	1.33	10.78	.15	4.57	5.41	2.82	3.57	2.1731	.3249	99.78	1.65	14.0	246	52.0	180	157	125	142	51	.0	61	736	315
SN-7(B)	54.05	14.29	1.32	10.69	.16	4.79	5.40	2.58	3.77	2.1308	.3413	99.51	1.65	15.0	251	53.0	171	172	129	152	49	.0	58	737	302
SN-8	53.82	14.37	1.28	10.40	.16	5.08	6.21	2.41	3.57	2.0784	.3362	99.73	2.02	13.0	245	53.0	197	170	134	291	51	.0	62	654	322
SN-9	53.65	14.22	1.41	11.44	.14	4.03	5.34	4.08	2.60	2.2855	.3102	99.51	1.43	14.0	254	53.0	203	108	113	159	52	.0	65	553	333

WHOLE ROCK GEOCHEMICAL DATA OF STRAUMSNUTANE VOLCANICS

MAJOR ELEMENTS IN WEIGHT PER CENT													TRACE ELEMENTS IN PPM											
SiO2	Al2O3	Fe2O3	FeO	MnO	MgO	CaO	Na2O	K2O	TiO2	P2O5	TOTAL	LOI	Nb	Zr	Y	Sr	Rb	Zn	Cu	Ni	Sc	Cr	Ba	V
SN-10(A)																								
50.87	13.99	1.42	11.48	.22	7.75	5.61	3.79	1.67	2.5182	.3976	99.73	2.69	17.0	254	57.0	92	43	183	220	53	.0	63	474	335
SN-10(B)																								
51.01	14.17	1.41	11.41	.21	7.30	5.63	3.82	1.88	2.5018	.3966	99.76	2.69	15.0	253	56.0	99	54	176	224	57	.0	59	567	327
SN-11																								
53.93	13.53	1.12	9.04	.18	7.98	8.21	3.44	1.12	.9541	.1539	99.65	2.28	8.0	126	26.0	136	33	97	109	47	.0	30	333	265
SN-12																								
54.80	14.11	1.08	8.72	.15	7.14	7.31	2.63	2.57	.9551	.1643	99.62	1.98	9.0	127	29.0	150	113	93	111	49	.0	34	632	261
SN-13																								
54.47	13.58	1.13	9.17	.16	7.71	7.73	2.29	2.02	.9615	.1568	99.39	2.11	9.0	129	28.0	184	82	101	104	49	.0	30	463	257
SN-14																								
55.12	12.93	1.10	8.91	.18	7.78	7.73	2.93	1.64	.9990	.1457	99.47	3.09	8.0	124	27.0	112	45	89	115	49	.0	23	467	258
SN-15																								
55.80	13.72	1.14	9.21	.16	6.56	5.09	3.60	2.77	1.3563	.2158	99.62	2.33	10.0	154	33.0	102	104	101	339	45	.0	24	871	286
SN-18																								
54.03	13.28	1.11	8.97	.16	9.14	6.19	2.86	2.61	1.1092	.1746	99.64	2.50	9.0	135	29.0	135	73	99	43	49	.0	32	860	277
SN-19																								
53.76	13.53	1.05	8.54	.19	7.91	8.10	4.09	1.35	1.0478	.1831	99.77	2.79	8.0	131	29.0	197	38	92	145	47	.0	32	529	277
SN-23																								
54.46	12.49	1.25	10.12	.21	7.36	7.47	3.34	1.15	1.5214	.1966	99.56	2.04	10.0	165	38.0	154	29	106	99	37	.0	17	288	290
SN-26																								
56.73	12.68	1.28	10.35	.18	5.87	5.82	3.32	1.64	1.4449	.1871	99.50	1.86	10.0	170	37.0	165	68	109	110	33	.0	15	526	285
SN-29																								
54.80	13.50	1.15	9.29	.17	8.04	7.07	2.90	1.71	.9870	.1526	99.76	2.51	9.0	129	28.0	214	63	93	100	48	35.7	38	597	258
SN-33																								
55.65	13.34	1.19	9.61	.18	6.03	6.14	3.54	2.07	1.4531	.1986	99.39	1.78	11.0	164	35.0	207	102	104	113	33	37.9	14	660	289
SN-39																								
56.01	12.94	1.27	10.25	.17	6.29	5.67	3.45	1.93	1.5323	.2043	99.72	1.68	10.0	169	34.0	146	81	110	203	35	.0	9	575	285
SN-40(A)																								
55.57	13.04	1.15	9.30	.20	8.42	4.76	2.37	3.15	1.5372	.2647	99.77	2.69	11.0	166	34.0	83	113	114	123	30	.0	8	1504	274
SN-41																								
55.82	13.18	1.30	10.53	.17	5.86	5.69	4.05	1.28	1.5329	.1955	99.62	1.73	11.0	171	33.0	209	49	105	115	33	.0	15	371	290
SN-45																								
53.38	13.53	1.14	9.20	.18	8.33	7.46	3.24	1.90	1.0893	.1747	99.63	2.92	9.0	132	27.0	58	55	97	339	52	.0	31	509	273
SN-75																								
54.22	13.24	1.16	9.36	.19	8.34	7.86	3.06	1.07	.9377	.1649	99.60	2.63	10.0	133	29.0	174	34	92	100	53	.0	32	306	244

WHOLE ROCK GEOCHEMICAL DATA OF STRAUMSNUTANE VOLCANICS

MAJOR ELEMENTS IN WEIGHT PER CENT													TRACE ELEMENTS IN PPM												
SI02	AL2O3	FE2O3	FEO	MNO	MGO	CAO	NA2O	K2O	TIO2	P2O5	TOTAL	LOI	NB	ZR	Y	SR	RB	ZN	CU	NI	SC	CR	BA	V	
SN-79(A)																									
53.91	12.78	1.37	11.13	.16	5.23	7.32	2.33	2.81	2.0552	.2831	99.38	2.97	12.0	230	46.0	269	122	124	197	61	.0	72	481	293	
SN-79(B)																									
53.82	13.02	1.38	11.18	.15	5.27	7.34	2.29	2.76	2.1127	.2783	99.60	2.97	14.0	235	48.0	275	123	128	200	62	.0	80	461	306	
ET-8																									
54.73	12.76	1.21	9.77	.23	6.23	6.53	2.38	3.30	2.1101	.3911	99.63	1.82	14.0	241	53.0	126	110	136	234	50	.0	54	1402	302	
ET-9																									
53.27	12.22	1.33	10.80	.26	8.33	5.04	1.55	4.02	2.2729	.4359	99.54	.00	15.0	264	54.0	86	121	227	110	52	.0	66	2146	339	
ET-11																									
52.43	14.20	1.48	11.95	.16	4.08	7.58	2.18	2.75	2.2203	.3753	99.40	1.51	15.0	259	53.0	158	93	139	235	50	34.0	63	575	300	
ET-18																									
50.39	13.01	1.53	12.38	.20	6.37	7.97	3.57	1.19	2.7236	.3584	99.69	.00	14.0	218	42.0	173	32	127	140	57	.0	81	226	311	
ET-19(A)																									
53.40	13.70	1.44	11.67	.16	4.52	6.85	2.42	2.89	2.1760	.2798	99.50	1.80	14.0	250	53.0	191	104	129	232	58	.0	63	676	297	
ET-19(B)																									
53.31	13.69	1.45	11.73	.16	4.48	6.92	2.45	2.85	2.1780	.2800	99.49	1.80	14.0	255	51.0	195	105	130	233	59	.0	65	621	297	
BT-1																									
53.08	11.79	1.33	10.76	.21	11.16	6.65	1.93	1.46	1.1147	.1548	99.62	3.04	9.0	147	37.0	49	47	134	30	91	.0	54	385	222	
BT-2																									
55.14	11.30	1.21	9.81	.19	9.15	6.56	2.80	2.32	.9669	.1144	99.55	1.92	7.0	137	34.0	63	78	102	51	84	.0	40	632	262	
BT-4																									
54.79	11.68	1.23	9.98	.17	8.67	5.86	3.19	2.96	1.0280	.1131	99.67	1.51	7.0	142	31.0	96	96	100	112	77	.0	42	733	265	
BT-11																									
55.25	12.41	1.17	9.47	.19	8.80	5.88	3.26	2.01	.9168	.1354	99.48	2.05	8.0	128	31.0	66	66	103	144	83	.0	62	535	246	
BT-14																									
55.74	13.21	1.11	9.01	.15	6.62	7.85	3.39	1.23	.9920	.1044	99.42	1.94	11.0	155	30.0	243	43	83	101	64	31.1	70	353	215	
BT-15																									
57.01	12.40	1.07	8.66	.16	7.72	7.75	2.77	1.05	.9578	.0824	99.63	2.29	10.0	144	29.0	152	35	90	111	66	.0	76	329	212	
BT-17																									
55.62	14.37	1.15	9.29	.14	6.38	6.82	2.13	2.79	1.0669	.1409	99.91	2.09	10.0	157	33.0	159	119	99	122	67	.0	94	561	265	
NN-1																									
56.33	12.56	1.09	8.82	.16	6.77	9.20	2.16	1.26	1.1487	.0621	99.56	2.42	9.0	152	30.0	346	75	83	99	61	.0	73	345	255	
NN-4																									
56.21	12.44	1.13	9.12	.17	7.11	8.34	2.54	1.21	1.1533	.1039	99.51	2.62	9.0	154	32.0	233	47	98	101	62	32.2	73	420	249	
NN-5																									
56.20	12.99	1.10	8.93	.17	6.98	7.75	2.79	1.47	1.1044	.1135	99.58	2.42	10.0	156	34.0	222	62	96	76	65	.0	72	466	254	

WHOLE ROCK GEOCHEMICAL DATA OF STRAUMSNUSTANE VOLCANICS

MAJOR ELEMENTS IN WEIGHT PER CENT														TRACE ELEMENTS IN PPM											
SiO2	Al2O3	Fe2O3	FeO	MnO	MgO	CaO	Na2O	K2O	TiO2	P2O5	TOTAL	LOI	Nb	Zr	Y	Sr	Rb	Zn	Cu	Ni	SC	CR	BA	V	
NN-8	54.37	12.35	1.07	8.66	.19	7.87	10.39	2.44	1.09	1.0655	.0828	99.57	2.58	9.0	130	29.0	203	41	85	110	67	.0	.75	247	273
NN-12	56.48	12.99	1.11	9.01	.16	7.45	6.67	3.05	1.21	1.1775	.1459	99.45	2.72	9.0	147	32.0	165	39	88	106	63	.0	.68	374	268
NN-15	55.09	11.36	1.20	9.72	.16	8.72	12.15	.10	.10	1.0759	.0410	99.72	4.73	9.0	119	28.0	35	4	101	142	63	.0	.77	81	237
NN-16	55.66	13.17	1.09	8.86	.16	7.88	6.63	3.04	1.75	1.0143	.1464	99.40	2.73	9.0	126	29.0	107	58	104	105	72	.0	.79	463	243
MG-1	54.24	13.64	1.17	9.44	.18	8.28	7.18	3.07	1.47	.9838	.1521	99.81	3.12	9.0	125	27.0	42	51	102	110	73	.0	.41	344	281
TN-1	54.88	13.51	1.03	8.35	.17	9.91	6.43	2.74	1.69	.8959	.1425	99.76	3.07	6.0	102	24.0	96	45	95	70	88	.0	.116	575	240
TN-3	55.12	13.59	1.04	8.45	.16	7.98	8.25	2.57	1.39	.8696	.1035	99.52	2.70	8.0	106	24.0	112	47	82	89	89	.0	.95	362	237
TN-4	52.92	13.39	1.05	8.50	.18	8.70	9.21	3.19	1.31	.9060	.1041	99.45	2.42	7.0	109	26.0	110	34	92	103	90	.0	.104	359	248
TN-4	53.00	14.30	1.07	8.70	.16	8.51	9.32	2.60	.99	.8339	.0824	99.58	2.58	5.0	88	22.0	235	50	83	102	91	.0	.143	211	249
TN-7	54.27	13.25	1.06	8.57	.16	8.00	9.52	2.30	1.33	.7893	.0526	99.31	2.60	8.0	93	22.0	243	69	82	96	91	.0	.134	276	227
TN-8	53.59	13.25	1.05	8.50	.17	8.67	8.77	3.08	1.42	.8725	.1039	99.49	2.75	7.0	105	25.0	125	36	81	147	93	.0	.94	319	244
TN-9	52.51	13.92	1.15	9.31	.19	7.72	8.17	4.63	.64	1.1751	.1649	99.57	1.98	9.0	140	32.0	269	13	92	135	75	.0	.81	171	244
RG-3	54.80	13.60	1.09	8.83	.17	7.74	7.43	3.35	1.39	.8773	.1253	99.40	2.47	8.0	101	25.0	122	47	87	90	97	.0	.98	425	225
RG-4	52.33	13.57	1.07	8.68	.17	8.27	10.75	3.37	.51	.9668	.0712	99.76	2.23	8.0	125	27.0	269	15	70	107	77	.0	.86	173	268
RG-5	53.63	13.78	1.07	8.63	.18	9.84	5.56	3.55	2.08	.9861	.1765	99.48	2.85	7.0	106	24.0	87	71	90	82	97	.0	.132	715	262
RG-10	52.28	13.70	1.13	9.13	.17	9.51	8.92	3.22	.72	.9141	.1016	99.79	2.98	6.0	100	23.0	52	20	88	102	90	.0	.134	196	238
RG-12	53.41	14.09	1.09	8.80	.16	8.20	8.90	2.61	1.46	.8515	.0718	99.64	2.62	7.0	101	24.0	166	68	81	104	90	36.1	.130	462	239
RG-13	54.18	13.25	1.18	9.53	.19	8.95	5.43	3.31	2.12	1.1341	.1977	99.46	2.76	9.0	145	28.0	40	62	117	54	86	.0	.65	583	248

WHOLE ROCK GEOCHEMICAL DATA OF STRAUMSNUTANE VOLCANICS

MAJOR ELEMENTS IN WEIGHT PER CENT													TRACE ELEMENTS IN PPM											
SiO2	Al2O3	Fe2O3	FeO	MnO	MgO	CaO	Na2O	K2O	TiO2	P2O5	TOTAL	LOI	Nb	Zr	Y	Sr	Rb	Zn	Cu	Ni	SC	CR	BA	V
RG-14																								
53.91	14.09	1.20	9.75	.17	7.52	6.18	4.27	1.31	1.1606	.1833	99.75	2.05	9.0	141	34.0	83	41	107	129	78	.0	66	355	256
RG-15																								
54.55	12.29	1.29	10.45	.17	9.17	8.92	.08	1.37	1.3802	.1319	99.82	4.06	8.0	137	31.0	41	53	106	100	81	.0	65	445	239
RG-16																								
53.62	12.77	1.10	8.89	.20	8.83	6.93	3.28	2.44	1.2295	.1876	99.46	1.96	8.0	154	33.0	96	80	94	142	77	.0	66	780	281
RG-17																								
54.26	12.44	1.16	9.36	.18	8.05	8.68	3.64	.64	1.0378	.0830	99.53	2.01	11.0	138	29.0	720	16	83	116	79	.0	83	196	251
RG-19																								
55.29	13.63	1.14	9.21	.15	6.75	5.35	3.57	3.11	1.1851	.1958	99.58	1.73	10.0	161	38.0	113	120	94	118	61	.0	93	810	281
LV-1																								
53.64	13.51	1.13	9.15	.17	8.06	8.99	2.13	1.69	.9717	.1034	99.54	2.42	8.0	120	28.0	261	95	95	103	74	.0	74	505	257
LV-4																								
53.39	13.99	1.11	8.97	.18	9.00	7.05	2.89	1.91	.9475	.1545	99.58	2.60	6.0	116	26.0	202	111	99	101	89	.0	92	667	250
LV-6																								
53.27	13.90	1.10	8.93	.17	7.80	10.03	2.29	.98	.8858	.0625	99.41	2.09	8.0	103	23.0	212	54	88	97	94	.0	118	234	242
LV-7																								
52.93	13.45	1.09	8.85	.17	8.36	10.55	2.11	1.00	.8755	.0625	99.43	2.40	8.0	105	24.0	198	47	84	100	87	.0	118	237	248
LV-8																								
52.93	14.21	1.18	9.54	.18	6.89	7.77	5.28	.47	1.1782	.1524	99.78	1.64	9.0	146	32.0	167	11	89	115	71	.0	64	147	270
LV-9																								
51.27	14.32	1.20	9.75	.20	8.25	8.25	4.64	.51	1.2088	.1727	99.77	2.45	8.0	146	31.0	44	10	89	114	81	.0	69	131	293
LV-10																								
54.69	13.20	1.14	9.27	.18	8.11	6.77	3.76	1.19	1.0295	.1352	99.47	2.37	8.0	134	31.0	181	33	90	98	81	.0	67	382	253
UK-2																								
52.12	12.64	1.14	9.21	.19	9.12	10.66	2.91	.49	.9283	.0626	99.46	2.55	7.0	111	25.0	117	12	80	145	96	.0	129	180	264
UK-3																								
53.50	13.72	1.09	8.83	.15	8.57	8.00	2.27	2.47	.9242	.0924	99.63	2.51	7.0	102	28.0	201	100	87	99	101	.0	122	650	251
UK-4																								
55.31	12.47	1.13	9.13	.17	8.43	7.05	3.28	1.50	.9756	.0934	99.53	2.04	7.0	123	26.0	158	55	87	93	90	.0	89	514	249
UK-5																								
54.98	12.68	1.11	8.99	.16	8.44	8.27	2.55	1.58	.9746	.0711	99.81	2.17	8.0	121	29.0	414	59	83	118	93	36.3	93	698	258
UK-8																								
53.90	12.22	1.10	8.94	.18	9.59	8.72	2.67	1.19	.9164	.0729	99.49	2.41	7.0	107	26.0	265	43	84	94	99	.0	124	462	255
UK-9																								
54.14	13.61	1.15	9.29	.16	8.50	7.39	2.13	2.38	.9542	.1015	99.79	2.56	8.0	125	30.0	164	106	98	82	91	.0	87	686	265

WHOLE ROCK GEOCHEMICAL DATA OF STRAUMSNUTTANE VOLCANICS

MAJOR ELEMENTS IN WEIGHT PER CENT

TRACE ELEMENTS IN PPM

SiO2	Al2O3	Fe2O3	FeO	MnO	MgO	CaO	Na2O	K2O	TiO2	P2O5	TOTAL	LOI	Nb	Zr	Y	Sr	Rb	Zn	Cu	Ni	SC	CR	BA	V
54.61	13.03	1.15	9.32	.18	7.92	5.41	3.59	2.77	1.30	99.2079	99.48	2.30	9.0	163	37.0	115	100	105	145	64	.0	98	880	271
TP-2																								
55.70	12.77	1.13	9.19	.17	7.58	7.26	2.70	1.65	1.17	99.1458	99.47	2.60	8.0	155	30.0	205	65	95	107	63	.0	77	506	242
TP-4																								
53.81	12.93	1.05	8.48	.20	7.49	9.78	3.36	1.29	1.08	99.1136	99.58	2.40	10.0	152	33.0	36	37	90	133	65	.0	74	206	257
TP-6																								
56.46	12.30	1.18	9.57	.16	6.78	8.97	2.05	.93	1.10	99.0621	99.57	2.47	8.0	157	33.0	354	46	88	105	62	.0	77	335	244
TP-8																								
54.38	12.23	1.16	9.40	.20	8.13	8.72	3.35	.80	1.16	99.1131	99.65	2.22	9.0	144	30.0	150	24	90	117	71	.0	78	206	240
TP-9																								
54.02	11.47	1.25	10.09	.19	9.54	10.39	.00	1.28	1.23	99.1140	99.59	3.24	7.0	141	30.0	19	44	96	120	70	34.5	70	396	241
TP-10																								
54.95	12.73	1.15	9.34	.19	7.48	7.22	3.76	1.10	1.32	99.1674	99.41	2.05	10.0	151	34.0	60	35	120	120	64	.0	65	295	243
TP-11																								
55.57	13.13	1.14	9.24	.18	7.53	5.63	3.79	1.92	1.19	99.1765	99.50	2.06	9.0	152	33.0	66	66	99	124	61	.0	91	449	268
TP-13																								
54.38	13.43	1.19	9.62	.16	7.29	6.85	2.76	2.35	1.41	99.1848	99.64	2.34	10.0	164	34.0	141	86	102	113	61	.0	91	619	300
TP-14																								
54.42	13.66	1.21	9.77	.17	7.05	5.83	3.87	1.74	1.46	99.2192	99.40	2.14	9.0	163	35.0	85	63	103	119	62	.0	93	427	280
TP-16																								
52.18	12.94	1.21	9.78	.19	7.72	10.02	3.03	1.11	1.22	99.1142	99.51	2.30	9.0	157	33.0	273	45	92	126	75	.0	81	302	258
TP-17																								
55.43	10.80	1.18	9.58	.19	7.82	11.17	1.71	.52	1.09	99.0104	99.52	2.11	8.0	139	30.0	379	26	83	113	67	.0	76	175	245
TP-19																								
53.97	12.35	1.10	8.88	.18	7.19	11.63	2.24	.95	1.05	99.0310	99.58	1.75	9.0	162	33.0	336	46	71	90	59	.0	83	205	254
TP-21																								
56.84	13.06	1.12	9.05	.15	6.89	6.40	2.72	2.22	1.15	99.1226	99.71	2.21	10.0	169	34.0	253	98	94	101	62	.0	77	646	249
TP-23																								
55.55	11.46	1.27	10.25	.18	7.96	9.14	1.62	.85	1.25	99.0725	99.60	2.79	8.0	150	34.0	261	41	87	108	74	.0	78	301	236
TP-24																								
55.42	11.58	1.19	9.67	.18	7.75	9.82	2.34	.66	.98	99.0207	99.61	2.19	8.0	140	30.0	451	19	77	108	82	.0	72	193	256
TP-25																								
53.67	12.24	1.19	9.60	.20	7.80	9.09	3.51	.98	1.15	99.0832	99.52	1.88	10.0	159	34.0	276	39	79	129	77	.0	80	283	249
TP-26																								
59.39	10.22	1.15	9.34	.16	6.79	11.53	.00	.07	.95	99.0000	99.61	4.00	8.0	120	27.0	24	11	104	170	58	.0	61	104	229
TP-27																								

WHOLE ROCK GEOCHEMICAL DATA OF STRAUMSUTANE VOLCANICS

MAJOR ELEMENTS IN WEIGHT PER CENT

MAJOR ELEMENTS IN WEIGHT PER CENT													TRACE ELEMENTS IN PPM											
SiO2	Al2O3	Fe2O3	FEO	MNO	MGO	CAO	NA2O	K2O	TiO2	P2O5	TOTAL	LOI	NB	ZR	Y	SR	RB	ZN	CU	NI	SC	CR	BA	V
TP-28																								
55.53	12.32	1.18	9.55	.15	8.36	8.31	.30	2.53	1.1373	.1148	99.47	3.60	8.0	138	31.0	39	96	87	116	71	.0	71	924	264
TP-29																								
56.62	11.89	1.06	8.58	.18	8.95	5.75	3.36	2.05	.9951	.1348	99.56	2.21	7.0	128	29.0	97	66	98	118	72	.0	63	740	254
TP-30																								
52.57	13.74	1.06	8.61	.17	9.49	7.79	3.38	1.59	.8873	.1148	99.40	2.56	7.0	94	22.0	129	57	88	108	101	.0	147	463	147
TP-32																								
52.28	14.18	1.08	8.77	.16	9.78	7.25	2.62	2.34	.9204	.1448	99.52	2.97	7.0	97	24.0	107	79	92	47	98	.0	140	609	259
TP-34(A)																								
54.44	12.73	1.09	8.83	.16	8.93	8.61	2.72	1.11	.8797	.0621	99.55	2.27	7.0	101	23.0	339	45	87	92	90	.0	127	327	266
TP-34(B)																								
53.93	12.30	1.09	8.81	.17	8.98	9.69	2.75	.82	.8779	.0418	99.44	2.27	7.0	99	24.0	436	29	83	123	95	.0	127	262	260
TP-35																								
56.54	11.76	1.13	9.14	.17	7.70	7.57	3.13	1.29	.9123	.0944	99.43	1.98	8.0	123	27.0	147	41	92	109	70	.0	66	303	250
TP-36																								
54.73	12.18	1.15	9.30	.18	9.41	6.61	3.17	1.60	.9932	.1359	99.45	2.81	8.0	123	29.0	108	44	103	120	77	.0	70	470	281
TP-38																								
53.48	13.58	1.16	9.38	.19	8.72	6.20	3.52	1.90	1.1998	.2172	99.53	2.47	9.0	140	31.0	52	63	107	99	76	.0	66	547	266
TP-39																								
56.89	12.71	1.03	8.33	.16	8.17	5.54	2.98	2.71	1.0043	.1537	99.69	2.23	8.0	124	28.0	65	89	98	107	74	.0	61	837	256
TP-40(B)																								
53.84	13.87	1.08	8.72	.16	8.79	5.16	2.11	4.52	1.2342	.2346	99.72	2.46	11.0	153	36.0	54	155	107	117	78	.0	57	1613	305
TP-42(2)																								
53.88	12.87	1.20	9.74	.17	8.26	7.50	3.02	1.62	1.0351	.1255	99.41	2.50	9.0	145	30.0	229	61	91	115	77	.0	72	475	265
TP-43																								
55.27	11.53	1.14	9.24	.18	9.29	7.53	2.72	1.60	.9661	.0935	99.55	2.51	8.0	134	30.0	197	49	91	106	84	.0	68	552	280
TP-44																								
51.60	14.02	1.24	10.08	.19	8.93	6.63	3.32	1.85	1.3529	.2185	99.43	2.61	10.0	150	34.0	84	49	109	168	83	.0	74	477	286
TP-46																								
55.17	13.06	1.10	8.95	.17	7.58	8.00	2.54	2.00	.9188	.0929	99.58	2.12	9.0	135	31.0	226	100	92	108	69	.0	56	562	263
TP-47																								
56.57	12.04	1.05	8.51	.16	9.04	5.22	3.06	2.95	.9539	.1436	99.69	2.19	8.0	127	28.0	99	101	103	124	74	.0	62	964	259
TP-49																								
52.81	12.69	1.08	8.78	.17	9.60	10.62	2.48	.52	.8333	.0412	99.63	3.34	7.0	90	25.0	112	17	75	121	90	.0	139	169	243
TP-50																								
52.75	13.80	1.14	9.22	.17	9.72	7.67	3.57	.59	.9594	.1225	99.71	3.17	6.0	92	24.0	128	16	91	119	97	.0	146	239	244

WHOLE ROCK GEOCHEMICAL DATA OF STRAUMSUTANE VOLCANICS

MAJOR ELEMENTS IN WEIGHT PER CENT										TRACE ELEMENTS IN PPM															
	SiO2	Al2O3	Fe2O3	FeO	MnO	MgO	CaO	Na2O	K2O	TiO2	P2O5	TOTAL	LOI	Nb	Zr	Y	Sr	Rb	Zn	Cu	Ni	SC	CR	BA	V
TP-53																									
53.90	14.35	1.03	8.35	.16	8.50	7.70	3.21	1.80	.7958	.0907	99.89	2.50	7.0	90	20.0	150	93	84	87	89	.0	132	367	246	
TP-54																									
54.83	11.72	1.14	9.21	.19	9.43	6.91	3.43	1.56	1.0357	.1346	99.58	2.41	8.0	142	32.0	123	40	101	115	76	.0	70	478	273	
TP-55																									
54.70	12.74	1.12	9.05	.18	7.87	6.59	4.78	1.28	.9820	.1358	99.43	1.39	9.0	140	28.0	157	32	81	92	71	.0	64	396	258	
TP-56																									
54.32	13.67	1.13	9.18	.17	7.35	8.75	2.60	1.34	1.0169	.0924	99.63	2.33	9.0	122	27.0	135	61	92	106	84	.0	78	306	262	
TP-61																									
55.03	14.52	1.10	8.93	.15	7.55	6.55	2.68	2.25	.9787	.1312	99.87	2.64	8.0	123	28.0	129	107	94	91	94	.0	95	515	249	
TP-62																									
54.84	12.82	1.11	9.00	.16	8.27	8.59	2.65	1.20	.9248	.0719	99.65	2.50	6.0	115	28.0	243	42	84	92	92	.0	92	327	244	
TP-63																									
53.90	13.68	1.09	8.86	.17	8.10	8.09	3.11	1.49	.9313	.0931	99.52	2.59	6.0	109	26.0	155	50	120	101	93	.0	120	409	253	
TP-64																									
54.64	12.13	1.10	8.94	.17	8.62	9.32	2.39	1.23	.9061	.0521	99.50	2.60	7.0	113	27.0	176	35	81	72	92	.0	91	315	262	
TP-67																									
55.48	13.19	1.08	8.72	.16	8.18	6.69	2.70	2.29	.9422	.1139	99.53	2.41	7.0	112	25.0	106	70	87	100	90	.0	92	562	241	
TP-68																									
6.33	13.38	2.36	19.15	.36	15.92	15.98	7.37	1.82	2.2377	.2322	85.13	2.30	8.0	129	31.0	140	30	92	127	79	.0	61	349	255	
TP-72																									
54.18	13.03	1.11	8.99	.17	8.52	8.48	2.54	1.41	.9289	.0835	99.43	2.72	6.0	101	23.0	174	58	89	100	93	.0	126	387	252	
TP-74																									
52.92	12.92	1.12	9.08	.17	9.10	9.74	2.65	.95	.8391	.0518	99.54	2.70	8.0	99	24.0	204	34	77	101	99	.0	136	225	240	
TP-75																									
52.93	11.71	1.11	9.02	.17	8.66	13.07	1.89	.30	.8109	.0103	99.69	2.28	8.0	103	22.0	434	10	67	93	88	.0	125	113	125	
TP-76																									
44.42	12.98	1.11	8.97	.17	8.39	8.25	2.94	1.19	.9195	.0836	99.42	2.71	7.0	104	25.0	130	45	89	101	91	36.8	126	346	235	

TABLE A2.3

RARE EARTH AND SELECTED TRACE ELEMENT DATA OF BORGMASSIVET INTRUSIONS AND STRAUMSNUTANE BASALTS

	A14/82	A27/82	JT10/82	JT23/82	G9/82	G18/82	J19/81	A7/82	R8/82	R16/82	ET-11	SJ-17
La	7.4	12.1	17.0	9.7	21.0	20.6	18.4	16.7	4.8	12.6	35.9	20.8
Ce	15.7	27.0	37.4	21.2	47.0	45.2	37.7	43	14	25	78.7	43.4
Nd	9.7	14.3	19.5	10.1	25.0	22.8	18.5	16	4	12	42.2	21.6
Sm	1.71	2.83	3.85	2.25	5.49	4.73	4.14	3.57	1.04	2.89	9.06	4.86
Eu	0.60	0.85	1.07	0.74	1.67	1.22	1.03	1.18	0.24	0.84	2.15	1.27
Gd	-	-	-	-	-	-	-	-	-	-	-	-
Tb	0.35	0.53	0.68	0.33	1.06	0.80	0.61	0.7	0.2	0.7	1.50	0.84
Ho	-	-	-	-	-	-	-	-	-	-	-	-
Tm	(0.25)	(0.29)	(0.42)	-	0.57	0.45	0.37	-	-	-	-	0.46
Yb	1.35	1.83	2.51	1.48	3.38	2.84	2.25	2.76	0.84	2.02	5.55	2.96
Lu	0.23	0.29	0.39	0.25	0.53	0.45	0.40	0.41	0.12	0.30	0.87	0.47
Hf	1.25	2.24	3.13	1.71	4.11	3.70	2.91	2.8	0.8	2.3	6.66	3.55
Ta	0.44	0.80	0.81	0.53	0.84	0.80	0.37	0.8	<0.5	<0.5	1.06	0.50
Th	2.42	4.54	6.22	3.46	4.91	7.04	6.40	5.0	0.7	2.6	11.6	6.5

Data supplied by B.R.Watters, Department of Geology, University of Regina, Saskatchewan, Canada.

TABLE A2.4

GEOCHEMISTRY OF ARCHAEOAN ROCKS

	A15/81	KA2	DK1	RD1
SiO ₂	72.98	68.04	69.63	72.85
Al ₂ O ₃	14.89	15.42	16.62	15.12
Fe ₂ O ₃	0.20	0.41	0.25	0.20
FeO	1.58	3.31	2.03	1.64
MnO	0.04	0.07	0.03	0.03
MgO	0.68	2.08	0.87	0.65
CaO	1.55	3.88	2.88	2.05
Na ₂ O	5.01	4.48	5.16	4.31
K ₂ O	2.54	1.57	1.61	2.77
TiO ₂	0.24	0.47	0.38	0.31
P ₂ O ₅	0.07	0.18	0.15	0.10
TOTAL	99.77	99.92	99.61	100.05
Nb	34.3	4.2	1.7	4.2
Zr	125	163	181	164
Y	22.3	11.1	7.6	10.9
Sr	258	339	805	319
Rb	194	76	80	104

A15/81: Annandagstoppane granite

KA2: Lüneburg tonalite gneiss; DK1: Leucotonalite

RD1: Granite, Lüneburg area.

Data on Lüneburg samples supplied by R.G.Smith,
Department of Geology and Mineralogy,
University of Natal, Pietermaritzburg.

TABLE A2.5

EXAMPLE OF DATA REDUCTION

SAMPLE NUMBER R1/82

ORIGINAL WEIGHT		PERCENT OXIDES													
SiO2	Al2O3	Fe2O3	FEO	MNO	MGO	CAO	NA2O	K2O	TiO2	P2O5	CR2O3	TOTAL			
51.93	15.08	.90	7.30	.16	8.05	11.41	1.90	.70	.67	.08	.09	98.27			

WEIGHT		PERCENT OXIDES		RECALCULATED TO 100 PERCENT									
SiO2	Al2O3	Fe2O3	FEO	MNO	MGO	CAO	NA2O	K2O	TiO2	P2O5	CR2O3	TOTAL	
52.85	15.35	.92	7.43	.16	8.19	11.61	1.93	.71	.68	.08	.09	100.00	

CATION PROPORTIONS IN ANALYSIS													
Si	Al	Fe(3)	Fe(2)	MN	MG	CA	NA	K	Ti	P	CR		
54.97	9.41	.36	6.46	.14	12.70	12.94	1.95	.47	.53	.04	.04		

CIPW NORM

	OTZ	COR	OR	AB	AN	LC	NE	KP
WEIGHT PERCENT	2.167	.000	4.209	16.356	31.090	.000	.000	.000
MOLE PERCENT	8.239	.000	4.211	14.249	25.528	.000	.000	.000
CATION PERCENT	2.008	.000	4.210	17.364	31.107	.000	.000	.000

	AC	NS	KS	D1	WO	HY	OL	CS
WEIGHT PERCENT	.000	.000	.000	21.133	.000	22.105	.000	.000
MOLE PERCENT	.000	.000	.000	21.332	.000	22.924	.000	.000
CATION PERCENT	.000	.000	.000	20.794	.000	22.345	.000	.000

	MT	CM	IL	HM	TN	PF	RU	AP
WEIGHT PERCENT	1.328	.132	1.289	.000	.000	.000	.000	.193
MOLE PERCENT	1.310	.135	1.941	.000	.000	.000	.000	.131
CATION PERCENT	.958	.099	.946	.000	.000	.000	.000	.170

MAFIC INDEX = 46.180
NORM TOTAL = 100.002

OLIVINE COMPOSITION
FORSTERITE .000 FAYALITE .000

ORTHOPYROXENE COMPOSITION
ENSTATITE 62.989 FERROSILITE 37.011

CLINOPYROXENE COMPOSITION
WOLLASTONITE 51.330 ENSTATITE 30.657 FERROSILITE 18.013

FELDSPAR COMPOSITION
ORTHOCASE 8.149 ALBITE 31.664 ANORTHITE 60.187
PLAGIOCLASE COMPOSITION (PERC AN) 65.527

THORNTON AND TUTTLE DIFFERENTIATION INDEX = 22.732
SOLIDIFICATION INDEX (100*MGO/(MGO+FEO+FE2O3+NA2O+K2O)) = 42.706
CRYSTALLIZATION INDEX (AN+MG.D1+FO+FO EOIV OF EN) = 54.823
LARSEN INDEX (1/3SI+K)-(CA+MG) = -6.844
ALBITE RATIO (100*(AB+AB EOIV IN NE)/PLAG) = 34.473
IRON RATIO ((FE2-MN)*100/(FE2+MN+MG)) = 54.427
MG NUMBER AS CATIONS MG/CATIONS (FE+MG) = 66.274
OXIDATION RATIO ACCORDING TO LE MAITRE (FEO/FEO+FE2O3) = .837
DENSITY OF DRY LIQUID OF THIS COMPOSITION (AT 1050 DEG) = 2.670
AFM RATIO

TOTAL ALKALIS 13.86 TOTAL FE 43.23 MG 42.91

QUARTZ - FELDSPAR RATIOS						
QUARTZ	4.03	ORTHOCLASE	7.82	PLAGIOCLASE	88.15	
QUARTZ	9.53	ORTHOCLASE	18.52	ALBITE	71.95	
CATION PROPORTIONS		CA	39.86	FE	21.01	MG 39.13
		CA	16.05	MG	15.76	SI 68.19
		SI	71.32	AL	12.20	MG 16.48
		2MG	50.77	2FE	27.26	SI/5 21.97
		CA	52.24	AL	37.98	NA+K 9.78

COORDINATES IN THE SYSTEM PLAGIOCLASE - OLIVINE - CLINOPYROXENE - QUARTZ (IN MOLE PERCENT)

PROPORTION OF ANALYSIS IN BASALT TETRAHEDRON IS 93.62 MOLE PERCENT

BASALT TETRAHEDRON	OL	17.90	CPX	22.21	PLAG	51.78	QTZ	8.11
CLINOPYROXENE PROJECTION		23.01		0.0		66.56		10.43
QUARTZ PROJECTION		19.48		24.17		56.35		0.0
PLAGIOCLASE PROJECTION		37.12		46.06		0.0		16.82
OLIVINE PROJECTION		0.0		20.87		48.65	OPX+(4QTZ)	30.48

CMAS PROJECTIONS

TETRAHEDRON COORDINATES	C	17.79	M	18.90	A	12.84	S	50.47
DIOPSIDE PROJECTION	C3A	32.76	M	15.09	S	52.16		
OLIVINE PROJECTION	CS	25.70	M	58.02	S	16.28		
ENSTATITE PROJECTION	M2S	28.53	C2S3	36.68	A2S3	34.79		
QUARTZ PROJECTION	CAS2	59.10	MS	23.19	CMS2	17.71		

C.I.P.W. NORM CALCULATION

ABBREVIATIONS --- O-QUARTZ, C-CORUNDUM, OR-ORTHACLASE, AB-ALBITE, AN-ANORTHITE, LC-LEUCITE, NE-NEPHELINE, KP-KALIOPHILITE, AC-ACMITE, NS-SODIUM METASILICATE, KS-POTASSIUM METASILICATE, DI-DIOPSIDE, WO-WOLLASTONITE, HY-HYPERSTHENE, OL-OLIVINE, CS-CALCIUM ORTHOSILICATE, MT-MAGNETITE, CM-CHROMITE, IL-ILMENITE, HM-HAEMATITE, TN-TITANITE, PF-PEROVSKITE, RU-RUTILE, AP-APATITE

APPENDIX 3

TABLES REFERENCED IN TEXT

TABLE 2.1
PROPOSED INFORMAL NAMES FOR NUNATAKS AT
ANNANDAGSTOPPANE AND JULETOPPANE

Identification in Krynauw <i>et al.</i> , 1984, Figures 2 and 3.	Proposed informal name
<u>Annandagstoppane</u>	
Nunatak A	Hammer Heads
B	Bravo
C	Feldspar Hill
D	Graphic Hill
E	Echo
F	Viper's Hill
G ¹	See comment below
H	Peeping Tom
<u>Juletoppane</u>	
Nunatak 1570	Giaever's Sentinel
North of 1680	Ebele
1680	Camp Hill
1740	Julepiggen
1770	Thandi
1800	Littlehead Nunatak

1. Nunatak G was shown on Van Zyl's (1974) map, but was subsequently found to be a blue-ice field with wind-sculpted ice forms.

TABLE 2.2

MODAL COMPOSITIONS: MAIN SUITE, ANNANDAGSTOPPANE, JULETOPPANE AND FORSTEFJELL

(Volume per cent)

SAMPLE	LOCALITY	ORTHOPYROXENE	CLINOPYROXENE	PIGEONITE ⁽¹⁾	PLAGIOCLASE	BIOTITE	FE-TI OXIDES	MICROGRAPHIC ⁽²⁾ INTERGROWTHS	OTHER ⁽³⁾
A1/82	W. Viper' Hill	40	10	-	40	+ 2	< 1	8	-
A2/82	W. Viper's Hill	41	15	-	36	+ 1	< 1	5	+ 2
A5/82	W. Viper's Hill	7	3	-	83	< 1	< 1	+ 2	5
A16/82	St. Viper's Hill	50	11	Tr	18	7	< 1	9	5
A20/82	Central Viper's Hill	29	6	7	51	+ 2	+ 1	4	-
A21/82	Central Viper's Hill	50	10	-	31	< 1	< 1	8	-
A22/82	Central Viper's Hill	5	7	25	52	+ 1	+ 1	6	3
A23/82	Echo	22	17	-	48	+ 2	< 1	9	+ 1
A27/82	Bravo	18	7	6	58	+ 1	< 1	10	-
A34/82	Hammer Heads	26	12	+ 1	45	+ 2	< 1	13	1
A39/82	Hammer Heads	33	9	3	50	< 1	+ 1	+ 2	+ 1
JT8/82	Julepiggen	11	14	10	53	< 1	< 1	12	-
JT12/82	Thandi	28	7	4	50	+ 1	+ 1	9	-
JT15/82	Thandi	10	8	27	40	3	< 1	9	3
JT22/82	Giaever's Sentinel	9	4	22	51	+ 1	< 1	13	-
JT24/82	Ebele	21	31	13	31	+ 2	< 1	+ 2	-
JT26/82	Ebele	21	5	7	55	+ 2	< 1	10	-
JT28/82	Camp Hill	31	3	1	60	< 1	< 1	6	-
F1/84	Förstefjell	7	23	6	50	< 1	+ 1	12	+ 1
F7/84	Förstefjell	10	6	13	48	3	< 1	17	3
F8/84	Förstefjell	13	9	8	44	+ 1	+ 2	18	5
F9/84	Förstefjell	3	9	16	48	+ 2	< 1	19	3

(1)

Pigeonite is inverted in all cases

(2)

Intergrowths of quartz and alkali feldspar

(3)

Mainly alteration products: sericite, chlorite, amphibole.

TABLE 2.3

SUMMARY OF PETROGRAPHIC FEATURES IN MAIN SUITE ROCKS

PETROGRAPHIC CHARACTERISTICS	ANNANDAGSTOPPANE	JULETOPPANE	FÖRSTEFJELL
Presence of orthopyroxene primocrysts	X	X	X
Reaction relationship between orthopyroxene primocrysts and clinopyroxene	(X)	-	-
Reaction relationship between orthopyroxene and pigeonite	(X)	X	X
Mantles of orthopyroxene over pigeonite	X	X	X
Reaction relationship between orthopyroxene mantles and clinopyroxene, and between pigeonite and clinopyroxene	X	X	X
Presence of plagioclase as a primocryst	X	X	X
Presence of postcumulus clinopyroxene oikocrysts with plagioclase inclusions	X	X	X
Presence of micrographic intergrowths of quartz and alkali feldspar	X	X	X
Reaction relationship between magnetite and biotite	X	X	X

TABLE 2.4

MODAL COMPOSITIONS: SILLS FROM JULETOPPANE AND FÖRSTEFJELL
(Volume per cent)

SAMPLE	PIGEONITE ⁽¹⁾	CLINOPYROXENE	PLAGIOCLASE	MICROGRAPHIC ⁽²⁾ INTERGROWTHS	BIOTITE	FE-TI OXIDES
JT19/82	6	34	35	23	< 1	< 1
JT31/82	7	31	59	\pm 2	< 1	< 1
F2/84	3	31	48	15	\pm 2	< 1
F3/84	-	31	56	12	< 1	< 1
F4/84	-	38	53	8	< 1	< 1

(¹) Pigeonite is inverted or shows inversion in parts.

(²) Intergrowths of quartz and alkali feldspar.

TABLE 2.5
 STATISTICAL DATA FOR GEOCHEMISTRY OF MAIN SUITE MAFIC INTRUSIONS
 AT ANNANDAGSTOPPANE, JULETOPPANE AND FÖRSTEFJELL⁽¹⁾

ELEMENT OR CHEMICAL PARAMETER	ROCK TYPE ⁽²⁾	NUMBER ⁽³⁾ OF DETERMINATIONS	MINIMUM	MAXIMUM	MEAN	VARIANCE	STANDARD DEVIATION
SiO ₂ ⁽⁴⁾	AT	24	52.66	54.12	53.37	.16	.40
	JT	13	52.44	55.15	53.53	.57	.76
	FF	4	54.10	54.86	54.51	.14	.37
Al ₂ O ₃	AT	24	11.44	15.99	14.49	1.98	1.41
	JT	13	13.30	17.51	15.33	1.90	1.38
	FF	4	14.54	15.91	15.16	.52	.72
FeO	AT	24	7.76	9.41	8.28	.27	.52
	JT	13	7.22	9.79	8.14	.46	.68
	FF	4	8.15	8.91	8.52	.10	.32
MnO	AT	24	.15	.21	.17	.00	.02
	JT	13	.14	.19	.17	.00	.02
	FF	4	.17	.19	.18	.00	.01
MgO	AT	24	8.27	13.62	10.61	2.06	1.44
	JT	13	4.30	11.76	8.41	6.02	2.45
	FF	4	7.18	9.49	8.04	1.10	1.05
Mg ⁽⁵⁾	AT	24	64.40	72.14	69.38	3.33	1.83
	JT	13	50.80	72.75	63.55	51.95	7.21
	FF	4	60.28	66.32	62.55	6.81	2.61
CaO	AT	24	7.43	9.16	8.59	.30	.55
	JT	13	8.57	10.38	9.69	.35	.60
	FF	4	8.94	9.26	9.07	.02	.15
Na ₂ O	AT	24	1.03	1.80	1.54	.06	.24
	JT	13	1.34	2.12	1.65	.05	.22
	FF	4	1.70	2.00	1.84	.02	.13
K ₂ O	AT	24	.50	1.02	.69	.01	.11
	JT	13	.41	1.28	.85	.06	.25
	FF	4	.78	1.24	1.06	.04	.21
TiO ₂	AT	24	.05	.08	.07	.00	.01
	JT	13	.06	.10	.08	.00	.01
	FF	4	.07	.10	.08	.00	.01
P ₂ O ₅	AT	24	.05	.08	.07	.00	.01
	JT	13	.06	.10	.08	.00	.01
	FF	4	.07	.10	.08	.00	.01

TABLE 2.5
(continued)

ELEMENT OR CHEMICAL PARAMETER	ROCK ⁽²⁾ TYPE	NUMBER OF DETERMINATIONS	MINIMUM	MAXIMUM	MEAN	VARIANCE	STANDARD DEVIATION
Nb ⁽⁴⁾	AT	24	1.1	7.0	3.5	1.5	1.2
	JT	13	2.6	7.5	4.8	2.7	1.7
	FF	4	2.8	3.8	3.4	.2	.5
Zr	AT	24	54	88	69	62	8
	JT	13	56	113	82	306	17
	FF	4	69	91	82	100	10
Y	AT	24	6.3	16.6	10.4	4.7	2.2
	JT	13	9.6	23.6	14.8	20.2	4.5
	FF	4	17.2	22.3	19.5	4.6	2.1
Sr	AT	24	97	136	120	153	12
	JT	13	119	156	136	136	12
	FF	4	126	152	140	130	11
Rb	AT	24	19	62	31	68	8
	JT	13	24	61	39	141	12
	FF	4	33	53	46	85	9
Zn	AT	24	65	85	73	31	6
	JT	13	61	78	71	26	5
	FF	4	78	85	82	10	3
Cu	AT	24	37	120	64	340	18
	JT	13	35	98	67	324	18
	FF	4	82	102	91	76	9
Ni	AT	24	94	164	121	312	18
	JT	13	41	110	84	607	25
	FF	4	85	124	101	292	17
Sc	AT	24	22.5	41.0	29.3	19.3	4.4
	JT	13	27.1	40.3	32.2	11.9	3.4
	FF	4	29.1	31.8	30.7	1.6	1.3
Cr	AT	19	281	531	413	4425	67
	JT	13	71	400	265	15172	123
	FF	4	223	310	254	1504	39
Ba	AT	4	146	208	189	853	29
	JT	4	177	301	234	2653	52
	FF	0	-	-	-	-	-
V	AT	19	146	211	177	218	15
	JT	13	83	220	184	1285	36
	FF	4	205	215	209	20	5

- (¹) Two anorthositic samples, A5/82 and A22/82 have been excluded.
- (²) AT: Annandagstoppane; JT: Juletoppane; FF: Förstefjell.
- (³) Concentrations below detection limit not considered.
- (⁴) Major elements in weight per cent.
- (⁵) $Mg' = 100 \text{ Mg} / (\text{Mg} + \text{Fe})$
- (⁶) Trace elements in ppm.

TABLE 2.6A
VARIABLE CORRELATION OF SELECTED ELEMENT PAIRS: MAIN SUITE, ANNANDAGSTOPPANE

ELEMENT X	ELEMENT Y	NUMBER ⁽¹⁾ OF DETERMINATIONS	R	R ²	SLOPE	STANDARD ERROR OF SLOPE	INTERCEPT ON Y	STANDARD ERROR OF INTERCEPT	DISPERSION ⁽²⁾
Mg	SiO ₂	24	-.37	.14	-.2206	-.0418	68.67	2.90	3.10
"	Al ₂ O ₃	24	-.72	.52	-.7714	-.1096	68.00	7.60	4.27
"	FeO	24	.58	.34	.2860	.0475	-11.56	3.29	1.74
"	MnO	24	.80	.63	.0094	.0012	-.48	.08	1.17
"	MgO	24	.90	.81	.7868	.0708	-43.98	4.91	1.05
"	CaO	24	-.62	.38	-.3017	-.0485	29.51	3.37	3.43
"	Na ₂ O	24	-.63	.40	-.1288	-.0203	10.48	1.41	3.33
"	K ₂ O	24	-.50	.25	-.0607	-.0108	4.90	.75	3.16
"	TiO ₂	24	-.88	.78	-.0357	-.0035	2.97	.24	3.54
"	P ₂ O ₅	24	-.56	.31	-.0054	-.0009	.45	.06	3.22
"	Nb	24	-.39	.15	-.6724	-.1264	50.2	8.8	3.7
"	Zr	24	-.87	.76	-4.3062	-.4351	368	30	16
"	Y	24	-.87	.76	-1.1840	-.1176	92.5	8.2	5.5
"	Sr	24	-.66	.43	-6.7650	-1.0392	590	72	23
"	Rb	24	-.25	.06	-4.5300	-.8961	345	62	13
"	Zn	24	.56	.31	3.0388	.5134	-138	36	5
"	Cu	24	-.31	.09	-10.1068	-1.9645	765	136	30
"	Ni	24	.82	.67	9.6712	1.1364	-550	79	11
"	Sc	24	.55	.30	2.4045	.4106	-137.5	28.5	4.5
"	Cr	19	.81	.65	32.4134	4.3732	-1838	304	41
"	Ba	4	-.59	.35	-11.0561	-4.4616	951	308	52
"	V	19	-.11	.01	-7.1939	-1.6400	676	114	22
Zr	SiO ₂	24	.35	.12	.0512	.0098	49.84	.68	9.01
"	Al ₂ O ₃	24	.57	.32	.1791	.0301	2.16	2.08	7.41
"	FeO	24	-.57	.32	-.0664	-.011	12.85	.77	13.96
"	MnO	24	-.72	.52	-.0022	-.0003	.33	.02	14.58
"	MgO	24	-.80	.64	-.1827	-.0223	23.19	1.54	15.17
"	CaO	24	.48	.23	.0701	.0125	3.76	.87	8.04
"	Na ₂ O	24	.63	.40	.0299	.0047	-.52	.33	6.73
"	K ₂ O	24	.74	.55	.0141	.0019	-.28	.13	5.65
"	TiO ₂	24	.94	.89	.0083	.0006	-.07	.04	2.67
"	P ₂ O ₅	24	.53	.28	.0013	.0002	-.02	.02	7.60

TABLE 2.6A

(continued)

ELEMENT X	ELEMENT Y	NUMBER ⁽¹⁾ OF DETERMINATIONS	R	R ²	SLOPE	STANDARD ERROR OF SLOPE	INTERCEPT ON Y	STANDARD ERROR OF INTERCEPT	DISPERSION ⁽²⁾
Zr	Nb	24	.33	.11	.1562	.0301	-7.2	2.1	9.2
"	Y	24	.93	.87	.2750	.0202	-8.6	1.4	3.0
"	Sr	24	.50	.25	1.5710	.2780	12	19	15
"	Rb	24	.50	.25	1.0520	.1861	-42	13	11
"	Zn	24	-.52	.27	-.7057	-.1230	122	9	17
"	Cu	24	.57	.32	2.3471	.3941	-.98	27	19
"	Ni	24	-.59	.35	-2.2459	-.3687	275	26	35
"	Sc	24	-.38	.14	-.5584	-.2054	67.7	7.3	15
"	Cr	19	-.66	.44	-7.5568	-1.3968	935	90	122
"	Ba	4	.92	.85	2.0651	.4045	40	30	13
"	V	19	.34	.11	1.6772	.3624	61	25	20
K ₂ O	TiO ₂	24	.72	.51	.5878	.0837	.09	.06	.10
"	P ₂ O ₅	24	.28	.08	.0895	.0175	.01	.01	.13
"	Nb	24	.35	.12	11.0736	2.1192	-4.1	1.5	1.4
"	Y	24	.68	.46	19.4982	2.9223	-3.0	2.0	1.7
"	Sr	24	.15	.02	111.4045	22.4977	44	16	16
"	Rb	24	.93	.87	74.5991	5.4429	-21	4	3
"	Ba	4	.77	.60	134.2362	42.4266	83	35	20
Ti	P ₂ O ₅	24	.63	.40	.0000	.0000	-.01	.01	334.55
"	Nb	24	.31	.10	.0031	.0006	-5.8	1.8	458.3
"	Y	24	.92	.84	.0055	.0005	-6.1	1.4	160.7
"	Sr	24	.43	.18	.0316	.0058	26	18	418
"	Rb	24	.48	.23	.0212	.0038	-.32	11	398
"	Ba	4	.89	.79	.0509	.0116	33	36	270
P ₂ O ₅	Nb	24	.09	.01	123.7712	25.1597	-5	1.7	1.7
"	Y	24	.61	.37	217.9343	35.2524	-4.6	2.4	1.9
"	Sr	24	.47	.22	1245.1816	223.8832	35	16	13
"	Rb	24	.06	.00	833.8040	169.9033	-27	12	11
"	Ba	4	.74	.55	5058.4013	1697.4250	-140	111	21

TABLE 2.6A
(continued)

ELEMENT X	ELEMENT Y	NUMBER ⁽¹⁾ OF DETERMINATIONS	R	R ²	SLOPE	STANDARD ERROR OF SLOPE	INTERCEPT ON Y INTERCEPT	STANDARD ERROR OF	DISPERSION ⁽²⁾
Nb	Y	24	.38	.15	1.7608	.3320	4.1	1.2	2.8
"	Sr	24	.15	.02	10.0603	2.0308	85	8	16
"	Rb	24	.35	.12	6.7367	1.2900	7	5	10
"	Ba	4	.86	.75	43.9032	11.0397	19	43	15
Y	Sr	24	.48	.23	5.7136	1.0250	61	11	13
"	Rb	24	.46	.21	3.8259	.6947	-9	7	9
"	Ba	4	.87	.76	10.2133	2.5147	81	27	15
Sr	Rb	24	-.40	.00	-.6696	-.1366	111	17	21
"	Ba	4	.56	.31	1.5823	.6580	2	79	33
Rb	Ba	4	.59	.35	1.6552	.6655	124	28	31

(1) Concentrations below detection limit not considered.
(2) Dispersion about the reduced major axes.

TABLE 2.6B

VARIABLE CORRELATION OF SELECTED ELEMENT PAIRS: MAIN SUITE, JULETOPPANE

ELEMENT X	ELEMENT Y	NUMBER ⁽¹⁾ OF DETERMINATIONS	R	R ²	SLOPE	STANDARD ERROR OF SLOPE	INTERCEPT ON Y	STANDARD ERROR OF INTERCEPT	DISPERSION ⁽²⁾
Mg	SiO ₂	13	-.66	.44	-.1051	-.0218	60.21	1.39	13.22
"	Al ₂ O ₃	13	-.61	.37	-.1912	-.0421	27.48	2.69	13.16
"	FeO	13	.29	.08	.0941	.0250	2.16	1.60	8.63
"	MnO	13	.62	.39	.0021	.0005	.03	.03	6.26
"	MgO	13	.96	.93	.3404	.0252	-13.22	1.61	2.05
"	CaO	13	-.57	.32	-.0826	-.0189	14.94	1.21	12.80
"	Na ₂ O	13	-.85	.71	-.0307	-.0045	3.60	.29	13.85
"	K ₂ O	13	-.80	.64	-.0341	-.0057	3.02	.36	13.67
"	TiO ₂	13	-.92	.86	-.0163	-.0017	1.61	.11	14.14
"	P ₂ O ₅	13	-.85	.72	-.0019	-.0003	.20	.02	13.87
"	Nb	13	-.66	.43	-.2294	-.0481	19.4	3.1	13.5
"	Zr	13	-.86	.74	-2.4253	-.3397	237	22	37
"	Y	13	-.87	.76	-.6234	-.0853	54.4	5.5	16.4
"	Sr	13	-.74	.55	-1.6196	-.3010	238	19	26
"	Rb	13	-.87	.76	-1.6489	-.2244	144	14	27
"	Zn	13	.45	.20	.7048	.1744	26	11	9
"	Cu	13	-.83	.68	-2.4966	-.3890	225	25	37
"	Ni	13	.93	.86	3.4179	.3574	-133	23	10
"	Sc	13	.36	.13	.4780	.1235	2.8	7.9	9
"	Cr	13	.90	.81	17.0894	2.0884	-821	134	56
"	Ba	4	-.73	.53	-5.8995	-2.0124	575	118	97
"	V	13	-.43	.18	-.49730	-1.2471	500	80	62
Zr	SiO ₂	13	.79	.63	.0434	.0073	49.96	.62	11.22
"	Al ₂ O ₃	13	.58	.34	.0788	.0178	8.83	1.49	15.99
"	FeO	13	-.45	.21	-.0388	-.0096	11.33	.81	29.82
"	MnO	13	-.66	.43	-.0009	-.0002	.24	.02	31.83
"	MgO	13	-.85	.72	-.1404	-.0206	19.97	1.74	33.94
"	CaO	13	.48	.23	.0340	.0083	6.88	.70	17.88
"	Na ₂ O	13	.70	.49	.0126	.0025	.61	.21	13.58
"	K ₂ O	13	.96	.92	.0141	.0011	-.31	.09	5.01
"	TiO ₂	13	.93	.87	.0067	.0007	.02	.06	6.51
"	P ₂ O ₅	13	.89	.79	.0008	.0001	.01	.01	8.26

TABLE 2.6B
(continued)

ELEMENT X	ELEMENT Y	NUMBER ⁽¹⁾ OF DETERMINATIONS	R	R ²	SLOPE	STANDARD ERROR OF SLOPE	INTERCEPT ON Y	STANDARD ERROR OF INTERCEPT	DISPERSION ⁽²⁾
Zr	Nb	13	.78	.61	.0946	.0164	-3	1.4	11.6
"	Y	13	.90	.81	.2570	.0307	-6.4	2.6	8
"	Sr	13	.73	.53	.6678	.1273	81	11	16
"	Rb	13	.96	.92	.6799	.0526	-17	4	6
"	Zn	13	-.36	.13	-.2906	-.0753	95	6	30
"	Cu	13	.95	.90	1.0294	.0917	-18	8	8
"	Ni	13	.90	.81	-1.4094	-.1694	200	14	59
"	Sc	13	-.55	.31	-.1971	-.0455	48.4	3.8	31.4
"	Cr	13	-.89	.78	-7.0462	-.9078	845	76	242
"	Ba	4	.80	.65	2.5185	.7501	-.2	72	35
"	V	13	.76	.57	2.0505	.3709	15	31	28
K ₂ O	TiO ₂	13	.84	.70	.4782	.0726	.17	.06	.16
"	P ₂ O ₅	13	.83	.68	.0566	.0088	.03	.01	.14
"	Nb	13	.67	.45	6.7327	1.3831	-.9	1.2	1.4
"	Y	13	.83	.70	18.2922	2.7975	-.8	2.5	2.6
"	Sr	13	.74	.55	47.5238	8.8691	95	8	8
"	Rb	13	.98	.95	48.3856	2.8589	-2	3	3
"	Ba	4	.79	.62	2221.8712	68.1968	11	71	33
Ti	P ₂ O ₅	13	.94	.89	.0000	.0000	.01	.01	239.03
"	Nb	13	.77	.60	.0024	.0004	-3.3	1.5	474.8
"	Y	13	.92	.84	.0064	.0007	-7.3	2.5	285.7
"	Sr	13	.64	.41	.0166	.0035	78	12	597
"	Rb	13	.89	.79	.0169	.0022	-19	8	334
"	Ba	4	.87	.75	.0523	.0130	30	53	510
P ₂ O ₅	Nb	13	.73	.54	118.8605	22.4754	-4.2	1.7	1.2
"	Y	13	.86	.74	322.9325	46.0160	-9.6	3.5	2.4
"	Sr	13	.61	.37	838.9921	184.9921	72	14	10
"	Rb	13	.85	.73	854.2064	123.5715	-25	9	6
"	Ba	4	.88	.78	3989.6748	929.5975	-105	80	25

TABLE 2.6B

(continued)

ELEMENT X	ELEMENT Y	NUMBER ⁽¹⁾ OF DETERMINATIONS	R	R ²	SLOPE	STANDARD ERROR OF SLOPE	INTERCEPT ON Y	STANDARD ERROR OF INTERCEPT	DISPERSION ⁽²⁾
Nb	Y	13	.85	.73	2.7169	.3912	1.7	2	2.6
"	Sr	13	.42	.17	7.0586	1.7794	102	9	13
"	Rb	13	.72	.52	7.1866	1.3852	5	7	9
"	Ba	4	.87	.76	34.0612	8.3433	50	47	26
Y	Sr	13	.67	.45	2.5980	.5337	97	8	10
"	Rb	13	.91	.83	2.6452	.3038	0	5	5
"	Ba	4	.87	.76	9.6140	2.3343	70	42	26
Sr	Rb	13	.74	.55	1.0181	.1889	-99	26	12
"	Ba	4	.84	.70	7.2660	1.9933	-828	292	30
Rb	Ba	4	.79	.62	3.9504	1.2205	49	60	35

(1) Concentrations below detection limit not considered.

(2) Dispersion about the reduced major axes.

TABLE 2.6C

VARIABLE CORRELATION OF SELECTED ELEMENT PAIRS: MAIN SUITE, JULETOPPANE

ELEMENT X	ELEMENT Y	NUMBER ⁽¹⁾ OF DETERMINATIONS	R	R ²	SLOPE	STANDARD ERROR OF SLOPE	INTERCEPT ON Y	STANDARD ERROR OF INTERCEPT	DISPERSION ⁽²⁾
Mg	SiO ₂	4	-.84	.71	-.1412	-.0383	63.34	2.40	5.06
"	Al ₂ O ₃	4	-.65	.42	-.2760	-.1048	32.43	6.56	4.92
"	FeO	4	.21	.04	.1215	.0594	.92	3.72	3.31
"	MnO	4	.92	.84	.0037	.0007	-.05	.05	1.07
"	MgO	4	.96	.93	.4014	.0531	.17.07	3.33	.75
"	CaO	4	-.51	.26	-.0575	-.0247	12.66	1.55	4.55
"	Na ₂ O	4	-.85	.73	-.0512	-.0134	5.05	.84	5.04
"	K ₂ O	4	.95	.91	-.0801	-.0122	6.07	.77	5.18
"	TiO ₂	4	-.96	.93	-.0196	-.0026	1.90	.16	5.18
"	P ₂ O ₅	4	-.33	.11	-.0049	-.0023	.39	.15	5.18
"	Nb	4	.42	.18	.1809	.0820	-7.9	5.1	2.9
"	Zr	4	-.92	.84	-3.8350	-.7756	321	49	20
"	Y	4	-.89	.79	-.8203	-.1896	70.9	11.9	6.6
"	Sr	4	-.91	.82	-4.3597	-.9223	412	58	23
"	Rb	4	-.98	.95	-3.5281	-.3769	267	24	19
"	Zn	4	.22	.05	1.1852	.5787	8	36	5
"	Cu	4	-.81	.66	-3.3304	-.9741	299	61	17
"	Ni	4	.96	.92	6.5377	.9115	-308	57	5
"	Sc	4	.69	.48	.4868	.1751	.3	11	2.3
"	Cr	4	.98	.96	14.8493	1.4896	-675	93	8
"	Ba	0	-	-	-	-	-	-	-
"	V	4	-.34	.11	-1.7229	-.8110	317	51	9
Zr	SiO ₂	4	.99	.97	.0368	.0029	51.51	.24	1.59
"	Al ₂ O ₃	4	.90	.80	.0720	.0160	9.30	1.31	4.57
"	FeO	4	-.58	.33	-.0317	-.0129	11.10	1.06	17.80
"	MnO	4	-.99	.98	-.0010	-.0001	.26	.01	19.99
"	MgO	4	-.98	.96	-.1047	-.0099	16.57	.82	20.05
"	CaO	4	.78	.62	.0150	.0046	7.85	.38	6.57
"	Na ₂ O	4	.97	.94	.0134	.0016	.75	.13	2.39
"	K ₂ O	4	.99	.98	.0209	.0015	-.64	.12	1.40
"	TiO ₂	4	.98	.97	.0051	.0005	.26	.04	1.79
"	P ₂ O ₅	4	.67	.45	.0013	.0005	-.02	.04	8.14

TABLE 2.6C

(continued)

ELEMENT X	ELEMENT Y	NUMBER ⁽¹⁾ OF DETERMINATIONS	R	R ²	SLOPE	STANDARD ERROR OF SLOPE	INTERCEPT ON Y	STANDARD ERROR OF INTERCEPT	DISPERSION ⁽²⁾
Zr	Nb	4	-.02	.00	-.0472	-.0236	7.3	1.9	14.3
"	Y	4	.94	.88	.2139	.0370	2.1	3	3.6
"	Sr	4	.99	.98	1.1368	.0773	47	6	2
"	Rb	4	.96	.91	.9200	.1362	-29	11	4
"	Zn	4	-.27	.08	-.3091	-.1486	107	12	17
"	Cu	4	.69	.48	.8684	.3133	20	26	10
"	Ni	4	-.99	.98	-1.7047	-.1142	240	9	40
"	Sc	4	-.88	.77	-.1269	-.0305	41.1	2.5	19.6
"	Cr	4	-.82	.67	-3.8720	-1.1204	570	92	76
"	Ba	0	-	-	-	-	-	-	-
"	V	4	-.07	.00	-.4493	-.2241	245	18	16
K ₂ O	TiO ₂	4	.99	.97	.2449	.0199	.42	.02	.04
"	P ₂ O ₅	4	.60	.36	.0617	.0247	.02	.03	.19
"	Nb	4	-.13	.02	-2.2592	-1.1200	5.9	1.2	.8
"	Y	4	.91	.83	10.2418	2.1147	8.7	2.3	.9
"	Sr	4	.97	.94	54.4357	6.5658	82	7	3
"	Rb	4	.99	.97	44.0520	3.5459	-1	4	1
"	Ba	0	-	-	-	-	-	-	-
Ti	P ₂ O ₅	4	.53	.28	.0000	.0000	-.09	.07	297.82
"	Nb	4	-.19	.03	-.0015	-.0008	9.7	3.1	4/2.6
"	Y	4	.96	.92	.0070	.0010	-8.8	3.9	85.6
"	Sr	4	.99	.97	.0371	.0031	-11	13	52
"	Rb	4	.97	.94	.0300	.0037	-76	15	76
"	Ba	0	-	-	-	-	-	-	-
P ₂ O ₅	Nb	4	.71	.50	36.6060	12.8841	.3	1.1	.4
"	Y	4	.51	.26	165.9518	71.5612	5.4	6.2	2.1
"	Sr	4	.63	.40	882.0434	340.7351	65	29	10
"	Rb	4	.49	.24	713.7930	311.0467	-14	27	9
"	Ba	0	-	-	-	-	-	-	-

TABLE 2.6C

(continued)

ELEMENT X	ELEMENT Y	NUMBER ⁽¹⁾ OF DETERMINATIONS	R	R ²	SLOPE	STANDARD ERROR OF SLOPE	INTERCEPT ON Y	STANDARD ERROR OF INTERCEPT	DISPERSION ⁽²⁾
Nb	Y	4	-.12	.01	-4.5335	-2.2516	35.2	7.8	3.3
"	Sr	4	-.03	.00	-24.0956	-12.0420	223	42	16
"	Rb	4	-.26	.07	-19.4993	-9.4036	114	33	15
"	Ba	0	-	-	-	-	-	-	-
Y	Sr	4	.98	.95	5.3151	.5839	36	11	3
"	Rb	4	.86	.75	4.3012	1.0842	-38	21	5
"	Ba	0	-	-	-	-	-	-	-
Sr	Rb	4	.93	.86	.8092	.1528	-67	21	6
"	Ba	0	-	-	-	-	-	-	-
Rb	Ba	0	-	-	-	-	-	-	-

TABLE 2.7
MODAL COMPOSITIONS: HAMMER HEADS SECTION
(Volume per cent)

	SAMPLE NUMBER	ORTHO- PYROXENE	PIGEONITE ⁽¹⁾	CLINO- PYROXENE	PLAGIO- CLASE	BIOTITE	FE-TI OXIDES	MICROGRAPHIC INTERGROWTHS	OTHER ⁽²⁾
UPPER UNIT	A44/84	28	-	14	51	± 2	± 1	5	-
	A42/84	28	< 1	10	52	3	< 1	6	-
	A41/84	26	-	19	44	3	< 1	8	< 1
	A39/84	30	Tr	8	53	± 2	< 1	6	-
	A37/84	28	-	12	48	± 2	< 1	10	< 1
	A36/84	30	-	18	43	± 1	± 1	5	± 1
	A35/84	35	-	9	45	± 2	< 1	7	± 2
	A33/84	24	-	11	54	± 2	< 1	9	< 1
	A32/84	24	-	13	53	± 2	< 1	6	± 1
	A30/84	27	Tr	11	54	± 2	< 1	6	< 1
	A29/84	27	-	14	51	± 2	Tr	6	< 1
	A27/84	29	-	9	51	3	± 1	7	< 1
	A26/84	27	-	9	54	± 2	< 1	7	< 1
	A25/84	25	± 1	13	51	± 2	± 2	6	< 1
	A24/84	28	± 1	8	54	± 2	< 1	6	± 1
	A22/84	25	± 2	11	53	± 1	< 1	7	± 1
	A21/84	26	± 2	14	52	± 1	± 1	3	< 1
	A19/84	23	< 1	12	58	± 2	Tr	4	± 1
	A18/84	27	± 1	8	54	± 2	< 1	6	± 2
	A17B/84	19	< 1	8	59	4	< 1	9	-
	A17A/84	23	3	13	50	± 2	± 1	8	± 1
	A16/84	21	4	8	60	± 2	1	5	< 1
LOWER UNIT	A15/84	25	± 2	7	47	6	< 1	7	6
	A14/84	21	4	8	51	5	< 1	9	± 2
	A13/84	24	± 2	10	51	± 2	± 1	10	< 1
	A12/84	24	4	7	59	± 2	< 1	4	< 1
	A11/84	22	6	5	53	± 2	< 1	9	3
	A10/84	21	10	11	47	± 2	± 1	7	± 1
	A9/84	14	8	8	62	± 3	< 1	5	< 1
	A7/84	18	8	8	50	± 1	< 1	9	7
	A6/84	17	8	12	54	± 2	< 1	6	< 1
	A5/84	15	11	10	50	± 2	< 1	9	3
	A3/84	19	6	9	59	± 2	< 1	4	± 1
	A2/84	17	9	9	47	± 2	< 1	14	± 2
	A0/84	19	7	56	7	± 2	< 1	9	< 1

⁽¹⁾ Inverted pigeonite.

⁽²⁾ Alteration products including calcite, quartz, and hematite.

TABLE 2.8
SUMMARY OF PLAGIOCLASE GRAIN SIZE MEASUREMENTS: HAMMER HEADS SECTION

SAMPLE	WIDTH								LENGTH								DIAMETER											
	$\bar{x}^{(1)}$	Mdn	St. Dev. ⁽¹⁾	Kurt	Skew	Range	Min.	Max.	$\bar{x}^{(1)}$	Mdn	St. Dev. ⁽¹⁾	Kurt	Skew	Range	Min.	Max.	\bar{x}	Mdn	St. Dev. ⁽¹⁾	Kurt	Skew	Range	Min.	Max.	$L/W^{(*)}$	$L/W^{(*)}$		
A44/B4	4.150	3.907	1.520	3.408	1.361	9	2	11	8.810	8.237	3.446	9.280	2.211	24	4	28	6.540	6.239	2.231	8.903	2.034	16	3	19	2.12	2.11		
A42/B4	3.840	3.500	1.475	1.479	1.187	7	2	9	7.760	7.206	2.992	6.155	2.019	19	3	22	5.800	5.313	2.089	3.969	1.601	12	3	15	2.02	2.06		
A39/B4	4.370	3.900	2.087	5.133	1.949	12	2	14	9.300	8.250	4.312	4.082	1.624	25	3	28	6.860	6.206	3.015	5.221	1.872	17	3	20	2.13	2.12		
A36/B4	4.550	4.000	2.484	8.395	2.133	17	1	18	8.740	8.045	3.445	2.349	1.306	19	3	22	6.689	6.192	2.715	5.179	1.665	18	2	20	1.92	2.01		
A33/B4	4.250	3.994	1.800	3.480	1.578	9	2	11	9.510	8.700	4.201	5.231	1.698	27	3	30	6.990	6.370	2.844	3.553	1.558	16	3	19	2.24	2.18		
A30/B4	3.920	3.473	1.822	8.844	2.193	13	1	14	8.440	7.714	4.357	8.698	2.401	27	3	30	6.240	5.763	2.868	9.632	2.446	19	2	21	2.15	2.22		
A27/B4	4.190	3.658	2.014	4.328	1.780	11	1	12	9.890	8.250	3.832	4.805	1.651	24	4	28	6.710	6.132	2.603	6.355	1.915	18	2	20	2.19	2.26		
A24/B4	3.700	3.473	1.299	1.097	.917	7	1	8	8.090	7.750	3.185	7.030	2.003	21	3	24	5.950	5.550	2.086	5.856	1.846	13	3	16	2.19	2.23		
A21/B4	3.930	3.500	2.051	8.324	2.311	14	1	15	8.470	7.967	3.719	5.576	1.860	23	3	26	6.300	5.875	2.754	7.183	2.116	18	2	20	2.16	2.28		
A18/B4	4.390	3.938	2.300	4.278	1.679	13	2	15	9.310	8.690	3.645	1.172	1.070	18	3	21	6.830	6.250	2.727	1.389	1.177	13	3	16	2.12	2.21		
A15/B4	4.670	4.029	2.411	5.929	2.036	15	1	16	9.940	8.577	4.674	4.800	1.869	28	4	32	7.310	6.182	3.407	4.862	1.930	20	2	23	2.128	2.129		
A12/B4	3.890	3.435	1.831	3.551	1.637	9	2	11	9.630	8.625	4.282	1.004	1.169	20	4	24	6.760	6.000	2.778	.834	1.113	12	3	15	2.476	2.51		
A9/B4	4.190	3.891	2.004	4.048	1.717	10	2	12	9.050	8.409	3.883	3.825	1.693	21	4	25	6.660	6.167	2.660	3.095	1.476	15	3	18	2.160	2.16		
A6/B4	3.840	3.412	1.674	.917	1.102	8	1	9	8.160	7.447	3.274	1.416	1.049	17	3	20	6.020	5.500	2.179	.203	.805	10	2	12	2.125	2.183		
A3/B4	3.310	3.159	1.152	2.624	1.185	7	1	8	7.580	7.200	2.779	3.214	1.245	17	2	19	5.500	5.273	1.823	2.946	1.194	11	2	13	2.29	2.279		
A0/B4	3.530	3.313	1.439	0.965	1.019	7	1	8	7.140	6.600	2.478	.797	.791	12	3	15	5.370	5.196	1.790	1.141	.772	9	2	11	2.023	1.992		

(¹) \bar{x} = Mean

(²) Std. Dev = Standard Deviation

(³) Length/Width of mean values

(⁴) Length/Width of median values

KEY: Mdn = Median Min. = Minimum

Kurt = Kurtosis Max. = Maximum

Skew = Skewness

Range = Range

TABLE 2.9

PEARSON'S COEFFICIENT OF CORRELATION, r^2 , STANDARD ERROR OF ESTIMATE AND SLOPE OF

GEOCHEMICAL VARIATION WITH HEIGHT: HAMMER HEADS SECTION

VARIABLE	LOWER UNIT (A15/B4 INCLUDED)				LOWER UNIT (A15/B4 EXCLUDED)				UPPER UNIT			
	r	r ²	STD ERROR ⁽¹⁾	SLOPE	r	r ²	STD ERROR ⁽¹⁾	SLOPE	r	r ²	STD ERROR ⁽¹⁾	SLOPE
SiO ₂	-0.569	0.322	0.26	-0.036	-0.408	0.166	0.19	-0.018	-0.266	0.071	0.27	-0.008
Al ₂ O ₃	0.164	0.027	0.46	0.016	0.479	0.229	0.27	0.043	-0.232	0.054	0.54	-0.015
FeO*	0.144	0.021	0.39	0.011	-0.377	0.142	0.22	-0.019	0.108	0.012	0.28	0.003
MnO	0.128	0.016	0.01	0.000	-0.157	0.025	0.01	-0.000	0.298	0.089	0.01	0.000
MgO	0.283	0.080	0.41	0.025	-0.063	0.004	0.29	-0.004	0.331	0.110	0.41	0.016
Mg	0.333	0.111	0.47	0.034	0.345	0.119	0.49	0.039	0.476	0.227	0.45	0.028
CaO	-0.099	0.010	0.21	-0.004	0.384	0.147	0.13	0.012	-0.156	0.024	0.25	-0.004
Na ₂ O	-0.303	0.092	0.11	-0.007	0.230	0.053	0.11	-0.006	-0.226	0.051	0.07	-0.002
K ₂ O	-0.327	0.107	0.05	-0.004	-0.172	0.030	0.05	-0.002	-0.371	0.138	0.04	-0.002
TiO ₂	-0.513	0.264	0.01	-0.002	-0.436	0.190	0.01	-0.001	-0.302	0.091	0.03	-0.001
P ₂ O ₅	-0.455	0.217	0.01	-0.000	-0.583	0.340	0.01	-0.001	-0.072	0.005	0.01	-0.000
Nb	0.515	0.266	0.3	0.035	0.390	0.152	0.3	0.025	-0.175	0.031	0.5	-0.011
Zr	-0.513	0.263	10	-1.263	-0.477	0.227	3	-0.314	-0.336	0.113	4	-0.162
Y	-0.467	0.218	0.7	-0.071	-0.510	0.261	0.7	-0.085	-0.141	0.020	0.9	-0.015
Sr	-0.309	0.095	5	-0.307	-0.191	0.037	5	-0.196	0.049	0.002	6	0.033
Rb	0.255	0.065	5	0.271	-0.037	0.001	4	-0.032	-0.220	0.049	3	-0.065
Zn	-0.371	0.138	4	-0.306	-0.467	0.218	4	-0.041	0.075	0.006	4	0.035
Cu	-0.453	0.205	5	-0.468	-0.345	0.119	5	-0.361	-0.164	0.027	7	-0.136
Ni	0.269	0.072	10	0.575	-0.045	0.002	8	-0.075	0.238	0.057	6	0.179
Sc	-0.112	0.012	1.5	-0.035	-0.522	0.273	1.1	-0.143	-0.015	0.000	1.7	-0.003
Cr	0.189	0.036	24	0.950	-0.266	0.071	15	-0.889	0.432	0.187	21	1.112
V	-0.176	0.031	5	-0.197	-0.472	0.223	4	-0.511	-0.334	0.111	7	-0.291
Nb/Zr	0.491	0.241	2.73	0.312	0.544	0.296	0.42	0.058	-0.062	0.004	0.84	-0.006
Y/Zr	0.418	0.175	12.4	1.161	-0.000	0.000	1.27	-0.000	0.297	0.088	1.39	0.049
Rb/Zr	0.436	0.190	41.32	4.058	0.178	0.032	5.30	0.206	0.103	0.011	3.63	0.042
Zn/Zr	0.415	0.173	60.91	5.644	-0.016	0.000	8.29	-0.029	0.350	0.122	10.16	0.428
Cu/Zr	0.420	0.176	49.66	4.658	0.032	0.001	8.51	0.058	0.058	0.003	9.45	0.063
K/Zr	0.440	0.193	41.37	4.112	0.201	0.040	5.94	0.263	-0.005	0.000	5.16	-0.003
Ti/Zr	0.439	0.191	23.96	2.373	0.320	0.103	1.76	0.128	0.206	0.043	1.90	0.045
Nb/Rb	0.168	0.028	1.21	0.042	0.282	0.079	1.20	0.076	-0.096	0.009	1.48	-0.016
Y/Rb	-0.385	0.148	4.96	-0.420	-0.182	0.033	4.37	-0.174	0.159	0.025	2.42	0.044
Zn/Rb	-0.334	0.112	28.16	-2.024	-0.165	0.027	26.78	-0.967	0.194	0.038	23.49	0.524
Cu/Rb	-0.344	0.118	29.99	-2.229	-0.129	0.017	26.42	-0.739	-0.039	0.002	19.68	-0.086
K/Rb	-0.399	0.159	18.40	-1.626	-0.096	0.009	11.34	-0.235	-0.213	0.045	7.85	-0.193
Ti/Rb	-0.328	0.108	10.23	-0.721	-0.070	0.005	8.34	-0.126	-0.028	0.001	6.06	-0.019
Cr/V	0.267	0.071	0.11	0.006	0.010	0.000	0.09	-0.000	0.669	0.448	0.10	0.010

$$(1) \quad \text{Standard error of estimate} = \sqrt{\frac{\sum (y - y^1)^2}{N - 2}}$$

where y = measured value of geochemical variable; y^1 = predicted value of geochemical variable

N = number of cases

NOTE: r = Pearson's coefficient of correlation. The geochemical parameter is considered as the dependent variable, hence the slope given here is reversed on Figures 2.34, 2.35 and 2.38.

TABLE 3.1
MODAL VARIATION WITH HEIGHT, GULLY SECTION, ICE AXE PEAK
(VOLUME PER CENT)

HEIGHT (M)	SAMPLE NO.	OLIVINE	ORTHO- PYROXENE	CLINO- PYROXENE	PLAGIO- CLASE	QUARTZ	BIOTITE/ PHLOGOPITE	Fe-Ti-Cr OXIDES	OTHER ²	ROCK TYPE ³
106.0	R45/84	-	8	29	54	4	< 1	± 1	2-3	G
102.0	R44/84	-	9	34	45	8	± 1	< 1	2	QG } QG }
98.0	R43/84	-	9	26	41	8	< 1	< 1	15	
94.0	R42/84	-	10	36	47	4	< 1	< 1	1-2	G
90.0	R41/84	-	10	34	50	4	< 1	< 1	-	G
86.0	R40/84	-	10	29	56	4	< 1	< 1	± 1	G
82.0	R39/84	-	11	36	51	1-2	< 1	< 1	-	G
78.0	R38/84	-	8	34	56	1-2	± 1	< 1	-	G
74.0	R37/84	-	16	35	48	± 1	< 1	< 1	-	GBN
70.0	R36/84	-	20	38	41	< 1	± 1	< 1	-	GBN
66.0	R35/84	-	16	33	48	3	< 1	< 1	-	GBN
62.0	R34/84	-	17	33	47	± 2	± 1	< 1	-	GBN
59.0	R33/84	-	15	31	48	< 1	< 1	< 1	5	GBN
56.0	R32/84	-	17	34	44	1-2	3	< 1	-	GBN
54.0	R31/84	-	13	31	53	± 2	< 1	± 1	-	GBN
52.0	R30b/84	-	15	25	55	± 2	± 2	± 1	-	GBN
51.5	R30a/84	-	19	56	24	< 1	± 1	< 1	-	MGN
50.0	R29/84	3-4	16	42	35	-	< 1	± 1	1-2	MGN
48.0	R28/84	2-3	26	40	28	-	4	< 1	-	MGN
42.0	R27/84	41	23	15	20	-	± 1	< 1	-	MOG
40.0	R26/84	20	38	20	17	-	3	< 1	± 2	MOG
38.0	R25/84	28	29	21	17	-	4	< 1	-	MOG
36.0	R24/84	13	45	20	21	-	± 1	< 1	-	MOG
34.5	R23/84	34	31	10	22	-	± 2	< 1	< 1	MON } PL }
34.0	R22/84	23	28	27	10	-	7	± 1	4	
32.0	R21/84	23	35	23	19	-	< 1	< 1	-	MOG
30.0	R20/84	12	37	23	25	-	3	< 1	-	MOG
28.0	R19/84	12	46	20	21	-	± 1	< 1	-	MOG
26.0	R18/84	19	44	11	20	-	5	< 1	-	MOG
24.0	R17/84	20	36	11	31	-	± 2	< 1	-	MOG
22.0	R16/84	16	46	10	23	-	3	± 2	-	MOG
20.0	R15/84	39	12	14	32	-	3	< 1	-	MOG
18.0	R14/84	44	21	6	22	-	5	2-3	-	MON }
16.0	R13/84	41	24	5	29	-	± 1	< 1	-	MON }
14.0	R12/84	38	23	13	22	-	2-3	1-2	-	MOG
12.0	R11/84	41	18	15	23	-	± 2	1-2	-	MOG
10.0	R10/84	34	20	11	30	-	4	± 1	-	MON }
8.0	R9/84	29	15	30	21	-	5	< 1	-	MOG
6.0	R8/84	33	17	18	28	-	3	1-2	-	MOG
4.0	R7/84	20	23	20	33	-	3	1-2	-	MOG
2.0	R6/84	21	29	14	31	-	5	< 1	-	MOG
0.0	R5/84	14	30	18	31	-	6	< 1	-	MOG

¹ Height above snow line (lowermost exposures) in eastern windscoop.

² Other: Alteration products: serpentine, sericite, etc.

³ G: Gabbro; QG: Quartz gabbro; GBN: Gabbro-norite; MGN: Melagabbro-norite; MON: Mela-olivine norite; PL: Plagioclase-bearing lherzolite; MOG: Mela-olivine gabbro-norite.

TABLE 3.2

SUMMARY OF PETROGRAPHIC FEATURES, GULLY SECTION, ROBERTSKOLLEN COMPLEX

ZONE	CR	OL	QZ	OPX(C)	OPX(PC)	CPX(C)	CPX(PC)	PLAG(C)	PLAG(PC)	COMMENTS
VI			X	(X)	X	X?	X	X	X	Poikilitic, quartz content increases upwards.
V		((X))	X	(X)	X	(X)	X	X	X	Poikilitic, ol rare at base of zone.
IV		(X)	(X)	X	X	X	X		(X)	Abundant uralitization of cpx.
III	X	X		X	X	X	X		X	Increase in grain size relative to Zone II.
II	X	X		X	X	X	X		X	Increase in total opx, decrease in ol relative to Zone I. Deuteric alteration at top of zone. Normal and Metastable (?) relationships between opx and cpx.
I	X	X		?	X	?	X	Ms?	X	Undercooling textures; metastable (?) crystallization of plag; normal and metastable relationships between opx and ol.

CR: Chromite; OL: Olivine; QZ: Quartz; OPX: Orthopyroxene; CPX: Clinopyroxene;

PLAG: Plagioclase; (C): Cumulus; (PC): Postcumulus; Ms: Metastable.

TABLE 3.3
STATISTICAL DATA FOR GEOCHEMISTRY OF ROBERTSKOLLEN
MAFIC AND ULTRAMAFIC UNITS

ELEMENT OR CHEMICAL PARAMETER	ROCK ⁽¹⁾ TYPE	NUMBER ⁽²⁾ OF DETERMINATIONS	MINIMUM	MAXIMUM	MEAN	VARIANCE	STANDARD DEVIATION
SiO ₂	MAFIC(M)	17	51.11	55.10	53.46	1.53	1.24
	ULTRA- MAFIC(U)	23	42.49	53.57	49.34	9.71	3.12
Al ₂ O ₃	M	17	7.97	15.81	14.07	3.15	1.77
	U	23	4.37	9.31	6.59	1.79	1.34
FeO	M	17	6.65	10.85	8.28	1.19	1.09
	U	23	7.73	11.52	9.77	1.30	1.14
MnO	M	17	.15	.20	.18	.00	.02
	U	23	.18	.22	.20	.00	.01
MgO	M	17	4.28	18.75	9.08	10.05	3.17
	U	23	15.92	32.31	23.41	22.62	4.76
Mg ⁺	M	17	41.28	78.87	64.77	81.25	9.01
	U	23	77.35	83.92	80.76	2.77	1.67
CaO	M	17	8.28	11.74	10.28	1.44	1.20
	U	23	3.70	11.03	6.57	6.04	2.46
Na ₂ O	M	17	1.20	2.78	1.92	.18	.43
	U	23	.50	1.18	.81	.04	.21
K ₂ O	M	17	.26	1.22	.64	.07	.26
	U	23	.10	.48	.25	.01	.09
TiO ₂	M	17	.47	1.39	.73	.06	.24
	U	23	.28	.61	.43	.01	.09
P ₂ O ₅	M	17	.05	.17	.10	.00	.03
	U	23	.04	.09	.06	.00	.01
Nb	M	17	1.0	11.1	4.6	5.9	2.4
	U	23	.9	6.2	3.3	2.3	1.5
Zr	M	17	40	146	78	593	24
	U	23	24	68	43	126	11
Y	M	17	10.4	29.3	16.7	30.0	5.5
	U	23	1.2	12.9	7.5	11.1	3.3
Sr	M	17	89	190	154	576	24
	U	23	42	95	66	257	16
Rb	M	17	11	44	25	98	10
	U	23	1	21	11	18	4
Zn	M	17	54	119	75	241	16
	U	23	61	89	77	64	8
Cu	M	17	45	155	82	837	29
	U	23	22	68	44	126	11
Ni	M	27	33	337	116	4509	67
	U	23	220	868	489	37622	194
Sc	M	17	29.0	43.3	37.4	14.9	3.9
	U	23	16.9	49.6	32.2	95.8	9.8
Cr	M	17	2	2641	612	381654	618
	U	23	2190	4363	3202	394358	628
Ba	M	5	138	237	183	1334	37
	U	4	79	124	105	398	20
V	M	17	160	359	221	2373	49
	U	23	104	219	156	1044	32

(¹) U: Ultramafic Unit

M: Mafic Unit

(²) Concentrations below detection limit not considered.

TABLE 3.4
VARIABLE CORRELATION OF SELECTED ELEMENT PAIRS:
ULTRAMAFIC UNIT, REGIONAL DATA, ROBERTSKOLLEN

ELEMENT X	ELEMENT Y	NUMBER ⁽¹⁾ OF DETERMINATIONS	R	R ²	SLOPE	STANDARD ERROR OF SLOPE	INTERCEPT ON Y	STANDARD ERROR OF INTERCEPT	DISPERSION ⁽²⁾
Mg	SiO ₂	23	-.65	.42	-1.8704	-.2962	200.40	23.92	6.42
"	Al ₂ O ₃	23	-.85	.72	-.8037	-.0882	71.49	7.12	4.11
"	FeO	23	.62	.38	.6847	.1120	-45.52	9.05	1.76
"	MnO	23	.52	.27	.0075	.0013	-.40	.11	1.63
"	MgO	23	.89	.80	2.8555	.2677	-207.20	21.62	2.33
"	CaO	23	-.74	.54	-1.4756	-.2082	125.74	16.82	5.53
"	Na ₂ O	23	-.75	.56	-.1271	-.0176	11.08	1.42	3.14
"	K ₂ O	23	-.27	.07	-.0558	-.0112	4.76	.90	2.66
"	TiO ₂	23	-.71	.50	-.0558	-.0082	4.93	.66	3.09
"	P ₂ O ₅	23	-.43	.19	-.0077	-.0015	.68	.12	2.82
"	Nb	23	-.48	.24	-.9086	-.1657	76.7	13.4	3.9
"	Zr	23	-.66	.44	-6.7393	-1.0505	588	85	21
"	Y	23	-.76	.58	-1.9237	-.2722	162.9	22.0	7.1
"	Sr	23	-.65	.42	-9.6195	-1.5257	843	123	29
"	Rb	23	-.38	.14	-2.5612	-.4945	218	40	8
"	Zn	23	.47	.22	4.8126	.8847	-312	71	8
"	Cu	23	-.58	.34	-6.7298	-1.1387	587	92	20
"	Ni	23	.71	.56	116.44	16.09	-8915	1300	137
"	Log Ni	23	.71	.50	.1065	.0156	-5.9462	1.2631	1.2756
"	Sc	23	-.65	.42	-5.8749	-.9346	506.7	75.5	18.0
"	Cr	23	.92	.85	377.00	30.12	-27244	2433	245
"	Log Cr	23	.92	.84	.0525	.0043	-.7406	.3492	.6728
"	Ba	4	-.85	.73	-7.2938	-1.9074	692	154	39
"	V	23	-.81	.66	-19.4012	-2.3566	1723	190	62
Zr	SiO ₂	23	.35	.12	.2775	.0541	37.33	2.42	13.25
"	Al ₂ O ₃	23	.74	.55	.1192	.0167	1.43	.75	8.14
"	FeO	23	-.58	.33	-.1016	-.0173	14.17	.77	20.04
"	MnO	23	-.76	.58	-.0011	-.0002	.25	.01	21.08
"	MgO	23	-.66	.43	-.4237	-.0665	41.74	2.97	22.20
"	CaO	23	.53	.28	.2189	.0386	-2.90	1.73	11.10
"	Na ₂ O	23	.75	.56	.0189	.0026	.00	.12	7.98
"	K ₂ O	23	.56	.32	.0083	.0014	-.11	.06	10.50
"	TiO ₂	23	-.86	.74	.0083	.0009	.07	.04	5.97

TABLE 3.4 continued

ELEMENT X	ELEMENT Y	NUMBER ⁽¹⁾ OF DETERMINATIONS	R	R ²	SLOPE	STANDARD ERROR OF SLOPE	INTERCEPT ON Y	STANDARD ERROR OF INTERCEPT	DISPERSION ⁽²⁾
Zr	P ₂ O ₅	23	.79	.62	.0011	.0000	.01	.01	7.32
"	Nb	23	.76	.62	.1348	.0181	-2.5	.8	7.8
"	Y	23	.51	.26	.3101	.0583	-6.3	2.7	11.2
"	Sr	23	.62	.38	1.4274	.2334	4	10	17
"	Rb	23	.76	.58	.3800	.0515	-5	2	8
"	Zn	23	-.47	.22	-.7141	-.1318	108	6	24
"	Cu	23	.77	.60	.9986	.1325	1	6	11
"	Ni	23	-.50	.25	-17.2784	-3.1211	1236	139	336
"	Log Ni	23	-.53	.28	-.0158	-.0028	3.3389	.1247	19.6534
"	Sc	23	.41	.16	.8717	.1661	-5.5	7.4	16.2
"	Cr	23	-.64	.41	-55.9405	-8.9318	5623	399	1139
"	Log Cr	23	-.66	.43	-.0078	-.0012	3.8341	.0546	20.4492
"	Ba	4	.55	.30	2.0614	.8617	5	42	21
"	V	23	.71	.50	2.8788	.4253	32	19	26
Ti	P O	23	.75	.57	.0000	.0000	.00	.01	391.14
"	Nb	23	.49	.24	.0027	.0005	-3.6	1.3	560.5
"	Y	23	.79	.63	.0062	.0008	-8.7	2.2	346.8
"	Sr	23	.81	.66	.0288	.0035	-8	9	344
"	Rb	23	.80	.64	.0077	.0010	-8	3	353
"	Ba	4	.70	.49	.0346	.0124	12	34	448
P ₂ O ₅	Nb	23	.43	.19	117.33	22.05	-3.6	1.3	1.6
"	Y	23	.37	.14	252.36	51.06	-7.5	3.1	3.7
"	Sr	23	.55	.30	1242.16	216.50	-7	13	15
"	Rb	23	.75	.56	330.73	45.63	-8	3	3
"	Ba	4	.17	.03	3453.98	1700.73	-120	111	26
Nb	Y	23	.13	.02	2.3025	.4982	-.5	1.9	4.8
"	Sr	23	.23	.05	10.5868	2.1502	31	8	20
"	Rb	23	.42	.18	2.8188	.5334	2	2	5
"	Ba	4	.78	.60	30.7705	9.9672	-28	42	13

TABLE 3.4 continued

ELEMENT X	ELEMENT Y	NUMBER ⁽¹⁾ OF DETERMINATIONS	R	R ²	SLOPE	STANDARD ERROR OF SLOPE	INTERCEPT ON Y	STANDARD ERROR OF INTERCEPT	DISPERSION ⁽²⁾
Y	Sr	23	.75	.56	4.1628	.5766	37	5	12
"	Rb	23	.67	.44	1.1084	.1726	4	1	5
"	Ba	4	.61	.37	4.9083	1.9483	72	15	18
Sr	Rb	23	.74	.55	.2663	.0373	-6	3	12
"	Ba	4	.98	.95	1.0639	.1146	32	8	6
Rb	Ba	4	.98	.97	7.7233	.6874	4	9	4

(¹) Concentrations below detection limit not considered.

(²) Dispersion about the reduced major axis.

TABLE 3.5
VARIABLE CORRELATION OF SELECTED ELEMENT PAIRS:
MAFIC UNIT, REGIONAL DATA, ROBERTSKOLLEN

ELEMENT X	ELEMENT Y	NUMBER ⁽¹⁾ OF DETERMINATIONS	R	R ²	SLOPE	STANDARD ERROR OF SLOPE	INTERCEPT ON Y	STANDARD ERROR OF INTERCEPT	DISPERSION ⁽²⁾
Mg	SiO ₂	17	-.68	.46	-.1372	-.0245	62.34	1.60	16.66
"	Al ₂ O ₃	17	-.32	.10	-.1968	-.0452	26.81	2.96	14.93
"	FeO	17	-.71	.51	-.1211	-.0206	16.12	1.35	16.80
"	MnO	17	-.38	.15	-.0018	-.0004	.29	.03	14.98
"	CaO	17	.29	.09	.1333	.0309	1.65	2.02	10.81
"	Na ₂ O	17	-.89	.80	-.0477	-.0052	5.01	.34	17.56
"	K ₂ O	17	-.79	.63	-.0288	-.0042	2.50	.28	17.09
"	TiO ₂	17	-.94	.88	-.0263	-.0022	2.43	.15	17.75
"	P ₂ O ₅	17	-.91	.83	-.0036	-.0004	.33	.02	17.63
"	Nb	17	-.64	.40	-.2697	-.0505	22.0	3.3	16.90
"	Zr	17	-.93	.86	-2.7010	-.2416	253	16	51
"	Y	17	-.93	.86	-.6078	-.0554	56.1	3.6	20.7
"	Sr	17	-.71	.51	-2.6631	-.4523	327	30	47
"	Rb	17	-.59	.35	-1.0958	-.2139	96	14	24
"	Zn	17	-.66	.43	-1.7218	-.3154	187	21	33
"	Cu	17	-.38	.77	-3.2092	.2744	290	24	59
"	Ni	17	.75	.56	7.4493	1.1943	-366	78	48
"	Log Ni	17	.91	.84	.0240	.0024	.4555	.1541	3.7228
"	Sc	17	-.39	.15	-.4282	-.0958	65.2	6.3	16.3
"	Cr	17	.74	.55	68.5367	11.1722	-3827	731	445
"	Log Cr	17	.94	.88	.0767	.0064	-2.4473	.4164	3.1426
"	Ba	5	-.91	.83	-9.6873	-1.7803	835	120	72
"	V	17	-.91	.82	-5.4047	-.5495	571	36	97
Zr	SiO ₂	17	.53	.28	.0508	.0104	49.48	.85	23.55
"	Al ₂ O ₃	17	.25	.06	.0729	.0171	8.36	1.40	29.86
"	FeO	17	.76	.58	.0448	.0070	4.76	.58	16.83
"	MnO	17	.34	.12	.0007	.0001	.12	.01	27.98
"	MgO	17	-.74	.55	-.1302	-.0212	19.28	1.74	45.80
"	CaO	17	-.49	.24	-.0493	-.0105	14.15	.86	42.01
"	Na ₂ O	17	.74	.54	.0177	.0029	.54	.24	17.71
"	K ₂ O	17	.82	.67	.0107	.0015	-.20	.12	14.59
"	TiO ₂	17	.90	.82	.0097	.0010	-.03	.08	10.62

TABLE 3.5 continued

ELEMENT X	ELEMENT Y	NUMBER ⁽¹⁾ OF DETERMINATIONS	R	R ²	SLOPE	STANDARD ERROR OF SLOPE	INTERCEPT ON Y	STANDARD ERROR OF INTERCEPT	DISPERSION ⁽²⁾
Zr	P ₂ O ₅	17	.91	.84	.0013	.0001	-.01	.01	10.08
"	Nb	17	.76	.58	.0999	.0157	-3.2	1.3	16.90
"	Y	17	.85	.73	.2250	.0258	-.9	2.3	13.5
"	Sr	17	.52	.27	.9860	.2045	77	17	34
"	Rb	17	.76	.49	.4057	.0704	-7	6	20
"	Zn	17	.66	.44	.6375	.1159	25	10	24
"	Cu	17	.83	.70	1.1882	.1589	-11	13	22
"	Ni	17	-.66	.43	-2.7580	-.5054	332	41	130
"	Log Ni	17	-.82	.67	-.0089	-.0012	2.7104	.1020	46.42
"	Sc	17	.21	.04	.1585	.0376	25.0	3.1	31.0
"	Cr	17	-.66	.43	-25.3748	-4.6500	2600	382	1125
"	Log Cr	17	-.87	.77	-.0284	-.0033	4.7443	.2739	47.16
"	Ba	5	.88	.77	2.9269	.6318	-40	49	19
"	V	17	.86	.74	2.0010	.2468	65	20	29
Ti	P ₂ O ₅	17	.97	.94	0.0000	.0000	.00	.01	362.73
"	Nb	17	.63	.40	.0017	.0003	2.9	1.5	1212.5
"	Y	17	.93	.86	.0039	.0004	-.2	1.6	548.5
"	Sr	17	.59	.35	.0169	.0033	80	15	1287
"	Rb	17	.41	.17	.0070	.0015	-5	7	1545
"	Ba	5	.87	.76	.0505	.0110	-26	46	366
P ₂ O ₅	Nb	17	.65	.42	74.9755	13.8405	-2.6	1.4	2.0
"	Y	17	.90	.82	168.9565	17.4614	.6	1.8	2.4
"	Sr	17	.56	.31	740.2936	149.2983	84	50	23
"	Rb	17	.45	.20	304.6033	65.9112	-4	7	10
"	Ba	5	.71	.50	1634.5986	534.0076	28	50	28
Nb	Y	17	.49	.24	2.2535	.4763	6.4	2.5	6.1
"	Sr	17	.30	.09	9.8738	2.2856	109	12	29
"	Rb	17	.46	.21	4.0627	.8763	6	5	11
"	Ba	5	.17	.03	22.0512	9.7174	53	59	47

TABLE 3.5 continued

ELEMENT X	ELEMENT Y	NUMBER ⁽¹⁾ OF DETERMINATIONS	R	R ²	SLOPE	STANDARD ERROR OF SLOPE	INTERCEPT ON Y	STANDARD ERROR OF INTERCEPT	DISPERSION ⁽²⁾
Y	Sr	17	.61	.37	4.3816	.8428	81	15	22
"	Rb	17	.51	.26	1.8029	.3756	-5	7	11
"	Ba	5	.97	.93	10.8851	1.2634	31	18	10
Sr	Rb	17	.25	.06	.4115	.0967	-38	15	32
"	Ba	5	.37	.14	2.6268	1.0895	-226	170	44
Rb	Ba	5	.841	.71	6.7470	1.6279	31	38	21

(¹) Concentrations below detection limit not considered.

(²) Dispersion about the reduced major axis.

TABLE 3.6
MEANS AND STANDARD DEVIATIONS OF TRACE ELEMENT RATIOS IN GULLY SECTION

Height ⁽¹⁾	K/Zr		Ti/Zr		P ₂ O ₅ /Zr		Rb/Zr		K/Rb		Ti/Rb		Y/Rb		P ₂ O ₅ /Nb		Zr/Nb		P ₂ O ₅ /Y	
	\bar{x} ⁽²⁾	SD ⁽³⁾	\bar{x}	SD	\bar{x}	SD	\bar{x}	SD	\bar{x}	SD	\bar{x}	SD	\bar{x}	SD	\bar{x}	SD	\bar{x}	SD	\bar{x}	SD
0-32 m	68.2	5.6	67.5	4.6	20.2	1.9	.325	.031	210.0	12.5	208.6	19.6	.760	.069	505.5	158.9	25.0	7.3	82.2	6.8
36-42 m	75.9	2.6	72.7	1.8	22.2	2.3	.324	.012	234.1	6.2	224.3	5.0	.851	.044	493.0	155.3	22.4	7.7	80.5	7.1
54-74 m	70.6	11.4	72.4	2.2	14.4	.9	.266	.043	266.1	19.5	280.1	57.1	1.103	.213	451.9	140.2	31.2	9.5	50.7	4.7
78-106 m	63.5	10.4	66.8	3.4	14.5	.7	.249	.046	257.3	29.4	276.5	50.6	1.101	.202	291.5	48.2	20.1	2.8	54.7	5.2

- (¹) Height above snow line
- (²) \bar{x} = Mean
- (³) SD = Standard deviation

(After Wolmarans and Krynauw, 1981a)



TABLE 4.1B

SUMMARY OF SEDIMENTARY STRUCTURES AND PALAEOGEOGRAPHY OF THE AHLMANNRYGGEN GROUP
(After Wolmarans and Kent, 1982)

FORMATION	SEDIMENTARY STRUCTURES	PALAEOGEOGRAPHIC RECONSTRUCTION
Raudberget	Rare raindrop impressions and abundant desiccation cracks in mudstones, distorted ripple marks.	Shallow water sedimentation, rare periodic emergence.
Jekselen	Abundant ripple marks	Shallow water sedimentation; provenance N and NW.
Högfonna	Table 4.2.	Table 4.2.
Schumacher-fjellet	Table 4.2.	Table 4.2.
Frammryggen	Cross-bedding well developed in greywackes; local, mudstone-filled erosion channel present with desiccation cracks in the mudstone.	Shallow water, low energy conditions.
Pyramiden	Mudcracks, raindrop impressions, ripple marks, a pronounced parting lineation and small-scale planar cross-bedding.	<p>Increased energy, shallow water sedimentation and periodic emergence. Provenance SW to SE.</p> <hr/> <p>Low energy sedimentation under deepwater, reducing conditions.</p>

TABLE 4.2

SEDIMENTARY STRUCTURES AND PALAEOGEOGRAPHY OF THE SCHUMACHERFJELLET AND HÖGFONNA FORMATIONS
IN THE GRUNEHOGNA AREA
(After E.P. Ferreira, pers. comm., 1985)

FORMATION	SEDIMENTARY STRUCTURES	PALAEOGEOGRAPHIC RECONSTRUCTION	
HÖGFONNA	<p>Arenites: Trough cross-bedding with locally planar and ripple cross-bedding and wavy and graded bedding.</p> <p>Bedding structures: Ripple marks, current lineations, desiccation cracks and deformed bedding.</p> <p>Mudcrack polygons up to 70 cm in diameter locally present.</p> <p>Rare overturned bedding.</p>	Higher energy environment; Meandering rivers.	Main provenance to SW; local source variations from NW to SW, resulting in variations in energy conditions of depositional environments.
SCHUMACHER-FJELLET	<p>Argillites: Small-scale planar and ripple cross-bedding; wavy and horizontally layered units.</p> <p>Arenites: Planar cross-bedding, locally trough cross- and graded-bedding.</p> <p>Ripple marks, current lineations, desiccation cracks and deformed bedding. Sole and load structures locally.</p>	Lower energy environment; Braided rivers.	

TABLE 4.3
MODAL COMPOSITIONS: GRUNEHOGNA AND KULLEN SILLS⁽¹⁾

SAMPLE ⁽²⁾	HEIGHT ⁽³⁾	ORTHOPYROXENE ⁽⁴⁾	CLINOPYROXENE ⁽⁵⁾	INV. PIGEONITE ⁽⁴⁾	PLAGIOCLASE ⁽⁶⁾	QUARTZ	FE-TI OXIDES	BIOTITE	CHLORITE	K-FELDSPAR	APATITE
G9/82	0	-	44.5	-	40.4	5.4	6.5	-	-	3.2	-
G10/82	35	-	29.8	-	50.2	9.3	1.7	-	1.7	7.3	-
G11/82	40	-	41.2	-	43.5	6.8	5.1	-	-	3.4	-
G13/82	45	-	30.2	-	44.4	14.5	3.0	1	-	-	<1.0
G14/82	50	-	29.2	-	42.8	13.6	2.6	2.1	2.7	6.5	<1.0
G17/82	-	-	33.2	-	46.8	9.7	2.0	3.2	2.7	2.4	-
G28/82	-	-	33.3	-	56.8	6.6	3.3	-	-	-	-
G32/82	-	4.5	21.2	13.3	52.3	5.4	<1.0	2.7	-	-	-
G64/82	60	-	29.4	-	67.7	Tr	1.7	<1	<1	-	-
G63/82	75	-	32.1	-	61.8	4.3	1.0	<1	-	-	-
G59/82	360	-	31.7	-	53.5	10.4	1.9	-	1.5	1.0	-
G67/82	400	-	37.9	-	45.1	13.3	2.5	<1	<1	-	-

(¹) See Appendix 4: Errors in Modal Data

(²) Numbers G9/82 to G14/82: Grunehogna sill, 1390 section; G17/82: Basal zone of Kullen sill, 1390 section; G28/82: Upper chill zone, Kullen sill, 1390 section; G31/84: Kullen sill, basal zone, Grunehogna windscoop south of 1390; G59/82 to G67/82: Kullen section, Peak 1550.

(³) Approximate heights above snow line.

(⁴) Altered to amphibole in most cases, and included in clinopyroxene total.

(⁵) Includes amphiboles.

(⁶) Plagioclase extensively saussuritized and sericitized.

TABLE 4.4

SUMMARY OF PETROGRAPHY OF SEDIMENTS AND GRANOSEDIMENTS ALONG THE 1285 SE CONTACT ZONE

SAMPLE NUMBER	HEIGHT ABOVE SILL CONTACT	SAMPLE DESCRIPTION	DISTINCTIVE AND CHARACTERISTIC FEATURES	COMMENTS
G14/84	7.0 m	Fine- to medium-grained arenite		Laminations defined by concentrations of Fe-Ti oxides in layers, 0.2 m thick, 6 mm apart.
G13/84	5.0 m	Medium-grained subarkose	Sporadic development PEQ texture	
G12/84	3.8 m	Coarse-grained, poorly sorted, carbonate-rich quartz arenite	Coarse (2 mm diameter) quartz grains show abundant PEQ texture	
G11/84	3.5 m	Subarkose	Extensive development of granophyric and pseudo-granophyric textures	Muscovite is abundant
G10/84	2.8 m	As for G9/84	SAPG textures	
G9/84	2.0 m	Fine- to medium-grained grano-sediment comprising \pm 60% quartz, 25% K-feldspar, 10% albite + muscovite + Fe-Ti oxides	SAPG textures	
G7/84	1.3 m	Medium-grained granular quartz arenite	PEQ, and EEQ textures; local development of veinlets comprising euhedral quartz, anhedral K-feldspar, carbonate, chlorite, epidote and zoisite	Lamination defined by variations in grain size and concentrations of Fe-Ti oxides
G5/84	0.3 m	As for G4/84	Quartz textures vary from recrystallized, with well-defined triple junctions at 120°, to EEQ	
G4/84	0.10 m	Granosediment, variable composition	Laminations, 5 to 10 mm thick which show either extensive EEQ and granophyric textures, or granitic textures similar to G3/84	Apatite is abundant, with smaller amounts of zircon, epidote, chlorite and sphene
G3/84	0.05 m	Medium-grained granophyric granite	Granular granophyric textured granite comprising albite laths, microperthitic, Fe-stained K-feldspar, and minor and trace amounts of chlorite, epidote, skeletal magnetite, haematite, apatite, sphene (minor constituent) and allanite	Fe-Ti oxides concentrated in narrow, 1 mm, laminations, defining crude layering

Abbreviations: PEQ, partially embayed quartz grains
 EEQ, extensively embayed quartz grains
 SAPQ, spherical aggregates of pseudo-granophyric, EEQ and PEQ textures
 See text for definitions

TABLE 4.5

STATISTICAL DATA FOR GEOCHEMISTRY OF GRUNEHOGNA INTRUSIONS AND GRANOSSEDIMENTS

ELEMENT OR CHEMICAL PARAMETER	ROCK TYPE ⁽¹⁾	NUMBER OF DETERMINATIONS ⁽²⁾	MINIMUM	MAXIMUM	MEAN	VARIANCE	STANDARD DEVIATION
SiO ₂ ⁽³⁾	1	20	53.62	57.01	55.35	.74	.86
	2	6	51.75	56.86	54.76	5.36	2.31
	3	5	64.09	72.25	68.08	8.83	2.97
	4	13	56.98	84.67	72.51	46.20	6.80
Al ₂ O ₃	1	20	14.02	16.81	15.47	.63	.79
	2	6	12.45	13.48	12.99	.17	.41
	3	5	11.32	12.76	12.24	.32	.57
	4	13	8.57	17.07	12.62	5.66	2.38
FeO	1	20	7.77	9.80	8.61	.24	.49
	2	6	11.68	14.73	13.07	1.72	1.31
	3	5	4.04	9.28	7.24	3.89	1.97
	4	13	1.02	9.57	4.36	8.90	2.98
MnO	1	20	.15	.22	.17	.00	.02
	2	6	.23	.30	.27	.00	.02
	3	5	.04	.17	.09	.00	.06
	4	13	.02	.15	.07	.00	.04
MgO	1	20	3.92	8.00	5.11	1.19	1.09
	2	6	1.89	3.93	2.75	.44	.66
	3	5	.26	1.12	.68	.11	.33
	4	13	.32	3.06	1.27	.71	.84
Mg ⁽⁴⁾	1	20	43.13	61.62	50.91	26.09	5.11
	2	6	20.7	32.34	27.08	14.59	3.82
	3	5	10.29	17.70	13.74	9.95	3.15
	4	13	5.99	53.55	38.31	292.77	17.11
CaO	1	20	7.51	10.31	8.94	.45	.67
	2	6	5.68	8.45	6.91	.80	.90
	3	5	1.52	3.60	2.38	.82	.90
	4	13	.49	7.91	1.87	3.47	1.86
Na ₂ O	1	20	1.67	2.72	2.12	.11	.33
	2	6	2.60	4.23	3.17	.36	.60
	3	5	2.99	4.03	3.46	.21	.46
	4	13	1.90	5.63	3.57	.81	.90
K ₂ O	1	20	.87	2.18	1.42	.14	.38
	2	6	1.18	1.88	1.64	.06	.25
	3	5	2.79	4.00	3.30	.20	.45
	4	13	.98	3.98	2.72	.97	.98

TABLE 4.5
continued

ELEMENT OR CHEMICAL PARAMETER	ROCK TYPE ⁽¹⁾	NUMBER ⁽²⁾ OF DETERMINATIONS	MINIMUM	MAXIMUM	MEAN	VARIANCE	STANDARD DEVIATION
TiO ₂	1	20	.63	1.24	.89	.02	.14
	2	6	1.78	2.87	2.15	.17	.41
	3	5	.27	1.01	.68	.08	.28
	4	13	.18	.95	.51	.03	.17
P ₂ O ₅	1	20	.09	.17	.12	.00	.02
	2	6	.14	.76	.30	.05	.23
	3	5	.04	.28	.17	.01	.09
	4	13	.06	.18	.13	.00	.04
Nb ⁽³⁾	1	20	6.3	10.9	8.9	1.4	1.2
	2	6	10.0	17.4	13.0	7.0	2.6
	3	5	16.2	25.2	21.4	12.5	3.5
	4	13	8.8	30.3	16.4	47.4	6.9
Zr	1	20	100	156	130	266	16
	2	6	138	231	191	953	31
	3	5	141	452	325	13669	117
	4	13	101	589	279	16817	130
Y	1	20	19.0	30.5	25.1	10.5	3.2
	2	6	30.7	53.4	40.2	59.4	7.7
	3	5	47.9	81.6	59.8	234.0	15.3
	4	13	17.4	92.6	43.3	505.6	22.5
Sr	1	20	127	289	170	1475	38
	2	6	139	222	191	789	28
	3	5	113	195	153	900	30
	4	13	43	344	183	8957	95
Rb	1	20	34	114	68	422	21
	2	6	44	66	54	54	7
	3	5	77	114	94	210	15
	4	13	51	123	81	601	25
Zn	1	19	67	107	86	134	12
	2	6	90	146	108	460	21
	3	5	9	93	42	1032	32
	4	4	18	79	45	645	25
Cu	1	19	74	136	106	339	18
	2	6	180	489	274	19203	139
	3	5	13	161	87	3439	59
	4	4	26	132	82	2824	53

TABLE 4.5

continued

ELEMENT OR CHEMICAL PARAMETER	ROCK ⁽¹⁾ TYPE	NUMBER ⁽²⁾ OF DETERMINATIONS	MINIMUM	MAXIMUM	MEAN	VARIANCE	STANDARD DEVIATION
Ni	1	19	31	79	45	213	15
	2	6	1	28	7	111	11
	3	5	1	5	3	2	1
	4	4	5	27	15	125	11
Sc	1	17	33.2	41.3	36.3	6.8	2.6
	2	6	31.7	44.9	40.4	24.3	4.9
	3	1	13.8	-	-	-	-
	4	4	11.8	32.5	17.3	102.8	10.1
Cr	1	17	8	219	90	4135	64
	2	4	2	17	8	41	6
	3	0	-	-	-	-	-
	4	3	1	169	63	8508	92
Ba	1	2	404	431	418	365	19
	2	2	402	479	441	2965	54
	3	5	1126	1580	1303	45597	214
	4	12	214	1408	826	144979	381
V	1	19	186	276	241	545	23
	2	6	22	693	192	63154	251
	3	5	5	34	19	126	11
	4	4	4	246	83	12977	114

(1) Rock type 1: Kullen sill; 2: Grunehogna sill; 3: Granites SE of Peak 1390; 4: Granosediments

(2) Concentrations below detection limit not considered

(3) Major elements in weight per cent

(4) $Mg^* = 100 \text{ Mg}/(\text{Mg} + \text{Fe})$

(5) Trace elements in ppm

TABLE 4.6
VARIABLE CORRELATION OF SELECTED ELEMENT PAIRS: KULLEN SILL

ELEMENT X	ELEMENT Y	NUMBER ⁽¹⁾ OF DETERMINATIONS	R	R ²	SLOPE	STANDARD ERROR OF SLOPE	INTERCEPT ON Y	STANDARD ERROR OF INTERCEPT	DISPERSION ⁽²⁾
Mg	SiO ₂	20	-.38	.15	-.17	-.03	63.91	1.78	8.61
"	Al ₂ O ₃	20	-.36	.13	-.15	-.03	23.36	1.65	8.54
"	FeO	20	-.16	.03	-.10	-.02	13.48	1.08	7.83
"	MnO	20	-.14	.02	-.0032	-.0007	.34	.04	7.70
"	MgO	20	.96	.91	.21	.01	-5.77	.72	1.55
"	CaO	20	.47	.22	.13	.03	2.24	1.33	5.33
"	Na ₂ O	20	-.53	.28	-.07	-.01	5.43	.63	8.95
"	K ₂ O	20	-.69	.48	-.07	-.01	5.17	.61	9.43
"	TiO ₂	20	-.70	.49	-.03	.00	2.29	.22	9.43
"	P ₂ O ₅	20	-.68	.47	.00	.32	.32	.03	9.37
"	Nb	20	-.71	.51	-.23	-.04	20.8	1.9	9.7
"	Zr	20	-.74	.55	-3.19	-.48	292	25	32
"	Y	20	-.72	.53	-.63	-.10	57.4	5.0	11.2
"	Sr	20	-.68	.47	-7.52	-1.23	553	63	71
"	Rb	20	-.58	.34	-4.02	-.73	272	37	38
"	Zn	19	-.36	.13	-2.21	-.47	199	24	21
"	Cu	19	-.48	.23	-3.52	-.71	285	36	33
"	Ni	19	.96	.91	2.79	.19	-96	10	5
"	Sc	17	-.22	.05	-.48	-.11	60.8	5.8	9.3
"	Cr	17	-.91	.83	11.93	1.18	-513	60	27
"	Ba	2	-1.00	1.00	-13.83	-.01	1073	1	38
"	V	19	-.48	.23	-4.50	-.91	469	46	41
Zr	SiO ₂	20	.81	.66	.0527	.0068	48.52	.89	9.97
"	Al ₂ O ₃	20	.05	.00	.05	.01	9.18	1.42	22.53
"	FeO	20	.09	.01	.03	.01	4.73	.87	22.06
"	MnO	20	.07	.00	.00	.00	.04	.03	22.25
"	MgO	20	-.70	.49	-.07	.01	13.78	1.39	30.16
"	CaO	20	-.78	.61	-.04	.01	14.27	.75	30.79
"	Na ₂ O	20	.25	.06	.02	.00	-.53	.58	19.96
"	K ₂ O	20	.86	.75	.02	.00	-1.56	.34	8.50
"	Ti	20	.42	.18	51.63	10.46	-1376	1366	9.05
"	P ₂ O ₅	20	.50	.25	.0012	.0002	-.04	.03	16.26
"	Nb	20	.64	.40	.07	.01	-.6	1.6	13.9
"	Y	20	.94	.89	.20	.01	-.7	1.9	5.6
"	Sr	20	.52	.27	2.36	.45	-135	59	41
"	Rb	20	.79	.63	1.26	.17	-96	22	17
"	Zn	19	.41	.17	.71	.15	-6	20	22
"	Cu	19	.30	.09	1.13	.25	-42	32	29
"	Ni	19	-.70	.48	-.90	-.15	162	19	40
"	Sc	17	.37	.14	.16	.04	16.0	4.6	18.9
"	Cr	17	-.56	.32	-3.87	-.78	590	101	117
"	Ba	2	1.00	1.00	3.00	.00	-13	0	0
"	V	19	.42	.18	1.40	.29	60	38	31

TABLE 4.6

continued

ELEMENT X	ELEMENT Y	NUMBER ⁽¹⁾ OF DETERMINATIONS	R	R ²	SLOPE	STANDARD ERROR OF SLOPE	INTERCEPT ON Y	STANDARD ERROR OF INTERCEPT	DISPERSION ⁽²⁾
Ti	P ₂ O ₅	20	.88	.78	.0000	.0000	-.01	.01	410.14
"	Nb	20	.51	.26	.0014	.0003	1.3	1.5	834.9
"	Y	20	.42	.18	.0039	.0008	4.6	4.2	906.6
"	Sr	20	.55	.30	.0456	.0085	-72	46	802
"	Rb	20	.09	.01	.0244	.0054	-62	29	1138
"	Ba	2	1.00	1.00	.0902	.0003	-74	2	1
P ₂ O ₅	Nb	20	.37	.14	59.80	12.24	1.7	1.5	1.3
"	Y	20	.43	.18	162.35	43.86	5.8	4.0	3.5
"	Sr	20	.51	.26	1922.58	369.20	-58	45	38
"	Rb	20	.16	.03	1027.90	226.77	-55	27	27
"	Ba	2	-1.00	1.00	-2700.00	.00	755	0	38
Nb	Y	20	.64	.41	2.71	.47	1.0	4.2	2.9
"	Sr	20	.59	.35	32.15	5.80	-115	52	35
"	Rb	20	.50	.25	17.19	3.32	-85	30	21
"	Ba	2	1.00	1.00	19.29	.03	244	0	0
Y	Sr	20	.44	.19	11.84	2.38	-127	60	41
"	Rb	20	.77	.59	6.33	.90	-91	23	14
"	Ba	2	1.00	1.00	16.87	.02	-45	0	0
Sr	Rb	20	.62	.39	.53	.09	-24	16	0
"	Ba	2	-1.00	1.00	-4.50	.00	1192	0	38
Rb	Ba	2	1.00	1.00	9.00	.00	-280	0	39

¹ Concentrations below detection limit not considered² Dispersion about the reduced major axes

TABLE 4.7
VARIABLE CORRELATION OF SELECTED ELEMENT PAIRS: GRUNEHOGNA SILL

ELEMENT X	ELEMENT Y	NUMBER ⁽¹⁾ OF DETERMINATIONS	R	R ²	SLOPE	STANDARD ERROR OF SLOPE	INTERCEPT ON Y	STANDARD ERROR OF INTERCEPT	DISPERSION ⁽²⁾
Mg	SiO ₂	6	-.46	.21	-.61	-.22	71.17	6.00	7.64
"	Al ₂ O ₃	6	.43	.19	.11	.04	10.08	1.08	4.09
"	FeO	6	.18	.03	.34	.14	3.77	3.77	5.18
"	MnO	6	.74	.55	-.0061	-.0017	.43	.05	7.13
"	MgO	6	.89	.79	.17	.03	-1.95	.89	1.83
"	CaO	6	.89	.79	.23	.04	.56	1.19	1.84
"	Na ₂ O	6	-.22	.05	-.16	-.06	7.43	1.72	6.04
"	K ₂ O	6	-.73	.53	-.07	-.02	3.44	.51	7.11
"	TiO ₂	6	.04	.00	.11	.04	-.78	1.21	5.32
"	P ₂ O ₅	6	-.78	.60	-.06	-.02	1.92	.42	7.21
"	Nb	6	-.78	.61	-.69	-.18	31.7	4.8	8.8
"	Zr	6	-.86	.74	-8.08	-1.68	410	46	60
"	Y	6	-.84	.71	-2.02	-.44	94.9	12.1	16.5
"	Sr	6	.53	.28	7.36	2.54	-8	70	27
"	Rb	6	-.91	.82	-1.91	-.33	105	9	16
"	Zn	6	.59	.34	5.62	1.86	-44	51	20
"	Cu	6	.48	.23	36.28	12.96	-709	354	141
"	Ni	6	.69	.48	2.76	.81	-68	22	9
"	Sc	6	.77	.59	1.29	.34	5.5	9.2	4.2
"	Cr	4	-.50	.25	-2.25	-.97	72	28	12
"	Ba	2	-1.00	1.00	-17.14	-.02	956	1	109
"	V	6	.71	.51	65.79	18.78	-1589	514	190
Zr	SiO ₂	6	.81	.66	.0750	.0179	40.41	3.47	19.01
"	Al ₂ O ₃	6	.02	.00	.01	.01	10.44	1.05	43.12
"	FeO	6	-.65	.42	-.04	-.01	21.20	2.57	56.04
"	MnO	6	.60	.36	.00	.00	.12	.05	27.53
"	MgO	6	-.99	.99	-.02	.00	6.87	.18	61.65
"	CaO	6	-.99	.98	-.03	.00	12.46	.35	61.57
"	Na ₂ O	6	.08	.01	.02	.01	-.56	1.54	41.90
"	K ₂ O	6	.92	.85	.01	.00	.07	.25	12.03
"	Ti	6	-.50	.25	-80.14	-28.39	28224	5503	4280
"	P ₂ O ₅	6	.70	.50	.0074	.0021	-1.1	.41	23.72
"	Nb	6	.90	.81	.09	.02	-3.4	3.0	13.9
"	Y	6	.93	.86	.25	.04	-7.6	7.3	12.0
"	Sr	6	-.47	.22	-.91	-.33	365	64	71
"	Rb	6	.84	.70	.24	.05	8	10	18
"	Zn	6	-.91	.82	-.70	-.12	241	23	73
"	Cu	6	-.85	.73	-4.49	-.95	1133	185	273
"	Ni	6	-.90	.81	-.34	-.06	72	12	64
"	Sc	6	-.79	.62	-.16	-.04	71.0	7.8	59.1
"	Cr	4	-.17	.03	-.22	-.11	48	20	45
"	Ba	2	1.00	1.00	1.17	.00	241	0	0
"	V	6	-.91	.83	-8.14	-1.37	1750	265	495

TABLE 4.7

continued

ELEMENT X	ELEMENT Y	NUMBER ⁽¹⁾ OF DETERMINATIONS	R	R ²	SLOPE	STANDARD ERROR OF SLOPE	INTERCEPT ON Y	STANDARD ERROR OF INTERCEPT	DISPERSION ⁽²⁾
Ti	P ₂ O ₅	6	-.36	.13	-.0001	.0000	1.49	.46	4076.84
"	Nb	6	-.62	.38	-.0011	-.0003	26.8	4.5	4446.6
"	Y	6	-.54	.30	-.0031	-.0011	80.4	14.0	4347.4
"	Sr	6	.37	.14	.0114	.0043	44	56	2770
"	Rb	6	-.24	.06	-.0030	-.0012	92	15	3894
"	Ba	2	-1.00	-1.00	-.0203	.0000	696	.0	5357
P ₂ O ₅	Nb	6	.90	.82	11.60	2.02	9.4	.8	1.2
"	Y	6	.91	.82	33.83	5.83	29.9	2.2	3.3
"	Sr	6	-.92	.85	-123.31	-19.51	228	7	55
"	Rb	6	.85	.73	32.10	6.82	44	3	4
"	Ba	2	1.00	1.00	962.50	.22	229	0	0
Nb	Y	6	.98	.97	2.92	.21	2.4	2.7	1.4
"	Sr	6	-.77	.60	-10.63	-2.75	329	36	53
"	Rb	6	.83	.69	2.77	.63	18	8	5
"	Ba	2	1.00	1.00	18.78	.01	214	0	0
Y	Sr	6	-.75	.56	-3.64	-.98	337	40	55
"	Rb	6	.89	.79	.95	.18	15	7	5
"	Ba	2	1.00	1.00	7.20	.00	181	0	0
Sr	Rb	6	-.60	.35	-.26	-.09	103	16	52
"	Ba	2	1.00	1.00	9.62	.00	-1398	0	0
Rb	Ba	2	1.00	1.00	12.83	.00	-163	0	0

¹ Concentrations below detection limit not considered.² Dispersion about the reduced major axes.

TABLE 4.8

VARIABLE CORRELATION OF SELECTED ELEMENT PAIRS: GRUNEHOGNA GRANITES

ELEMENT X	ELEMENT Y	NUMBER ⁽¹⁾ OF DETERMINATIONS	R	R ²	SLOPE	STANDARD ERROR OF SLOPE	INTERCEPT ON Y	STANDARD ERROR OF INTERCEPT	DISPERSION ⁽²⁾
Mg	SiO ₂	5	-.93	.87	-.94	-.15	81.02	2.12	8.52
"	Al ₂ O ₃	5	.89	.80	.18	.04	9.76	.51	1.48
"	FeO	5	.86	.73	.62	.14	-1.35	2.04	2.00
"	MnO	5	.99	.97	.0174	.0013	-.15	.02	.51
"	MgO	5	.98	.96	.11	.01	-.76	.13	.60
"	CaO	5	.97	.95	.29	.03	-1.56	.41	.75
"	Na ₂ O	5	-.27	.07	-.15	-.06	5.46	.89	5.08
"	K ₂ O	5	-.80	.64	-.14	-.04	5.26	.54	6.04
"	TiO ₂	5	.92	.85	.09	.01	-.52	.21	1.24
"	P ₂ O ₅	5	.94	.88	.03	.00	-.22	.06	1.13
"	Nb	5	-.86	.74	-1.12	-.25	36.8	3.6	9.2
"	Zr	5	-.89	.80	-37.06	-7.40	834	104	228
"	Y	5	-.82	.68	-4.85	-1.23	126.4	17.4	29.8
"	Sr	5	-.17	.03	-9.51	-4.19	283	59	46
"	Rb	5	-.85	.73	-4.60	-1.08	157	15	29
"	Zn	5	.92	.84	10.18	1.83	-98	26	13
"	Cu	5	-.12	.01	-18.59	-8.26	343	116	88
"	Ni	5	.65	.43	.47	.16	-4	2	3
"	Sc	1	-	-	-	-	-	-	-
"	Cr	0	-	-	-	-	-	-	-
"	Ba	5	-.06	0.00	-67.69	-30.22	2233	426	310
"	V	5	.87	.76	3.56	.78	-30	11	6
Zr	SiO ₂	5	.95	.91	.0254	.0034	59.81	1.17	35.25
"	Al ₂ O ₃	5	-.82	.67	0.00	.00	13.82	.43	223.01
"	FeO	5	-.88	.77	-.02	.00	12.72	1.25	226.61
"	MnO	5	-.94	.88	.00	.00	.25	.03	230.06
"	MgO	5	-.94	.89	.00	.00	1.61	.15	230.53
"	CaO	5	-.92	.84	-.01	.00	4.90	.48	228.93
"	Na ₂ O	5	.07	.00	.00	.00	2.18	.61	159.40
"	K ₂ O	5	.90	.81	.00	.00	2.05	.26	51.93
"	Ti	5	-.89	.79	-14.15	-2.92	8700	1009	3222
"	P ₂ O ₅	5	-.93	.87	-.0008	-.0001	.41	.04	229
"	Nb	5	.93	.86	.03	.01	11.5	1.7	44.4
"	Y	5	.78	.61	.13	.04	17.3	12.6	78.1
"	Sr	5	.30	.09	.26	.11	69	38	143
"	Rb	5	.92	.85	.12	.02	53	7	46
"	Zn	5	-.94	.89	-.27	-.04	131	14	239
"	Cu	5	.06	.00	.50	.22	-76	77	179
"	Ni	5	-.62	.39	-.01	.00	7	2	211
"	Sc	1	-	-	-	-	-	-	-
"	Cr	0	-	-	-	-	-	-	-
"	Ba	5	-.09	.01	-1.83	-.81	1897	281	359
"	V	5	-.81	.71	-.10	-.02	50	8	225

TABLE 4.8

continued

ELEMENT X	ELEMENT Y	NUMBER ⁽¹⁾ OF DETERMINATIONS	R	R ²	SLOPE	STANDARD ERROR OF SLOPE	INTERCEPT ON Y	STANDARD ERROR OF INTERCEPT	DISPERSION ⁽²⁾
Ti	P ₂ O ₅	5	.99	.99	.0001	.0000	-.05	.01	192.28
"	Nb	5	-.72	.52	-.0021	-.0007	30.1	2.9	3069.0
"	Y	5	-.83	.69	-.0092	-.0023	97.7	10.2	3164.6
"	Sr	5	-.54	.29	-.0181	-.0068	227	30	2900
"	Rb	5	-.89	.79	-.0088	-.0018	130	8	3217
"	Ba	5	-.30	.09	-.1291	-.0551	1832	243	2689
P ₂ O ₅	Nb	5	-.79	.62	-40.15	-11.02	28.1	2.1	6.7
"	Y	5	-.86	.73	-173.53	-40.23	89.0	7.6	29.5
"	Sr	5	-.49	.24	-340.39	-132.94	210	25	52
"	Rb	5	-.93	.86	-164.52	-27.09	121	5	28
"	Ba	5	-.23	.05	-2422.46	-1054.02	1710	200	335
Nb	Y	5	.76	.57	4.32	1.26	-32.6	27.4	10.9
"	Sr	5	-.07	.00	-8.48	-3.78	334	82	44
"	Rb	5	.85	.73	4.10	.96	6	21	8
"	Ba	5	-.28	.08	-60.33	-25.90	2593	561	342
Y	Sr	5	.28	.08	1.96	.84	35	52	40
"	Rb	5	.95	.90	.95	.14	37	8	7
"	Ba	5	.41	.16	13.96	5.71	468	352	234
Sr	Rb	5	.38	.15	.48	.20	20	31	37
"	Ba	5	.63	.39	7.12	2.48	217	385	186
Rb	Ba	5	.23	.05	14.72	6.41	-75	607	266

¹ Concentrations below detection limit not considered.² Dispersion about the reduced major axes.

TABLE 4.9

VARIABLE CORRELATION OF SELECTED ELEMENT PAIRS: GRUNEHOGNA GRANOSSEDIMENTS

ELEMENT X	ELEMENT Y	NUMBER ⁽¹⁾ OF DETERMINATIONS	R	R ²	SLOPE	STANDARD ERROR OF SLOPE	INTERCEPT ON Y	STANDARD ERROR OF INTERCEPT	DISPERSION ⁽²⁾
Mg	SiO ₂	13	.29	.08	.40	.11	57.29	4.42	21.94
"	Al ₂ O ₃	13	.15	.02	.14	.04	7.29	1.60	22.95
"	FeO	13	-.82	.67	-.17	-.03	11.04	1.16	33.15
"	MnO	13	.38	.15	.0022	.0006	-.02	.02	19.03
"	MgO	13	.49	.24	.05	.01	-.61	.50	17.30
"	CaO	13	.10	.01	.11	.03	-2.30	1.26	23.03
"	Na ₂ O	13	-.32	.10	-.05	-.01	5.58	.58	27.88
"	K ₂ O	13	.18	.03	.06	.02	.51	.66	21.93
"	TiO ₂	13	-.27	.07	-.01	.00	.89	.11	27.30
"	P ₂ O ₅	13	.71	.51	.00	.00	.05	.02	12.94
"	Zr	13	-.73	.53	-.40	-.08	31.8	3.2	34.3
"	Nb	13	-.77	.60	-7.58	-1.33	57.0	56	246
"	Y	13	-.85	.73	-1.31	-.19	93.6	8.0	54.4
"	Sr	13	.27	.07	5.53	1.48	-29	62	116
"	Rb	13	.20	.04	1.43	.39	26	16	38
"	Zn	4	.71	.50	1.17	.41	15	14	26
"	Cu	4	-.24	.06	-2.44	-1.19	146	40	90
"	Ni	4	.99	.99	.51	.03	2	1	2
"	Sc	4	.46	.21	.47	.21	5.1	7.1	25.0
"	Cr	3	.74	.55	4.40	1.71	-82	67	68
"	Ba	12	.04	.00	21.57	6.22	15	258	528
"	V	4	.68	.47	5.23	1.91	-54	65	92
Zr	SiO ₂	13	-.17	.03	-.0524	-.0143	87.5	4.41	198.84
"	Al ₂ O ₃	13	-.04	.00	-.02	-.01	17.74	1.57	186.77
"	FeO	13	.51	.26	.02	.01	-2.06	1.69	128.98
"	MnO	13	-.32	.10	.00	.00	.15	.02	210.71
"	MgO	13	-.46	.21	-.01	.00	3.08	.49	221.26
"	CaO	13	-.28	.08	-.01	.00	5.88	1.18	207.91
"	Na ₂ O	13	.50	.25	.01	.00	1.64	.51	129.79
"	K ₂ O	13	-.04	.00	-.01	.00	4.84	.65	187.02
"	Ti	13	.12	.01	7.90	2.17	828	669	1368
"	P ₂ O ₅	13	-.45	.21	-.0003	-.0001	.21	.02	221.05
"	Nb	13	.55	.30	.05	.01	1.5	3.8	123.3
"	Y	13	.67	.45	.17	.04	-5.1	11.0	106.6
"	Sr	13	.15	.02	.73	.20	-21	62	210
"	Rb	13	-.19	.03	-.19	-.05	134	16	203
"	Zn	4	-.89	.79	-.21	-.05	107	15	243
"	Cu	4	-.16	.03	-.43	-.21	210	68	203
"	Ni	4	-.90	.81	-.09	-.02	42	6	239
"	Sc	4	-.79	.62	-.08	-.03	41.8	8.1	232.2
"	Cr	3	-.30	.09	-.73	-.40	254	117	252
"	Ba	12	.08	.01	2.84	.82	16	258	549
"	V	4	-.93	.86	-.93	-.17	358	55	328

TABLE 4.9

continued

ELEMENT X	ELEMENT Y	NUMBER ⁽¹⁾ OF DETERMINATIONS	R	R ²	SLOPE	STANDARD ERROR OF SLOPE	INTERCEPT ON Y	STANDARD ERROR OF INTERCEPT	DISPERSION ⁽²⁾
Ti	P ₂ O ₅	13	.02	.00	.0000	.0000	.02	.03	1431.89
"	Nb	13	.27	.07	.0067	.0018	-4.0	5.7	1235.8
"	Y	13	.31	.10	.0220	.0058	-23.3	18.5	1204.4
"	Sr	13	.01	.00	.0924	.0256	-97	82	1449
"	Rb	13	.05	.00	.0239	.0066	9	21	1413
"	Ba	13	-.24	.06	-.3613	-.1012	1939	329	1767
P ₂ O ₅	Nb	13	-.31	.10	-188.42	-49.68	41.3	6.8	11.1
"	Y	13	-.44	.20	-615.18	-153.05	124.7	21.0	38.2
"	Sr	13	.02	.00	2589.38	-717.96	-159	99	132
"	Rb	13	.35	.12	670.53	174.51	-8	24	28
"	Ba	12	.12	.02	9994.05	2863.15	-490	392	504
Nb	Y	13	.89	.80	3.26	.41	-10.1	7.2	10.8
"	Sr	13	-.34	.12	-13.74	-3.58	408	63	156
"	Rb	13	-.10	.01	-3.56	-.98	139	17	38
"	Ba	12	-.06	.00	-54.22	-15.62	1735	284	555
Y	Sr	13	-.36	.13	-4.21	-1.09	365	53	160
"	Rb	13	-.19	.04	-1.09	-.30	128	14	51
"	Ba	12	.09	.01	16.64	4.78	82	240	515
Sr	Rb	13	-.19	.04	-.26	-.07	129	15	151
"	Ba	12	-.19	.04	-3.89	-1.10	1524	225	608
Rb	Ba	12	.62	.39	15.24	3.44	-389	287	331

¹ Concentrations below detection limit not considered.² Dispersion about the reduced major axes.

TABLE 4.10

COMPARISONS OF GEOCHEMICAL VARIATION IN GRUNEHOGNA AND KULLEN SILLS
USING Z VALUES

ELEMENT X	ELEMENT Y	ABSOLUTE Z OF SLOPES	% EXPECTED ⁽¹⁾ DIFFERENCE	X ₀	ABSOLUTE Z AT X ₀	% EXPECTED DIFFERENCE
Mg	SiO ₂	1.98	4.8	-	-	-
"	Al ₂ O ₃	5.20	<0.3	-	-	-
"	FeO	3.11	<0.3	-	-	-
"	MnO	1.58	11.0	60	1.49	<u>14.0</u>
"	MgO	1.27	21.0	60	1.43	<u>15.0</u>
"	CaO	2.0	4.6	-	-	-
"	Na ₂ O	1.48	14.0	60	1.72	<u>8.5</u>
"	K ₂ O	0.00	100.0	60	2.60	0.9
"	TiO ₂	3.50	<0.3	-	-	-
"	P ₂ O ₅	3.00	0.3	-	-	-
"	Nb	2.50	1.2	-	-	-
"	Zr	2.80	0.5	-	-	-
"	Y	3.08	<0.3	-	-	-
"	Sr	5.27	<0.3	-	-	-
"	Rb	2.63	0.9	-	-	-
"	Zn	4.08	<0.3	-	-	-
"	Cu	3.07	<0.3	-	-	-
"	Ni	0.004	100.00	60	0.98	<u>32.00</u>
"	Sc	4.95	<0.3	-	-	-
"	Cr	9.28	<0.3	-	-	-
"	Ba ⁽²⁾	-	-	-	-	-
"	V	3.74	<0.3	-	-	-
Zr	SiO ₂	0.89	37.0	60	11.42	0.3
"	Al ₂ O ₃	2.83	0.4	-	-	-
"	FeO	4.95	<0.3	-	-	-
"	MnO ⁽¹⁾	-	-	-	-	-
"	MgO	5.00	<0.3	-	-	-
"	CaO	1.00	32.0	60	13.31	0.3
"	Na ₂ O	0.00	100.0	60	.09	<u>92.0</u>
"	K ₂ O ²	-	-	-	-	-
"	Ti	4.35	<0.3	-	-	-
"	P ₂ O ₅	2.94	3.2	-	-	-
"	Nb	0.89	37.0	60	2.41	1.6
"	Y	1.21	22.0	60	2.96	0.3
"	Sr	5.86	<0.3	-	-	-
"	Rb	5.76	<0.3	-	-	-
"	Zn	7.34	<0.3	-	-	-
"	Cu	5.72	<0.3	-	-	-
"	Ni	3.47	<0.3	-	-	-
"	Sc	5.66	<0.3	-	-	-
"	Cr	4.63	<0.3	-	-	-
"	Ba ⁽²⁾	-	-	-	-	-
"	V	6.81	<0.3	-	-	-

TABLE 4.10

continued

ELEMENT X	ELEMENT Y	ABSOLUTE Z OF SLOPES	% EXPECTED DIFFERENCE ⁽¹⁾	X ₀	ABSOLUTE Z AT X ₀	% EXPECTED DIFFERENCE
Ti	P ₂ O ₅	-	-	-	-	-
"	Nb	5.89	<0.3	-	-	-
"	Y	5.15	<0.3	-	-	-
"	Sr	3.59	<0.3	-	-	-
"	Rb	4.95	<0.3	-	-	-
"	Ba ⁽²⁾	-	-	-	-	-
P ₂ O ₅	Nb	3.83	<0.3	-	-	-
"	Y	3.85	<0.3	-	-	-
"	Sr	5.53	<0.3	-	-	-
"	Rb	4.39	0.3	-	-	-
"	Ba ⁽²⁾	-	-	-	-	-
Nb	Y	0.41	68.0	60	1.72	<u>8.5</u>
"	Sr	6.67	<0.3	-	-	-
"	Rb	4.27	<0.3	-	-	-
"	Ba ⁽²⁾	-	-	-	-	-
Y	Sr	6.01	<0.3	-	-	-
"	Rb	5.86	<0.3	-	-	-
"	Ba ⁽²⁾	-	-	-	-	-
Sr	Rb	6.21	<0.3	-	-	-
"	Ba ⁽²⁾	-	-	-	-	-
Rb	Ba ⁽²⁾	-	-	-	-	-

NOTES:

Element variations which show no significant differences for both slopes and growth lines at X₀ are underlined in the righthand column.

1. The relative number of cases (expressed in per cent) expected to be larger than that observed when drawing pairs of samples from a homogeneous population, is determined by the absolute value of Z.
2. Z values not computed either because $\sqrt{0.0}$ in calculation, or not sufficient data available.

TABLE 4.11
COMPARISONS OF GEOCHEMICAL VARIATION IN THE GRUNEHOGNA SILL
AND GRUNEHOGNA GRANITES

ELEMENT X	ELEMENT Y	ABSOLUTE Z OF SLOPES	% EXPECTED ⁽¹⁾ DIFFERENCE	X ₀	ABSOLUTE Z AT X ₀	% EXPECTED DIFFERENCE
Mg ⁺	SiO ₂	1.24	22.0	10	1.72	8.5
"	Al ₂ O ₃	1.24	22.0	35	2.35	1.8
"	FeO	1.41	15.0	10	.948	34.0
"	MnO	10.98	<0.3	-	-	-
"	MgO	1.90	5.8	10	1.15	25.0
"	CaO	1.20	23.0	10	2.20	2.8
"	Na ₂ O	0.118	91.0	10	1.78	7.5
"	K ₂ O	1.57	12.0	10	3.00	<0.3
"	TiO ₂	0.485	63.0	10	0.0088	92.0
"	P ₂ O ₅	4.50	<0.3	-	-	-
"	Nb	1.40	16.0	10	1.81	7.0
"	Zr	3.82	<0.3	-	-	-
"	Y	2.17	3.0	-	-	-
"	Sr	3.44	<0.3	-	-	-
"	Rb	2.38	17.0	10	3.62	0.3
"	Zn	1.75	8.0	35	2.42	1.1
"	Cu	3.57	<0.3	-	-	-
"	Ni	2.77	0.0	-	-	-
"	Sc ⁽²⁾	-	-	-	-	-
"	Cr ⁽²⁾	-	-	-	-	-
"	Ba ⁽²⁾	-	-	-	-	-
"	V	3.31	<0.3	-	-	-
Zr	SiO ₂	2.72	0.7	-	-	-
"	Al ₂ O ₃	3.29	<0.3	-	-	-
"	FeO	1.87	6.1	10	3.64	0.3
"	MnO	5.81	<0.3	-	-	-
"	MgO	18.99	<0.3	-	-	-
"	CaO	9.34	<0.3	-	-	-
"	Na ₂ O	1.93	5.4	10	19.13	0.3
"	K ₂ O	2.91	0.4	-	-	-
"	Ti	2.31	2.1	-	-	-
"	P ₂ O ₅	3.90	<0.3	-	-	-
"	Nb	2.68	0.7	-	-	-
"	Y	2.12	3.4	-	-	-
"	Sr	3.36	<0.3	-	-	-
"	Rb	2.23	2.6	-	-	-
"	Zn	3.40	<0.3	-	-	-
"	Cu	5.12	<0.3	-	-	-
"	Ni	5.50	<0.3	-	-	-
"	Sc ⁽²⁾	-	-	-	-	-
"	Cr ⁽²⁾	-	-	-	-	-
"	Ba ⁽²⁾	-	-	-	-	-
"	V	5.87	<0.3	-	-	-

TABLE 4.11

continued

ELEMENT X	ELEMENT Y	ABSOLUTE Z OF SLOPES	% EXPECTED ⁽¹⁾ DIFFERENCE	X ₀	ABSOLUTE Z AT X ₀	% EXPECTED DIFFERENCE
Ti	P ₂ O ₅	-	-	-	-	-
"	Nb	1.31	19	19	.698	<u>49.0</u>
"	Y	2.39	<0.3	-	-	-
"	Sr	4.04	<0.3	-	-	-
"	Rb	2.68	0.74	-	-	-
"	Ba ⁽²⁾	-	-	-	-	-
P ₂ O ₅	Nb	4.62	<0.3	-	-	-
"	Y	5.10	<0.3	-	-	-
"	Sr	1.62	11.0	10	3.66	<0.3
"	Rb	7.04	<0.3	-	-	-
"	Ba ⁽²⁾	-	-	-	-	-
Nb	Y	1.10	27.0	10	3.55	<0.3
"	Sr	0.46	64.0	35	0.96	<u>33</u>
"	Rb	1.16	24.0	35	1.64	<u>10</u>
"	Ba ⁽²⁾	-	-	-	-	-
Y	Sr	4.34	<0.3	-	-	-
"	Rb	0.00	100.0	10	7.06	<0.3
"	Ba ⁽²⁾	-	-	-	-	-
Sr	Rb	3.37	<0.3	-	-	-
	Ba ⁽²⁾	-	-	-	-	-
Rb	Ba ⁽²⁾	-	-	-	-	-

NOTES:

Element variations which show no significant differences for both slopes and growth lines at X₀ are underlined in the righthand column.

1. The relative number of cases (expressed in per cent) expected to be larger than that observed when drawing pairs of samples from a homogeneous population is determined by the absolute value of Z.
2. Z values not computed either because $\sqrt{0.0}$ in calculation, or not sufficient data available.

TABLE 5.1

STATISTICAL DATA FOR GEOCHEMISTRY OF BORGMASSIVET INTRUSIONS AT KRYLEN

ELEMENT OR CHEMICAL PARAMETER	SAMPLE ⁽¹⁾ GROUPING	NUMBER ⁽²⁾ OF DETERMINATIONS	MINIMUM	MAXIMUM	MEAN	VARIANCE	STANDARD DEVIATION
SiO ₂ ⁽³⁾	1	9	54.38	55.49	54.99	.14	.38
	2	10	48.56	55.49	54.34	4.26	2.06
Al ₂ O ₃	1	9	14.76	16.53	15.62	.33	.58
	2	10	9.52	16.53	15.01	4.02	2.00
FeO	1	9	7.96	8.59	8.32	.05	.22
	2	10	7.96	9.48	8.44	.18	.42
MnO	1	9	.17	.18	.17	.00	.00
	2	10	.17	.18	.17	.00	.00
MgO	1	9	5.62	6.29	5.90	.06	.24
	2	10	5.62	20.69	7.38	21.92	4.68
Mg ⁽⁴⁾	1	9	54.21	56.95	55.81	1.06	1.03
	2	10	54.21	79.55	58.19	57.26	7.57
CaO	1	9	9.03	9.96	9.64	.11	.33
	2	10	7.34	9.96	9.41	.62	.79
Na ₂ O	1	9	1.52	1.77	1.66	.01	.07
	2	10	1.38	1.77	1.63	.01	.11
K ₂ O	1	9	1.00	1.44	1.13	.02	.13
	2	10	.61	1.44	1.08	.04	.20
TiO ₂	1	9	.69	.84	.77	.00	.05
	2	10	.69	.84	.76	.00	.05
P ₂ O ₅	1	7	.10	.12	.11	.00	.01
	2	7	.10	.12	.11	.00	.01
Nb ⁽⁵⁾	1	9	6.1	8.2	7.1	.6	.8
	2	10	4.1	8.2	6.8	1.4	1.2
Zr	1	9	105	125	117	45	7
	2	10	70	125	112	260	16
Y	1	9	19.1	23.4	21.5	2.2	1.5
	2	10	11.3	23.4	20.5	12.4	3.5
Sr	1	9	132	156	144	49	7
	2	10	95	156	139	279	17
Rb	1	9	46	67	52	38	6
	2	10	26	67	49	101	10
Zn	1	9	63	102	84	120	11
	2	10	63	102	82	135	12
Cu	1	9	39	94	80	311	18
	2	10	39	94	77	344	19
Ni	1	9	48	59	53	11	3
	2	10	48	814	129	57990	241
Sc	1	9	30.8	38.0	33.3	4.4	2.1
	2	10	23.3	38.0	32.3	13.9	3.7
Ba	1	4	277	321	292	408	20
	2	5	158	321	265	3871	62
V	1	9	201	235	211	115	11
	2	10	186	235	209	166	13

(1) Sample Grouping: 1. Excluding Mela-olivine gabbroonorite
2. Including Mela-olivine gabbroonorite

(2) Concentrations below detection limit not considered

(3) Major elements in weight per cent

(4) $Mg^* = 100 Mg / (Mg + Fe^{2+})$

(5) Trace elements in ppm

TABLE 6.1

STATISTICAL DATA FOR GEOCHEMISTRY OF JEKSELEN COMPLEX:

ZONE III AND APOPHYSES

ELEMENT OR CHEMICAL PARAMETER	NUMBER OF DETERMINATIONS	MINIMUM	MAXIMUM	MEAN	VARIANCE	STANDARD DEVIATION
SiO ₂	9	55.12	57.35	56.05	.70	.84
Al ₂ O ₃	9	14.82	16.73	15.21	.35	.60
FeO	9	7.64	8.47	8.30	.07	.26
MnO	9	.15	.18	.16	.00	.01
MgO	9	5.77	6.85	6.23	.16	.40
Mg ⁽¹⁾	9	55.16	59.27	57.18	2.49	1.58
CaO	9	4.97	8.28	7.02	1.27	1.13
Na ₂ O	9	1.65	5.61	2.99	1.23	1.11
K ₂ O	9	.16	2.51	1.73	.43	.66
TiO ₂	9	.75	.83	.81	.00	.03
P ₂ O ₅	9	.10	.12	.11	.00	.01
Nb	9	5.2	11.18	8.1	3.5	1.9
Zr	9	122	155	130	94	10
Y	9	22.1	30.3	23.8	6.6	2.6
Sr	9	173	399	245	7297	85
Rb	9	9	89	62	540	23
Zu	9	61	91	84	83	9
Cu	9	14	101	78	630	25
Ni	9	59	76	66	36	6
Sc	9	30	34.3	31.8	1.6	1.3
Cr	0	-	-	-	-	-
Ba	3	109	431	285	26566	163
V	9	213	232	222	35	6

⁽¹⁾ Mg⁺ = Mg/(Mg + Fe²⁺)

TABLE 7.1
SUMMARY OF CORRELATION COEFFICIENTS (R^2) OF INCOMPATIBLE ELEMENTS:
BORGMASSIVET INTRUSIONS AND STRAUMSNUTANE BASALTS

A. ALL INTRUSIONS AND LAVAS

	K ₂ O	TiO ₂	P ₂ O ₅	Nb	Zr	Y	Sr	Rb	Ba
K ₂ O	-								
TiO ₂	.40	-							
P ₂ O ₅	.42	.70	-						
Nb	.46	.70	.56	-					
Zr	.53	.80	.66	.90	-				
Y	.54	.84	.66	.82	.93	-			
Sr	.00	.04	.00	.09	.09	.07	-		
Rb	.86	.31	.30	.38	.44	.44	.01	-	
Ba	.75	.11	.32	.17	.20	.22	.04	.47	-

D. INTRUSIONS (EXCLUDING JEKSELEN COMPLEX AND GRUNEHOGNA SILL) AND LAVAS

	K ₂ O	TiO ₂	P ₂ O ₅	Nb	Zr	Y	Sr	Rb	Ba
K ₂ O	-								
TiO ₂	.48	-							
P ₂ O ₅	.55	.80	-						
Nb	.51	.78	.58	-					
Zr	.59	.88	.70	.90	-				
Y	.60	.89	.68	.83	.94	-			
Sr	.00	.04	.00	.07	.06	.06	-		
Rb	.87	.38	.40	.44	.50	.50	.01	-	
Ba	.75	.15	.35	.16	.22	.25	.05	.50	-

B. ALL INTRUSIONS

	K ₂ O	TiO ₂	P ₂ O ₅	Nb	Zr	Y	Sr	Rb	Ba
K ₂ O	-								
TiO ₂	.26	-							
P ₂ O ₅	.20	.52	-						
Nb	.49	.51	.46	-					
Zr	.52	.61	.54	.86	-				
Y	.47	.68	.58	.70	.86	-			
Sr	.24	.21	.16	.29	.41	.41	-		
Rb	.83	.21	.11	.39	.45	.42	.16	-	
Ba	.85	.01	.23	.52	.31	.27	.26	.40	-

E. INTRUSIONS EXCLUDING JEKSELEN COMPLEX AND GRUNEHOGNA SILL

	K ₂ O	TiO ₂	P ₂ O ₅	Nb	Zr	Y	Sr	Rb	Ba
K ₂ O	-								
TiO ₂	.53	-							
P ₂ O ₅	.38	.78	-						
Nb	.51	.63	.37	-					
Zr	.73	.78	.60	.81	-				
Y	.69	.80	.48	.53	.77	-			
Sr	.40	.38	.19	.19	.35	.47	-		
Rb	.94	.47	.26	.51	.70	.65	.34	-	
Ba	.90	.71	.26	.61	.90	.86	.49	.78	-

C. ALL BASALTS

	K ₂ O	TiO ₂	P ₂ O ₅	Nb	Zr	Y	Sr	Rb	Ba
K ₂ O	-								
TiO ₂	.15	-							
P ₂ O ₅	.37	.75	-						
Nb	.18	.78	.63	-					
Zr	.24	.83	.70	.86	-				
Y	.26	.84	.72	.82	.95	-			
Sr	.07(-)	.00	.09(-)	.00	.00	.00	-		
Rb	.83	.13	.24	.18	.23	.24	.02(-)	-	
Ba	.72	.08	.30	.08	.13	.15	.08(-)	.46	-